

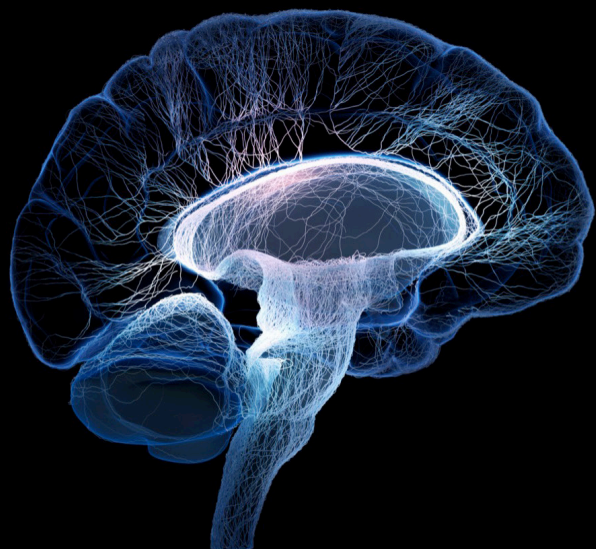
# Advances and challenges in studying brain disorders: From development to aging

**Edited by**

Subashika Govindan, Fiona Francis and  
Esther Klingler

**Published in**

Frontiers in Neuroscience



## FRONTIERS EBOOK COPYRIGHT STATEMENT

The copyright in the text of individual articles in this ebook is the property of their respective authors or their respective institutions or funders. The copyright in graphics and images within each article may be subject to copyright of other parties. In both cases this is subject to a license granted to Frontiers.

The compilation of articles constituting this ebook is the property of Frontiers.

Each article within this ebook, and the ebook itself, are published under the most recent version of the Creative Commons CC-BY licence. The version current at the date of publication of this ebook is CC-BY 4.0. If the CC-BY licence is updated, the licence granted by Frontiers is automatically updated to the new version.

When exercising any right under the CC-BY licence, Frontiers must be attributed as the original publisher of the article or ebook, as applicable.

Authors have the responsibility of ensuring that any graphics or other materials which are the property of others may be included in the CC-BY licence, but this should be checked before relying on the CC-BY licence to reproduce those materials. Any copyright notices relating to those materials must be complied with.

Copyright and source acknowledgement notices may not be removed and must be displayed in any copy, derivative work or partial copy which includes the elements in question.

All copyright, and all rights therein, are protected by national and international copyright laws. The above represents a summary only. For further information please read Frontiers' Conditions for Website Use and Copyright Statement, and the applicable CC-BY licence.

ISSN 1664-8714  
ISBN 978-2-8325-4440-2  
DOI 10.3389/978-2-8325-4440-2

## About Frontiers

Frontiers is more than just an open access publisher of scholarly articles: it is a pioneering approach to the world of academia, radically improving the way scholarly research is managed. The grand vision of Frontiers is a world where all people have an equal opportunity to seek, share and generate knowledge. Frontiers provides immediate and permanent online open access to all its publications, but this alone is not enough to realize our grand goals.

## Frontiers journal series

The Frontiers journal series is a multi-tier and interdisciplinary set of open-access, online journals, promising a paradigm shift from the current review, selection and dissemination processes in academic publishing. All Frontiers journals are driven by researchers for researchers; therefore, they constitute a service to the scholarly community. At the same time, the *Frontiers journal series* operates on a revolutionary invention, the tiered publishing system, initially addressing specific communities of scholars, and gradually climbing up to broader public understanding, thus serving the interests of the lay society, too.

## Dedication to quality

Each Frontiers article is a landmark of the highest quality, thanks to genuinely collaborative interactions between authors and review editors, who include some of the world's best academicians. Research must be certified by peers before entering a stream of knowledge that may eventually reach the public - and shape society; therefore, Frontiers only applies the most rigorous and unbiased reviews. Frontiers revolutionizes research publishing by freely delivering the most outstanding research, evaluated with no bias from both the academic and social point of view. By applying the most advanced information technologies, Frontiers is catapulting scholarly publishing into a new generation.

## What are Frontiers Research Topics?

Frontiers Research Topics are very popular trademarks of the *Frontiers journals series*: they are collections of at least ten articles, all centered on a particular subject. With their unique mix of varied contributions from Original Research to Review Articles, Frontiers Research Topics unify the most influential researchers, the latest key findings and historical advances in a hot research area.

Find out more on how to host your own Frontiers Research Topic or contribute to one as an author by contacting the Frontiers editorial office: [frontiersin.org/about/contact](https://frontiersin.org/about/contact)



# Advances and challenges in studying brain disorders: From development to aging

## Topic editors

Subashika Govindan — Wellcome Trust DBT India Alliance, India

Fiona Francis — INSERM U839 Institut du Fer à Moulin (IFM), France

Esther Klingler — VIB & KU Leuven Center for Brain & Disease Research, Belgium

## Citation

Govindan, S., Francis, F., Klingler, E., eds. (2024). *Advances and challenges in studying brain disorders: From development to aging*. Lausanne: Frontiers Media SA. doi: 10.3389/978-2-8325-4440-2

## Table of contents

- 05 **Editorial: Advances and challenges in studying brain disorders: from development to aging**  
Esther Klingler, Subashika Govindan and Fiona Francis
- 07 **Neurons gating behavior—developmental, molecular and functional features of neurons in the Substantia Nigra pars reticulata**  
Juha Partanen and Kaia Achim
- 20 **Identification of the common differentially expressed genes and pathogenesis between neuropathic pain and aging**  
Qingqing Ye, Zhensheng Huang, Weicheng Lu, Fang Yan, Weian Zeng, Jingdun Xie and Weiqiang Zhong
- 36 **Differential impacts of *Cntnap2* heterozygosity and *Cntnap2* null homozygosity on axon and myelinated fiber development in mouse**  
Carmen Cifuentes-Díaz, Giorgia Canali, Marta Garcia, Mélanie Druart, Taylor Manett, Mythili Savariradjane, Camille Guillaume, Corentin Le Magueresse and Laurence Goutebroze
- 56 **From attention-deficit hyperactivity disorder to sporadic Alzheimer's disease—Wnt/mTOR pathways hypothesis**  
Edna Grünblatt, Jan Homolák, Ana Babic Perhoc, Virag Davor, Ana Knezovic, Jelena Osmanovic Barilar, Peter Riederer, Susanne Walitza, Christian Tackenberg and Melita Salkovic-Petrisic
- 78 **Multifaceted microglia during brain development: Models and tools**  
Cécile Bridlance and Morgane Sonia Thion
- 88 **Novel patients with NHLRC2 variants expand the phenotypic spectrum of FINCA disease**  
Antti Tallgren, Leo Kager, Gina O'Grady, Hannu Tuominen, Jarmo Körkkö, Outi Kuismin, Martha Feucht, Callum Wilson, Jana Behunova, Eleina England, Mitja I. Kurki, Aarno Palotie, Mikko Hallman, Riitta Kaarteenaho, Franco Laccone, Kaan Boztug, Reetta Hinttala and Johanna Uusimaa
- 100 **The human brain through the lens of somatic mosaicism**  
Sara Bizzotto
- 109 **Opening the black box of traumatic brain injury: a holistic approach combining human 3D neural tissue and an *in vitro* traumatic brain injury induction device**  
Céline Loussert-Fonta, Luc Stoppini, Yoan Neuenschwander, Ophélie Righini, Denis Prim, Cédric Schmidt, Marc O. Heuschkel, Loris Gomez Baisac, Milica Jovic, Marc E. Pfeifer, Jérôme Extermann and Adrien Roux

- 121 **Knockout of angiotensin converting enzyme-2 receptor leads to morphological aberrations in rodent olfactory centers and dysfunctions associated with sense of smell**  
Sarang Mahajan, Deepshikha Sen, Anantu Sunil, Priyadharshini Srikanth, Shruti D. Marathe, Karishma Shaw, Mahesh Sahare, Sanjeev Galande and Nixon M. Abraham
- 139 **Intracellular traffic and polarity in brain development**  
Martina Polenghi and Elena Taverna



## OPEN ACCESS

## EDITED BY

Guo-Yuan Yang,  
Shanghai Jiao Tong University, China

## REVIEWED BY

Eunju Jenny Shin,  
Keele University, United Kingdom  
Zhi Zhang,  
University of Michigan–Dearborn,  
United States

## \*CORRESPONDENCE

Esther Klingler  
✉ esther.klingler@kuleuven.be  
Subashika Govindan  
✉ g.subashika@gmail.com  
Fiona Francis  
✉ fiona.francis@inserm.fr

RECEIVED 20 November 2023

ACCEPTED 15 January 2024

PUBLISHED 29 January 2024

## CITATION

Klingler E, Govindan S and Francis F (2024)  
Editorial: Advances and challenges in studying  
brain disorders: from development to aging.  
*Front. Neurosci.* 18:1341410.  
doi: 10.3389/fnins.2024.1341410

## COPYRIGHT

© 2024 Klingler, Govindan and Francis. This is  
an open-access article distributed under the  
terms of the [Creative Commons Attribution  
License \(CC BY\)](#). The use, distribution or  
reproduction in other forums is permitted,  
provided the original author(s) and the  
copyright owner(s) are credited and that the  
original publication in this journal is cited, in  
accordance with accepted academic practice.  
No use, distribution or reproduction is  
permitted which does not comply with these  
terms.

# Editorial: Advances and challenges in studying brain disorders: from development to aging

Esther Klingler<sup>1,2\*</sup>, Subashika Govindan<sup>3,4\*</sup> and Fiona Francis<sup>5,6,7\*</sup>

<sup>1</sup>Department of Neuroscience, VIB-KU Leuven Center for Brain and Disease Research, Leuven, Belgium, <sup>2</sup>Leuven Brain Institute, KU Leuven, Leuven, Belgium, <sup>3</sup>Wellcome Trust/DBT - India Alliance, Hyderabad, India, <sup>4</sup>Indian Institute of Technology - Madras, Chennai, Tamil Nadu, India, <sup>5</sup>Institut du Fer à Moulin, Paris, France, <sup>6</sup>Institut National de Santé et de Recherche Médicale (INSERM) UMR-S 1270, Paris, France, <sup>7</sup>Sorbonne Universités, Paris, France

## KEYWORDS

brain development, brain aging, neurodegenerative diseases, neurodevelopmental diseases, intrinsic - extrinsic, cell-type susceptibilities, genetic mutation, *in vitro in vivo*

## Editorial on the Research Topic

[Advances and challenges in studying brain disorders: from development to aging](#)

Development and function of the human brain depends on multiple molecular programs, the fine balance of heterogeneous cell types and coordination of distinct anatomical structures. The human brain is vulnerable to a range of diseases that manifest at different life stages, affecting various cell types and structures. Despite the protection provided by the blood-brain barrier in adulthood, neurons, the fundamental unit of the brain, which receive, integrate and transmit signals, are highly susceptible to developmental and cumulative defects or injuries due to very limited renewal. Although brain disorders are traditionally categorized as “neurodevelopmental,” “neuropsychiatric,” and “neurodegenerative,” there is some evidence that these conditions share common molecular and cellular pathways with diverse outcomes based on region- and cell-type-specific susceptibilities. In this Research Topic, we have compiled hypotheses and research articles, along with reviews, to shed light on current and complementary approaches of studying brain diseases from development to aging.

Brain development relies on the production of neurons from neural progenitor cells, which, when affected, lead to various neurodevelopmental disorders. For instance, abnormal regulation of neural progenitor polarity can lead to not only abnormal division, neuron production and microcephaly, but also to epilepsy and/or autism spectrum disorders (ASD). These defects can stem from mutations in genes coding for trafficking-related structural proteins and enzymes within the endoplasmic reticulum and the Golgi apparatus of progenitors, as discussed in [Polenghi and Taverna](#).

Once neurons are generated, their migration, differentiation, and establishment of connections are crucial for correctly forming functional circuits. Identifying the developmental origins of neurons in a specific brain region is essential for fully understanding connectivity and function, in both normal and diseased conditions. For example, neurons of distinct parts of the *substantia nigra pars reticulata* (SNpr) have different connectivities and are differentially involved in seizures. Those originating from

diencephalon/midbrain respond to short-term flexible reward, while neurons originating from the hindbrain and colonizing a more posterior part of the SNpr, play a role in long-term high-value reward encoding (Partanen and Achim). Establishment of proper brain connectivity also relies on precise controls over gene expression levels. For example, different levels of the Caspr2 protein encoded by the *CNTNAP2* gene (whose mutations can lead to several brain disorders, from neurodevelopmental to peripheral neuropathies) lead to different abnormalities in connectivity tracts. In mice, *Cntnap2* heterozygosity can even lead to a stronger phenotype than null homozygosity in the case of callosal axon diameters or cortical neuron intrinsic excitability (Cifuentes-Diaz et al.). With respect to disease causing mutations, a diversity of phenotypes can also occur even with a single pathogenic variant: patients with the *NHLRC2* pathogenic variant c.442G > T (either homozygous or heterozygous) have various defects in multiple organs (including the brain) affecting development and function, and leading to Fibrosis, Neurodegeneration and Cerebral Angiomatosis (FINCA) (Tallgren et al.). The FINCA disease is a good example of how perturbation of single molecule can manifest both with neurodevelopmental and neurodegenerative phenotypes.

It is not only cell origins which are important in defining cell development and later function, but also the changes which can arise after birth. Somatic mutations occur throughout cell life and particularly affect brain functions. These have been implicated in several brain disorders, from developmental, such as focal cortical dysplasia, autism spectrum disorders and schizophrenia, to neurodegenerative conditions, such as Alzheimer's disease. In her review, Bizzotto explores cutting edge discoveries from the last 5 years that utilize single-cell and next generation sequencing, and sheds light on how accumulation of somatic mutations in aging brain cells can inform on cell-type-specific disease predisposition.

The correct production, migration, growth of axons and synapse development of neurons are also all sensitive to extrinsic factors, e.g., via immune-responsive cell types, such as microglia. Microglia, originating outside the central nervous system, invade the brain during early embryogenesis, before any other glial cell is present, and influence both brain development and later function. Their involvement has been associated with various brain disorders, including ASD, schizophrenia, and neurodegenerative diseases such as Alzheimer's disease, as discussed by Bridance and Thion. To further explore the effect of environmental factors such as viral infections on brain function, Mahajan et al. show that the loss of function of Angiotensin Converting Enzyme-2 (ACE2) receptor, one of the key molecular factors mediating SARS-CoV-2 entry into the central nervous system, leads to distinct morphological changes, abnormal odor processing and associated cognitive disability.

In summary, a diversity of mechanisms can contribute to a single disease, and distinct deficits in one specific cell type can contribute to a range of brain diseases, which highlights the need to strengthen the bridge between neurodevelopmental and neurodegenerative studies. This can be achieved through cross-comparisons of animal models and different datasets to uncover common and specific mechanisms/pathways, aiding in

drug discovery. For example, Grünblatt et al. emphasize the links between Alzheimer's disease and attention deficit hyperactivity disorder (ADHD), proposing a common dysregulation of molecular pathways involving the Wnt/mTOR pathway at different life stages. Additionally, leveraging transcriptomics datasets allows for the comparison of disease-related pathways, as demonstrated by Ye et al., who provide new insights on the immune microenvironment, but also the transcription factors and miRNA regulation networks at play in neuropathic pain and aging animal models. Finally, using *in vitro* technologies, such as induced pluripotent stem (iPS) cells derived from patients, also provides new avenues for modeling brain diseases, as discussed by Loussert-Fonta et al. in their approach to model traumatic brain injury in a dish.

Altogether, our Research Topic elucidates the multifaceted etiology of numerous brain disorders, converging on a range of factors, from point mutations at the genome level, to gene expression changes at the molecular level, to perturbation at the cellular and anatomical level, to environmental factors such as infectious diseases and immune responses. This Research Topic further reveals how we can leverage on latest cutting-edge technologies such as next generation sequencing, single-cell sequencing, CRISPR-Cas9 based gene editing, iPS technologies and tissue engineering to put ourselves in the forefront of studying brain disorders.

## Author contributions

EK: Writing – original draft. SG: Writing – review & editing. FF: Writing – review & editing.

## Funding

The author(s) declare that no financial support was received for the research, authorship, and/or publication of this article.

## Conflict of interest

The authors declare that the research was conducted in the absence of any commercial or financial relationships that could be construed as a potential conflict of interest.

## Publisher's note

All claims expressed in this article are solely those of the authors and do not necessarily represent those of their affiliated organizations, or those of the publisher, the editors and the reviewers. Any product that may be evaluated in this article, or claim that may be made by its manufacturer, is not guaranteed or endorsed by the publisher.



## OPEN ACCESS

EDITED BY  
Esther Klingler,  
Université de Genève, Switzerland

REVIEWED BY  
Sandra Blaess,  
University of Bonn, Germany  
Jeroen Pasterkamp,  
Utrecht University, Netherlands

\*CORRESPONDENCE  
Juha Partanen  
juha.m.partanen@helsinki.fi

SPECIALTY SECTION  
This article was submitted to  
Translational Neuroscience,  
a section of the journal  
Frontiers in Neuroscience

RECEIVED 23 June 2022  
ACCEPTED 15 August 2022  
PUBLISHED 06 September 2022

CITATION  
Partanen J and Achim K (2022)  
Neurons gating  
behavior—developmental, molecular  
and functional features of neurons  
in the Substantia Nigra pars reticulata.  
*Front. Neurosci.* 16:976209.  
doi: 10.3389/fnins.2022.976209

COPYRIGHT  
© 2022 Partanen and Achim. This is an  
open-access article distributed under  
the terms of the [Creative Commons  
Attribution License \(CC BY\)](https://creativecommons.org/licenses/by/4.0/). The use,  
distribution or reproduction in other  
forums is permitted, provided the  
original author(s) and the copyright  
owner(s) are credited and that the  
original publication in this journal is  
cited, in accordance with accepted  
academic practice. No use, distribution  
or reproduction is permitted which  
does not comply with these terms.

# Neurons gating behavior—developmental, molecular and functional features of neurons in the Substantia Nigra pars reticulata

Juha Partanen\* and Kaia Achim

Molecular and Integrative Biosciences Research Programme, Faculty of Biological  
and Environmental Sciences, University of Helsinki, Helsinki, Finland

The Substantia Nigra pars reticulata (SNpr) is the major information output site of the basal ganglia network and instrumental for the activation and adjustment of movement, regulation of the behavioral state and response to reward. Due to both overlapping and unique input and output connections, the SNpr might also have signal integration capacity and contribute to action selection. How the SNpr regulates these multiple functions remains incompletely understood. The SNpr is located in the ventral midbrain and is composed primarily of inhibitory GABAergic projection neurons that are heterogeneous in their properties. In addition, the SNpr contains smaller populations of other neurons, including glutamatergic neurons. Here, we discuss regionalization of the SNpr, in particular the division of the SNpr neurons to anterior (aSNpr) and posterior (pSNpr) subtypes, which display differences in many of their features. We hypothesize that unique developmental and molecular characteristics of the SNpr neuron subtypes correlate with both region-specific connections and notable functional specializations of the SNpr. Variation in both the genetic control of the SNpr neuron development as well as signals regulating cell migration and axon guidance may contribute to the functional diversity of the SNpr neurons. Therefore, insights into the various aspects of differentiation of the SNpr neurons can increase our understanding of fundamental brain functions and their defects in neurological and psychiatric disorders, including movement and mood disorders, as well as epilepsy.

## KEYWORDS

Substantia Nigra pars reticulata, basal ganglia, GABAergic neuron, neurogenesis, movement, seizure, sleep, reward



## Introduction

Basal ganglia, a network of brain structures and nuclei in the forebrain and anterior brainstem, evaluate external and internal signals and use this information to select, activate and invigorate appropriate behavior, often including voluntary movement (Dudman and Krakauer, 2016; Klaus et al., 2019). These brain functions are of paramount importance for the fitness of an organism and the various underlying cell types and circuits have aggregated to form the basal ganglia system early in the evolution (Grillner and Robertson, 2016).

The basal ganglia include separate structures for information input, modulation and output. The main input areas sending afferent projections to the basal ganglia are the striatum and the subthalamic nucleus (STN), which in turn receive projections from the cortex and thalamic nuclei (Figure 1C). The modulatory components include the dopaminergic nuclei in the ventral midbrain. These structures and their incorporation to the basal ganglia network have been extensively reviewed earlier (Deniau et al., 2007; Takakusaki, 2008; Grillner and Robertson, 2016; Hikosaka et al., 2019; Klaus et al., 2019; Arber and Costa, 2022). The output of the basal ganglia is funneled through two brain centers: the internal segment of Globus Pallidus (GPi) and Substantia Nigra pars reticulata (SNpr). These nuclei contain GABAergic projection neurons that tonically inhibit their targets in the dorsal midbrain, anterior brainstem and thalamus, to control activation of movement and other aspects of behavior. Thus, the basal ganglia participate in the control of behavior by disinhibition: upstream components of the basal ganglia network suppress the GPi and SNpr, resulting in activation of the GPi and SNpr targets under excitatory cortical stimulation, leading to the effective behaviors (Hikosaka, 2007). This model has extensive experimental support, but the SNpr neuron function also appears more complex. While the activity of some SNpr neurons decreases during the activation of behavior, many others increase their firing, suggesting that in addition to allowing the desired behavior, the SNpr also suppresses competing actions (Mink, 1996; Gulley et al., 2002; Meyer-Luehmann et al., 2002). Furthermore, recent studies suggest that disinhibition may not be the only operational mechanism of the SNpr, and that the SNpr neurons can also elicit activation of their target neurons by rebound depolarization (Villalobos and Basso, 2022). In addition, there also are some excitatory glutamatergic neurons in the SNpr (Antal et al., 2014; Morales and Root, 2014). Importantly, both earlier and recent studies promote a view that to regulate various types of behaviors, the SNpr is divided into discrete modules, differing in their connectivity and function (Deniau et al., 2007; McElvain et al., 2021).

How the basal ganglia output is controlled by specialized SNpr neurons, responsible for distinct behavioral outcomes, remains incompletely understood. A prerequisite for

understanding the cell type-specific output is to have information on the properties and diversity of the output neurons at multiple levels (Arber and Costa, 2022). In this review, we focus on the cellular composition of the SNpr. We discuss the embryonic development of the molecularly distinct subtypes of SNpr neurons, and give an overview of information available about their connectivity patterns as well as region-specific functions. The focus of this review is on the possible correlations between the neuronal subtype-specific developmental, neuroanatomical and functional features, which have remained largely overlooked to date. Insights to the SNpr composition and function are central for understanding fundamental aspects of behavioral regulation and have implications for understanding several brain diseases such as movement disorders, attention deficit and hyperactivity, as well as epilepsy.

## The Substantia Nigra pars reticulata neurons and their development

The SNpr is an anatomically easily recognizable nucleus in the most ventral brainstem, next to the dopaminergic neurons in the Substantia Nigra pars compacta (SNpc) and Ventral Tegmental Area (VTA) (Figure 1A). In the mouse, the SNpr extends from the posterior diencephalon to the midbrain, with its posterior limit at the midbrain-hindbrain border (Figure 1B). The majority of the SNpr neurons are inhibitory GABAergic neurons, but the SNpr also contains glutamatergic and dopaminergic neurons, as well as neurons using both glutamate and dopamine as neurotransmitters (Nair-Roberts et al., 2008; Yamaguchi et al., 2013; Antal et al., 2014). In addition, few cholinergic neurons are also located in the posterior SNpr (Gould and Butcher, 1986). The SNpr neurons are mostly projection neurons and local interneurons appear very few in number (Deniau et al., 2007). Most of the research discussed here has focused on the GABAergic component of the SNpr, although some of the SNpr glutamatergic neurons may be both developmentally and functionally related to these neurons.

## Developmental origins of the Substantia Nigra pars reticulata GABAergic neurons

Although located primarily in the ventral midbrain in the mature brain, the SNpr GABAergic neurons are largely derived outside the embryonic midbrain neuroepithelium. The first indication of this was the observation that abundant SNpr GABAergic neurons were still present in mouse mutants where the midbrain GABAergic neurogenesis completely failed

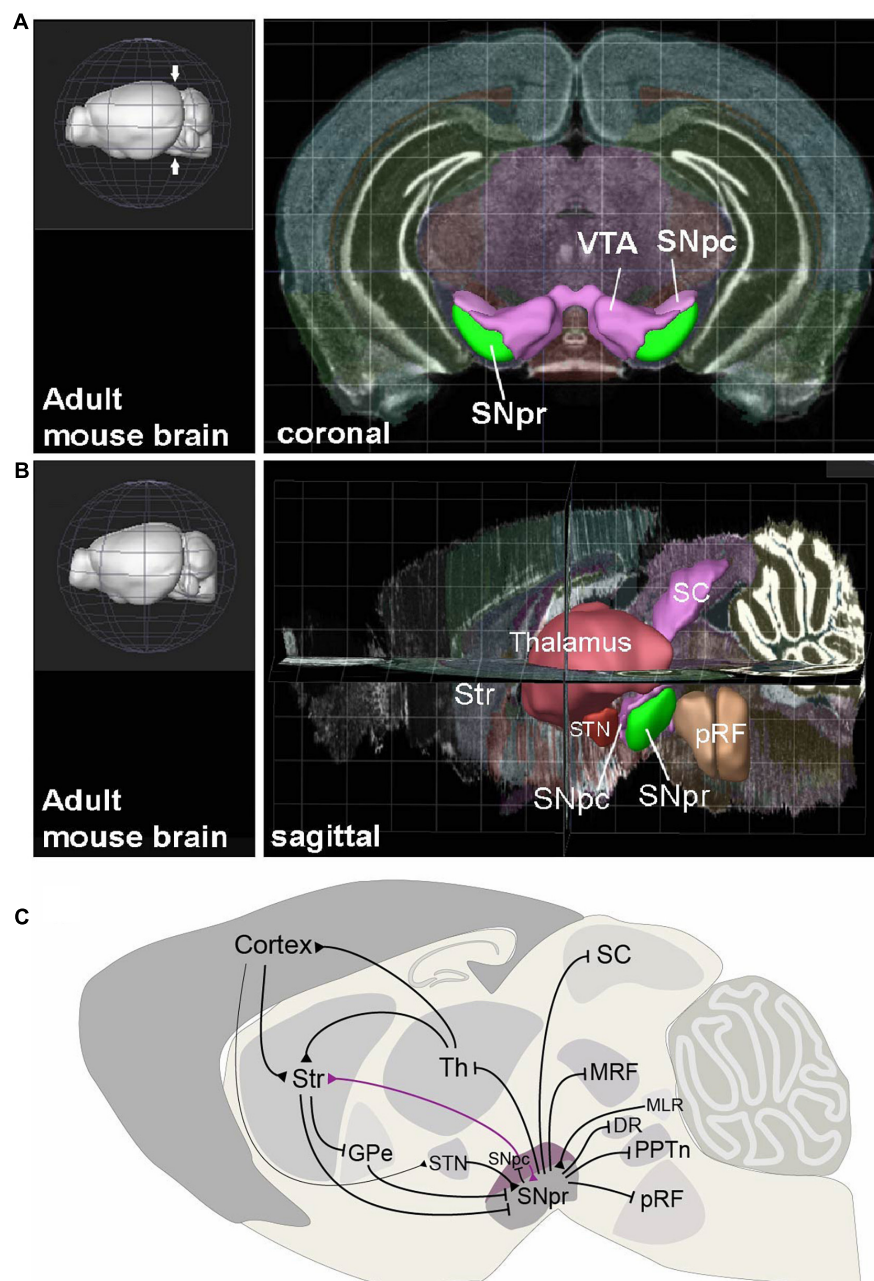


FIGURE 1

The anatomical context and connectivity of Substantia Nigra. **(A)** Coronal view to the adult mouse brain at the level on midbrain (level indicated with arrows on the 3D image in left). The Substantia Nigra pars reticulata (SNpr), pars compacta (SNpc) and Ventral Tegmental Area (VTA) are highlighted. **(B)** Sagittal view to adult mouse brain, showing the positions of SNpr and its interconnected structures. Str, striatum; STN, Subthalamic nucleus; SC, Superior colliculus; pRF, pontine reticular formation. **(C)** Input and output structures of the SNpr and their interconnections in mature mouse brain. Black arrows represent inhibitory GABAergic (blunt arrowhead) and excitatory glutamatergic (triangular arrowhead) projections. The dopaminergic neuron projection from SNpc to striatum (Str) is shown in violet. Th, Thalamus; GPe, Globus Pallidus, external segment; MRF, midbrain reticular formation; MLR, midbrain locomotor region; DR, Dorsal Raphe nucleus; PPTn, pedunculopontine tegmental nucleus. The views in **(A,B)** are created using the Brain Explorer 2 app (Allen Institute for Brain Science, <https://mouse.brain-map.org/static/brainexplorer>).

(Kala et al., 2009). Cre-recombinase driven fate-mapping in the mouse subsequently indicated an origin for some SNpr GABAergic neurons in the hindbrain (Achim et al., 2012).

Importantly, a hindbrain-specific Cre-driver (*Gbx2<sup>CreERT2</sup>*) labeled the posterior part of the SNpr (pSNpr), but not its anterior part (aSNpr). Studies of the development of

GABAergic neuron subtypes in the rhombomere 1 (r1) of the anterior hindbrain have further refined the origin of the pSNpr neurons in the ventrolateral r1 neuroepithelium expressing the homeodomain transcription factor (TF) NKX6-1, and in particular the anterior part of this neuroepithelial region close to the midbrain-hindbrain border (Morello et al., 2020a; Figure 2A). On the other hand, fate mapping with the *Nkx6-2<sup>CreERT2</sup>* -driver suggested that the aSNpr neurons are derived from the *Nkx6-2* expressing neuronal progenitors or precursors found in the ventrolateral midbrain-diencephalon region (Qiu et al., 1998; Moreno-Bravo et al., 2010; Madrigal et al., 2016). The exact origin of aSNpr neurons remains to be established with regionally more restricted progenitor cell labeling (Qiu et al., 1998; Moreno-Bravo et al., 2010; Madrigal et al., 2016).

In summary, the SNpr is divided into two developmentally independent GABAergic components, termed aSNpr and pSNpr in this review, each of which originates in distinct antero-posterior brain compartments (Figure 2A). The ventrolateral neuroepithelial domains giving rise to the aSNpr and pSNpr neurons are marked by the expression of specific homeodomain TFs. Interestingly, in addition to the GABAergic neurons of the pSNpr, the precursors in the ventrolateral r1 also produce developmentally related glutamatergic neuron types, some of which may also contribute to the SNpr (Figure 2A, blue).

## Regulation of the differentiation of the Substantia Nigra pars reticulata GABAergic neurons

GABAergic neurogenesis, production of post-mitotic GABAergic neuron precursors from proliferative progenitor cells, is regulated by different proneural TFs in the diencephalon/midbrain and the hindbrain, giving rise to aSNpr and pSNpr, respectively. In the diencephalon/midbrain *Ascl1* and *Helt* are required for GABAergic precursor production (Song et al., 2015; Wende et al., 2015). In turn, similar to spinal cord, GABAergic neurogenesis in the ventrolateral hindbrain may be controlled by *Foxn4* and *Ascl1* (Li et al., 2005; Misra et al., 2014; Figure 2A).

The differentiation of postmitotic pSNpr and aSNpr neurons is guided by related, but somewhat different sets of TFs. Members of the GATA zinc finger TF family, GATA2 and GATA3, as well as members of the Tal/Scl bHLH TF family, TAL1 and TAL2, interact in a heteromeric TF complex and are important for the acquisition of GABAergic neuron identity in the spinal cord, r1 and midbrain (Zhou et al., 2000; Joshi et al., 2009; Kala et al., 2009; Achim et al., 2012, 2013; Porcher et al., 2017). These TF genes act as developmental selector genes (Hobert and Kratsios, 2019). The differentiation of the pSNpr neurons is regulated by *Tal1*, *Gata2*, and *Gata3*, the latter two functioning redundantly (Achim et al., 2012; Lahti

et al., 2016; Figure 2A). During the embryonic development, most of the pSNpr GABAergic neuron precursors exit the cell cycle between E11.5-E12.5, slightly after the GABAergic neurons of the midbrain reticular formation, but before the GABAergic neurons of the dorsal midbrain (superior colliculi) (Achim et al., 2012). The expression of *Tal1*, *Gata2* and *Gata3* is robustly activated at this stage in the neuronal precursors of the ventrolateral r1 as these cells exit the cell cycle and migrate out of the neuroepithelium. At later stages, *Gata2* expression decreases while *Gata3* expression is maintained in the GABAergic neurons. Importantly, the ventrolateral r1 comprises *Nkx6-1* expressing progenitors that can give rise to post-mitotic precursors differentiating into either GABAergic or glutamatergic neurons. TAL1, GATA2, and GATA3 act as selectors of the GABAergic identity, preventing the alternative glutamatergic differentiation (Lahti et al., 2016). It is also known that in the pSNpr precursors, *Gata2* and *Gata3* genes are activated independent of each other and either one of them is required for GABAergic differentiation. In turn, the expression of *Nkx6-1* is maintained only in the differentiating glutamatergic precursors. Asymmetric Notch signaling, probably mediated by NOTCH1 receptor and its ligands DLL3 and DLL4, is associated with the activation of selector gene expression and GABAergic fate acquisition in the post-mitotic precursors in the ventrolateral r1 (Morello et al., 2020a). Similar role for NOTCH1-DLL4 signaling has been demonstrated in the ventrolateral V2 region of the spinal cord (Del Barrio et al., 2007; Peng et al., 2007).

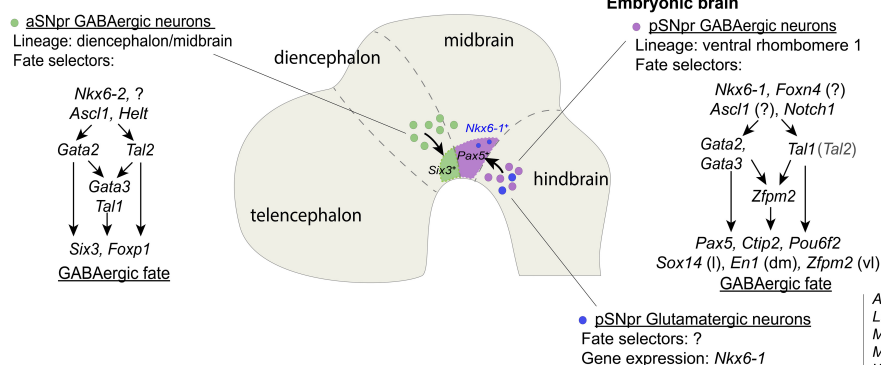
The differentiation of the aSNpr GABAergic neurons is also initiated by *Gata2* function, *Gata2* being the main selector gene for GABAergic identity in early postmitotic precursors in the midbrain and posterior diencephalon (P1–P2) (Kala et al., 2009; Achim et al., 2012; Virolainen et al., 2012). In contrast to the pSNpr precursors where *Gata2* and *Gata3* operate redundantly, *Gata2* function is essential for *Gata3* expression in the midbrain and diencephalon, and inactivation of *Gata2* alone is sufficient to prevent GABAergic differentiation of the aSNpr precursors (Achim et al., 2012; Lahti et al., 2016). Furthermore, unlike in the pSNpr precursors, *Tal1* is not required for the development of aSNpr precursors, where the requirement of a bHLH selector function may be compensated by a related TF TAL2 (Achim et al., 2013).

Thus, the early precursors of the pSNpr and aSNpr neurons are dependent on different combinations of GATA and TAL TFs that function as GABAergic fate selectors.

## Molecular subtypes of the Substantia Nigra pars reticulata GABAergic neurons

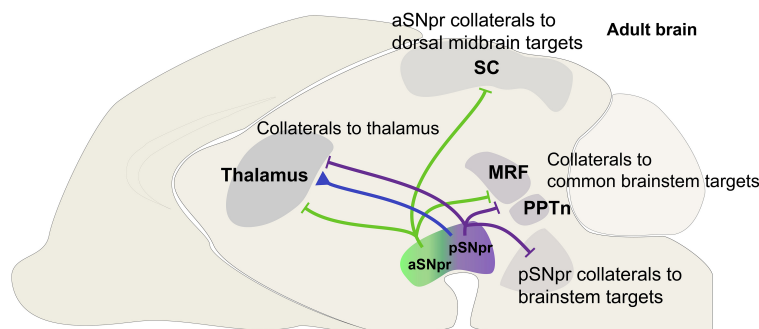
The SNpr GABAergic neurons are heterogeneous in their cytoarchitecture and expression of neurochemical markers,

## A DEVELOPMENT and GENE EXPRESSION in aSNpr and pSNpr



Achim et al, 2012  
Lahti et al, 2016  
Morello et al, 2020  
Madrigal et al, 2016  
Wende et al, 2015  
Song et al, 2015

## B CONNECTIVITY: OUTPUTS of aSNpr and pSNpr



McElvain et al, 2021  
Liu et al, 2020  
Foster et al, 2021  
Antal et al, 2014

## C BEHAVIORAL FUNCTIONS

BEHAVIOR	SUBTYPE MARKER / REGION	KNOWN FUNCTION(S)
MOVEMENT, MODE OF ACTIVITY, SLEEP	PVALB	Active during movement High baseline activity and firing rate
	GAD2	Active during low-activity period, transition to sleep Regulation of arousal
SEIZURES	PVALB	Activation induces seizures Inhibition alleviates seizures
	anterior SNpr	Activation induces seizures, inhibition alleviates
MOTIVATION AND REWARD	posterior SNpr	Varied effects on seizures
	CD(h)-aSNpr	Short-term flexible reward
	CD(t)-pSNpr	Long-term high-value reward
	all SNpr	Opioid reward

Rizzi and Tan, 2019  
Galaj et al, 2020  
Hikosaka et al, 2014  
Liu et al, 2020  
Wicker et al, 2019  
Chen et al, 2020  
Broer, 2020

FIGURE 2

The development, connectivity and function of the anterior and posterior SNpr neurons. **(A)** Developmental origin and differential gene expression in the aSNpr GABAergic neurons and the pSNpr GABAergic and glutamatergic neurons. The aSNpr GABAergic neurons originate in the *Nkx6-2* expressing neuronal progenitors in the ventrolateral midbrain or posterior diencephalon (green), and are characterized by the expression of *Six3* and *Foxp1*. aSNpr neurons require the function of the proneural genes *Ascl1* and *Helt* and the selector genes *Tal1* and *Gata2* in order to acquire GABAergic neuron phenotype. In early precursors, *Gata2* and *Tal2* are activated independently of each other and can have both common and separate target genes. The pSNpr GABAergic neurons (violet) and glutamatergic neurons (blue) originate in the *Nkx6-1* expressing neuronal progenitors in the anterior ventrolateral hindbrain. pSNpr progenitors express *Foxn4*, *Ascl1* and *Notch1*. pSNpr GABAergic neurons are characterized by the expression of *Pax5*, *Ctbp2* and *Pou6f2*, and require the function of *Tal1* and *Gata2/Gata3* to acquire GABAergic neuron phenotype. *Sox14*, *En1* and *Zfp2* expression marks further subtypes of pSNpr neurons, which are located in distinct spatial positions: lateral (l), dorsomedial (dm) or ventrolateral (vl) pSNpr. The transcription factors involved in the fate specification of pSNpr glutamatergic neurons are not known. The relatively minor populations of dopaminergic and cholinergic SNpr neurons are not shown. **(B)** Differences in the output connectivity of aSNpr and pSNpr neurons. One of the hallmarks of SNpr neurons are the axon-collaterals. The common targets of the aSNpr and pSNpr are thalamus, MRF (midbrain and pontine reticular formation) and PPTn (pedunculopontine nucleus). In addition to projections to the common targets, the aSNpr neuron axon-collaterals (green) project to superior colliculus (SC), while the pSNpr axon-collaterals (violet) more often project to brainstem. Thalamus is one of the major targets of the SNpr glutamatergic neurons (blue). SNpr glutamatergic neurons specifically project to the nucleus reticularis of thalamus (nRT, see text). **(C)** Variety of functions of the SNpr neuron subtypes. The table summarizes the known functions of the *Pvalb*- or *Gad2*-expressing SNpr GABAergic neurons in the control of motor activity and behavioral state, and the functions of the anterior and posterior parts of the SNpr in the seizure activity, motivation, and reward. How these functions are related to specific molecularly defined SNpr neuron subtypes remains to be shown.



including Parvalbumin (PVALB), Calretinin, and Nitric oxide synthase, with the subtypes differing in their spatial distribution along the medio-lateral and antero-posterior axes of the SNpr (Gonzalez-Hernandez and Rodriguez, 2000; Lee and Tepper, 2007).

The developmental regulation leads to a unique molecular profile in a cell or cell type, defining its functional properties. Both pSNpr and aSNpr neurons robustly express genes required for the GABAergic neurotransmission, such as Glutamic acid decarboxylase 1 (*Gad1*), and markers of the GABAergic neurons in the posterior diencephalon-midbrain-ventral hindbrain region, such as *Gata3* (Lahti et al., 2016). However, the developmentally distinct SNpr neuron populations also differ in other TF gene expression. For example, the pSNpr neurons express TF genes *Pax5*, *Ctip2*, and *Pou6f2*, whereas the aSNpr neurons express *Six3* and *Foxp1* (Achim et al., 2013; Lahti et al., 2016; Madrigal et al., 2016; Saunders et al., 2018; Morello et al., 2020a). Developmentally, the pSNpr neurons are likely derived from the *Pax5* expressing precursors located close to the midbrain-hindbrain border in the ventrolateral r1. The early regulation of differentiation and *Pax5* expression in the r1 precursors is probably subject to the antero-posterior patterning and other signals from the midbrain-hindbrain/isthmic organizer (Wurst and Bally-Cuif, 2001).

Besides the two main SNpr neuron subtypes, aSNpr and pSNpr, there is further molecular heterogeneity in the SNpr, especially among the pSNpr neurons. For example, the most lateral pSNpr is distinguished by *Sox14* expression, and *En1* and *Zfp62* expression marks additional dorsomedial and ventrolateral pSNpr neuron subtypes (Lahti et al., 2016; Saunders et al., 2018; Zeisel et al., 2018). Anatomically, the molecularly distinct aSNpr and pSNpr neurons are clearly segregated in the embryonic brain (Lahti et al., 2016; Morello et al., 2020a) and despite partial intermingling during later development, the aSNpr and pSNpr neurons retain their regional bias and can be identified based on subtype-specific gene expression in the adult brain.

The distinct TF expression profiles described above likely manifest in the expression of subtype-specific gene products that determine neuronal function, but to date, this remains incompletely understood. Interestingly, the calcium-binding protein PVALB, used for mapping the SNpr connections and functions (see below), is preferentially, although not exclusively, expressed in the *Foxp1* positive putative aSNpr neurons and the lateral SNpr (Saunders et al., 2018; Liu et al., 2020). Also GAD2, an enzyme involved in GABA biosynthesis, is expressed at different levels in several SNpr GABAergic neuron subpopulations and, in contrast to PVALB, its expression is enriched in the medial part of the SNpr (Liu et al., 2020).

In summary, the SNpr GABAergic neurons are molecularly heterogeneous. The subtypes of mature SNpr neurons that differ in their developmental origins and regulation can also be distinguished by differential gene expression (Figure 2A).

Recent scRNAseq studies (La Manno et al., 2016; Lutas et al., 2016; Saunders et al., 2018; Agarwal et al., 2020; Morello et al., 2020a) have contributed to the understanding of the molecular features and subtypes among the SNpr neurons, but the full resolution seems to not be achieved yet.

## Migration of the Substantia Nigra pars reticulata GABAergic neuron precursors

The later developmental mechanisms, including the molecular cues guiding the migration of the SNpr GABAergic precursors to their correct location in the ventral midbrain are beginning to be elucidated. The SNpr GABAergic neurons move to the ventral midbrain mostly between E14.5-E16.5 (Achim et al., 2012; Vasudevan et al., 2012; Brignani et al., 2020). In the ventral midbrain the GABAergic neurons are preceded by the SNpc and VTA dopaminergic neurons, but different conclusions have been reached considering the role of dopaminergic neurons in the guidance of GABAergic precursor migration (Vasudevan et al., 2012; Brignani et al., 2020). Several cell adhesion and migration associated proteins, such as DCC, Netrin-1 (NTN1), Ephrins and Plexins are expressed across the SNpr area. Furthermore, NTN1, released by striatal axons in the cerebral peduncle crossing the ventral midbrain, is required for the migration of SIX3<sup>+</sup> aSNpr neurons to their location ventral to SNpc dopaminergic neurons (Brignani et al., 2020). The aSNpr neurons express *Dcc*, *Neogenin* and *Dscam*, of which DSCAM is the main functional NTN1 receptor in migrating aSNpr precursors (Brignani et al., 2020). Importantly, in contrast to the aSNpr precursors, migration of the GABAergic precursors of the posterior SNpr is not affected by depletion of the NTN1 expression in the striatal axons. The specific mechanisms guiding the pSNpr neuron migration remain less understood. A guidance molecule EPHB1 is expressed in the SNpr GABAergic neurons during development, and *Ephb1* mutant mice show reduced numbers of SNpr cells at both anterior and posterior levels, and display locomotor hyperactivity (Richards et al., 2007). How the dopaminergic and GABAergic neurons interact in the ventral midbrain to form the SNpc and SNpr components of the Substantia Nigra still remains an open question.

## Development and molecular subtypes of the other Substantia Nigra pars reticulata neurons

Compared to the GABAergic neurons, less is known about the other neuron types in SNpr, including glutamatergic neurons, and the neurons co-releasing glutamate and dopamine.

Many SNpr glutamatergic neurons express the TF gene *Nkx6-1* (Lahti et al., 2016; Saunders et al., 2018) and are located in the dorsomedial and posterior regions of the SNpr (Antal et al., 2014; Morales and Root, 2014; Figures 2A,B). Similar to the pSNpr GABAergic neurons, these neurons likely have their embryonic origin in the ventrolateral r1, as their numbers are markedly increased by inactivation of *Tal1* or *Gata2/3* and the resulting GABAergic-to-glutamatergic fate transformation of the r1 precursors (Lahti et al., 2016). These NKX6-1 positive neurons may represent the SNpr glutamatergic neurons that do not co-express dopaminergic neuron characteristics (Antal et al., 2014) (see below). The SNpr neurons co-releasing dopamine and glutamate seem to be molecularly and developmentally related to the SNpc and VTA dopamine neuron subgroups (Poulin et al., 2020).

## Connections of the Substantia Nigra pars reticulata neurons and their regional specification

### Input to the Substantia Nigra pars reticulata GABAergic neurons

The SNpr receives GABAergic input from the striatum and the external segment of Globus Pallidus (GPe), and glutamatergic input from the STN and a subset of neurons in the midbrain locomotor region (MLR) (the RBP4 expressing glutamatergic neurons in the midbrain reticular formation) (Grillner and Robertson, 2016; Ferreira-Pinto et al., 2021; Arber and Costa, 2022). The striatal input to the SNpr is organized into the direct inhibitory pathway, and the indirect excitatory pathway through the STN (Kravitz et al., 2010). The direct striatal and indirect striatopallidal inputs converge in SNpr, maintaining the features of the striatal topographical organization as demonstrated by systematic tracing studies in rodents (Deniau et al., 1996, 2007; Lee et al., 2020; Foster et al., 2021). In the SNpr, the striatal input is directed to at least six identifiable longitudinal columns spanning the entire antero-posterior extent of the SNpr. Thus, the columns receiving information from the striatum do not strictly correlate with the developmental aSNpr/pSNpr division. Instead, distinct striatal areas preferentially connect to different medio-lateral regions in the SNpr: the dorsolateral striatum connecting to more lateral SNpr and ventromedial striatum to more medial SNpr, to regulate various aspects of movement (Deniau et al., 2007; Lee et al., 2020). Basal ganglia nuclei, including the striatum, GPe and STN, were found to be the main source of input to both *Pvalb*- and *Gad2*-expressing SNpr

neurons. Compared to the *Pvalb*-expressing neurons, the *Gad2*-expressing neurons receive more variable inputs, including connections from the anterior brainstem regions implicated in the regulation of both movement and brain state, such as SC, MLR, dorsal raphe (DR), and periaqueductal gray (PAG) (Liu et al., 2020).

The striatal input to the SNpr is also topographically organized in primates. The dorsal striatum in primates is composed of two nuclei, the Caudate and the Putamen. Of these, the Putamen projects primarily to the GPi, whereas the main target of the Caudate nucleus is the SNpr (Parent et al., 1984; Smith and Parent, 1986). The Caudate nucleus is further divided into sub-regions that project to non-overlapping targets in the SNpr and have been shown to be preferentially activated during distinct assays of object recognition in primates. The projections from the head of the Caudate nucleus CD(h) are directed toward the anterior (rostro-ventral-medial) region of the SNpr, whereas the tail of the Caudate nucleus CD(t) projects to the posterior (caudal-dorsal-lateral) SNpr (Hikosaka et al., 2014; Yasuda and Hikosaka, 2015).

In addition to these inhibitory and excitatory projections, the SNpr receives dopamine released by the dendrites of adjacent SNpc dopaminergic neurons (Cheramy et al., 1981; Levey et al., 1993). SNpr GABAergic neurons express dopamine receptors D1R and D5R, and the direct dopamine signaling might contribute to tonic firing of SNpr neurons (Zhou et al., 2009). In addition to the SNpr neurons, dopamine may affect local astrocytes, which strongly express D1R in the SNpr (Nagatomo et al., 2017). As discussed above, the SNpr neurons receive extensive indirect dopamine regulation *via* striatonigral GABAergic projection neurons, which also express D1R.

### Output from the Substantia Nigra pars reticulata GABAergic neurons

The SNpr sends GABAergic output to the dorsal midbrain (the superior colliculi, SC, and the inferior colliculi, IC), brainstem nuclei and the thalamus (Deniau and Chevalier, 1992). This output affects downstream targets regulating behavior and may provide feedback and efference copy information to the upstream basal ganglia structures, the cortex and to the SNpr itself. Systematic anterograde mapping of the SNpr projections revealed 42 different output sites of the SNpr, including several targets in the brainstem region (McElvain et al., 2021). Among these targets, the relative SNpr output varies greatly, two-thirds of it being directed to the brainstem reticular formation and the colliculi. One prominent feature of the SNpr output are the axon collaterals. Using the axon-collaterals, the SNpr neurons can have both specific targets, for example in the dorsal midbrain and the brainstem, as well as



shared targets in thalamus, pedunculopontine nucleus (PPTn) and midbrain reticular formation (Liu et al., 2020; McElvain et al., 2021). There are also non-collateralising SNpr neuron populations, such as the projections to pontine and midbrain reticular formation.

The SNpr projections to the dorsal midbrain and the brainstem send information out of the basal ganglia loop circuits toward action initiation. Interestingly, SNpr neurons projecting to specific targets in the dorsal midbrain and the brainstem are spatially clustered, showing enrichment in different areas of SNpr. The neurons sending projections to the superior and inferior colliculi (SC and IC) in the dorsal midbrain are located in the anterolateral SNpr, whereas the neurons sending projections to the brainstem nuclei in the hindbrain, including the dorsal raphe and pontomedullary reticular formation, are located in the posteromedial SNpr (Deniau and Chevalier, 1992; McElvain et al., 2021; Figure 2B). This is further supported by distinct projection patterns: lateral *Pvalb*-expressing neurons are connected to the SC and MLR, brain regions related to locomotion, while medial *Gad2*-expressing SNpr neurons project more widely to brainstem regions involved in brain-state regulation (Saunders et al., 2018; Liu et al., 2020). It is possible that these differences in the regional projection patterns are corollary to the distinct molecular properties and developmental histories of the inherent neuron subtypes. Interestingly, the origin of the pSNpr neurons in the embryonic r1 parallels the projection of the posterior and medial SNpr neurons to the brainstem nuclei located in the hindbrain. It is thus possible that the translocation of the cell bodies of the pSNpr neurons is associated with establishment of their connectivity, as seen in some other neuronal subtypes in the developing brain (Lambert de Rouvroit and Goffinet, 2001).

In addition to SNpr neurons having region-specific output targets, there is regional specification also within the shared targets. In particular, most SNpr neurons are characterized by a projection to the thalamus. The target areas in the thalamus, however, differ between the SNpr neurons connected to the dorsal midbrain and the brainstem: the SNpr neurons projecting to the dorsal midbrain send collaterals to the more lateral thalamus, whereas the SNpr neurons projecting to brainstem send collaterals to the more medial regions of the motor and intralaminar thalamic nuclei (McElvain et al., 2021). These connections appear to be involved in parallel closed-loop circuits between the cortex, striatum, SNpr and thalamus (Foster et al., 2021). Thus, the SNpr contains parallel modules that can affect both ascending and descending targets regulating behavior.

As mentioned above, the SNpr is thought to contain only sparse local interneurons. Rather than local interneurons, the axon-collaterals of the SNpr projection neurons provide feedback and mutual inhibitory interactions within the SNpr,

as well as project to the adjacent dopaminergic SNpc (Tepper et al., 1995; Mailly et al., 2003; Lee and Tepper, 2007; Brown et al., 2014; Galaj et al., 2020). The SNpr neurons projecting to the SNpc are characterized with a relatively high level of PVALB expression (Rizzi and Tan, 2019).

In summary, the SNpr receives region-specific input and is a source of region-specific output. The regional organization of the input and output show similarities, suggesting separate information channels (Deniau et al., 2007), but the regional maps may not fully overlap, providing some input integration capacity. Although there are clear differences in the connectivity along the antero-posterior, dorso-ventral and medio-lateral axes of the SNpr, the extent of correlation between the distinct projection patterns and the molecularly defined SNpr neuron subtypes is not yet shown.

## Connections of the Substantia Nigra pars reticulata glutamatergic neurons

Similar to the SNpr GABAergic neurons, the SNpr glutamatergic neurons also receive inhibitory input from the striatum and project to the thalamus (Antal et al., 2014; Figure 2B). However, the thalamic targets of the GABAergic and glutamatergic neurons differ. Whereas the SNpr GABAergic neurons provide inhibitory input to the ventral thalamic area (the ventroposterolateral nucleus), the glutamatergic projection provides excitatory input to the nucleus reticularis of thalamus (nRT), and both GABAergic and glutamatergic neurons project to the posterior nucleus group (Antal et al., 2014). The specific function of the SNpr glutamatergic neurons is unknown.

## Signaling properties of the Substantia Nigra pars reticulata neurons

The SNpr GABAergic neurons are spontaneously active suppressing their targets. They display a broad range of activity characteristics. Importantly, the topographically organized SNpr neuron subtypes, differing in their projections to the collicular and brainstem targets, are also specialized in their intrinsic electrophysiological properties (McElvain et al., 2021). The neurons projecting to the lateral and central SC, involved in sensorimotor function, show higher level of activity and narrow action potentials, whereas the projection neurons to the neuromodulatory dorsal raphe are the slowest population. These electrophysiological specializations further support the existence of molecularly and functionally segregated SNpr neuron subtypes. Consistent with this, the

*Pvalb*-expressing SNpr neurons, were also shown to fire at higher frequencies and have higher baseline activity than the *Gad2*- and *Vgat* (*Slc32a1*) expressing SNpr neurons (Rizzi and Tan, 2019; Liu et al., 2020; Figure 2C). Recent studies have addressed fine aspects of the ion channel expression and function in the SNpr GABAergic neurons (Zhou et al., 2009; Zhou and Lee, 2011; Lutas et al., 2016), demonstrating notable diversity in ion channel gene expression, but this information has not been linked to spatial positions. Those findings could, in future, be carefully compared with the recent single-cell sequencing data. One especially promising approach here would be to use spatial transcriptomics studies as reference.

## Behavioral functions of the Substantia Nigra pars reticulata neurons

### Movement, action selection and decision making

The hallmark feature of the basal ganglia output is the inhibition of movement, combined with selective activation of a movement by disinhibition when a tonic inhibitory output from the SNpr is paused (Chevalier and Deniau, 1990). This principle may be extended to selection of series of movements, behaviors and behavioral patterns. Different regions of the SNpr appear to regulate different types of movement, such as orofacial movement (licking) or body movements (turning), as suggested by the topographically organized projections from the striatum to the SNpr, and the behavioral consequences of stimulation of distinct striatal regions (Lee et al., 2020). The SNpr GABAergic neurons are thought to integrate “Go” signals (inhibitory direct input from the striatum) and “Stop” signals (excitatory input from the STN, a target of the striatal indirect pathway, and MLR) (Ferreira-Pinto et al., 2021). Activation of both the *Pvalb*-expressing and the *Gad2*-expressing neurons suppresses movement (Liu et al., 2020). However, during normal behavior, the *Pvalb*-expressing neurons have been shown to be more active during high motor activity, which is thought to reflect their function in suppression of unwanted movements (Liu et al., 2020). The pathways involving medial or lateral SNpr may affect movement differently, and earlier studies have indeed suggested that the lateral and medial regions of the SNpr differentially control locomotion and postural muscle tone (Takakusaki et al., 2003). Interestingly, the SNpr contains a specific region enriched in neurons that are associated with correct “Stop” signaling (Schmidt et al., 2013). This “hotspot” of “Stop” signaling is located in the dorsolateral SNpr and may comprise specific aSNpr/pSNpr neurons

subgroups, such as the *Sox14* positive lateral pSNpr neurons (Lahti et al., 2016).

### Mode of activity and sleep

The SNpr also controls transitions between behavioral states, such as different levels of motor activity and sleep (Figure 2C). In particular, the *Gad2*-expressing neurons in the medial SNpr have been shown to fire more during behavioral states of low motor activity, immobility, and sleep. Furthermore, activation of the *Gad2*-expressing cells, in addition to suppression of movement, also induced behavioral transition to sleep. This is in contrast to the *Pvalb*-expressing cells, whose activation suppressed movement but had no direct effect on sleep. Consistently, inactivation of the *Gad2*-expressing neurons more strongly inhibited sleep. These findings correlate with the projection of the *Gad2*-expressing cells to the brainstem neuromodulatory centers, including dorsal raphe and locus coeruleus, which regulate the behavioral state (Liu et al., 2020) (see above).

### Seizures

Perhaps related to its role in action selection, the SNpr function has been associated with the control of seizures. Already 40 years ago, it was found that the injection of GABA agonist muscimol into the SNpr has anticonvulsant effects (Iadarola and Gale, 1982). Interestingly, multiple studies have reported anterior-posterior differences in how SNpr is involved in seizure control. The anterior and posterior SNpr are differentially active during seizures (Gernert et al., 2004; Veliskova et al., 2005). Moreover, modulation of neuronal activity in distinct regions of the SNpr have different effects on seizure predisposition. Several studies have found pharmacological suppression of the anterior SNpr to be anticonvulsive, whereas suppression of the posterior SNpr has been reported to have both anticonvulsive and proconvulsive effects (Broer, 2020; Figure 2C). Consistent with this, opto- or chemogenetic activation of the *Pvalb*-expressing SNpr neurons was found to amplify seizures, whereas their inhibition alleviated seizure activity (Chen et al., 2020). Optogenetic inhibition of the GABAergic neurons in the anterior SNpr neurons was also found to suppress different kinds of seizures in rats (Wicker et al., 2019). Furthermore, suppression of the SNpr projections to the SC recapitulated these effects. In contrast, suppression of the SNpr projection to the PPTn, a target of the posterior SNpr, had more varied effects and even amplified some of the seizure types (Wicker et al., 2019). Thus, the anterior and posterior regions of the SNpr, and their

region-specific output targets, have distinct roles in the control of seizures.

## Reward

In addition to the GABAergic and dopaminergic neurons in the VTA that have been extensively studied in the context of reward, the SNpr GABAergic neurons have also been shown to mediate avoidance and reward function, and are especially important for opioid action (Rizzi and Tan, 2019; Galaj et al., 2020). Compared to the VTA, the SNpr GABAergic neurons more abundantly express  $\mu$ -opioid receptors and their optogenetic activation more potently inhibits opioid reward. These neurons may be related to the *Pvalb*-expressing SNpr GABAergic neurons that project to the adjacent SNpc and regulate both movement and reward (Rizzi and Tan, 2019).

The function of basal ganglia and SNpr in value-based behavior and decision making has been elucidated by the studies in primates. Interestingly, different roles have been assigned to the anterior and posterior parts of the SNpr that receive differential innervation from the CD(h) and CD(t) (see above). In primates, the activity of the CD(t)-pSNpr circuit was specifically observed during the saccade toward previously learned high-value objects, while the activity of the CD(h)-aSNpr circuit was associated with the selection of objects with short-term, changing value (Hikosaka et al., 2014; Yasuda and Hikosaka, 2015; Figure 2C).

## Conclusion and relevance for brain disease

A number of recent studies have addressed the region-specific functions of the SNpr neurons in the context of selecting appropriate behavior, initiation of specific movements and the regulation of behavioral states. The regional differences and specific functions are likely to match the molecularly distinct cell types, as demonstrated by specific manipulation of the activity of the *Pvalb*- and *Gad2*-expressing SNpr neurons (Figure 2C). In addition to acute optogenetic manipulation, behavioral studies of animal models with defects in differentiation of specific SNpr neuron subtypes would be important for understanding behavioral disorders, which often have a developmental basis. For example, mice carrying a mutation in the *Tall* gene lack pSNpr neurons and show ADHD-like behaviors (Morello et al., 2020b). However, these mice also have defects in other brainstem nuclei, underlining the importance of finding strategies for more specific manipulation of the SNpr cell types.

SNpr has been shown to gate different types of behaviors, and studies reviewed here have addressed its broad (for example controlling the state of behavioral activity) as well as more

focused (for example activating a specific movement) functions. The functional repertoire of SNpr appears to be based on distinct SNpr neuron subtypes and their cell-type specific connectivity that form parallel, segregated pathways regulating specific behaviors (Lee et al., 2020). We have discussed here how the SNpr neurons differ by their development, gene expression, connectivity and functions. We propose existence of two main categories of the SNpr GABAergic neurons, the anterolateral aSNpr and posteromedial pSNpr neurons, the features of which reflect their distinct developmental histories in the embryonic brain and suggest that the functional differences of these main SNpr neuron subtypes are intrinsically defined already in the early precursors. It appears that this division represents just the first level of SNpr GABAergic neuron heterogeneity and that both aSNpr and pSNpr contain diverse subcategories, in particular along their medio-lateral axis. This heterogeneity can arise from intrinsic differences in the early precursors, or later extrinsic influences from the neuronal environment and circuitry. Although both aspects likely contribute to the diversity, the fact that molecularly distinct pSNpr neuron subtypes are found in the embryonic brain suggests that at least to some extent their differences are determined early during precursor differentiation. It should be noted that anatomical correlates, although suggestive, are only first approximations, and future studies using cell-type-specific labeling should directly test how the regional differences in the various properties of the SNpr neurons are related to each other. Better understanding of the SNpr neurons also requires more focused and deeper gene expression profiling. This can be expected to reveal SNpr neuron subtypes and their specific markers that would be useful tools for mapping SNpr neuron input and output connections, patterns of activity, and physiological functions in the regulation of behavior. Thus, developmental and genetic studies are expected to guide deeper analyses of the SNpr neurons by viral tracing, electrophysiological techniques, and optogenetic methods.

As a center for behavioral gating, understanding the SNpr has broad implications for brain disease (Figure 2C). A defect in the control of the activity state is a fundamental characteristic of the sleep disorders and attention deficit hyperactivity disorders. Epilepsy reflects a failure to control the overall brain activity pattern and to carry out normal action selection process resulting in seizures (Salpekar, 2018; Broer, 2020). Movement disorders involve more focused defects in the activation of motor activity, and GABAergic basal ganglia output is thought to be overactive in Parkinson's disease (Wichmann and DeLong, 2003; Takakusaki, 2008). The primary cause of these diseases may not lay in the SNpr. However, understanding the basic principles of the basal ganglia function has allowed development of strategies, such as deep brain stimulation for modulation of the SNpr/GPi output and symptomatic treatment of the

movement disorders (Bergman et al., 1990; Limousin and Foltynie, 2019). As the SNpr appears to contain neuron types with different or even opposite functions, access to the subtypes of the SNpr neurons may lead to more focused and effective therapies. As the SNpr gates many types of behaviors, it could even be targeted to treat symptoms of various neuropsychiatric disease including epilepsy, hyperactivity or even sleep disorders.

## Author contributions

JP and KA wrote the article and compiled the figure. JP conceptualized the study. Both authors contributed to the article and approved the submitted version.

## Funding

KA was funded by the Academy of Finland (Finland). JP was funded by the Academy of Finland, the Sigrid Juselius Foundation, and the Magnus Ehrnrooth Foundation (Finland).

## References

- Achim, K., Peltopuro, P., Hui-Hsin, T., Zachariah, A., Åstrand, M., Rowitch, D., et al. (2013). The role of Tal2 and Tal1 in the differentiation of midbrain GABAergic neuron precursors. *Biol. Open* 2, 990–997. doi: 10.1242/bio.20135041
- Achim, K., Peltopuro, P., Lahti, L., Li, J., Salminen, M., and Partanen, J. (2012). Distinct developmental origins and regulatory mechanisms for GABAergic neurons associated with dopaminergic nuclei in the ventral mesodiencephalic region. *Development* 139, 2360–2370. doi: 10.1242/dev.076380
- Agarwal, D., Sandor, C., Volpato, V., Caffrey, T. M., Monzon-Sandoval, J., Bowden, R., et al. (2020). A single-cell atlas of the human substantia nigra reveals cell-specific pathways associated with neurological disorders. *Nat. Commun.* 11:4183. doi: 10.1038/s41467-020-17876-0
- Antal, M., Beneduce, B. M., and Regehr, W. G. (2014). The substantia nigra conveys target-dependent excitatory and inhibitory outputs from the basal ganglia to the thalamus. *J. Neurosci.* 34, 8032–8042. doi: 10.1523/JNEUROSCI.0236-14.2014
- Arber, S., and Costa, R. M. (2022). Networking brainstem and basal ganglia circuits for movement. *Nat. Rev. Neurosci.* 23, 342–360.
- Bergman, H., Wichmann, T., and DeLong, M. R. (1990). Reversal of experimental parkinsonism by lesions of the subthalamic nucleus. *Science* 249, 1436–1438.
- Brignani, S., Raj, D. D. A., Schmidt, E. R. E., Dudukcu, O., Adolfs, Y., De Ruiter, A. A., et al. (2020). Remotely produced and axon-derived netrin-1 instructs GABAergic neuron migration and dopaminergic substantia nigra development. *Neuron* 107:e689. doi: 10.1016/j.neuron.2020.05.037
- Broer, S. (2020). Not Part of the Temporal Lobe, but Still of Importance? Substantia Nigra and Subthalamic Nucleus in Epilepsy. *Front. Syst. Neurosci.* 14:581826. doi: 10.3389/fnins.2020.581826
- Brown, J., Pan, W. X., and Dudman, J. T. (2014). The inhibitory microcircuit of the substantia nigra provides feedback gain control of the basal ganglia output. *Elife* 3:e02397. doi: 10.7554/eLife.02397
- Chen, B., Xu, C., Wang, Y., Lin, W., Wang, Y., Chen, L., et al. (2020). A disinhibitory nigra-parafascicular pathway amplifies seizure in temporal lobe epilepsy. *Nat. Commun.* 11:923. doi: 10.1038/s41467-020-14648-8
- Cheramy, A., Leviel, V., and Glowinski, J. (1981). Dendritic release of dopamine in the substantia nigra. *Nature* 289, 537–542.
- Chevalier, G., and Deniau, J. M. (1990). Disinhibition as a basic process in the expression of striatal functions. *Trends Neurosci.* 13, 277–280.
- Del Barrio, M. G., Taveira-Marques, R., Muroyama, Y., Yuk, D. I., Li, S., Wines-Samuelson, M., et al. (2007). A regulatory network involving Foxn4, Mash1 and delta-like 4/Notch1 generates V2a and V2b spinal interneurons from a common progenitor pool. *Development* 134, 3427–3436. doi: 10.1242/dev.005868
- Deniau, J. M., and Chevalier, G. (1992). The lamellar organization of the rat substantia nigra pars reticulata: Distribution of projection neurons. *Neuroscience* 46, 361–377.
- Deniau, J. M., Mailly, P., Maurice, N., and Charpier, S. (2007). The pars reticulata of the substantia nigra: A window to basal ganglia output. *Prog. Brain Res.* 160, 151–172. doi: 10.1016/S0079-6123(06)60009-5
- Deniau, J. M., Menetrey, A., and Charpier, S. (1996). The lamellar organization of the rat substantia nigra pars reticulata: Segregated patterns of striatal afferents and relationship to the topography of corticostriatal projections. *Neuroscience* 73, 761–781. doi: 10.1016/0306-4522(96)00088-7
- Dudman, J. T., and Krakauer, J. W. (2016). The basal ganglia: From motor commands to the control of vigor. *Curr. Opin. Neurobiol.* 37, 158–166. doi: 10.1016/j.conb.2016.02.005
- Ferreira-Pinto, M. J., Kanodia, H., Falasconi, A., Sigrist, M., Esposito, M. S., and Arber, S. (2021). Functional diversity for body actions in the mesencephalic locomotor region. *Cell* 184:e4518. doi: 10.1016/j.cell.2021.07.002
- Foster, N. N., Barry, J., Korobkova, L., Garcia, L., Gao, L., Becerra, M., et al. (2021). The mouse cortico-basal ganglia-thalamic network. *Nature* 598, 188–194.
- Galaj, E., Han, X., Shen, H., Jordan, C. J., He, Y., Humburg, B., et al. (2020). Dissecting the Role of GABA Neurons in the VTA versus SNr in Opioid Reward. *J. Neurosci.* 40, 8853–8869. doi: 10.1523/JNEUROSCI.0988-20.2020
- Gernert, M., Fedrowitz, M., Wlaz, P., and Loscher, W. (2004). Subregional changes in discharge rate, pattern, and drug sensitivity of putative GABAergic nigral neurons in the kindling model of epilepsy. *Europ. J. Neurosci.* 20, 2377–2386. doi: 10.1111/j.1460-9568.2004.03699.x
- Gonzalez-Hernandez, T., and Rodriguez, M. (2000). Compartmental organization and chemical profile of dopaminergic and GABAergic neurons in the substantia nigra of the rat. *J. Comp. Neurol.* 421, 107–135. doi: 10.1002/(sici)1096-9861(20000522)421:1&lt;107::aid-cne78>3.3.co;2-6

## Acknowledgments

We thank Svetlana Molchanova for reading and commenting the manuscript.

## Conflict of interest

The authors declare that the research was conducted in the absence of any commercial or financial relationships that could be construed as a potential conflict of interest.

## Publisher's note

All claims expressed in this article are solely those of the authors and do not necessarily represent those of their affiliated organizations, or those of the publisher, the editors and the reviewers. Any product that may be evaluated in this article, or claim that may be made by its manufacturer, is not guaranteed or endorsed by the publisher.



- Gould, E., and Butcher, L. L. (1986). Cholinergic neurons in the rat substantia nigra. *Neurosci. Lett.* 63, 315–319.
- Grillner, S., and Robertson, B. (2016). The basal ganglia over 500 million years. *Curr. Biol.* 26, R1088–R1100.
- Gulley, J. M., Kosobud, A. E., and Rebec, G. V. (2002). Behavior-related modulation of substantia nigra pars reticulata neurons in rats performing a conditioned reinforcement task. *Neuroscience* 111, 337–349. doi: 10.1016/s0306-4522(02)00018-0
- Hikosaka, O. (2007). GABAergic output of the basal ganglia. *Prog. Brain Res.* 160, 209–226.
- Hikosaka, O., Kim, H. F., Amita, H., Yasuda, M., Isoda, M., Tachibana, Y., et al. (2019). Direct and indirect pathways for choosing objects and actions. *Europ. J. Neurosci.* 49, 637–645.
- Hikosaka, O., Kim, H. F., Yasuda, M., and Yamamoto, S. (2014). Basal ganglia circuits for reward value-guided behavior. *Annu. Rev. Neurosci.* 37, 289–306.
- Hubert, O., and Kratsios, P. (2019). Neuronal identity control by terminal selectors in worms, flies, and chordates. *Curr. Opin. Neurobiol.* 56, 97–105. doi: 10.1016/j.conb.2018.12.006
- Iadarola, M. J., and Gale, K. (1982). Substantia nigra: Site of anticonvulsant activity mediated by gamma-aminobutyric acid. *Science* 218, 1237–1240.
- Joshi, K., Lee, S., Lee, B., Lee, J. W., and Lee, S. K. (2009). LMO4 controls the balance between excitatory and inhibitory spinal V2 interneurons. *Neuron* 61, 839–851. doi: 10.1016/j.neuron.2009.02.011
- Kala, K., Haugas, M., Lillevali, K., Guimera, J., Wurst, W., Salminen, M., et al. (2009). Gata2 is a tissue-specific post-mitotic selector gene for midbrain GABAergic neurons. *Development* 136, 253–262. doi: 10.1242/dev.029900
- Klaus, A., Alves da Silva, J., and Costa, R. M. (2019). What, If, and When to Move: Basal Ganglia Circuits and Self-Paced Action Initiation. *Annu. Rev. Neurosci.* 42, 459–483. doi: 10.1146/annurev-neuro-072116-031033
- Kravitz, A. V., Freeze, B. S., Parker, P. R., Kay, K., Thwin, M. T., Deisseroth, K., et al. (2010). Regulation of parkinsonian motor behaviours by optogenetic control of basal ganglia circuitry. *Nature* 466, 622–626.
- La Manno, G., Gyllborg, D., Codeluppi, S., Nishimura, K., Salto, C., Zeisel, A., et al. (2016). Molecular diversity of midbrain development in mouse, human, and stem cells. *Cell* 167:e519.
- Lahti, L., Haugas, M., Tikker, L., Airavaara, M., Voutilainen, M. H., Anttila, J., et al. (2016). Differentiation and molecular heterogeneity of inhibitory and excitatory neurons associated with midbrain dopaminergic nuclei. *Development* 143, 516–529. doi: 10.1242/dev.129957
- Lambert de Rouvroit, C., and Goffinet, A. M. (2001). Neuronal migration. *Mech. Dev.* 105, 47–56.
- Lee, C. R., and Tepper, J. M. (2007). Morphological and physiological properties of parvalbumin- and calretinin-containing gamma-aminobutyric acidergic neurons in the substantia nigra. *J. Comp. Neurol.* 500, 958–972. doi: 10.1002/cne.21220
- Lee, J., Wang, W., and Sabatini, B. L. (2020). Anatomically segregated basal ganglia pathways allow parallel behavioral modulation. *Nat. Neurosci.* 23, 1388–1398. doi: 10.1038/s41593-020-00712-5
- Levey, A. I., Hersch, S. M., Rye, D. B., Sunahara, R. K., Niznik, H. B., Kitt, C. A., et al. (1993). Localization of D1 and D2 dopamine receptors in brain with subtype-specific antibodies. *Proc. Natl. Acad. Sci. U.S.A.* 90, 8861–8865.
- Li, S., Misra, K., Matisse, M. P., and Xiang, M. (2005). Foxn4 acts synergistically with Mash1 to specify subtype identity of V2 interneurons in the spinal cord. *Proc. Natl. Acad. Sci. U.S.A.* 102, 10688–10693. doi: 10.1073/pnas.0504799102
- Limousin, P., and Foltyniec, T. (2019). Long-term outcomes of deep brain stimulation in Parkinson disease. *Nat. Rev. Neurol.* 15, 234–242.
- Liu, D., Li, W., Ma, C., Zheng, W., Yao, Y., Tso, C. F., et al. (2020). A common hub for sleep and motor control in the substantia nigra. *Science* 367, 440–445. doi: 10.1126/science.aaz0956
- Lutas, A., Lahmann, C., Soumillon, M., and Yellen, G. (2016). The leak channel NALCN controls tonic firing and glycolytic sensitivity of substantia nigra pars reticulata neurons. *Elife* 5:e15271. doi: 10.7554/eLife.15271
- Madrigal, M. P., Moreno-Bravo, J. A., Martinez-Lopez, J. E., Martinez, S., and Puellas, E. (2016). Mesencephalic origin of the rostral Substantia nigra pars reticulata. *Brain Struct. Funct.* 221, 1403–1412.
- Mailly, P., Charpier, S., Menetrey, A., and Deniau, J. M. (2003). Three-dimensional organization of the recurrent axon collateral network of the substantia nigra pars reticulata neurons in the rat. *J. Neurosci.* 23, 5247–5257. doi: 10.1523/JNEUROSCI.23-12-05247.2003
- McElvain, L. E., Chen, Y., Moore, J. D., Brigidi, G. S., Bloodgood, B. L., Lim, B. K., et al. (2021). Specific populations of basal ganglia output neurons target distinct brain stem areas while collateralizing throughout the diencephalon. *Neuron* 109:e1724. doi: 10.1016/j.neuron.2021.03.017
- Meyer-Luehmann, M., Thompson, J. F., Berridge, K. C., and Aldridge, J. W. (2002). Substantia nigra pars reticulata neurons code initiation of a serial pattern: Implications for natural action sequences and sequential disorders. *Europ. J. Neurosci.* 16, 1599–1608. doi: 10.1046/j.1460-9568.2002.02210.x
- Mink, J. W. (1996). The basal ganglia: Focused selection and inhibition of competing motor programs. *Prog. Neurobiol.* 50, 381–425.
- Misra, K., Luo, H., Li, S., Matisse, M., and Xiang, M. (2014). Asymmetric activation of Dll4-Notch signaling by Foxn4 and proneural factors activates BMP/TGFbeta signaling to specify V2b interneurons in the spinal cord. *Development* 141, 187–198. doi: 10.1242/dev.092536
- Morales, M., and Root, D. H. (2014). Glutamate neurons within the midbrain dopamine regions. *Neuroscience* 282C, 60–68.
- Morello, F., Borshagovski, D., Survila, M., Tikker, L., Sadik-Ogli, S., Kirjavainen, A., et al. (2020a). molecular fingerprint and developmental regulation of the tegmental GABAergic and glutamatergic neurons derived from the anterior hindbrain. *Cell Rep.* 33:108268. doi: 10.1016/j.celrep.2020.108268
- Morello, F., Voikar, V., Parkkinen, P., Panhelainen, A., Rosenholm, M., Makkonen, A., et al. (2020b). ADHD-like behaviors caused by inactivation of a transcription factor controlling the balance of inhibitory and excitatory neuron development in the mouse anterior brainstem. *Transl. Psychiatry* 10:357. doi: 10.1038/s41398-020-01033-8
- Moreno-Bravo, J. A., Perez-Balaguer, A., Martinez, S., and Puellas, E. (2010). Dynamic expression patterns of Nkx6.1 and Nkx6.2 in the developing mesencephalic basal plate. *Dev. Dyn.* 239, 2094–2101. doi: 10.1002/dvdy.22327
- Nagatomo, K., Suga, S., Saitoh, M., Kogawa, M., Kobayashi, K., Yamamoto, Y., et al. (2017). Dopamine D1 Receptor Immunoreactivity on Fine Processes of GFAP-Positive Astrocytes in the Substantia Nigra Pars Reticulata of Adult Mouse. *Front. Neuroanat.* 11:3. doi: 10.3389/fnana.2017.00003
- Nair-Roberts, R. G., Chatelain-Badie, S. D., Benson, E., White-Cooper, H., Bolam, J. P., and Ungless, M. A. (2008). Stereological estimates of dopaminergic, GABAergic and glutamatergic neurons in the ventral tegmental area, substantia nigra and retrorubral field in the rat. *Neuroscience* 152, 1024–1031. doi: 10.1016/j.neuroscience.2008.01.046
- Parent, A., Bouchard, C., and Smith, Y. (1984). The striatopallidal and striatonigral projections: Two distinct fiber systems in primate. *Brain Res.* 303, 385–390. doi: 10.1016/0006-8993(84)91224-1
- Peng, C. Y., Yajima, H., Burns, C. E., Zon, L. I., Sisodia, S. S., Pfaff, S. L., et al. (2007). Notch and MAML signaling drives Scl-dependent interneuron diversity in the spinal cord. *Neuron* 53, 813–827. doi: 10.1016/j.neuron.2007.02.019
- Porcher, C., Chagraoui, H., and Kristiansen, M. S. (2017). SCL/TAL1: A multifaceted regulator from blood development to disease. *Blood* 129, 2051–2060. doi: 10.1182/blood-2016-12-754051
- Poulin, J. F., Gaertner, Z., Moreno-Ramos, O. A., and Awatramani, R. (2020). Classification of midbrain dopamine neurons using single-cell gene expression profiling approaches. *Trends Neurosci.* 43, 155–169.
- Qiu, M., Shimamura, K., Sussel, L., Chen, S., and Rubenstein, J. L. (1998). Control of anteroposterior and dorsoventral domains of Nkx-6.1 gene expression relative to other Nkx genes during vertebrate CNS development. *Mech. Dev.* 72, 77–88. doi: 10.1016/s0925-4773(98)00018-5
- Richards, A. B., Scheel, T. A., Wang, K., Henkemeyer, M., and Kromer, L. F. (2007). EphB1 null mice exhibit neuronal loss in substantia nigra pars reticulata and spontaneous locomotor hyperactivity. *Europ. J. Neurosci.* 25, 2619–2628. doi: 10.1111/j.1460-9568.2007.05523.x
- Rizzi, G., and Tan, K. R. (2019). Synergistic nigral output pathways shape movement. *Cell Rep.* 27:e2184. doi: 10.1016/j.celrep.2019.04.068
- Salpekar, J. (2018). Links between epilepsy and ADHD: Time to focus and act. *Epilepsy Curr.* 18, 160–161. doi: 10.5698/1535-7597.18.3.160
- Saunders, A., Macosko, E. Z., Wysoker, A., Goldman, M., Krienen, F. M., de Rivera, H., et al. (2018). Molecular diversity and specializations among the cells of the adult mouse brain. *Cell* 174, 1015–1030.e1016.
- Schmidt, R., Leventhal, D. K., Mallet, N., Chen, F., and Berke, J. D. (2013). Canceling actions involves a race between basal ganglia pathways. *Nat. Neurosci.* 16, 1118–1124.
- Smith, Y., and Parent, A. (1986). Differential connections of caudate nucleus and putamen in the squirrel monkey (*Saimiri sciureus*). *Neuroscience* 18, 347–371. doi: 10.1016/0306-4522(86)90159-4
- Song, H., Lee, B., Pyun, D., Guimera, J., Son, Y., Yoon, J., et al. (2015). Ascl1 and Helt act combinatorially to specify thalamic neuronal identity by repressing Dlx5 activation. *Dev. Biol.* 398, 280–291. doi: 10.1016/j.ydbio.2014.12.003

- Takakusaki, K. (2008). Forebrain control of locomotor behaviors. *Brain Res. Rev.* 57, 192–198.
- Takakusaki, K., Habaguchi, T., Ohtinata-Sugimoto, J., Saitoh, K., and Sakamoto, T. (2003). Basal ganglia efferents to the brainstem centers controlling postural muscle tone and locomotion: A new concept for understanding motor disorders in basal ganglia dysfunction. *Neuroscience* 119, 293–308. doi: 10.1016/s0306-4522(03)00095-2
- Tepper, J. M., Martin, L. P., and Anderson, D. R. (1995). GABAA receptor-mediated inhibition of rat substantia nigra dopaminergic neurons by pars reticulata projection neurons. *J. Neurosci.* 15, 3092–3103.
- Vasudevan, A., Won, C., Li, S., Erdelyi, F., Szabo, G., and Kim, K. S. (2012). Dopaminergic neurons modulate GABA neuron migration in the embryonic midbrain. *Development* 139, 3136–3141. doi: 10.1242/dev.078394
- Veliskova, J., Miller, A. M., Nunes, M. L., and Brown, L. L. (2005). Regional neural activity within the substantia nigra during peri-ictal flurothyl generalized seizure stages. *Neurobiol. Dis.* 20, 752–759. doi: 10.1016/j.nbd.2005.05.007
- Villalobos, C. A., and Basso, M. A. (2022). Optogenetic activation of the inhibitory nigro-collicular circuit evokes contralateral orienting movements in mice. *Cell Rep.* 39:110699. doi: 10.1016/j.celrep.2022.110699
- Virolainen, S. M., Achim, K., Peltopuro, P., Salminen, M., and Partanen, J. (2012). Transcriptional regulatory mechanisms underlying the GABAergic neuron fate in different diencephalic prosomeres. *Development* 139, 3795–3805. doi: 10.1242/dev.075192
- Wende, C. Z., Zoubaa, S., Blak, A., Echevarria, D., Martinez, S., Guillemot, F., et al. (2015). Hairy/Enhancer-of-Split MEGANE and Proneural MASH1 factors cooperate synergistically in midbrain GABAergic neurogenesis. *PLoS One* 10:e0127681. doi: 10.1371/journal.pone.0127681
- Wichmann, T., and DeLong, M. R. (2003). Pathophysiology of Parkinson's disease: The MPTP primate model of the human disorder. *Ann. N.Y. Acad. Sci.* 991, 199–213.
- Wicker, E., Beck, V. C., Kulick-Soper, C., Kulick-Soper, C. V., Hyder, S. K., Campos-Rodriguez, C., et al. (2019). Descending projections from the substantia nigra pars reticulata differentially control seizures. *Proc. Natl. Acad. Sci. U.S.A.* 116, 27084–27094. doi: 10.1073/pnas.1908176117
- Wurst, W., and Bally-Cuif, L. (2001). Neural plate patterning: Upstream and downstream of the isthmus organizer. *Nat. Rev. Neurosci.* 2, 99–108. doi: 10.1038/35053516
- Yamaguchi, T., Wang, H. L., and Morales, M. (2013). Glutamate neurons in the substantia nigra compacta and retrorubral field. *Europ. J. Neurosci.* 38, 3602–3610.
- Yasuda, M., and Hikosaka, O. (2015). Functional territories in primate substantia nigra pars reticulata separately signaling stable and flexible values. *J. Neurophysiol.* 113, 1681–1696. doi: 10.1152/jn.00674.2014
- Zeisel, A., Hochgerner, H., Lonnerberg, P., Johnsson, A., Memic, F., van der Zwan, J., et al. (2018). Molecular architecture of the mouse nervous system. *Cell* 174, 999–1014e1022.
- Zhou, F. M., and Lee, C. R. (2011). Intrinsic and integrative properties of substantia nigra pars reticulata neurons. *Neuroscience* 198, 69–94.
- Zhou, F. W., Jin, Y., Matta, S. G., Xu, M., and Zhou, F. M. (2009). An ultra-short dopamine pathway regulates basal ganglia output. *J. Neurosci.* 29, 10424–10435.
- Zhou, Y., Yamamoto, M., and Engel, J. D. (2000). GATA2 is required for the generation of V2 interneurons. *Development* 127, 3829–3838. doi: 10.1242/dev.127.17.3829





## OPEN ACCESS

## EDITED BY

Subashika Govindan,  
Wellcome Trust DBT India Alliance,  
India

## REVIEWED BY

Huaqiang Zhou,  
Sun Yat-sen University Cancer Center  
(SYSUCC), China  
Enrico Capobianco,  
Jackson Laboratory, United States

## \*CORRESPONDENCE

Jingdun Xie  
xiejd6@mail.sysu.edu.cn  
Weiqiang Zhong  
zhongwq@sysucc.org.cn

†These authors have contributed  
equally to this work and share first  
authorship

## SPECIALTY SECTION

This article was submitted to  
Translational Neuroscience,  
a section of the journal  
Frontiers in Neuroscience

RECEIVED 15 July 2022

ACCEPTED 04 October 2022

PUBLISHED 19 October 2022

## CITATION

Ye Q, Huang Z, Lu W, Yan F, Zeng W,  
Xie J and Zhong W (2022)  
Identification of the common  
differentially expressed genes  
and pathogenesis between  
neuropathic pain and aging.  
*Front. Neurosci.* 16:994575.  
doi: 10.3389/fnins.2022.994575

## COPYRIGHT

© 2022 Ye, Huang, Lu, Yan, Zeng, Xie  
and Zhong. This is an open-access  
article distributed under the terms of  
the [Creative Commons Attribution  
License \(CC BY\)](#). The use, distribution  
or reproduction in other forums is  
permitted, provided the original  
author(s) and the copyright owner(s)  
are credited and that the original  
publication in this journal is cited, in  
accordance with accepted academic  
practice. No use, distribution or  
reproduction is permitted which does  
not comply with these terms.

# Identification of the common differentially expressed genes and pathogenesis between neuropathic pain and aging

Qingqing Ye<sup>†</sup>, Zhensheng Huang<sup>†</sup>, Weicheng Lu<sup>†</sup>, Fang Yan,  
Weian Zeng, Jingdun Xie\* and Weiqiang Zhong\*

State Key Laboratory of Oncology in Southern China, Department of Anesthesiology, Collaborative Innovation for Cancer Medicine, Sun Yat-sen University Cancer Center, Guangzhou, China

**Background:** Neuropathic pain is a debilitating disease caused by damage or diseases of the somatosensory nervous system. Previous research has indicated potential associations between neuropathic pain and aging. However, the mechanisms by which they are interconnected remain unclear. In this study, we aim to identify the common differentially expressed genes (co-DEGs) between neuropathic pain and aging through integrated bioinformatics methods and further explore the underlying molecular mechanisms.

**Methods:** The microarray datasets GSE24982, GSE63442, and GSE63651 were downloaded from Gene Expression Omnibus (GEO) database. Differentially expressed genes (DEGs) and co-DEGs were first identified. Functional enrichment analyses, protein-protein Interaction (PPI) network, module construction and hub genes identification were performed. Immune infiltration analysis was conducted. Targeted transcription factors (TFs), microRNAs (miRNAs) and potential effective drug compounds for hub genes were also predicted.

**Results:** A total of 563 and 1,250 DEGs of neuropathic pain and aging were screened, respectively. 16 genes were further identified as co-DEGs. The functional analysis emphasizes the vital roles of the humoral immune response and complement and coagulation cascades in these two diseases. Cxcl14, Fblim1, RT1-Da, Serping1, Cfd, and Fcgr2b were identified as hub genes. Activated B cell, mast cell, activated dendritic cell, CD56 bright natural killer cell, effector memory CD8+ T cell, and type 2 T helper cell were significantly up-regulated in the pain and aging condition. Importantly, hub genes were found to correlate with the activated B cell, activated dendritic cell, Gamma delta T cell, central memory CD4+ T cell and mast cell in pain and aging diseases. Finally, Spic, miR-883-5p, and miR-363-5p et al. were predicted as the potential vital regulators for hub genes. Aldesleukin, Valziflocept, MGD-010, Cinryze, and Rhucin were the potential effective drugs in neuropathic pain and aging.

**Conclusion:** This study identified co-DEGs, revealed molecular mechanisms, demonstrated the immune microenvironment, and predicted the possible TFs, miRNAs regulation networks and new drug targets for neuropathic pain and aging, providing novel insights into further research.

#### KEYWORDS

neuropathic pain, aging, co-DEGs, immune infiltration, regulation network

## Introduction

Neuropathic pain is a debilitating neurobiological disease caused by damage or diseases of the somatosensory nervous system and characterized by spontaneous pain or amplified pain responses (Jensen et al., 2011). It is a major socioeconomic problem that affects 7–10% of the population (van Hecke et al., 2014). Patients with neuropathic pain are often accompanied by sleep disturbances, depression, and severe impairment of daily life (Finnerup et al., 2021). Its prevalence has been projected to increase with the aging population, which is directly associated with suffering, disability, and higher costs to health care systems (Domenichiello and Ramsden, 2019).

Aging is a progressive loss of physiological integrity that leads to diminished function and increased mortality (López-Otín et al., 2013). It is one of the leading risk factors for most neurodegenerative diseases, including Alzheimer's disease (AD) and Parkinson's disease (PD) (Hou et al., 2019). Numerous studies have also indicated the strong relationship between neuropathic pain and aging. Persistent pain has been associated with aging (Saraiva et al., 2018), and aging may contribute to descending inhibition of pain pathways (Karp et al., 2008). Additionally, older adults with pain conditions are more likely to age than pain-free individuals (Karp et al., 2008). However, the underlying mechanisms involved in neuropathic pain and aging remain elusive.

In recent years, advances in microarray chip technology and other bioinformatics tools have made it possible to explore the common molecular mechanisms of disease–disease interaction. Here, We explored common differentially expressed genes (co-DEGs) and underlying molecular mechanisms between neuropathic pain and aging models. Three gene expression datasets (GSE24982, GSE63442, and GSE63651) were downloaded from the Gene Expression Omnibus (GEO) database. Through integrated bioinformatics analyses, co-DEGs and their functional roles in neuropathic pain and aging were identified. PPI network, critical modules and hub genes were predicted. The immune microenvironment was further revealed, and the potential roles of hub genes in immune regulation were demonstrated. Finally, we investigated these genes' TFs, associated miRNAs and predicted possible effective target drug compounds. The present study sought to

provide new insights into the molecular mechanisms underlying neuropathic pain and aging.

## Materials and methods

### Data acquisition

Three microarray datasets were first downloaded and analyzed from the GEO database.<sup>1</sup> The GSE24982 dataset contains 10 pairs of contralateral and 10 pairs of ipsilateral L4 or L5 Dorsal Root Ganglion (DRG) tissue samples with sham surgery or Spinal Nerve Ligation (SNL) surgery (von Schack et al., 2011). GSE63442 dataset consists of 6 sham surgery samples and 6 SNL surgery samples from the rat DRG tissue. GSE63651 consists of 4 young (6 months-old) normal-fed rats, 4 old (25–28 months-old) normal-fed rats, and 4 old (25–28 months-old) fed restrictively. We further selected 10 ipsilateral post-sham DRG tissue in the GSE24982 dataset as the control group and 10 ipsilateral SNL post-op DRG tissue as the experimental group. The six sham-operated DRG samples in the GSE63442 dataset were regarded as the control group, and the other six SNL postoperative DRG samples were regarded as the experimental group. The four young samples of GSE63651 were used as the control group, and the four old samples were used as the experimental group. All three datasets were generated from transcriptome microarray arrays.

### Identification of differentially expressed genes and common differentially expressed genes

Using the R language, we normalized the raw data using the `normalizeBetweenArrays` function, in which the data would be log2 transformed if needed. Differentially expressed genes (DEGs) were identified based on R packages “limma” and “impute” (Ritchie et al., 2015; Hastie et al., 2021). DEGs were defined as genes with adjusted *P*-value < 0.05 and | logFC

<sup>1</sup> <http://www.ncbi.nlm.nih.gov/geo>

(fold change)  $|\geq 0.58$  in the pain datasets, and genes with  $p\text{-value} < 0.05$  and  $|\log\text{FC (fold change)}| \geq 0.58$  in the aging dataset. After screening the DEGs, we first intersected the two pain datasets to collect intersecting genes and then identify the overlapping genes among neuropathic pain and the aging dataset. Genes with opposite expression trends between neuropathic pain and aging datasets were removed.

## Tissue-most expressed gene analysis

We next identified the most related systems/tissues in neuropathic pain and aging by exploring co-DEGs' distribution. We used the online resource BioGPS<sup>2</sup> to analyze the most related systems/tissues with high expression of the co-DEGs. The most related systems/tissues should be the top two expressed systems/tissues, which can be identified as having a certain degree of specificity: (1) the most related tissues-expression level was more than the three multiples of the median, and (2) the second related tissue expression was more than the two multiples of the median.

## Functional enrichment pathway analysis

We performed Gene Ontology (GO) and Kyoto Encyclopedia of Genes and Genomes (KEGG) pathway analyses by “clusterProfiler” R package on the intersection DEGs of GSE24982 and GSE63442, the DEGs of GSE63651, and the co-DEGs of the two phenotypes (Wu et al., 2021). Results with  $P\text{-value} < 0.05$  were indicated as significant. The “ggplot2” package was used to draw the bubble chart (Wickham, 2016). Gene Set Enrichment Analysis (GSEA) was further performed to validate the significant pathway based on GSE24982, GSE63442, and GSE63651, respectively (Subramanian et al., 2005).

## Construction of protein-protein interaction network

We applied the GeneMANIA online database<sup>3</sup> to predict co-DEGs' PPI network (Warde-Farley et al., 2010). It is an online analysis tool that widely used to demonstrate and evaluate gene interactions (Jiang et al., 2022; Tian et al., 2022). Given a query list of genes, GeneMANIA will find more genes like those. Most importantly, with a long enough list (currently five or more genes), GeneMANIA will weight data sources based on their predictive value for reconstructing the query list by default (Franz et al., 2018). We searched the 16 co-DEGs in

GeneMANIA with the search parameters of the organism as *Rattus norvegicus* and network weighting as an automatically selected weighting method. The network was then imported into Cytoscape (Version: 3.7.1) (Shannon et al., 2003) for visualization. To identify the interaction between co-DEGs, we further extracted co-DEGs networks with interactions from the PPI network. The cytoHubba plug-in was then applied to identify the hub genes based on co-DEGs in Cytoscape using the degree algorithm. In addition, the Minimal Common Oncology Data Elements (MCODE) plug-in was used to identify the potential vital modules. Default criteria in MCODE plug-in were set as follows: Degree Cutoff = 2, Node Score Cutoff = 0.2, K-Core = 2, and Max. Depth = 100.

## Immune infiltration analysis

ssGSEA (single-sample GSEA) algorithm was applied to evaluate the immune infiltration in pain and aging based on GSE24982 and GSE63651. It is a rank-based method that defines a score representing the degree of absolute enrichment of a particular gene set in each sample (Bindea et al., 2013; Finotello and Trajanoski, 2018). The correlations between co-DEGs and 28 immune cells were further determined using Spearman correlation analysis (Zhang et al., 2020a).

## Identification of transcription factors and microRNAs

TRRUST<sup>4</sup> is a database for predicting transcription factors. We obtained hub genes' TFs through this database. After downloading the results, we constructed a TF-gene interaction network in Cytoscape. The website miRDB<sup>5</sup> is a comprehensive database of microRNAs. Compared with other databases, the microRNAs collected by miRDB are more complete and fully annotated. Through the Target mining module, we submitted hub genes as gene targets and then downloaded predicted miRNAs with scores greater than 50 points. The results were also visualized by Cytoscape.

## Drug prediction of hub genes

The drug prediction database DGIdb<sup>6</sup> can predict gene-related drugs. We used the drug-gene interaction search module with parameters (source database = 22, gene category = 43, interaction type = 31) to predict drugs for the hub genes. The Cytoscape software conducted further visualization.

<sup>2</sup> <http://biogps.org>

<sup>3</sup> <http://genemania.org/search/>

<sup>4</sup> <https://www.grnpedia.org/trrust/>

<sup>5</sup> <http://mirdb.org/>

<sup>6</sup> <https://dgidb.org/>



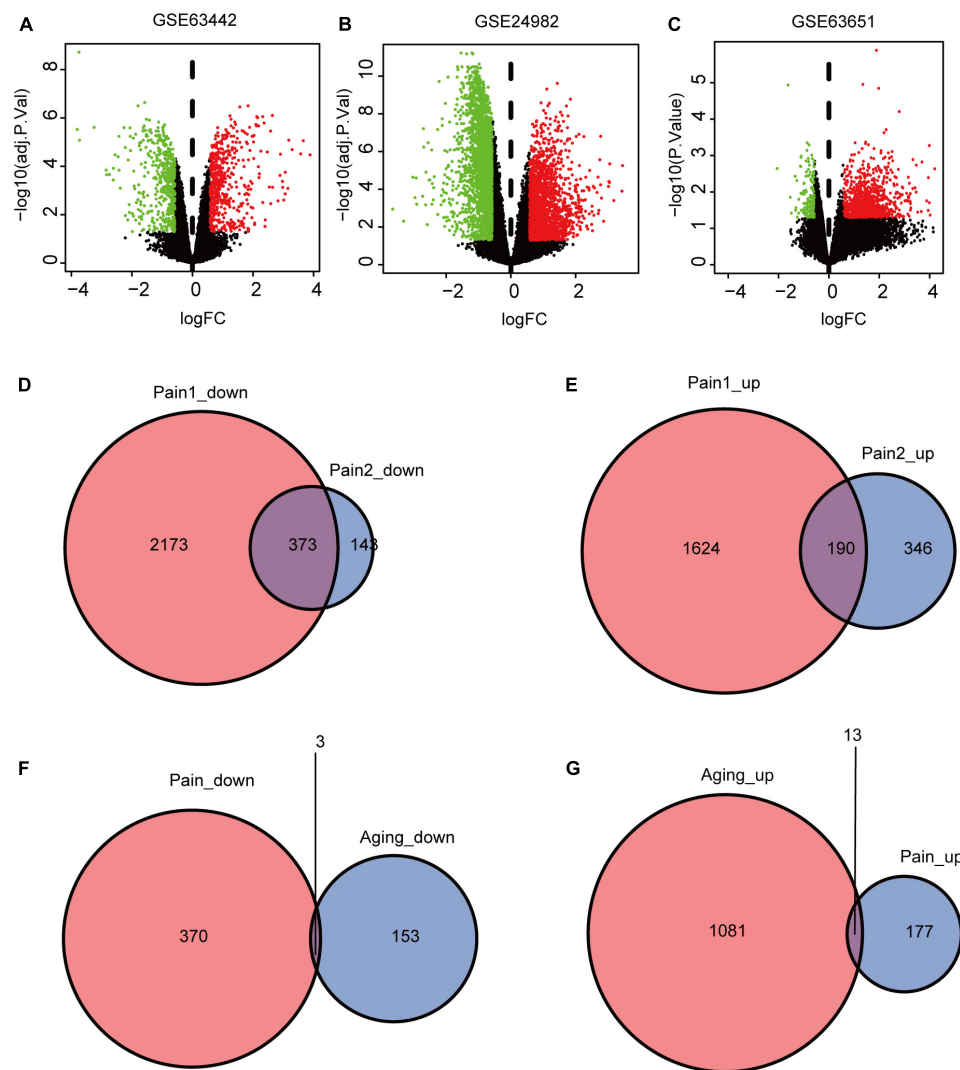


FIGURE 2

DEGs and co-DEGs identification. (A–C) The volcano plots of pain1: GSE63442, pain2: GSE24982 and aging: GSE63651. (D,E) The two pain datasets showed an overlap of 373 down-regulated DEGs and 190 upregulated DEGs. (F,G) The two neuropathic pain and aging datasets showed an overlap of 16 co-DEGs (3 down-regulated and 13 upregulated). DEGs, differentially expressed genes; co-DEGs, common differential expressed genes.

## Results

### Identification of differentially expressed genes in neuropathic pain and aging

The flowchart of this research is shown in Figure 1. We first downloaded two pain datasets numbered GSE24982, GSE63442, and an aging dataset GSE63651 from the GEO database. According to the previously set criteria, we first identified the DEGs of the two pain datasets (Figures 2A,B). A total of 1,250 DEGs (1,094 upregulated and 156 downregulated) were obtained from the aging dataset (Figure 2C). An intersection

was conducted and we obtained 563 common DEGs (190 upregulated and 373 downregulated) between the pain datasets (Figures 2D,E). After excluding genes with opposite expression trends, we performed a Venn diagram analysis. Finally, 16 co-DEGs (13 upregulated and 3 downregulated) were identified (Figures 2F,G and Table 1).

### Tissue-most expressed gene analysis

To better identify tissue- and organ-specific expressed co-DEGs, we searched our co-DEGs in BioGPS. The most highly tissue-related expression system was the hematologic/immune system. The neurologic systems, including pineal, ventral



TABLE 1 16 co-DEGs between neuropathic pain and aging.

Gene	Terms	Pain1		Pain2		Aging	
		LogFc	adj.P.Val	LogFc	adj.P.Val	LogFc	P.Val
Cxcl14	C-X-C motif chemokine ligand 14	3.66	8.73E-06	3.43	1.26E-04	2.19	2.36E-04
Gpnmb	Glycoprotein nmb	2.03	4.75E-05	0.62	1.21E-02	1.57	5.05E-04
Bmp7	Bone morphogenetic protein 7	0.72	6.79E-03	1.57	2.49E-05	1.19	8.29E-04
Ramp1	Receptor activity modifying protein 1	0.87	2.49E-05	1.23	1.94E-04	0.87	6.51E-03
Lilrb4	Leukocyte immunoglobulin like receptor B4	1.53	4.72E-03	1.31	5.77E-06	0.63	9.95E-03
Reg3b	Regenerating islet-derived 3 beta	1.81	4.69E-06	2.52	1.59E-02	1.67	9.99E-03
Cfd	Complement factor D	0.84	1.60E-03	1.74	8.95E-03	1.47	1.60E-02
Serpinb2	Serpin family B member 2	2.98	7.40E-04	1.84	1.68E-09	2.44	1.97E-02
Clec4a3	C-type lectin domain family 4, member a3	1.45	1.02E-05	0.99	2.91E-02	0.60	2.30E-02
Serping1	Serpin family G member 1	1.04	2.36E-03	0.95	1.59E-02	1.07	2.44E-02
RT1-Da	RT1 class II, locus Da	0.86	4.37E-02	2.01	9.06E-05	0.86	2.99E-02
Fcgr2b	Fc gamma receptor IIb	3.02	2.48E-03	1.82	4.93E-05	0.96	3.31E-02
Fblim1	Filamin binding LIM protein 1	0.63	4.63E-02	0.65	4.63E-03	1.50	3.58E-02
Abcd2	ATP binding cassette subfamily D member 2	-1.08	8.68E-05	-0.97	1.85E-06	-0.75	1.39E-02
Hs3st2	Heparan sulfate-glucosamine 3-sulfotransferase 2	-1.47	8.92E-06	-1.97	5.34E-05	-0.73	3.70E-02
Rem2	RRAD and GEM like GTPase 2	-1.69	8.04E-05	-1.06	3.59E-02	-0.89	9.97E-03

striatum, and primary cortical neurons ranked second. Furthermore, the digestive system and others like the cornea ranked third, while the circulatory system and urinary had another similar level of enrichment (Table 2). The results indicated the possible related systems across pain and aging.

## Functional enrichment pathway analysis

GO and KEGG enrichment analyses of the DEGs and co-DEGs above were performed in R using the “clusterProfiler” package. Results showed that DEGs in pain datasets were mainly enriched in membrane potential, metal ion transport, wound healing, sensory perception of pain, action potential, transmembrane transport, complement, and coagulation cascades etc. (Figures 3A,B and Supplementary Tables 1, 2),

while the DEGs in the aging dataset were mainly enriched in regulation of cell-cell adhesion, negative regulation of cell activation, cytokine-cytokine receptor interaction etc. (Figures 3C,D and Supplementary Tables 3, 4). Further functional enrichments analyses indicated that the co-DEGs between pain and aging were principally associated with humoral immune response, negative regulation of cytokine production, antigen processing, and presentation of exogenous peptide antigen, antigen processing, and presentation of exogenous antigen, antigen processing and presentation of peptide antigen, negative regulation of tumor necrosis factor production, negative regulation of tumor necrosis factor superfamily cytokine production, negative regulation of lymphocyte proliferation, negative regulation of mononuclear cell proliferation, and negative regulation of leukocyte proliferation (Figure 3E and Supplementary Table 5). Furthermore, two KEGG pathways were identified, including the complement cascade and Staphylococcus aureus infection (Figure 3F and Supplementary Table 6).

The results of GSEA analyses consistently indicated the importance of immune regulation across pain and aging. Complement binding (NES = 1.87,  $P = 0.003$ ; NES, normalized enrichment scores;  $P$ ,  $P$ -value), antigen processing and presentation of peptide antigen via MHC class II (NES = 1.97,  $P < 0.001$ ), regulation of immune response (NES = 1.95,  $P < 0.001$ ), complement and coagulation cascades (NES = 2.18,  $P < 0.001$ ) and B cell receptor signaling (NES = 1.58,  $P = 0.012$ ) pathway were significantly enriched in pain based on GSE24982 (Figures 4A–E). The cellular

TABLE 2 Tissue-most expressed gene identified by BioGPS.

System	Tissue/Cell	Gene
Hematologic/immune	Spleen, thymus, bone marrow	Fcgr2b, RT1-Da, Reg3b, Cfd
Circulatory	Endothelial cell	Fblim1
Neurologic	Pineal, ventral striatum, primary cortical neurons	Serping1, Cxcl14, Bmp7
Digestive	Small intestine, large intestine	Reg3b, Fblim1
Urinary	Kidney	Serping1
Others	Cornea	Cxcl14, Bmp7



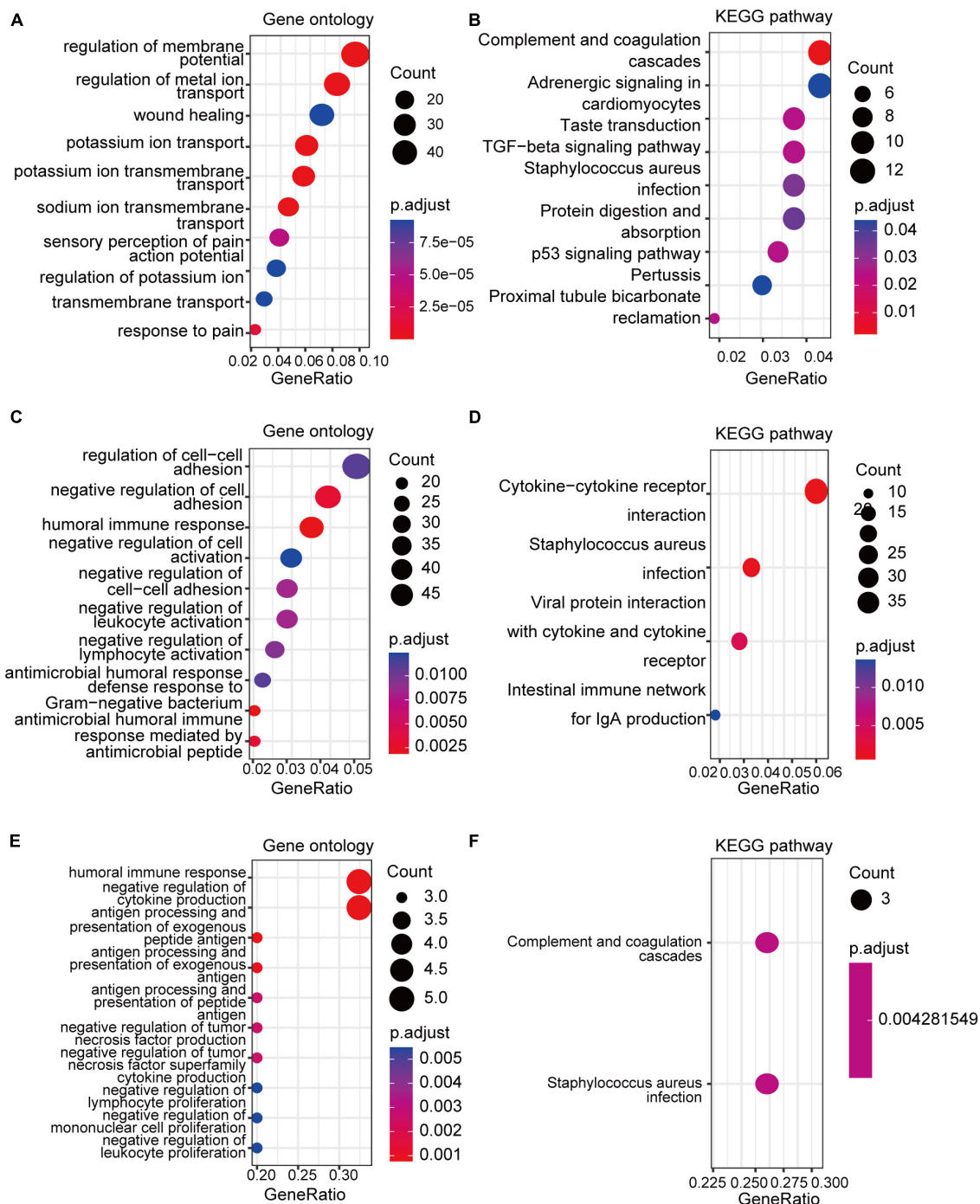


FIGURE 3

GO and KEGG analyses of the DEGs and co-DEGs. (A,B) GO analysis and KEGG pathways analysis of the co-DEGs of the pain datasets. (C,D) GO analysis and KEGG pathways analysis of the DEGs of the aging dataset. (E,F) GO analysis and KEGG pathways analysis of the co-DEGs between the pain and aging datasets. GO, Gene Ontology; KEGG, Kyoto Encyclopedia of Genes and Genomes; DEGs, differential expressed genes; co-DEGs, common differential expressed genes.

senescence item was also upregulated considerably ( $NES = 1.76$ ,  $P < 0.001$ ) (Figure 4F). Meanwhile, Complement binding ( $NES = 1.88$ ,  $P = 0.006$ ), MHC protein complex binding ( $NES = 2.13$ ,  $P < 0.001$ ), CXCR chemokine receptor binding

( $NES = 2.05$ ,  $P < 0.001$ ), complement and coagulation cascades ( $NES = 2.32$ ,  $P < 0.001$ ), antigen processing and presentation ( $NES = 2.04$ ,  $P < 0.001$ ) and cytokine—cytokine receptor interaction ( $NES = 3.02$ ,  $P < 0.001$ ) were enriched

in pain based on GSE63442 (Figures 4G–I). Complement activation ( $NES = 1.58$ ,  $P < 0.001$ ), humoral immune response ( $NES = 1.49$ ,  $P < 0.001$ ), immune receptor activity ( $NES = 1.41$ ,  $P < 0.001$ ), complement and coagulation cascades ( $NES = 1.57$ ,  $P < 0.001$ ), intestinal immune network for IgA production ( $NES = 1.41$ ,  $P = 0.019$ ), and cytokine–cytokine receptor interaction ( $NES = 1.32$ ,  $P < 0.001$ ) were enriched in aging based on GSE6365 (Figures 4M–R).

## Protein-protein interaction network construction and analysis

GeneMANIA database was first used to perform the PPI network construction. From the results, 15 co-DEGs except Hs3st2, and 20 related genes with 950 total links were demonstrated. Approximately 95.10% of the interactions were based on co-expression data, 3.11% of them were based on shared protein domains, while only 1.8% of them were predicted based on co-localization. The networks of co-DEGs and their co-expressed genes were drawn (Figure 5A). We further extracted co-DEGs networks with interactions (Figure 5B). From the results, 15 co-DEGs except Hs3st2 showed a significant interaction, most of which were based on co-expression data. Plug-in cytoHubba was then used to identify the potential hub genes. We further screened 6 hub genes including Cxcl14, Fblim1, RT1-Da, Serping1, Cfd, and Fcgr2b (Figure 5C). MCODE was then applied to identify potential key gene cluster modules. The result demonstrated one connected gene module (Figure 5D) containing 4 co-DEGs, including Ramp1, Cxcl14, Fcgr2b, and RT1-Da.

## Immune infiltration analysis

Based on the GSE24982 and GSE63651 datasets, we applied the ssGSEA method to decode the relative infiltration abundance of 28 immune cell subpopulations in pain and normal controls as well as aging and normal controls. Compared with normal controls, both pain and aging group exhibited a higher infiltration abundance of most immune cells, suggesting a microenvironment of immune activation (Figures 6A,B). Among the results, activated B cell, mast cell, activated dendritic cell, CD56 bright natural killer cell, effector memory CD8+ T cell and type 2 T helper cell were consistently up-regulated in the pain and aging condition. Moreover, correlations between co-DEGs and 28 immune cells were shown. We were surprised to find that hub genes here correlate simultaneously with the activated B cell, activated dendritic cell, Gamma delta T cell, central memory CD4+ T cell and mast cell in pain and aging diseases (Figures 6C,D), suggesting their immunity roles across the disorders.

## Target transcription factors and microRNAs prediction and network construction

Based on the TRRUST database, Spic, a TF (Figure 7A) that may regulate the gene Fcgr2b was identified. According to the miRDB database, 36 target miRNAs were also predicted to interact with genes (Figure 7B). The TF-genes and miRNA-genes interaction networks were visualized by Cytoscape software.

## Prediction of targeted drugs

According to the DGIdb database, 5 potential drugs (Aldesleukin, Valziflocept, MGD-010, Cinryze, and Rhucin) were predicted to target the hub genes (Figure 7C). Cytoscape was used to visualize the drug-genes interaction.

## Discussion

Nowadays, many studies have confirmed the correlation between neuropathic pain and aging. The incidence of pain gradually increases with aging (Koc and Kutsal, 2015). Meanwhile, many studies have shown that the occurrence of pain may accelerate the progression of aging. Miaskowski et al. (2020) showed that older adults with chronic pain in multiple locations have a significantly increased risk of developing disability over time and are at risk for decreased mobility. Morrison and his colleagues revealed that many inflammatory factors, such as tumor necrosis factor- $\alpha$  (TNF- $\alpha$ ), nuclear transcription factors (NF- $\kappa$ B), and interleukin-6 (IL-6), are both significantly correlated with chronic pain and aging, which play an important role in pain sensitization and cell senescence (Morrison et al., 2013). However, the direct link and specific mechanisms remain unclear. Therefore, it's urgent to explore the molecular mechanisms and pinpoint the particular links between pain and aging.

Our study was conducted based on three datasets, two of which were associated with pain while another was related to aging. We first analyzed the DEGs in each pain dataset and took the intersection after eliminating the opposite trend of the DEGs in the two datasets, and then we obtained the common DEGs of pain. Then we analyzed the aging dataset and followed the same method as above to take the intersection. Finally, we identified 16 co-DEGs in pain and aging datasets (13 upregulated and 3 downregulated).

BioGPS was an online tool that created as a centralized gene-annotation portal for clustering distributed genes (Wu et al., 2009). It has been widely used to explore tissue- and organ-specific genes, indicating the correlated systems in diseases (Fang et al., 2022; Li et al., 2022; Xing et al., 2022). According

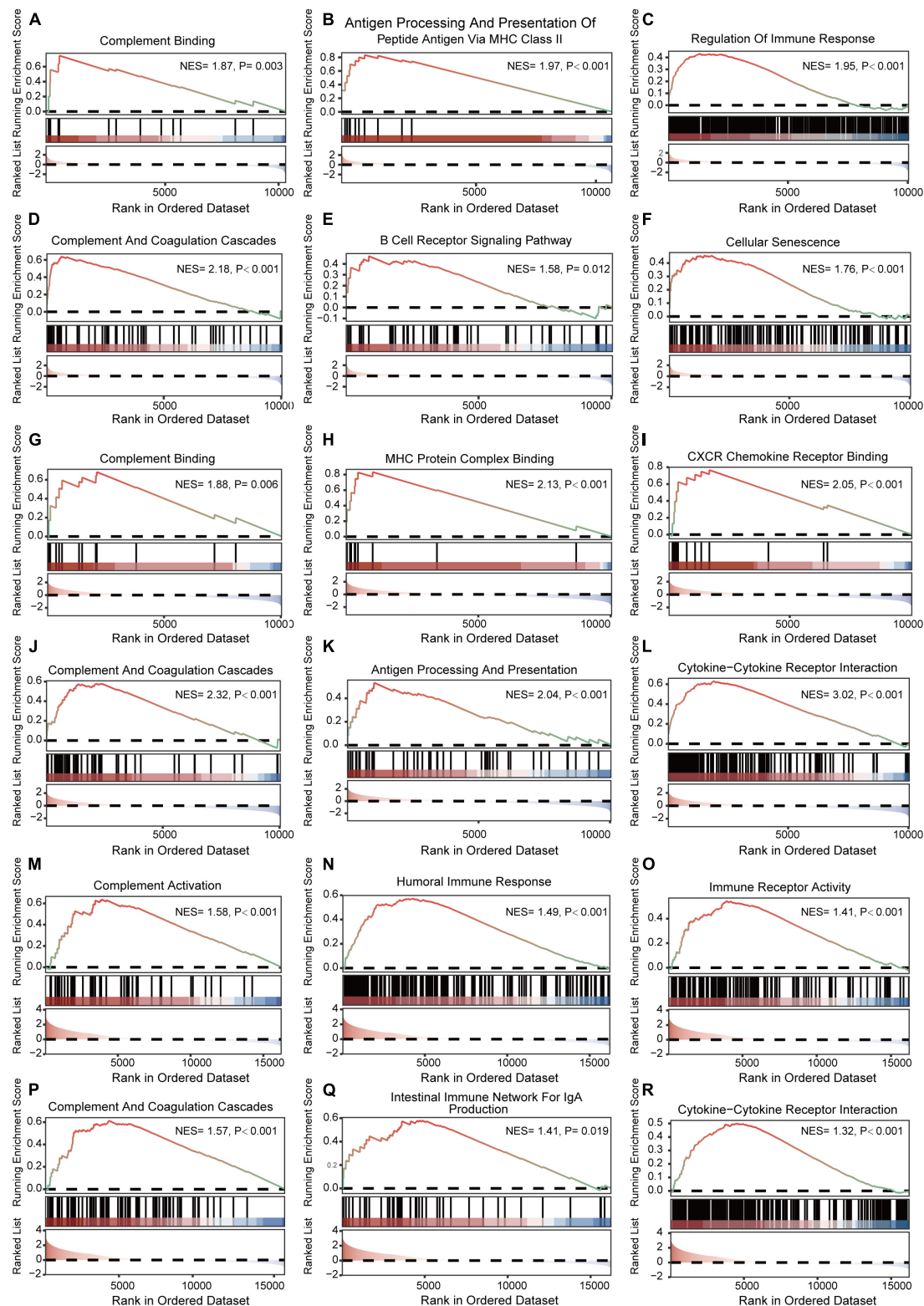
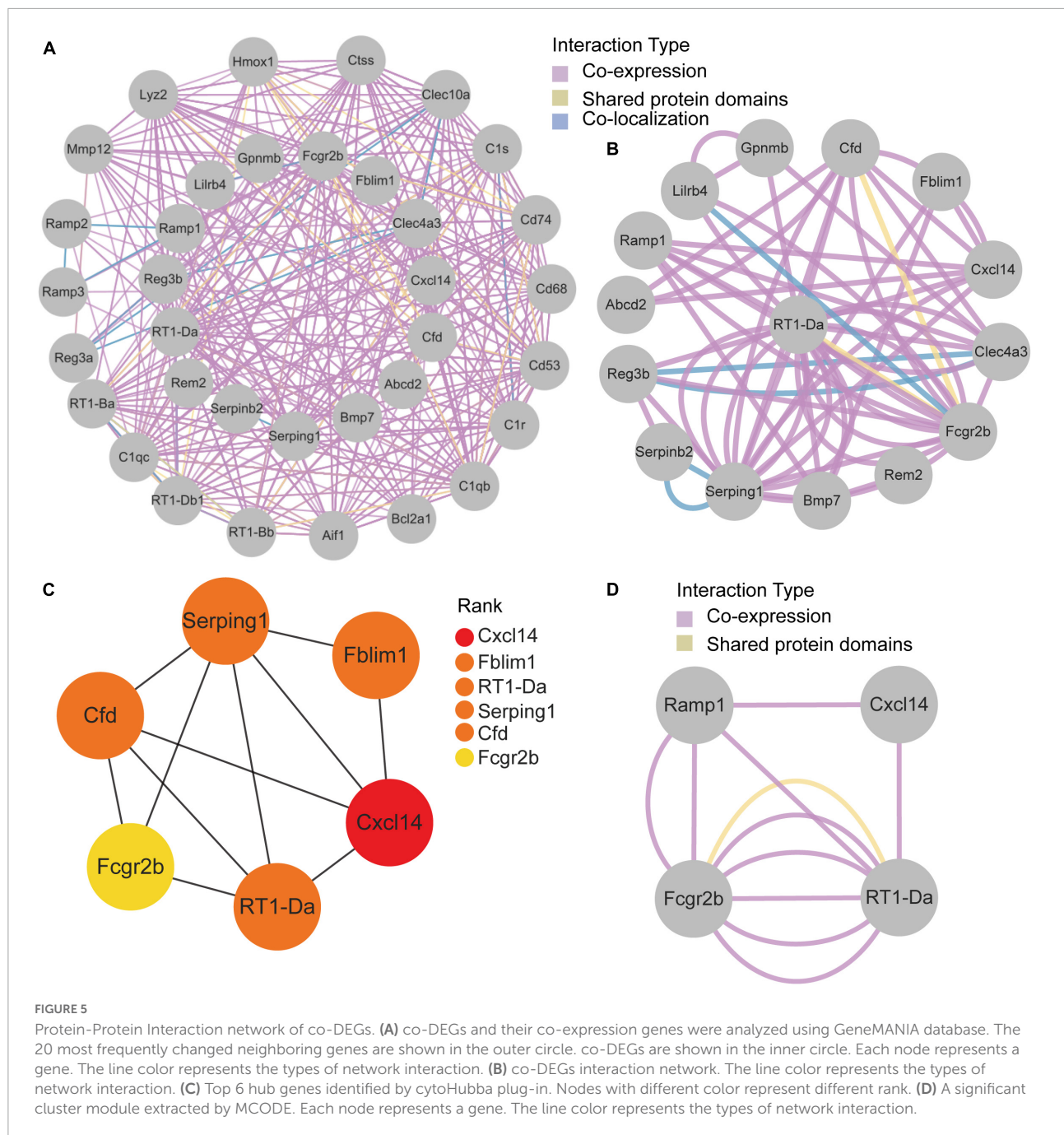


FIGURE 4

GSEA enrichment analyses of GSE24982, GSE63442, and GSE63651. (A–C) Immunity-related GO items enriched in pain based on GSE24982. (D–F) Immunity-related KEGG pathways and cellular senescence enriched in pain based on GSE24982. (G–I) Immunity-related GO items enriched in pain based on GSE63442. (J–L) Immunity-related KEGG pathways enriched in pain based on GSE63442. (M–O) Immunity-related GO items enriched in aging based on GSE63651. (P–R) Immunity-related KEGG pathways enriched in aging based on GSE63651. GSEA, Gene set enrichment analysis; NES, Normalized enrichment score; P, p-value.



to BioGPS, the co-DEGs above were mainly expressed in the hematologic/immune system and neurologic system, which highlights the immune system's role in neuropathic pain and aging. However, though many studies have also indicated the potential significance of immune response in neuropathic pain and aging (Scholz and Woolf, 2007; Kavelaars and Heijnen, 2021), the underlying mechanisms remain to be further elucidated.

We performed a series of bioinformatic analyses to investigate the function of the DEGs. According to GO and

KEGG enrichment analyses, DEGs in pain datasets were majorly enriched in regulating membrane potential, metal ion transport, wound healing, sensory perception of pain, action potential and transmembrane transport, consistent with the fact that pain is mainly associated with sensory conduction and ion transport. DEGs in aging were enriched in regulation of cell-cell adhesion, humoral immune response, negative regulation of cell activation, and antimicrobial humoral response, which showed that aging is linked to immune response and the activation of immune cells. Most importantly, we found that



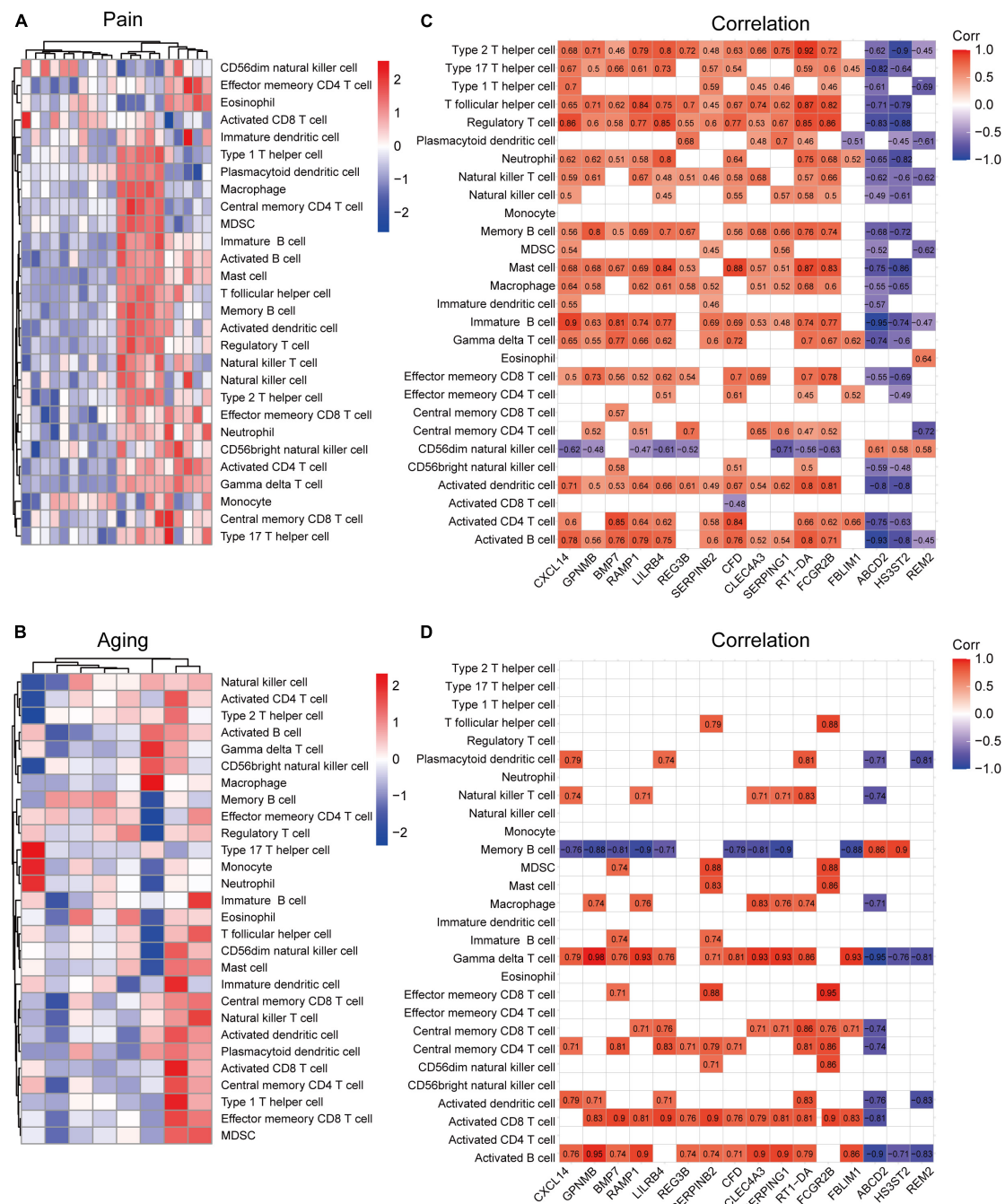


FIGURE 6

Immune infiltration and correlations with co-DEGs. **(A)** Relative infiltration abundance of 28 immune cell subpopulations in pain. **(B)** Relative infiltration abundance of 28 immune cell subpopulations in aging. **(C)** The correlations between co-DEGs and immune cells infiltration in pain. **(D)** The correlations between co-DEGs and immune cells infiltration in aging.

the co-DEGs in both pain and aging datasets were mainly enriched in immune function and pathways. KEGG pathway analysis demonstrated that the co-DEGs were enriched in complement and coagulation cascades and *Staphylococcus aureus* infection, which is primarily related to immunity and inflammation.

Further GSEA enrichment analysis also validated the importance of immune regulation in pain and aging. The results showed that complement binding, antigen processing and presentation, complement and coagulation cascades, B cell receptors, MHC protein complex binding, CXCR chemokine, and cytokine receptors were mainly enriched in pain conditions.

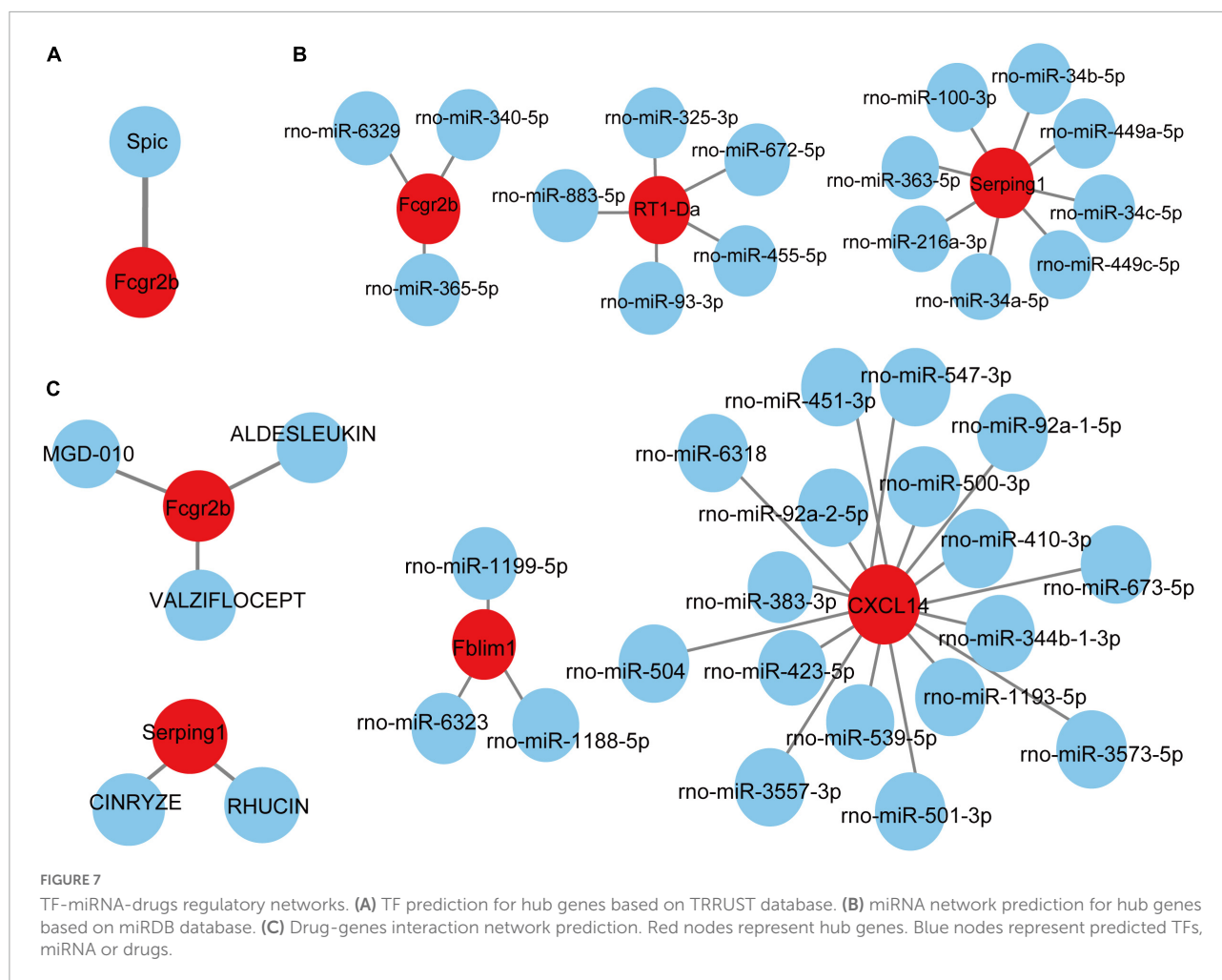


FIGURE 7

TF-miRNA-drugs regulatory networks. (A) TF prediction for hub genes based on TRRUST database. (B) miRNA network prediction for hub genes based on miRDB database. (C) Drug-genes interaction network prediction. Red nodes represent hub genes. Blue nodes represent predicted TFs, miRNA or drugs.

Besides, it was worth noting that cellular senescence, a hallmark of aging (Childs et al., 2015), was also activated in pain, indicating the correlation between pain and aging. Meanwhile, complement activation, humoral immune response, immune receptor activity and complement and coagulation cascades were upregulated in aging. As the hypersensitivity caused by inflammatory immune response is one of the crucial factors of neuropathic pain (Li et al., 2020), and immune dysregulation has also emerged as a vital component of aging (Borgoni et al., 2021), we speculate that immune homeostasis may play a crucial role across pain and aging. Therefore, immune targeting therapies might be a potent approach for solving pain and aging. It was different from previous studies that we here paid extra attention to the functional analyses of the co-DEGs across the pain and aging datasets, thus providing new ideas for mechanisms and treatments for the comorbidity of the two diseases.

Subsequently, we constructed the PPI network and applied CytoHubba and MCODE plug-ins to identify the hub genes and critical modules. *Cxcl14*, *Fblim1*, *RT1-Da*, *Serping1*, *Cfd*, and *Fcgr2b* were further screened. It's worth noting that these genes

were upregulated in both pain and aging datasets, suggesting their essential roles in pain and aging.

*Cxcl14* (C-X-C motif chemokine ligand 14) is a CXC chemokine ligand that constitutively expressed in immune cells and throughout the central nervous system. Lu et al. (2016) have summarized its significant role in immunity as an emerging immune and inflammatory modulator. It has been reported that deletion of *Cxcl14* in mice could accelerate skeletal myogenesis by promoting cell cycle withdrawal, which may be a promising target for developing therapeutics to treat aging-related muscle wasting (Waldemer-Streyer et al., 2017). And it has also been identified as a candidate marker for endometrial aging (Kawamura et al., 2021). Besides, *cxcl14* is an essential factor in the initial and maintenance of pain. Previous studies showed that *cxcl14* contributes to the modulation of somatosensation in concert with somatostatin (Yamamoto et al., 2020). And it has been demonstrated that NFATc2-dependent epigenetic upregulation of *cxcl14* is involved in the development of neuropathic pain induced by paclitaxel (Liu et al., 2020). Moreover, a microarray analysis of rat sensory ganglia after



local inflammation also implicates the significant upregulation of cxcl14 in pain (Strong et al., 2012).

Fblim1 (Filamin binding LIM protein 1) encodes a protein with an N-terminal filamin-binding domain, a central proline-rich domain, and multiple C-terminal LIM domains that can serve as an anchoring site for cell-ECM adhesion proteins and filamin-containing actin filaments. It has been implicated in the pathogenesis of sterile bone inflammation (Cox et al., 2017). Meanwhile, migfilin, a protein encoded by Fblim1, is widely expressed in different adherent and circulating blood cells and can regulate integrin activation in naturally occurring vascular cells, endothelial cells and neutrophils. Besides, tightly regulated expression of migfilin is also essential for neuronal development (Ishizuka et al., 2018). However, the role of Fblim1 in the pathogenesis of pain and aging remains unknown.

RT1-Da (RT1 class II, locus Da) is a protein-coding gene that enables T cell receptor binding activity, MHC class II protein complex binding activity and peptide antigen-binding activity. Prior studies have shown that RT1-Da is significantly associated with diseases mediated by the immune system (Vestberg et al., 1998). And it was also identified as an intermediate marker for bilateral hippocampal response to mild traumatic brain injury (Almeida-Suhett et al., 2014).

Serping1 (Serp Family G Member 1) encodes a highly glycosylated plasma protein regulating the complement cascade. Its protein product inhibits activated C1r and C1s of the first complement component, thus regulating complement activation (Murray-Rust et al., 2009). It has been demonstrated to be associated with hereditary angioneurotic edema (Canonica and Rossi, 2012).

Cfd (Complement Factor D) encodes a member of the S1, or chymotrypsin, family of serine peptidases. As a serine protease of the alternative complement pathway, Cfd is required to form C3 convertase, which is the rate-limiting enzyme (Barratt and Weitz, 2021). Mutations in Cfd might result in the deficiency of complement factor D, which is associated with recurrent bacterial meningitis infections in human patients (Wiles et al., 2020).

Fcgr2b (Fc Gamma Receptor IIb) is a protein-coding gene associated with Systemic Lupus Erythematosus and Malaria (Su et al., 2004). It has been reported to play an important role in the B cell receptor signaling pathway and immune response. Evidence has suggested that Fcgr2b is closely associated with arthritis-related joint pain (Bersellini Farinotti et al., 2019), anterior cingulate cortex and prefrontal cortex alteration after nerve injury (Poh et al., 2012; Zhang et al., 2022), and stroke in aged rats (Buga et al., 2012). However, few studies have demonstrated its role in the interconnection between pain and aging. Our work further highlights its significant role in pain and aging interconnection.

Neuroinflammation is one of the crucial factors promoting the occurrence of neuropathic pain. It is usually characterized by the activation and infiltration of leukocytes, the activation

of glial cells, and the increasing inflammatory mediators (Ji et al., 2016). Meanwhile, immunity and inflammation were also dispensable in aging (Ovadya et al., 2018; Wu et al., 2019). For example, senescent cells usually accelerate aging phenotypes through a senescence-associated secretory phenotype (SASP), inducing amounts of inflammatory mediators (IL-1 $\beta$ , IL-6, and TNF- $\alpha$ , etc.). It has also been proved that some critical cytokines and immune cells in aging are indeed neuromodulators of the peripheral and central nervous systems (Atzeni et al., 2019; Durante et al., 2021). Consistently, we found that in both pain and aging condition, there exhibited a higher infiltration abundance of most immune cells, including the activated B cell, mast cell, activated dendritic cell, CD56 bright natural killer cell, effector memory CD8+ T cell and type 2 T helper cell, suggesting a microenvironment of immune activation. Furthermore, we were surprised that those hub genes simultaneously demonstrated a close correlation with the activated B cell, activated dendritic cell, Gamma delta T cell, central memory CD4+ T cell and mast cell in pain and aging diseases, indicating their importance across pain and aging.

TFs are proteins that can bind to DNA and regulate the transcription of DNA into RNA by attaching to the transcription factor binding site, representing the point of convergence of multiple signaling pathways within eukaryotic cells (Kontos et al., 2013). MiRNAs are a class of small and non-coding RNAs that function as post-transcriptional gene regulators by inducing mRNA degradation or repressing mRNA translation (He and Hannon, 2004). The roles of TFs and microRNAs in the pathophysiology of pain and aging have been emerging (Andersen et al., 2014; Zhang and Chi, 2018; Kinser and Pincus, 2020). Here, we constructed TFs- and miRNAs- related regulatory networks for hub genes and module-related key genes to show the potential interactions under pain and aging conditions. As shown on the network, we obtained Spic (Spi-C Transcription Factor) as the key regulatory factor for gene Fcgr2b expression. Besides, 36 miRNAs were predicted to regulate the above genes.

Based on the DGIdb database, drug compounds were put forward. Aldesleukin, Valziflocept, MGD-010, Cinryze, and Rhucin were highlighted among the potential effective drugs. Aldesleukin is an interleukin-2 that FDA approved for the treatment of adults with metastatic renal cell carcinoma (metastatic RCC) and metastatic melanoma (Clement and McDermott, 2009). Song et al. (2002) found that IL-2 can produce analgesic effects in morphine-insensitive mice (Song et al., 2002). Zhang et al. (2020b) found that low doses of IL-2 can also effectively prevent and reverse behavioral development associated with acute and chronic headaches. And IL-2 has also been reported in modulating the inflammation-related senescence of hippocampal neurons. Considering the significance of IL-2, we speculated that Aldesleukin might have a potential value in treating pain and aging. Valziflocept is a recombinant soluble Fc $\gamma$ IIb receptor that targets Fc and

FcγR (Zuercher et al., 2019). FcγR has been reported as a potential therapeutic target for pain in autoimmune diseases (Bersellini Farinotti et al., 2019; Peyrin-Biroulet et al., 2019), and it was also crucial in aging neutrophils (Gasparoto et al., 2021). There is no doubt that Valziflocept may benefit patients with comorbidities of pain and aging to some extent. MGD-010 is a DART (Dual Affinity Retargeting) antibody molecule with great potential in autoimmune disease treatment, which can downregulate B cell receptors and finally reduces signaling. As ssGSEA indicated the upregulation of activated B cells in pain and aging, MGD-010 might also be an effective drug in pain and aging by targeting B cell. Besides, Rhucin, and Cinryze are C1 esterase inhibitors that target hereditary angioedema with FDA approval (Gompels and Lock, 2011). And Chen et al. (2013) found that neutralizing antibodies against the globular heads of the complement protein's C1q receptor (gC1qR) could also alleviate mechanical hyperalgesia in rats with partial sciatic nerve ligation. Though the efficacy of predictive drugs needs further validation, it provides a new direction that targeting the hub genes *via* various mechanisms may help alleviate pain and aging conditions.

Nevertheless, there are still several issues to be addressed starting from our preliminary evidence. Firstly, it is a retrospective study that requires more extensive data analysis before addressing external validation. Secondly, some predictive results are limited in significance due to the knowledge base currently available to database users. Thirdly, the expressions of the hub genes and their roles in pain and aging need to be further explored and assessed. Finally, detailed molecular mechanisms and the regulatory networks still lack research efforts to establish characterization *in vitro* and *in vivo*.

## Conclusion

This is the first study using integrated transcriptome analyses to explore the relationship between neuropathic pain and aging. We put forward ideas to explore and identify the co-DEGs, hub genes to support our understanding of their potential roles in the immune microenvironment, and find specific players among TFs, miRNAs and potential drugs in neuropathic pain and aging. Humoral immune response, especially the regulation of the immune cells like activated B cells, might be the critical mechanism of the interaction. Cxcl14, Fblim1, RT1-Da, Serping1, Cfd, and Fcgr2b might play a significant role in the process. Spic, miR-883-5p, miR-363-5p et al. and potential drugs including Aldesleukin, Valziflocept, MGD-010, Cinryze, and Rhucin were further predicted. In conclusion, our work proposed to explore the correlation between pain and aging, and the preliminary findings highlighted a feasible strategy to identify potential co-DEGs targets addressing early diagnosis and therapy aspects.

## Data availability statement

The datasets presented in this study can be found in online repositories. The names of the repository/repositories and accession number(s) can be found in the article/**Supplementary material**.

## Author contributions

WZ and JX designed the study. QY, ZH, and WL collated the data, carried out data analyses, and produced the initial draft of the manuscript. FY and WZ helped perform the analysis with constructive discussions. All authors have read and approved the final submitted manuscript.

## Funding

This study was supported by the Guangdong Natural Science Foundation for Distinguished Young Scholars (2019B151502010), the National Natural Science Foundation of China (81870878), and the Guangdong Natural Science Foundation (2020A1515110087).

## Conflict of interest

The authors declare that the research was conducted in the absence of any commercial or financial relationships that could be construed as a potential conflict of interest.

The reviewer HZ declared a shared affiliation with the authors to the handling editor at the time of review.

## Publisher's note

All claims expressed in this article are solely those of the authors and do not necessarily represent those of their affiliated organizations, or those of the publisher, the editors and the reviewers. Any product that may be evaluated in this article, or claim that may be made by its manufacturer, is not guaranteed or endorsed by the publisher.

## Supplementary material

The Supplementary Material for this article can be found online at: <https://www.frontiersin.org/articles/10.3389/fnins.2022.994575/full#supplementary-material>

## References

- Almeida-Suhett, C. P., Li, Z., Marini, A. M., Braga, M. F. M., and Eiden, L. E. (2014). Temporal course of changes in gene expression suggests a cytokine-related mechanism for long-term hippocampal alteration after controlled cortical impact. *J. Neurotrauma* 31, 683–690. doi: 10.1089/neu.2013.3029
- Andersen, H. H., Duroux, M., and Gazerani, P. (2014). MicroRNAs as modulators and biomarkers of inflammatory and neuropathic pain conditions. *Neurobiol. Dis.* 71, 159–168. doi: 10.1016/j.nbd.2014.08.003
- Atzeni, F., Nucera, V., Masala, I. F., Sarzi-Puttini, P., and Bonitta, G. (2019). IL-6 Involvement in pain, fatigue and mood disorders in rheumatoid arthritis and the effects of IL-6 inhibitor sarilumab. *Pharmacol. Res.* 149:104402. doi: 10.1016/j.phrs.2019.104402
- Barratt, J., and Weitz, I. (2021). Complement factor d as a strategic target for regulating the alternative complement pathway. *Front. Immunol.* 12:712572. doi: 10.3389/fimmu.2021.712572
- Bersellini Farinotti, A., Wigerblad, G., Nascimento, D., Bas, D. B., Morado Urbina, C., Nandakumar, K. S., et al. (2019). Cartilage-binding antibodies induce pain through immune complex-mediated activation of neurons. *J. Exp. Med.* 216, 1904–1924. doi: 10.1084/jem.20181657
- Bindea, G., Mlecnik, B., Tosolini, M., Kirilovsky, A., Waldner, M., Obenauf, A. C., et al. (2013). Spatiotemporal dynamics of intratumoral immune cells reveal the immune landscape in human cancer. *Immunity* 39, 782–795. doi: 10.1016/j.immuni.2013.10.003
- Borgoni, S., Kudryashova, K. S., Burka, K., and de Magalhães, J. P. (2021). Targeting immune dysfunction in aging. *Ageing Res. Rev.* 70:101410. doi: 10.1016/j.arr.2021.101410
- Buga, A.-M., Scholz, C. J., Kumar, S., Herndon, J. G., Alexandru, D., Cojocaru, G. R., et al. (2012). Identification of new therapeutic targets by genome-wide analysis of gene expression in the ipsilateral cortex of aged rats after stroke. *PLoS One* 7:e50985. doi: 10.1371/journal.pone.0050985
- Canonica, G. W., and Rossi, O. (2012). Diagnosis and treatment of hereditary angioedema. *Panminerva Med.* 54, 241–253.
- Chen, Y.-C., Pristerá, A., Ayub, M., Swanwick, R. S., Karu, K., Hamada, Y., et al. (2013). Identification of a receptor for neuropeptide VGF and its role in neuropathic pain. *J. Biol. Chem.* 288, 34638–34646. doi: 10.1074/jbc.M113.510917
- Childs, B. G., Durik, M., Baker, D. J., and van Deursen, J. M. (2015). Cellular senescence in aging and age-related disease: From mechanisms to therapy. *Nat. Med.* 21, 1424–1435. doi: 10.1038/nm.4000
- Clement, J. M., and McDermott, D. F. (2009). The high-dose aldesleukin (IL-2) "Select" Trial: A trial designed to prospectively validate predictive models of response to high-dose IL-2 treatment in patients with metastatic renal cell carcinoma. *Clin. Genitourin. Cancer* 7, E7–E9. doi: 10.3816/CGC.2009.n.014
- Cox, A. J., Darbro, B. W., Laxer, R. M., Velez, G., Bing, X., Finer, A. L., et al. (2017). Recessive coding and regulatory mutations in FBLIM1 underlie the pathogenesis of chronic recurrent multifocal osteomyelitis (CRMO). *PLoS One* 12:e0169687. doi: 10.1371/journal.pone.0169687
- Domenichiello, A. F., and Ramsden, C. E. (2019). The silent epidemic of chronic pain in older adults. *Prog. Neuro Psychopharmacol. Biol. Psychiatry* 93, 284–290. doi: 10.1016/j.pnpb.2019.04.006
- Durante, M., Squillace, S., Lauro, F., Giancotti, L. A., Coppi, E., Cherchi, F., et al. (2021). Adenosine A3 agonists reverse neuropathic pain via T cell-mediated production of IL-10. *J. Clin. Invest.* 131:e139299. doi: 10.1172/JCI139299
- Fang, D., Fang, Y., Zhang, W., Xiang, Y., Cheng, X., Liang, M., et al. (2022). Comprehensive analysis of quantitative proteomics with dia mass spectrometry and ceRNA network in intrahepatic cholestasis of pregnancy. *Front. Cell Dev. Biol.* 10:854425. doi: 10.3389/fcell.2022.854425
- Finnerup, N. B., Kuner, R., and Jensen, T. S. (2021). Neuropathic pain: From mechanisms to treatment. *Physiol. Rev.* 101, 259–301. doi: 10.1152/physrev.00045.2019
- Finotello, F., and Trajanoski, Z. (2018). Quantifying tumor-infiltrating immune cells from transcriptomics data. *Cancer Immunol. Immunother.* CII 67, 1031–1040. doi: 10.1007/s00262-018-2150-z
- Franz, M., Rodriguez, H., Lopes, C., Zuberi, K., Montojo, J., Bader, G. D., et al. (2018). GeneMANIA update 2018. *Nucleic Acids Res.* 46, W60–W64. doi: 10.1093/nar/gky311
- Gasparoto, T. H., Dalboni, T. M., Amôr, N. G., Abe, A. E., Perri, G., Lara, V. S., et al. (2021). Fcγ receptors on aging neutrophils. *J. Appl. Oral Sci. Revista FOB* 29:e20200770. doi: 10.1590/1678-7757-2020-0770
- Gompels, M. M., and Lock, R. J. (2011). Cinryze (C1-inhibitor) for the treatment of hereditary angioedema. *Exp. Rev. Clin. Immunol.* 7, 569–573. doi: 10.1586/eci.11.50
- Hastie, T., Tibshirani, R., Narasimhan, B., and Chu, G. (2021). *Impute: Imputation for microarray data*. Available online at: <https://bioconductor.org/packages/release/bioc/html/impute.html>
- He, L., and Hannon, G. J. (2004). MicroRNAs: Small RNAs with a big role in gene regulation. *Nat. Rev. Genet.* 5, 522–531.
- Hou, Y., Dan, X., Babbar, M., Wei, Y., Hasselbalch, S. G., Croteau, D. L., et al. (2019). Ageing as a risk factor for neurodegenerative disease. *Nat. Rev. Neurol.* 15, 565–581. doi: 10.1038/s41582-019-0244-7
- Ishizuka, K., Tabata, H., Ito, H., Kushima, I., Noda, M., Yoshimi, A., et al. (2018). Possible involvement of a cell adhesion molecule, Migfilin, in brain development and pathogenesis of autism spectrum disorders. *J. Neurosci. Res.* 96, 789–802. doi: 10.1002/jnr.24194
- Jensen, T. S., Baron, R., Haanpää, M., Kalso, E., Loeser, J. D., Rice, A. S. C., et al. (2011). A new definition of neuropathic pain. *Pain* 152, 2204–2205. doi: 10.1016/j.pain.2011.06.017
- Ji, R. R., Chameissian, A., and Zhang, Y. Q. (2016). Pain regulation by non-neuronal cells and inflammation. *Science* 354, 572–577. doi: 10.1126/science.aaf8924
- Jiang, Y., Han, D., Zhao, Y., Zhang, C., Shi, X., and Gu, W. (2022). Multi-omics analysis of the prognosis and biological function for trpv channel family in clear cell renal cell carcinoma. *Front. Immunol.* 13:872170. doi: 10.3389/fimmu.2022.872170
- Karp, J. F., Shega, J. W., Morone, N. E., and Weiner, D. K. (2008). Advances in understanding the mechanisms and management of persistent pain in older adults. *Br. J. Anaesthesia* 101, 111–120. doi: 10.1093/bja/aen090
- Kavelaars, A., and Heijnen, C. J. (2021). Immune regulation of pain: Friend and foe. *Sci. Trans. Med.* 13:eabj7152. doi: 10.1126/scitranslmed.aab7152
- Kawamura, T., Tomari, H., Onoyama, I., Araki, H., Yasunaga, M., Lin, C., et al. (2021). Identification of genes associated with endometrial cell ageing. *Mol. Hum. Reprod.* 27:gaaa078. doi: 10.1093/molehr/gaaa078
- Kinser, H. A., and Pincus, Z. A. (2020). MicroRNAs as modulators of longevity and the aging process. *Hum. Genet.* 139, 291–308. doi: 10.1007/s00439-019-02046-0
- Koc, M., and Kutsal, A. (2015). Vascular aging. *Turk. J. Geriatr.* 18, 156–161.
- Kontos, C. K., Scorilas, A., and Papavassiliou, A. G. (2013). The role of transcription factors in laboratory medicine. *Clin. Chem. Lab. Med.* 51, 1563–1571. doi: 10.1515/cclm-2013-0077
- Li, H.-L., Huang, Y., Zhou, Y.-L., Teng, R.-H., Zhou, S.-Z., Lin, J.-P., et al. (2020). C-X-C motif chemokine 10 contributes to the development of neuropathic pain by increasing the permeability of the blood-spinal cord barrier. *Front. Immunol.* 11:477. doi: 10.3389/fimmu.2020.00477
- Li, Y., Huang, C., Yang, Z., Wang, L., Luo, D., Qi, L., et al. (2022). Identification of potential biomarkers of gout through competitive endogenous RNA network analysis. *Eur. J. Pharmaceut. Sci.* 173:106180. doi: 10.1016/j.ejps.2022.106180
- Liu, M., Zhang, S.-B., Luo, Y.-X., Yang, Y.-L., Zhang, X.-Z., Li, B., et al. (2020). NFATc2-dependent epigenetic upregulation of CXCL14 is involved in the development of neuropathic pain induced by paclitaxel. *J. Neuroinflamm.* 17:310. doi: 10.1186/s12974-020-01992-1
- López-Otín, C., Blasco, M. A., Partridge, L., Serrano, M., and Kroemer, G. (2013). The hallmarks of aging. *Cell* 153, 1194–1217. doi: 10.1016/j.cell.2013.05.039
- Lu, J., Chatterjee, M., Schmid, H., Beck, S., and Gawaz, M. (2016). CXCL14 as an emerging immune and inflammatory modulator. *J. Inflamm. (London, England)*. 13:1. doi: 10.1186/s12950-015-0109-9
- Miaskowski, C., Blyth, F., Nicosia, F., Haan, M., Keefe, F., Smith, A., et al. (2020). A biopsychosocial model of chronic pain for older adults. *Pain Med.* 21, 1793–1805. doi: 10.1093/pm/pnz329
- Morrison, G., Van Langenberg, D. R., Gibson, S. J., and Gibson, P. R. (2013). Chronic pain in inflammatory bowel disease: Characteristics and associations of a hospital-based cohort. *Inflamm. Bowel Dis.* 19, 1210–1217. doi: 10.1097/MIB.0b013e318280e729
- Murray-Rust, T. A., Kerr, F. K., Thomas, A. R., Wu, T., Yongqing, T., Ong, P. C., et al. (2009). Modulation of the proteolytic activity of the complement protease C1s by polyanions: Implications for polyanion-mediated acceleration of

- interaction between C1s and SERPING1. *Biochem. J.* 422, 295–303. doi: 10.1042/bj20090198
- Ovadya, Y., Landsberger, T., Leins, H., Vadai, E., Gal, H., Biran, A., et al. (2018). Impaired immune surveillance accelerates accumulation of senescent cells and aging. *Nat. Commun.* 9:5435. doi: 10.1038/s41467-018-07825-3
- Peyrin-Biroulet, L., Demarest, S., and Nirula, A. (2019). Bispecific antibodies: The next generation of targeted inflammatory bowel disease therapies. *Autoimmun. Rev.* 18, 123–128. doi: 10.1016/j.autrev.2018.07.014
- Poh, K.-W., Yeo, J.-F., Stohler, C. S., and Ong, W.-Y. (2012). Comprehensive gene expression profiling in the prefrontal cortex links immune activation and neutrophil infiltration to antinociception. *J. Neurosci.* 32, 35–45. doi: 10.1523/JNEUROSCI.2389-11.2012
- Ritchie, M. E., Phipson, B., Wu, D., Hu, Y., Law, C. W., Shi, W., et al. (2015). Limma powers differential expression analyses for RNA-sequencing and microarray studies. *Nucleic Acids Res.* 43, e47–e47. doi: 10.1093/nar/gkv007
- Saraiva, M. D., Suzuki, G. S., Lin, S. M., de Andrade, D. C., Jacob-Filho, W., and Suemoto, C. K. (2018). Persistent pain is a risk factor for frailty: A systematic review and meta-analysis from prospective longitudinal studies. *Age Ageing* 47, 785–793. doi: 10.1093/ageing/afy104
- Scholz, J., and Woolf, C. J. (2007). The neuropathic pain triad: Neurons, immune cells and glia. *Nat. Neurosci.* 10, 1361–1368.
- Shannon, P., Markiel, A., Ozier, O., Baliga, N. S., Wang, J. T., Ramage, D., et al. (2003). Cytoscape: A software environment for integrated models of biomolecular interaction networks. *Genome Res.* 13, 2498–2504. doi: 10.1101/gr.123930
- Song, P., Liu, X. Y., and Zhao, Z. Q. (2002). Interleukin-2-induced antinociception in morphine-insensitive rats. *Acta Pharmacol. Sin.* 23, 981–984.
- Strong, J. A., Xie, W., Coyle, D. E., and Zhang, J.-M. (2012). Microarray analysis of rat sensory ganglia after local inflammation implicates novel cytokines in pain. *PLoS One* 7:e40779. doi: 10.1371/journal.pone.0040779
- Su, K. H., Wu, J. M., Edberg, J. C., Li, X. L., Ferguson, P., Cooper, G. S., et al. (2004). A promoter haplotype of the immunoreceptor tyrosine-based inhibitory motif-bearing Fc gamma RIIb alters receptor expression and associates with autoimmunity. I. Regulatory FCGR2B polymorphisms and their association with systemic lupus erythematosus. *J. Immunol.* 172, 7186–7191. doi: 10.4049/jimmunol.172.11.7186
- Subramanian, A., Tamayo, P., Mootha, V. K., Mukherjee, S., Ebert, B. L., Gillette, M. A., et al. (2005). Gene set enrichment analysis: A knowledge-based approach for interpreting genome-wide expression profiles. *Proc. Natl. Acad. Sci. U.S.A.* 102, 15545–15550.
- Tian, Y., Bai, F., and Zhang, D. (2022). HIF1: A novel biomarker with potential prognostic and immunotherapy in pan-cancer. *Oxi. Med. Cell. Longev.* 2022:1246267. doi: 10.1155/2022/1246267
- van Hecke, O., Austin, S. K., Khan, R. A., Smith, B. H., and Torrance, N. (2014). Neuropathic pain in the general population: A systematic review of epidemiological studies. *Pain* 155, 654–662. doi: 10.1016/j.pain.2013.11.013
- Vestberg, M., Brunsberg, U., Bergsteinsdottir, K., Karlsson, M., Gustafsson, K., Wedekind, D., et al. (1998). Limited polymorphism in the first domain of the rat MHC class II RT1-D molecule. *Immunogenetics* 48, 344–349. doi: 10.1007/s002510050442
- von Schack, D., Agostino, M. J., Murray, B. S., Li, Y., Reddy, P. S., Chen, J., et al. (2011). Dynamic changes in the microRNA expression profile reveal multiple regulatory mechanisms in the spinal nerve ligation model of neuropathic pain. *PLoS One* 6:e17670. doi: 10.1371/journal.pone.0017670
- Waldemer-Streyer, R. J., Reyes-Ordoñez, A., Kim, D., Zhang, R., Singh, N., and Chen, J. (2017). Cxcl14 depletion accelerates skeletal myogenesis by promoting cell cycle withdrawal. *NPJ Regen. Med.* 2:16017. doi: 10.1038/npjregenmed.2016.17
- Warde-Farley, D., Donaldson, S. L., Comes, O., Zuberi, K., Badrawi, R., Chao, P., et al. (2010). The GeneMANIA prediction server: Biological network integration for gene prioritization and predicting gene function. *Nucleic Acids Res.* 38, W214–W220. doi: 10.1093/nar/gkq537
- Wickham, H. (2016). *ggplot2: Elegant graphics for data analysis*. New York, NY: Springer-Verlag.
- Wiles, J. A., Galvan, M. D., Podos, S. D., Geffner, M., and Huang, M. (2020). Discovery and development of the oral complement factor d inhibitor danicopan (ACH-4471). *Curr. Med. Chem.* 27, 4165–4180. doi: 10.2174/0929867326666191001130342
- Wu, C., Orozco, C., Boyer, J., Leglise, M., Goodale, J., Batalov, S., et al. (2009). BioGPS: An extensible and customizable portal for querying and organizing gene annotation resources. *Genome Biol.* 10:R130. doi: 10.1186/gb-2009-10-11-r130
- Wu, T., Hu, E., Xu, S., Chen, M., Guo, P., Dai, Z., et al. (2021). clusterProfiler 4.0: A universal enrichment tool for interpreting omics data. *Innovation* 2:100141. doi: 10.1016/j.xinn.2021.100141
- Wu, Z., Isik, M., Moroz, N., Steinbaugh, M. J., Zhang, P., and Blackwell, T. K. (2019). Dietary restriction extends lifespan through metabolic regulation of innate immunity. *Cell Metabol.* 29, 1192.e–1205.e. doi: 10.1016/j.cmet.2019.02.013
- Xing, X., Xia, Q., Gong, B., Shen, Z., and Zhang, Y. (2022). Identification of tissue-specific expressed hub genes and potential drugs in rheumatoid arthritis using bioinformatics analysis. *Front. Genet.* 13:855557. doi: 10.3389/fgene.2022.855557
- Yamamoto, T., Sasaguri, K., Mizumoto, N., and Suzuki, H. (2020). The Chemokine CXCL14-like Immunoreactivity Co-exists with Somatostatin, but not NPY in the rat dorsal horn and has intimate association with GABAergic neurons in the lateral spinal nucleus. *Acta Histochemica Cytochemica* 53, 121–129. doi: 10.1267/ahc.20-00004
- Zhang, B., Wu, Q., Li, B., Wang, D., Wang, L., and Zhou, Y. L. (2020a). mA regulator-mediated methylation modification patterns and tumor microenvironment infiltration characterization in gastric cancer. *Mol. Cancer* 19:53. doi: 10.1186/s12943-020-01170-0
- Zhang, J., Czerpaniak, K., Huang, L., Liu, X., Cloud, M. E., Unsinger, J., et al. (2020b). Low-dose interleukin-2 reverses behavioral sensitization in multiple mouse models of headache disorders. *Pain* 161, 1381–1398. doi: 10.1097/j.pain.0000000000001818
- Zhang, Y., and Chi, D. (2018). Overexpression of SIRT2 alleviates neuropathic pain and neuroinflammation through deacetylation of transcription factor nuclear factor-kappa B. *Inflammation* 41, 569–578. doi: 10.1007/s10753-017-0713-3
- Zhang, Y., Jiang, S., Liao, F., Huang, Z., Yang, X., Zou, Y., et al. (2022). A transcriptomic analysis of neuropathic pain in the anterior cingulate cortex after nerve injury. *Bioengineered* 13, 2058–2075. doi: 10.1080/21655979.2021.2021710
- Zuercher, A. W., Spirig, R., Baz Morelli, A., Rowe, T., and Kasermann, F. (2019). Next-generation Fc receptor-targeting biologics for autoimmune diseases. *Autoimmun. Rev.* 18:102366. doi: 10.1016/j.autrev.2019.102366





## OPEN ACCESS

## EDITED BY

Subashika Govindan,  
DBT/Wellcome Trust India Alliance, India

## REVIEWED BY

Ricardo Scott,  
University of Alicante, Spain  
Dries Meijer,  
The University of Edinburgh, United Kingdom

## \*CORRESPONDENCE

Laurence Goutebroze  
✉ laurence.goutebroze@inserm.fr

## †PRESENT ADDRESS

Mélanie Druart,  
Department of Psychiatry,  
Physiology and Neuroscience, New York  
University Grossman School of Medicine,  
New York, NY, United States

‡These authors have contributed equally to this work

## SPECIALTY SECTION

This article was submitted to  
Translational Neuroscience,  
a section of the journal  
Frontiers in Neuroscience

RECEIVED 16 November 2022

ACCEPTED 09 January 2023

PUBLISHED 30 January 2023

## CITATION

Cifuentes-Diaz C, Canali G, Garcia M, Druart M,  
Manett T, Savariradjane M, Guillaume C,  
Le Magueresse C and Goutebroze L (2023)  
Differential impacts of *Cntnap2* heterozygosity  
and *Cntnap2* null homozygosity on axon  
and myelinated fiber development in mouse.  
*Front. Neurosci.* 17:1100121.  
doi: 10.3389/fnins.2023.1100121

## COPYRIGHT

© 2023 Cifuentes-Diaz, Canali, Garcia, Druart,  
Manett, Savariradjane, Guillaume, Le  
Magueresse and Goutebroze. This is an  
open-access article distributed under the terms  
of the [Creative Commons Attribution License](https://creativecommons.org/licenses/by/4.0/)  
(CC BY). The use, distribution or reproduction in  
other forums is permitted, provided the original  
author(s) and the copyright owner(s) are  
credited and that the original publication in this  
journal is cited, in accordance with accepted  
academic practice. No use, distribution or  
reproduction is permitted which does not  
comply with these terms.

# Differential impacts of *Cntnap2* heterozygosity and *Cntnap2* null homozygosity on axon and myelinated fiber development in mouse

Carmen Cifuentes-Diaz<sup>1,2,3†</sup>, Giorgia Canali<sup>1,2,3†</sup>, Marta Garcia<sup>1,2,3</sup>,  
Mélanie Druart<sup>1,2,3†</sup>, Taylor Manett<sup>1,2,3</sup>, Mythili Savariradjane<sup>1,2,3</sup>,  
Camille Guillaume<sup>1,2,3</sup>, Corentin Le Magueresse<sup>1,2,3</sup> and  
Laurence Goutebroze<sup>1,2,3\*</sup>

<sup>1</sup>Inserm, Unité Mixte de Recherche (UMR)-S 1270, Paris, France, <sup>2</sup>Faculté des Sciences et Ingénierie, Sorbonne University, Paris, France, <sup>3</sup>Institut du Fer à Moulin, Paris, France

Over the last decade, a large variety of alterations of the *Contactin Associated Protein 2 (CNTNAP2)* gene, encoding Caspr2, have been identified in several neuronal disorders, including neurodevelopmental disorders and peripheral neuropathies. Some of these alterations are homozygous but most are heterozygous, and one of the current challenges is to estimate to what extent they could affect the functions of Caspr2 and contribute to the development of these pathologies. Notably, it is not known whether the disruption of a single *CNTNAP2* allele could be sufficient to perturb the functions of Caspr2. To get insights into this issue, we questioned whether *Cntnap2* heterozygosity and *Cntnap2* null homozygosity in mice could both impact, either similarly or differentially, some specific functions of Caspr2 during development and in adulthood. We focused on yet poorly explored functions of Caspr2 in axon development and myelination, and performed a morphological study from embryonic day E17.5 to adulthood of two major brain interhemispheric myelinated tracts, the anterior commissure (AC) and the corpus callosum (CC), comparing wild-type (WT), *Cntnap2*<sup>-/-</sup> and *Cntnap2*<sup>+/-</sup> mice. We also looked for myelinated fiber abnormalities in the sciatic nerves of mutant mice. Our work revealed that Caspr2 controls the morphology of the CC and AC throughout development, axon diameter at early developmental stages, cortical neuron intrinsic excitability at the onset of myelination, and axon diameter and myelin thickness at later developmental stages. Changes in axon diameter, myelin thickness and node of Ranvier morphology were also detected in the sciatic nerves of the mutant mice. Importantly, most of the parameters analyzed were affected in *Cntnap2*<sup>+/-</sup> mice, either specifically, more severely, or oppositely as compared to *Cntnap2*<sup>-/-</sup> mice. In addition, *Cntnap2*<sup>+/-</sup> mice, but not *Cntnap2*<sup>-/-</sup> mice, showed motor/coordination deficits in the grid-walking test. Thus, our observations show that both *Cntnap2* heterozygosity and *Cntnap2* null homozygosity impact axon and central and

peripheral myelinated fiber development, but in a differential manner. This is a first step indicating that *CNTNAP2* alterations could lead to a multiplicity of phenotypes in humans, and raising the need to evaluate the impact of *Cntnap2* heterozygosity on the other neurodevelopmental functions of Caspr2.

#### KEYWORDS

Caspr2, corpus callosum, anterior commissure, sciatic nerve, axon diameter, myelin thickness, node of Ranvier, neuronal activity

## Introduction

The *Contactin Associated Protein 2* gene (*CNTNAP2*), encoding the neuronal cell-adhesion transmembrane glycoprotein Caspr2, has gained prominence over the last decade in the field of neurological disabilities. A duplication of exon 4 of *CNTNAP2* was identified in two sisters suffering from Charcot-Marie-Tooth type 2, a peripheral motor and sensory neuropathy (Hoyer et al., 2015). Additionally, an increasing number of *CNTNAP2* alterations have been reported in patients with various neurodevelopmental disorders, including autism spectrum disorders (ASD), schizophrenia, intellectual disability, obsessive compulsive disorder, Pitt-Hopkins-like syndrome, attention deficit hyperactivity disorder, Gilles de la Tourette syndrome and cortical dysplasia focal epilepsy (Rodenas-Cuadrado et al., 2014; Poot, 2015, 2017; Saint-Martin et al., 2018). The genetic alterations identified in these disorders comprise a large diversity ranging from complex genomic rearrangements, homozygous and compound-heterozygous deletions and mutations, homozygous truncating non-sense mutations or deletions, and a large number of heterozygous missense variants found mainly in ASD patients. Currently, one of the major challenges is to estimate to what extent *CNTNAP2* alterations could affect the molecular and cellular functions of Caspr2, and therefore contribute to the development of the pathologies.

Caspr2 was initially identified as a component of the juxtaparanodal domains (juxtaparanodes) of the nodes of Ranvier in mature myelinated neurons, both in the central (CNS) and peripheral (PNS) nervous system (Poliak et al., 1999). Within the juxtaparanodes, Caspr2 is involved in the organization of specific axo-glial contacts, forming complexes with the cell-adhesion molecule Contactin2/TAG-1. These complexes are required for the clustering of the *Shaker*-type Kv1 (Kv1.1 and Kv1.2) channels (Poliak et al., 2003; Traka et al., 2003; Scott et al., 2017). Since Caspr2's identification, several studies conducted in *Cntnap2*<sup>-/-</sup> (KO) mice revealed that Caspr2 also plays critical roles in contributing to neuronal network formation during brain development, notably in neuronal migration (Penagarikano et al., 2011), dendritic arborization (Anderson et al., 2012; Gao et al., 2018), spine formation and maintenance (Gdalyahu et al., 2015; Varea et al., 2015; Lazaro et al., 2019), and synapse development and function (Anderson et al., 2012; Pinatel et al., 2015; Varea et al., 2015; Fernandes et al., 2019; Gao et al., 2019). Electrophysiological and imaging approaches further demonstrated that Caspr2 contributes to local and long-range brain connectivity (Penagarikano et al., 2011; Scott et al., 2017; Liska et al., 2018; Vogt et al., 2018; Zerbi et al., 2018; Antoine et al., 2019). Moreover, behavioral studies showed deficits in KO mice, some of which replicate clinical ASD phenotypes and are rescued by normalizing altered circuit connectivity (Penagarikano et al., 2011;

Brunner et al., 2015; Scott et al., 2017; Choe et al., 2022). These data revealed mechanisms through which some *CNTNAP2* alterations may contribute to the development of neurological pathologies in humans.

However, studies in KO mice do not accurately replicate the genetic situations in patients and are not sufficient to fully explore the potential impact of the multiple *CNTNAP2* alterations identified thus far. Most of the genetic alterations are heterozygous and it is currently not known whether disruption of a single *CNTNAP2* allele could be sufficient to perturb the functions of Caspr2. Our recent observations indicate that some Caspr2 functions could be modulated by the level of the protein and affected by some ASD missense variants in a *Cntnap2*<sup>+/-</sup> (HET) background (Canali et al., 2018). We showed that Caspr2 plays a dose-dependent function in cortical neuron axon growth *in vitro*, and that certain variants impinge Caspr2 cell adhesive properties and display loss of function, while others lead to protein retention in the endoplasmic reticulum and display a dominant-negative effect through oligomerization with wild-type (WT) Caspr2. Vogt et al. (2018) also found that HET fast-spiking PV<sup>+</sup> cortical interneurons exhibit an intermediate electrophysiological phenotype between WT and KO interneurons. Nevertheless, whether or not the level of Caspr2 could more broadly modulate its functions remains to be determined.

In this study, we addressed this question, focusing on poorly explored functions of Caspr2 in axon development and myelination *in vivo*, whose disturbances could contribute to the development of both peripheral and central neurological disabilities. We performed a morphological study from embryonic day E17.5 to adulthood of two major brain interhemispheric myelinated tracts, the anterior commissure (AC) and the corpus callosum (CC), comparing WT, *Cntnap2* HET and KO mice. We also characterized myelinated fiber abnormalities in the sciatic nerves of mutant mice. Overall, our observations indicate that the level of Caspr2 modulates the development and organization of myelinated fibers both in the CNS and in the PNS.

## Materials and methods

### Animals

*Contactin Associated Protein 2* (*Cntnap2*) mutant mice, previously described (Poliak et al., 2003), were obtained from the Jackson Laboratory and maintained in a C57BL/6J background. They were group-housed with *ad libitum* access to food and water and a 12–12 h light–dark cycle (light phase onset at 7 a.m.). For staging of embryos, the day of vaginal plug was considered E0.5.



## Tissue processing

For brain morphology analyses, E17.5 embryos were rapidly decapitated. Pups (P2, P7), juvenile (P30), and adult (P90) mice were deeply anesthetized by intraperitoneal injection of ketamine (100 mg/kg) and xylazine (10 mg/kg) and transcardially perfused with 4% paraformaldehyde (PFA) in 0.12 M phosphate buffer pH 7.4. Brains were fixed (embryos) or post-fixed (P2, P7, P30, P90) overnight (O/N) at 4°C in 4% PFA. Embryonic, P2 and P7 brains were washed in sodium phosphate buffered saline (PBS), embedded in 75 g/l gelatin and 100 g/l sucrose in PBS or in 15 g/l agarose and 20 g/l sucrose in PBS, and serial coronal (E17.5, P2, P7, 60 µm-thick) and sagittal (E17.5, 60 µm-thick; P7, 45 µm-thick) sections were obtained using a vibratome (Leica, France). Thirty-five µm-thick serial sagittal sections of P30 and P90 brains embedded in 35 g/l agarose and 80 g/l sucrose in PBS were obtained similarly. Forty µm-thick serial coronal sections of P30 and P90 brains and 500 µm-thick horizontal sections of P90 brains were performed without inclusion. All floating sections were conserved at 4°C in PBS with 1 g/l sodium azide until use.

For sciatic nerve immunostainings, 2-month-old mice were perfused as described above, sciatic nerves were dissected, fibers were teased apart on slides to yield single fiber preparations, air-dried and kept at −20°C.

## Immunostainings

For morphological analysis of the CC and AC, brain sections of E17.5, P2 and P7 animals were incubated in a permeabilization/saturation solution (PS1: PBS, 5 ml/l Triton X-100, 100 ml/l normal goat serum) for 1 h at room temperature (RT) and then O/N at 4°C (72 h for P7) with the anti-L1CAM antibody (Millipore, rat clone 324, #MAB5272, 1:400) diluted in PS1. Sections were then washed three times for 10 min in PBS/5 ml/l Triton X-100 (WS1) and incubated for 2 h at RT with adequate fluorophore-conjugated-secondary antibodies (Molecular Probes, Invitrogen, Waltham, MA, USA) diluted in PS1. For brain sections of P30 and P90 animals, permeabilization and saturation were performed in PBS supplemented with 2 g/l porcine skin gelatin and 2.5 ml/l Triton X-100 (PS2 solution), before incubation O/N at 4°C with the anti-NF-M antibody (Sigma, mouse clone NN18, #N5264, 1:300) diluted in PS2. The following day, sections were washed three times for 10 min in PBS/2.5 ml/l Triton X-100 (WS2) and incubated for 2 h at RT with secondary antibodies diluted in PS2. For all ages, after secondary antibody incubation, sections were washed three times for 10 min in WS1 (E17.5, P2, P7) or WS2 (P30, P90), and nuclei were stained for 10 min with Hoechst before mounting with Fluoromount-G medium (Invitrogen, Waltham, MA, USA). For neuron counting in the cortex, E17.5 sections were incubated with the anti-L1CAM antibody (1:750) together with the anti-Satb2 (Abcam, Cambridge, UK, mouse clone SATBA4B10, #ab51502, 1:750) and the anti-Ctip2 (Abcam, Cambridge, UK, rabbit #ab28448, 1:500) antibodies diluted in PS1.

Immunofluorescent staining of sciatic nerves was performed as described previously (Martin et al., 2017). Briefly, slides were treated with 0.1 M glycine for 30 min at RT or with methanol 50%/acetone 50% for 20 min at −20°C, pre-incubated for 1 h at room temperature in PS2, before incubation with primary antibodies diluted in PS2 overnight at 4°C ( $K_v1.2$   $\alpha$  subunit, mouse clone

K67/25 #75-075, NeuroMab, 1:400; F3, goat #AF904, R&D Systems, 1:400; NrCAM, rabbit #ab24344, Abcam, Cambridge, UK, 1:300; TAG-1, goat #AF4439, R&D Systems, 1:500; Caspr (L51, 1:500) and Caspr2 (191, 1:400) previously described) (Menegoz et al., 1997; Denisenko-Nehrbass et al., 2003). After washing with PBS, coverslips were incubated for 2 h at room temperature with secondary antibodies diluted in PS2, washed again with PBS, and mounted with Fluoromount-G medium.

## Image acquisition and analysis

Images of immunostained brain sections or phase-contrast images were acquired using a macroscope MVX10 (Olympus, Tokyo, Japan). Thickness and area measurements were performed using the ImageJ software, for six mice/genotype/condition, except for AC area at E17.5 (four embryos/genotype). CC and cortex thicknesses were measured on one coronal section per brain per animal for E17.5 and P2 stages and three consecutive sections per animal for P90. Measurements were performed independently on both hemispheres and averaged; the measures were further averaged between the three consecutive sections for P90. Anterior branch (ACa) thickness at P90 was measured independently on both hemispheres on one horizontal section per brain per animal, and averaged. Measurements of CC and AC areas were performed on three consecutive sagittal sections per animal at all ages, and averaged.

For quantification of Satb2- or Ctip2-positive neurons at E17.5, images were acquired using a Leica SP5 confocal laser-scanning microscope (Leica microsystems, Wetzlar, Germany, Z stack 1 µm, 25 stacks, 40× immersion objective) at the level of the somatosensory cortex of both hemispheres for two successive medial coronal sections per animal ( $n = 4$  animals/genotype). The density of Satb2- or Ctip2-positive neurons was estimated using the Imaris software (Bitplane, Zurich, CH). To do so, images were cropped to exclude the region corresponding to the intermediate zone and the subplate layer, using L1CAM immunostaining to delineate these regions. The average volume of Satb2- and Ctip2-positive nuclei was calculated by averaging the volumes of 15 isolated nuclei. Masks were built to obtain the total volumes occupied by Satb2- and Ctip2-positive nuclei, respectively, excluding objects with a volume lower than the smallest volume out of the 15 used for averaging. The density of Satb2- or Ctip2-positive neurons was then calculated by dividing these total volumes by the average nucleus volume (Hoechst staining).

Images of stained sciatic nerve fibers were acquired using a Zeiss Celldiscoverer 7 imaging system for quantification analyzes, and a STELLARIS 5 confocal laser-scanning microscope (Leica Microsystems, Wetzlar, Germany) to acquire representative images. Measurements of node length and node axonal diameter were performed manually on NrCAM stainings using the ImageJ software (3 mice/genotype, 81 nodes/mouse).

## Electron microscopy

For ultrastructural studies of the CC and the AC, P7 animals (3 pups/genotype) were deeply anesthetized by intraperitoneal injection of ketamine (100 mg/kg) and xylazine (10 mg/kg), and transcardially perfused with 4% PFA (EMS) and 2.5% glutaraldehyde

(Microm Microtech, G003) in phosphate buffer 0.1 M pH 7.4. Brains were removed and post-fixed in the same fixative solution O/N at 4°C. P30 animals (3 mice/genotype) were anesthetized as above and transcardially perfused with 3% glutaraldehyde in Millonig's phosphate buffer 0.1 M pH 7.4. Brains were removed and immediately processed. For the two ages, 1 mm-thick brain sagittal sections were produced and post-fixed for 1 h at 4°C in fresh fixative solution, washed once with phosphate buffer 0.1 M pH 7.4 (P7) or Millonig's phosphate buffer 0.1 M (P30), and three times for 10 min with Palade buffer. Samples were then incubated in 2% osmium tetroxide in Palade buffer for 1 h at RT, rinsed in Palade buffer for 3 min and three times for 3 min in distilled water, dehydrated in a series of ethanol baths, and flat embedded in epoxy resin (EPON 812, Polysciences). After polymerization, 0.5 µm-thick semi-thin sections stained with toluidine blue to locate the CC and the AC. Then, blocks containing the CC and the AC were cut in 50 nm-thick ultrathin sections using an ultramicrotome (Ultracut E, Leica). Sections were examined with a Philips CM100 electron microscope and digital images acquired with a CCD camera (Gatan Orius). Diameters were calculated from areas measured manually using the Image J software (P7, ACa/ACp 300 axons/pup, CC 360 axons/pup; P30, ACa/ACp 147 myelinated fibers/mouse, CC 150 myelinated fibers/mouse). The percentage of myelinated fibers was determined by counting the numbers of unmyelinated and myelinated axons on 18 photos at magnification 9700×. The percentage of myelinated axons containing mitochondria was measured on six photos at magnification 2500×.

For ultrastructural analyses of peripheral myelinated fibers, the sciatic nerves were fixed *in situ* for ~1 min with 3% glutaraldehyde in Millonig's phosphate buffer 0.1 M pH 7.4, dissected out, placed in fixative O/N at 4°C, rinsed in PB, post-fixed in 2% osmium tetroxide in PB, dehydrated in an ascending series of ethanol, and embedded in epoxy resin. The global morphology of the nerves was evaluated on 0.5 µm-thick semi-thin transversal sections stained with toluidine blue and visualized with a DM6000 Leica microscope. Morphometric analyzes were performed on ultra-thin sections (50 nm) and examined as above (4 mice/genotype, 47 myelinated fibers/mouse).

## Brain lysate preparation and immunoblotting

To analyze protein levels, brains (six mice/genotype/age) were lysed in RIPA buffer containing proteases inhibitors and immunoblotting was performed as previously described (Canali et al., 2018). Briefly, equal amounts of proteins (40 µg) were loaded on NuPAGE 8–12% Bis-Tris gels (Thermo Fisher Scientific, Waltham, MA, USA) and transferred to 0.45 µm Nitrocellulose membranes. Membranes were blocked with 50 g/l non-fat dry milk in Tris-Buffered Saline solution/0.1 ml/l Tween 20 for 1 h at RT, incubated with primary antibodies in the same solution for 2 h at RT or O/N at 4°C, 1 h at RT with appropriate IRDye-conjugated secondary antibodies, and imaged and quantified using Odyssey Imaging System (LiCOR Biosciences, Lincoln, NE, USA). The commercial antibodies were from the following sources: anti-MBP, Serotec, rat clone 82–87, #MCA409S, 1:250; anti-PLP, Novus Biochemicals, rabbit, #NBP1-87781, 1:1000; anti-MAG, Zymed, rabbit, #34–6200, 1:1000; anti-GAPDH, Millipore, chicken, #AB2302, 1:5000. The anti-TAG-1

antibody has been described previously (Traka et al., 2003). The anti-Caspr2 was the same as the one used for immunostainings.

## RT-qPCR experiments

For mRNA expression analysis, total mRNA was extracted from brains (six mice/genotype/age) using the TRIzol™ Reagent (Invitrogen, Waltham, MA, USA) following the manufacturer's recommendations. Reverse transcription was performed with the SuperScript II reverse transcriptase (Invitrogen, Waltham, MA, USA, #18064-022) and random primers, and qPCR in a Stratagene™ Mx3005P qPCR instrument (Agilent Technologies, Santa Clara, CA, USA) using the Brilliant II SYBR® Green QPCR Master Mix (Agilent Technologies, Santa Clara, CA, USA, #600828). The MxPro QPCR Software (Agilent Technologies, Santa Clara, CA, USA) was used to perform expression analyses. The expression level of *Cntnap2* mRNA was normalized to *Psap* mRNA level. Primers for *Cntnap2* were designed on two 5' exons: primer sense 5'CAGCGCTCTCGCTCTGGATT (accession number NM\_001004357, nucleotides 261–280), primer anti-sense 5'CCCCAGCACCTCCTCGTTTATT (nucleotides 425–446), amplified DNA fragment 186 bp. Primers for *Psap* were the following: primer sense 5'CTGGTGTGAGAACATGGAGACTG (accession number NM\_001146120, nucleotides 1708–1730), primer anti-sense 5'TGACTTCTGCAGCTGGGAAA (nucleotides 1781–1800), amplified DNA fragment 93 bp.

## Electrophysiology

### Acute slice preparation

A total of 250 µm-thick coronal slices of the somatosensory cortex were prepared from brains of KO, HET, and WT littermates aged P10–P12. Acute coronal slices were cut using a vibroslicer (HM 650 V, Microm) in ice-cold artificial cerebrospinal fluid (ACSF) containing the following (in mM): 125 NaCl, 2.5 KCl, 25 glucose, 25 NaHCO<sub>3</sub>, 1.25 NaH<sub>2</sub>PO<sub>4</sub>, 2 CaCl<sub>2</sub>, and 1 MgCl<sub>2</sub>, continuously bubbled with 95% O<sub>2</sub>–5% CO<sub>2</sub>. Slices were incubated in ACSF at 32°C for 20 min and then at room temperature (20–25°C). For patch-clamp recordings, slices were transferred to the recording chamber where they were continuously superfused with ACSF (30–32°C).

### Patch-clamp

Patch-clamp pipettes (4–6 Mohm resistance) were prepared from borosilicate glass (BF150-86-10; Harvard Apparatus, Holliston, MA, USA) using a DMZ pipette puller (Zeitz). Patch-clamp recordings were performed using an EPC-10 amplifier (HEKA Elektronik GmbH, Reutlingen, Germany) with the following intracellular solution (in mM): 105 K-gluconate, 10 HEPES, 10 phosphocreatine-Na, 4 ATP-Na<sub>2</sub>, 30 KCl (pH 7.25, adjusted with KOH). Intrinsic excitability was measured in current-clamp using depolarizing current steps of increasing amplitude (0–500 pA, 500 ms) at an interstimulus interval of 6 s, from a cell potential set to –70 mV, in the presence of SR95531 hydrobromide (Gabazine, 10 µm, Hello Bio) to block GABA<sub>A</sub> receptor-mediated synaptic transmission, 6-cyano-7-nitroquinoxaline-2,3-dione (CNQX, 10 µm, Biotrend, Köln, Germany) to block AMPA receptor-mediated synaptic transmission and D-2-amino-5-phosphonopentanoic acid (D-APV, 50 µm, Hello Bio) to block NMDA receptor-mediated synaptic transmission.

## Data acquisition and analysis

Stimulus delivery and data acquisition were performed using the Patchmaster software (HEKA Elektronik GmbH, Reutlingen, Germany). The junction potential ( $-5$  mV) was left uncorrected. Signals were sampled at 20 kHz and filtered at 4 kHz. Offline analysis was performed using Igor Pro (WaveMetrics).

## Grid-walking test

Coordination between forelimbs and hind limbs and accurate limb placement were examined by assessing the ability to walk on metal grid bars with 1.5 cm gaps on the bottom of a  $30 \times 20 \times 20$  cm box (8–9 6-month-old males/genotype). The performance of each animal was analyzed by counting and averaging the number of errors in foot placement/total number of steps, during 2-min sessions, once a day, for three consecutive days. On the day before data collection, each mouse was allowed to walk on the grid for 2 min.

## Statistical analysis

Statistical analyses were performed with the GraphPad Prism 9 Software (GraphPad Software, San Diego, CA, USA). Results are provided as mean  $\pm$  SEM or median  $\pm$  quartile (Violin plot, medium smoothing). The normality of the samples was tested using the Shapiro–Wilk test. When the variables followed a normal distribution, statistical analyses were carried out using the unpaired *t*-test to compare 2 genotypes and the one-way ANOVA test to compare the three genotypes, followed by a Tukey's multiple comparisons test. When the variables did not follow a normal distribution, the Mann–Whitney test was used to compare two genotypes and the Kruskal–Wallis test to compare the three genotypes, followed by a Dunn's multiple comparisons test. The thicknesses of the CC measured on coronal section and the firings of cortical neurons were compared between genotypes using Two-way RM ANOVA tests, followed by a Tukey's multiple comparisons test or a Sidak *post-hoc* test. Statistical analyses to compare the distributions of two quantitative variables were carried out using the Kolmogorov–Smirnov test. Linear regression analyzes were performed after checking the correlations between the variables (Pearson coefficient). The significance was established at a *P*-value  $< 0.05$ .

## Results

### Caspr2 level modulates CC morphology during development

The CC is the most prominent white matter structure in the brain, formed by  $\sim 80\%$  of axons coming from neocortical neurons in layers II/III and  $\sim 20\%$  of axons coming from cortical neurons in layer V (Ku and Torii, 2020). A potential implication of Caspr2 in the development of this tract was suggested by our previous *in vitro* study showing a role for Caspr2 in axon growth of embryonic neocortical neurons (Canali et al., 2018). The morphology of the CC was first examined in WT, HET and KO mice at postnatal day P90 on brain coronal sections selected at Bregma +1.1, +0.55, and 0, and on mid-brain sagittal sections. Brain slices were immunostained with

antibodies directed against the neurofilament subunit NF-M, which is expressed in commissural axons at late stages of development. From this point onward in the manuscript, the analyses were performed by comparing the three genotypes to investigate dose-dependent effects, but also by comparing HET and KO mice individually to WT mice to reveal potential effects of *Cntnap2* heterozygosity and/or null homozygosity, which would not be revealed by three-genotype comparisons. Main statistical results were reported on figures in black for three-genotype comparisons, and in color for individual comparisons to WT conditions when the difference was significant (HET, orange; KO, blue; all statistical analyses reported in **Supplementary Table 1**). When measuring the thickness of the CC in different positions from the brain midline to the lateral parts of coronal brain sections (**Figure 1B**, inset), we did not detect significant differences when comparing the three genotypes at the three Bregma levels, but a significant decrease in KO mice as compared to WT mice when comparing the two at Bregma + 0.50 (**Figures 1A, B**; data not shown for brain sections at Bregma +1.1 and 0). Decreased thickness was particularly pronounced at the midline of the brain (**Figure 1C**). Immunostainings of mid-sagittal sections consistently showed a decrease of CC area in KO mice as compared to WT and HET mice, as well as a decreased minimum caliper as compared to WT mice (**Figures 1D–G**). In HET mice, none of the morphometric parameters were significantly different from those in WT mice.

Decreased CC thickness and area in adult KO mice were likely not due to a major decrease in the number of axons forming this tract since a previous study showed a normal distribution of the neocortical neurons projecting their axon through the CC in these mice (Scott et al., 2017). We attempted to find the temporal origin of the phenotype by characterizing the morphology of the CC through development. In mice, E15 pioneering axons from the cingulate cortex are the first axons forming the CC to reach the midline, followed later by neocortical projections at around E17.5 (Suarez et al., 2014). The formation of the CC continues after birth, until some axons begin to be myelinated by oligodendrocytes (OLs) (Suarez et al., 2014). The first myelinated sheaths are observable at P11 and a rapid phase of myelination occurs between P14 and P45 (Sturrock, 1980). We characterized CC morphology at P30 when myelination is ongoing, at P7 before the onset of myelination, at an early stage of axon development (E17.5), and at an intermediate developmental stage (P2). Morphometric analyzes were performed on mid-sagittal sections at P30 and P7, and on coronal sections at P2 and E17.5 because the structure of the CC at these stages did not allow measuring its area with confidence on sagittal sections. At P7, P2, and E17.5, brain sections were immunostained with antibodies directed against the cell-adhesion molecule L1CAM, which is widely expressed in commissural axons at embryonic and early post-natal developmental stages. The observations at P30 were comparable to those at P90, with a decrease in CC area and minimum and maximum calipers in KO mice as compared to WT (**Figure 2A**). In contrast, no difference was observed between the three genotypes either at P7 (**Figure 2B**) or at P2 (**Figures 2C–E**). Moreover, the thickness of the CC was remarkably increased in both HET and KO embryos at E17.5 as compared to WT embryos, with no significant difference between HET and KO embryos (**Figures 2F, G**). CC thickness at the brain midline was significantly increased in HET embryos as compared to WT embryos (**Figure 2H**). This increase was likely not due to an increased number of axons, since neither the thickness of the cortex nor the



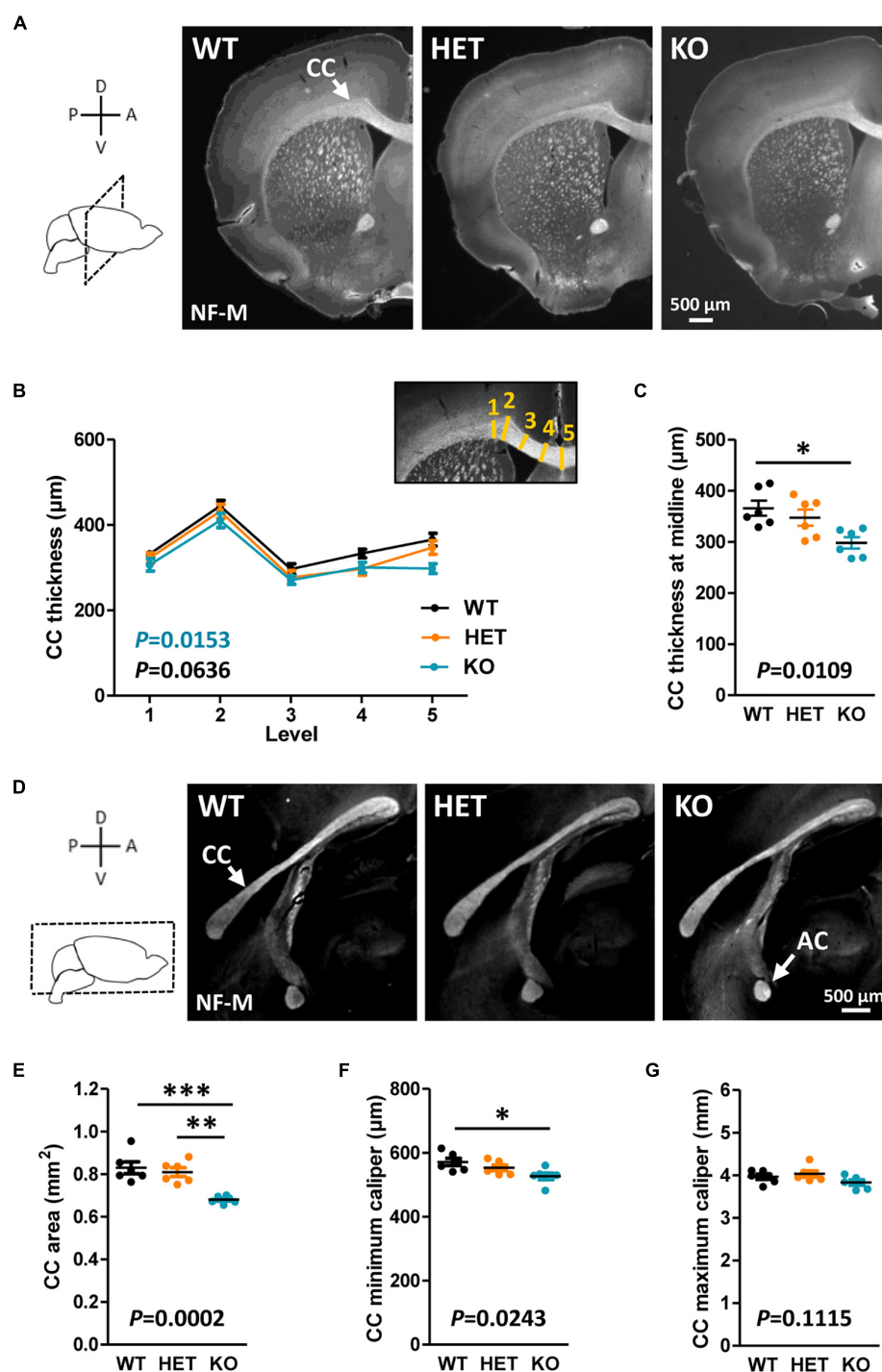


FIGURE 1

Corpus callosum (CC) morphology in adult mice. Representative images of brain coronal sections (Bregma + 0.50) of wild-type (WT), HET, and KO P90 mice showing CC immunostained with anti-NF-M antibodies (A). CC thickness measured at different levels on coronal sections (B); inset, schematic representation of the levels (yellow lines) where CC thickness measurements were performed. CC thickness at the midline of the brains (C). Representative images of mid-sagittal brain sections of WT, HET, and KO P90 mice, showing the CC and the AC immunostained with anti-NF-M antibodies (D). CC area (E), minimum caliper (F), and maximum caliper (G) measured on mid-sagittal brain sections. (B,C,E–G) Six animals/genotype, (B) average of measurements on both hemispheres on three consecutive sections/animal, (C,E–G) average of measurements on three consecutive sections/animal. Statistical tests: (B) Two-way RM ANOVA test; (C,E–G) Unpaired *t*-test to compare HET or KO mice to WT mice, and one-way ANOVA test to compare the three genotypes; \**P* < 0.05, \*\**P* < 0.01, \*\*\**P* < 0.001.

densities of callosal Ctip2<sup>+</sup> and Satb2<sup>+</sup> projecting neurons in the cortex were different between the three genotypes (Supplementary Figure 1). These observations demonstrate that the level of Caspr2 modulates the morphology of the CC during development, with

a remarkable “switch” at P7, immediately before the onset of myelination. Furthermore, they strongly suggested that Caspr2 could play previously unidentified functions in axon development and/or myelination.

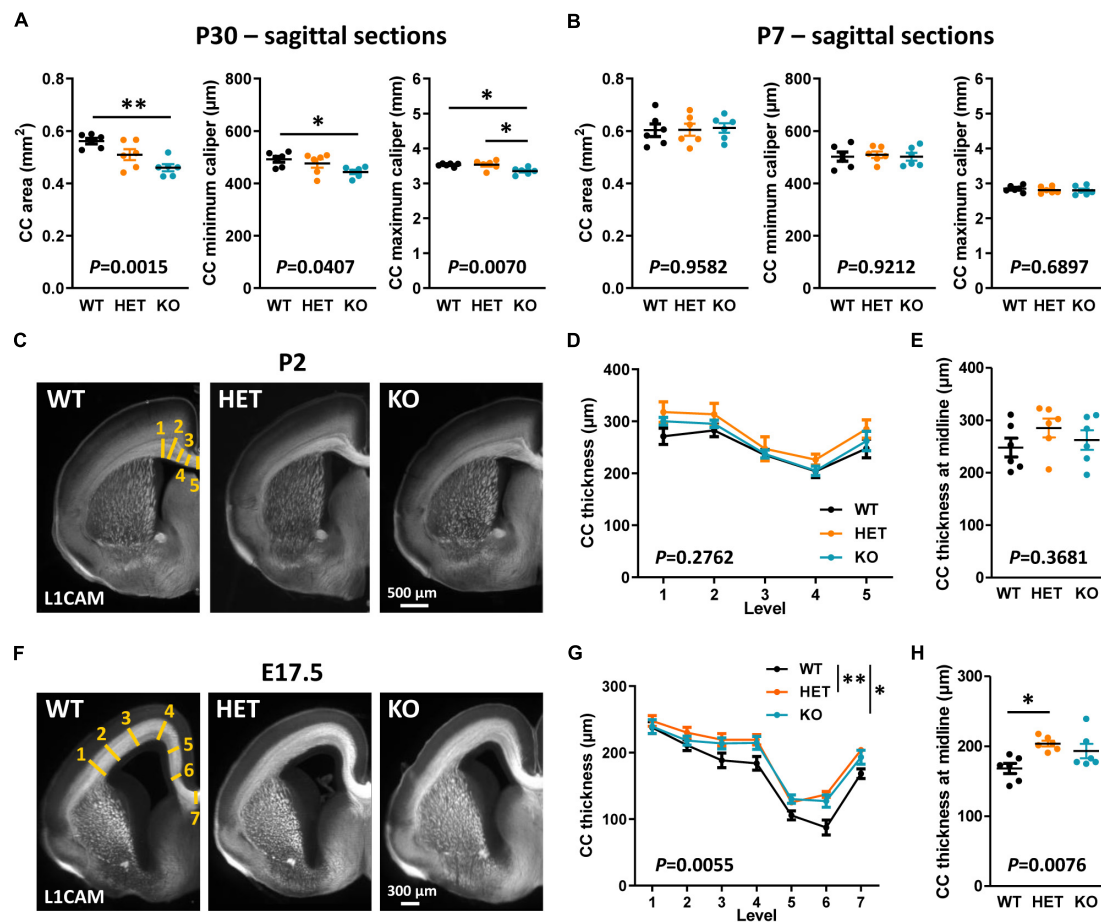


FIGURE 2

Corpus callosum (CC) morphology during development. CC area, minimum caliper, and maximum caliper measured on mid-sagittal brain sections of wild-type (WT), HET, and KO P30 mice (A) and P7 pups (B). Representative images of brain coronal sections of WT, HET, and KO P2 pups (C) and E17.5 embryos (F) showing CC immunostained with anti-L1-CAM antibodies; the levels where CC thickness measurements were performed are schematized on the images of WT mice (yellow lines). CC thickness measured on coronal sections of P2 pups (D) and E17.5 embryos (G) at the levels indicated in panels (C,F). CC thickness at the midline of the brains of P2 pups (E) and E17.5 embryos (H). (A,B,D,E,G,H) Six animals/genotype, (A,B) average of measurements on three consecutive sections/animal, (D,G) average of measurements on both hemispheres on one section/animal, (E,H) measurements on one section/animal. Statistical tests: Unpaired *t*-test (A,B,E) or Mann–Whitney test (H) to compare HET or KO mice to WT mice, and one-way ANOVA test (A,B,E) or Kruskal–Wallis test (H) to compare the three genotypes; (D,G) Two-way RM ANOVA test followed by a Tukey's multiple comparisons test (G);  $*P < 0.05$ ,  $**P < 0.01$ .

## Caspr2 level modulates AC morphology during development

The AC is formed by two main branches, contacting each other at the midline of the brain (Figure 3A). The ACa is composed mainly of axons from the anterior piriform cortex and the anterior olfactory nucleus, whereas the posterior branch (ACp) is composed mostly of axons from the posterior piriform cortex and the amygdala. We assumed that Caspr2 could contribute to the development and organization of this tract because *Cntnap2* expression was previously detected in the piriform cortex (Penagarikano et al., 2011; Gordon et al., 2016). As the AC follows a developmental timeline comparable to that of the CC in mice (Martin-Lopez et al., 2018), we characterized its morphology at the same developmental stages—P90, P30, P7, and E17.5. Phase-contrast images of 500 μm-thick horizontal brain sections did not reveal gross morphological defects in adult mutant mice (Figure 3A). However, we detected an increased thickness of the ACa in HET mice as compared to WT and KO mice, while the thickness tended to be decreased in KO mice, although not

significantly different from that in WT mice (Figures 3A, B). This tendency turned out to be significant when considering the area of the whole AC on mid-sagittal sections (Figures 1D, 3D), suggesting that both the ACa and the ACp were thinner in KO mice as compared to WT mice. The area of the AC in KO mice appeared also significantly smaller than in HET mice. The AC area in HET mice was not significantly different from that in WT mice, but showed a strong tendency to increase (unpaired *t*-test,  $P = 0.0571$ ), which was consistent with the increased thickness of the ACa. Results following a similar trend were observed in juvenile mice at P30 (Figures 3C, E). In contrast, no major differences were observed between the three genotypes in P7 pups (Figures 3C, F). In addition, the AC area was significantly increased in KO mice as compared to WT and HET mice in E17.5 embryos (Figures 3C, G). These data demonstrated that the level of Caspr2 also modulates the morphology of the AC during development, with a switch immediately before the onset of myelination as for the CC. They also suggested that Caspr2 could display functions in axon development and/or myelination extended to several myelinated tracts.



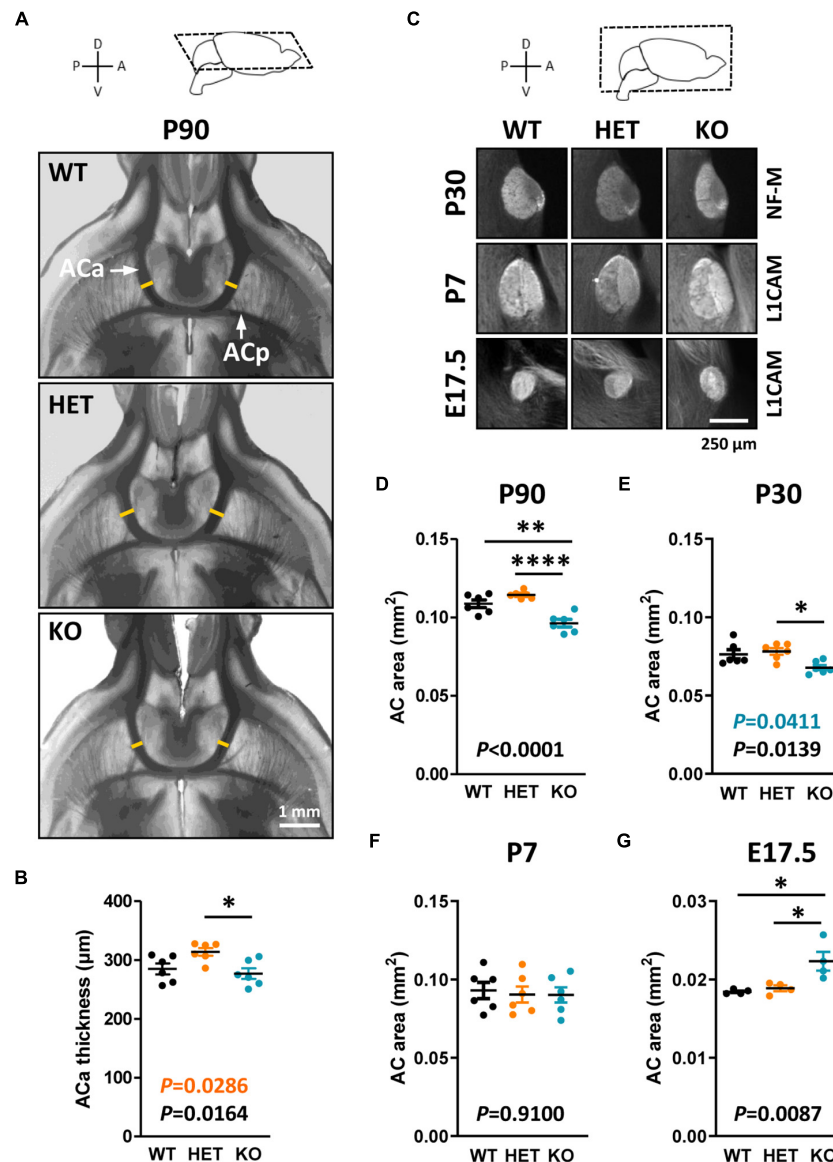


FIGURE 3

Anterior commissure (AC) morphology during development and at adulthood. Representative phase-contrast images of horizontal brain sections of wild-type (WT), HET, and KO P90 mice, showing the two branches of the AC (A); yellow lines, levels where the thickness of the anterior branch (ACa) was measured. ACa thickness measured on horizontal brain sections of P90 mice (B). Representative images of mid-sagittal brain sections of WT, HET, and KO mice at P30, P7, and E17.5, showing AC immunostained with anti-NF-M (P30) or L1CAM (P7, E17.5) antibodies (C). AC area measured on mid-sagittal brain sections of P90 (D) and P30 (E) mice, P7 pups (F), and E17.5 embryos (G). (B,D–F) Six animals/genotype, (G) four animals/genotype, (B) average of measurements on both hemispheres on one section/animal, (D–G) average of measurements on three consecutive sections/animal. Statistical tests: Unpaired t-test (B,D,F,G) or Mann–Whitney test (E) to compare HET or KO mice to WT mice, and one-way ANOVA test (B,D,F,G) or Kruskal–Wallis test (E) to compare the three genotypes; \* $P < 0.05$ , \*\* $P < 0.01$ , \*\*\*\* $P < 0.0001$ .

## Caspr2 level modulates axon diameter and myelin thickness of CC myelinated fibers in P30 mice

To further investigate the potential functions of Caspr2 in axon development and myelination, we first evaluated the timeline of overall myelination in HET and KO mice at four developmental stages from the onset of myelination (P10) to adulthood, by quantifying the levels of myelin proteins in whole brain extracts. Immunoblots showed a significant decrease of MBP, PLP, and MAG levels in KO mice at P30 as compared to WT mice, but not in P10, P15, and P90 mice (Supplementary Figures 2A–C), suggesting

a potential widespread myelination delay in KO mice at P30. No alterations of myelin protein levels were detectable in HET mice, regardless of the developmental stage. We then performed tissue microdissection to compare myelin protein levels in the CC and the neocortex of P30 mice. Immunoblots revealed a significant decrease of MBP and MAG levels in the neocortex of KO mice as compared to WT mice (Supplementary Figures 2D, E), which was consistent with a delay of myelination previously reported in the neocortex of KO mice at P21 (Scott et al., 2017). However, no alteration of myelin protein level was detected in the CC of KO mice, in agreement with two previous studies showing similar MBP-immunoreactivity of the CC on brain coronal sections of WT and KO mice (Scott et al., 2017;

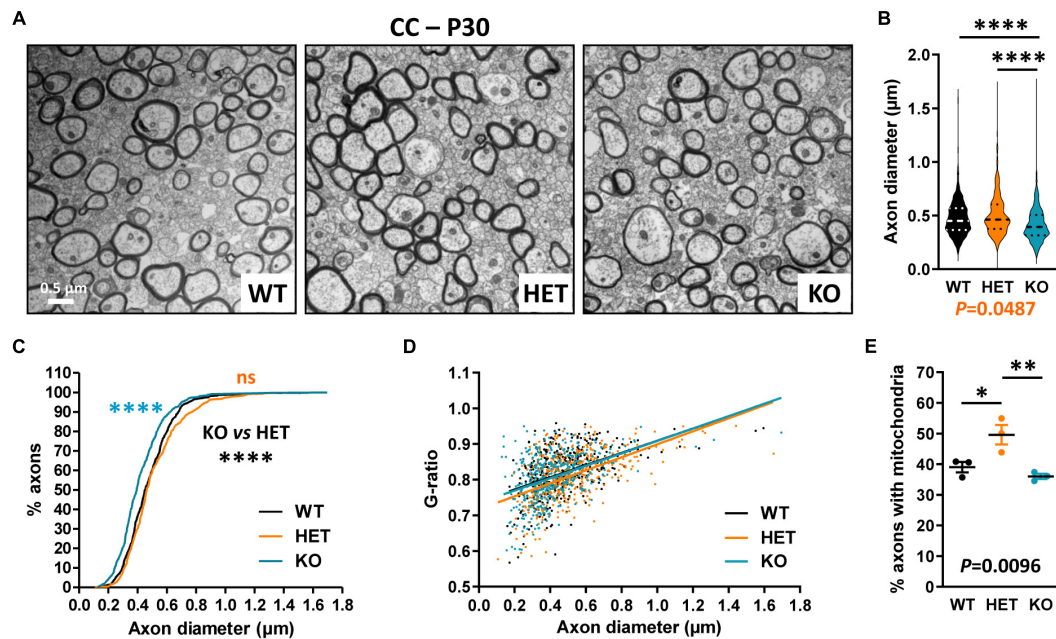


FIGURE 4

Ultrastructural abnormalities of corpus callosum (CC) myelinated fibers in P30 mice. Electron micrographs of transversal sections of the CC at brain midline, from wild-type (WT), HET, and KO P30 mice (A). Axonal diameters of CC myelinated fibers (B). Cumulative frequency distribution of axonal diameters (in %) (C). Scatter plot graph displaying G-ratios of individual myelinated axons as a function of the respective axon diameters, and linear regression of the G-ratio measurements for each genotype (D). Percentage of myelinated axons containing mitochondria (E). (B–D) 450 myelinated fibers/genotype, 3 mice/genotype, 150 myelinated fibers/mouse; (E) 3 mice/genotype, % of mitochondria counted on ~2000 axons/mouse. Statistical tests: (B) Mann–Whitney test to compare HET or KO mice to WT mice, and Kruskal–Wallis test to compare the three genotypes; (C) Kolmogorov–Smirnov test for pairwise comparisons; (D) Linear regression (WT  $R^2 = 0.2102$ , HET  $R^2 = 0.2871$ , KO  $R^2 = 0.1959$ ) for pairwise comparisons, HET vs. WT elevation  $P < 0.0001$ , HET vs. KO elevation  $P = 0.0005$ ; (E) Unpaired  $t$ -test to compare HET or KO mice to WT mice, and one-way ANOVA test to compare the three genotypes; \* $P < 0.05$ , \*\* $P < 0.01$ , \*\*\*\* $P < 0.0001$ ; ns, non-significant.

Liska et al., 2018). No alteration of myelin protein level was detected in the CC of HET mice either.

We further evaluated CC myelination in P30 mice at the ultrastructural level by measuring myelinated fiber and axon diameters, to subsequently calculate the G-ratio, which is the ratio of axon diameter to fiber diameter whose variations can reveal myelin thickness defects. Transversal sections were observed at  $\sim$ Bregma + 0.02, in dorsal projection of the AC. We detected a significant decrease in axon diameters in KO mice as compared both to WT and HET (Figures 4A–C), which was consistent with previous observations at Bregma  $-2.46$  (Zerbi et al., 2018). No difference between KO and WT mice was detectable when plotting the G-ratios as a function of axon diameters, indicating absence of major myelination changes in KO mice (Figure 4D). No significant difference was observed either in the % of myelinated fibers between KO and WT mice (WT  $16.5 \pm 0.6775$ , KO  $13.84 \pm 2.594$ , unpaired  $t$ -test  $P = 0.3775$ , three mice/genotype), thus confirming that P30 KO mice do not present major myelination defects of the CC. In contrast, the % of myelinated fibers appeared significantly decreased in HET mice when compared to WT mice (WT  $16.5 \pm 0.6775$ , HET  $8.747 \pm 1.709$ , unpaired  $t$ -test  $P = 0.0135$ , three mice/genotype). In parallel, axon diameters were slightly decreased as compared to WT mice (Figures 4B, C). A significant difference was also detectable between WT and HET mice when plotting the G-ratios as a function of axon diameters (Figure 4D). The mean G-ratio was consistently decreased in HET mice as compared to WT mice, reflecting hypermyelination (WT  $0.8200 \pm 0.003069$ , HET  $0.8099 \pm 0.003189$ , Mann–Whitney

test  $P = 0.0271$ , 450 fibers/genotype, three mice/genotype, 150 fibers/mouse). Interestingly, we also noticed a significant increase in the % of myelinated axons containing mitochondria in HET mice as compared to WT and KO mice (Figure 4E). Thus, our observations showed alterations of myelinated fibers in the CC of P30 HET mice which were not suspected by myelin protein level analyses, perhaps because the hypermyelination was masked by the decrease in the myelinated fiber number. Overall, axon diameter and myelin thickness modifications observed in mutant mice confirm the assumption that Caspr2 could play roles in axon development and/or myelination, which could be modulated by the protein level.

## Caspr2 level modulates axon diameter and myelin thickness of AC myelinated fibers in P30 mice

We further evaluated whether Caspr2 could also display functions in axon development and/or myelination in the AC, searching similar axonal and/or myelination defects in mutant mice at P30. Ultrastructural analyses of the ACa and the ACp were performed separately, since the two branches are distinguishable on mid-brain transversal sections (Figures 5A, F, insets). No significant difference in the % of myelinated fibers was observed between the three genotypes, either in the ACa (WT  $18.2 \pm 1.554$ , HET  $21.24 \pm 0.611$ , KO  $13.4 \pm 3.022$ , one-way ANOVA test  $P = 0.0818$ , three mice/genotype) or in the ACp (WT  $11.8 \pm 1.02$ , HET  $9.716 \pm 0.7453$ , KO  $7.655 \pm 0.8618$ , Kruskal–Wallis test  $P = 0.0857$ ,

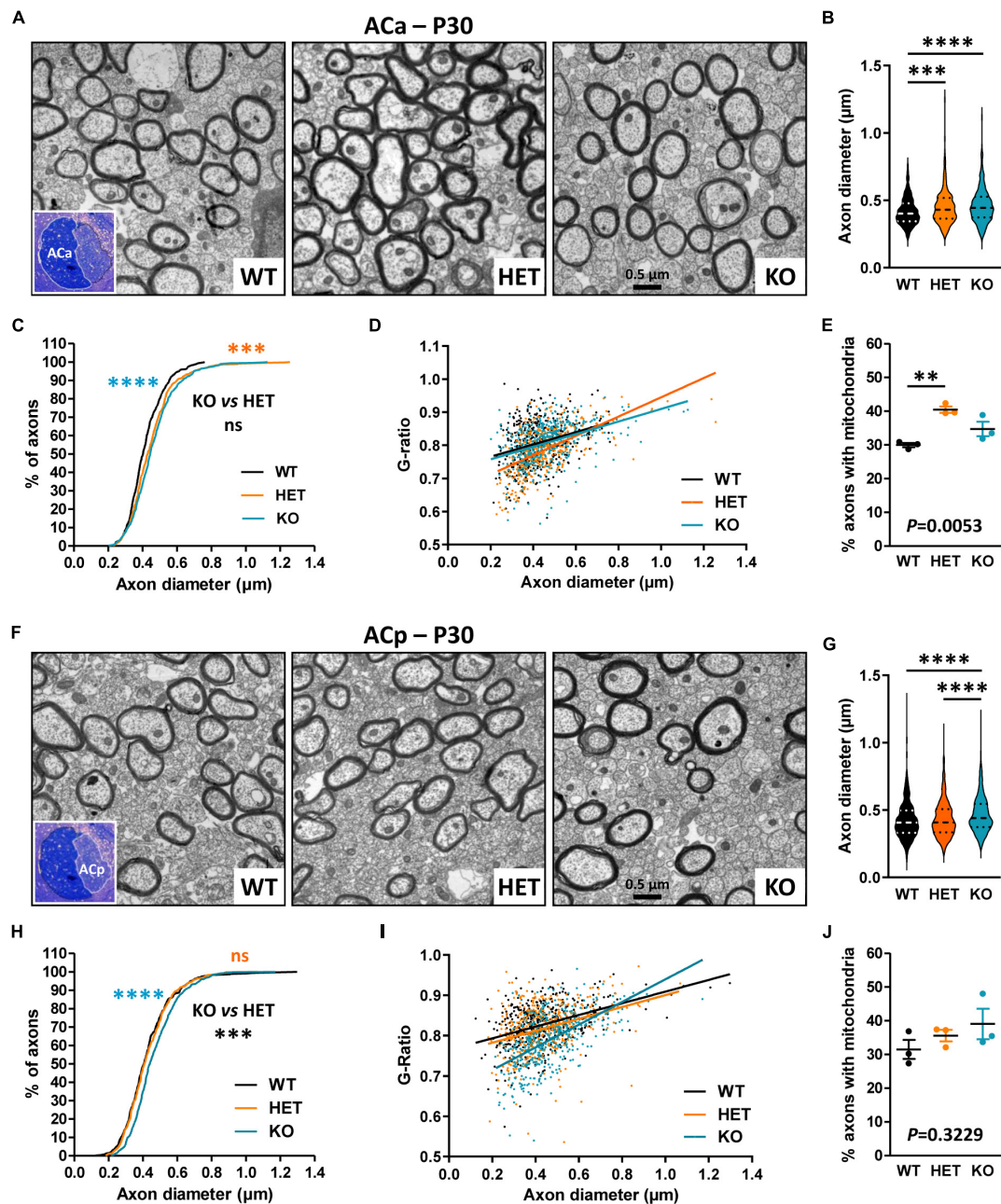


FIGURE 5

Ultrastructural abnormalities of anterior branch (ACa) and posterior branch (ACp) myelinated fibers in P30 mice. Electron micrographs of transversal sections of the ACa (**A**) and ACp (**F**) at brain midline, from wild-type (WT), HET, and KO P30 mice; insets, semi-thin transversal sections of the AC stained with toluidine blue, showing the ACa and the ACp. Axonal diameters of ACa (**B**) and ACp (**G**) myelinated fibers. Cumulative frequency distribution of axonal diameters (in %) of ACa (**C**) and ACp (**H**) myelinated fibers. Scatter plot graphs displaying G-ratios of individual myelinated axons as a function of the respective axon diameters, and the linear regression of the G-ratio measurements for each genotype, for the ACa (**D**) and the ACp (**I**). Percentage of myelinated axons containing mitochondria in the ACa (**E**) and the ACp (**J**). (**B–D, G–I**) 441 myelinated fibers/genotype, 3 mice/genotype, 147 myelinated fibers/mouse; (**E**) 3 mice/genotype, % of mitochondria counted on ~2000 axons/mouse; (**J**) 3 mice/genotype, % of mitochondria counted on ~1000 axons/mouse. Statistical tests: (**B, G**) Mann–Whitney test to compare HET or KO mice to WT mice, and Kruskal–Wallis test to compare the three genotypes; (**C, H**) Kolmogorov–Smirnov test for pairwise comparisons; (**D**) Linear regression (WT  $R^2 = 0.08121$ , HET  $R^2 = 0.3458$ , KO  $R^2 = 0.1727$ ) for pairwise comparisons, HET vs. WT slope  $P = 0.0024$ , HET vs. KO slope  $P = 0.0003$ ; (**I**) Linear regression (WT  $R^2 = 0.1589$ , HET  $R^2 = 0.1062$ , KO  $R^2 = 0.3420$ ) for pairwise comparisons, HET vs. WT elevation  $P = 0.0047$ , KO vs. WT slope  $P < 0.0001$ , HET vs. KO slope  $P < 0.0001$ ; (**E, J**) Unpaired t-test (**E**) or Mann–Whitney test (**J**) to compare HET or KO mice to WT mice, and one-way ANOVA test (**E**) or Kruskal–Wallis test (**J**) to compare the three genotypes; \*\* $P < 0.01$ , \*\*\* $P < 0.001$ , \*\*\*\* $P < 0.0001$ ; ns, non-significant.

three mice/genotype). In contrast, we detected modifications in axon diameters and myelination, which were remarkably different between the ACa and the ACp. While axon diameters of the ACa were significantly increased in both HET and KO mice as compared to

WT mice, with an intermediate phenotype in HET mice (Figures 5B, C), axon diameters of the ACp were increased in KO mice only (Figures 5G, H). Additionally, plotting of the G-ratios as a function of axon diameters revealed a significant difference between HET mice



and WT and KO mice for the ACa (**Figure 5D**), while both HET and KO mice were significantly different from WT mice for the ACp (**Figure 5I**). These observations were consistent with decreases of the mean G-ratios, demonstrating hypermyelination of ACa fibers in HET mice (WT  $0.8060 \pm 0.003146$ , HET  $0.7854 \pm 0.003246$ , KO  $0.8077 \pm 0.002936$ , Kruskal–Wallis test  $P < 0.0001$ , HET vs. WT  $P < 0.0001$ , HET vs. KO  $P < 0.0001$ , 441 fibers/genotype, 3 mice/genotype, 147 fibers/mouse), and of ACp fibers in both HET and KO mice, with an intermediate phenotype in HET mice (WT  $0.8264 \pm 0.005555$ , HET  $0.8167 \pm 0.002880$ , KO  $0.7899 \pm 0.003097$ , Kruskal–Wallis test  $P < 0.0001$ , KO vs. WT  $P < 0.0001$ , KO vs. HET  $P < 0.0001$ , HET vs. WT  $P = 0.0169$ , 441 fibers/genotype, 3 mice/genotype, 147 fibers/mouse). The % of myelinated axons of the ACa containing mitochondria was also significantly higher in HET mice than in WT (**Figure 5E**), while no difference was observed between the three genotypes for the ACp (**Figure 5J**). Altogether these data reinforce the assumption that Caspr2 could display functions in axon development and/or myelination of several myelinated tracts. In addition, they suggest that the underlying mechanisms may be different, depending on myelinated fiber type, and may therefore be differentially affected by variations in Caspr2 level.

## Caspr2 level modulates axon diameter and neuronal activity before and at the onset of myelination

Myelination in the CNS relies on a complex sequence of cellular events, which includes proliferation and migration of oligodendrocyte precursor cells (OPCs) in white matter tracts, recognition of target axons, and axon–glia signaling, differentiation of OPCs into mature myelinating OLs, axonal ensheathment, and myelin compaction. This sequence is controlled by intrinsic factors that are responsive to extracellular cues, including signaling molecules released by neurons or glial cells and cell-surface expressed proteins, and by neuronal activity, which regulates OPC proliferation and survival potentiating OL differentiation, and drives the extent of myelin formation (Stassart et al., 2018; de Faria et al., 2019). The changes in the morphology of the CC and AC in mutant mice at P7 suggested that Caspr2 could regulate some neuronal parameters immediately before and/or at the onset of myelination, which could control axo–glial cross-talk and, later, axon diameter and myelin thickness. To evaluate this hypothesis, we first compared the diameter of the axons between WT, HET, and KO pups at P7. Ultrastructural analyses did not reveal significant axon diameter difference between the three genotypes for the ACp (**Figures 6A, C, F**), but a slight decrease of axon diameters of the ACa in KO pups as compared to WT and HET pups (**Figures 6A, B, E**). In addition, axon diameters of the CC were significantly increased in HET pups as compared to WT and KO pups, and decreased in KO pups as compared to WT pups (**Figures 6A, D, G**).

Following this observation, we explored whether Caspr2 could regulate the intrinsic excitability of layers III cortical neurons which project their axons in the CC at the onset of myelination, i.e., the propensity of neurons to fire action potentials when subjected to an input current. We measured the firing frequency of action potentials in response to 500 ms depolarizing current steps from a membrane potential of  $-70$  mV, in the presence of blockers of synaptic activity.

We found that intrinsic excitability was significantly increased in HET and KO neurons as compared to WT neurons (**Figures 7A, B**), while the resting membrane potential was unchanged (**Figure 7C**). The intrinsic excitability did not significantly differ between HET and KO mice. These results may, at least in part, reflect a role of Caspr2 at the axon initial segment, the site of initiation of action potentials, since Caspr2 has been detected in the axon initial segment of both pyramidal cells of human temporal neocortex (Inda et al., 2006) and rat hippocampal neurons in culture (Ogawa et al., 2008). Altogether our observations suggest that decreased Caspr2 dosage may indirectly control myelination through activity-dependent mechanisms, and by regulating axon diameter.

## Caspr2 levels are downregulated in HET mouse brain before the onset of myelination

The impacts of *Cntnap2* heterozygosity on myelinated tract morphology, axon diameter, myelin thickness, and neuronal activity, either specific, opposite, or stronger than those of *Cntnap2* null homozygosity, led us to question Caspr2 levels in HET mice at different stages from E17.5 to adulthood. These levels were expected to be  $\sim 50\%$  relative to levels in WT brains. Immunoblots on whole brain extracts showed that this was the case at P15, P30, and P90, but not earlier during development (**Figures 8A, B**). Caspr2 levels were indeed reduced to  $\sim 35\%$  at E17.5, P2, P7, and P10, and significantly different from those in P90 HET mice. RT-qPCR experiments showed that this reduction may not be due to a decrease in gene expression (**Figure 8C**). *Cntnap2* mRNA level at P10 was actually increased and higher than that at P30 (unpaired *t*-test,  $P = 0.0564$ , six mice/genotype), indicating a need for cells to increase the level of Caspr2 around this developmental stage.

Decreased levels of cell-surface expressed proteins can be due to increased turnover and degradation, reflecting potential modifications in their interactions with their partners. We investigated this possibility, postulating that TAG-1 could be a partner of Caspr2 not only at juxtaparanodes of mature myelinated axons but also throughout development. Immunoblots on whole brain extracts of KO mice supported this assumption, showing that TAG-1 levels in these mice started to decrease from P2, to reach  $\sim 33\text{--}42\%$  decrease from P7 to P15, and  $\sim 90\%$  decrease at P30 and P90, as compared to WT mice (**Figures 8A, D**). In contrast, TAG-1 levels were not significantly affected in HET mice, except at P30. This indicates that the association of Caspr2 and TAG-1 are mostly preserved in HET mice and that the mechanisms which regulate Caspr2 levels at early developmental stages are probably independent of TAG-1. However, these data also suggest that the differential phenotypes observed in HET and KO could be partly due to the fact that the functions of TAG-1 are preserved in HET mice while they are highly perturbed in KO mice.

## Caspr2 level also modulates the organization of myelinated fibers in peripheral nerves

The identification of a *CNTNAP2* genetic alteration in Charcot–Marie–Tooth patients led us to finally question whether *Cntnap2*

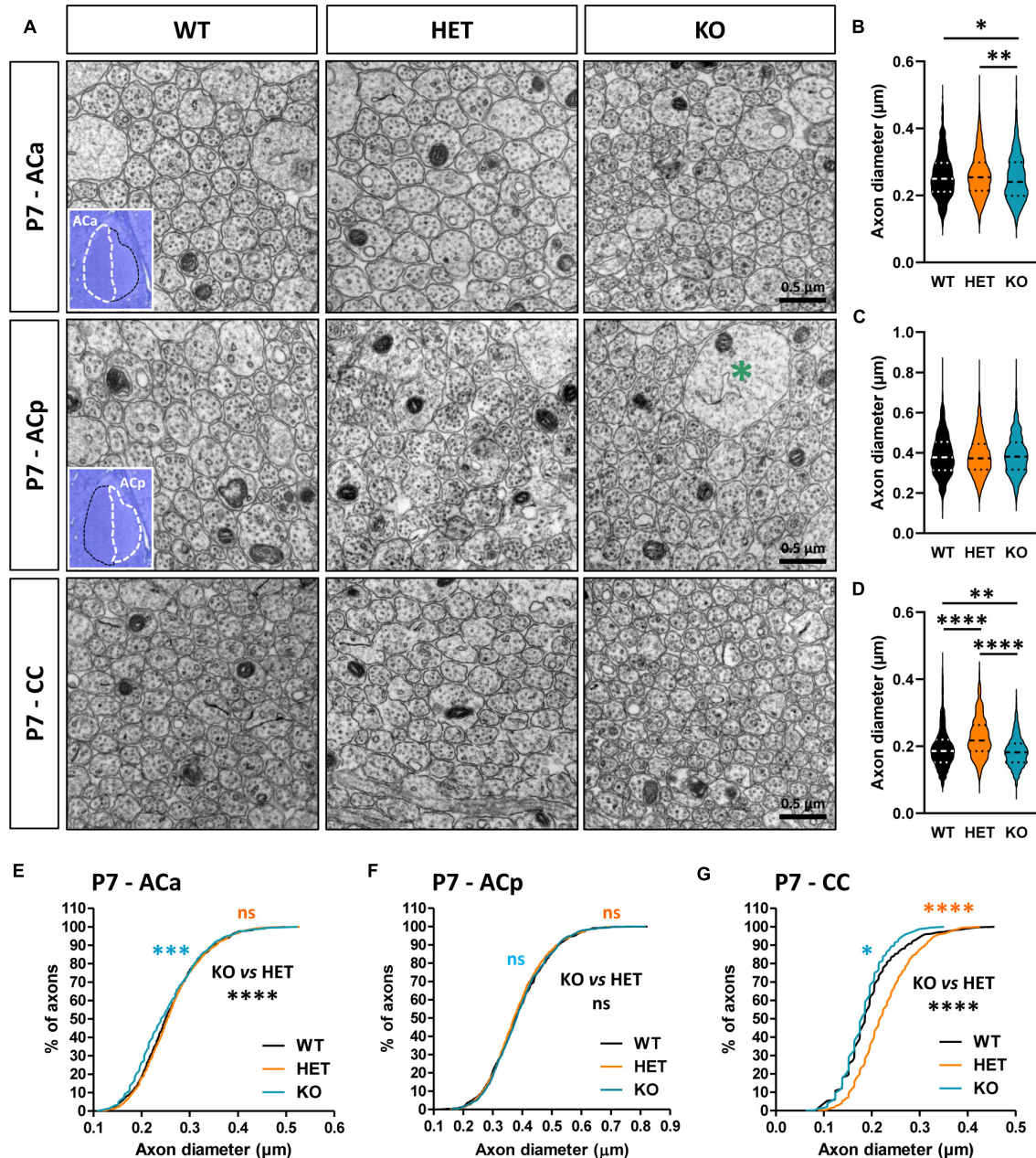


FIGURE 6

Anterior commissure (AC) and corpus callosum (CC) axon diameter abnormalities in P7 pups. Electron micrographs of transverse sections of the anterior branch (ACa), posterior branch (ACp), and CC at brain midline, from wild-type (WT), HET, and KO P7 pups; insets, semi-thin transverse sections of the AC stained with toluidine blue, showing the ACa and the ACp; the green asterisk indicates a growth cone (A). Axonal diameters of the ACa (B), ACp (C), and CC (D). Cumulative frequency distribution of axonal diameters (in %) of the ACa (E), ACp (F), and CC (G). (B,C,E,F) 900 axons/genotype, 3 pups/genotype, 300 axons/pup; (D,G) 1080 axons/genotype, 3 pups/genotype, 360 axons/pup. Statistical tests: (B–D) Mann–Whitney test to compare HET or KO mice to WT mice, and Kruskal–Wallis test to compare the three genotypes; (E–G) Kolmogorov–Smirnov test for pairwise comparisons; \* $P < 0.05$ , \*\* $P < 0.01$ , \*\*\* $P < 0.001$ , \*\*\*\* $P < 0.0001$ ; ns, non-significant.

heterozygosity and null homozygosity could also perturb the organization of peripheral myelinated fibers in adult mice. Semi-thin transversal sections of sciatic nerves stained with toluidine blue did not reveal any major difference in the global morphology of the nerves between adult WT, HET, and KO mice, nor in the total number of axons (data not shown). The structure of the myelin appeared normal both in HET and KO mice (Figure 9A). A previous study reported comparable values of axon diameters and G-ratios in the sciatic nerves of WT and KO adult mice (Poliak et al.,

2003). We re-evaluated these data by focusing our ultrastructural analysis on large caliber motor fibers only. We found that the axonal diameters were increased in HET and KO mice as compared to WT mice, with an intermediate phenotype in HET mice (Figure 9B). When plotting the G-ratios as a function of axon diameter, we did not detect any difference between KO and WT mice, but a significant difference between HET and WT mice (Figure 9C). The mean G-ratio was consistently increased in HET mice as compared to WT mice, reflecting hypomyelination (WT  $0.6948 \pm 0.003826$ ,



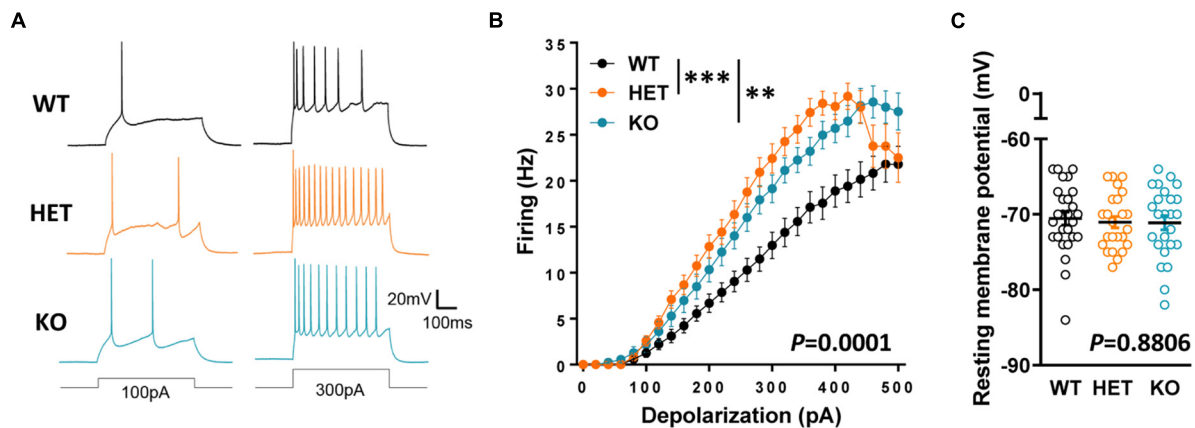


FIGURE 7

Intrinsic excitability in cortical pyramidal cells from P10–P12 pups. Sample spike trains evoked by a 100-pA (left) or a 300-pA somatic current injection (right) in a WT (top), HET (middle) and KO (bottom) neuron (A). Mean f-i curve for WT ( $n = 27$  cells from three mice), HET ( $n = 24$  cells from three mice), and KO ( $n = 27$  cells from three mice) (B). Resting membrane potential of the recorded neurons (C). Statistical tests: (B) Two-way RM ANOVA followed by Sidak's post-hoc test; (C) One-way ANOVA to compare the three genotypes;  $**P < 0.01$ ,  $***P < 0.001$ .

HET  $0.7244 \pm 0.004060$ , Mann–Whitney test  $P < 0.0001$ , 141 fibers/genotype, 4 mice/genotype, 47 fibers/mouse). Furthermore, fluorescent immunolabelings on teased myelinated fibers confirmed a drastic reduction of TAG-1 and Kv1.2 channel enrichment in the juxtaparanodes of KO mice (Figure 9D), as previously described (Poliak et al., 2003), but did not reveal obvious modification in the enrichment of Caspr2, TAG-1, and Kv1.2 in HET mice (proteins detected in more than 90% of the juxtaparanodes). The levels of TAG-1 and Kv1.2 in nerve extracts were not affected either in HET mice as compared to WT mice (data not shown). However, a morphometric analysis showed an unexpected decrease in the length of the nodes (labeled for NrCAM) in both HET and KO mice, with an intermediate phenotype for HET mice (Figures 9E, F), while no difference was observed for the axonal diameters of the nodes (WT  $2.640 \pm 0.045 \mu\text{m}$ , HET  $2.535 \pm 0.036 \mu\text{m}$ , KO  $2.677 \pm 0.054 \mu\text{m}$ , Kruskal–Wallis test  $P = 0.5342$ , three mice/genotype). We questioned whether defects in sciatic nerve organization could lead to motor and coordination deficits in a grid-walking test. Interestingly, adult HET mice made significantly more slips than WT and KO mice during the 2 min of the test (Figure 9G). Altogether these observations demonstrate that Caspr2 level also modulates the organization of mature peripheral myelinated fibers, with potential functional consequences in HET mice.

## Discussion

A large variety of homozygous and heterozygous genetic alterations of the *CNTNAP2* gene have been identified in several neuronal disorders (Rodenias-Cuadrado et al., 2014; Hoyer et al., 2015; Poot, 2015, 2017; Saint-Martin et al., 2018). However, the impact of these mutations on Caspr2 functions remains unknown. To better elucidate this issue, we questioned whether *Cntnap2* heterozygosity and *Cntnap2* null homozygosity could impact, either similarly or differentially, some specific functions of Caspr2 during development and in adulthood. Our study indicates that Caspr2 levels influence the gross morphology of both CC and AC, as well as axon diameter at early developmental stages, cortical neuronal activity

at the onset of myelination, and axon diameter, myelin thickness and nodal length at later developmental stages (Figure 10). Our observations also highlight Caspr2 functions in axon development and myelination, through which the protein could contribute to normal neuronal network connectivity.

Two previous studies proposed that some functions of Caspr2 in the CNS could be modulated by the level of the protein (Canali et al., 2018; Vogt et al., 2018). Our study reinforces this assumption and further shows that *Cntnap2* heterozygosity and *Cntnap2* null homozygosity lead to complex phenotypes in myelinated fibers. Among all the parameters that we quantified, some present an intermediate phenotype in HET mice as compared to WT and KO mice, some show an opposite phenotype in HET and KO mice, some others are affected in HET or KO mice only, while few tend to be more severely affected in HET mice than in KO mice (Figure 10). The diversity of the phenotypes does not only illustrate differences between HET and KO mice, but also demonstrates that *Cntnap2* heterozygosity and *Cntnap2* null homozygosity impact different types of myelinated fibers differentially. This diversity may be due to the complexity of the mechanisms involved in the bi-directional axo-glial signaling regulating axon and myelin dimensions (which might be disparately affected by the level of protein), and to differences in the molecular mechanisms in which Caspr2 could be implicated from one axon to another. Our observations suggest that these mechanisms could involve the protein TAG-1, which is expressed in both CC and AC axons during development (Kastriti et al., 2019). Caspr2 could also very likely be associated with one or more additional partners among the numerous membranous proteins differentially expressed in CC and AC axons.

According to our observations, Caspr2 could intervene at several time points during the myelination process in the CNS. A handful of elements points to potential roles at the onset of myelination. This includes the switch in morphologies of the CC and AC observed at P7 in mutant pups. Also, as aforementioned, myelination in the CNS relies on a complex sequence of cellular events, which is controlled by OLs intrinsic factors but is also modulated by extrinsic factors, including neuronal activity (Stassart et al., 2018; de Faria et al., 2019). We observed increased neuronal activities in layer

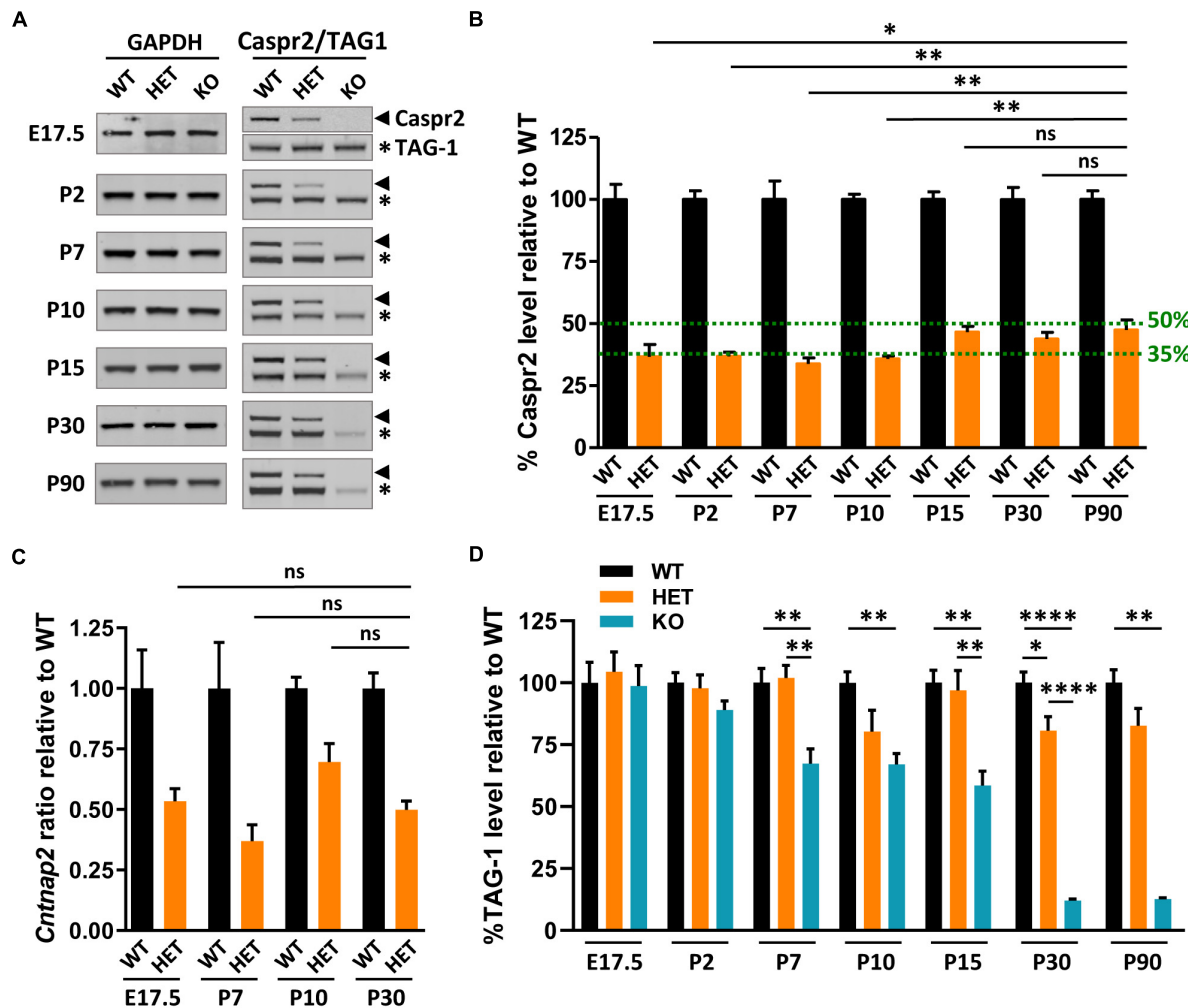


FIGURE 8

Caspr2, TAG-1, and *Cntnap2* mRNA levels in mouse brains during development. Representative immunoblots showing Caspr2, TAG-1, and GAPDH levels in brain lysates of wild-type (WT), HET, and KO mice at different developmental stages and at adulthood (A). Levels of Caspr2 normalized to GAPDH levels and relative to mean WT (in %) (B). Levels of *Cntnap2* mRNAs normalized to the *Psap* gene and relative to mean WT (ratio) in brain of WT, HET, and KO mice at E17.5, P7, P10, and P30 (C). Levels of TAG-1 normalized to GAPDH levels and relative to mean WT (in %) (D). (B–D) Six animals/genotype/age. Statistical tests: (B) Mann–Whitney test to compare Caspr2 levels in HET mice at stages E17.5, P2, P7, P10, P15, or P30, to Caspr2 level in HET mice at P90. (C) Unpaired *t*-test to compare *Cntnap2* mRNA levels in HET mice at stages E17.5, P7, or P10, to *Cntnap2* mRNA level in HET mice at P30. (D) One-way ANOVA test or Kruskal–Wallis test to compare the three genotypes at different ages; \**P* < 0.05, \*\**P* < 0.01, \*\*\*\**P* < 0.0001; ns, non-significant.

III cortical neurons in mutant pups at P10–P12, supporting the possibility that Caspr2 might participate in the cross-talk between the axons of the CC and the OLs at these stages, and possibly later in myelin sheath growth. Caspr2 is involved in the formation and stabilization of neuronal synapses, and in the trafficking of the GluA1 subunits of the AMPA receptors (Gdalyahu et al., 2015; Varea et al., 2015). Of interest, myelination is thought to be modulated by the establishment of axon-oligodendroglial cell synapses and synaptic-like interactions, which respond to the electrical activity of those axons (Bergles and Richardson, 2015). The OPCs display expression of ionotropic neurotransmitter receptors and receive direct glutamatergic and GABAergic synaptic inputs from unmyelinated or partially myelinated axons. In addition, myelin sheath growth involves the establishment of specialized synaptic-like micro-domains at the axon-myelin interface and is regulated by the activity-dependent vesicular release of neurotransmitters along axons (Mensch et al., 2015; Hughes and Appel, 2019). Thus it is possible that Caspr2 plays functions at axon/OLs connections, and possibly also

in OL differentiation since single-cell RNA sequencing experiments indicate that Caspr2 is expressed in OLs at different differentiation stages (Marques et al., 2016).

The wrapping of OLs around the axons and the extension of myelin along its length are intrinsically regulated, but modulated by the diameter of the axon they wrap (Stassart et al., 2018). Our data showing axon diameter modifications in the CC and the Aca at P7 indicate that Caspr2 likely contributes to the regulation of the axon diameters of unmyelinated axons before and at the onset of myelination. When considering a single axon, its diameter depends on the axonal cytoskeleton, which is made up of neurofilaments, microtubules, deep dynamic actin trails, and a submembranous actin-spectrin network—which is composed of actin rings regularly spaced by spectrin tetramers (Costa and Sousa, 2021). This membrane periodic skeleton (MPS) can organize transmembrane cell adhesion molecules along neurites and has been shown to regulate multiple aspects of neuronal physiology, including axon diameter, axon-axon interactions, axonal

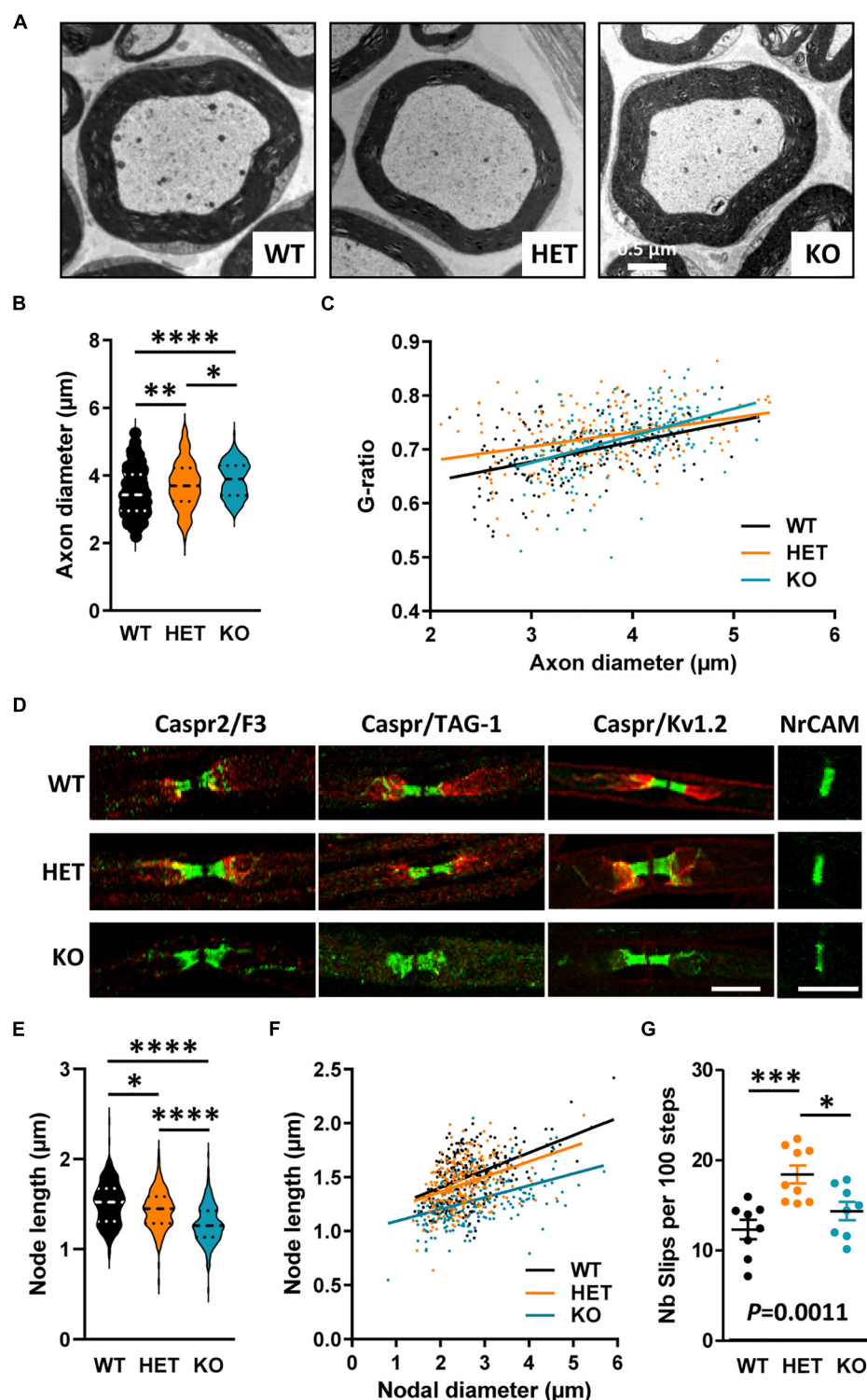


FIGURE 9

Myelinated fiber abnormalities in sciatic nerves of adult mice. Electron micrographs of transversal sections of the sciatic nerve of wild-type (WT), HET, and KO adult mice, showing a single myelinated fiber for each genotype (A). Axonal diameters of myelinated fibers (B). Scatter plot graph displaying G-ratios of individual myelinated axons as a function of the respective axon diameters, and the linear regression of the G-ratio measurements for each genotype (C). Representative confocal images of immunostainings of sciatic nerves fibers from WT, HET, and KO adult mice, for nodal (NrCAM), paranodal (Caspr, F3), and juxtaparanodal (Caspr2, TAG-1, Kv1.2) proteins (D). Length of the nodes measured on NrCAM immunostainings (E). Scatter plot graph displaying length of individual node as a function of the respective nodal diameters, and the linear regression of the node length measurements for each genotype (F). Number of slips per 100 steps made by WT, HET, and KO adult males during the grid-walking test (G). (B,C) 141 myelinated fibers/genotype, 4 mice/genotype, 47 myelinated fibers/mouse, (E,F) 243 nodes/genotype, 3 mice/genotype, 81 nodes/mouse, (G) 8–9 mice/genotype. Statistical tests: (B,E) Kruskal–Wallis test to compare the three genotypes; (C) Linear regression (WT  $R^2 = 0.2093$ , HET  $R^2 = 0.1143$ , KO  $R^2 = 0.2022$ ) for pairwise comparisons, HET vs. WT elevation  $P < 0.0001$ , HET vs. KO slope  $P = 0.019$ ; (F) Linear regression (WT  $R^2 = 0.2295$ , HET  $R^2 = 0.1368$ , KO  $R^2 = 0.1935$ ) for pairwise comparisons, HET vs. WT elevation  $P = 0.0052$ , KO vs. WT slope  $P = 0.0315$ , HET vs. KO elevation  $P < 0.0001$ ; (G) one-way ANOVA test to compare the three genotypes; \* $P < 0.05$ , \*\* $P < 0.01$ , \*\*\* $P < 0.001$ , \*\*\*\* $P < 0.0001$ . Bar scales, 10 μm (E).

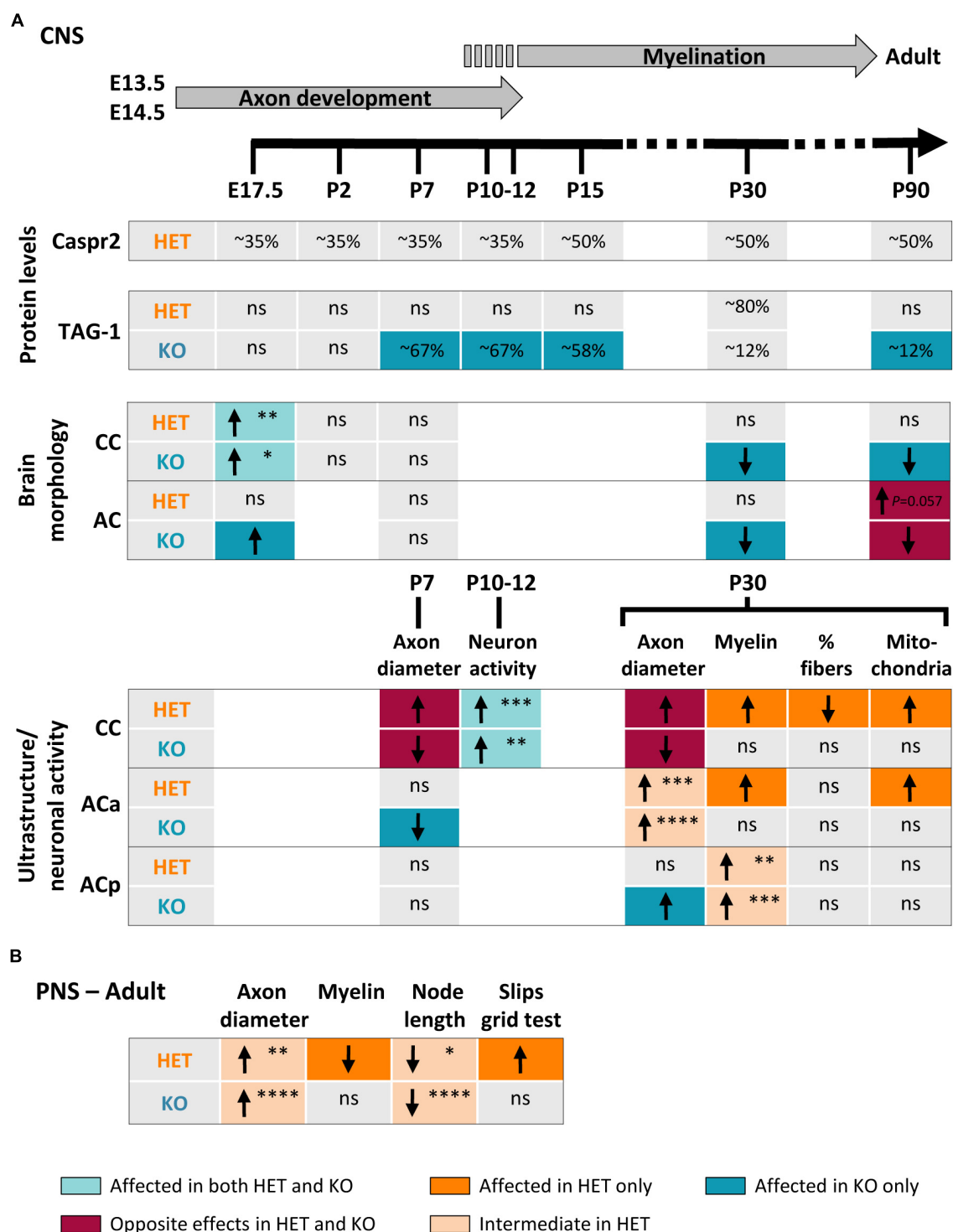


FIGURE 10

Summary of changes observed in HET and KO mice as compared to wild-type (WT) mice. Changes observed in the brain during development and in adulthood (A). Upper part, timeline of axonal development and myelination in mouse. Changes observed in the sciatic nerves and in the grid test performance (B). Arrows indicate increase (↑) or decrease (↓) in the parameters; ns, non-significant changes. The colors of the boxes underline the nature of the differences between HET and KO (color code at the bottom of the figure). The P-values are indicated when HET mice present an intermediate phenotype or tend to be more affected than KO mice (\* $P < 0.05$ , \*\* $P < 0.01$ , \*\*\* $P < 0.001$ , \*\*\*\* $P < 0.0001$ ). Corpus callosum (CC) E17.5, P-values for coronal sections; posterior branch (ACp) myelin P30, P-values for G-ratios.

transport, and microtubule stability (Zhou et al., 2022). We previously showed that Caspr2 presents the capacity to interact with actin/spectrin-associated proteins of the 4.1 family (Denisenko-Nehrbass et al., 2003). So, it is tempting to speculate that Caspr2

could participate in the regulation of axon diameter by interacting with the MPS through a 4.1 protein, although it cannot be excluded that Caspr2 could also regulate neurofilament and/or microtubule organization.



Morphological modifications at the ultrastructural levels undoubtedly contribute to the alterations of the gross morphology of the CC and the ACa observed in HET and KO mice during development and at adulthood, but no strict correlation can be established. This is probably due to the fact that, at late development stages, myelinated axons represent only a small percentage of all the axons composing the tracts. In addition, at all developmental stages, the morphology of the tracts may not be dependent on axon diameters only, but also on the compaction of unmyelinated axons. A close observation of the electron micrographs of the CC and AC at P7 seems to show that the organization of the contacts between the axons could be different between WT, HET, and KO conditions (see [Figure 6A](#), compare for example ACa WT and KO), suggesting that Caspr2 could also participate in the regulation of axon-axon contacts. Dedicated image analyses and *in vitro* cellular approaches will have to be developed to investigate this hypothesis. We didn't analyze the ultrastructure of the CC and AC at E17.5 because their morphology was not sufficiently well-defined to ensure confident measurements. However, it is very likely that the enlargement of the tracts at this stage is also due to an increase in axon diameter and/or modifications in axon-axon contacts, possibly combined with perturbations in the mechanisms guiding growing axons across the midline at early embryonic stages ([Nishikimi et al., 2013](#); [Suarez et al., 2014](#); [Fenlon et al., 2021](#)).

The changes in the morphology of the CC and ACa in HET and KO mice during development are interesting with regard to the neurodevelopmental disorders in which *CNTNAP2* alterations have been identified, notably ASD. This disorder is characterized by atypical brain connectivity associated with neural alterations in white matter production and myelination in diverse brain regions ([Galvez-Contreras et al., 2020](#)). Numerous structural MRI studies indicate that transient CC overgrowth could be among the earliest neural signatures of ASD in young toddlers ([Wolff et al., 2015](#); [Fingher et al., 2017](#)), while disproportionally small CCs relative to overall brain size are among the most replicated imaging findings in older patients ([Frazier and Hardan, 2009](#)). We intriguingly observed a similar trend, with an increased thickness in HET and KO embryos at E17.5 and a decreased thickness in KO juvenile and adult mice. Beyond that, our observations support the possibility that the *CNTNAP2* alterations could contribute broadly to myelin defects in ASD patients. Of interest, performing an integrative multi-omics analysis, [Jang et al. \(2022\)](#) recently identified *Cntnap2*-associated ASD networks and found a downregulation in the prefrontal cortex of KO mice of proteins implicated in the formation of the myelin sheath, axon growth, and axonal transport. These data are in line with our current observations and support the role of Caspr2 in axon growth that we described previously ([Canali et al., 2018](#)). In addition, they strongly suggest that the increased percentages of myelinated axons containing mitochondria that we observed in the CC and ACa of HET mice could reflect defects in axonal transport.

Finally, we showed that the level of Caspr2 also modulates the organization of peripheral myelinated fibers in adult mice. *Cntnap2* heterozygosity and *Cntnap2* null homozygosity impact the diameter of the axons, the G-ratio, and the length of the nodes differentially. The increase in axon diameters that we observed, notably in KO mice, was not previously reported ([Poliak et al., 1999](#)), either because only the diameters of the large-caliber fibers are increased, or because the phenotype was masked in previous morphometric analyses performed on fibers of wide range calibers. The decrease in the nodal length was not previously detected either, although

a decreased tendency in the nodal length-to-axonal diameter ratio was reported in KO mice as compared to WT mice ([Gordon et al., 2014](#)). When calculating this ratio with our data, it turns out that the decrease measured in KO mice is significant (WT  $0.596 \pm 0.008$ , KO  $0.510 \pm 0.008$ , Mann-Whitney test  $P < 0.0001$ ), probably because we analyzed a larger number of nodes. Similar to our observations in central myelinated fibers, these abnormalities reveal that Caspr2 plays previously unidentified functions in the development of peripheral myelinated fibers as well. These functions might be similar but also distinct from those in the CNS, since there are substantial differences between the PNS and CNS in the intrinsic and extrinsic signals that dictate axonal ensheathment, myelin thickness, and the formation of the nodes of Ranvier ([Nave and Werner, 2014](#); [Salzer, 2015](#); [Rasband and Peles, 2021](#)). Of great interest, we observed that the perturbations of the peripheral functions of Caspr2 have functional consequences in HET mice which present motor and coordination deficits, suggesting that such perturbations in humans could lead to the development of peripheral neuropathies, especially non-demyelinating Charcot-Marie-Tooth disease type 2.

## Conclusion

In conclusion, our study demonstrates that both *Cntnap2* heterozygosity and *Cntnap2* null homozygosity impact axon and myelinated fiber development both in the CNS and the PNS, but in a differential manner. It is a first step indicating that *CNTNAP2* alterations may lead to multiple phenotypes. Further experiments will have to be developed to evaluate the consequences on functional connectivity, especially for HET mice. Another challenge will be understanding how a decrease in Caspr2 level in HET mice on one side, and a total absence of the protein in KO mice on the other side, can eventually lead to different or opposite effects. This will require the characterization of the molecular and cellular mechanisms in which Caspr2 is implicated during axon development and myelination. The switch in the level of Caspr2 in whole brain extracts of HET mice from ~35% at early developmental stages to ~50% at later development stages, when compared to WT, supports the possibility that Caspr2 plays major functions before and at the onset of myelination. However, it is unlikely that this switch could be attributed to the functions of Caspr2 in axon and myelin development only. On the contrary, it strongly suggests that *Cntnap2* heterozygosity probably impacts the developmental functions of the protein more broadly. Active phases of dendritic spine formation and synapse development occur from the second week of post-natal development ([Farhy-Tselnicker and Allen, 2018](#)). Therefore, our study raises the need to evaluate the impact of *Cntnap2* heterozygosity on the functions of Caspr2 in these processes as well, to further assess the possible consequences of *CNTNAP2* alterations in neurodevelopmental disorders. It would also be of great interest to conduct similar studies for other members of the Contactin Associated Protein family, which have also been associated with neurodevelopmental disorders such as ASD, especially Caspr3/*CNTNAP3* ([Vaags et al., 2012](#); [Turner et al., 2017](#)), Caspr4/*CNTNAP4* ([Wang et al., 2010](#); [O'Roak et al., 2012](#); [Costa et al., 2022](#)), and Caspr5/*CNTNAP5* ([Pagnamenta et al., 2010](#); [Aleo et al., 2020](#); [Ludington et al., 2020](#)). Little is known about the functions of these three proteins compared to Caspr2. However, Caspr3 and Caspr4 have been implicated in synapse formation and/or



transmission. Very interestingly Caspr4 was shown to act in a gene dose-dependent manner in the structural maturation of interneuron synapses (Karayannis et al., 2014; Shangguan et al., 2018; Tong et al., 2019), suggesting that the modulation of the biological functions by protein levels could be a common feature to the Contactin Associated Proteins.

## Data availability statement

The original contributions presented in this study are included in the article/**Supplementary material**, further inquiries can be directed to the corresponding author.

## Ethics statement

This animal study was reviewed and approved by French Ministry of Higher Education, Research and Innovation (Institute agreement D750522; project agreements APAFIS#5496-2016051915148075 v8 and APAFIS#31520-2021051709364077 v3).

## Author contributions

CC-D was responsible for the preparation of the samples for electron microscopy and for image acquisition, before performing measurements with GC and MS. GC, CG, and LG performed the brain sections and immunostainings to characterize brain morphology. GC and LG were responsible for the conception or design of the work and carried out the measurements. MG and LG performed the other experiments: sciatic nerve teasing and immunostaining and image acquisition and quantification. GC performed Ctip2<sup>+</sup> and Satb2<sup>+</sup> immunostainings and image acquisition and quantification. MD performed electrophysiological recordings. TM performed RT-qPCR experiments. LG performed immunoblots on brain and sciatic extracts and grid-walking test and drafted the work. GC, MG, MD, CL, and LG analyzed the data. All the authors approved the final version of the manuscript.

## Funding

Our salaries and lab were supported by Centre National de la Recherche Scientifique (CNRS), Sorbonne University, Institut National de la Santé et de la Recherche Médicale (Inserm), the French Ministry of Higher Education, Research and Innovation (Ph.D. fellowship GC and MD), the Fondation pour la sclérose en plaques (ARSEP, grant and Ph.D. fellowship GC), the Fédération pour la Recherche sur la Cerveau (FRC, grant), and the Fondation pour la Recherche Médicale (FRM, Ph.D. fellowship TM). The tissue imaging platform at the Institut du Fer à Moulin was supported in part by the Région Ile-de-France and the FRC Rotary. The team was associated during the period of this work with the BioPsy Labex project and the Ecole des Neurosciences de Paris Ile-de-France network.

## Acknowledgments

We thank all members of the lab for their comments and discussions. We are grateful to all the members of the animal facility and of the cellular and tissue imaging platforms for animal care and assistance with microscope. We also thank G. Martinez Lorenzana for help in electron microscopy experiments.

## Conflict of interest

The authors declare that the research was conducted in the absence of any commercial or financial relationships that could be construed as a potential conflict of interest.

## Publisher's note

All claims expressed in this article are solely those of the authors and do not necessarily represent those of their affiliated organizations, or those of the publisher, the editors and the reviewers. Any product that may be evaluated in this article, or claim that may be made by its manufacturer, is not guaranteed or endorsed by the publisher.

## Supplementary material

The Supplementary Material for this article can be found online at: <https://www.frontiersin.org/articles/10.3389/fnins.2023.1100121/full#supplementary-material>

### SUPPLEMENTARY FIGURE 1

Density of callosal projecting neurons in the somatosensory cortex and cortex thickness of E17.5 embryos. Representative images (stacks of 10 confocal images) of the somatosensory cortex (coronal sections) of wild-type (WT), HET, and KO E17.5 embryos immunostained with antibodies directed against Satb2 (green), Ctip2 (red), and L1CAM (white) (A); IZ, intermediate zone; SPL, subplate layer; CP, cortical plate; MZ, marginal zone. Density of Satb2-positive (B) and Ctip2-positive (C) cells in the somatosensory cortex. Cortex thickness measured at the same levels as corpus callosum (CC) thickness (Figure 2G, levels 1 to 5) (D). (B,C) Four animals/genotype, average of measurements on both hemispheres/animal, 25 confocal 1  $\mu$ m-stacks/hemisphere; (D) Six animals/genotype, average of measurements on both hemispheres on one section/animal. Statistical tests: (B,C) One-way ANOVA; (D) Two-way RM ANOVA.

### SUPPLEMENTARY FIGURE 2

Myelin protein levels in brain extracts. Representative immunoblots showing MBP, MAG, PLP, and GAPDH levels in brain extracts of wild-type (WT), HET, and KO mice at P30 and P90 (A). Levels of MBP normalized to GAPDH levels and relative to mean WT (in %) in brain extracts of mice at P10, P15, P30, and P90 (B). Levels of PLP and MAG normalized to GAPDH levels and relative to mean WT (in %) in brain extracts of mice at P30 and P90 (C). Representative immunoblots showing MBP, MAG, and GAPDH levels in extracts from the neocortex and the corpus callosum (CC) of WT, HET, and KO mice at P30 (D). Levels of MBP and MAG normalized to GAPDH levels and relative to mean WT (in %) in extracts from the neocortex and the CC of mice at P30 (E). (A,D) Molecular mass markers positions are shown in kDa on the left of the panels. (B,C,E) 6 animals/genotype/age. Statistical tests: Unpaired *t*-test (E, CC-P30 MAG, Neocortex-P30 MBP and MAG) or Mann-Whitney test (B,E, CC-P30 MBP) to compare HET or KO mice to WT mice, and one-way ANOVA test (B, P10, P30 and P90; E, CC-P30 MAG, Neocortex-P30 MBP and MAG) or Kruskal-Wallis test (A, P15; B,E, CC-P30 MBP) to compare the three genotypes; \**P* < 0.05, \*\**P* < 0.01.

### SUPPLEMENTARY TABLE 1

Statistical tests and results (*P*-values for genotype effect).

## References

- Aleo, S., Milani, D., Pansa, A., Marchisio, P., Guerneri, S., and Silipigni, R. (2020). Autism spectrum disorder and intellectual disability in an inherited 2q14.3 micro-deletion involving CNTNAP5. *Am. J. Med. Genet. A* 182, 3071–3073. doi: 10.1002/ajmg.a.61881
- Anderson, G. R., Galfin, T., Xu, W., Aoto, J., Malenka, R. C., and Sudhof, T. C. (2012). Candidate autism gene screen identifies critical role for cell-adhesion molecule CASPR2 in dendritic arborization and spine development. *Proc. Natl. Acad. Sci. U.S.A.* 109, 18120–18125. doi: 10.1073/pnas.1216398109
- Antoine, M. W., Langberg, T., Schnepel, P., and Feldman, D. E. (2019). Increased excitation-inhibition ratio stabilizes synapse and circuit excitability in four autism mouse models. *Neuron* 101, 648.e4–661.e4. doi: 10.1016/j.neuron.2018.12.026
- Bergles, D. E., and Richardson, W. D. (2015). Oligodendrocyte development and plasticity. *Cold Spring Harb. Perspect. Biol.* 8:a020453. doi: 10.1101/cshperspect.a020453
- Brunner, D., Kabitzke, P., He, D., Cox, K., Thiede, L., Hanania, T., et al. (2015). Comprehensive analysis of the 16p11.2 deletion and null cntnap2 mouse models of autism spectrum disorder. *PLoS One* 10:e0134572. doi: 10.1371/journal.pone.0134572
- Canali, G., Garcia, M., Hivert, B., Pinatel, D., Goullancourt, A., Oguievetskaia, K., et al. (2018). Genetic variants in autism-related CNTNAP2 impair axonal growth of cortical neurons. *Hum. Mol. Genet.* 27, 1941–1954. doi: 10.1093/hmg/ddy102
- Choe, K. Y., Bethlehem, R. A. I., Safrin, M., Dong, H., Salman, E., Li, Y., et al. (2022). Oxytocin normalizes altered circuit connectivity for social rescue of the Cntnap2 knockout mouse. *Neuron* 110, 795.e6–808.e6. doi: 10.1016/j.neuron.2021.11.031
- Costa, A. R., and Sousa, M. M. (2021). The role of the membrane-associated periodic skeleton in axons. *Cell Mol. Life Sci.* 78, 5371–5379. doi: 10.1007/s00018-021-03867-x
- Costa, C. I. S., da Silva Montenegro, E. M., Zarrei, M., de Sa Moreira, E., Silva, I. M. W., de Oliveira Scliar, M., et al. (2022). Copy number variations in a Brazilian cohort with autism spectrum disorders highlight the contribution of cell adhesion genes. *Clin. Genet.* 101, 134–141. doi: 10.1111/cge.14072
- de Faria, O. Jr., Gonsalves, D. G., Nicholson, M., and Xiao, J. (2019). Activity-dependent central nervous system myelination throughout life. *J. Neurochem.* 148, 447–461. doi: 10.1111/jnc.14592
- Denisenko-Nehrbass, N., Oguievetskaia, K., Goutebroze, L., Galvez, T., Yamakawa, H., Ohara, O., et al. (2003). Protein 4.1B associates with both Caspr/paranodin and Caspr2 at paranodes and juxtaparanodes of myelinated fibres. *Eur. J. Neurosci.* 17, 411–416. doi: 10.1046/j.1460-9568.2003.02441.x
- Farhy-Tselnicker, I., and Allen, N. J. (2018). Astrocytes, neurons, synapses: a tripartite view on cortical circuit development. *Neural Dev.* 13:7. doi: 10.1186/s13064-018-0104-y
- Fenlon, L. R., Suarez, R., Lynton, Z., and Richards, L. J. (2021). The evolution, formation and connectivity of the anterior commissure. *Semin. Cell Dev. Biol.* 118, 50–59. doi: 10.1016/j.semcdb.2021.04.009
- Fernandes, D., Santos, S. D., Coutinho, E., Whitt, J. L., Beltrao, N., Rondao, T., et al. (2019). Disrupted AMPA receptor function upon genetic- or antibody-mediated loss of autism-associated CASPR2. *Cereb. Cortex* 29, 4919–4931. doi: 10.1093/cercor/bhz032
- Fingher, N., Dinstein, I., Ben-Shachar, M., Haar, S., Dale, A. M., Eyler, L., et al. (2017). Toddlers later diagnosed with autism exhibit multiple structural abnormalities in temporal corpus callosum fibers. *Cortex* 97, 291–305. doi: 10.1016/j.cortex.2016.12.024
- Frazier, T. W., and Hardan, A. Y. (2009). A meta-analysis of the corpus callosum in autism. *Biol. Psychiatry* 66, 935–941. doi: 10.1016/j.biopsych.2009.07.022
- Galvez-Contreras, A. Y., Zarate-Lopez, D., Torres-Chavez, A. L., and Gonzalez-Perez, O. (2020). Role of Oligodendrocytes and myelin in the pathophysiology of autism spectrum disorder. *Brain Sci.* 10:951. doi: 10.3390/brainsci10120951
- Gao, R., Piguel, N. H., Melendez-Zaidi, A. E., Martin-de-Saavedra, M. D., Yoon, S., Forrest, M. P., et al. (2018). CNTNAP2 stabilizes interneuron dendritic arbors through CASK. *Mol. Psychiatry* 23, 1832–1850. doi: 10.1038/s41380-018-0027-3
- Gao, R., Zaccard, C. R., Shapiro, L. P., Dionisio, L. E., Martin-de-Saavedra, M. D., Piguel, N. H., et al. (2019). The CNTNAP2-CASK complex modulates GluA1 subcellular distribution in interneurons. *Neurosci. Lett.* 701, 92–99. doi: 10.1016/j.neulet.2019.02.025
- Gdalyahu, A., Lazaro, M., Penagarikano, O., Golshani, P., Trachtenberg, J. T., and Geschwind, D. H. (2015). The autism related protein contactin-associated protein-like 2 (CNTNAP2) stabilizes new spines: an *in vivo* mouse study. *PLoS One* 10:e0125633. doi: 10.1371/journal.pone.0125633
- Gordon, A., Adamsky, K., Vainshtein, A., Frechter, S., Dupree, J. L., Rosenbluth, J., et al. (2014). Caspr and caspr2 are required for both radial and longitudinal organization of myelinated axons. *J. Neurosci.* 34, 14820–14826. doi: 10.1523/JNEUROSCI.3369-14.2014
- Gordon, A., Salomon, D., Barak, N., Pen, Y., Tsoory, M., Kimchi, T., et al. (2016). Expression of Cntnap2 (Caspr2) in multiple levels of sensory systems. *Mol. Cell. Neurosci.* 70, 42–53. doi: 10.1016/j.mcn.2015.11.012
- Hoyer, H., Braathen, G. J., Eek, A. K., Nordang, G. B., Skjelbred, C. F., and Russell, M. B. (2015). Copy number variations in a population-based study of Charcot-Marie-Tooth disease. *BioMed. Res. Int.* 2015:960404. doi: 10.1155/2015/960404
- Hughes, A. N., and Appel, B. (2019). Oligodendrocytes express synaptic proteins that modulate myelin sheath formation. *Nat. Commun.* 10:4125. doi: 10.1038/s41467-019-12059-y
- Inda, M. C., DeFelipe, J., and Munoz, A. (2006). Voltage-gated ion channels in the axon initial segment of human cortical pyramidal cells and their relationship with chandelier cells. *Proc. Natl. Acad. Sci. U.S.A.* 103, 2920–2925. doi: 10.1073/pnas.0511197103
- Jang, W. E., Park, J. H., Park, G., Bang, G., Na, C. H., Kim, J. Y., et al. (2022). Cntnap2-dependent molecular networks in autism spectrum disorder revealed through an integrative multi-omics analysis. *Mol. Psychiatry* [Epub ahead of print]. doi: 10.1038/s41380-022-01822-1
- Karayannis, T., Au, E., Patel, J. C., Kruglikov, I., Markx, S., Delorme, R., et al. (2014). Cntnap4 differentially contributes to GABAergic and dopaminergic synaptic transmission. *Nature* 511, 236–240. doi: 10.1038/nature13248
- Kastriti, M. E., Stratigi, A., Mariatos, D., Theodosiou, M., Savvaki, M., Kavkova, M., et al. (2019). Ablation of CNTN2+ pyramidal neurons during development results in defects in neocortical size and axonal tract formation. *Front. Cell. Neurosci.* 13:454. doi: 10.3389/fncel.2019.00454
- Ku, R. Y., and Torii, M. (2020). New molecular players in the development of callosal projections. *Cells* 10:29. doi: 10.3390/cells10010029
- Lazaro, M. T., Taxis, J., Shuman, T., Bachmutsky, I., Ikrar, T., Santos, R., et al. (2019). Reduced prefrontal synaptic connectivity and disturbed oscillatory population dynamics in the CNTNAP2 model of Autism. *Cell Rep.* 27, 2567.e6–2578.e6. doi: 10.1016/j.celrep.2019.05.006
- Liska, A., Bertero, A., Gomolka, R., Sabbioni, M., Galbusera, A., Barsotti, N., et al. (2018). Homozygous loss of autism-risk gene CNTNAP2 results in reduced local and long-range prefrontal functional connectivity. *Cereb. Cortex* 28, 1141–1153. doi: 10.1093/cercor/bhx022
- Ludington, E. G., Yu, S., Bae, H. A., and Barnett, C. P. (2020). Novel de novo 2q14.3 deletion disrupting CNTNAP5 in a girl with intellectual impairment, thin corpus callosum, and microcephaly. *Am. J. Med. Genet. A* 182, 1824–1828. doi: 10.1002/ajmg.a.61592
- Marques, S., Zeisel, A., Codeluppi, S., van Bruggen, D., Mendanha Falcao, A., Xiao, L., et al. (2016). Oligodendrocyte heterogeneity in the mouse juvenile and adult central nervous system. *Science* 352, 1326–1329. doi: 10.1126/science.aaf6463
- Martin, P. M., Cifuentes-Diaz, C., Devaux, J., Garcia, M., Bureau, J., Thomasseau, S., et al. (2017). Schwannomin-interacting protein 1 isoform IQCJ-SCHIP1 is a multipartner ankyrin- and spectrin-binding protein involved in the organization of nodes of Ranvier. *J. Biol. Chem.* 292, 2441–2456. doi: 10.1074/jbc.M116.758029
- Martin-Lopez, E., Meller, S. J., and Greer, C. A. (2018). Development of piriform cortex interhemispheric connections via the anterior commissure: progressive and regressive strategies. *Brain Struct. Funct.* 223, 4067–4085. doi: 10.1007/s00429-018-1741-y
- Menegoz, M., Gaspar, P., Le Bert, M., Galvez, T., Burgaya, F., Palfrey, C., et al. (1997). Paranodin, a glycoprotein of neuronal paranodal membranes. *Neuron* 19, 319–331. doi: 10.1016/s0896-6273(00)80942-3
- Mensch, S., Baraban, M., Almeida, R., Czopka, T., Ausborn, J., El Manira, A., et al. (2015). Synaptic vesicle release regulates myelin sheath number of individual oligodendrocytes in vivo. *Nat. Neurosci.* 18, 628–630. doi: 10.1038/nn.3991
- Nave, K. A., and Werner, H. B. (2014). Myelination of the nervous system: mechanisms and functions. *Annu. Rev. Cell Dev. Biol.* 30, 503–533. doi: 10.1146/annurev-cellbio-100913-013101
- Nishikimi, M., Oishi, K., and Nakajima, K. (2013). Axon guidance mechanisms for establishment of callosal connections. *Neural Plast.* 2013:149060. doi: 10.1155/2013/149060
- Ogawa, Y., Horresh, I., Trimmer, J. S., Bredt, D. S., Peles, E., and Rasband, M. N. (2008). Postsynaptic density-93 clusters Kv1 channels at axon initial segments independently of Caspr2. *J. Neurosci.* 28, 5731–5739. doi: 10.1523/JNEUROSCI.4431-07.2008
- O’Roak, B. J., Vives, L., Girirajan, S., Karakoc, E., Krumm, N., Coe, B. P., et al. (2012). Sporadic autism exomes reveal a highly interconnected protein network of de novo mutations. *Nature* 485, 246–250. doi: 10.1038/nature10989
- Pagnamenta, A. T., Bacchelli, E., de Jonge, M. V., Mirza, G., Scerri, T. S., Minopoli, F., et al. (2010). Characterization of a family with rare deletions in CNTNAP5 and DOK4 suggests novel risk loci for autism and dyslexia. *Biol. Psychiatry* 68, 320–328. doi: 10.1016/j.biopsych.2010.02.002
- Penagarikano, O., Abrahams, B. S., Herman, E. I., Winden, K. D., Gdalyahu, A., Dong, H., et al. (2011). Absence of CNTNAP2 leads to epilepsy, neuronal migration abnormalities, and core autism-related deficits. *Cell* 147, 235–246. doi: 10.1016/j.cell.2011.08.040
- Pinatel, D., Hivert, B., Boucraut, J., Saint-Martin, M., Rogemond, V., Zoupi, L., et al. (2015). Inhibitory axons are targeted in hippocampal cell culture by anti-Caspr2 autoantibodies associated with limbic encephalitis. *Front. Cell. Neurosci.* 9:265. doi: 10.3389/fncel.2015.00265
- Poliak, S., Gollan, L., Martinez, R., Custer, A., Einheber, S., Salzer, J. L., et al. (1999). Caspr2, a new member of the neurexin superfamily, is localized at the juxtaparanodes of myelinated axons and associates with K+ channels. *Neuron* 24, 1037–1047. doi: 10.1016/s0896-6273(00)81049-1
- Poliak, S., Salomon, D., Elhanany, H., Sabanay, H., Kiernan, B., Pevny, L., et al. (2003). Juxtaparanodal clustering of Shaker-like K+ channels in myelinated axons depends on Caspr2 and TAG-1. *J. Cell Biol.* 162, 1149–1160. doi: 10.1083/jcb.200305018

- Poot, M. (2015). Connecting the CNTNAP2 networks with neurodevelopmental disorders. *Mol. Syndromol.* 6, 7–22. doi: 10.1159/000371594
- Poot, M. (2017). Intragenic CNTNAP2 deletions: a bridge too far? *Mol. Syndromol.* 8, 118–130. doi: 10.1159/000456021
- Rasband, M. N., and Peles, E. (2021). Mechanisms of node of Ranvier assembly. *Nat. Rev. Neurosci.* 22, 7–20. doi: 10.1038/s41583-020-00406-8
- Rodenas-Cuadrado, P., Ho, J., and Vernes, S. C. (2014). Shining a light on CNTNAP2: complex functions to complex disorders. *Eur. J. Hum. Genet.* 22, 171–178. doi: 10.1038/ejhg.2013.100
- Saint-Martin, M., Joubert, B., Pelletier-Monnin, V., Pascual, O., Noraz, N., and Honnorat, J. (2018). Contactin-associated protein-like 2, a protein of the neuroligin family involved in several human diseases. *Eur. J. Neurosci.* 48, 1906–1923. doi: 10.1111/ejn.14081
- Salzer, J. L. (2015). Schwann cell myelination. *Cold Spring Harb. Perspect. Biol.* 7:a020529. doi: 10.1101/cshperspect.a020529
- Scott, R., Sanchez-Aguilera, A., van Elst, K., Lim, L., Dehorter, N., Bae, S. E., et al. (2017). Loss of Cntnap2 causes axonal excitability deficits, developmental delay in cortical myelination, and abnormal stereotyped motor behavior. *Cereb. Cortex* 29, 1–12. doi: 10.1093/cercor/bhx341
- Shangguan, Y., Xu, X., Ganbat, B., Li, Y., Wang, W., Yang, Y., et al. (2018). CNTNAP4 impacts epilepsy through GABAA receptors regulation: evidence from temporal lobe epilepsy patients and mouse models. *Cereb. Cortex* 28, 3491–3504. doi: 10.1093/cercor/bhx215
- Stassart, R. M., Mobius, W., Nave, K. A., and Edgar, J. M. (2018). The axon-myelin unit in development and degenerative disease. *Front. Neurosci.* 12:467. doi: 10.3389/fnins.2018.00467
- Sturrock, R. R. (1980). Myelination of the mouse corpus callosum. *Neuropathol. Appl. Neurobiol.* 6, 415–420. doi: 10.1111/j.1365-2990.1980.tb00219.x
- Suarez, R., Gobius, I., and Richards, L. J. (2014). Evolution and development of interhemispheric connections in the vertebrate forebrain. *Front. Hum. Neurosci.* 8:497. doi: 10.3389/fnhum.2014.00497
- Tong, D. L., Chen, R. G., Lu, Y. L., Li, W. K., Zhang, Y. F., Lin, J. K., et al. (2019). The critical role of ASD-related gene CNTNAP3 in regulating synaptic development and social behavior in mice. *Neurobiol. Dis.* 130:104486. doi: 10.1016/j.nbd.2019.104486
- Traka, M., Goutebroze, L., Denisenko, N., Bessa, M., Nifli, A., Havaki, S., et al. (2003). Association of TAG-1 with Caspr2 is essential for the molecular organization of juxtaparanodal regions of myelinated fibers. *J. Cell Biol.* 162, 1161–1172.
- Turner, T. N., Coe, B. P., Dickel, D. E., Hoekzema, K., Nelson, B. J., Zody, M. C., et al. (2017). Genomic patterns of de novo mutation in simplex autism. *Cell* 171, 710.e2–722.e2. doi: 10.1016/j.cell.2017.08.047
- Vaags, A. K., Lionel, A. C., Sato, D., Goodenberger, M., Stein, Q. P., Curran, S., et al. (2012). Rare deletions at the neuroligin 3 locus in autism spectrum disorder. *Am. J. Hum. Genet.* 90, 133–141. doi: 10.1016/j.ajhg.2011.11.025
- Varea, O., Martin-de-Saavedra, M. D., Kopeikina, K. J., Schurmann, B., Fleming, H. J., Fawcett-Patel, J. M., et al. (2015). Synaptic abnormalities and cytoplasmic glutamate receptor aggregates in contactin associated protein-like 2/Caspr2 knockout neurons. *Proc. Natl. Acad. Sci. U.S.A.* 112, 6176–6181. doi: 10.1073/pnas.1423205112
- Vogt, D., Cho, K. K. A., Shelton, S. M., Paul, A., Huang, Z. J., Sohal, V. S., et al. (2018). Mouse Cntnap2 and human CNTNAP2 ASD alleles cell autonomously regulate PV+ cortical interneurons. *Cereb. Cortex* 28, 3868–3879. doi: 10.1093/cercor/bhx248
- Wang, L. S., Hranilovic, D., Wang, K., Lindquist, I. E., Yurcaba, L., Petkovic, Z. B., et al. (2010). Population-based study of genetic variation in individuals with autism spectrum disorders from Croatia. *BMC Med. Genet.* 11:134. doi: 10.1186/1471-2350-11-134
- Wolff, J. J., Gerig, G., Lewis, J. D., Soda, T., Styner, M. A., Vachet, C., et al. (2015). Altered corpus callosum morphology associated with autism over the first 2 years of life. *Brain* 138, 2046–2058. doi: 10.1093/brain/awv118
- Zerbi, V., Ielacqua, G. D., Markicevic, M., Haberl, M. G., Ellisman, M. H., A-Bhaskaran, A., et al. (2018). Dysfunctional autism risk genes cause circuit-specific connectivity deficits with distinct developmental trajectories. *Cereb. Cortex* 28, 2495–2506. doi: 10.1093/cercor/bhy046
- Zhou, R., Han, B., Nowak, R., Lu, Y., Heller, E., Xia, C., et al. (2022). Proteomic and functional analyses of the periodic membrane skeleton in neurons. *Nat. Commun.* 13:3196. doi: 10.1038/s41467-022-30720-x



## OPEN ACCESS

## EDITED BY

Fiona Francis,  
INSERM U839 Institut du Fer à Moulin (IFM),  
France

## REVIEWED BY

Marie-Claude Potier,  
Centre National de la Recherche Scientifique  
(CNRS), France  
Marika Nosten-Bertrand,  
Institut National de la Santé et de la Recherche  
Médicale (INSERM), France  
Shinji Hirotsune,  
Osaka City University, Japan

## \*CORRESPONDENCE

Edna Grünblatt  
✉ edna.gruenblatt@kjp.d.uzh.ch

## SPECIALTY SECTION

This article was submitted to  
Translational Neuroscience,  
a section of the journal  
Frontiers in Neuroscience

RECEIVED 22 November 2022

ACCEPTED 31 January 2023

PUBLISHED 16 February 2023

## CITATION

Grünblatt E, Homolak J, Babic Perhoc A,  
Davor V, Knezovic A, Osmanovic Barilar J,  
Riederer P, Walitza S, Tackenberg C and  
Salkovic-Petrisic M (2023) From  
attention-deficit hyperactivity disorder  
to sporadic Alzheimer's disease—Wnt/mTOR  
pathways hypothesis.  
*Front. Neurosci.* 17:1104985.  
doi: 10.3389/fnins.2023.1104985

## COPYRIGHT

© 2023 Grünblatt, Homolak, Babic Perhoc,  
Davor, Knezovic, Osmanovic Barilar, Riederer,  
Walitza, Tackenberg and Salkovic-Petrisic. This  
is an open-access article distributed under the  
terms of the [Creative Commons Attribution  
License \(CC BY\)](https://creativecommons.org/licenses/by/4.0/). The use, distribution or  
reproduction in other forums is permitted,  
provided the original author(s) and the  
copyright owner(s) are credited and that the  
original publication in this journal is cited, in  
accordance with accepted academic practice.  
No use, distribution or reproduction is  
permitted which does not comply with  
these terms.

# From attention-deficit hyperactivity disorder to sporadic Alzheimer's disease—Wnt/mTOR pathways hypothesis

Edna Grünblatt<sup>1,2,3\*</sup>, Jan Homolak<sup>4</sup>, Ana Babic Perhoc<sup>4</sup>,  
Virag Davor<sup>4</sup>, Ana Knezovic<sup>4</sup>, Jelena Osmanovic Barilar<sup>4</sup>,  
Peter Riederer<sup>5,6</sup>, Susanne Walitza<sup>1,2,3</sup>, Christian Tackenberg<sup>2,7</sup>  
and Melita Salkovic-Petrisic<sup>4</sup>

<sup>1</sup>Department of Child and Adolescent Psychiatry and Psychotherapy, Psychiatric University Hospital Zurich (PUK), University of Zurich, Zurich, Switzerland, <sup>2</sup>Neuroscience Center Zurich, University of Zurich and the Swiss Federal Institute of Technology (ETH) Zurich, Zurich, Switzerland, <sup>3</sup>Zurich Center for Integrative Human Physiology, University of Zurich, Zurich, Switzerland, <sup>4</sup>Department of Pharmacology and Croatian Institute for Brain Research, University of Zagreb School of Medicine, Zagreb, Croatia, <sup>5</sup>Department of Psychiatry, Psychosomatics and Psychotherapy, Center of Mental Health, University Hospital Würzburg, Würzburg, Germany, <sup>6</sup>Department and Research Unit of Psychiatry, Institute of Clinical Research, University of Southern Denmark, Odense, Denmark, <sup>7</sup>Institute for Regenerative Medicine (IREM), University of Zurich, Schlieren, Switzerland

Alzheimer's disease (AD) is the most common neurodegenerative disorder with the majority of patients classified as sporadic AD (sAD), in which etiopathogenesis remains unresolved. Though sAD is argued to be a polygenic disorder, apolipoprotein E (APOE) ε4, was found three decades ago to pose the strongest genetic risk for sAD. Currently, the only clinically approved disease-modifying drugs for AD are aducanumab (Aduhelm) and lecanemab (Leqembi). All other AD treatment options are purely symptomatic with modest benefits. Similarly, attention-deficit hyperactivity disorder (ADHD), is one of the most common neurodevelopmental mental disorders in children and adolescents, acknowledged to persist in adulthood in over 60% of the patients. Moreover, for ADHD whose etiopathogenesis is not completely understood, a large proportion of patients respond well to treatment (first-line psychostimulants, e.g., methylphenidate/MPH), however, no disease-modifying therapy exists. Interestingly, cognitive impairments, executive, and memory deficits seem to be common in ADHD, but also in early stages of mild cognitive impairment (MCI), and dementia, including sAD. Therefore, one of many hypotheses is that ADHD and sAD might have similar origins or that they intercalate with one another, as shown recently that ADHD may be considered a risk factor for sAD. Intriguingly, several overlaps have been shown between the two disorders, e.g., inflammatory activation, oxidative stress, glucose and insulin pathways, wingless-INT/mammalian target of rapamycin (Wnt/mTOR) signaling, and altered lipid metabolism. Indeed, Wnt/mTOR activities were found to be modified by MPH in several ADHD studies. Wnt/mTOR was also found to play a role in sAD and in animal models of the disorder. Moreover, MPH treatment in the MCI phase was shown to be successful for apathy including some improvement in cognition, according to a recent meta-analysis. In several AD animal models, ADHD-like behavioral phenotypes have been observed indicating a possible interconnection between ADHD and AD. In this concept paper, we will discuss



the various evidence in human and animal models supporting the hypothesis in which ADHD might increase the risk for sAD, with common involvement of the Wnt/mTOR-pathway leading to lifespan alteration at the neuronal levels.

#### KEYWORDS

Alzheimer's disease, Wnt/mTOR, cognitive impairment, glucose/insulin, oxidative stress, methylphenidate, attention-deficit hyperactivity disorder (ADHD), mild cognitive impairment (MCI)

## 1. Introduction

The orchestration of brain development, maturation, plasticity, repair, and survival is highly complex, in which any imbalance in one or more of these processes may induce disruptions manifested at different stages of life, from the neurodevelopmental disorders at the early stages to neurodegeneration of the brain in late stage (Feldes et al., 2015). These opposite ends of the timeline may appear unrelated, as in the case of attention-deficit hyperactivity disorder (ADHD) and Alzheimer's disease (AD), which represent mental disorders affecting the early and late ends of lifespan, respectively. However, literature data indicates there are some overlaps between ADHD and AD (Kakuszi et al., 2020; Zhang et al., 2022). In this article, we will lay down the current evidence proposing the involvement of important pathways, participating in many of the above lifelong processes in the brain, i.e., the wingless-INT (Wnt), and the mammalian target of rapamycin (mTOR) (Wnt/mTOR) pathway, as a common link between ADHD and AD, and a target for a drug that can therefore act therapeutically in both diseases (Kovacs et al., 2014; Lee, 2015; Noelanders and Vleminckx, 2017; Palomer et al., 2019; Marchetti et al., 2020; Ishikawa and Ishikawa, 2022).

Before delving deep into our hypothesis, some comparisons between ADHD and AD are presented in **Table 1**. ADHD is the most common neurodevelopmental mental disorder in children and adolescents that presents as inattentiveness, hyperactivity, impulsivity, and emotional dysregulation (Faraone et al., 2015). Though considered a childhood disorder, in about 60% of the cases it persists into adulthood (Franke et al., 2018; Di Lorenzo et al., 2021; Song et al., 2021). ADHD is characterized by high heritability (77–88%) (Faraone and Larsson, 2019), however, current evidence suggests that the development of the disease is driven by complex interactions of composite polygenic and multiple environmental factors that undermine developmental processes resulting in altered brain connectivity and structure (Castellanos and Tannock, 2002; Faraone et al., 2015). On the other hand, AD is the most common neurodegenerative disorder that poses a substantial socioeconomic burden on society (Sontheimer et al., 2021; Velandia et al., 2022). A fully penetrant autosomal dominant inheritance of amyloid precursor protein (APP), presenilin-1 (PS1), or presenilin-2 (PS2) mutations drives the development of the disease in a small fraction of patients [0.5–1%; familial AD (fAD)], however for the remaining 99% classified as sporadic AD (sAD), the etiopathogenesis remains unresolved (Reitz et al., 2020). Although, sAD seems to be a polygenic disorder, the most prominent locus, apolipoprotein E (APOE), found already three decades ago, was confirmed to have

the strongest genetic risk for sAD in the most recent and largest genome-wide association meta-analysis study (meta-GWAS), with APOE  $\epsilon 4$  as the risk allele4 (de Rojas et al., 2021; Wightman et al., 2021; Bellenguez et al., 2022). At first glance, no common mechanism seems to link these two diseases together. However, several recent overviews have discussed their complementary phenomena (Feldes et al., 2015; Callahan et al., 2017), and possible genetic overlaps (Garcia-Argibay et al., 2022; Leffa et al., 2022).

In the current paper, we present our hypothesis of the Wnt/mTOR pathway playing a role both in ADHD and sAD pathophysiology, which may explain the recent findings of ADHD as a risk for sAD (Tzeng et al., 2019; Dobrosavljevic et al., 2021; Zhang et al., 2022). Furthermore, we discuss the possible therapeutic potentials of the psychostimulant methylphenidate (MPH) which, by affecting the Wnt/mTOR pathway, might be beneficial in both disorders.

## 2. Current knowledge of Alzheimer's disease pathology, insulin resistance, and diabetes mellitus

Alzheimer's disease is a neurodegenerative disorder and the most common form of dementia with an estimated number of 55 million people currently suffering from AD worldwide, predicted to reach 78 million in 2030 and 139 million in 2050 (Alzheimer's Disease International, 2022). The well-known neuropathological hallmarks of AD are an accumulation of misfolded proteins, amyloid  $\beta$  ( $A\beta$ ) in the forms of extracellular plaques and hyperphosphorylated Tau protein in the form of neurofibrillary tangles, accompanied by synaptic loss (Sanabria-Castro et al., 2017; **Table 1**). Less common early onset disease (predominantly fAD) is associated with autosomal dominant missense gene mutations in PS1 and PS2 or APP. On the contrary, the most common, late-onset or sAD form (>95% of all AD cases) is of unknown origin, and is considered polygenic (de Rojas et al., 2020; Wightman et al., 2021; Bellenguez et al., 2022; **Table 1**). Though the sAD etiopathogenesis is still unclear, several hypotheses in addition to the most prominent, the amyloid hypothesis (Hampel et al., 2021), have been suggested. Recently, sAD has been acknowledged as a metabolic disease with characteristic neurodegenerative processes possibly being caused by brain insulin resistance (BIR) and metabolic dysfunction in the brain (De Felice et al., 2014; Bloom et al., 2018; Kellar and Craft, 2020; Alves et al., 2021). Current epidemiological and environmental studies suggest that type 2

TABLE 1 Current knowledge in attention-deficit hyperactivity disorder (ADHD) and Alzheimer's disease (AD)- A comparison.

	ADHD		AD	
Definition	Neurodevelopmental mental disorder	<a href="#">American Psychiatric Association (2013)</a>	–	
	–		Neurodegenerative mental disorder	<a href="#">American Psychiatric Association (2013)</a>
Demographics	Prevalence ca 5% world-wide in child and adolescent	<a href="#">Sayal et al. (2018)</a>	Prevalence ca 0.7% old dementia world-wide in old aged individuals	<a href="#">GBD 2019 Dementia Forecasting Collaborators (2022)</a>
	Persisting into adulthood ca 60% of pediatric ADHD	<a href="#">Fayyad et al. (2017)</a> ; <a href="#">Franke et al. (2018)</a>	–	
	Childhood: male to female 3:1 Adulthood: male to female 1.6:1	<a href="#">Willcutt (2012)</a> ; <a href="#">Sayal et al. (2018)</a>	– Old age: male to female 1:1.67	<a href="#">Podcasy and Epperson (2016)</a>
Genetics	n.a.		1% Familial AD ( <i>APP</i> , <i>PS1</i> and <i>PS2</i> )	<a href="#">Serretti et al. (2007)</a>
	Heritability ( $h^2$ ) ca 70% and polygenic	<a href="#">Demontis et al. (2019, 2023)</a> ; <a href="#">Faraone and Larsson (2019)</a>	Heritability ( $h^2$ ) ca 58–70% and polygenic including <i>APOEε4</i> as risk allele	<a href="#">Sims et al. (2020)</a> ; <a href="#">de Rojas et al. (2021)</a> ; <a href="#">Wightman et al. (2021)</a>
Main clinical phenotypes	Inattention, hyperactivity, impulsivity	<a href="#">American Psychiatric Association (2013)</a>	–	
	–		Cognitive decline	<a href="#">American Psychiatric Association (2013)</a>
	Executive dysfunction	<a href="#">Pineda et al. (1998)</a> ; <a href="#">Willcutt et al. (2005)</a>	Executive dysfunction	<a href="#">Swanberg et al. (2004)</a> ; <a href="#">Baudic et al. (2006)</a>
Comorbidity	Depression Anxiety ASD Bipolar in adulthood Sleep disorder	<a href="#">Jensen and Steinhausen (2015)</a> ; <a href="#">Wajszilber et al. (2018)</a> ; <a href="#">Mayer et al. (2021)</a> ; <a href="#">Sandstrom et al. (2021)</a> ; <a href="#">Schweck et al. (2021)</a>	Depression Anxiety – – Sleep disorder	<a href="#">Zhao et al. (2016)</a> ; <a href="#">Kuring et al. (2020)</a>
	T2DM Metabolic syndrome Hypertension	<a href="#">Chen et al. (2018)</a> ; <a href="#">Landau and Pinhas-Hamiel (2019)</a> ; <a href="#">Wang et al. (2021)</a> ; <a href="#">Ai et al. (2022)</a>	T2DM Metabolic syndrome Hypertension	<a href="#">Wang et al. (2018)</a> ; <a href="#">Qin J. et al. (2021)</a> ; <a href="#">Zuin et al. (2021)</a> ; <a href="#">Antal et al. (2022)</a>
Treatment	Only reducing symptoms: psychostimulants (e.g., methylphenidate, dexamphetamine, lisdexamphetamine), non-psychostimulants (e.g., atomoxetine, guanfacine)	<a href="#">Banaschewski et al. (2018)</a>	Only reducing symptoms: acetylcholinesterase (AChE) inhibitors and memantine	<a href="#">National Institute on Aging (2021)</a>
	n.a.		Possible disease-modifying: aducanumab	<a href="#">National Institute on Aging (2021)</a>
Affected brain regions	Cerebral cortex (forebrain) Basal ganglia Amygdala Hippocampus	<a href="#">Hoogman et al. (2017)</a>	Cerebral cortex (medial and superior frontal gyrus) Putamen Amygdala Hippocampus	<a href="#">Li et al. (2012, 2015)</a> ; <a href="#">Lupton et al. (2016)</a> ; <a href="#">Roe et al. (2021)</a> ; <a href="#">Planche et al. (2022)</a>
Current hypothesis to etiopathology	Neuronal maturation delays	<a href="#">Shaw et al. (2007)</a> ; <a href="#">Hoogman et al. (2017)</a>	–	
	–		Pathological Amyloid- $\beta$	<a href="#">Hampel et al. (2021)</a>
	Dopaminergic deficit theory	<a href="#">Gonon (2009)</a>	–	
	–		Pathological Tau forms and neurofibrillary tangles	<a href="#">Hasani et al. (2021)</a>
	–		Cholinergic neuronal damage	<a href="#">Lyness et al. (2003)</a>
	–		APOE cascade hypothesis	<a href="#">Martens et al. (2022)</a>
	Excitatory/inhibitory imbalance theory	<a href="#">Selten et al. (2018)</a>	Excitatory/inhibitory imbalance theory	<a href="#">Shu et al. (2022)</a> ; <a href="#">van den Berg et al. (2022)</a> ; <a href="#">Wood et al. (2022)</a>
	Oxidative stress and mitochondria dysfunction	<a href="#">Corona (2020)</a>	Oxidative stress and mitochondria dysfunction	<a href="#">Mittal et al. (2022)</a>
	Neuroinflammation	<a href="#">Misiak et al. (2022)</a>	Neuroinflammation	<a href="#">Kinney et al. (2018)</a>
	Energy metabolism- cerebral glucose hypometabolism	<a href="#">Zametkin et al. (1990)</a>	Energy metabolism- cerebral glucose hypometabolism; brain insulin resistance	<a href="#">Kellar and Craft (2020)</a> ; <a href="#">Strom et al. (2022)</a>

APOE, apolipoprotein E; ASD, autism spectrum disorder; n.a., not available; –, not relevant; T2DM, Type 2 diabetes mellitus.

diabetes mellitus (T2DM) increases the risk of developing sAD (Xue et al., 2019; Rebelos et al., 2021). Recently, a polygenic risk score (PRS) for T2DM was found to predict the conversion of amnesic mild cognitive impairment (MCI) to sAD, with shared genes highly expressed in cortical neurons; neuronal development and generation, cell junction and projection, and phosphatidylinositol 3-kinase (PI3K), protein kinase B (Akt) and mitogen-activated protein kinase (MAPK) signaling pathway (Yang et al., 2022). There are many shared pathological findings in the brain of sAD and T2DM patients that should not be overlooked. These include impaired glucose metabolism, impaired insulin signaling, the accumulation of advanced glycation end products, mitochondrial dysfunction, increased inflammation and elevated oxidative stress, which altogether support the hypothesis of sAD as a specific form of metabolic brain disorder (Kubis-Kubiak et al., 2019; Austad et al., 2022; Pakdin et al., 2022).

Brain insulin resistance is characterized by a reduced response to insulin signaling downstream of the insulin receptor (IR) in the brain, consequently leading to metabolic alteration, neurodegeneration, and cognitive impairment (Kullmann et al., 2017; Kellar and Craft, 2020). 18F-fluorodeoxyglucose-positron emission tomography (FDG-PET), revealed that individuals with reduced FDG-PET brain metabolism are prone to a much faster cognitive decline and brain atrophy compared to individuals without significantly impaired FDG-PET uptake (Ou et al., 2019), indicating the importance of glucose hypometabolism and BIR in sAD development. In postmortem studies, sAD patients demonstrate decreased brain insulin levels, diminished levels of IR protein and mRNA, as well as altered levels of components downstream of the IR signaling cascade (Frölich et al., 1998; Bartl et al., 2013a; Riederer et al., 2017). BIR has been analyzed in the hippocampal fields CA1–CA3, the dentate gyrus, and the subiculum, which develop marked AD pathology starting in the early phase of the disease, and in the cerebellar cortex, which develops limited pathology seen only in the late phase of AD (Talbot et al., 2012). The markedly reduced insulin signaling downstream of the IR→IR substrate-1 (IRS-1)→PI3K signaling pathway was found postmortem in the hippocampal and cerebellar cortex in sAD patients without diabetes (Talbot et al., 2012). The major finding was the elevated Serine phosphorylation of IRS-1 on epitopes pS616 and pS636 in the hippocampal and cerebellar cortex, which is a feature of insulin resistance in peripheral tissues (Talbot et al., 2012; Yarchan et al., 2014).

The state of BIR, clinically defined as failure of insulin (delivered into the brain *via* the intranasal route to bypass the blood-brain barrier) to elicit a neuroimaging (FDG-PET or functional magnetic resonance imaging) or neurophysiological (e.g., electroencephalography) appears to be an early and common feature in human AD patients (Henri et al., 2015; Kullmann et al., 2016; Kellar and Craft, 2020). BIR can lead to energy misbalance manifesting as mitochondrial dysfunction and an increase in oxidative stress (Reddy, 2014). This may shed new light on the previously proposed hypotheses of sAD, which have emphasized the involvement of oxidative stress and mitochondria dysfunction as well as neuroinflammation in the disease etiopathogenesis (Munch et al., 1998; Bachiller et al., 2018; Monterey et al., 2021). As the mitochondria are the power suppliers of the cell, their damage observed in sAD can be deleterious for neurons, astrocytes,

and microglia. The decrease in functionality and changes in the morphology of mitochondria is observed postmortem in the brains of AD patients (Moreira, 2012; Macdonald et al., 2018). Altogether, different studies found a decrease in complex I, III, and IV, as well as the decreased expression of subunits from all complexes in the entorhinal cortex of AD patients postmortem (Kim et al., 2000; Armand-Ugon et al., 2017; Macdonald et al., 2018; Holper et al., 2019). All of the above leads to impaired oxidative phosphorylation, decreased production of ATP, and an increase in oxidative stress, features well documented in AD (Wang et al., 2014; Flannery and Trushina, 2019). Additionally, changes in the mitochondrial turnover (fusion and fission) were detected, causing the irregular distribution and function of mitochondria in neurons and microglia (Wilkins et al., 2017). BIR and consequent mitochondrial dysfunction lead to energy deprivation and oxidative stress, causing neuronal damage and activation of astrocytes and microglial cells (Wilkins et al., 2017). Dysregulated microglial and astrocyte function and alterations in their morphology have been related to inflammatory changes observed in sAD (Damani et al., 2011; Mosher and Wyss-Coray, 2014; Monterey et al., 2021). Moreover, aged astrocytes and microglia show altered responses to extracellular ATP signals compared to young cells (Damani et al., 2011; Monterey et al., 2021). Degenerated neurons appear to be surrounded by activated astrocytes and microglia in aging and neurodegenerative diseases (Bachiller et al., 2018; Monterey et al., 2021). Eventually, damaged astrocytes and microglia also undergo metabolic reprogramming due to glucose deprivation, shifting their glucose preference to fatty acids for energy production. This profound metabolic change can be directly linked to oxidative stress and inflammation (Flowers et al., 2017; Monterey et al., 2021).

So far, the anti-Aβ antibodies aducanumab and lecanemab are the only clinically approved disease-modifying drugs for the treatment of AD. Both were recently granted accelerated approval by the U.S. Food and Drug Administration (U.S. Food & Drugs Administration, 2021, 2023). This procedure allows for earlier approval of drugs to treat serious conditions and highlights the unmet medical need for AD treatment options. Thus, there is still the demand for further effective therapies for sAD and involvement of BIR, together with the integration of all of these changes found in sAD, might be crucial in developing novel prevention and treatment strategies.

### 3. Attention-deficit hyperactivity disorder current genetic and etiology hypothesis

As indicated in the introduction, ADHD is a highly heritable neurodevelopmental disorder (Faraone and Larsson, 2019), currently known to be associated with a polygenetic predisposition. In the most recent GWAS, including a total of 38'691 ADHD patients and 186'843 controls, 27 genome-wide significant loci were found to associate with ADHD risk (Demontis et al., 2023). As found previously using neuroimaging meta-analysis (Hoogman et al., 2017), frontal cortex and midbrain dopaminergic neurons were highly associated with ADHD genes (Demontis et al., 2023). Indeed, ADHD was found to be highly

polygenic, with around seven thousand gene variants explaining 90% of the single nucleotide polymorphism (SNP) heritability ( $h^2$ ) (Demontis et al., 2023). Moreover, gene enrichment analysis found enrichment in genes upregulated during early embryonic brain development as well as genes of cognition-related phenotypes (Demontis et al., 2023). As found in the previous GWAS results (Demontis et al., 2019), as well as in the current large meta-GWAS, several genes (e.g., *DUSP6*, *SEMA6D*, *ST3GAL3*, *FOXP1* and *FOXP2*, and *SORCS3*) linked to the Wnt pathways (canonical and non-canonical) were found to be associated with ADHD (Demontis et al., 2023). Interestingly, some of these genes were also found to associate with dementia or/and with pathological hallmarks of sAD (Liao et al., 2018; Balabanski et al., 2021; Blue et al., 2021; Tang et al., 2021).

Although the etiopathology of the disorder is still unknown, several hypotheses have been suggested (Table 1), proposing factors leading to neurodevelopmental delays observed in ADHD patients (Shaw et al., 2007; Hoogman et al., 2017). As psychostimulants (first-line ADHD treatment; e.g., MPH, amphetamine) (Banaschewski et al., 2018), demonstrate large effect sizes, the dopaminergic deficit theory has been studied for many years (Gonon, 2009). However, the paradoxical calming effects of psychostimulants in ADHD have still not been fully understood (Robbins and Sahakian, 1979; Harris et al., 2022). Recently, the excitatory/inhibitory imbalance theory has gained interest (Selten et al., 2018), in which GABAergic and parvalbumin-interneurons are hypothesized to play a role in some of the circuits (Bakhtiari et al., 2012; Morello et al., 2020; Sousa et al., 2022). Two hypotheses, extensively studied, are the involvement of oxidative stress (Corona, 2020), particularly mitochondrial dysfunction, and the neuroinflammatory hypothesis (Corona, 2020; Misiak et al., 2022). Both may be a result of long-lasting alterations in neurodevelopmental processes, but may also be one of the etiopathogenic factors. Partially linked with mitochondrial dysfunction, the energy metabolism imbalance in ADHD has been discussed as a possible source of neurodevelopmental delays (Cannon Homaei et al., 2022; Foschiera et al., 2022; Radtke et al., 2022). Cerebral glucose hypometabolism has been found in childhood-onset adult ADHD patients (Zametkin et al., 1990), however, this may also be a consequence of deficits in impulse control leading to metabolic syndrome (di Girolamo et al., 2022). Indeed, a recent meta-analysis found a bidirectional association between ADHD and T2DM (Ai et al., 2022), pointing to long-lasting BIR effects. Interestingly, some significant genetic correlations with insulin-related phenotypes were found for ADHD and AD that provide the foundations for the hypothesis of insulinopathies in the brains of such disorders (Fanelli et al., 2022). Lastly, the involvement of Wnt/mTOR pathways in ADHD has been hypothesized (Yde Ohki et al., 2020), with evidence at the genetic, molecular, and pharmacological levels. This hypothesis will be discussed in more detail in the Wnt/mTOR chapter.

In summary, although an effective treatment exists for ADHD, the long-term effects of drug treatment, the consequences of persistent ADHD in adult patients, as well as the etiopathology of the disorder are not fully understood. Nevertheless, metabolic and Wnt/mTOR pathway alterations may be a common factor in ADHD and AD, and a potential target for preventive measures in both diseases.

## 4. Epidemiological evidence for attention-deficit hyperactivity disorder risk for dementia

Epidemiological studies on the link between ADHD and dementia face several prominent methodological challenges – e.g., the required duration of the follow-up in prospective cohorts from childhood to very old age and substantial spatiotemporal variability in diagnostic criteria and therapeutic guidelines (particularly for ADHD). Nevertheless, although there are only a handful of studies investigating the association between ADHD and AD in humans, some evidence point to a possible link suggesting that ADHD might increase the risk for AD. Earlier clinical research on the frequency of ADHD in the aging population suggested that attentional deficits in geriatric subjects with cognitive impairment might not necessarily imply the existence of an underlying neurodegenerative disorder (Ivanchak et al., 2011). However, recent epidemiological and genetic studies indicate that ADHD is a potential risk factor for sAD and MCI (Fluegge and Fluegge, 2018; Tzeng et al., 2019; Dobrosavljevic et al., 2021). A recent multi-generation nationwide cohort study from Sweden provided strong evidence that ADHD is associated with AD (and other dementias) across generations (Zhang et al., 2022), indicating that elucidation of the overlapping molecular pathways in models of ADHD and AD may uncover relevant etiopathogenic mechanisms and reveal novel drug targets. Literature data on factors that might reduce this risk indicates that adjustment for psychiatric disorders (depression, anxiety, substance use disorder, and bipolar disorder) substantially attenuated the associations (Dobrosavljevic et al., 2021). Conversely, there is inconsistency regarding metabolic disorders like T2DM, obesity, and hypertension reported to have both a limited impact (Dobrosavljevic et al., 2021) and a strong risk-increasing effect (Fluegge and Fluegge, 2018). A recent study (Kakuszi et al., 2020), provided findings consistent with the “last in, first out” hypothesis, which refers to a mirroring pattern of brain development and aging, i.e., relatively late-developing brain regions with age become the early degenerating ones, indicating that, in addition to delayed neurodevelopment, ADHD may also be associated with a premature age-related deterioration. On the other hand, in a very small longitudinal study of 6 ADHD adults with an average of 135 months of follow-up data, no memory decline was observed, however, this might be due to the small sample size and the effect of medication (3/6 participants were taking MPH and 5/6 were taking unspecified antidepressants) not taken into account (Callahan et al., 2021). The same group conducted cognitive and neuroimaging assessments of adults (age 50–85 years) with ADHD ( $n = 40$ ), MCI ( $n = 29$ ), and controls ( $N = 37$ ) (Callahan et al., 2022). In the study, the authors reported memory impairment in both ADHD and MCI groups, however, the first was due to an encoding deficit (frontal lobe thinning) while the second was due to a storage deficit (smaller hippocampi). The authors concluded that the resembling phenotype was caused by distinct pathophysiological factors (Callahan et al., 2022). However, some limitations should be taken into account—namely the significant age differences between ADHD and MCI (mean age was 64 and 73.7, respectively), as well as sex differences with a greater proportion of females in the MCI group (72.4% in comparison with 52.5% in the ADHD group), which might play a role in the current



findings. Mendonca et al. (2021) reported in a cross-sectional study of older patients with ADHD ( $n = 26$ ), MCI ( $n = 40$ ) and controls ( $n = 41$ ), that ADHD individuals have poorer performance than controls in episodic memory and executive function. These findings were comparable between MCI and ADHD for all domains, which, for clinicians, may result in misdiagnosis (Mendonca et al., 2021). Then again, the study by Leffa et al. (2022) in which 212 cognitively healthy controls were followed up for 6 years, including baseline and longitudinal AD biomarkers assessment (e.g., amyloid- $\beta$  PET, MRI, cognitive assessments etc.), showed an association between higher ADHD-PRS and cognitive decline. Interestingly, a combined effect of brain A $\beta$  deposits and a high ADHD-PRS [that predicted longitudinal increases in cerebrospinal fluid (CSF) phosphorylated-Tau<sub>131</sub>] score demonstrated a larger effect on cognitive dysfunction than each did individually.

The current epidemiological and clinical association studies on ADHD, MCI, and AD, provide some evidence that those suffering from ADHD may be at an increased risk for the development of MCI and, thereafter, AD, possibly mediated by a common mechanism. However, there is still a great need for studies that may elucidate common pathways and provide an explanation for the temporal pattern of occurrence of ADHD, MCI, and AD in long-lasting longitudinal prospective cohorts.

## 5. Wnt/mTOR pathways evidence in Alzheimer's disease and attention-deficit hyperactivity disorder

Recent evidence suggests the dysregulation of the Wnt/mTOR signaling pathways as a potential common mechanism in the etiopathogenesis of both ADHD and AD (Boonen et al., 2009; Inestrosa and Varela-Nallar, 2014; Tramutola et al., 2015; Tapia-Rojas and Inestrosa, 2018; Yde Ohki et al., 2020; Perluigi et al., 2021; Nagu et al., 2022; Narvaes and Furini, 2022). Based on the involvement of  $\beta$ -catenin, Wnt signaling can be generally divided into the canonical ( $\beta$ -catenin-dependent) and non-canonical ( $\beta$ -catenin-independent) pathway, activated by binding of different Wnt proteins to their receptors (Wan et al., 2014), which all play an important role in modulation of physiological processes crucial for both developing and mature brain (Jia et al., 2019). During development, Wnt signaling regulates the balance between the proliferation and differentiation of neuronal progenitor and precursor cells (Noelanders and Vleminckx, 2017). In the mature brain, it affects neuronal stem cell proliferation and differentiation (Bengoa-Vergniory and Kypta, 2015). The Wnt pathway has a positive developmental role in the maturation of dendrites and dendritic spines (Hussaini et al., 2014) and an additional role in neurotransmission. Interestingly, recent results also demonstrate that at least some of the effects of Wnt on axonal and dendritic growth may be mediated by APP (Liu et al., 2021). The mTOR pathway plays a key role in maintaining energy homeostasis by regulating nutrient availability and cellular stress information, both intracellularly and extracellularly (Mannaa et al., 2013). Both signaling pathways have some common effectors, like glycogen synthase kinase-3 $\beta$  (GSK3 $\beta$ ), which independently participates

in both signaling cascades regulating different cellular processes (Kaidanovich-Beilin and Woodgett, 2011). In addition, Wnt ligands can regulate mTOR and insulin signaling pathways (Ackers and Malgor, 2018). The involvement of the aforementioned pathways in ADHD and AD is discussed in the following text (see overview Figure 1).

### 5.1. Canonical Wnt pathway

A pivotal role of Wnt signaling in physiological processes implies that its imbalance may be significant in the pathophysiology of both neurodevelopmental disorders including ADHD (Yde Ohki et al., 2020) and neurodegenerative disorders such as AD (Boonen et al., 2009; Inestrosa and Varela-Nallar, 2014). Therefore, the downstream components of Wnt signaling might be important candidates in both disorders. In the Wnt canonical signaling, activation of the pathway occurs by the binding of Wnt glycoproteins to Frizzled receptors and the lipoprotein receptor-related protein 5 (LRP5) or LRP6 co-receptor, which determine the downstream signaling cascade by the intracellular level and phosphorylation status of  $\beta$ -catenin, modulated by GSK3 $\beta$  (Liu et al., 2002; Jia et al., 2019). In the presence of Dickkopf-1 (Dkk1), a Wnt-inhibitor, GSK3 $\beta$  phosphorylates  $\beta$ -catenin and thus targets it for rapid ubiquitin-dependent degradation by a “destruction complex,” consequently resulting in a low cellular level of  $\beta$ -catenin (Wu and Pan, 2010). On the other hand, activation of Wnt signaling leads to inhibition of GSK3 $\beta$ , disassembly of the  $\beta$ -catenin-containing “destruction complex,” and release of  $\beta$ -catenin, which consequently accumulates and stabilizes in the cytosol, and is then translocated into the nucleus triggering expression of target genes crucial for neuronal survival, neurogenesis, and synaptic plasticity (Jia et al., 2019).

Increased activity of GSK3 $\beta$  has been found in the brain of sAD patients (Llorens-Martin et al., 2014) and increased activation of GSK3 $\beta$  is inversely associated with a significant decrease in  $\beta$ -catenin levels in the prefrontal cortex of AD patients (Folke et al., 2019). Decreased  $\beta$ -catenin levels are unable to suppress the transcription of the  $\beta$ -site APP cleaving enzyme (BACE1), consequently promoting A $\beta$  production and aggregation (Parr et al., 2015), while accumulation of A $\beta$  stimulates the activation of the endogenous Wnt pathway inhibitor, Dkk1, contributing to the decreased  $\beta$ -catenin-dependent triggering of various genes' expression (Caricasole et al., 2004). Furthermore, since GSK3 $\beta$  is the main kinase involved in the phosphorylation of the Tau protein (Hernandez et al., 2013), a convincing body of evidence indicates that hyperactivity of GSK3 $\beta$  is linked to pathological Tau hyperphosphorylation (Llorens-Martin et al., 2014), thus supporting a link between dysfunctional Wnt/ $\beta$ -catenin signaling with the two major AD hallmarks (Jia et al., 2019). Several AD susceptibility genes are linked to aberrant Wnt signaling, such as APOE  $\epsilon$ 4, a major genetic risk factor for late-onset sAD, which inhibits canonical Wnt signaling in cell lines (Caruso et al., 2006). Liu et al. (2021) recently reported a direct interaction between Wnt (Wnt3a and Wnt5a) with the cysteine-rich domain in the extracellular portion of APP, a genetic risk factor for fAD. Binding of Wnt3a promoted APP stability, while Wnt5a reduced APP by stimulating lysosomal degradation (Liu et al., 2021). It was

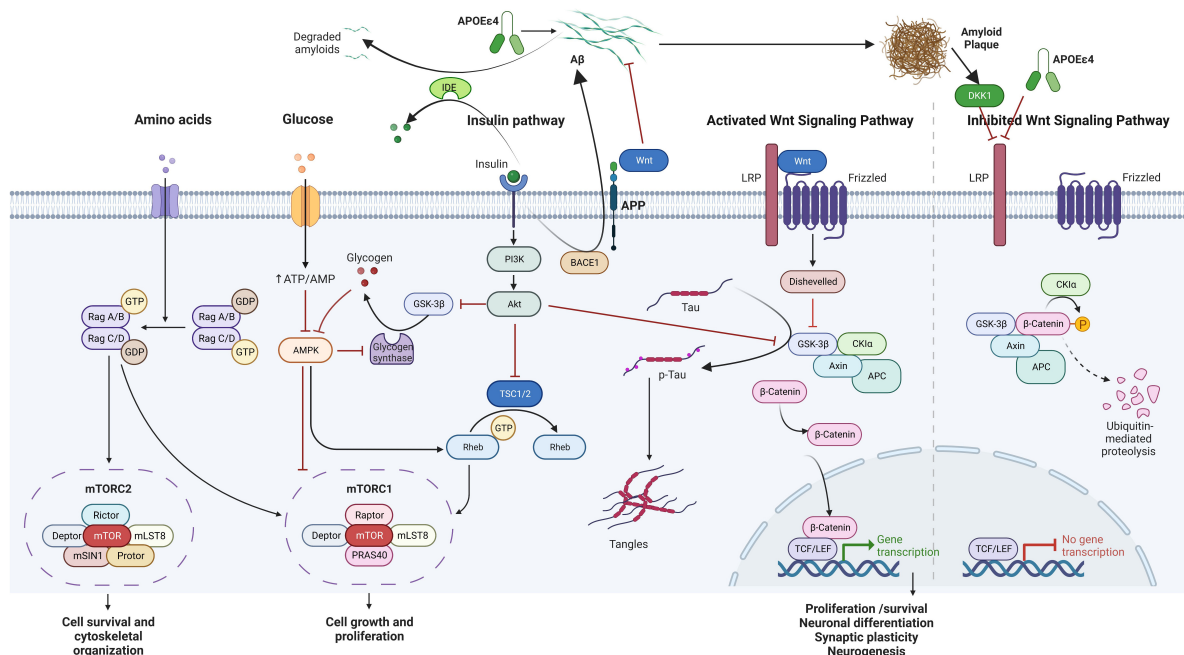


FIGURE 1

Overview of the Wnt/β-catenin/mTOR signaling pathway hypothesized to be involved in attention-deficit hyperactivity disorder (ADHD) and Alzheimer's disease (AD) over the lifespan. The two pathways work in a concomitant manner with some common molecules, including energy metabolism and insulin signaling. In the short term, disruption in the pathways may influence growth, differentiation, and synaptic plasticity, while in the long-term, accumulation of p-Tau and amyloid plaques may lead to cell death and decreased neurogenesis. Aβ, amyloid β; Akt, protein kinase B; AMP, adenosine monophosphate; AMPK, adenosine monophosphate-activated protein kinase; APC, adenomatous polyposis coli; APOE, apolipoprotein; APP, amyloid precursor protein; ATP, adenosine triphosphate; DKK1, Dickkopf WNT signaling pathway inhibitor 1; GDP, guanosine diphosphate; GSK3β, glycogen synthase kinase-3β; GTP, guanosine-5'-triphosphate; IDE, insulin-degrading enzyme; LRP, LDL receptor related protein; MAPK, mitogen-activated protein kinase; mTOR, mammalian target of rapamycin; PI3K, phosphatidylinositol 3-kinase; Tau, tubulin associated unit; TCF/LEF, T cell factor/lymphoid enhancer factor family; TSC1/2, tuberous sclerosis proteins 1 and 2; Wnt, wingless-INT. The figure was created using BioRender (<https://biorender.com/>).

shown that both Frizzled1 and Frizzled7 are downregulated in early human AD stages, as well as in the hAPP<sup>NLGF/NLGF</sup> mouse model (depicting a knock-in of the hAPP Swedish mutation of a fAD), and concomitantly increase Sirtuin2-induced deacetylation (Palomer et al., 2022). Inhibiting Sirt2 *in vivo* and *in vitro* rescued Frizzled expression and synaptic loss (Palomer et al., 2022). The Wnt pathway plays an important role in the regulation of brain insulin signaling. Activation of Wnt upregulates brain-derived insulin in the hypothalamus (Lee et al., 2016) and restores insulin sensitivity in insulin-resistant neurons (Tian et al., 2021). In the rat model of sAD induced by intracerebroventricular streptozotocin (STZ-icv), dysregulation of the IR-PI3K-Akt signaling pathway is associated with increased activity of GSK3β (Barilar et al., 2015). In the STZ-icv mice, increased activity of GSK3β in the hippocampus was accompanied with increased β-catenin (Qi et al., 2021) and decreased Wnt3a and β-catenin (Salem et al., 2021). Furthermore, a recent study modeling sAD using induced pluripotent stem cell (iPSC)-derived cortical neurons from sAD patients and controls, and comparing them to postmortem brain samples from sAD and controls, found at the transcriptomic level, after mapping the findings to the Kyoto Encyclopedia of Genes and Genomes (KEGG) AD map, that pathways of the PI3K and the Wnt-mediated activation of Dishevelled, a key component of Wnt signaling, are altered (Verheijen et al., 2022). This provides further support for the involvement of the IR and Wnt pathways in sAD even at an early stage of sAD

as iPSC-derived neurons usually represent less mature aging neurons.

Dysregulation in the canonical Wnt signaling pathway in ADHD and its alteration after MPH therapy was confirmed by various researchers as reviewed elsewhere (Yde Ohki et al., 2020). In a mouse model overexpressing the thyroid hormone-responsive protein with defining characteristics of ADHD, a proteomic analysis of the hippocampus found an altered network of proteins involved in Wnt signaling; catenin β1 was found to be upregulated, and hippocampal gene expression of Wnt ligands, inhibitors, receptors, and co-receptors: i.e., significant reductions of the *Wnt7a* gene, as well as upregulation of Wnt inhibitors *Dkk4* and *Igfbp5* and enhanced *Lrp6* expression was found (Custodio et al., 2023). In humans, a significant association was found between sex-specific genetic variations of *LRP5* or *LRP6* co-receptors and child and adolescent ADHD (Grünblatt et al., 2019). As already mentioned in the previous chapter, in a large meta-GWAS, several genes (e.g., *DUSP6*, *SEMA6D*, *ST3GAL3*, *FOXP1* and *FOXP2*, and *SORCS3*) linked to the Wnt-pathways (canonical and non-canonical) were found to be associated with ADHD, further supporting a role of this pathway (Demontis et al., 2023). In a study of Chinese families with a child diagnosed with ADHD, analysis of whole-genome sequencing data showed an increased frequency of single nucleotide variants in several ADHD-susceptible genes, including *LRP6* (Li et al., 2022). Recent comprehensive analysis of mononuclear blood transcriptomic data

of 270 ADHD and 279 controls, revealed enrichment of genes involved in the  $\beta$ -catenin-T-cell factors (TCF) complex assembly, AD as well as insulin signaling pathways (Cabana-Dominguez et al., 2022). Interestingly, the *FZD1* gene was significantly down-regulated in ADHD patients compared to controls, similarly to the reported reduction in sAD [internal communication with Cabana-Dominguez et al. (2022)]. Finally, it was also found that MPH enhances neuronal differentiation and reduces proliferation in human SH-SY5Y-cells through activation of the Wnt/ $\beta$ -catenin pathway (Grünblatt et al., 2018). On the other hand, differential regulation by prolonged MPH treatment was found in GSK3 $\beta$  signaling responses in different brain regions (Mines and Jope, 2012; Mines et al., 2013).

## 5.2. mTOR pathway

The serine/threonine kinase mTOR is present in two structurally and functionally distinct protein complexes referred to as mTOR complex 1 (mTORC1) and mTOR complex 2 (mTORC2). mTORC1 integrates signals from multiple growth factors, nutrients, and energy supply, to promote cell growth when energy is sufficient, and catabolism in the absence of nutrients. The mTOR pathway has been found to hold a central role in a variety of cell processes, ranging from promoting protein synthesis to determining the extent of autophagy, and is consequently largely implicated in disease; dysregulation of the pathway has been confirmed in the aging process, cancer, and metabolic disorders like diabetes (Saxton and Sabatini, 2017). mTORC1 is composed of mTOR, the scaffolding protein raptor (regulatory associated protein of TOR), the GTPase  $\beta$ -subunit-like protein (G $\beta$ L/mLST8) and deptor (Dowling et al., 2010). mTORC2 mainly controls cell proliferation and survival and is comprised of mTOR, Rictor, G $\beta$ L, Proline Rich 5 (PRR5/Protector), deptor, and mammalian stress-activated protein kinase interacting protein (SIN1) (Zou et al., 2020). mTOR is involved in many signaling pathways in the body and coordinates or interacts with several upstream signal components, including insulin, growth factors, 5-AMP-activated protein kinase (AMPK), PI3K/Akt, and GSK3 (Cai et al., 2015). Due to its extensive presence in different cellular processes, changes in the function of the mTOR pathway activity significantly alter cell homeostasis. On the one hand, decreases in protein synthesis rates driven by inhibition of the mTOR pathway governing mRNA translation may allow for improved cellular proteostasis, whereas increases in the activity of the autophagy-lysosomal pathway due to mTOR inhibition leads to degradation of damaged organelles and macromolecules (Johnson et al., 2015). Indeed, diminished activation of the PI3K/Akt/mTOR pathway was found to augment longevity in mice. Likewise, increased insulin sensitivity in centenarians has been associated with decreased mTOR activity (Sharp and Bartke, 2005). Therefore, longevity appears to be associated with the reduced activity of insulin or insulin-like growth factor (IGF)-mediated PI3K/Akt/mTOR pathway, suggesting that these signaling cascades may be important targets for pharmacological manipulation (Blagosklonny, 2006). However, since insulin and IGF-1 activate mTOR through the PI3K pathway, ultimately regulating cell growth and proliferation in neuronal progenitor cells and neuronal differentiation (Han et al.,

2008), as well as synaptic plasticity, glucose, and lipid metabolism, and protein homeostasis (Bedse et al., 2015), chronic inhibition of the pathway is bound to result in deleterious effects, including carcinogenesis and metabolic dysfunction (Ali et al., 2022). Therefore, finely balanced activation of mTOR is of equal interest, e.g., in the context of neurodegeneration, intact mTOR signaling is vital for long-lasting forms of synaptic plasticity and hippocampal memory consolidation and maintenance, by supporting protein synthesis in dendrites and their synapses (Querfurth and Lee, 2021).

Abnormal regulation of the mTOR-pathway is seen in the brain of individuals affected by AD as well as various tissues of patients with T2DM (Mannaa et al., 2013). Although many antidiabetic drugs can affect the mTOR pathway (and introduce bias), current evidence supports the hypothesis that its hyperactivation plays the role in the etiopathogenesis of the disease (Jia et al., 2014; Ong et al., 2016; Ali et al., 2017; Guillen and Benito, 2018). Furthermore, increased levels of pIRS1<sup>Ser636</sup> and pGSK3 $\beta$ <sup>Ser9</sup>, and hyperactivation of the Akt/mTOR/p70S6K pathway was reported in neuronal-derived extracellular vesicles from patients with Down syndrome (Perluigi et al., 2022) with an increased risk of AD (Zigman and Lott, 2007). Hyperactivation of the mTOR pathway in the brain of AD patients was shown in a number of studies (Uddin et al., 2020), however on the contrary, reduced mTOR signaling was also reported in patients as well as animal models and cell cultures (Lafay-Chebassier et al., 2005). In sAD, neuronal resistance to insulin and IGF-1 is promoted by the over-activation of the PI3K/mTOR axis *via* a negative feedback mechanism that inhibits IRS1 (Tramutola et al., 2015). Moreover, neuronal insulin resistance is also associated with neuroinflammation *via* the tumor necrosis factor- $\alpha$  (TNF $\alpha$ )/c-Jun N-terminal kinases (JNK) pathway, which, in AD, is activated by A $\beta$  oligomers and misfolded Tau that consequently alter the IRS1/mTOR signaling pathway (Liang et al., 2019).

Animal models provide further evidence of the ambiguous role of mTOR activation/inhibition in neurodegeneration and AD. Brain gene expression of several components of the mTOR complex was found to be downregulated in both transgenic (3xTg-AD) and non-transgenic (STZ-icv rat and mice) AD models (Chen et al., 2012; Qin G. et al., 2021). Downregulation of mTOR signaling was found to mediate impairment in synaptic plasticity of the Tg2576 mouse model and increasing mTOR signaling was found to be protective against A $\beta$ -related impairment in long-term potentiation (Ma et al., 2010). In pre-symptomatic and middle-aged APPSwe/PS1 $\Delta$ E9 (APP/PS1) mice, generation of reactive oxygen species was found to lead to oxidative modification of Akt1 in the synapse resulting in reduction of Akt1-mTOR signaling and deficiency in activity-dependent protein translation; moreover, a similar attenuation of synaptoneurosomal protein translation was found in postmortem AD brains (Ahmad et al., 2017). In cell cultures, STZ-injured oligodendrocytes showed significantly lower expression of PI3K, Akt, p-Akt, mTOR, and p-mTOR proteins than the control group (Liu et al., 2020).

Conversely, inhibition of mTOR was studied for the mitigation of AD symptoms in different AD models. Improvement of cognitive functions and reduction of cortical A $\beta$  levels were found in hAPP(J20) mice after rapamycin (canonical mTOR inhibitor) treatment, along with restoration of neurovascular coupling (Van Skike et al., 2021). Increased hippocampal expression of p-mTOR



was reported in the STZ-icv model of AD (El Sayed et al., 2021), while mTOR inhibition by everolimus showed improvements in cognition, as well as lowered TNF $\alpha$  levels in the brain accompanied by increases of insulin and IGF-1 levels and correction of STZ-icv-induced alterations of mRNA expression of PI3K/Akt/mTOR pathway genes (Bansal et al., 2021).

The mTOR pathway's ubiquitous presence in cell processes implies a role in other disorders, including ADHD. Large-scale computational analysis of the S-nitrosylation proteome pointed to the mTORC1 signaling pathway as one of the shared molecular mechanisms between the autism spectrum disorder (ASD) animal model (InsG3680) and P301S AD mouse model (Mencer et al., 2021). As ADHD is the most common comorbidity in ASD patients (Hours et al., 2022), and ADHD is associated with sAD and any dementia across generations (Zhang et al., 2022), the mTOR pathway may be one of special interest in linking these two disorders. A meta-analysis of GWAS data by Rovira et al. (2020) identified nine new loci indicating a common genetic basis for ADHD in childhood and persistent ADHD in adults, among which was also the *FRAT1/FRAT2* gene regulating the Wnt signaling pathway. In a multi-step analysis aimed to identify and characterize modules of co-expressed genes associated with ADHD using data from peripheral blood mononuclear cells, both *RICTOR* and *MTOR* genes were found to be significantly upregulated in ADHD patients compared to controls further internal discussion with authors regarding data presented in Cabana-Dominguez et al. (2022). In addition, it has been shown by Schmitz et al. (2019) that the Akt-mTOR pathway was affected by MPH treatment in PC12 cells. Short-term MPH treatment decreased pAkt(Thr308)/Akt, p-mTOR/mTOR, and pS6K/S6K ratios, as well as pFoxO1 levels, although long-term treatment increased pAkt(Thr308)/Akt, pmTOR/mTOR and pGSK-3 $\beta$ /GSK-3 $\beta$  ratios (Schmitz et al., 2019). A study of ADHD-susceptible variants by Li et al. (2022) identified genes corresponding to single-nucleotide variants labeled as possibly or probably damaging including *CACNA1H*, *PKD1*, *DYNC2H1*, *LRP6*, and *RGS11*. The *CACNA1H* gene encodes for the  $\alpha 1$ -subunit of the T-type low voltage-dependent calcium (Ca $^{2+}$ ) channel Cav3.2 (Leresche and Lambert, 2017), and mTORC1 pathway regulation may be driven by intracellular Ca $^{2+}$  levels (Li et al., 2016). Other than ADHD, voltage-gated calcium channels have also been implicated in other neuropsychiatric disorders, like schizophrenia, ASD, anxiety, etc. (Nanou and Catterall, 2018; Andrade et al., 2019). Only a few studies investigated the mTOR pathway in ADHD, but both the mTOR and Wnt pathways are implicated in cellular metabolism and energy balance, and emerging data suggests a positive association between ADHD, obesity, and T2DM (Landau and Pinhas-Hamiel, 2019).

Therefore, a growing body of evidence points to a harmful vicious cycle in which impaired Wnt/mTOR-signaling is intertwined with the major AD and ADHD pathophysiology hallmarks at the protein and gene level for each of the pathways and individual diseases, respectively. However, searching for the alterations of those Wnt/mTOR signaling-related parameters found both in AD and ADHD, might reveal a common point of weakness in their respective etiopathogenesis and thus not only help clarify the overlap of sAD and ADHD pathophysiology at the molecular level but also offer possible shared target(s) for disease-modifying drug intervention in their therapy. Elucidation

of the Wnt/mTOR signaling dysfunction underlying ADHD-AD overlapping pathophysiology is very important also as a contribution to understanding its role in the pathophysiology of other neurodegenerative disorders like Parkinson's disease (Huang et al., 2022; Serafino and Cozzolino, 2023).

## 6. Evidence of the link between attention-deficit hyperactivity disorder and Alzheimer's disease in the context of animal model phenotypic traits

Although most animal models of ADHD and AD do not fulfill all the validation criteria [face, construct, and predictive validity (Willner, 1986)], they are invaluable in elucidating pathomechanism in these disorders. The face validity criteria of both models seem to be satisfied as they relatively faithfully reflect the key symptoms of ADHD (inattention, hyperactivity, and impulsivity) and AD (progressive cognitive deficits). Nevertheless, both models frequently also demonstrate additional phenotypic traits that may or may not reflect the comorbidity/complex presentation in humans. The construct validity of the models is often challenging to determine considering that the etiopathogenesis of ADHD and AD is still not fully understood. In this regard, some pathological and molecular correlates suggest some models may be valid, e.g., most animal models of AD demonstrate accumulation of A $\beta$  and tau hyperphosphorylation. Additionally, a low attentive, low vigilance, and high response disinhibition model of ADHD shows improved vigilance and reduced probability of false alarms upon administration of an agonist of the dopamine D4 receptor (Hayward et al., 2016) associated with adult ADHD (Franke et al., 2012). However, the models also seem to present with features that do not reflect the natural course of AD and ADHD in humans, e.g., Tg2576 animals -fAD model, overexpress a mutant form of APP with a Swedish mutation (KM670/671NL) throughout their life (representing at best ~1% of familial AD cases) and do not show signs of neuronal loss and neurofibrillary tangles (Irizarry et al., 1997). Similar to that, dopamine transporter (DAT)-knockout mice (ADHD model), show solid face and predictive validity, however, DAT seems to be increased, and not decreased in ADHD patients (Rahi and Kumar, 2021). Finally, ADHD and AD models demonstrate variable positive and negative predictive validity as many drugs that work in animal models (McKean et al., 2021; Dougnon and Matsui, 2022; Kantak, 2022), unfortunately, show little benefits in humans, while some drugs that are successfully used in patients, fail to improve symptoms in some animal models.

Regardless of the aforementioned limitations, animal models sometimes offer unexpected insight into diseases with shared molecular pathobiology offering the opportunity for a better understanding of genetic and environmental risk factors and comorbidities, as well as the development of new working models and identification of novel (shared) drug targets. Here we propose that a careful evaluation of ADHD and AD models, particularly from the perspective of face validity, provides evidence for potentially shared pathomechanisms and risk factors.



## 6.1. Evidence for Alzheimer's disease-like behavioral traits in animal models of attention-deficit hyperactivity disorder

As the etiopathogenesis of ADHD remains largely unknown (construct validity), most animal models focus on replicating the symptomatology (face validity), which classically consists of hyperactivity, impulsivity, and inattention (Sontag et al., 2010), i.e., executive dysfunction.

A link between ADHD and AD may be found in the dysfunction of working memory as one of the core executive functions (Roth and Saykin, 2004; Diamond, 2013). In 2000, Baddeley suggested the working memory's "episodic buffer" as a stage in long-term episodic learning (Baddeley, 2000). A key component of AD symptomatology is the loss of long-term episodic memory (Salkovic-Petrisic et al., 2021), which seems to arise from a deficit in the encoding of new memories (Germano and Kinsella, 2005), implicating a working memory deficit antecedent to long-term memory dysfunction [confirming the "hypothesis 1" by Callahan et al. (2017)]. However, longitudinal studies are necessary. Even though they are sorely lacking in animal models, there is some evidence that the above is precisely the case in at least two different models of ADHD: Sprague–Dawley rats selected for high impulsivity, and the spontaneously hypertensive rat (SHR) model.

In Dellu-Hagedorn et al. (2004) divided 3-month-old Sprague–Dawley rats by impulsivity—at this point, no differences in working memory among groups could be observed (radial arm maze). At middle age (15 months), the difference in impulsivity between groups was retained, but impulsivity decreased overall. In the working memory assessment, the highly impulsive group performed worse in the training phase up until the last day, when it reached the non-impulsive group's performance. Two years later, Dellu-Hagedorn again divided 3-month-old rats by impulsivity and reproduced these results (Dellu-Hagedorn, 2006). While rats in the hyperactive group made more errors in training, after 6 days they managed to reach the same level of performance as the hypoactive group, indicating a surmountable working memory deficit among the hyperactive animals in this scenario. Another ADHD model, the SHR (Sagvolden and Johansen, 2012), has originally been developed as a model for studying hypertension in 1963 by selectively breeding Wistar-Kyoto rats (Okamoto and Aoki, 1963). The increased locomotor activity of these animals seems to be highly age-dependent, peaking in a juvenile phase around 8 weeks of age (van den Bergh et al., 2006), and again in an older age of 45 weeks (Hendley et al., 1985). Most ADHD research using this model, therefore, focuses on this juvenile period, when no cognitive deficits seem to be present (Langen and Dost, 2011). Young, 7–8-week-old male SHR rats exhibiting increased locomotor activity do not seem to show cognitive impairments in the novel object recognition test (Langen and Dost, 2011). It seems that, in older SHR rats, the hyperactive (in terms of increased locomotor activity) phenotype diminishes as cognitive deficits begin to appear, and spatial memory dysfunction has been observed in 3-month-old SHR rats (Sontag et al., 2013). Another study examining 3- and 7-month-old SHR rats links these deficits to brain IR dysfunction, a phenomenon linked to AD (Grünblatt et al., 2015). A third study working with older (26–30 weeks) SHR rats describes a similar phenotype accompanied by vascular

dysfunction in the hippocampus (Johnson et al., 2020), another neuropathology commonly found in AD (Govindpani et al., 2019). While there is also evidence of neuropathology less specific to AD in particular, such as neuroinflammation (Tayebati et al., 2016; Cohen et al., 2019) and increased oxidative stress (Corona, 2020), parenchymal A $\beta$  formation, a hallmark of AD, has also been observed in this model at 20–44 weeks of age with conventional histology and immunohistochemistry, showing an age-dependent increase in parenchymal  $\beta$ -amyloid load (Schreiber et al., 2014).

The aforementioned cognitive deficits developing at a later age provide face validity to the hypothesis that, with age, an ADHD model may serve as a sAD model, and the neuropathological markers found therein thought to be closely related to AD, lend construct validity. Unfortunately, there is little data on therapies in older ADHD model animals to provide a statement on predictive validity.

## 6.2. Evidence for attention-deficit hyperactivity disorder-like behavioral traits in animal models of Alzheimer's disease

Accumulating evidence suggests that animal models of AD demonstrate some phenotypic traits resembling ADHD. van Swinderen (2007) has shown that mutations in genes involved in short and long-term memory formation (van Swinderen et al., 2009), and memory consolidation (van Swinderen and Brembs, 2010) all result in deficits in attention-like processes in *Drosophila melanogaster*. Furthermore, the attention deficits were accompanied by well-defined behavioral hyperactivity and phenotypic alterations were successfully alleviated by MPH treatment (van Swinderen and Brembs, 2010) providing evidence for both face and predictive validity (in the context of ADHD-like symptoms). The results from Zhang et al. (2015) illustrate the presence of phenotypic traits of ADHD in AD even more clearly as they observed clear ADHD-like behavior in flies generated as a model of AD. Zhang et al. (2015) generated flies with inducible expression of low levels of human APP and BACE1 to overcome methodological problems associated with the overexpression of AD-associated transgenes. Unexpectedly, inducing low levels of human APP and BACE1 resulted in a phenotype resembling ADHD with: (i) a marked increase in overall motor activity; (ii) male predominance; (iii) carbohydrate-induced aggravation of symptoms; (iv) the phenotype mitigated with age; (v) delayed, but a steep reduction in nocturnal activity; (all strongly indicative of high face validity of the model for ADHD) and; (vi) a reversible reduction in hyperactivity by dextroamphetamine (with the absence of the effect in non-ADHD-like fly controls)—strongly indicative of good predictive validity of the model (Zhang et al., 2015). The construct validity of the proposed model for ADHD remains to be explored, however, based on strong evidence in support of both face and predictive validity, the authors proposed its use for elucidation of the etiopathogenesis of ADHD. The presence of ADHD-like symptoms has also been reported in other, more complex, animal models of AD. For example, Tg2576 mice demonstrate locomotor hyperactivity (Gorman and Yellon, 2010; Bardgett et al., 2011) and increased exploratory behavior (Babic Perhoc et al., 2019) providing some evidence for face validity.

Locomotor hyperactivity has also been reported in other transgenic models of AD—e.g., Swedish-APP (Bedrosian et al., 2011), 3xTg-AD (only in male mice) (Pietropaolo et al., 2008; Sterniczuk et al., 2010), Swedish APP on a 129 genetic background (Rustay et al., 2010), TgCRND8 (Walker et al., 2011), APP+PS1 (Arendash et al., 2001), and APP23 (Van Dam et al., 2003) models. Unfortunately, data on ADHD predictive validity in AD models is scarce as most studies utilizing ADHD drugs in AD models focused on cognitive rather than ADHD symptoms. Nevertheless, some reports suggest that treatments that show beneficial effects in ADHD models [e.g., an H3 antagonist ciproxifan (Fox et al., 2002)] also attenuate hyperactive behavior in some models of AD (Bardgett et al., 2011).

Pronounced locomotor hyperactivity of AD animal models has been reported by different groups, as it was recognized as an important confounder precluding valid behavioral analysis. For example, Jankowsky et al. generated a tetracycline-responsive transgenic APP mouse model to study the effects of A $\beta$  production arrest expected from the treatment with inhibitors of secretases. However, mice overexpressing APP throughout their development demonstrated severe locomotor hyperactivity (with 100% penetrance), incompatible with cognitive testing (Jankowsky et al., 2005). Interestingly, the same model has been used to elucidate the effects of the APP overexpression onset on behavioral phenotype, showing that overexpression during early postnatal development resulted in the most pronounced hyperactivity (Rodgers et al., 2012). In contrast, delaying the overexpression of APP until adulthood resulted in a substantial attenuation of the hyperlocomotor phenotype (Rodgers et al., 2012). The latter provides indirect evidence that ADHD and AD may represent two points along a single pathophysiological continuum [i.e., “hypothesis 1” proposed by Callahan et al. (2017)] and suggests that similar noxious stimuli may result in the development of either ADHD or AD depending on the developmental period during which they occur.

Behavioral alterations in the non-transgenic STZ-icv rat model of sAD provide additional evidence in support of the overlapping phenotype of ADHD and AD in animal models with the advantage of the absence of altered gene expression during brain development (as is often the case with transgenic models). In the STZ-icv model, a complex phenotype characterized by a combination of ADHD and AD-like symptoms develops after icv administration of a diabetogenic compound (streptozotocin) in the period in which neural circuits are already fully formed (excluding the possibility of purely neurodevelopmental origin). The STZ-icv model is characterized by a chronic and progressive cognitive decline (Knezovic et al., 2015) (AD face validity) accompanied by neuropathological and metabolic hallmarks of AD [i.e., BIR state (Grünblatt et al., 2007), neuroinflammation (Knezovic et al., 2017), accumulation of A $\beta$  (Salkovic-Petrisic et al., 2011), hyperphosphorylated Tau (Li et al., 2020), mitochondrial dysfunction (Correia et al., 2011), oxidative stress (Sharma and Gupta, 2001), and glucose hypometabolism (Knezovic et al., 2018)] (AD construct validity) (Salkovic-Petrisic et al., 2021). Interestingly, apart from symptoms and molecular alterations resembling AD, the STZ-icv model also develops attentional deficits and locomotor hyperactivity (ADHD face validity). The development of the hyperlocomotor phenotype was first observed by Mayer and Hoyer during the initial behavioral characterization of the STZ-icv model (Mayer et al., 1990), and it was later (similarly

as was the case with the transgenic AD models) recognized as an important confounder for behavioral analyses (Homolak et al., 2021). The STZ-icv rats also demonstrate several common features of ADHD: pronounced circadian dysrhythmia [present already in the very early (24–48 h) post-induction period preliminary data—Supplementary Figure 1A; (WASAD Congress, 2021)], increased stress response (Virag et al., 2021), increased social interaction preference [commonly reported in ADHD models—e.g. (Hopkins et al., 2009; Robinson et al., 2012; Gauthier et al., 2015)] (preliminary data—Supplementary Figure 1B), dysfunctional attention dynamics and hesitancy/impulsivity (unpublished preliminary results see Supplementary Figures 1C–F).

In summary, although a more thorough exploration of the pre-cognitive ADHD-like behavioral phenotype of the STZ-icv model is needed, it seems that non-transgenic models of AD may also recapitulate the behavioral aspect of the hypothesized ADHD-AD continuum (Callahan et al., 2017). Experiments testing ADHD predictive validity (mainly the ability of ADHD drugs to counteract ADHD-like symptoms) utilizing the early ADHD-like pre-cognitive stage of the disease in the STZ-icv model may provide critical information to support or reject the hypothesis. Such experiments, planned to be performed in our lab in the near future, will hopefully elucidate this open question. Furthermore, if such experiments confirm the efficacy of ADHD drugs in treating ADHD-like symptoms in the pre-cognitive stage of the disease, they may also provide a platform for testing the hypothesis that a timely introduction of ADHD therapy may delay or even prevent neurodegeneration and cognitive decline in the context of the proposed ADHD-AD pathophysiological continuum.

Altogether, data from both ADHD and AD animal models support the hypothesis of overlapping pathophysiology and the existence of the ADHD-AD continuum. In both cases, the strongest evidence comes from the experiments reporting a complex ADHD/AD phenotype (face validity), however, the data on construct and predictive validity are still scarce. One of the reasons, for the paucity of construct and predictive validity evidence, may be a time-period restricted use of ADHD and AD models and consequent failure to acknowledge the overlapping symptoms and identify them as a rationale to explore molecular patterns of AD in ADHD and vice versa (construct validity), and test ADHD drugs in AD models and vice versa (predictive validity). The animal models of ADHD are mostly examined when the animals are relatively young to faithfully mimic human disease that usually presents at a relatively young age in most patients. Accordingly, most researchers use old animals to model the AD-like phenotype in rodents. Consequently, most research on ADHD models is done at a time point in which cognitive deficits are not yet evident, and most animal studies with AD models fail to acknowledge a potential early ADHD-like stage of the disease. The evidence supporting this hypothesis comes from relatively rare longitudinal studies on ADHD models with behavioral follow-up after dissipation of the hyperactive phenotype (Dellu-Hagedorn, 2006), and the studies on AD that focus on the developmental/early aspect of AD-like pathophysiology that resembles ADHD e.g., overexpression of APP during brain development (Rodgers et al., 2012). A more mindful and less time-restricted approach to behavioral and molecular patterns in models of ADHD and AD may provide additional evidence in support of the overlapping phenotype and motivate researchers to conduct experiments designed to address the lack

of construct and predictive validity evidence for the ADHD-AD continuum. Finally, animal research addressing the ADHD-AD continuum hypothesis will inevitably have to deal with the impact of sex on the etiopathogenesis and the progression of the

disease actively explored both in the context of ADHD (Ramtekkar et al., 2010; Cortese et al., 2016; Greven et al., 2018) and sAD (Li and Singh, 2014; Toro et al., 2019). In childhood, a great number of females are undiagnosed for ADHD until reaching

TABLE 2 Wnt/mTOR pathway and behavioral alterations in rodent models of attention-deficit hyperactivity disorder (ADHD) and Alzheimer's disease (AD).

Animal model	Wnt/mTOR alterations	ADHD-like behavioral alterations	AD-like behavioral alterations
<b>AD models</b>			
TgCRND8/APP J20	↑DKK, GSK-3α/β, ↓Wnt, β-catenin (Rosi et al., 2010) ↑DKK, ↓β-catenin (Tong et al., 2022)	locomotor hyperactivity (Walker et al., 2011) circadian dysrhythmia, hyperarousal (Colby-Milley et al., 2015)	+
APP/PS1	↑GSK3β, ↓β-catenin (Xiang et al., 2021) ↓Wnt4 (Yan et al., 2022) ↓Wnt3a, β-catenin, ↑GSK3β (Zhu et al., 2018) ↓mTOR (Ahmad et al., 2017) ↓mTOR (Francois et al., 2014) ↑DKK-1 (Rosi et al., 2010)	locomotor hyperactivity (Arendash et al., 2001)	+
APP23	↓β-catenin, ↑GSK3β (cells isolated from APP23 mice) (He and Shen, 2009)	locomotor hyperactivity (Van Dam et al., 2003)	+
Tg2576	↓mTOR (Ma et al., 2010) ↑DKK-1 (Rosi et al., 2010)	locomotor hyperactivity (Gorman and Yellon, 2010; Rustay et al., 2010; Bardgett et al., 2011; Bedrosian et al., 2011) increased exploratory behavior (Babic Perhoc et al., 2019)	+
3xTg	↓mTOR (Chen et al., 2012) ↓active β-catenin, β-catenin mRNA, ↑inactive β-catenin, GSK3β mRNA, GSK3β activity (Huang et al., 2018)	locomotor hyperactivity (Pietropaolo et al., 2008; Sterniczuk et al., 2010) increased locomotor and exploratory activity (Chen et al., 2013)	+
P301S	↑mTOR (Mencer et al., 2021) ↑non-canonical Wnt (Amal et al., 2019) ↑DKK-1 (Rosi et al., 2010)	increased locomotor activity and exploration (Scattoni et al., 2010; Takeuchi et al., 2011)	+
5xFAD	↓mTOR, ↓β-catenin, ↑GSK3β (Avrahami et al., 2013)	locomotor hyperactivity (Oblak et al., 2021; Sil et al., 2022)	+
STZ-icv mice	↓mTOR (STZ icv 3 months) (Qin G. et al., 2021) ↑mTOR (STZ icv 3 weeks) (El Sayed et al., 2021) ↑β-catenin, ↑GSK3β (STZ 3 mg/kg bilateral hippocampal injection) (Qi et al., 2021) ↓β-catenin, ↓Wnt3a; ↑GSK3β, ↑mTOR (Salem et al., 2021)	decreased locomotor activity and exploration (Qi et al., 2021) increased locomotor activity and exploration (Chen et al., 2013)	+
STZ-icv rats	↑GSK3β (Barilar et al., 2015) ↓mTOR (Chen et al., 2012)	locomotor hyperactivity (Mayer et al., 1990; Homolak et al., 2021), <b>Supplementary Figure 1</b> (WASAD Congress, 2021) increased stress response (Virag et al., 2021) circadian dysrhythmia [ <b>Supplementary Figure 1</b> (WASAD Congress, 2021)]	+
<b>ADHD models</b>			
SHR	↑GSK3β activity, ↓β-catenin (Cheng et al., 2015) ↑GSK3β (Grünblatt et al., 2015)	+	spatial, object, and aversive memory deficits (Sontag et al., 2013; Grünblatt et al., 2015; Johnson et al., 2020)
THRSP OE	↑β-catenin, <i>Dkk4</i> , <i>Igfbp5</i> , <i>Lrp6</i> ; ↓ <i>Wnt7a</i> (Custodio et al., 2023)	+	recognition memory deficits (Custodio et al., 2018)
Neonatal MSG	↓Wnt3a, β-catenin, ↑GSK3β mRNA (Abu-Elfotuh et al., 2022)	+	spatial memory deficits (Abu-Elfotuh et al., 2022)

Standardly present cognitive alterations in animal models of AD and ADHD-like traits in animal models of ADHD were marked with a "+". APP, amyloid precursor protein; APP23, B6-Tg/Thy1APP23Sdz; APP/PS1, APP/PS1 double transgenic; DKK, Dickkopf; 5xFAD, APP/PS1, Tg6799, Tg-5xFAD [APP K670\_M671delinsNL (Swedish), APP I716V (Florida), APP V717I (London), PSEN1 M146L (A > C), PSEN1 L286V]; GSK3, glycogen synthase kinase 3; mTOR, mammalian target of rapamycin; *Igfbp*, insulin-like growth factor-binding protein; *Lrp*, low-density lipoprotein receptor-related protein; MSG, monosodium glutamate; P301S, Tau PS19Tg (MAPT P301S mutation); PS1, presenilin 1; SHR, spontaneously hypertensive rat; STZ-icv, streptozotocin intracerebroventricular; Tg, transgenic; 3xTg, 3xTg-AD, the Laferla mouse [APP K670\_M671delinsNL (Swedish), MAPT P301L, PSEN1 M146V]; Tg2576, hsaio mice, App-Swe, App-sw, APP(sw), APPSwe; TgCRND8, APP(swe/ind) CRND8; THRSP OE, thyroid hormone-responsive gene overexpression.

adulthood which leads to the male prominence that disappears in adult ADHD. Nevertheless, the latter must be acknowledged in a broader context since the exact causes driving the apparent sexual dimorphism of both diseases are yet to be understood and it is possible that at least some of the factors are more cultural and not biological. For example, there is evidence that female children are underdiagnosed in the community setting resulting in biased and overemphasized estimates pertaining to male predominance (Ramtekkar et al., 2010). Furthermore, regardless of the female predominance of sAD, some animal models of the disease demonstrate the male predominance of some ADHD-like phenotypic traits. For example, female 3xTg mice demonstrate less circadian dysrhythmia in comparison with male transgenic animals (Wu et al., 2018).

Summarizing the aforementioned, the analysis of behavioral traits and phenotypes in animal models of ADHD and AD provides additional evidence in favor of the hypothesis of shared etiopathogenesis. Furthermore, considering molecular similarities, primarily related to Wnt and mTOR pathways (described in detail in chapters 5.1 and 5.2), data from animal models support the existence of a common pathophysiological phenomenon involved in the development of both AD and ADHD (Table 2). As studies indicate that manifestation of primary phenotypic characteristics (ADHD predominant—e.g., animal models of ADHD when tested at a young age, some AD models when tested before the development of cognitive deficits; AD-predominant—e.g., animal models of AD in the late phase, some ADHD animal models after locomotor hyperactivity subsides) is dependent on age. Therefore, molecular alterations ensue, longitudinal studies with animal models of both diseases focused on the temporal association of molecular and behavioral alterations will be necessary to fully entangle the association between ADHD and AD.

## 7. Methylphenidate in attention-deficit hyperactivity disorder and Alzheimer's disease and the link to Wnt/mTOR

Unlike for AD, pharmacological interventions for ADHD have shown a high level of efficacy supported by decades of clinical use and thousands of research studies (Banaschewski et al., 2018; Cortese et al., 2018). In child and adolescent, the efficacy lowering total symptoms following meta-analysis of total 22 studies with 1,603 patients treated with MPH vs. 1,251 placebo controls was estimated to be 0.77 (Faraone and Buitelaar, 2010). For MPH immediate release, the long-term effects of MPH following meta-analysis of seven studies (444 patients) resulted in efficacy of 0.96 and 1.12 for inattention and hyperactivity/impulsivity, respectively (Maia et al., 2017). Moreover, in a recent meta-analysis of 31 studies (804 children), dose-dependent effect of MPH on neurocognitive functioning in children with ADHD showed beneficial effects on all neurocognitive functions ( $d = 0.20$ – $0.73$ ) with linear dosing effects (Vertessen et al., 2022). In adults with ADHD, meta-analysis in eight studies (2,036 patients) found that MPH treatment efficacy of up to 0.58, with increase efficacy of 0.12 for every 10 mg increment of MPH (Castells et al., 2011). MPH is the first-line treatment for

ADHD in children and adolescents according to the NICE and the German guidelines (Banaschewski et al., 2018; Cortese et al., 2018). Safety and efficacy have also been demonstrated in adults with ADHD (Castells et al., 2011; Cortese et al., 2018; Solmi et al., 2020), however, despite evidence based guidelines, only half of the European countries have approved the use of MPH for the management of adult ADHD (Chappuy et al., 2020). In AD, MPH has been used as a treatment for apathy (Ruthirakuhan et al., 2018; Kishi et al., 2020; Mintzer et al., 2021), and although it was shown to be a safe and efficacious medication, this use is still off-label. Indeed, in a very small meta-analysis of three double-blind, randomized, placebo-controlled trials (RCTs) investigating MPH treatment of apathy as a primary or secondary outcome in people with AD ( $n = 145$ ), it was shown that MPH treatment is associated with small improvements (in apathy scores) in AD patients (Ruthirakuhan et al., 2018). Interestingly, a slight improvement in cognition measured using mini-mental state examination (MMSE) was observed as well (mean difference of 1.98, CI 1.06–2.91), however, due to a low number of studies, no conclusion could be made. In another meta-analysis including modafinil as a psychostimulant treatment of apathy in AD patients (3 MPH and 1 modafinil study,  $n = 156$ ), an increase in cognitive scores (MMSE) was found alongside improvement of apathy (Kishi et al., 2020). In the recently published RCT with a 6 month follow-up ( $n = 301$ ), MPH improved apathy scores compared to placebo, with improved Alzheimer's Disease Cooperative Study Clinical Global Impression at 6 months (Mintzer et al., 2021). However, there was no apparent difference in comparison with the placebo group in cognitive performance nor the quality of life (Mintzer et al., 2021). The absence of the effects on cognition in some AD trials may be due to timing, as a small RCT with MCI patients ( $n = 15$ ) demonstrated a beneficial effect of MPH on memory tests (Press et al., 2021). The latter might be due to the neurogenic capacity still available in MCI compared to AD patients.

Despite its well-known clinical efficacy, the exact molecular mechanisms responsible for the beneficial effects of MPH in ADHD remain elusive (Yde Ohki et al., 2020). The effects of MPH are usually attributed to its ability to block the reuptake of dopamine, noradrenaline, and (in low affinity) serotonin to potentiate the effects of monoamines in the synaptic cleft (Quintero et al., 2022). Nevertheless, accumulating evidence suggests that the ability of MPH to stimulate cortical maturation [responsible for its long-term effects (Shaw et al., 2009; Walhovd et al., 2020)] may be mediated by a separate mechanism not related to the inhibition of monoamine transporters (Bartl et al., 2010, 2013b, 2017; Grünblatt et al., 2018; Yde Ohki et al., 2020). It has been reported that MPH can inhibit proliferation and enhance neuronal differentiation both *in vitro* (Bartl et al., 2013b; Grünblatt et al., 2018) and *in vivo* (Lee et al., 2012; Oakes et al., 2019) via an unknown molecular mechanism. One possible molecular pathway hypothesized to be responsible for these effects is the Wnt pathway (Yde Ohki et al., 2020). MPH was demonstrated to activate Wnt signaling in three distinct neuronal cell lines (murine stem cells, rat PC12, and human SH-SY5Y cells), independently of its action on the dopamine transporter (considering that the selective dopamine transporter inhibitor GBR-12909 exerted opposite effects) (Grünblatt et al., 2018). The ability of MPH to activate Wnt *in vitro* (Grünblatt et al., 2018) is in line with the reports from *in vivo* studies where the ability of low-dose MPH to promote cell proliferation



and survival was associated with increased activity of the Wnt-signaling pathway (Mines and Jope, 2012; Sadasivan et al., 2012; Dela Pena et al., 2013; Oakes et al., 2019; Yde Ohki et al., 2020). The signaling pathway revolving around the mTOR pathway with complementary biological functions to Wnt was proposed as another potential mediator of the effects of MPH on cortical maturation (Yde Ohki et al., 2020). Although mechanisms by which MPH regulates the mTORC1 signaling pathway remain elusive, its ability to modulate the activity of its components (e.g., Akt, GSK3 $\beta$ , p70S6K, 4E-BP1, CREB) has been demonstrated both *in vitro* (Schmitz et al., 2019) and *in vivo* (Warren et al., 2011).

Briefly, MPH is beneficial in treating childhood ADHD while showing beneficial effects in early AD patients, which, following the current evidence, might be also due to its influence on the Wnt/mTOR-pathway. However, longitudinal clinical studies will be required to confirm this hypothesis.

## 8. Conclusion

Following the aforementioned evidence regarding ADHD-AD being a continuum, with several overlapping pathways and mechanisms, it would be of high urgency to move into research over the lifespan in humans and animal models, as well as at the molecular and cellular levels modeling both disorders *in vitro* using e.g., iPSC-derived neural cells (2D and 3D). Moreover, the common Wnt/mTOR pathways that have been altered both in ADHD and AD, and the fact that some drug treatments may influence them, should be studied more in-depth, to explore the possibilities of prevention and/or rescue in these two frequent neurological disorders. Although out of scope of the current hypothesis paper, it should be noted that neurodevelopmental disorders in general also were argued to be linked to sAD (Folsom and Fatemi, 2013; Delhay and Bardoni, 2021; Ebstein et al., 2021) while neurodegenerative disease with cognitive decline have some overlap to ADHD (Golimstok et al., 2011; Gehricke et al., 2017; Prentice et al., 2021). In particular, keeping in mind all the above and the recent literature proposing normalization of altered Wnt/mTOR signaling as a novel mechanism of action for MPH used as ADHD-treatment, the accumulated evidence provide a convincing argument and an encouragement to explore the idea that a timely introduction of ADHD therapy may delay/prevent neurodegeneration and cognitive decline in AD.

## Data availability statement

The original contributions presented in this study are included in this article/**Supplementary material**, further inquiries can be directed to the corresponding author.

## References

Abu-Elfotuh, K., Abdel-Sattar, S. A., Abbas, A. N., Mahran, Y. F., Alshani, A. R., Hamdan, A. M. E., et al. (2022). The protective effect of thymoquinone or/and thymol against monosodium glutamate-induced attention-deficit/hyperactivity disorder (ADHD)-like behavior in rats: Modulation of Nrf2/HO-1, TLR4/NF-kappaB/NLRP3/caspase-1 and Wnt/beta-Catenin signaling pathways in rat model. *Biomed. Pharmacother.* 155:113799. doi: 10.1016/j.biopha.2022.113799

## Author contributions

EG, JH, PR, CT, and MS-P contributed to the conception and substantiation of the hypothesis. AB, VD, AK, and JO collected the literature evidence on animal modeling. PR, SW, EG, CT, and MS-P collected the literature evidence on clinical aspects. EG wrote the first draft of the manuscript. EG, JH, AB, VD, AK, JO, CT, and MS-P wrote sections of the manuscript. All authors contributed to the manuscript revision, read, and approved the submitted version.

## Funding

The presented research was funded by the Croatian Science Foundation (IP-2018-01-8938) and co-financed by the Scientific Centre of Excellence for Basic, Clinical, and Translational Neuroscience (project “Experimental and clinical research of hypoxic-ischemic damage in perinatal and adult brain”; GA KK01.1.1.01.0007 funded by the European Union through the European Regional Development Fund).

## Conflict of interest

The authors declare that the research was conducted in the absence of any commercial or financial relationships that could be construed as a potential conflict of interest.

## Publisher's note

All claims expressed in this article are solely those of the authors and do not necessarily represent those of their affiliated organizations, or those of the publisher, the editors and the reviewers. Any product that may be evaluated in this article, or claim that may be made by its manufacturer, is not guaranteed or endorsed by the publisher.

## Supplementary material

The Supplementary Material for this article can be found online at: <https://www.frontiersin.org/articles/10.3389/fnins.2023.1104985/full#supplementary-material>

Ackers, I., and Malgor, R. (2018). Interrelationship of canonical and non-canonical Wnt signalling pathways in chronic metabolic diseases. *Diab Vasc Dis Res* 15, 3–13. doi: 10.1177/1479164117738442

Ahmad, F., Singh, K., Das, D., Gowaikar, R., Shaw, E., Ramachandran, A., et al. (2017). Reactive oxygen species-mediated loss of synaptic Akt1 signaling leads to

- deficient activity-dependent protein translation early in Alzheimer's disease. *Antioxid. Redox. Signal.* 27, 1269–1280. doi: 10.1089/ars.2016.6860
- Ai, Y., Zhao, J., Liu, H., Li, J., and Zhu, T. (2022). The relationship between diabetes mellitus and attention deficit hyperactivity disorder: A systematic review and meta-analysis. *Front. Pediatr.* 10:936813. doi: 10.3389/fped.2022.936813
- Ali, E. S., Mitra, K., Akter, S., Ramproshad, S., Mondal, B., Khan, I. N., et al. (2022). Recent advances and limitations of mTOR inhibitors in the treatment of cancer. *Cancer Cell Int.* 22:284. doi: 10.1186/s12935-022-02706-8
- Ali, M., Bukhari, S. A., Ali, M., and Lee, H. W. (2017). Upstream signalling of mTORC1 and its hyperactivation in type 2 diabetes (T2D). *BMB Rep.* 50, 601–609.
- Alves, S. S., Silva-Junior, R., Servilha-Menezes, G., Homolák, J., Salkovic-Petrisic, M., and Garcia-Cairasco, N. (2021). Insulin resistance as a common link between current Alzheimer's disease hypotheses. *J. Alzheimers Dis.* 82, 71–105. doi: 10.3233/JAD-210234
- Alzheimer's Disease International (2022). *Dementia statistics [Online]*. Alzheimer's disease international. Available online at: <https://www.alz.co.uk/research/statistics> (accessed October 24, 2022).
- Amal, H., Gong, G., Gjonesta, E., Lewis, S. M., Wishnok, J. S., Tsai, L. H., et al. (2019). S-nitrosylation of E3 ubiquitin-protein ligase RNF213 alters non-canonical Wnt/Ca<sup>2+</sup> signaling in the P301S mouse model of tauopathy. *Transl. Psychiatry* 9:44. doi: 10.1038/s41398-019-0388-7
- American Psychiatric Association (2013). *Diagnostic and statistical manual of mental disorders: DSM-5*. Washington, DC: American Psychiatric Association.
- Andrade, A., Brennecke, A., Mallat, S., Brown, J., Gomez-Rivadeneira, J., Czepl, N., et al. (2019). Genetic associations between voltage-gated calcium channels and psychiatric disorders. *Int. J. Mol. Sci.* 20:3537. doi: 10.3390/ijms20143537
- Antal, B., McMahon, L. P., Sultan, S. F., Lithen, A., Wexler, D. J., Dickerson, B., et al. (2022). Type 2 diabetes mellitus accelerates brain aging and cognitive decline: Complementary findings from UK Biobank and meta-analyses. *Elife* 11:e73138. doi: 10.7554/eLife.73138
- Arendash, G. W., King, D. L., Gordon, M. N., Morgan, D., Hatcher, J. M., Hope, C. E., et al. (2001). Progressive, age-related behavioral impairments in transgenic mice carrying both mutant amyloid precursor protein and presenilin-1 transgenes. *Brain Res.* 891, 42–53. doi: 10.1016/S0006-8993(00)03186-3
- Armand-Ugon, M., Ansoleaga, B., Berjaoui, S., and Ferrer, I. (2017). Reduced mitochondrial activity is early and steady in the entorhinal cortex but it is mainly unmodified in the frontal cortex in Alzheimer's disease. *Curr. Alzheimer Res.* 14, 1327–1334. doi: 10.2174/1567205014666170505095921
- Austad, S. N., Ballinger, S., Buford, T. W., Carter, C. S., Smith, D. L. Jr., Darley-Usmar, V., et al. (2022). Targeting whole body metabolism and mitochondrial bioenergetics in the drug development for Alzheimer's disease. *Acta Pharm. Sin. B* 12, 511–531. doi: 10.1016/j.apsb.2021.06.014
- Avrami, L., Farfara, D., Shaham-Kol, M., Vassar, R., Frenkel, D., and Eldar-Finkelman, H. (2013). Inhibition of glycogen synthase kinase-3 ameliorates beta-amyloid pathology and restores lysosomal acidification and mammalian target of rapamycin activity in the Alzheimer disease mouse model: In vivo and in vitro studies. *J. Biol. Chem.* 288, 1295–1306. doi: 10.1074/jbc.M112.409250
- Babic Perhoc, A., Osmanovic Barilar, J., Knezovic, A., Farkas, V., Bagaric, R., Svarc, A., et al. (2019). Cognitive, behavioral and metabolic effects of oral galactose treatment in the transgenic Tg2576 mice. *Neuropharmacology* 148, 50–67. doi: 10.1016/j.neuropharm.2018.12.018
- Bachiller, S., Jimenez-Ferrer, I., Paulus, A., Yang, Y., Swanberg, M., Deierborg, T., et al. (2018). Microglia in neurological diseases: A road map to brain-disease dependent-inflammatory response. *Front. Cell. Neurosci.* 12:488. doi: 10.3389/fncel.2018.00488
- Baddeley, A. (2000). The episodic buffer: A new component of working memory? *Trends Cogn. Sci.* 4, 417–423.
- Bakhtiari, R., Mohammadi Sepahvand, N., Nili Ahmadabadi, M., Nadjar Araabi, B., and Esteki, H. (2012). Computational model of excitatory/inhibitory ratio imbalance role in attention deficit disorders. *J. Comput. Neurosci.* 33, 389–404. doi: 10.1007/s10827-012-0391-y
- Balabanski, L., Serbezov, D., Atanasoska, M., Karachanak-Yankova, S., Hadjidekova, S., Nikolova, D., et al. (2021). Rare genetic variants prioritize molecular pathways for semaphorin interactions in Alzheimer's disease patients. *Biotechnol. Biotechnol. Equip.* 35, 1256–1262. doi: 10.1080/13102818.2021.1964382
- Banaschewski, T., Hohmann, S., and Millenet, S. (2018). *Aufmerksamkeitsdefizit-/hyperaktivitätsstörung (ADHS) im Kindes- jugend- und erwachsenenalter*. Duesseldorf: AWMF.
- Bansal, S., Agrawal, M., Mahendiratta, S., Kumar, S., Arora, S., Joshi, R., et al. (2021). Everolimus: A potential therapeutic agent targeting PI3K/Akt pathway in brain insulin system dysfunction and associated neurobehavioral deficits. *Fundam. Clin. Pharmacol.* 35, 1018–1031. doi: 10.1111/fcp.12677
- Bardgett, M. E., Davis, N. N., Schultheis, P. J., and Griffith, M. S. (2011). Ciproxifan, an H3 receptor antagonist, alleviates hyperactivity and cognitive deficits in the APP Tg2576 mouse model of Alzheimer's disease. *Neurobiol. Learn. Mem.* 95, 64–72. doi: 10.1016/j.nlm.2010.10.008
- Barilar, J. O., Knezovic, A., Grünblatt, E., Riederer, P., and Salkovic-Petrisic, M. (2015). Nine-month follow-up of the insulin receptor signalling cascade in the brain of streptozotocin rat model of sporadic Alzheimer's disease. *J. Neural Transm. (Vienna)* 122, 565–576. doi: 10.1007/s00702-014-1323-y
- Bartl, J., Link, P., Schlosser, C., Gerlach, M., Schmitt, A., Walitz, S., et al. (2010). Effects of methylphenidate: The cellular point of view. *Atten. Defic. Hyperact. Disord.* 2, 225–232. doi: 10.1007/s12402-010-0039-6
- Bartl, J., Monoranu, C. M., Wagner, A. K., Kolter, J., Riederer, P., and Grünblatt, E. (2013a). Alzheimer's disease and type 2 diabetes: Two diseases, one common link? *World J. Biol. Psychiatry* 14, 233–240. doi: 10.3109/15622975.2011.650204
- Bartl, J., Mori, T., Riederer, P., Ozawa, H., and Grünblatt, E. (2013b). Methylphenidate enhances neural stem cell differentiation. *J. Mol. Psychiatry* 1:5. doi: 10.1186/2049-9256-1-5
- Bartl, J., Palazzesi, F., Parrinello, M., Hommers, L., Riederer, P., Walitz, S., et al. (2017). The impact of methylphenidate and its enantiomers on dopamine synthesis and metabolism in vitro. *Prog. Neuropsychopharmacol. Biol. Psychiatry* 79(Pt B), 281–288. doi: 10.1016/j.pnpbp.2017.07.002
- Baudic, S., Barba, G. D., Thibaudet, M. C., Smaghe, A., Remy, P., and Traykov, L. (2006). Executive function deficits in early Alzheimer's disease and their relations with episodic memory. *Arch. Clin. Neuropsychol.* 21, 15–21. doi: 10.1016/j.acn.2005.07.002
- Bedrosian, T. A., Herring, K. L., Weil, Z. M., and Nelson, R. J. (2011). Altered temporal patterns of anxiety in aged and amyloid precursor protein (APP) transgenic mice. *Proc. Natl. Acad. Sci. U.S.A.* 108, 11686–11691. doi: 10.1073/pnas.1103098108
- Bedse, G., Di Domenico, F., Serviddio, G., and Cassano, T. (2015). Aberrant insulin signaling in Alzheimer's disease: Current knowledge. *Front. Neurosci.* 9:204. doi: 10.3389/fnins.2015.00204
- Bellenguez, C., Kucukali, F., Jansen, I. E., Klei, E. D., Moreno-Grau, S., Amin, N., et al. (2022). New insights into the genetic etiology of Alzheimer's disease and related dementias. *Nat. Genet.* 54, 412–436. doi: 10.1038/s41588-022-01024-z
- Bengoa-Vergniory, N., and Kypta, R. M. (2015). Canonical and noncanonical Wnt signaling in neural stem/progenitor cells. *Cell. Mol. Life Sci.* 72, 4157–4172. doi: 10.1007/s00018-015-2028-6
- Blagosklonny, M. V. (2006). Aging and immortality: Quasi-programmed senescence and its pharmacologic inhibition. *Cell Cycle* 5, 2087–2102. doi: 10.4161/cc.5.18.3288
- Bloom, G. S., Lazo, J. S., and Norambuena, A. (2018). Reduced brain insulin signaling: A seminal process in Alzheimer's disease pathogenesis. *Neuropharmacology* 136(Pt B), 192–195. doi: 10.1016/j.neuropharm.2017.09.016
- Blue, E. E., Thornton, T. A., Kooperberg, C., Liu, S., Wactawski-Wende, J., Manson, J., et al. (2021). Non-coding variants in MYH11, FZD3, and SORCS3 are associated with dementia in women. *Alzheimers Dement.* 17, 215–225. doi: 10.1002/alz.12181
- Boonen, R. A., van Tijn, P., and Zivkovic, D. (2009). Wnt signaling in Alzheimer's disease: Up or down, that is the question. *Ageing Res. Rev.* 8, 71–82. doi: 10.1016/j.arr.2008.11.003
- Cabana-Dominguez, J., Soler Artigas, M., Arribas, L., Alemany, S., Vilar-Ribo, L., Llonga, N., et al. (2022). Comprehensive analysis of omics data identifies relevant gene networks for Attention-Deficit/Hyperactivity Disorder (ADHD). *Transl. Psychiatry* 12:409. doi: 10.1038/s41398-022-02182-8
- Cai, Z., Chen, G., He, W., Xiao, M., and Yan, L. J. (2015). Activation of mTOR: A culprit of Alzheimer's disease? *Neuropsychiatr. Dis. Treat.* 11, 1015–1030. doi: 10.2147/NDT.S75717
- Callahan, B. L., Bierstone, D., Stuss, D. T., and Black, S. E. (2017). Adult ADHD: Risk factor for dementia or phenotypic mimic? *Front. Aging Neurosci.* 9:260. doi: 10.3389/fnagi.2017.00260
- Callahan, B. L., Ramakrishnan, N., Shammi, P., Bierstone, D., Taylor, R., Ozzoude, M., et al. (2022). Cognitive and neuroimaging profiles of older adults with attention deficit/hyperactivity disorder presenting to a memory clinic. *J. Atten. Disord.* 26, 1118–1129. doi: 10.1177/10870547211060546
- Callahan, B. L., Shammi, P., Taylor, R., Ramakrishnan, N., and Black, S. E. (2021). Longitudinal cognitive performance of older adults with ADHD presenting to a cognitive neurology clinic: A case series of change up to 21 years. *Front. Aging Neurosci.* 13:726374. doi: 10.3389/fnagi.2021.726374
- Cannon Homaei, S., Barone, H., Kleppe, R., Betari, N., Reif, A., and Haavik, J. (2022). ADHD symptoms in neurometabolic diseases: Underlying mechanisms and clinical implications. *Neurosci. Biobehav. Rev.* 132, 838–856. doi: 10.1016/j.neubiorev.2021.11.012
- Caricasole, A., Copani, A., Caraci, F., Aronica, E., Rozemuller, A. J., Caruso, A., et al. (2004). Induction of Dickkopf-1, a negative modulator of the Wnt pathway, is associated with neuronal degeneration in Alzheimer's brain. *J. Neurosci.* 24, 6021–6027. doi: 10.1523/JNEUROSCI.1381-04.2004
- Caruso, A., Motolese, M., Iacovelli, L., Caraci, F., Copani, A., Nicoletti, F., et al. (2006). Inhibition of the canonical Wnt signaling pathway by apolipoprotein E4 in PC12 cells. *J. Neurochem.* 98, 364–371. doi: 10.1111/j.1471-4159.2006.03867.x

- Castellanos, F. X., and Tannock, R. (2002). Neuroscience of attention-deficit/hyperactivity disorder: The search for endophenotypes. *Nat. Rev. Neurosci.* 3, 617–628. doi: 10.1038/nrn896
- Castells, X., Ramos-Quiroga, J. A., Rigau, D., Bosch, R., Nogueira, M., Vidal, X., et al. (2011). Efficacy of methylphenidate for adults with attention-deficit hyperactivity disorder: A meta-regression analysis. *CNS Drugs* 25, 157–169. doi: 10.2165/11539440-000000000-00000
- Chappuy, M., Boulanger, A., Nourredine, M., Fournier, P., and Rolland, B. (2020). Disparate regulatory status of methylphenidate for adults with ADHD across Europe. *Lancet Psychiatry* 7, e1–e2. doi: 10.1016/S2215-0366(19)30482-1
- Chen, Q., Hartman, C. A., Haavik, J., Harro, J., Klungsoyr, K., Hegvik, T. A., et al. (2018). Common psychiatric and metabolic comorbidity of adult attention-deficit/hyperactivity disorder: A population-based cross-sectional study. *PLoS One* 13:e0204516. doi: 10.1371/journal.pone.0204516
- Chen, Y., Liang, Z., Blanchard, J., Dai, C. L., Sun, S., Lee, M. H., et al. (2013). A non-transgenic mouse model (icv-STZ mouse) of Alzheimer's disease: Similarities to and differences from the transgenic model (3xTg-AD mouse). *Mol. Neurobiol.* 47, 711–725. doi: 10.1007/s12035-012-8375-5
- Chen, Y., Tian, Z., Liang, Z., Sun, S., Dai, C. L., Lee, M. H., et al. (2012). Brain gene expression of a sporadic (icv-STZ Mouse) and a familial mouse model (3xTg-AD mouse) of Alzheimer's disease. *PLoS One* 7:e51432. doi: 10.1371/journal.pone.0051432
- Cheng, P. W., Chen, Y. Y., Cheng, W. H., Lu, P. J., Chen, H. H., Chen, B. R., et al. (2015). Wnt signaling regulates blood pressure by downregulating a GSK-3 $\beta$ -mediated pathway to enhance insulin signaling in the central nervous system. *Diabetes* 64, 3413–3424. doi: 10.2337/db14-1439
- Cohen, E. M., Mohammed, S., Kavurma, M., Nedobov, P. E., Cartland, S., Farnham, M. M. J., et al. (2019). Microglia in the RVLm of SHR have reduced P2Y<sub>12</sub>R and CX3CR1 expression, shorter processes, and lower cell density. *Auton. Neurosci.* 216, 9–16. doi: 10.1016/j.autneu.2018.12.002
- Colby-Milley, J., Cavanagh, C., Jegu, S., Breitner, J. C., Quirion, R., and Adamantidis, A. (2015). Sleep-wake cycle dysfunction in the TgCRND8 mouse model of Alzheimer's disease: From early to advanced pathological stages. *PLoS One* 10:e0130177. doi: 10.1371/journal.pone.0130177
- Congress, W. (2021). Abstracts of the WASAD Congress, 2021: An international congress of the world association for stress related and anxiety disorders, held on 20–22 September 2021 in Vienna, Austria. *J. Neural Transm. (Vienna)* 128, 1767–1812. doi: 10.1007/s00702-021-02422-z
- Corona, J. C. (2020). Role of oxidative stress and neuroinflammation in attention-deficit/hyperactivity disorder. *Antioxidants (Basel)* 9:1039. doi: 10.3390/antiox9111039
- Correia, S. C., Santos, R. X., Perry, G., Zhu, X., Moreira, P. I., and Smith, M. A. (2011). Insulin-resistant brain state: The culprit in sporadic Alzheimer's disease? *Ageing Res. Rev.* 10, 264–273. doi: 10.1016/j.arr.2011.01.001
- Cortese, S., Adamo, N., Del Giovane, C., Mohr-Jensen, C., Hayes, A. J., Carucci, S., et al. (2018). Comparative efficacy and tolerability of medications for attention-deficit hyperactivity disorder in children, adolescents, and adults: A systematic review and network meta-analysis. *Lancet Psychiatry* 5, 727–738. doi: 10.1016/S2215-0366(18)30269-4
- Cortese, S., Faraone, S. V., Bernardi, S., Wang, S., and Blanco, C. (2016). Gender differences in adult attention-deficit/hyperactivity disorder: Results from the national epidemiologic survey on alcohol and related conditions (NESARC). *J. Clin. Psychiatry* 77, e421–e428. doi: 10.4088/JCP.14m09630
- Custodio, R. J. P., Botanas, C. J., de la Pena, J. B., Dela Pena, I. J., Kim, M., Sayson, L. V., et al. (2018). Overexpression of the thyroid hormone-responsive (THRSP) Gene in the striatum leads to the development of inattentive-like phenotype in mice. *Neuroscience* 390, 141–150. doi: 10.1016/j.neuroscience.2018.08.008
- Custodio, R. J. P., Kim, H. J., Kim, J., Ortiu D. M., Kim, M., Buctot, D. et al. (2023). Hippocampal dentate gyri proteomics reveals Wnt signaling involvement in the behavioral impairment in the THRSP-overexpressing ADHD mouse model. *Commun. Biol.* 6. doi: 10.1038/s42003-022-04387-5
- Damani, M. R., Zhao, L., Fontainhas, A. M., Amaral, J., Fariss, R. N., and Wong, W. T. (2011). Age-related alterations in the dynamic behavior of microglia. *Ageing Cell* 10, 263–276. doi: 10.1111/j.1474-9726.2010.00660.x
- De Felice, F. G., Lourenco, M. V., and Ferreira, S. T. (2014). How does brain insulin resistance develop in Alzheimer's disease? *Alzheimers Dement.* 10(1 Suppl), S26–S32. doi: 10.1016/j.jalz.2013.12.004
- de Rojas, I., Moreno-Grau, S., Tesi, N., Grenier-Boley, B., Andrade, V., Jansen, I., et al. (2020). Common variants in Alzheimer's disease: Novel association of six genetic variants with AD and risk stratification by polygenic risk scores. *medRxiv* [Preprint]. doi: 10.1101/19012021
- de Rojas, I., Moreno-Grau, S., Tesi, N., Grenier-Boley, B., Andrade, V., Jansen, I. E., et al. (2021). Common variants in Alzheimer's disease and risk stratification by polygenic risk scores. *Nat. Commun.* 12:3417. doi: 10.1038/s41467-021-22491-8
- Dela Pena, I., Jeon, S. J., Lee, E., Ryu, J. H., Shin, C. Y., Noh, M., et al. (2013). Neuronal development genes are key elements mediating the reinforcing effects of methamphetamine, amphetamine, and methylphenidate. *Psychopharmacology (Berl)* 230, 399–413. doi: 10.1007/s00213-013-3168-8
- Delhaye, S., and Bardoni, B. (2021). Role of phosphodiesterases in the pathophysiology of neurodevelopmental disorders. *Mol. Psychiatry* 26, 4570–4582. doi: 10.1038/s41380-020-00997-9
- Dellu-Hagedorn, F. (2006). Relationship between impulsivity, hyperactivity and working memory: A differential analysis in the rat. *Behav. Brain Funct.* 2:10. doi: 10.1186/1744-9081-2-10
- Dellu-Hagedorn, F., Trunet, S., and Simon, H. (2004). Impulsivity in youth predicts early age-related cognitive deficits in rats. *Neurobiol. Aging* 25, 525–537. doi: 10.1016/j.neurobiolaging.2003.06.006
- Demontis, D., Walters, G. B., Athanasiadis, G., Walters, R., Therrien, K., Nielsen, T. T., et al. (2023). Genome-wide analyses of ADHD identify 27 risk loci, refine the genetic architecture and implicate several cognitive domains. *Nat. Genet.* [Epub ahead of print]. doi: 10.1038/s41588-022-01285-8
- Demontis, D., Walters, R. K., Martin, J., Mattheisen, M., Als, T. D., Agerbo, E., et al. (2019). Discovery of the first genome-wide significant risk loci for attention deficit/hyperactivity disorder. *Nat. Genet.* 51, 63–75. doi: 10.1038/s41588-018-0269-7
- di Girolamo, G., Bracco, I. F., Portigliatti Pomeri, A., Puglisi, S., and Oliva, F. (2022). Prevalence of metabolic syndrome and insulin resistance in a sample of adult ADHD outpatients. *Front. Psychiatry* 13:891479. doi: 10.3389/fpsyt.2022.891479
- Di Lorenzo, R., Balducci, J., Poppi, C., Arcolin, E., Cutino, A., Ferri, P., et al. (2021). Children and adolescents with ADHD followed up to adulthood: A systematic review of long-term outcomes. *Acta Neuropsychiatr.* 33, 283–298. doi: 10.1017/neu.2021.23
- Diamond, A. (2013). Executive functions. *Annu. Rev. Psychol.* 64, 135–168. doi: 10.1146/annurev-psych-113011-143750
- Dobrosavljevic, M., Zhang, L., Garcia-Argibay, M., Du Rietz, E., Andershed, H., Chang, Z., et al. (2021). Attention-deficit/hyperactivity disorder as a risk factor for dementia and mild cognitive impairment: A population-based register study. *Eur. Psychiatry* 65, 1–19. doi: 10.1192/j.eurpsy.2021.2261
- Dougnon, G., and Matsui, H. (2022). Modelling autism spectrum disorder (ASD) and attention-deficit/hyperactivity disorder (ADHD) using mice and zebrafish. *Int. J. Mol. Sci.* 23:7550. doi: 10.3390/ijms23147550
- Dowling, R. J., Topisirovic, I., Fonseca, B. D., and Sonenberg, N. (2010). Dissecting the role of mTOR: Lessons from mTOR inhibitors. *Biochim. Biophys. Acta* 1804, 433–439. doi: 10.1016/j.bbapap.2009.12.001
- Ebstein, F., Kury, S., Papendorf, J. J., and Kruger, E. (2021). Neurodevelopmental disorders (n.d.) caused by genomic alterations of the ubiquitin-proteasome system (UPS): The possible contribution of immune dysregulation to disease pathogenesis. *Front. Mol. Neurosci.* 14:733012. doi: 10.3389/fnmol.2021.733012
- El Sayed, N. S., Kandil, E. A., and Ghoneum, M. H. (2021). Enhancement of insulin/PI3K/Akt signaling pathway and modulation of gut microbiome by probiotics fermentation technology, a kefir grain product, in sporadic Alzheimer's disease model in mice. *Front. Pharmacol.* 12:666502. doi: 10.3389/fphar.2021.666502
- Fanelli, G., Franke, B., De Witte, W., Ruisch, I. H., Haavik, J., van Gils, V., et al. (2022). Insulinopathies of the brain? Genetic overlap between somatic insulin-related and neuropsychiatric disorders. *Transl. Psychiatry* 12:59. doi: 10.1038/s41398-022-01817-0
- Faraone, S. V., and Buitelaar, J. (2010). Comparing the efficacy of stimulants for ADHD in children and adolescents using meta-analysis. *Eur. Child Adolesc. Psychiatry* 19, 353–364. doi: 10.1007/s00787-009-0054-3
- Faraone, S. V., and Larsson, H. (2019). Genetics of attention deficit hyperactivity disorder. *Mol. Psychiatry* 24, 562–575. doi: 10.1038/s41380-018-0070-0
- Faraone, S. V., Asherson, P., Banaschewski, T., Biederman, J., Buitelaar, J. K., Ramos-Quiroga, J. A., et al. (2015). Attention-deficit/hyperactivity disorder. *Nat. Rev. Dis. Primers* 1:15020. doi: 10.1038/nrdp.2015.20
- Fayyad, J., Sampson, N. A., Hwang, I., Adamowski, T., Aguilar-Gaxiola, S., Al-Hamzawi, A., et al. (2017). The descriptive epidemiology of DSM-IV Adult ADHD in the World Health Organization World Mental Health Surveys. *Atten. Defic. Hyperact. Disord.* 9, 47–65. doi: 10.1007/s12402-016-0208-3
- Feltes, B. C., de Faria Poloni, J., and Bonatto, D. (2015). Development and aging: Two opposite but complementary phenomena. *Interdiscip. Top. Gerontol.* 40, 74–84. doi: 10.1159/000364932
- Flannery, P. J., and Trushina, E. (2019). Mitochondrial dysfunction in Alzheimer's disease and progress in mitochondria-targeted therapeutics. *Curr. Behav. Neurosci. Rep.* 6, 88–102. doi: 10.1007/s40473-019-00179-0
- Flowers, A., Bell-Temin, H., Jalloh, A., Stevens, S. M. Jr., and Bickford, P. C. (2017). Proteomic analysis of aged microglia: Shifts in transcription, bioenergetics, and nutrient response. *J. Neuroinflammation* 14, 96. doi: 10.1186/s12974-017-0840-7



- Fluegge, K., and Fluegge, K. (2018). Antecedent ADHD, dementia, and metabolic dysregulation: A U.S. based cohort analysis. *Neurochem. Int.* 112, 255–258. doi: 10.1016/j.neuint.2017.08.005
- Folke, J., Pakkenberg, B., and Brudek, T. (2019). Impaired Wnt signaling in the prefrontal cortex of Alzheimer's disease. *Mol. Neurobiol.* 56, 873–891. doi: 10.1007/s12035-018-1103-z
- Folsom, T. D., and Fatemi, S. H. (2013). The involvement of reelin in neurodevelopmental disorders. *Neuropharmacology* 68, 122–135. doi: 10.1016/j.neuropharm.2012.08.015
- Foschiera, L. N., Schmitz, F., and Wyse, A. T. S. (2022). Evidence of methylphenidate effect on mitochondria, redox homeostasis, and inflammatory aspects: Insights from animal studies. *Prog. Neuropsychopharmacol. Biol. Psychiatry* 116:110518. doi: 10.1016/j.pnpbp.2022.110518
- Fox, G. B., Pan, J. B., Esbenshade, T. A., Bennani, Y. L., Black, L. A., Faghii, R., et al. (2002). Effects of histamine H3 receptor ligands GT-2331 and ciproxifan in a repeated acquisition avoidance response in the spontaneously hypertensive rat pup. *Behav. Brain Res.* 131, 151–161. doi: 10.1016/S0166-4328(01)00379-5
- Francois, A., Rioux Bilan, A., Quillard, N., Fernandez, B., Janet, T., Chassaing, D., et al. (2014). Longitudinal follow-up of autophagy and inflammation in brain of APPswePS1dE9 transgenic mice. *J. Neuroinflammation* 11:139. doi: 10.1186/s12974-014-0139-x
- Franke, B., Faraone, S. V., Asherson, P., Buitelaar, J., Bau, C. H., Ramos-Quiroga, J. A., et al. (2012). The genetics of attention deficit/hyperactivity disorder in adults, a review. *Mol. Psychiatry* 17, 960–987. doi: 10.1038/mp.2011.138
- Franke, B., Michelini, G., Asherson, P., Banaschewski, T., Bilbow, A., Buitelaar, J. K., et al. (2018). Live fast, die young? A review on the developmental trajectories of ADHD across the lifespan. *Eur. Neuropsychopharmacol.* 28, 1059–1088. doi: 10.1016/j.euroneuro.2018.08.001
- Frölich, L., Blum-Degen, D., Bernstein, H. G., Engelsberger, S., Humrich, J., Laufer, S., et al. (1998). Brain insulin and insulin receptors in aging and sporadic Alzheimer's disease. *J. Neural Transm. (Vienna)* 105, 423–438. doi: 10.1007/s007020050068
- Garcia-Argibay, M., du Rietz, E., Lu, Y., Martin, J., Haan, E., Lehto, K., et al. (2022). The role of ADHD genetic risk in mid-to-late life somatic health conditions. *Transl. Psychiatry* 12, 152. doi: 10.1038/s41398-022-01919-9
- Gauthier, A. C., DeAngeli, N. E., and Bucci, D. J. (2015). Cross-fostering differentially affects ADHD-related behaviors in spontaneously hypertensive rats. *Dev. Psychobiol.* 57, 226–236. doi: 10.1002/dev.21286
- GBD 2019 Dementia Forecasting Collaborators (2022). Estimation of the global prevalence of dementia in 2019 and forecasted prevalence in 2050: An analysis for the Global Burden of Disease Study 2019. *Lancet Public Health* 7, e105–e125. doi: 10.1016/S2468-2667(21)00249-8
- Gehricke, J. G., Kruggel, F., Thampipop, T., Alejo, S. D., Tatos, E., Fallon, J., et al. (2017). The brain anatomy of attention-deficit/hyperactivity disorder in young adults – A magnetic resonance imaging study. *PLoS One* 12:e0175433. doi: 10.1371/journal.pone.0175433
- Germano, C., and Kinsella, G. J. (2005). Working memory and learning in early Alzheimer's disease. *Neuropsychol. Rev.* 15, 1–10. doi: 10.1007/s11065-005-3583-7
- Golinstok, A., Rojas, J. I., Romano, M., Zurru, M. C., Doctorovich, D., and Cristiano, E. (2011). Previous adult attention-deficit and hyperactivity disorder symptoms and risk of dementia with Lewy bodies: A case-control study. *Eur. J. Neurol.* 18, 78–84. doi: 10.1111/j.1468-1331.2010.03064.x
- Gonon, F. (2009). The dopaminergic hypothesis of attention-deficit/hyperactivity disorder needs re-examining. *Trends Neurosci.* 32, 2–8. doi: 10.1016/j.tins.2008.09.010
- Gorman, M. R., and Yellon, S. (2010). Lifespan daily locomotor activity rhythms in a mouse model of amyloid-induced neuropathology. *Chronobiol. Int.* 27, 1159–1177. doi: 10.3109/07420528.2010.485711
- Govindpani, K., McNamara, L. G., Smith, N. R., Vinnakota, C., Waldvogel, H. J., Faull, R. L., et al. (2019). Vascular dysfunction in Alzheimer's disease: A prelude to the pathological process or a consequence of it? *J. Clin. Med.* 8:651. doi: 10.3390/jcm8050651
- Greven, C. U., Richards, J. S., and Buitelaar, J. K. (2018). “Sex differences in ADHD,” in *Oxford textbook of attention deficit hyperactivity disorder*, eds T. Banaschewski, D. Coghill, and A. Zuddas (Oxford: Oxford University Press).
- Grünblatt, E., Bartl, J., and Walitza, S. (2018). Methylphenidate enhances neuronal differentiation and reduces proliferation concomitant to activation of Wnt signal transduction pathways. *Transl. Psychiatry* 8:51. doi: 10.1038/s41398-018-0096-8
- Grünblatt, E., Bartl, J., Iuhos, D. I., Knezovic, A., Trkulja, V., Riederer, P., et al. (2015). Characterization of cognitive deficits in spontaneously hypertensive rats, accompanied by brain insulin receptor dysfunction. *J. Mol. Psychiatry* 3:6. doi: 10.1186/s40303-015-0012-6
- Grünblatt, E., Nemoda, Z., Werling, A. M., Roth, A., Angyal, N., Tarnok, Z., et al. (2019). The involvement of the canonical Wnt-signaling receptor LRP5 and LRP6 gene variants with ADHD and sexual dimorphism: Association study and meta-analysis. *Am. J. Med. Genet. Part B* 180, 365–376. doi: 10.1002/ajmg.b.32695
- Grünblatt, E., Salkovic-Petrisic, M., Osmanovic, J., Riederer, P., and Hoyer, S. (2007). Brain insulin system dysfunction in streptozotocin intracerebroventricularly treated rats generates hyperphosphorylated tau protein. *J. Neurochem.* 101, 757–770. doi: 10.1111/j.1471-4159.2006.04368.x
- Guillen, C., and Benito, M. (2018). mTORC1 overactivation as a key aging factor in the progression to Type 2 diabetes mellitus. *Front. Endocrinol. (Lausanne)* 9:621. doi: 10.3389/fendo.2018.00621
- Hampel, H., Hardy, J., Blennow, K., Chen, C., Perry, G., Kim, S. H., et al. (2021). The amyloid-beta pathway in Alzheimer's disease. *Mol. Psychiatry* 26, 5481–5503. doi: 10.1038/s41380-021-01249-0
- Han, J., Wang, B., Xiao, Z., Gao, Y., Zhao, Y., Zhang, J., et al. (2008). Mammalian target of rapamycin (mTOR) is involved in the neuronal differentiation of neural progenitors induced by insulin. *Mol. Cell Neurosci.* 39, 118–124. doi: 10.1016/j.mcn.2008.06.003
- Harris, S. S., Green, S. M., Kumar, M., and Urs, N. M. (2022). A role for cortical dopamine in the paradoxical calming effects of psychostimulants. *Sci. Rep.* 12:3129. doi: 10.1038/s41598-022-07029-2
- Hasani, S. A., Mayeli, M., Salehi, M. A., and Barzegar Parizi, R. (2021). A systematic review of the association between amyloid-beta and tau pathology with functional connectivity alterations in the Alzheimer dementia spectrum utilizing PET Scan and rsfMRI. *Dement. Geriatr. Cogn. Dis. Extra* 11, 78–90. doi: 10.1159/000516164
- Hayward, A., Tomlinson, A., and Neill, J. C. (2016). Low attentive and high impulsive rats: A translational animal model of ADHD and disorders of attention and impulse control. *Pharmacol. Ther.* 158, 41–51. doi: 10.1016/j.pharmthera.2015.11.010
- He, P., and Shen, Y. (2009). Interruption of  $\beta$ -catenin signaling reduces neurogenesis in Alzheimer's disease. *J. Neurosci.* 29, 6545–6557. doi: 10.1523/jneurosci.0421-09.2009
- Hendley, E. D., Wessel, D. J., Atwater, D. G., Gellis, J., Whitehorn, D., and Low, W. C. (1985). Age, sex and strain differences in activity and habituation in SHR and WKY Rats. *Physiol. Behav.* 34, 379–383. doi: 10.1016/0031-9384(85)90199-4
- Heni, M., Kullmann, S., Preissl, H., Fritsche, A., and Haring, H. U. (2015). Impaired insulin action in the human brain: Causes and metabolic consequences. *Nat. Rev. Endocrinol.* 11, 701–711. doi: 10.1038/nrendo.2015.173
- Hernandez, F., Lucas, J. J., and Avila, J. (2013). GSK3 and tau: Two convergence points in Alzheimer's disease. *J. Alzheimers Dis.* 33(Suppl. 1), S141–S144. doi: 10.3233/JAD-2012-129025
- Holper, L., Ben-Shachar, D., and Mann, J. J. (2019). Multivariate meta-analyses of mitochondrial complex I and IV in major depressive disorder, bipolar disorder, schizophrenia, Alzheimer disease, and Parkinson disease. *Neuropsychopharmacology* 44, 837–849. doi: 10.1038/s41386-018-0090-0
- Homolak, J., Perhoc, A. B., Knezovic, A., Osmanovic Barilar, J., and Salkovic-Petrisic, M. (2021). Additional methodological considerations regarding optimization of the dose of intracerebroventricular streptozotocin A response to: “Optimization of intracerebroventricular streptozotocin dose for the induction of neuroinflammation and memory impairments in rats” by Ghosh et al., *Metab Brain Dis* 2020 July 21. *Metab. Brain Dis.* 36, 97–102. doi: 10.1007/s11011-020-00637-9
- Hoogman, M., Bralten, J., Hibar, D. P., Mennes, M., Zwiers, M. P., Schwen, L. S. J., et al. (2017). Subcortical brain volume differences in participants with attention deficit hyperactivity disorder in children and adults: A cross-sectional mega-analysis. *Lancet Psychiatry* 4, 310–319. doi: 10.1016/S2215-0366(17)30049-4
- Hopkins, M. E., Sharma, M., Evans, G. C., and Bucci, D. J. (2009). Voluntary physical exercise alters attentional orienting and social behavior in a rat model of attention-deficit/hyperactivity disorder. *Behav. Neurosci.* 123, 599–606. doi: 10.1037/a0015632
- Hours, C., Recasens, C., and Baleyte, J. M. (2022). ASD and ADHD comorbidity: What are we talking about? *Front. Psychiatry* 13:837424. doi: 10.3389/fpsy.2022.837424
- Huang, M., Liang, Y., Chen, H., Xu, B., Chai, C., and Xing, P. (2018). The role of fluoxetine in activating Wnt/beta-catenin signaling and repressing beta-amyloid production in an Alzheimer mouse model. *Front. Aging Neurosci.* 10:164. doi: 10.3389/fnagi.2018.00164
- Huang, Y. L., Zhang, J. N., Hou, T. Z., Gu, L., Yang, H. M., and Zhang, H. (2022). Inhibition of Wnt/beta-catenin signaling attenuates axonal degeneration in models of Parkinson's disease. *Neurochem. Int.* 159, 105389. doi: 10.1016/j.neuint.2022.105389
- Hussaini, S. M., Choi, C. I., Cho, C. H., Kim, H. J., Jun, H., and Jang, M. H. (2014). Wnt signaling in neuropsychiatric disorders: Ties with adult hippocampal neurogenesis and behavior. *Neurosci. Biobehav. Rev.* 47, 369–383. doi: 10.1016/j.neubiorev.2014.09.005
- Inestrosa, N. C., and Varela-Nallar, L. (2014). Wnt signaling in the nervous system and in Alzheimer's disease. *J. Mol. Cell Biol.* 6, 64–74. doi: 10.1093/jmcb/mjt051
- Irizarry, M. C., McNamara, M., Fedorchak, K., Hsiao, K., and Hyman, B. T. (1997). APPSw transgenic mice develop age-related A beta deposits and neuropil



- abnormalities, but no neuronal loss in CA1. *J. Neuropathol. Exp. Neurol.* 56, 965–973. doi: 10.1097/00005072-199709000-00002
- Ishikawa, S., and Ishikawa, F. (2022). “To G0 or Not to G0: Cell cycle paradox in senescence and brain aging,” in *Aging mechanisms I : Longevity, metabolism, and brain aging*, ed. N. Mori (Singapore: Springer Nature Singapore), 97–113.
- Ivanchak, N., Abner, E. L., Carr, S. A., Freeman, S. J., Seybert, A., Ranseen, J., et al. (2011). Attention-deficit/hyperactivity disorder in childhood is associated with cognitive test profiles in the geriatric population but not with mild cognitive impairment or Alzheimer's disease. *J. Aging Res.* 2011, 729801. doi: 10.4061/2011/729801
- Jankowsky, J. L., Slunt, H. H., Gonzales, V., Savonenko, A. V., Wen, J. C., Jenkins, N. A., et al. (2005). Persistent amyloidosis following suppression of Abeta production in a transgenic model of Alzheimer disease. *PLoS Med.* 2:e355. doi: 10.1371/journal.pmed.0020355
- Jensen, C. M., and Steinhausen, H. C. (2015). Comorbid mental disorders in children and adolescents with attention-deficit/hyperactivity disorder in a large nationwide study. *Atten. Defic. Hyperact. Disord.* 7, 27–38. doi: 10.1007/s12402-014-0142-1
- Jia, G., Aroor, A. R., Martinez-Lemus, L. A., and Sowers, J. R. (2014). Overnutrition, mTOR signaling, and cardiovascular diseases. *Am. J. Physiol. Regul. Integr. Comp. Physiol.* 307, R1198–R1206. doi: 10.1152/ajpregu.00262.2014
- Jia, L., Pina-Crespo, J., and Li, Y. (2019). Restoring Wnt/beta-catenin signaling is a promising therapeutic strategy for Alzheimer's disease. *Mol. Brain* 12:104. doi: 10.1186/s13041-019-0525-5
- Johnson, A. C., Miller, J. E., and Cipolla, M. J. (2020). Memory impairment in spontaneously hypertensive rats is associated with hippocampal hypoperfusion and hippocampal vascular dysfunction. *J. Cereb. Blood Flow Metab.* 40, 845–859. doi: 10.1177/0271678X19848510
- Johnson, S. C., Sangesland, M., Kaerberlein, M., and Rabinovitch, P. S. (2015). Modulating mTOR in aging and health. *Interdiscip. Top. Gerontol.* 40, 107–127. doi: 10.1159/000364974
- Kaidanovich-Beilin, O., and Woodgett, J. R. (2011). GSK-3: Functional insights from cell biology and animal models. *Front. Mol. Neurosci.* 4:40. doi: 10.3389/fnmol.2011.00040
- Kakuszi, B., Szuromi, B., Bitter, I., and Czobor, P. (2020). Attention deficit hyperactivity disorder: Last in, first out – Delayed brain maturation with an accelerated decline? *Eur. Neuropsychopharmacol.* 34, 65–75. doi: 10.1016/j.euroneuro.2020.03.011
- Kantak, K. M. (2022). Rodent models of attention-deficit hyperactivity disorder: An updated framework for model validation and therapeutic drug discovery. *Pharmacol. Biochem. Behav.* 216:173378. doi: 10.1016/j.pbb.2022.173378
- Kellar, D., and Craft, S. (2020). Brain insulin resistance in Alzheimer's disease and related disorders: Mechanisms and therapeutic approaches. *Lancet Neurol.* 19, 758–766. doi: 10.1016/S1474-4422(20)30231-3
- Kim, S. H., Vlkolinsky, R., Cairns, N., and Lubec, G. (2000). Decreased levels of complex III core protein I and complex V beta chain in brains from patients with Alzheimer's disease and down syndrome. *Cell Mol. Life Sci.* 57, 1810–1816. doi: 10.1007/pl00000661
- Kinney, J. W., Bemiller, S. M., Murtishaw, A. S., Leisgang, A. M., Salazar, A. M., and Lamb, B. T. (2018). Inflammation as a central mechanism in Alzheimer's disease. *Alzheimers Dement.* (N. Y.) 4, 575–590. doi: 10.1016/j.trci.2018.06.014
- Kishi, T., Sakuma, K., and Iwata, N. (2020). Efficacy and safety of psychostimulants for Alzheimer's disease: A systematic review and meta-analysis. *Pharmacopsychiatry* 53, 109–114. doi: 10.1055/a-1076-8228
- Knezovic, A., Loncar, A., Homoljak, J., Smailovic, U., Osmanovic Barilar, J., Ganoci, L., et al. (2017). Rat brain glucose transporter-2, insulin receptor and glial expression are acute targets of intracerebroventricular streptozotocin: Risk factors for sporadic Alzheimer's disease? *J. Neural Transm. (Vienna)* 124, 695–708. doi: 10.1007/s00702-017-1727-6
- Knezovic, A., Osmanovic Barilar, J., Babic, A., Bagaric, R., Farkas, V., Riederer, P., et al. (2018). Glucagon-like peptide-1 mediates effects of oral galactose in streptozotocin-induced rat model of sporadic Alzheimer's disease. *Neuropharmacology* 135, 48–62. doi: 10.1016/j.neuropharm.2018.02.027
- Knezovic, A., Osmanovic-Barilar, J., Curlin, M., Hof, P. R., Simic, G., Riederer, P., et al. (2015). Staging of cognitive deficits and neuropathological and ultrastructural changes in streptozotocin-induced rat model of Alzheimer's disease. *J. Neural Transm. (Vienna)* 122, 577–592. doi: 10.1007/s00702-015-1394-4
- Kovacs, G. G., Adle-Biasette, H., Milenkovic, I., Cipriani, S., van Scheppingen, J., and Aronica, E. (2014). Linking pathways in the developing and aging brain with neurodegeneration. *Neuroscience* 269, 152–172. doi: 10.1016/j.neuroscience.2014.03.045
- Kubis-Kubiak, A. M., Rorbach-Dolata, A., and Piwowar, A. (2019). Crucial players in Alzheimer's disease and diabetes mellitus: Friends or foes? *Mech. Ageing Dev.* 181, 7–21. doi: 10.1016/j.mad.2019.03.008
- Kullmann, S., Fritsche, A., Wagner, R., Schwab, S., Haring, H. U., Preissl, H., et al. (2017). Hypothalamic insulin responsiveness is associated with pancreatic insulin secretion in humans. *Physiol. Behav.* 176, 134–138. doi: 10.1016/j.physbeh.2017.03.036
- Kullmann, S., Heni, M., Hallschmid, M., Fritsche, A., Preissl, H., and Haring, H. U. (2016). Brain insulin resistance at the crossroads of metabolic and cognitive disorders in humans. *Physiol. Rev.* 96, 1169–1209. doi: 10.1152/physrev.00032.2015
- Kuring, J. K., Mathias, J. L., and Ward, L. (2020). Risk of dementia in persons who have previously experienced clinically-significant depression, anxiety, or PTSD: A systematic review and meta-analysis. *J. Affect. Disord.* 274, 247–261. doi: 10.1016/j.jad.2020.05.020
- Lafay-Chebassier, C., Paccalin, M., Page, G., Barc-Pain, S., Perault-Pochat, M. C., Gil, R., et al. (2005). mTOR/p70S6k signalling alteration by Abeta exposure as well as in APP-PS1 transgenic models and in patients with Alzheimer's disease. *J. Neurochem.* 94, 215–225. doi: 10.1111/j.1471-4159.2005.03187.x
- Landau, Z., and Pinhas-Hamiel, O. (2019). Attention deficit/hyperactivity, the metabolic syndrome, and type 2 diabetes. *Curr. Diab. Rep.* 19:46. doi: 10.1007/s11892-019-1174-x
- Langen, B., and Dost, R. (2011). Comparison of SHR, WKY and Wistar rats in different behavioural animal models: effect of dopamine D1 and alpha2 agonists. *Atten. Defic. Hyperact. Disord.* 3, 1–12. doi: 10.1007/s12402-010-0034-y
- Lee, D. Y. (2015). Roles of mTOR signaling in brain development. *Exp. Neurobiol.* 24, 177–185. doi: 10.5607/en.2015.24.3.177
- Lee, J., Kim, K., Yu, S. W., and Kim, E. K. (2016). Wnt3a upregulates brain-derived insulin by increasing NeuroD1 via Wnt/beta-catenin signaling in the hypothalamus. *Mol. Brain* 9:24. doi: 10.1186/s13041-016-0207-5
- Lee, T. H., Lee, C. H., Kim, I. H., Yan, B. C., Park, J. H., Kwon, S. H., et al. (2012). Effects of ADHD therapeutic agents, methylphenidate and atomoxetine, on hippocampal neurogenesis in the adolescent mouse dentate gyrus. *Neurosci. Lett.* 524, 84–88. doi: 10.1016/j.neulet.2012.07.029
- Leffa, D. T., Ferrari-Souza, J. P., Bellaver, B., Tissot, C., Ferreira, P. C. L., Brum, W. S., et al. (2022). Genetic risk for attention-deficit/hyperactivity disorder predicts cognitive decline and development of Alzheimer's disease pathophysiology in cognitively unimpaired older adults. *medRxiv [Preprint]*. doi: 10.1101/2022.04.05.22273464
- Leresche, N., and Lambert, R. C. (2017). T-type calcium channels in synaptic plasticity. *Channels (Austin)* 11, 121–139. doi: 10.1080/19336950.2016.1238992
- Li, H. J., Hou, X. H., Liu, H. H., Yue, C. L., He, Y., and Zuo, X. N. (2015). Toward systems neuroscience in mild cognitive impairment and Alzheimer's disease: A meta-analysis of 75 fMRI studies. *Hum. Brain Mapp.* 36, 1217–1232. doi: 10.1002/hbm.22689
- Li, J., Pan, P., Huang, R., and Shang, H. (2012). A meta-analysis of voxel-based morphometry studies of white matter volume alterations in Alzheimer's disease. *Neurosci. Biobehav. Rev.* 36, 757–763. doi: 10.1016/j.neubiorev.2011.12.001
- Li, Q., Meng, Y., Wang, J., Xie, Y., Li, T., and Sun, W. (2022). A systematic screening of ADHD-susceptible variants from 25 chinese parents-offspring trios. *Front. Genet.* 13:878036. doi: 10.3389/fgene.2022.878036
- Li, R. J., Xu, J., Fu, C., Zhang, J., Zheng, Y. G., Jia, H., et al. (2016). Regulation of mTORC1 by lysosomal calcium and calmodulin. *Elife* 5:e19360. doi: 10.7554/eLife.19360
- Li, R., and Singh, M. (2014). Sex differences in cognitive impairment and Alzheimer's disease. *Front. Neuroendocrinol.* 35:385–403. doi: 10.1016/j.yfrne.2014.01.002
- Li, Y., Xu, P., Shan, J., Sun, W., Ji, X., Chi, T., et al. (2020). Interaction between hyperphosphorylated tau and pyroptosis in forskolin and streptozotocin induced AD models. *Biomed. Pharmacother.* 121:109618. doi: 10.1016/j.biopha.2019.109618
- Liang, H., Nie, J., Van Skike, C. E., Valentine, J. M., and Orr, M. E. (2019). Mammalian target of rapamycin at the crossroad between Alzheimer's disease and diabetes. *Adv. Exp. Med. Biol.* 1128, 185–225. doi: 10.1007/978-981-13-3540-2\_10
- Liao, W., Zheng, Y., Fang, W., Liao, S., Xiong, Y., Li, Y., et al. (2018). Dual specificity phosphatase 6 protects neural stem cells from beta-amyloid-induced cytotoxicity through ERK1/2 Inactivation. *Biomolecules* 8:181. doi: 10.3390/biom8040181
- Liu, C., Li, Y., Semenov, M., Han, C., Baeg, G. H., Tan, Y., et al. (2002). Control of beta-catenin phosphorylation/degradation by a dual-kinase mechanism. *Cell* 108, 837–847. doi: 10.1016/s0092-8674(02)00685-2
- Liu, T., Zhang, T., Nicolas, M., Boussicault, L., Rice, H., Soldano, A., et al. (2021). The amyloid precursor protein is a conserved Wnt receptor. *Elife* 10:e69199. doi: 10.7554/eLife.69199
- Liu, Z., Qin, G., Mana, L., Huang, S., Wang, Y., and Wang, P. (2020). Shenzhiling oral liquid protects STZ-injured oligodendrocyte through PI3K/Akt-mTOR pathway. *Evid. Based Complement. Alternat. Med.* 2020, 4527283. doi: 10.1155/2020/4527283
- Llorens-Martin, M., Jurado, J., Hernandez, F., and Avila, J. (2014). GSK-3beta, a pivotal kinase in Alzheimer disease. *Front. Mol. Neurosci.* 7:46. doi: 10.3389/fnmol.2014.00046

- Lupton, M. K., Strike, L., Hansell, N. K., Wen, W., Mather, K. A., Armstrong, N. J., et al. (2016). The effect of increased genetic risk for Alzheimer's disease on hippocampal and amygdala volume. *Neurobiol. Aging* 40, 68–77. doi: 10.1016/j.neurobiolaging.2015.12.023
- Lyneess, S. A., Zarow, C., and Chui, H. C. (2003). Neuron loss in key cholinergic and aminergic nuclei in Alzheimer disease: A meta-analysis. *Neurobiol. Aging* 24, 1–23. doi: 10.1016/s0197-4580(02)00057-x
- Ma, T., Hoeffler, C. A., Capetillo-Zarate, E., Yu, F., Wong, H., Lin, M. T., et al. (2010). Dysregulation of the mTOR pathway mediates impairment of synaptic plasticity in a mouse model of Alzheimer's disease. *PLoS One* 5:e12845. doi: 10.1371/journal.pone.0012845
- Macdonald, R., Barnes, K., Hastings, C., and Mortiboys, H. (2018). Mitochondrial abnormalities in Parkinson's disease and Alzheimer's disease: Can mitochondria be targeted therapeutically? *Biochem. Soc. Trans.* 46, 891–909. doi: 10.1042/BST20170501
- Maia, C. R., Cortese, S., Caye, A., Deakin, T. K., Polanczyk, G. V., Polanczyk, C. A., et al. (2017). Long-term efficacy of methylphenidate immediate-release for the treatment of childhood ADHD. *J. Atten. Disord.* 21, 3–13. doi: 10.1177/1087054714559643
- Mannaa, M., Kramer, S., Boschmann, M., and Gollasch, M. (2013). mTOR and regulation of energy homeostasis in humans. *J. Mol. Med. (Berl)* 91, 1167–1175. doi: 10.1007/s00109-013-1057-6
- Marchetti, B., Tirollo, C., L'Episcopo, F., Caniglia, S., Testa, N., Smith, J. A., et al. (2020). Parkinson's disease, aging and adult neurogenesis: Wnt/beta-catenin signalling as the key to unlock the mystery of endogenous brain repair. *Aging Cell* 19:e13101. doi: 10.1111/accel.13101
- Martens, Y. A., Zhao, N., Liu, C. C., Kanekiyo, T., Yang, A. J., Goate, A. M., et al. (2022). ApoE Cascade Hypothesis in the pathogenesis of Alzheimer's disease and related dementias. *Neuron* 110, 1304–1317. doi: 10.1016/j.neuron.2022.03.004
- Mayer, G., Nitsch, R., and Hoyer, S. (1990). Effects of changes in peripheral and cerebral glucose metabolism on locomotor activity, learning and memory in adult male rats. *Brain Res.* 532, 95–100. doi: 10.1016/0006-8993(90)91747-5
- Mayer, J. S., Bernhard, A., Fann, N., Boxhoorn, S., Hartman, C. A., Reif, A., et al. (2021). Cognitive mechanisms underlying depressive disorders in ADHD: A systematic review. *Neurosci. Biobehav. Rev.* 121, 307–345. doi: 10.1016/j.neubiorev.2020.12.018
- McKean, N. E., Handley, R. R., and Snell, R. G. (2021). A review of the current mammalian models of Alzheimer's disease and challenges that need to be overcome. *Int. J. Mol. Sci.* 22:13168. doi: 10.3390/ijms222313168
- Mencer, S., Kartawy, M., Lendenfeld, F., Soluh, H., Tripathi, M. K., Khaliulin, I., et al. (2021). Proteomics of autism and Alzheimer's mouse models reveal common alterations in mTOR signaling pathway. *Transl. Psychiatry* 11:480. doi: 10.1038/s41398-021-01578-2
- Mendonca, F., Sudo, F. K., Santiago-Bravo, G., Oliveira, N., Assuncao, N., Rodrigues, F., et al. (2021). Mild cognitive impairment or attention-deficit/hyperactivity disorder in older adults? A cross sectional study. *Front. Psychiatry* 12:737357. doi: 10.3389/fpsy.2021.737357
- Mines, M. A., and Jope, R. S. (2012). Brain region differences in regulation of Akt and GSK3 by chronic stimulant administration in mice. *Cell Signal.* 24, 1398–1405. doi: 10.1016/j.cellsig.2012.03.001
- Mines, M. A., Beurel, E., and Jope, R. S. (2013). Examination of methylphenidate-mediated behavior regulation by glycogen synthase kinase-3 in mice. *Eur. J. Pharmacol.* 698, 252–258. doi: 10.1016/j.ejphar.2012.10.018
- Mintzer, J., Lancot, K. L., Scherer, R. W., Rosenberg, P. B., Herrmann, N., van Dyck, C. H., et al. (2021). Effect of methylphenidate on apathy in patients with Alzheimer disease: The ADMET 2 randomized clinical trial. *JAMA Neurol.* 78, 1324–1332. doi: 10.1001/jamaneurol.2021.3356
- Misiak, B., Wojta-Kempa, M., Samochowiec, J., Schiweck, C., Aichholzer, M., Reif, A., et al. (2022). Peripheral blood inflammatory markers in patients with attention deficit/hyperactivity disorder (ADHD): A systematic review and meta-analysis. *Prog. Neuropsychopharmacol. Biol. Psychiatry* 118, 110581. doi: 10.1016/j.pnpbp.2022.110581
- Mittal, A., Sharma, R., Sardana, S., Goyal, P. K., Piplani, M., and Pandey, A. (2022). A systematic review of updated mechanistic insights towards Alzheimer's disease. *CNS Neurol. Disord. Drug Targets*. doi: 10.2174/1871527321666220510144127
- Monterey, M. D., Wei, H., Wu, X., and Wu, J. Q. (2021). The many faces of astrocytes in Alzheimer's disease. *Front. Neurol.* 12:619626. doi: 10.3389/fneur.2021.619626
- Moreira, P. I. (2012). Alzheimer's disease and diabetes: an integrative view of the role of mitochondria, oxidative stress, and insulin. *J. Alzheimers Dis.* 30(Suppl. 2), S199–S215. doi: 10.3233/JAD-2011-111127
- Morello, F., Voikar, V., Parkkinen, P., Panhelainen, A., Rosenholm, M., Makkonen, A., et al. (2020). ADHD-like behaviors caused by inactivation of a transcription factor controlling the balance of inhibitory and excitatory neuron development in the mouse anterior brainstem. *Transl. Psychiatry* 10:357. doi: 10.1038/s41398-020-01033-8
- Mosher, K. I., and Wyss-Coray, T. (2014). Microglial dysfunction in brain aging and Alzheimer's disease. *Biochem. Pharmacol.* 88, 594–604. doi: 10.1016/j.bcp.2014.01.008
- Munch, G., Schinzel, R., Loske, C., Wong, A., Durany, N., Li, J. J., et al. (1998). Alzheimer's disease—synergistic effects of glucose deficit, oxidative stress and advanced glycation endproducts. *J. Neural Transm. (Vienna)* 105, 439–461. doi: 10.1007/s007020050069
- Nagu, P., Sharma, V., Behl, T., Pathan, A. K. A., and Mehta, V. (2022). Molecular insights to the wnt signaling during Alzheimer's disorder: A potential target for therapeutic interventions. *J. Mol. Neurosci.* 72, 679–690. doi: 10.1007/s12031-021-01940-5
- Nanou, E., and Catterall, W. A. (2018). Calcium channels, synaptic plasticity, and neuropsychiatric disease. *Neuron* 98, 466–481. doi: 10.1016/j.neuron.2018.03.017
- Narvaez, R. F., and Furini, C. R. G. (2022). Role of Wnt signaling in synaptic plasticity and memory. *Neurobiol. Learn. Mem.* 187, 107558. doi: 10.1016/j.nlm.2021.107558
- National Institute on Aging (2021). *Treatment of Alzheimer's disease: How is Alzheimer's disease treated?*. NIH National Institute on Aging. Available online at: <https://www.nia.nih.gov/health/how-alzheimers-disease-treated#:~:text=Aducanumab%20is%20the%20only%20disease,brain%20lesions%20associated%20with%20Alzheimer's> (accessed September 23, 2022).
- Noelenders, R., and Vleminckx, K. (2017). How Wnt signaling builds the brain: Bridging development and disease. *Neuroscientist* 23, 314–329. doi: 10.1177/1073858416667270
- Oakes, H. V., DeVee, C. E., Farmer, B., Allen, S. A., Hall, A. N., Ensley, T., et al. (2019). Neurogenesis within the hippocampus after chronic methylphenidate exposure. *J. Neural Transm. (Vienna)* 126, 201–209. doi: 10.1007/s00702-018-1949-2
- Oblak, A. L., Lin, P. B., Kotredes, K. P., Pandey, R. S., Garceau, D., Williams, H. M., et al. (2021). Comprehensive evaluation of the 5XFAD mouse model for preclinical testing applications: A model-AD study. *Front. Aging Neurosci.* 13:713726. doi: 10.3389/fnagi.2021.713726
- Okamoto, K., and Aoki, K. (1963). Development of a strain of spontaneously hypertensive rats. *Jpn. Circ. J.* 27, 282–293. doi: 10.1253/cj.27.282
- Ong, P. S., Wang, L. Z., Dai, X., Tseng, S. H., Loo, S. J., and Sethi, G. (2016). Judicious toggling of mTOR activity to combat insulin resistance and cancer: Current evidence and perspectives. *Front. Pharmacol.* 7:395. doi: 10.3389/fphar.2016.00395
- Ou, Y. N., Xu, W., Li, J. Q., Guo, Y., Cui, M., Chen, K. L., et al. (2019). FDG-PET as an independent biomarker for Alzheimer's biological diagnosis: A longitudinal study. *Alzheimers Res. Ther.* 11:57. doi: 10.1186/s13195-019-0512-1
- Pakdin, M., Toutounchian, S., Namazi, S., Arabpour, Z., Pouladi, A., Afsahi, S., et al. (2022). Type 2 diabetes mellitus and Alzheimer's disease: A review of the potential links. *Curr. Diabetes Rev.* 18:e051121197760. doi: 10.2174/1573399818666211105122545
- Palomer, E., Buechler, J., and Salinas, P. C. (2019). Wnt signaling deregulation in the aging and Alzheimer's brain. *Front. Cell Neurosci.* 13:227. doi: 10.3389/fncel.2019.00227
- Palomer, E., Martin-Flores, N., Jolly, S., Pascual-Vargas, P., Benvegno, S., Podpolny, M., et al. (2022). Epigenetic repression of Wnt receptors in AD: A role for Sirtuin2-induced H4K16ac deacetylation of Frizzled1 and Frizzled7 promoters. *Mol. Psychiatry* 27, 3024–3033. doi: 10.1038/s41380-022-01492-z
- Parr, C., Mirzaei, N., Christian, M., and Sastre, M. (2015). Activation of the Wnt/beta-catenin pathway represses the transcription of the beta-amyloid precursor protein cleaving enzyme (BACE1) via binding of T-cell factor-4 to BACE1 promoter. *FASEB J.* 29, 623–635. doi: 10.1096/fj.14-253211
- Perluigi, M., Di Domenico, F., Barone, E., and Butterfield, D. A. (2021). mTOR in Alzheimer disease and its earlier stages: Links to oxidative damage in the progression of this dementing disorder. *Free Radic. Biol. Med.* 169, 382–396. doi: 10.1016/j.freeradbiomed.2021.04.025
- Perluigi, M., Picca, A., Montanari, E., Calvani, R., Marini, F., Matassa, R., et al. (2022). Aberrant crosstalk between insulin signaling and mTOR in young Down syndrome individuals revealed by neuronal-derived extracellular vesicles. *Alzheimers Dement.* 18, 1498–1510. doi: 10.1002/alz.12499
- Pietropaolo, S., Feldon, J., and Yee, B. K. (2008). Age-dependent phenotypic characteristics of a triple transgenic mouse model of Alzheimer disease. *Behav. Neurosci.* 122, 733–747. doi: 10.1037/a0012520
- Pineda, D., Ardila, A., Rosselli, M., Cadavid, C., Mancheno, S., and Mejia, S. (1998). Executive dysfunction in children with attention deficit hyperactivity disorder. *Int. J. Neurosci.* 96, 177–196. doi: 10.3109/00207459808986466
- Planche, V., Manjon, J. V., Mansencal, B., Lanuza, E., Tourdias, T., Catheline, G., et al. (2022). Structural progression of Alzheimer's disease over decades: The MRI staging scheme. *Brain Commun.* 4:fca109. doi: 10.1093/braincomms/fca109

- Podcasy, J. L., and Epperson, C. N. (2016). Considering sex and gender in Alzheimer disease and other dementias. *Dialogues Clin. Neurosci.* 18, 437–446.
- Prentice, J. L., Schaeffer, M. J., Wall, A. K., and Callahan, B. L. (2021). A systematic review and comparison of neurocognitive features of late-life attention-deficit/hyperactivity disorder and dementia with lewy bodies. *J. Geriatr. Psychiatry Neurol.* 34, 466–481. doi: 10.1177/0891988720944251
- Press, Y., PUNCHIK, B., Kagan, E., Berzak, A., Freud, T., and Dwolatzky, T. (2021). Methylphenidate for mild cognitive impairment: An exploratory 3-day, randomized, double-blind, placebo-controlled trial. *Front. Med. (Lausanne)* 8:594228. doi: 10.3389/fmed.2021.594228
- Qi, C. C., Chen, X. X., Gao, X. R., Xu, J. X., Liu, S., and Ge, J. F. (2021). Impaired learning and memory ability induced by a bilaterally hippocampal injection of streptozotocin in mice: Involved with the adaptive changes of synaptic plasticity. *Front. Aging Neurosci.* 13:633495. doi: 10.3389/fnagi.2021.633495
- Qin, G., Wang, Y., Liu, Z., Mana, L., Huang, S., and Wang, P. (2021). Shenzhiling oral solution promotes myelin repair through PI3K/Akt-mTOR pathway in STZ-induced SAD mice. *3 Biotech* 11:361. doi: 10.1007/s13205-021-02900-x
- Qin, J., He, Z., Wu, L., Wang, W., Lin, Q., Lin, Y., et al. (2021). Prevalence of mild cognitive impairment in patients with hypertension: A systematic review and meta-analysis. *Hypertens. Res.* 44, 1251–1260. doi: 10.1038/s41440-021-00704-3
- Querfurth, H., and Lee, H. K. (2021). Mammalian/mechanistic target of rapamycin (mTOR) complexes in neurodegeneration. *Mol. Neurodegener.* 16, 44. doi: 10.1186/s13024-021-00428-5
- Quintero, J., Gutierrez-Casares, J. R., and Alamo, C. (2022). Molecular characterisation of the mechanism of action of stimulant drugs lisdexamfetamine and methylphenidate on ADHD neurobiology: A review. *Neurol. Ther.* 11, 1489–1517. doi: 10.1007/s40120-022-00392-2
- Radtke, F., Palladino, V. S., McNeill, R. V., Chiochetti, A. G., Haslinger, D., Leyh, M., et al. (2022). ADHD-associated PARK2 copy number variants: A pilot study on gene expression and effects of supplementary deprivation in patient-derived cell lines. *Am. J. Med. Genet. B Neuropsychiatr. Genet.* 189, 257–270. doi: 10.1002/ajmg.b.32918
- Rahi, V., and Kumar, P. (2021). Animal models of attention-deficit hyperactivity disorder (ADHD). *Int. J. Dev. Neurosci.* 81, 107–124. doi: 10.1002/jdn.10089
- Ramtekkar, U. P., Reiersen, A. M., Todorov, A. A., and Todd, R. D. (2010). Sex and age differences in attention-deficit/hyperactivity disorder symptoms and diagnoses: Implications for DSM-V and ICD-11. *J. Am. Acad. Child Adolesc. Psychiatry* 49, 217–228.e1–e3.
- Rebelos, E., Bucci, M., Karjalainen, T., Oikonen, V., Bertoldo, A., Hannukainen, J. C., et al. (2021). Insulin resistance is associated with enhanced brain glucose uptake during euglycemic hyperinsulinemia: A large-scale PET cohort. *Diabetes Care* 44, 788–794. doi: 10.2337/dc20-1549
- Reddy, P. H. (2014). Inhibitors of mitochondrial fission as a therapeutic strategy for diseases with oxidative stress and mitochondrial dysfunction. *J. Alzheimers Dis.* 40, 245–256. doi: 10.3233/JAD-132060
- Reitz, C., Rogaeva, E., and Beecham, G. W. (2020). Late-onset vs nonmendelian early-onset Alzheimer disease: A distinction without a difference? *Neurol. Genet.* 6:e512. doi: 10.1212/NXG.0000000000000512
- Riederer, P., Korczyn, A. D., Ali, S. S., Bajenaru, O., Choi, M. S., Chopp, M., et al. (2017). The diabetic brain and cognition. *J. Neural Transm. (Vienna)* 124, 1431–1454. doi: 10.1007/s00702-017-1763-2
- Robbins, T. W., and Sahakian, B. J. (1979). “Paradoxical” effects of psychomotor stimulant drugs in hyperactive children from the standpoint of behavioural pharmacology. *Neuropharmacology* 18, 931–950. doi: 10.1016/0028-3908(79)90157-6
- Robinson, A. M., Eggleston, R. L., and Bucci, D. J. (2012). Physical exercise and catecholamine reuptake inhibitors affect orienting behavior and social interaction in a rat model of attention-deficit/hyperactivity disorder. *Behav. Neurosci.* 126, 762–771. doi: 10.1037/a0030488
- Rodgers, S. P., Born, H. A., Das, P., and Jankowsky, J. L. (2012). Transgenic APP expression during postnatal development causes persistent locomotor hyperactivity in the adult. *Mol. Neurodegener.* 7:28. doi: 10.1186/1750-1326-7-28
- Roe, J. M., Vidal-Pineiro, D., Sorensen, O., Brandmaier, A. M., Duzel, S., Gonzalez, H. A., et al. (2021). Asymmetric thinning of the cerebral cortex across the adult lifespan is accelerated in Alzheimer’s disease. *Nat. Commun.* 12:721. doi: 10.1038/s41467-021-21057-y
- Rosi, M. C., Luccarini, I., Grossi, C., Fiorentini, A., Spillantini, M. G., Prisco, A., et al. (2010). Increased Dickkopf-1 expression in transgenic mouse models of neurodegenerative disease. *J. Neurochem.* 112, 1539–1551. doi: 10.1111/j.1471-4159.2009.06566.x
- Roth, R. M., and Saykin, A. J. (2004). Executive dysfunction in attention-deficit/hyperactivity disorder: Cognitive and neuroimaging findings. *Psychiatr. Clin. North Am.* 27, 83–96, ix. doi: 10.1016/S0193-953X(03)00112-6
- Rovira, P., Demontis, D., Sanchez-Mora, C., Zayats, T., Klein, M., Mota, N. R., et al. (2020). Shared genetic background between children and adults with attention deficit/hyperactivity disorder. *Neuropsychopharmacology* 45, 1617–1626. doi: 10.1038/s41386-020-0664-5
- Rustay, N. R., Cronin, E. A., Curzon, P., Markosyan, S., Bitner, R. S., Ellis, T. A., et al. (2010). Mice expressing the Swedish APP mutation on a 129 genetic background demonstrate consistent behavioral deficits and pathological markers of Alzheimer’s disease. *Brain Res.* 1311, 136–147. doi: 10.1016/j.brainres.2009.11.040
- Ruthirakuhan, M. T., Herrmann, N., Abraham, E. H., Chan, S., and Lancot, K. L. (2018). Pharmacological interventions for apathy in Alzheimer’s disease. *Cochrane Database Syst. Rev.* 5:CD012197. doi: 10.1002/14651858.CD012197.pub2
- Sadasivan, S., Pond, B. B., Pani, A. K., Qu, C., Jiao, Y., and Smeyne, R. J. (2012). Methylphenidate exposure induces dopamine neuron loss and activation of microglia in the basal ganglia of mice. *PLoS One* 7:e33693. doi: 10.1371/journal.pone.0033693
- Sagvolden, T., and Johansen, E. B. (2012). Rat models of ADHD. *Curr. Top. Behav. Neurosci.* 9, 301–315. doi: 10.1007/7854\_2011\_126
- Salem, M. A., Budzynska, B., Kowalczyk, J., El Sayed, N. S., and Mansour, S. M. (2021). Tadalafil and bergapten mitigate streptozotocin-induced sporadic Alzheimer’s disease in mice via modulating neuroinflammation, PI3K/Akt, Wnt/beta-catenin, AMPK/mTOR signaling pathways. *Toxicol. Appl. Pharmacol.* 429, 115697. doi: 10.1016/j.taap.2021.115697
- Salkovic-Petrisic, M., Osmanovic-Barilar, J., Bruckner, M. K., Hoyer, S., Arendt, T., and Riederer, P. (2011). Cerebral amyloid angiopathy in streptozotocin rat model of sporadic Alzheimer’s disease: A long-term follow up study. *J. Neural Transm. (Vienna)* 118, 765–772. doi: 10.1007/s00702-011-0651-4
- Salkovic-Petrisic, M., Perhoc, A. B., Homolak, J., Knezovic, A., Osmanovic Barilar, J., and Riederer, P. (2021). “Experimental approach to Alzheimer’s disease with emphasis on insulin resistance in the brain,” in *Handbook of neurotoxicity*, ed. R. M. Kostzewa (Cham: Springer International Publishing), 1–52. doi: 10.1016/j.pharmthera.2022.108277
- Sanabria-Castro, A., Alvarado-Echeverria, I., and Monge-Bonilla, C. (2017). Molecular Pathogenesis of Alzheimer’s disease: An update. *Ann. Neurosci.* 24, 46–54. doi: 10.1159/000464422
- Sandstrom, A., Perroud, N., Alda, M., Uher, R., and Pavlova, B. (2021). Prevalence of attention-deficit/hyperactivity disorder in people with mood disorders: A systematic review and meta-analysis. *Acta Psychiatr. Scand.* 143, 380–391. doi: 10.1111/acps.13283
- Saxton, R. A., and Sabatini, D. M. (2017). mTOR signaling in growth, metabolism, and disease. *Cell* 168, 960–976. doi: 10.1016/j.cell.2017.02.004
- Sayal, K., Prasad, V., Daley, D., Ford, T., and Coghill, D. (2018). ADHD in children and young people: prevalence, care pathways, and service provision. *Lancet Psychiatry* 5, 175–186. doi: 10.1016/S2215-0366(17)30167-0
- Scattoni, M. L., Gasparini, L., Alleva, E., Goedert, M., Calamandrei, G., and Spillantini, M. G. (2010). Early behavioural markers of disease in P301S tau transgenic mice. *Behav. Brain Res.* 208, 250–257. doi: 10.1016/j.bbr.2009.12.002
- Schiweck, C., Arteaga-Henriquez, G., Aichholzer, M., Edwin Thanarajah, S., Vargas-Caceres, S., Matura, S., et al. (2021). Comorbidity of ADHD and adult bipolar disorder: A systematic review and meta-analysis. *Neurosci. Biobehav. Rev.* 124, 100–123. doi: 10.1016/j.neubiorev.2021.01.017
- Schmitz, F., Chao, M. V., and Wyse, A. T. S. (2019). Methylphenidate alters Akt-mTOR signaling in rat pheochromocytoma cells. *Int. J. Dev. Neurosci.* 73, 10–18. doi: 10.1016/j.ijdevneu.2018.12.004
- Schreiber, S., Drukarch, B., Garz, C., Niklass, S., Stanaszek, L., Kropf, S., et al. (2014). Interplay between age, cerebral small vessel disease, parenchymal amyloid-beta, and tau pathology: Longitudinal studies in hypertensive stroke-prone rats. *J. Alzheimers Dis.* 42(Suppl. 3), S205–S215. doi: 10.3233/JAD-132618
- Selten, M., van Bokhoven, H., and Nadif Kasri, N. (2018). Inhibitory control of the excitatory/inhibitory balance in psychiatric disorders. *F1000Research* 7:23. doi: 10.12688/f1000research.12155.1
- Serafino, A., and Cozzolino, M. (2023). The Wnt/beta-catenin signaling: A multifunctional target for neuroprotective and regenerative strategies in Parkinson’s disease. *Neural Regen. Res.* 18, 306–308. doi: 10.4103/1673-5374.343908
- Serretti, A., Olgiati, P., and De Ronchi, D. (2007). Genetics of Alzheimer’s disease. A rapidly evolving field. *J. Alzheimers Dis.* 12, 73–92. doi: 10.3233/jad-2007-12108
- Sharma, M., and Gupta, Y. K. (2001). Intracerebroventricular injection of streptozotocin in rats produces both oxidative stress in the brain and cognitive impairment. *Life Sci.* 68, 1021–1029. doi: 10.1016/S0024-3205(00)01005-5
- Sharp, Z. D., and Bartke, A. (2005). Evidence for down-regulation of phosphoinositide 3-kinase/Akt/mammalian target of rapamycin (PI3K/Akt/mTOR)-dependent translation regulatory signaling pathways in Ames dwarf mice. *J. Gerontol. A Biol. Sci. Med. Sci.* 60, 293–300. doi: 10.1093/gerona/60.3.293
- Shaw, P., Eckstrand, K., Sharp, W., Blumenthal, J., Lerch, J. P., Greenstein, D., et al. (2007). Attention-deficit/hyperactivity disorder is characterized by a delay in cortical maturation. *Proc. Natl. Acad. Sci. U.S.A.* 104, 19649–19654. doi: 10.1073/pnas.0707741104



- Shaw, P., Sharp, W. S., Morrison, M., Eckstrand, K., Greenstein, D. K., Clasen, L. S., et al. (2009). Psychostimulant treatment and the developing cortex in attention deficit hyperactivity disorder. *Am. J. Psychiatry* 166, 58–63. doi: 10.1176/appi.ajp.2008.08050781
- Shu, S., Xu, S. Y., Ye, L., Liu, Y., Cao, X., Jia, J. Q., et al. (2022). Prefrontal parvalbumin interneurons deficits mediate early emotional dysfunction in Alzheimer's disease. *Neuropsychopharmacology* 48, 391–401. doi: 10.1038/s41386-022-01435-w
- Sil, A., Erfani, A., Lamb, N., Copland, R., Riedel, G., and Platt, B. (2022). Sex differences in behavior and molecular pathology in the 5XFAD model. *J. Alzheimers Dis.* 85, 755–778. doi: 10.3233/JAD-210523
- Sims, R., Hill, M., and Williams, J. (2020). The multiplex model of the genetics of Alzheimer's disease. *Nat. Neurosci.* 23, 311–322. doi: 10.1038/s41593-020-0599-5
- Solmi, M., Fornaro, M., Ostinelli, E. G., Zangani, C., Croatto, G., Monaco, F., et al. (2020). Safety of 80 antidepressants, antipsychotics, anti-attention-deficit/hyperactivity medications and mood stabilizers in children and adolescents with psychiatric disorders: A large scale systematic meta-review of 78 adverse effects. *World Psychiatry* 19, 214–232. doi: 10.1002/wps.20765
- Song, P., Zha, M., Yang, Q., Zhang, Y., Li, X., and Rudan, I. (2021). The prevalence of adult attention-deficit hyperactivity disorder: A global systematic review and meta-analysis. *J. Glob. Health* 11:04009. doi: 10.7189/jogh.11.04009
- Sontag, T. A., Fuermaier, A. B., Hauser, J., Kaunzinger, I., Tucha, O., and Lange, K. W. (2013). Spatial memory in spontaneously hypertensive rats (SHR). *PLoS One* 8:e74660. doi: 10.1371/journal.pone.0074660
- Sontag, T. A., Tucha, O., Walitz, S., and Lange, K. W. (2010). Animal models of attention deficit/hyperactivity disorder (ADHD): A critical review. *Atten. Defic. Hyperact. Disord.* 2, 1–20. doi: 10.1007/s12402-010-0019-x
- Sontheimer, N., Konnopka, A., and König, H. H. (2021). The excess costs of dementia: A systematic review and meta-analysis. *J. Alzheimers Dis.* 83, 333–354. doi: 10.3233/JAD-210174
- Sousa, B., Martins, J., Castelo-Branco, M., and Goncalves, J. (2022). Transcranial direct current stimulation as an approach to mitigate neurodevelopmental disorders affecting excitation/inhibition balance: Focus on autism spectrum disorder, schizophrenia, and attention deficit/hyperactivity disorder. *J. Clin. Med.* 11:2839. doi: 10.3390/jcm11102839
- Sterniczuk, R., Dyck, R. H., Laferla, F. M., and Antle, M. C. (2010). Characterization of the 3xTg-AD mouse model of Alzheimer's disease: part 1. Circadian changes. *Brain Res.* 1348, 139–148. doi: 10.1016/j.brainres.2010.05.013
- Strom, A., Iaccarino, L., Edwards, L., Lesman-Segev, O. H., Soleimani-Meigooni, D. N., Pham, J., et al. (2022). Cortical hypometabolism reflects local atrophy and tau pathology in symptomatic Alzheimer's disease. *Brain* 145, 713–728. doi: 10.1093/brain/awab294
- Swanberg, M. M., Tractenberg, R. E., Mohs, R., Thal, L. J., and Cummings, J. L. (2004). Executive dysfunction in Alzheimer disease. *Arch. Neurol.* 61, 556–560. doi: 10.1001/archneur.61.4.556
- Takeuchi, H., Iba, M., Inoue, H., Higuchi, M., Takao, K., Tsukita, K., et al. (2011). P301S mutant human tau transgenic mice manifest early symptoms of human tauopathies with dementia and altered sensorimotor gating. *PLoS One* 6:e21050. doi: 10.1371/journal.pone.0021050
- Talbot, K., Wang, H. Y., Kazi, H., Han, L. Y., Bakshi, K. P., Stucky, A., et al. (2012). Demonstrated brain insulin resistance in Alzheimer's disease patients is associated with IGF-1 resistance, IRS-1 dysregulation, and cognitive decline. *J. Clin. Invest.* 122, 1316–1338. doi: 10.1172/JCI59903
- Tang, X., Lebrilla, C., Jin, L.-W., Maezawa, I., Harvey, D., and Zivkovic, A. (2021). Brain-region-specific, glycosylation-related transcriptomic alterations in Alzheimer's disease. *Alzheimers Dement.* 17(Suppl. 3), e051117. doi: 10.1002/alz.051117
- Tapia-Rojas, C., and Inestrosa, N. C. (2018). Loss of canonical Wnt signaling is involved in the pathogenesis of Alzheimer's disease. *Neural Regen. Res.* 13, 1705–1710. doi: 10.4103/1673-5374.238606
- Tayebati, S. K., Tomassoni, D., and Amenta, F. (2016). Neuroinflammatory markers in spontaneously hypertensive rat brain: An immunohistochemical study. *CNS Neurol. Disord. Drug Targets* 15, 995–1000. doi: 10.2174/1871527315666160527155014
- Tian, S., Tan, S., Jia, W., Zhao, J., and Sun, X. (2021). Activation of Wnt/beta-catenin signaling restores insulin sensitivity in insulin resistant neurons through transcriptional regulation of IRS-1. *J. Neurochem.* 157, 467–478. doi: 10.1111/jnc.15277
- Tong, X. K., Royea, J., and Hamel, E. (2022). Simvastatin rescues memory and granule cell maturation through the Wnt/beta-catenin signaling pathway in a mouse model of Alzheimer's disease. *Cell Death Dis.* 13:325. doi: 10.1038/s41419-022-04784-y
- Toro, C. A., Zhang, L., Cao, J., and Cai, D. (2019). Sex differences in Alzheimer's disease: Understanding the molecular impact. *Brain Res.* 1719, 194–207. doi: 10.1016/j.brainres.2019.05.031
- Tramutola, A., Triplett, J. C., Di Domenico, F., Niedowicz, D. M., Murphy, M. P., Coccia, R., et al. (2015). Alteration of mTOR signaling occurs early in the progression of Alzheimer disease (AD): Analysis of brain from subjects with pre-clinical AD, amnesic mild cognitive impairment and late-stage AD. *J. Neurochem.* 133, 739–749. doi: 10.1111/jnc.13037
- Tzeng, N. S., Chung, C. H., Lin, F. H., Yeh, C. B., Huang, S. Y., Lu, R. B., et al. (2019). Risk of dementia in adults with ADHD: A nationwide, population-based cohort study in taiwan. *J. Atten. Disord.* 23, 995–1006. doi: 10.1177/1087054717714057
- U.S. Food & Drugs Administration. (2021). *Aducanumab (marketed as Aduhelm) information* [Online]. FDA. Available online at: <https://www.fda.gov/drugs/postmarket-drug-safety-information-patients-and-providers/aducanumab-marketed-aduhelm-information> (accessed September 23, 2022).
- U.S. Food & Drugs Administration (2023). *FDA grants accelerated approval for Alzheimer's disease treatment* [Online]. FDA. Available online at: <https://www.fda.gov/news-events/press-announcements/fda-grants-accelerated-approval-alzheimers-disease-treatment> (accessed January 24, 2023).
- Uddin, M. S., Rahman, M. A., Kabir, M. T., Behl, T., Mathew, B., Perveen, A., et al. (2020). Multifarious roles of mTOR signaling in cognitive aging and cerebrovascular dysfunction of Alzheimer's disease. *IUBMB Life* 72, 1843–1855. doi: 10.1002/iub.2324
- Van Dam, D., D'Hooge, R., Staufenbiel, M., Van Ginneken, C., Van Meir, F., and De Deyn, P. P. (2003). Age-dependent cognitive decline in the APP23 model precedes amyloid deposition. *Eur. J. Neurosci.* 17, 388–396. doi: 10.1046/j.1460-9568.2003.02444.x
- van den Berg, M., Adhikari, M. H., Verschuuren, M., Pintelon, I., Vasilkovska, T., Van Audekerke, J., et al. (2022). Altered basal forebrain function during whole-brain network activity at pre- and early-plaque stages of Alzheimer's disease in TgF344-AD rats. *Alzheimers Res. Ther.* 14:148. doi: 10.1186/s13195-022-01089-2
- van den Bergh, F. S., Bloemarts, E., Chan, J. S., Groenink, L., Olivier, B., and Oosting, R. S. (2006). Spontaneously hypertensive rats do not predict symptoms of attention-deficit hyperactivity disorder. *Pharmacol. Biochem. Behav.* 83, 380–390. doi: 10.1016/j.pbb.2006.02.018
- Van Skike, C. E., Hussong, S. A., Hernandez, S. F., Banh, A. Q., DeRosa, N., and Galvan, V. (2021). mTOR attenuation with rapamycin reverses neurovascular uncoupling and memory deficits in mice modeling Alzheimer's disease. *J. Neurosci.* 41, 4305–4320. doi: 10.1523/JNEUROSCI.2144-20.2021
- van Swinderen, B. (2007). Attention-like processes in *Drosophila* require short-term memory genes. *Science* 315, 1590–1593. doi: 10.1126/science.1137931
- van Swinderen, B., and Brembs, B. (2010). Attention-like deficit and hyperactivity in a *Drosophila* memory mutant. *J. Neurosci.* 30, 1003–1014. doi: 10.1523/JNEUROSCI.4516-09.2010
- van Swinderen, B., McCartney, A., Kauffman, S., Flores, K., Agrawal, K., Wagner, J., et al. (2009). Shared visual attention and memory systems in the *Drosophila* brain. *PLoS One* 4:e5989. doi: 10.1371/journal.pone.0005989
- Velandia, P. P., Miller-Petrie, M. K., Chen, C., Chakrabarti, S., Chapin, A., Hay, S., et al. (2022). Global and regional spending on dementia care from 2000–2019 and expected future health spending scenarios from 2020–2050: An economic modelling exercise. *EclinicalMedicine* 45:101337. doi: 10.1016/j.eclinm.2022.101337
- Verheijen, M. C. T., Krauskopf, J., Caiment, F., Nazark, M., Wen, Q. F., van Herwijnen, M. H. M., et al. (2022). iPSC-derived cortical neurons to study sporadic Alzheimer disease: A transcriptome comparison with post-mortem brain samples. *Toxicol. Lett.* 356, 89–99. doi: 10.1016/j.toxlet.2021.12.009
- Vertessen, K., Luman, M., Staff, A., Bet, P., de Vries, R., Twisk, J., et al. (2022). Meta-analysis: Dose-dependent effects of methylphenidate on neurocognitive functioning in children with attention-deficit/hyperactivity disorder. *J. Am. Acad. Child Adolesc. Psychiatry* 61, 626–646. doi: 10.1016/j.jaac.2021.08.023
- Virag, D., Homolák, J., Kodvanj, I., Babic Perhoc, A., Knezovic, A., Osmanovic Barilar, J., et al. (2021). Repurposing a digital kitchen scale for neuroscience research: A complete hardware and software cookbook for PASTA. *Sci. Rep.* 11:2963. doi: 10.1038/s41598-021-82710-6
- Wajszilber, D., Santiseban, J. A., and Gruber, R. (2018). Sleep disorders in patients with ADHD: Impact and management challenges. *Nat. Sci. Sleep* 10, 453–480. doi: 10.2147/NSS.S163074
- Walhovd, K. B., Amlen, I., Schranke, A., Rohani, D. A., Groote, I., Bjørnerud, A., et al. (2020). Methylphenidate effects on cortical thickness in children and adults with attention-deficit/hyperactivity disorder: A randomized clinical trial. *AJNR Am. J. Neuroradiol.* 41, 758–765. doi: 10.3174/ajnr.A6560
- Walker, J. M., Fowler, S. W., Miller, D. K., Sun, A. Y., Weisman, G. A., Wood, W. G., et al. (2011). Spatial learning and memory impairment and increased locomotion in a transgenic amyloid precursor protein mouse model of Alzheimer's disease. *Behav. Brain Res.* 222, 169–175. doi: 10.1016/j.bbr.2011.03.049
- Wan, W., Xia, S., Kalionis, B., Liu, L., and Li, Y. (2014). The role of Wnt signaling in the development of Alzheimer's disease: A potential therapeutic target? *Biomed. Res. Int.* 2014:301575. doi: 10.1155/2014/301575



- Wang, H., Laszlo, K. D., Gissler, M., Li, F., Zhang, J., Yu, Y., et al. (2021). Maternal hypertensive disorders and neurodevelopmental disorders in offspring: A population-based cohort in two Nordic countries. *Eur. J. Epidemiol.* 36, 519–530. doi: 10.1007/s10654-021-00756-2
- Wang, J. H., Wu, Y. J., Tee, B. L., and Lo, R. Y. (2018). Medical comorbidity in Alzheimer's disease: A nested case-control study. *J. Alzheimers Dis.* 63, 773–781. doi: 10.3233/JAD-170786
- Wang, X., Wang, W., Li, L., Perry, G., Lee, H. G., and Zhu, X. (2014). Oxidative stress and mitochondrial dysfunction in Alzheimer's disease. *Biochim. Biophys. Acta* 1842, 1240–1247. doi: 10.1016/j.bbdis.2013.10.015
- Warren, B. L., Iniguez, S. D., Alcantara, L. F., Wright, K. N., Parise, E. M., Weakley, S. K., et al. (2011). Juvenile administration of concomitant methylphenidate and fluoxetine alters behavioral reactivity to reward- and mood-related stimuli and disrupts ventral tegmental area gene expression in adulthood. *J. Neurosci.* 31, 10347–10358. doi: 10.1523/JNEUROSCI.1470-11.2011
- Wightman, D. P., Jansen, I. E., Savage, J. E., Shadrin, A. A., Bahrami, S., Holland, D., et al. (2021). A genome-wide association study with 1,126,563 individuals identifies new risk loci for Alzheimer's disease. *Nat. Genet.* 53, 1276–1282. doi: 10.1038/s41588-021-00921-z
- Wilkins, H. M., Weidling, I. W., Ji, Y., and Swerdlow, R. H. (2017). Mitochondria-derived damage-associated molecular patterns in neurodegeneration. *Front. Immunol.* 8:508. doi: 10.3389/fimmu.2017.00508
- Willcutt, E. G. (2012). The prevalence of DSM-IV attention-deficit/hyperactivity disorder: A meta-analytic review. *Neurotherapeutics* 9, 490–499. doi: 10.1007/s13311-012-0135-8
- Willcutt, E. G., Doyle, A. E., Nigg, J. T., Faraone, S. V., and Pennington, B. F. (2005). Validity of the executive function theory of attention-deficit/hyperactivity disorder: A meta-analytic review. *Biol. Psychiatry* 57, 1336–1346. doi: 10.1016/j.biopsych.2005.02.006
- Willner, P. (1986). Validation criteria for animal models of human mental disorders: Learned helplessness as a paradigm case. *Prog. Neuropsychopharmacol. Biol. Psychiatry* 10, 677–690. doi: 10.1016/0278-5846(86)90051-5
- Wood, O. W. G., Yeung, J. H. Y., Faull, R. L. M., and Kwakowsky, A. (2022). EAAT2 as a therapeutic research target in Alzheimer's disease: A systematic review. *Front. Neurosci.* 16:952096. doi: 10.3389/fnins.2022.952096
- Wu, D., and Pan, W. (2010). GSK3: A multifaceted kinase in Wnt signaling. *Trends Biochem. Sci.* 35, 161–168. doi: 10.1016/j.tibs.2009.10.002
- Wu, M., Zhou, F., Cao, X., Yang, J., Bai, Y., Yan, X., et al. (2018). Abnormal circadian locomotor rhythms and Per gene expression in six-month-old triple transgenic mice model of Alzheimer's disease. *Neurosci. Lett.* 676, 13–18. doi: 10.1016/j.neulet.2018.04.008
- Xiang, J., Ran, L. Y., Zeng, X. X., He, W. W., Xu, Y., Cao, K., et al. (2021). LiCl attenuates impaired learning and memory of APP/PS1 mice, which in mechanism involves  $\alpha 7$  nAChRs and Wnt/ $\beta$ -catenin pathway. *J. Cell Mol. Med.* 25, 10698–10710. doi: 10.1111/jcmm.17006
- Xue, M., Xu, W., Ou, Y. N., Cao, X. P., Tan, M. S., Tan, L., et al. (2019). Diabetes mellitus and risks of cognitive impairment and dementia: A systematic review and meta-analysis of 144 prospective studies. *Ageing Res. Rev.* 55:100944. doi: 10.1016/j.arr.2019.100944
- Yan, H., Yan, Y., Gao, Y., Zhang, N., Kumar, G., Fang, Q., et al. (2022). Transcriptome analysis of fasudil treatment in the APPswe/PSEN1dE9 transgenic (APP/PS1) mice model of Alzheimer's disease. *Sci. Rep.* 12:6625. doi: 10.1038/s41598-022-10554-9
- Yang, J., Wang, Z., Fu, Y., Xu, J., Zhang, Y., Qin, W., et al. (2022). Prediction value of the genetic risk of type 2 diabetes on the amnesic mild cognitive impairment conversion to Alzheimer's disease. *Front. Aging Neurosci.* 14:964463. doi: 10.3389/fnagi.2022.964463
- Yarchoan, M., Toledo, J. B., Lee, E. B., Arvanitakis, Z., Kazi, H., Han, L. Y., et al. (2014). Abnormal serine phosphorylation of insulin receptor substrate 1 is associated with tau pathology in Alzheimer's disease and tauopathies. *Acta Neuropathol.* 128, 679–689. doi: 10.1007/s00401-014-1328-5
- Yde Ohki, C. M., Grossmann, L., Alber, E., Dwivedi, T., Berger, G., Werling, A. M., et al. (2020). The stress-Wnt-signaling axis: A hypothesis for attention-deficit hyperactivity disorder and therapy approaches. *Transl. Psychiatry* 10:315. doi: 10.1038/s41398-020-00999-9
- Zametkin, A. J., Nordahl, T. E., Gross, M., King, A. C., Semple, W. E., Rumsey, J., et al. (1990). Cerebral glucose metabolism in adults with hyperactivity of childhood onset. *N. Engl. J. Med.* 323, 1361–1366. doi: 10.1056/NEJM199011153232001
- Zhang, L., Du Rietz, E., Kuja-Halkola, R., Dobrosavljevic, M., Johnell, K., Pedersen, N. L., et al. (2022). Attention-deficit/hyperactivity disorder and Alzheimer's disease and any dementia: A multi-generation cohort study in Sweden. *Alzheimers Dement.* 18, 1155–1163. doi: 10.1002/alz.12462
- Zhang, Q., Du, G., John, V., Kapahi, P., and Bredesen, D. E. (2015). Alzheimer's model develops early ADHD syndrome. *J. Neurol. Neurophysiol.* 6, 1–6.
- Zhao, Q. F., Tan, L., Wang, H. F., Jiang, T., Tan, M. S., Tan, L., et al. (2016). The prevalence of neuropsychiatric symptoms in Alzheimer's disease: Systematic review and meta-analysis. *J. Affect. Disord.* 190, 264–271. doi: 10.1016/j.jad.2015.09.069
- Zhu, L., Chi, T., Zhao, X., Yang, L., Song, S., Lu, Q., et al. (2018). Xanthoceraside modulates neurogenesis to ameliorate cognitive impairment in APP/PS1 transgenic mice. *J. Physiol. Sci.* 68, 555–565. doi: 10.1007/s12576-017-0561-9
- Zigman, W. B., and Lott, I. T. (2007). Alzheimer's disease in Down syndrome: neurobiology and risk. *Ment. Retard. Dev. Disabil. Res. Rev.* 13, 237–246. doi: 10.1002/mrdd.20163
- Zou, Z., Tao, T., Li, H., and Zhu, X. (2020). mTOR signaling pathway and mTOR inhibitors in cancer: progress and challenges. *Cell Biosci.* 10:31.
- Zuin, M., Roncon, L., Passaro, A., Cervellati, C., and Zuliani, G. (2021). Metabolic syndrome and the risk of late onset Alzheimer's disease: An updated review and meta-analysis. *Nutr. Metab. Cardiovasc. Dis.* 31, 2244–2252. doi: 10.1016/j.numecd.2021.03.020



## OPEN ACCESS

## EDITED BY

Subashika Govindan,  
DBT/Wellcome Trust India Alliance, India

## REVIEWED BY

Deborah R. Winter,  
Northwestern University, United States  
Kathryn M. Lenz,  
The Ohio State University, United States

## \*CORRESPONDENCE

Morgane Sonia Thion  
✉ thion@biologie.ens.fr

## SPECIALTY SECTION

This article was submitted to  
Translational Neuroscience,  
a section of the journal  
Frontiers in Neuroscience

RECEIVED 16 December 2022

ACCEPTED 24 February 2023

PUBLISHED 23 March 2023

## CITATION

Bridlance C and Thion MS (2023) Multifaceted  
microglia during brain development: Models  
and tools.  
*Front. Neurosci.* 17:1125729.  
doi: 10.3389/fnins.2023.1125729

## COPYRIGHT

© 2023 Bridlance and Thion. This is an  
open-access article distributed under the terms  
of the [Creative Commons Attribution License](#)  
(CC BY). The use, distribution or reproduction  
in other forums is permitted, provided the  
original author(s) and the copyright owner(s)  
are credited and that the original publication in  
this journal is cited, in accordance with  
accepted academic practice. No use,  
distribution or reproduction is permitted which  
does not comply with these terms.

# Multifaceted microglia during brain development: Models and tools

Cécile Bridlance<sup>1,2,3</sup> and Morgane Sonia Thion<sup>1,2\*</sup>

<sup>1</sup>Institut de Biologie de l'École Normale Supérieure (IBENS), École Normale Supérieure, CNRS, INSERM, Université PSL, Paris, France, <sup>2</sup>Center for Interdisciplinary Research in Biology, Collège de France, CNRS, INSERM, Université PSL, Paris, France, <sup>3</sup>Collège Doctoral, Sorbonne Université, Paris, France

Microglia, the brain resident macrophages, are multifaceted glial cells that belong to the central nervous and immune systems. As part of the immune system, they mediate innate immune responses, regulate brain homeostasis and protect the brain in response to inflammation or injury. At the same time, they can perform a wide array of cellular functions that relate to the normal functioning of the brain. Importantly, microglia are key actors of brain development. Indeed, these early brain invaders originate outside of the central nervous system from yolk sac myeloid progenitors, and migrate into the neural folds during early embryogenesis. Before the generation of oligodendrocytes and astrocytes, microglia thus occupy a unique position, constituting the main glial population during early development and participating in a wide array of embryonic and postnatal processes. During this developmental time window, microglia display remarkable features, being highly heterogeneous in time, space, morphology and transcriptional states. Although tremendous progress has been made in our understanding of their ontogeny and roles, there are several limitations for the investigation of specific microglial functions as well as their heterogeneity during development. This review summarizes the current murine tools and models used in the field to study the development of these peculiar cells. In particular, we focus on the methodologies used to label and deplete microglia, monitor their behavior through live-imaging and also discuss the progress currently being made by the community to unravel microglial functions in brain development and disorders.

## KEYWORDS

microglia, brain, development, models, tools

## Introduction

Microglia, the central nervous system (CNS) resident macrophages remained poorly studied until an exponential growth in interest during the last two decades led to fascinating insights into the origin of microglia, their functions, as well as dysfunctions in pathological conditions (Mosser et al., 2017; Hammond et al., 2018; Hoeffel and Ginhoux, 2018; Li and Barres, 2018; Thion et al., 2018a; Prinz et al., 2019). Contrary to most brain cells, microglia were shown to originate from mesodermal yolk sac (YS) macrophage progenitors that travel to reach the CNS during early embryonic development, around Embryonic day (E)9 in mice and gestational week 4/5 in humans (Monier et al., 2007; Ginhoux et al., 2010; Verney et al., 2010; Menassa et al., 2022). As such, these brain invaders constitute the main glial population before the emergence of other glial cells such as oligodendrocytes and astrocytes. After closure of the blood brain barrier around E14 in mice, microglia are believed to be

enclosed in the brain under steady-state conditions. These pioneer microglia thus proliferate, seed the entire parenchyma and progressively mature in symbiosis with the neural tissue microenvironment (Matcovitch-Natan et al., 2016; Thion et al., 2018b; Kracht et al., 2020) before self-renewing throughout life. This situation is different in zebrafish where microglia are fully replaced by another source of microglia by adulthood (Xu et al., 2015; Ferrero et al., 2018). A key aspect of their development is the high heterogeneity in their colonization patterns, morphologies and molecular properties. In particular, microglial colonization of the brain parenchyma is a long-lasting process that spans embryogenesis until the end of the second postnatal week, following a very stereotypical and uneven spatiotemporal pattern (Swinnen et al., 2013; Squarzone et al., 2014; Menassa et al., 2022). These cells transiently accumulate at specific hotspots such as the cortico-striatal-amygdalar boundary and are excluded from others regions such as the cortical plate. In addition, they display a variety of morphologies (ameboid, poorly ramified, and elongated) associated with different brain localizations. Finally, owing to high throughput approaches, microglia have been shown to exhibit different transcriptomic states, specifically during development, in both mice and humans (Hammond et al., 2019; Li et al., 2019; Sankowski et al., 2019; Kracht et al., 2020). This high developmental heterogeneity contrasts with a relatively uniform distribution in the whole parenchyma alongside homogeneously ramified morphologies and molecular signatures at adult stages. Finally, sex-specific microglial features have been highlighted in postnatal steady-state conditions but also in response to environmental challenges (Schwarz et al., 2012; Lenz et al., 2013; Rebuli et al., 2016; Hanamsagar et al., 2017; Guneykaya et al., 2018; Thion et al., 2018b; Villa et al., 2018; VanRyzin et al., 2019).

Several seminal studies have demonstrated that, beyond their immune functions, microglia also perform a wide array of cellular functions that relate to the normal functioning of the brain and importantly to its development. In particular, they interact with synapses to mediate remodeling, pruning and transmission but have also been involved in synaptogenesis (Andoh and Koyama, 2021). They further participate to neurogenesis and oligodendrogenesis, partly through their regulation of cell death and survival (Sierra et al., 2010; Cunningham et al., 2013; Hagemeyer et al., 2017; Wlodarczyk et al., 2017; Nemes-Baran et al., 2020; Sherafat et al., 2021; Cserep et al., 2022). They also contribute to the refinement of axonal tracts (Pont-Lezica et al., 2014; Squarzone et al., 2014) and to the development of cortical inhibitory circuits (Squarzone et al., 2014; Thion et al., 2019; Favuzzi et al., 2021; Yu et al., 2022). Besides, microglia express various pattern recognition, purinergic, chemokine and cytokine receptors, collectively described as the sensome (Hickman et al., 2013), enabling them to detect and integrate environmental changes. Importantly and consistently with their wide array of cellular functions, microglial dysfunction has been associated with the etiology of neurodevelopmental disorders, including autism spectrum disorders and schizophrenia in humans and mouse models (Lukens and Eyo, 2022). Therefore, during this crucial period of development, it is key to better grasp their functions, the regulatory mechanisms underpinning their heterogeneity and how their molecular states may regulate their roles. Furthermore, elucidating how external signals can impact on these fundamental processes is a major challenge. This will be crucial to illuminate specific and diverse microglial contributions to brain wiring as well

as shed light on pathological mechanisms of neurodevelopmental disorders.

Beside microglia, other non-parenchymal macrophages called Border-Associated Macrophages (BAMs) are present at the interfaces of the brain: the meninges, choroid plexus and perivascular space (Lee et al., 2021; Figure 1). Although microglia and BAMs originate from yolk-sac derived progenitors and seed the brain during embryogenesis, some of them are further replaced by monocyte-derived cells, arising from hematopoietic stem cells (Goldmann et al., 2016; Mrdjen et al., 2018; Van Hove et al., 2019; Utz et al., 2020; Masuda et al., 2022). Moreover, while generally referred to as BAMs, they display age- and tissue-specific signatures (Kierdorf et al., 2019; Mildner et al., 2022). Most of the well-recognized microglial markers, reporter mouse lines and models that currently exist to label and deplete microglia can also target a large part of macrophages such as the BAMs in the CNS but also populations of peripheral macrophages (Green et al., 2020). Consequently, despite intense research efforts, these limitations prevent the identification and characterization of specific microglia functions, especially during development. Herein, we discuss about the current murine tools and models available to label or deplete microglia and subsequently assess their developmental functions in physiological and disease conditions.

## From broad microglial targeting to specific states labeling

### Catch me if you can: Microglia and other brain macrophages

Historically, microglia were mainly identified either through Iba1 immunostaining or using the *Cx3cr1<sup>GFP/+</sup>* (Jung et al., 2000) that labels many macrophages, including microglia and BAMs. Similarly, the well-established *Cx3cr1<sup>creERT2</sup>* mouse lines have been very useful to inactivate genes in these cells (Parkhurst et al., 2013; Yona et al., 2013). Nevertheless, they are not specific to microglia and may trigger microglial reactivity in neonates upon tamoxifen administration (Sahasrabudhe and Ghosh, 2022). Recent studies, including single cell RNA sequencing analyses, highlighted more specific homeostatic microglia markers including *p2ry12*, *Sall1*, *Tmem119*, *Hexb*, *Siglech* (Gautier et al., 2012; Buttgerit et al., 2016; Satoh et al., 2016; Cserep et al., 2020; Masuda et al., 2020) allowing the use of specific antibodies to label either microglia (*P2ry12*, *Tmem119*, and *Siglech*) or BAMs (*CD206*, *Lyve1*, and *Siglec1*) (Mrdjen et al., 2018; Figure 1). Fluorescent *In Situ* Hybridization (FISH) has also been used to circumvent the absence of specific antibodies, particularly by taking advantage of the RNAscope technique (Matcovitch-Natan et al., 2016; Hammond et al., 2019). To specifically visualize, manipulate and assess microglia functions, reporter and *creERT2*-expressing lines were generated with minor recombination in BAMs: *Tmem119<sup>eGFP</sup>* and *Tmem119<sup>creERT2</sup>* (Kaiser and Feng, 2019), *Tmem119<sup>tdTomato</sup>* (Ruan et al., 2020), *Hexb<sup>tdTomato</sup>* and *Hexb<sup>creERT2</sup>* (Masuda et al., 2020), *p2ry12<sup>creERT2</sup>* (McKinsey et al., 2020), *Sall1<sup>GFP</sup>*, and *Sall1<sup>creERT2</sup>* (Buttgerit et al., 2016), the latter recombining in neurons and other glia (Chappell-Maor et al., 2020; Table 1). Nonetheless, since most of these genes start to be expressed as microglia mature (Bennett et al., 2016), it is important to stress that there are so far no

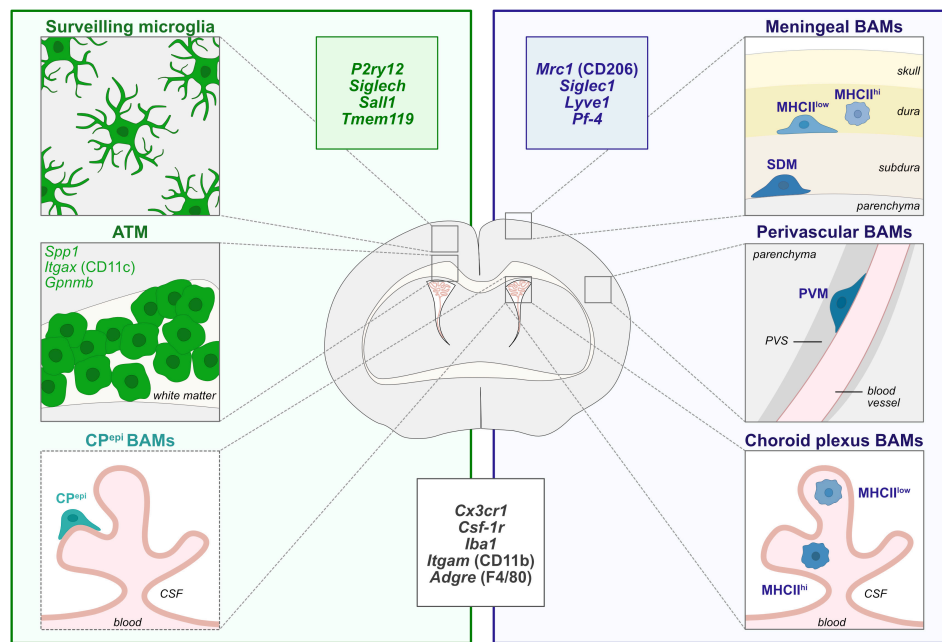


FIGURE 1

Diversity of CNS macrophages in steady-state conditions. During steady-state, microglia are localized within the brain parenchyma and are highly heterogeneous in morphologies, localization and molecular signatures throughout brain development. In particular, axon tract-associated microglia (ATM)/proliferative-region-associated microglia (PAM)/Cd11c-positive microglia have been described during early postnatal development in the corpus callosum and other white matter regions. Border-associated macrophages (BAMs) reside at distinct interfaces of the CNS such as the meninges, choroid plexus and perivascular space (Goldmann et al., 2016; Mrdjen et al., 2018; Van Hove et al., 2019; Utz et al., 2020; Masuda et al., 2022). Non-parenchymal microglia-like Kolmer's epilexus BAMS (CP<sup>epi</sup>) reside in the apical surface of the choroid plexus facing the cerebrospinal fluid (CSF) and share some transcriptional features with microglia and ATM signature (Van Hove et al., 2019). In particular, meningeal MHCII<sup>low</sup> and MHCII<sup>hi</sup> macrophages are localized in the dura matter while subdural macrophages (SDM) are restrained to the subdural area. Finally, while perivascular macrophages (PVM) are found in the perivascular space, between the vascular basement membrane and the glia limitans of the parenchyma, choroid plexus contains MHCII<sup>low</sup> and MHCII<sup>hi</sup> BAMS. The insets depict the most commonly used markers for microglia (green), BAMS (blue), and common markers to both populations (black). ATM, axon tract-associated microglia; BAMS, border-associated macrophages; CP<sup>epi</sup>, Kolmer's epilexus; CSF, cerebrospinal fluid; MHCII, major histocompatibility complex class II; PVS, perivascular space; PVM, perivascular macrophage; SDM, subdural macrophage.

alternatives to the *Cx3cr1*<sup>GFP/+</sup> or *Cx3cr1*<sup>creERT2</sup> lines to efficiently target early embryonic microglia.

Targeting microglia more specifically is crucial, since studies often assign a variety of roles to microglia using depletion models that target both microglia and BAMS. Kim et al. (2021) took advantage of an elegant “split cre” binary genetic construct to generate the *Cx3cr1*<sup>cre</sup>:*Sall1*<sup>ncr</sup> and *Cx3cr1*<sup>cre</sup>:*Lyve1*<sup>ncr</sup>, to selectively target microglia and BAMS, respectively. Furthermore, several mouse lines including the *Siglec1*<sup>cre</sup> (Utz et al., 2020), *Pf4*-*Cre* (McKinsey et al., 2020), *Lyve1*<sup>creERT2</sup>, and *Mrc1*<sup>CreERT2</sup> lines (Masuda et al., 2022) have been shown to specifically label BAMS during development and thereby enable to follow their trajectory (Table 1). In addition, while no circulating cells are thought to enter in the brain parenchyma during steady-state after BBB closure, monocyte infiltration can occur in disease, aging and injury, and can be monitored using bone marrow chimeras (Mills et al., 2022). These new tools will be important to decipher the relative contributions of microglia, BAMS or infiltrating myeloid cells, but still require thorough characterization with regards to efficiency and rate of spontaneous recombination at different timepoints along development.

Finally, cell-specific viral gene delivery has been extensively used to target different CNS population but robust transduction in microglia remained quite inefficient until recently (Maes et al., 2019). In a ground-breaking study, Lin et al. (2022)

successfully targeted 80% of microglia *in vivo* using adeno-associated viruses without inducing microglia reactivity or changes in gene expression, although it remains elusive to what extent BAMS were also affected. Such approach opens new avenues to study microglia but also have tremendous translational potential.

## Looking with new eyes

Along with new markers, mouse lines and viral approaches to target microglia, technical advances in diverse fields shed new light on ways to study microglia, in particular going from fixed immobile imaging in brain slices to dynamic and global approaches. First, tissue clearing methods are constantly improving, with some of them perfectly preserving the signal from reporter lines and antibodies [reviewed in Eme-Scolan and Dando (2020)]. This allows visualization of microglia in whole intact brains. However, while these techniques are becoming well-established and easier to use routinely, the difficulty lies in the analysis of the generated data. Annotated 3D atlases of the developing brain will offer many exciting possibilities toward a more comprehensive study of microglia development.

Another revolution in the field of microglia came with two-photon live-imaging experiments, which revealed never resting microglia with their processes constantly surveilling their



TABLE 1 Tools to label, target and deplete microglia and BAMs.

Tagging models	Microglia	BAMs	Prenatal and early postnatal	Adulthood	Remarks	References
<i>Cx3cr1<sup>GFP/+</sup></i>	Yes	Yes	GFP expressed by E9.5	>99%	Targets peripheral immune cells and myeloid BM progenitors	Jung et al., 2000
<i>Cx3cr1<sup>creERT2</sup></i> (1,2)	Yes	Yes	40H-Tam. E9.0: 99% efficiency at E10.5 (2)	>99%	Spontaneous recombination reported	Parkhurst et al., 2013 (1); Yona et al., 2013 (2)
<i>Tmem119<sup>creGFP</sup></i>	Yes	Few	GFP expressed by P1	>99%	Transiently labels blood vessels at P1	Kaiser and Feng, 2019
<i>Tmem119<sup>creERT2</sup></i>	Yes	Few	Tam. P2, P3 and P4: 90% efficiency by P14	>99%	Targets few CD45+ cells in blood	
<i>Tmem119<sup>tdTomato</sup></i>	Yes	Few	N.A.	>95%		Ruan et al., 2020
<i>Hexb<sup>tdTomato</sup></i>	Yes	Few	TdTomato expressed by E12.5	>99%	Labels few meningeal and perivascular BAMs	Masuda et al., 2020
<i>Hexb<sup>creERT2</sup></i>	Yes	Few	Tam. P1 and P3: 90% efficiency at P42	~80%	Targets peripheral macrophages in kidney	
<i>P2ry12<sup>creERT2</sup></i>	Yes	Few	Tam. E13.5, E15.5 and E17.5: robust efficiency by E18.5 in microglia and subsets of BAMs (40% in choroid plexus, 10% in meninges, few PVM)	90–95%	Targets 20–25% of BAMs in choroid plexus and meninges	McKinsey et al., 2020
<i>Sall1<sup>GFP</sup></i>	Yes	No	GFP expressed in 20% microglia by E12.5, 69% by E14.5, 90% by P2	>95%	Targets <10% other CNS cells	Buttgereit et al., 2016; Utz et al., 2020
<i>Sall1<sup>creERT2</sup></i>	Yes	No	Tam. E14.5 and E16.5: 75% efficiency at E18.5	>95%	Targets <10% other CNS cells	
<i>Cx3cr1<sup>ccre</sup>:Sall1<sup>ncre</sup></i>	Yes	No	N.A.	~90%		Kim et al., 2021
<i>Cx3cr1<sup>ccre</sup>:Lyve1<sup>ncre</sup></i>	No	Yes	N.A.	20% of Lyve1+ cells		
<i>Lyve1<sup>CreERT2</sup></i>	No	Yes	40H-Tam. E16.5: 50% efficiency in meningeal and perivascular macrophages at P14	N.A.	Targets lymphatic endothelial cells	Masuda et al., 2022
<i>Siglec1<sup>cre</sup></i>	No	Yes	Efficiently floxes gene in BAMs at E18.5	N.A.	<i>Siglec1</i> expressed by 60% BAMs at E14.5, 100% at E18.5	Utz et al., 2020
<i>Pf4-Cre</i>	Few	Yes	N.A.	>99%		McKinsey et al., 2020
<i>Mrc1<sup>CreERT2</sup></i>	No	Yes	40H-Tam. E9.0: 10% efficiency in BAMs and 5% in microglia by E18.5	>95%		Masuda et al., 2022
Adenoviruses	Yes	N.A.	N.A.	80%		Lin et al., 2022

(Continued)

TABLE 1 (Continued)

Depletion models	Microglia	BAMs	Prenatal and early postnatal	Adulthood	Remarks	References
<b>Killing by numbers</b>						
<i>Cx3cr1<sup>CreER</sup>;R26<sup>iDTR</sup></i>	Yes	Yes	N.A.	> 99%	Fast repopulation	Parkhurst et al., 2013
<i>IBA1-tTA::DTA<sup>tetO</sup>/tetO</i>	Yes	Yes	Withdrawal of doxycycline from maternal diet from P5: 50% depletion at P8	~90% in retina	Fast repopulation	Miyamoto et al., 2016; Takeda et al., 2018
<i>Siglech<sup>DTR/DTR</sup></i>	Yes	No	Injection at E10.5: 80% depletion at E12.5, 60% at E14.5	80–85%	Fast repopulation	Konishi et al., 2017; Li et al., 2021
<b>CSF-1R inhibitors</b>						
Anti CSF-1R antibodies	Yes	Yes	Injections at E6 and E7: > 98% depletion at E14.5	No effect	Fast repopulation	MacDonald et al., 2010; Squarzoni et al., 2014
Anti CSF-1 antibodies	Yes	No	Injections at E6 and E7: > 50% depletion at P0.5	60% in white matter region	Dose-dependent efficiency	Easley-Neal et al., 2019
Anti IL-34 antibodies	Yes	No	Injections at E6 and E7: no effect at P0.5. Injection at P0.5: 30% depletion at P4	50% in grey matter region	Dose-dependent efficiency	
PLX5622	Yes	Yes	Chow PLX from E3.5: 99% depletion at E15.5	> 95% within 7 days	Fast repopulation	Huang et al., 2018; Rosin et al., 2018; Marsters et al., 2020
PLX3397	Yes	Yes	Chow PLX from E14 followed by s.c. injections in pups: 90% depletion at P5 in spinal cord	> 99% within 7 days	Fast repopulation	Elmore et al., 2014; Li et al., 2020
<b>Genetic models</b>						
<i>Pu.1<sup>-/-</sup></i>	Yes	Yes	100%	100%	Homozygotes die shortly after birth	McKercher et al., 1996
<i>Csf1<sup>op/op</sup></i>	Yes	Yes	N.A.	0–30%	Abnormal brain development	Michaelson et al., 1996
<i>Il34<sup>LacZ/LacZ</sup> (1,2)</i>	Yes	N.A.	> 80% decrease at P2 (1); normal colonization of the brain from E10.5 to newborn (2)	50% (1; 2)		Wang et al., 2012 (1); Greter et al., 2012 (2)
<i>Csf1r<sup>-/-</sup></i>	Yes	Yes	> 99%	100%	Shortened lifespan and abnormal brain development	Erblich et al., 2011
<i>Sall1<sup>CreER</sup>;Csf1r<sup>fl/fl</sup></i>	Yes	No	N.A.	70–90%	Spatial variability in efficiency	Buttgereit et al., 2016
<i>Hexb<sup>CreERT2</sup>;Csf1r<sup>fl/fl</sup></i>	Yes	No	N.A.	60%		Masuda et al., 2020
<i>Csf1r<sup>ΔFIRE/ΔFIRE</sup></i>	Yes	Few	Absence of CPepi in the choroid plexus, other BAMs reduced	100%		Rojo et al., 2019; Munro et al., 2020
<i>Nestin<sup>cre</sup>;Csf1r<sup>fl/fl</sup></i>	Yes	N.A.	60% decrease in E17.5 cerebellum	~50% in cerebellum		Kana et al., 2019
<i>Nestin<sup>cre</sup>;Il34<sup>fl/fl</sup></i>	Yes	N.A.	N.A.	~85% in striatum		Badimon et al., 2020

Table summarizing the main mouse lines and tools available to label, target and deplete microglia and BAMs, indicating their specificity and efficiency in development and adulthood. BAMs, border-associated macrophages; BM, bone marrow; CNS, central nervous system; CPepi, Kolmer's epiplexus; DTA, diphtheria toxin fragment A; DTR, diphtheria toxin receptor; iDTR, inducible diphtheria toxin receptor; i.p., intraperitoneal; N.A., non-applicable; PVM, perivascular macrophages; s.c., subcutaneous; Tam, tamoxifen; 40H-Tam, 4-hydroxytamoxifen.

environment as well as rapidly reacting in case of injury (Davalos et al., 2005; Nimmerjahn et al., 2005). In combination with other markers, it is thus possible to monitor microglial interaction with blood vessels (Csaszar et al., 2022), radial glia (Rosin et al., 2021), neuronal populations as well as track microglial processes and their specific contact with synapses (Wake et al., 2009) or nodes of Ranvier (Ronzano et al., 2021). While some experiments are performed on brain slices, inducing tissue damage and possibly altering microglial behavior, most studies use cranial windows or skull thinning that allows microglial observation in their homeostatic environment. For pups, adapted approaches are being developed taking advantage of the thinness of the embryonic skull to perform *ex utero* live-imaging of microglia and macrophages in the brain of intact embryos (Hattori et al., 2020, 2022; Munz et al., 2022), that will probably be critical to better characterize key aspects of microglia development such as their entry in the brain parenchyma (Stremmel et al., 2018).

As a self-renewing population arising from a restricted pool of pioneer cells, the questions of microglial expansion during development, their migration and turnover were raised—and still retain some mystery. The “Microfetti” mice developed by Tay et al. (2017) in which microglia express randomly one out of four fluorophores after tamoxifen induction, highlighted clonal expansion of adult microglia in pathology. In addition, Ratz et al. (2022) developed the new TREX technique, which combines single-cell and spatial transcriptomic coupled to early (E9.5) *in vivo* barcoding, in order to analyze the lineage relationships between mature cells and progenitors. Thereby, they highlighted drastic microglial expansion from a limited pool of progenitors. Though not extensively used yet, these tools for clonal analysis and lineage tracing will be valuable in the context of development to better understand microglial expansion, migration and final distribution in the brain.

## Targeting the different flavors of microglia

Historically, microglia were classified as displaying either a neurotoxic pro-inflammatory M1 or neuroprotective anti-inflammatory M2 phenotype but this binary perspective has been largely revisited (Paolicelli et al., 2022). The development of high throughput technologies such as single cell and single nucleus RNA sequencing (sc/snRNA-seq), cytometry by time-of-flight (CyTOF), or multiplex error-robust fluorescent *in situ* hybridization (MERFISH) revealed a richer heterogeneity in microglial profiles. While microglia constitute a relatively homogeneous population in adulthood, they display a striking heterogeneity during prenatal/early postnatal development, aging and neurodegeneration (Deczkowska et al., 2018; Hammond et al., 2019; Li et al., 2019; Masuda et al., 2019; Sankowski et al., 2019; Kracht et al., 2020; Marschallinger et al., 2020; Safaiyan et al., 2021; Stogsdill et al., 2022). Nevertheless, we should not underestimate the experimental bias introduced by cell dissociation and sorting-strategies, sequencing technologies and subsequent analyzes selected to characterize microglial heterogeneity (Marsh et al., 2022; Paolicelli et al., 2022; Sankowski et al., 2022). To avoid extensive confusion in the field, it remains crucial to be cautious about the semantic implication of microglial heterogeneity and the

subsequent functional diversity associated with it (Paolicelli et al., 2022).

Specific developmental microglial states are thus starting to be described such as the Axon Tract-associated Microglia (ATM), also known as Proliferative-region-Associated Microglia (PAM), Cd11c-positive microglia, and Youth-Associated Microglia (YAM). They are characterized by the expression of several genes such as *Spp1*, *Itgax*, *Gpnmb* and were initially identified in the postnatal white matter as regulators of the development of oligodendrocyte precursors and of subsequent myelinogenesis (Hagemeyer et al., 2017; Wlodarczyk et al., 2017; Hammond et al., 2019; Li et al., 2019; Silvin et al., 2022). Interestingly, there are remarkable similarities in transcriptomic signatures between ATM and Disease Associated Microglia (DAM), initially characterized in mouse models of Alzheimer’s disease (Keren-Shaul et al., 2017; Krasemann et al., 2017), raising the question of their potential similarities, differences—and relationship. Apart from the use of specific antibodies or *in situ* hybridization probes, the field lacks genetic tools to specifically label and target microglia states. So far, only a *CD11c<sup>cre</sup>* line has been used to target ATM (Wlodarczyk et al., 2017), but was unsuccessful in depleting ATM in combination with Diphtheria Toxin strategies. In addition, a novel *Spp1<sup>tdTomato</sup>* mouse line has been generated and used to monitor SPP1 from perivascular macrophages (De Schepper et al., 2022), and could constitute an interesting tool for ATM-lineage studies. Based on their emerging molecular characterization, novel mouse lines or viral approaches will enable specific depletion or inactivation of microglial states to further assess their fates and functions. Moreover, in-depth characterization of transcriptomic, epigenomic, and metabolomic landscapes in microglia would enable to better understand their regulatory mechanisms, the transientness of these states and to which extent they can be induced by the microenvironment at different stages of life. Along these lines, the progress of spatial transcriptomics toward increased structural resolution should lead to a tremendous breakthrough to characterize microglial heterogeneity (Stogsdill et al., 2022), in particular at hotspots of accumulating microglia during development. Altogether, the field is moving onto a specific targeting of developmental microglial states which should shed new light on their regulatory mechanisms, their plasticity and functions in steady-state and disease conditions.

## En route for specific depletion approaches

Microglial functions in brain development, homeostasis and diseases were historically assessed using *in vivo* depletion strategies summarized in Table 1. Though a lot of techniques have been developed, their diversity illustrates the difficulty to obtain a specific, efficient and long-lasting depletion of microglia while limiting its off-target effects.

## Killing by numbers

The first strategies employed were aiming to directly trigger microglial apoptosis by administration of clodronate liposomes,

that are specifically phagocytosed by microglia and BAMs and induce cell death upon cytoplasmic release (Green et al., 2020). This approach is efficient in the early post-natal brain and in adults, but the inability of the clodronate liposomes to cross the blood brain barrier requires an intracerebral injection, inducing an injury and possible release of inflammatory cytokines (Han et al., 2019). Another approach uses the diphtheria-toxin (DT) based systems, either with direct expression of the DTA or with DT receptor, the latter needing administration of DT. The first studies were performed in *Cx3cr1<sup>CreER</sup>;R26<sup>iDTR</sup>* and *Iba1-tTA:DTA<sup>tetO</sup>/tetO* targeting both microglia and BAMs (Parkhurst et al., 2013; Miyamoto et al., 2016; Takeda et al., 2018). On the contrary, the use of the *Siglech<sup>dtr/+</sup>* mice led to specific and transient depletion of embryonic microglia, without affecting BAMs (Li et al., 2021). Thus, the constitutive or inducible DTR/DTA expression, combined with specific microglial lines provides a better temporal control as well as selective effect, though their efficiency remains variable.

## CSF-1R inhibitors

The CSF-1 receptor (CSF-1R) is expressed by microglia, macrophages and their progenitors and its signaling is essential for their survival and proliferation. It thus became a preferential target in the quest for microglial depletion methods. Injections of an anti-CSF-1R antibody performed at E6.5 and E7.5 lead to a drastic depletion of myeloid progenitors, macrophages and microglia, while repopulation spans the first postnatal week (Squarzoni et al., 2014; Hoeffel and Ginhoux, 2015; Thion et al., 2019). On the other hand, embryonic targeting of CSF-1, one of the two CSF-1R ligands, through anti-CSF-1 antibody, leads to a drastic depletion of forebrain microglia (Easley-Neal et al., 2019), with possible off-target effects of the circulating antibodies. Pharmacological inhibitors of the CSF-1R injected or delivered non-invasively *via* food pellets have been broadly developed to deplete adult microglia, such as PLX3397 and PLX5622, the latter having a higher specificity and improved brain penetrance (Elmore et al., 2014; Green et al., 2020) while it efficiently depletes embryonic microglia, enabling a temporal control of the depletion during gestation (Rosin et al., 2018; Marsters et al., 2020). Nevertheless, as this treatment can affect lactation by depleting maternal macrophages essential for mammary gland development (O'Brien et al., 2012), it can impact pup survival following birth. For early postnatal depletion, direct subcutaneous injections of PLX3397 or PLX5622 during the first post-natal week allows for an efficient depletion of microglia (Li et al., 2020; Favuzzi et al., 2021; Gesuita et al., 2022). Although beyond the scope of this review, CSF-1R inhibitors are also used in other species including humans, bringing novel therapeutic approaches [reviewed in Han et al. (2022)]. Overall, targeting the CSF-1R pathway has proven to be efficient and convenient, but also affects peripheral macrophages and BAMs, preventing the identification of specific microglial functions.

## Genetic models

Different genetic models, including constitutive knock-outs of fundamental transcription or survival factors, like *Pu.1<sup>-/-</sup>*

(McKercher et al., 1996) and *Csf1r<sup>-/-</sup>* (Erblich et al., 2011), fail to develop microglia as well as most macrophages (Green et al., 2020). This results in many off-target effects and early death in *Pu.1<sup>-/-</sup>* and *Csf1r<sup>-/-</sup>*. On the other hand, the *Csf1r<sup>fl/fl</sup>* allows for a more specific targeting of microglia, thanks to the microglia specific mouse lines now available and their possible temporal induction. This strategy has been used with *Sall1<sup>CreER</sup>;Csf1r<sup>fl/fl</sup>* (Buttgereit et al., 2016) and *Hexb<sup>CreERT2</sup>;Csf1r<sup>fl/fl</sup>* mice (Masuda et al., 2020), with a respective efficiency varying across brain regions from 70% to 90% and of 60%.

An additional important model is the *Csf1r<sup>ΔFIRE/ΔFIRE</sup>* mice, in which a *Csf1r* enhancer is deleted (Rojo et al., 2019; Munro et al., 2020). This leads to the absence of microglia from the brain parenchyma, and of resident macrophages of the skin, kidney, heart and peritoneum; while other macrophages and monocytes are unaffected. Importantly, these mice are healthy and fertile in a mixed B6CBAF1/C57BL/6J background, and do not display strong developmental defects described in the *Csf1r<sup>-/-</sup>*. So far, they were used to investigate the role of resident microglia in Alzheimer disease mice (Kiani Shabestari et al., 2022) and they will provide a more specific and long-lasting model to explore microglial functions.

Finally, full inactivation of CSF-1R ligands, *Csf-1* (Chang et al., 1994; Kondo and Duncan, 2009) or *Il34* (Greter et al., 2012; Wang et al., 2012), expressed by the neural tissue, results in time- and region-dependent partial depletion of microglia albeit there are still some controversies amongst studies and major impact on peripheral macrophages (Green et al., 2020; Table 1). Nevertheless, under the pan neuronal driver *Nestin<sup>cre</sup>* that restricts depletion to the nervous system, thus mainly affecting microglia, the *Nestin<sup>cre</sup>;Csf1r<sup>fl/fl</sup>* and *Nestin<sup>cre</sup>;Il34<sup>fl/fl</sup>* are respectively deprived of microglia in the white matter and cerebellum or in the gray matter highlighting region-specific dependency (Kana et al., 2019; Badimon et al., 2020). On the other hand, macrophages are unaffected in the yolk sac, fetal liver and fetal limbs. Last, because the CSF-1R ligands are differentially expressed and required from microglia through development, these lines provide promising models to investigate local microglial functions.

## Concluding remarks

Microglia now appear as key actors of brain development, interacting with most brain cells and regulating several crucial developmental processes. Nevertheless, these exciting advances were done in models affecting both microglia and BAMs. Thus, dissecting their respective contributions thanks to new specific tools will be key to the field. In addition, further understanding microglial diversity during development and the functions played by specific states should bring new light on their importance in neurodevelopmental pathologies and open new avenues for therapeutic intervention.

## Author contributions

CB and MST wrote the review. Both authors contributed to the article and approved the submitted version.



## Funding

The laboratories acknowledge support from the INSERM, CNRS, École Normale Supérieure, Collège de France and Fondation du Collège de France. CB was supported by an AMX doctoral fellowship and an ARC fellowship. MST is a CNRS investigator supported by the Foundation for Brain Research (FRC).

## Acknowledgments

We are grateful to members of the Thion and Garel laboratories for stimulating discussions and comments on the manuscript.

## References

- Andoh, M., and Koyama, R. (2021). Microglia regulate synaptic development and plasticity. *Dev. Neurobiol.* 81, 568–590. doi: 10.1002/dneu.22814
- Badimon, A., Strasburger, H. J., Ayata, P., Chen, X., Nair, A., Ikegami, A., et al. (2020). Negative feedback control of neuronal activity by microglia. *Nature* 586, 417–423. doi: 10.1038/s41586-020-2777-8
- Bennett, M. L., Bennett, F. C., Liddelow, S. A., Ajami, B., Zamanian, J. L., Fernhoff, N. B., et al. (2016). New tools for studying microglia in the mouse and human CNS. *Proc. Natl. Acad. Sci. U.S.A.* 113, E1738–E1746. doi: 10.1073/pnas.1525528113
- Buttgereit, A., Lelios, I., Yu, X., Vrohligs, M., Krakoski, N. R., Gautier, E. L., et al. (2016). Sall1 is a transcriptional regulator defining microglia identity and function. *Nat. Immunol.* 17, 1397–1406. doi: 10.1038/ni.3585
- Chang, Y., Albright, S., and Lee, F. (1994). Cytokines in the central nervous system: Expression of macrophage colony stimulating factor and its receptor during development. *J. Neuroimmunol.* 52, 9–17. doi: 10.1016/0165-5728(94)90156-2
- Chappell-Maor, L., Kolesnikov, M., Kim, J. S., Shemer, A., Haimon, Z., Grozovski, J., et al. (2020). Comparative analysis of CreER transgenic mice for the study of brain macrophages: A case study. *Eur. J. Immunol.* 50, 353–362. doi: 10.1002/eji.201948342
- Csaszar, E., Lenart, N., Cserep, C., Kornyei, Z., Fekete, R., Posfai, B., et al. (2022). Microglia modulate blood flow, neurovascular coupling, and hypoperfusion via purinergic actions. *J. Exp. Med.* 219:e20211071. doi: 10.1084/jem.20211071
- Cserep, C., Posfai, B., Lenart, N., Fekete, R., Laszlo, Z. I., Lele, Z., et al. (2020). Microglia monitor and protect neuronal function through specialized somatic purinergic junctions. *Science* 367, 528–537. doi: 10.1126/science.aax6752
- Cserep, C., Schwarcz, A. D., Posfai, B., Laszlo, Z. I., Kellermayer, A., Kornyei, Z., et al. (2022). Microglial control of neuronal development via somatic purinergic junctions. *Cell Rep.* 40:111369. doi: 10.1016/j.celrep.2022.111369
- Cunningham, C. L., Martinez-Cerdeno, V., and Noctor, S. C. (2013). Microglia regulate the number of neural precursor cells in the developing cerebral cortex. *J. Neurosci.* 33, 4216–4233. doi: 10.1523/JNEUROSCI.3441-12.2013
- Davalos, D., Grutzendler, J., Yang, G., Kim, J. V., Zuo, Y., Jung, S., et al. (2005). ATP mediates rapid microglial response to local brain injury in vivo. *Nat. Neurosci.* 8, 752–758. doi: 10.1038/nn1472
- De Schepper, S., Ge, J. G., Crowley, G., Ferreira, L. S. S., Garceau, D., Toomey, C. E., et al. (2022). Perivascular SPP1 mediates microglial engulfment of synapses in Alzheimer's disease models. *bioRxiv* [Preprint]. doi: 10.1101/2022.04.04.486547
- Deczkowska, A., Keren-Shaul, H., Weiner, A., Colonna, M., Schwartz, M., and Amit, I. (2018). Disease-associated microglia: A universal immune sensor of neurodegeneration. *Cell* 173, 1073–1081. doi: 10.1016/j.cell.2018.05.003
- Easley-Neal, C., Foreman, O., Sharma, N., Zarrin, A. A., and Weimer, R. M. (2019). CSF1R ligands IL-34 and CSF1 are differentially required for microglia development and maintenance in white and gray matter brain regions. *Front. Immunol.* 10:2199. doi: 10.3389/fimmu.2019.02199
- Elmore, M. R., Najafi, A. R., Koike, M. A., Dagher, N. N., Spangenberg, E. E., Rice, R. A., et al. (2014). Colony-stimulating factor 1 receptor signaling is necessary for microglia viability, unmasking a microglia progenitor cell in the adult brain. *Neuron* 82, 380–397. doi: 10.1016/j.neuron.2014.02.040
- Eme-Scolan, E., and Dando, S. J. (2020). Tools and approaches for studying microglia in vivo. *Front. Immunol.* 11:583647. doi: 10.3389/fimmu.2020.583647
- Erblich, B., Zhu, L., Etgen, A. M., Dobrenis, K., and Pollard, J. W. (2011). Absence of colony stimulation factor-1 receptor results in loss of microglia, disrupted brain development and olfactory deficits. *PLoS One* 6:e26317. doi: 10.1371/journal.pone.0026317
- Favuzzi, E., Huang, S., Saldi, G. A., Binan, L., Ibrahim, L. A., Fernandez-Otero, M., et al. (2021). GABA-receptive microglia selectively sculpt developing inhibitory circuits. *Cell* 184, 4048–4063.e32. doi: 10.1016/j.cell.2021.06.018
- Ferrero, G., Mahony, C. B., Dupuis, E., Yvernogeu, L., Di Ruggiero, E., Misericocchi, M., et al. (2022). Embryonic microglia derive from primitive macrophages and are replaced by cmyb-dependent definitive microglia in zebrafish. *Cell Rep.* 24, 130–141. doi: 10.1016/j.celrep.2021.05.066
- Gautier, E. L., Shay, T., Miller, J., Greter, M., Jakubzick, C., Ivanov, S., et al. (2012). Gene-expression profiles and transcriptional regulatory pathways that underlie the identity and diversity of mouse tissue macrophages. *Nat. Immunol.* 13, 1118–1128. doi: 10.1038/ni.2419
- Gesuita, L., Cavaccini, A., Argunsah, A. O., Favuzzi, E., Ibrahim, L. A., Stachniak, T. J., et al. (2022). Microglia contribute to the postnatal development of cortical somatostatin-positive inhibitory cells and to whisker-evoked cortical activity. *Cell Rep.* 40:111209. doi: 10.1016/j.celrep.2022.111209
- Ginhoux, F., Greter, M., Leboeuf, M., Nandi, S., See, P., Gokhan, S., et al. (2010). Fate mapping analysis reveals that adult microglia derive from primitive macrophages. *Science* 330, 841–845. doi: 10.1126/science.1194637
- Goldmann, T., Wieghofer, P., Jordao, M. J., Prutek, F., Hagemeyer, N., Frenzel, K., et al. (2016). Origin, fate and dynamics of macrophages at central nervous system interfaces. *Nat. Immunol.* 17, 797–805. doi: 10.1038/ni.3423
- Green, K. N., Crapser, J. D., and Hohsfield, L. A. (2020). To kill a microglia: A case for CSF1R Inhibitors. *Trends Immunol.* 41, 771–784. doi: 10.1016/j.it.2020.07.001
- Greter, M., Lelios, I., Pelczar, P., Hoeffel, G., Price, J., Leboeuf, M., et al. (2012). Stroma-derived interleukin-34 controls the development and maintenance of langerhans cells and the maintenance of microglia. *Immunity* 37, 1050–1060. doi: 10.1016/j.immuni.2012.11.001
- Guneykaya, D., Ivanov, A., Hernandez, D. P., Haage, V., Wojtas, B., Meyer, N., et al. (2018). Transcriptional and translational differences of microglia from male and female brains. *Cell Rep.* 24, 2773–2783.e6. doi: 10.1016/j.celrep.2018.08.001
- Hagemeyer, N., Hanft, K. M., Akriditou, M. A., Unger, N., Park, E. S., Stanley, E. R., et al. (2017). Microglia contribute to normal myelinogenesis and to oligodendrocyte progenitor maintenance during adulthood. *Acta Neuropathol.* 134, 441–458. doi: 10.1007/s00401-017-1747-1
- Hammond, T. R., Dufort, C., Dissing-Olesen, L., Giera, S., Young, A., Wysoker, A., et al. (2019). Single-Cell RNA sequencing of microglia throughout the mouse lifespan and in the injured brain reveals complex cell-state changes. *Immunity* 50, 253–271.e6. doi: 10.1016/j.immuni.2018.11.004
- Hammond, T. R., Robinton, D., and Stevens, B. (2018). Microglia and the brain: Complementary partners in development and disease. *Annu. Rev. Cell Dev. Biol.* 34, 523–544. doi: 10.1146/annurev-cellbio-100616-060509
- Han, J., Chitu, V., Stanley, E. R., Wszolek, Z. K., Karrenbauer, V. D., and Harris, R. A. (2022). Inhibition of colony stimulating factor-1 receptor (CSF-1R) as a potential therapeutic strategy for neurodegenerative diseases: Opportunities and challenges. *Cell Mol. Life Sci.* 79, 219. doi: 10.1007/s00018-022-04225-1

## Conflict of interest

The authors declare that the research was conducted in the absence of any commercial or financial relationships that could be construed as a potential conflict of interest.

## Publisher's note

All claims expressed in this article are solely those of the authors and do not necessarily represent those of their affiliated organizations, or those of the publisher, the editors and the reviewers. Any product that may be evaluated in this article, or claim that may be made by its manufacturer, is not guaranteed or endorsed by the publisher.

- Han, X., Li, Q., Lan, X., El-Mufti, L., Ren, H., and Wang, J. (2019). Microglial depletion with clodronate liposomes increases proinflammatory cytokine levels, induces astrocyte activation, and damages blood vessel integrity. *Mol. Neurobiol.* 56, 6184–6196. doi: 10.1007/s12035-019-1502-9
- Hanamsagar, R., Alter, M. D., Block, C. S., Sullivan, H., Bolton, J. L., and Bilbo, S. D. (2017). Generation of a microglial developmental index in mice and in humans reveals a sex difference in maturation and immune reactivity. *Glia* 65, 1504–1520. doi: 10.1002/glia.23176
- Hattori, Y., Kato, D., Murayama, F., Koike, S., Naito, Y., Kawaguchi, A., et al. (2022). Border-associated macrophages transventricularly infiltrate the early embryonic cerebral wall to differentiate into microglia. *bioRxiv* [Preprint]. doi: 10.1101/2022.07.27.501563
- Hattori, Y., Naito, Y., Tsugawa, Y., Nonaka, S., Wake, H., Nagasawa, T., et al. (2020). Transient microglial absence assists postmigratory cortical neurons in proper differentiation. *Nat. Commun.* 11:1631. doi: 10.1038/s41467-020-15409-3
- Hickman, S. E., Kingery, N. D., Ohsumi, T. K., Borowsky, M. L., Wang, L. C., Means, T. K., et al. (2013). The microglial sensome revealed by direct RNA sequencing. *Nat. Neurosci.* 16, 1896–1905. doi: 10.1038/nn.3554
- Hoeffel, G., and Ginhoux, F. (2015). Ontogeny of tissue-resident macrophages. *Front Immunol.* 6:486. doi: 10.3389/fimmu.2015.00486
- Hoeffel, G., and Ginhoux, F. (2018). Fetal monocytes and the origins of tissue-resident macrophages. *Cell Immunol.* 330, 5–15. doi: 10.1016/j.cellimm.2018.01.001
- Huang, Y., Xu, Z., Xiong, S., Sun, F., Qin, G., Hu, G., et al. (2018). Repopulated microglia are solely derived from the proliferation of residual microglia after acute depletion. *Nat. Neurosci.* 21, 530–540. doi: 10.1038/s41593-018-0090-8
- Jung, S., Aliberti, J., Graemmel, P., Sunshine, M. J., Kreutzberg, G. W., Sher, A., et al. (2000). Analysis of fractalkine receptor CX(3)CR1 function by targeted deletion and green fluorescent protein reporter gene insertion. *Mol. Cell Biol.* 20, 4106–4114. doi: 10.1128/MCB.20.11.4106-4114.2000
- Kaiser, T., and Feng, G. (2019). Tmem119-EGFP and tmem119-CreERT2 transgenic mice for labeling and manipulating microglia. *eNeuro* 6, ENEURO.0448–18.2019. doi: 10.1523/ENEURO.0448-18.2019
- Kana, V., Desland, F. A., Casanova-Acebes, M., Ayata, P., Badimon, A., Nabel, E., et al. (2019). CSF-1 controls cerebellar microglia and is required for motor function and social interaction. *J. Exp. Med.* 216, 2265–2281. doi: 10.1084/jem.20182037
- Keren-Shaul, H., Spinrad, A., Weiner, A., Matcovitch-Natan, O., Dvir-Szternfeld, R., Ulland, T. K., et al. (2017). A unique microglia type associated with restricting development of Alzheimer's disease. *Cell* 169, 1276–1290.e17. doi: 10.1016/j.cell.2017.05.018
- Kiani Shabestari, S., Morabito, S., Danhash, E. P., McQuade, A., Sanchez, J. R., Miyoshi, E., et al. (2022). Absence of microglia promotes diverse pathologies and early lethality in Alzheimer's disease mice. *Cell Rep.* 39:110961. doi: 10.1016/j.celrep.2022.110961
- Kierdorf, K., Masuda, T., Jordao, M. J. C., and Prinz, M. (2019). Macrophages at CNS interfaces: Ontogeny and function in health and disease. *Nat. Rev. Neurosci.* 20, 547–562. doi: 10.1038/s41583-019-0201-x
- Kim, J. S., Kolesnikov, M., Peled-Hajaj, S., Scheyltjens, I., Xia, Y., Trzebanski, S., et al. (2021). A binary Cre transgenic approach dissects microglia and CNS border-associated macrophages. *Immunity* 54, 176–190.e7. doi: 10.1016/j.immuni.2020.11.007
- Kondo, Y., and Duncan, I. D. (2009). Selective reduction in microglia density and function in the white matter of colony-stimulating factor-1-deficient mice. *J. Neurosci. Res.* 87, 2686–2695. doi: 10.1002/jnr.22096
- Konishi, H., Kobayashi, M., Kunisawa, T., Imai, K., Sayo, A., Malissen, B., et al. (2017). Siglec-H is a microglia-specific marker that discriminates microglia from CNS-associated macrophages and CNS-infiltrating monocytes. *Glia* 65, 1927–1943. doi: 10.1002/glia.23204
- Kracht, L., Borggrewe, M., Eskandar, S., Brouwer, N., Chuva de Sousa Lopes, S. M., Laman, J. D., et al. (2020). Human fetal microglia acquire homeostatic immune-sensing properties early in development. *Science* 369, 530–537. doi: 10.1126/science.aba5906
- Krasemann, S., Madore, C., Cialic, R., Baufeld, C., Calcagno, N., El Fatimy, R., et al. (2017). The TREM2-APOE pathway drives the transcriptional phenotype of dysfunctional microglia in neurodegenerative diseases. *Immunity* 47, 566–581.e9. doi: 10.1016/j.immuni.2017.08.008
- Lee, E., Eo, J. C., Lee, C., and Yu, J. W. (2021). Distinct features of brain-resident macrophages: Microglia and non-parenchymal brain macrophages. *Mol. Cells* 44, 281–291. doi: 10.14348/molcells.2021.0060
- Lenz, K. M., Nugent, B. M., Haliyur, R., and McCarthy, M. M. (2013). Microglia are essential to masculinization of brain and behavior. *J. Neurosci.* 33, 2761–2772. doi: 10.1523/JNEUROSCI.1268-12.2013
- Li, C., Konishi, H., Nishiwaki, K., Sato, K., Miyata, T., and Kiyama, H. (2021). A mouse model of microglia-specific ablation in the embryonic central nervous system. *Neurosci. Res.* 173, 54–61. doi: 10.1016/j.neures.2021.06.002
- Li, Q., and Barres, B. A. (2018). Microglia and macrophages in brain homeostasis and disease. *Nat. Rev. Immunol.* 18, 225–242. doi: 10.1038/nri.2017.125
- Li, Q., Cheng, Z., Zhou, L., Darmanis, S., Neff, N. F., Okamoto, J., et al. (2019). Developmental heterogeneity of microglia and brain myeloid cells revealed by deep single-cell RNA sequencing. *Neuron* 101, 207–223.e10. doi: 10.1016/j.neuron.2018.12.006
- Li, Y., He, X., Kawaguchi, R., Zhang, Y., Wang, Q., Monavarfeshani, A., et al. (2020). Microglia-organized scar-free spinal cord repair in neonatal mice. *Nature* 587, 613–618. doi: 10.1038/s41586-020-2795-6
- Lin, R., Zhou, Y., Yan, T., Wang, R., Li, H., Wu, Z., et al. (2022). Directed evolution of adeno-associated virus for efficient gene delivery to microglia. *Nat. Methods* 19, 976–985. doi: 10.1038/s41592-022-01547-7
- Lukens, J. R., and Eyo, U. B. (2022). Microglia and neurodevelopmental disorders. *Annu. Rev. Neurosci.* 45, 425–445. doi: 10.1146/annurev-neuro-110920-023056
- MacDonald, K. P., Palmer, J. S., Cronau, S., Seppanen, E., Olver, S., Raffelt, N. C., et al. (2010). An antibody against the colony-stimulating factor 1 receptor depletes the resident subset of monocytes and tissue- and tumor-associated macrophages but does not inhibit inflammation. *Blood* 116, 3955–3963. doi: 10.1182/blood-2010-02-266296
- Maes, M. E., Colombo, G., Schulz, R., and Siegert, S. (2019). Targeting microglia with lentivirus and AAV: Recent advances and remaining challenges. *Neurosci. Lett.* 707:134310. doi: 10.1016/j.neulet.2019.134310
- Marschallinger, J., Iram, T., Zardeneta, M., Lee, S. E., Lehallier, B., Haney, M. S., et al. (2020). Lipid-droplet-accumulating microglia represent a dysfunctional and proinflammatory state in the aging brain. *Nat. Neurosci.* 23, 194–208. doi: 10.1038/s41593-019-0566-1
- Marsh, S. E., Walker, A. J., Kamath, T., Dissing-Olesen, L., Hammond, T. R., de Soysa, T. Y., et al. (2022). Dissection of artifactual and confounding glial signatures by single-cell sequencing of mouse and human brain. *Nat. Neurosci.* 25, 306–316. doi: 10.1038/s41593-022-01022-8
- Marsters, C. M., Nesan, D., Far, R., Klenin, N., Pittman, Q. J., and Kurrasch, D. M. (2020). Embryonic microglia influence developing hypothalamic glial populations. *J. Neuroinflammation* 17:146. doi: 10.1186/s12974-020-01811-7
- Masuda, T., Amann, L., Monaco, G., Sankowski, R., Staszewski, O., Krueger, M., et al. (2022). Specification of CNS macrophage subsets occurs postnatally in defined niches. *Nature* 604, 740–748. doi: 10.1038/s41586-022-04596-2
- Masuda, T., Amann, L., Sankowski, R., Staszewski, O., Lenz, M., d'Errico, P., et al. (2020). Novel Hexb-based tools for studying microglia in the CNS. *Nat. Immunol.* 21, 802–815. doi: 10.1038/s41590-020-0707-4
- Masuda, T., Sankowski, R., Staszewski, O., Bottcher, C., Amann, L., Sagar, et al. (2019). Spatial and temporal heterogeneity of mouse and human microglia at single-cell resolution. *Nature* 566, 388–392. doi: 10.1038/s41586-019-0924-x
- Matcovitch-Natan, O., Winter, D. R., Giladi, A., Vargas Aguilar, S., Spinrad, A., Sarrazin, S., et al. (2016). Microglia development follows a stepwise program to regulate brain homeostasis. *Science* 353:aad8670. doi: 10.1126/science.aad8670
- McKercher, S. R., Torbett, B. E., Anderson, K. L., Henkel, G. W., Vestal, D. J., Baribault, H., et al. (1996). Targeted disruption of the PU.1 gene results in multiple hematopoietic abnormalities. *EMBO J.* 15, 5647–5658.
- McKinsey, G. L., Lizama, C. O., Keown-Lang, A. E., Niu, A., Santander, N., Larphavesarp, A., et al. (2020). A new genetic strategy for targeting microglia in development and disease. *Elife* 9:e54590. doi: 10.7554/eLife.54590
- Menassa, D. A., Muntslag, T. A. O., Martin-Estebane, M., Barry-Carroll, L., Chapman, M. A., Adorjan, I., et al. (2022). The spatiotemporal dynamics of microglia across the human lifespan. *Dev. Cell* 57, 2127–2139.e6. doi: 10.1016/j.devcel.2022.07.015
- Michaelson, M. D., Bieri, P. L., Mehler, M. F., Xu, H., Arezzo, J. C., Pollard, J. W., et al. (1996). CSF-1 deficiency in mice results in abnormal brain development. *Development* 122, 2661–2672. doi: 10.1242/dev.122.9.2661
- Mildenberger, W., Stifter, S. A., and Greter, M. (2022). Diversity and function of brain-associated macrophages. *Curr. Opin. Immunol.* 76:102181. doi: 10.1016/j.coi.2022.102181
- Mills, J., Ladner, L., Soliman, E., Leonard, J., Morton, P. D., and Theus, M. H. (2022). Cross-talk and subset control of microglia and associated myeloid cells in neurological disorders. *Cells* 11:3364. doi: 10.3390/cells11213364
- Miyamoto, A., Wake, H., Ishikawa, A. W., Eto, K., Shibata, K., Murakoshi, H., et al. (2016). Microglia contact induces synapse formation in developing somatosensory cortex. *Nat. Commun.* 7:12540. doi: 10.1038/ncomms12540
- Monier, A., Adle-Biasette, H., Delezoide, A. L., Evrard, P., Gressens, P., and Verney, C. (2007). Entry and distribution of microglial cells in human embryonic and fetal cerebral cortex. *J. Neuropathol. Exp. Neurol.* 66, 372–382. doi: 10.1097/nen.0b013e3180517b46
- Mosser, C. A., Baptista, S., Arnoux, I., and Audinat, E. (2017). Microglia in CNS development: Shaping the brain for the future. *Prog. Neurobiol.* 14, 1–20. doi: 10.1016/j.pneurobio.2017.01.002
- Mrdjen, D., Pavlovic, A., Hartmann, F. J., Schreiner, B., Utz, S. G., Leung, B. P., et al. (2018). High-dimensional single-cell mapping of central nervous system immune

cells reveals distinct myeloid subsets in health, aging, and disease. *Immunity* 48:599. doi: 10.1016/j.immuni.2018.02.014

Munro, D. A. D., Bradford, B. M., Mariani, S. A., Hampton, D. W., Vink, C. S., Chandran, S., et al. (2020). CNS macrophages differentially rely on an intronic CSf1r enhancer for their development. *Development* 147:dev194449. doi: 10.1242/dev.194449

Munz, M., Bharioke, A., Kosche, G., Moreno-Juan, V., Brignall, A., Graff-Meyer, A., et al. (2022). Embryonic cortical layer 5 pyramidal neurons form an active, transient circuit motif perturbed by autism-associated mutations. *bioRxiv* [Preprint]. doi: 10.1101/2022.08.31.506080

Nemes-Baran, A. D., White, D. R., and DeSilva, T. M. (2020). Fractalkine-dependent microglial pruning of viable oligodendrocyte progenitor cells regulates myelination. *Cell Rep.* 32:108047. doi: 10.1016/j.celrep.2020.108047

Nimmerjahn, A., Kirchhoff, F., and Helmchen, F. (2005). Resting microglial cells are highly dynamic surveillants of brain parenchyma in vivo. *Science* 308, 1314–1318. doi: 10.1126/science.1110647

O'Brien, J., Martinson, H., Durand-Rougely, C., and Schedin, P. (2012). Macrophages are crucial for epithelial cell death and adipocyte repopulation during mammary gland involution. *Development* 139, 269–275. doi: 10.1242/dev.071696

Paolicelli, R. C., Sierra, A., Stevens, B., Tremblay, M. E., Aguzzi, A., Ajami, B., et al. (2022). Microglia states and nomenclature: A field at its crossroads. *Neuron* 110, 3458–3483. doi: 10.1016/j.neuron.2022.10.020

Parkhurst, C. N., Yang, G., Ninan, I., Savas, J. N., Yates, J. R. III, Lafaille, J. J., et al. (2013). Microglia promote learning-dependent synapse formation through brain-derived neurotrophic factor. *Cell* 155, 1596–1609. doi: 10.1016/j.cell.2013.11.030

Pont-Lezica, L., Beumer, W., Colasse, S., Drexhage, H., Versnel, M., and Bessis, A. (2014). Microglia shape corpus callosum axon tract fasciculation: Functional impact of prenatal inflammation. *Eur. J. Neurosci.* 39, 1551–1557. doi: 10.1111/ejn.12508

Prinz, M., Jung, S., and Priller, J. (2019). Microglia biology: One century of evolving concepts. *Cell* 179, 292–311. doi: 10.1016/j.cell.2019.08.053

Ratz, M., von Berlin, L., Larsson, L., Martin, M., Westholm, J. O., La Manno, G., et al. (2022). Clonal relations in the mouse brain revealed by single-cell and spatial transcriptomics. *Nat. Neurosci.* 25, 285–294. doi: 10.1038/s41593-022-01011-x

Rebula, M. E., Gibson, P., Rhodes, C. L., Cushing, B. S., and Patisaul, H. B. (2016). Sex differences in microglial colonization and vulnerabilities to endocrine disruption in the social brain. *Gen. Comp. Endocrinol.* 238, 39–46. doi: 10.1016/j.ygcen.2016.04.018

Rojo, R., Raper, A., Ozdemir, D. D., Lefevre, L., Grabert, K., Wollscheid-Lengeling, E., et al. (2019). Deletion of a Csf1r enhancer selectively impacts CSF1R expression and development of tissue macrophage populations. *Nat. Commun.* 10:3215. doi: 10.1038/s41467-019-11053-8

Ronzano, R., Roux, T., Thetiot, M., Aigrot, M. S., Richard, L., Lejeune, F. X., et al. (2021). Microglia-neuron interaction at nodes of Ranvier depends on neuronal activity through potassium release and contributes to remyelination. *Nat. Commun.* 12:5219. doi: 10.1038/s41467-021-25486-7

Rosin, J. M., Marsters, C. M., Malik, F., Far, R., Adnani, L., Schuurmans, C., et al. (2019). Embryonic microglia interact with hypothalamic radial glia during development and upregulate the TAM receptors MERTK and AXL following an insult. *Cell Rep.* 34:108587. doi: 10.1016/j.celrep.2020.108587

Rosin, J. M., Vora, S. R., and Kurrasch, D. M. (2018). Depletion of embryonic microglia using the CSF1R inhibitor PLX5622 has adverse sex-specific effects on mice, including accelerated weight gain, hyperactivity and anxiolytic-like behaviour. *Brain Behav. Immun.* 73, 682–697. doi: 10.1016/j.bbi.2018.07.023

Ruan, C., Sun, L., Kroshilina, A., Beckers, L., De Jager, P., Bradshaw, E. M., et al. (2020). A novel Tmem119-tdTomato reporter mouse model for studying microglia in the central nervous system. *Brain Behav. Immun.* 83, 180–191. doi: 10.1016/j.bbi.2019.10.009

Safaiyan, S., Besson-Girard, S., Kaya, T., Cantuti-Castelvetri, L., Liu, L., Ji, H., et al. (2021). White matter aging drives microglial diversity. *Neuron* 109, 1100–1117.e10. doi: 10.1016/j.neuron.2021.01.027

Sahasrabudde, V., and Ghosh, H. S. (2022). Cx3Cr1-Cre induction leads to microglial activation and IFN-1 signaling caused by DNA damage in early postnatal brain. *Cell Rep.* 38:110252. doi: 10.1016/j.celrep.2021.110252

Sankowski, R., Bottcher, C., Masuda, T., Geirsdottir, L., Sagar, Sindram, E., et al. (2019). Mapping microglia states in the human brain through the integration of high-dimensional techniques. *Nat. Neurosci.* 22, 2098–2110. doi: 10.1038/s41593-019-0532-y

Sankowski, R., Monaco, G., and Prinz, M. (2022). Evaluating microglial phenotypes using single-cell technologies. *Trends Neurosci.* 45, 133–144. doi: 10.1016/j.tins.2021.11.001

Satoh, J., Kino, Y., Asahina, N., Takitani, M., Miyoshi, J., Ishida, T., et al. (2016). TMEM119 marks a subset of microglia in the human brain. *Neuropathology* 36, 39–49. doi: 10.1111/neup.12235

Schwarz, J. M., Sholar, P. W., and Bilbo, S. D. (2012). Sex differences in microglial colonization of the developing rat brain. *J. Neurochem.* 120, 948–963. doi: 10.1111/j.1471-4159.2011.07630.x

Sherafat, A., Pfeiffer, F., Reiss, A. M., Wood, W. M., and Nishiyama, A. (2021). Microglial neuropilin-1 promotes oligodendrocyte expansion during development and remyelination by trans-activating platelet-derived growth factor receptor. *Nat. Commun.* 12:2265. doi: 10.1038/s41467-021-22532-2

Sierra, A., Encinas, J. M., Deudero, J. J., Chancey, J. H., Enikolopov, G., Overstreet-Wadiche, L. S., et al. (2010). Microglia shape adult hippocampal neurogenesis through apoptosis-coupled phagocytosis. *Cell Stem Cell* 7, 483–495. doi: 10.1016/j.stem.2010.08.014

Silvin, A., Uderhardt, S., Piot, C., Da Mesquita, S., Yang, K., Geirsdottir, L., et al. (2022). Dual ontogeny of disease-associated microglia and disease inflammatory macrophages in aging and neurodegeneration. *Immunity* 55, 1448–1465.e6. doi: 10.1016/j.immuni.2022.07.004

Squarzone, P., Oller, G., Hoeffel, G., Pont-Lezica, L., Rostaing, P., Low, D., et al. (2014). Microglia modulate wiring of the embryonic forebrain. *Cell Rep.* 8, 1271–1279. doi: 10.1016/j.celrep.2014.07.042

Stogsdill, J. A., Kim, K., Binan, L., Farhi, S. L., Levin, J. Z., and Arlotta, P. (2022). Pyramidal neuron subtype diversity governs microglia states in the neocortex. *Nature* 608, 750–756. doi: 10.1038/s41586-022-05056-7

Stremmel, C., Schuchert, R., Wagner, F., Thaler, R., Weinberger, T., Pick, R., et al. (2018). Yolk sac macrophage progenitors traffic to the embryo during defined stages of development. *Nat. Commun.* 9:75. doi: 10.1038/s41467-017-02492-2

Swinnen, N., Smolders, S., Avila, A., Notelaers, K., Paesen, R., Ameloot, M., et al. (2013). Complex invasion pattern of the cerebral cortex by microglial cells during development of the mouse embryo. *Glia* 61, 150–163. doi: 10.1002/glia.22421

Takeda, A., Shinozaki, Y., Kashiwagi, K., Ohno, N., Eto, K., Wake, H., et al. (2018). Microglia mediate non-cell-autonomous cell death of retinal ganglion cells. *Glia* 66, 2366–2384. doi: 10.1002/glia.23475

Tay, T. L., Mai, D., Dautzenberg, J., Fernandez-Klett, F., Lin, G., Sagar, et al. (2017). A new fate mapping system reveals context-dependent random or clonal expansion of microglia. *Nat. Neurosci.* 20, 793–803. doi: 10.1038/nn.4547

Thion, M. S., Ginhoux, F., and Garel, S. (2018a). Microglia and early brain development: An intimate journey. *Science* 362, 185–189. doi: 10.1126/science.aat0474

Thion, M. S., Low, D., Silvin, A., Chen, J., Grisel, P., Schulte-Schrepping, J., et al. (2018b). Microbiome influences prenatal and adult microglia in a sex-specific manner. *Cell* 172, 500–516.e16. doi: 10.1016/j.cell.2017.11.042

Thion, M. S., Mosser, C. A., Ferezou, I., Grisel, P., Baptista, S., Low, D., et al. (2019). Biphasic impact of prenatal inflammation and macrophage depletion on the wiring of neocortical inhibitory circuits. *Cell Rep.* 28, 1119–1126.e14. doi: 10.1016/j.celrep.2019.06.086

Utz, S. G., See, P., Mildnerberger, W., Thion, M. S., Silvin, A., Lutz, M., et al. (2020). Early fate defines microglia and non-parenchymal brain macrophage development. *Cell* 181, 557–573.e18. doi: 10.1016/j.cell.2020.03.021

Van Hove, H., Martens, L., Scheyltjens, I., De Vlaminck, K., Pombo Antunes, A. R., De Prieck, S. E., et al. (2019). A single-cell atlas of mouse brain macrophages reveals unique transcriptional identities shaped by ontogeny and tissue environment. *Nat. Neurosci.* 22, 1021–1035. doi: 10.1038/s41593-019-0393-4

VanRyzin, J. W., Marquardt, A. E., Argue, K. J., Vecchiarelli, H. A., Ashton, S. E., Arambula, S. E., et al. (2019). Microglial phagocytosis of newborn cells is induced by endocannabinoids and sculpt sex differences in juvenile rat social play. *Neuron* 102, 435–449.e6. doi: 10.1016/j.neuron.2019.02.006

Verney, C., Monier, A., Fallet-Bianco, C., and Gressens, P. (2010). Early microglial colonization of the human forebrain and possible involvement in periventricular white-matter injury of preterm infants. *J. Anat.* 217, 436–448. doi: 10.1111/j.1469-7580.2010.01245.x

Villa, A., Gelosa, P., Castiglioni, L., Cimino, M., Rizzi, N., Pepe, G., et al. (2018). Sex-specific features of microglia from adult mice. *Cell Rep.* 23, 3501–3511. doi: 10.1016/j.celrep.2018.05.048

Wake, H., Moorhouse, A. J., Jinno, S., Kohsaka, S., and Nabekura, J. (2009). Resting microglia directly monitor the functional state of synapses in vivo and determine the fate of ischemic terminals. *J. Neurosci.* 29, 3974–3980. doi: 10.1523/JNEUROSCI.4363-08.2009

Wang, Y., Szretter, K. J., Vermi, W., Gilfillan, S., Rossini, C., Cella, M., et al. (2012). IL-34 is a tissue-restricted ligand of CSF1R required for the development of Langerhans cells and microglia. *Nat. Immunol.* 13, 753–760. doi: 10.1038/ni.2360

Włodarczyk, A., Holtman, I. R., Krueger, M., Yogeve, N., Bruttger, J., Khorooshi, R., et al. (2017). A novel microglial subset plays a key role in myelinogenesis in developing brain. *EMBO J.* 36, 3292–3308. doi: 10.15252/embj.201696056

Xu, J., Zhu, L., He, S., Wu, Y., Jin, W., Yu, T., et al. (2015). Temporal-spatial resolution fate mapping reveals distinct origins for embryonic and adult microglia in zebrafish. *Dev. Cell* 34, 632–641. doi: 10.1016/j.devcel.2015.08.018

Yona, S., Kim, K. W., Wolf, Y., Mildner, A., Varol, D., Breker, M., et al. (2013). Fate mapping reveals origins and dynamics of monocytes and tissue macrophages under homeostasis. *Immunity* 38, 79–91. doi: 10.1016/j.immuni.2012.12.001

Yu, D., Li, T., Delpech, J. C., Zhu, B., Kishore, P., Koshi, T., et al. (2022). Microglial GPR56 is the molecular target of maternal immune activation-induced parvalbumin-positive interneuron deficits. *Sci. Adv.* 8:eabm2545. doi: 10.1126/sciadv.abm2545





## OPEN ACCESS

## EDITED BY

Paola Tognini,  
University of Pisa, Italy

## REVIEWED BY

Tiziana Pisano,  
Meyer Children's Hospital, Italy  
Ellen Roy Elias,  
Children's Hospital Colorado, United States

## \*CORRESPONDENCE

Johanna Uusimaa  
✉ johanna.uusimaa@oulu.fi

†These authors have contributed equally to this work

## SPECIALTY SECTION

This article was submitted to  
Neurodevelopment,  
a section of the journal  
Frontiers in Neuroscience

RECEIVED 13 December 2022

ACCEPTED 08 February 2023

PUBLISHED 27 April 2023

## CITATION

Tallgren A, Kager L, O'Grady G, Tuominen H,  
Körkkö J, Kuismin O, Feucht M, Wilson C,  
Behunova J, England E, Kurki M, Palotie A,  
Hallman M, Kaarteenaho R, Laccone F,  
Boztug K, Hinttala R and Uusimaa J (2023)  
Novel patients with NHLRC2 variants expand  
the phenotypic spectrum of FINCA disease.  
*Front. Neurosci.* 17:1123327.  
doi: 10.3389/fnins.2023.1123327

## COPYRIGHT

© 2023 Tallgren, Kager, O'Grady, Tuominen,  
Körkkö, Kuismin, Feucht, Wilson, Behunova,  
England, Kurki, Palotie, Hallman, Kaarteenaho,  
Laccone, Boztug, Hinttala and Uusimaa. This is  
an open-access article distributed under the  
terms of the [Creative Commons Attribution  
License \(CC BY\)](https://creativecommons.org/licenses/by/4.0/). The use, distribution or  
reproduction in other forums is permitted,  
provided the original author(s) and the  
copyright owner(s) are credited and that the  
original publication in this journal is cited, in  
accordance with accepted academic practice.  
No use, distribution or reproduction is  
permitted which does not comply with  
these terms.

# Novel patients with NHLRC2 variants expand the phenotypic spectrum of FINCA disease

Antti Tallgren<sup>1</sup>, Leo Kager<sup>2,3,4†</sup>, Gina O'Grady<sup>5†</sup>,  
Hannu Tuominen<sup>6</sup>, Jarmo Körkkö<sup>7</sup>, Outi Kuismin<sup>1,8</sup>,  
Martha Feucht<sup>9</sup>, Callum Wilson<sup>10</sup>, Jana Behunova<sup>11</sup>,  
Eleina England<sup>12</sup>, Mitja I. Kurki<sup>13,14,15</sup>, Aarno Palotie<sup>13,16,17,18,19</sup>,  
Mikko Hallman<sup>1,20</sup>, Riitta Kaarteenaho<sup>21,22</sup>, Franco Laccone<sup>11</sup>,  
Kaan Boztug<sup>2,3,4,23</sup>, Reetta Hinttala<sup>1,24†</sup> and Johanna Uusimaa<sup>1,20\*</sup><sup>1</sup>Research Unit of Clinical Medicine and Medical Research Center, Oulu University Hospital, University of Oulu, Oulu, Finland, <sup>2</sup>St. Anna Children's Hospital, Vienna, Austria, <sup>3</sup>Department of Pediatrics and Adolescent Medicine, Medical University of Vienna, Vienna, Austria, <sup>4</sup>St. Anna Children's Cancer Research Institute (CCRI), Vienna, Austria, <sup>5</sup>Paediatric Neuroservices, Starship Children's Health, Te Whatu Ora Health New Zealand, Auckland, New Zealand, <sup>6</sup>Department of Pathology, Oulu University Hospital, University of Oulu, Oulu, Finland, <sup>7</sup>Center for Intellectual Disability Care, Oulu University Hospital, Oulu, Finland, <sup>8</sup>Department of Clinical Genetics, Oulu University Hospital, Oulu, Finland, <sup>9</sup>Department of Paediatrics, Center for Rare and Complex Epilepsies, Medical University of Vienna, Vienna, Austria, <sup>10</sup>National Metabolic Service, Auckland City Hospital, Auckland, New Zealand, <sup>11</sup>Department of Medical Genetics, Medical University of Vienna, Vienna, Austria, <sup>12</sup>Mendelian Genomics, Programme in Medical and Population Genetics, Broad Institute of MIT and Harvard, Cambridge, MA, United States, <sup>13</sup>Programme in Medical and Population Genetics, Broad Institute of MIT and Harvard, Cambridge, MA, United States, <sup>14</sup>Analytic and Translational Genetics Unit, Massachusetts General Hospital, Boston, MA, United States, <sup>15</sup>Stanley Center for Psychiatric Research, Broad Institute of MIT and Harvard, Cambridge, MA, United States, <sup>16</sup>Psychiatric and Neurodevelopmental Genetics Unit, Department of Psychiatry, Massachusetts General Hospital, Boston, MA, United States, <sup>17</sup>Analytic and Translational Genetics Unit, Department of Medicine, Massachusetts General Hospital, Boston, MA, United States, <sup>18</sup>Department of Neurology, Massachusetts General Hospital, Boston, MA, United States, <sup>19</sup>Institute for Molecular Medicine Finland (FIMM), University of Helsinki, Helsinki, Finland, <sup>20</sup>Clinic for Children and Adolescents, Oulu University Hospital, Oulu, Finland, <sup>21</sup>Research Unit of Internal Medicine, University of Oulu, Oulu, Finland, <sup>22</sup>Center of Internal Medicine and Respiratory Medicine and Medical Research Center Oulu, Oulu University Hospital, Oulu, Finland, <sup>23</sup>CeMM Research Center for Molecular Medicine of the Austrian Academy of Sciences, Vienna, Austria, <sup>24</sup>Biocenter Oulu, University of Oulu, Oulu, Finland**Purpose:** FINCA disease (Fibrosis, Neurodegeneration and Cerebral Angiomatosis, OMIM 618278) is an infantile-onset neurodevelopmental and multiorgan disease. Since our initial report in 2018, additional patients have been described. FINCA is the first human disease caused by recessive variants in the highly conserved *NHLRC2* gene. Our previous studies have shown that *Nhlrc2*-null mouse embryos die during gastrulation, indicating the essential role of the protein in embryonic development. Defect in *NHLRC2* leads to cerebral neurodegeneration and severe pulmonary, hepatic and cardiac fibrosis. Despite having a structure suggestive of an enzymatic role and the clinical importance of *NHLRC2* in multiple organs, the specific physiological role of the protein is unknown.



**Methods:** The clinical histories of five novel FINCA patients diagnosed with whole exome sequencing were reviewed. Segregation analysis of the biallelic, potentially pathogenic *NHLRC2* variants was performed using Sanger sequencing. Studies on neuropathology and *NHLRC2* expression in different brain regions were performed on autopsy samples of three previously described deceased FINCA patients.

**Results:** One patient was homozygous for the pathogenic variant c.442G > T, while the other four were compound heterozygous for this variant and two other pathogenic *NHLRC2* gene variants. All five patients presented with multiorgan dysfunction with neurodevelopmental delay, recurrent infections and macrocytic anemia as key features. Interstitial lung disease was pronounced in infancy but often stabilized. Autopsy samples revealed widespread, albeit at a lower intensity than the control, *NHLRC2* expression in the brain.

**Conclusion:** This report expands on the characteristic clinical features of FINCA disease. Presentation is typically in infancy, and although patients can live to late adulthood, the key clinical and histopathological features are fibrosis, infection susceptibility/immunodeficiency/intellectual disability, neurodevelopmental disorder/neurodegeneration and chronic anemia/cerebral angiomas (hence the acronym FINCA) that enable an early diagnosis confirmed by genetic investigations.

#### KEYWORDS

*NHLRC2*, whole exome sequencing, FINCA disease, neurodevelopmental disorder, macrocytic anemia

## 1. Introduction

FINCA is an infantile-onset disease characterized by severe interstitial pulmonary fibrosis, progressive neurodegeneration, recurrent infections and chronic hemolytic anemia (Uusimaa et al., 2018). Previously, we reported two Finnish families with three affected patients with a novel early-onset multiorgan disease associated with biallelic pathogenic variants in the *NHLRC2* gene (Uusimaa et al., 2018). All had infantile-onset severe progressive disease with tissue fibrosis and progressive neurodegeneration and leptomeningeal and cerebral revascularisation on autopsy. Based on the clinical manifestations of fibrosis, neurodegeneration and cerebral angiomas, we proposed the acronym FINCA for the name of the disease. The defect of *NHLRC2* leads to cerebral neurodegeneration and severe pulmonary, hepatic and cardiac fibrosis. However, the physiological role of the *NHLRC2* protein is unknown.

Since our initial report, more FINCA patients have been diagnosed worldwide (Brodsky et al., 2020; Rapp et al., 2021; Badura-Stronka et al., 2022). Interstitial lung disease and recurrent infections are pronounced in almost all patients during infancy and can lead to death before the age of 2–3 years. Alternatively, in some cases, the progressive disease stabilizes and the neurodevelopmental disorder (NDD) evolves as the key clinical finding (Rapp et al., 2021; Badura-Stronka et al., 2022). FINCA is the first human disease known to be caused by recessive variants in the highly conserved *NHLRC2*. The protein has a

structure suggesting an enzymatic role (Biterova et al., 2018) with three domains: an N-terminal thioredoxin-like (Trx-like) domain, followed by a six-bladed NHL repeat containing a  $\beta$ -propeller domain and a C-terminal  $\beta$ -stranded domain. The N-terminal Trx-like domain contains an unusual CCINC motif at the position of the CXXC motif, which is characteristic of oxidoreductases of the thioredoxin superfamily and commonly involved in thiol-disulfide exchange. However, no classical thioredoxin activity has been detected for *NHLRC2* (Uusimaa et al., 2018; Yeung et al., 2019).

Our studies have shown that *Nhlrc2* knockout (KO) mouse embryos die during gastrulation, indicating an essential role for the protein in embryonic development (Hiltunen et al., 2022). This gastrulation or early neurulation defect is consistent with the anatomic malformations called development duplications (DD, OMIA 002103-9913)<sup>1</sup> that have been observed in association with the *NHLRC2* variant p.Val311Ala in Angus cattle, highlighting its function in the development of the central nervous system (Polkoff et al., 2017). Our previous findings from the compound heterozygote FINCA knockin and *Nhlrc2* KO mouse model associated hnRNP C2 and RNA metabolism with the FINCA disease pathology, suggesting that *NHLRC2* plays an important role in the hippocampus (Hiltunen et al., 2020). FINCA/KO mice had increased hnRNP C2 in embryonic cortical neuronal precursor cells

<sup>1</sup> <https://omia.org/OMIA002103/9913/>

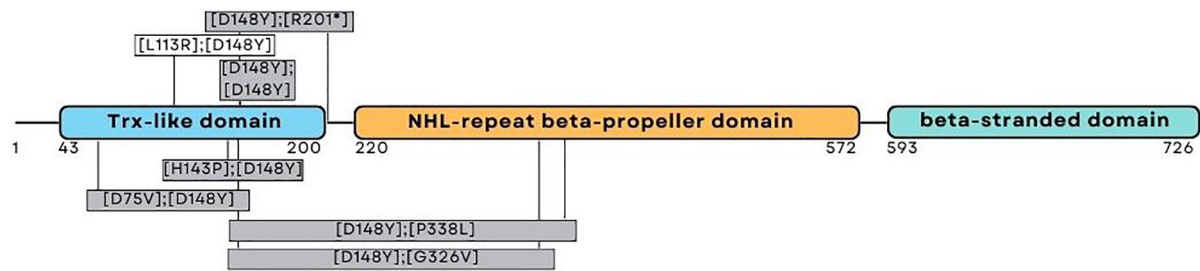


FIGURE 1

Schematic representation of the NHLRC2 domain composition and amino acid substitutions identified from the FINCA patients. The patients reported here harbored variants presented above the corresponding domain; the variants presented in gray boxes have been described previously (Uusimaa et al., 2018; Brodsky et al., 2020; Rapp et al., 2021; Badura-Stronka et al., 2022).

H.Sapiens (NP_940916.2)	79	KIVVLDFFTYCCINCIIHLLPDLHALEHTYSDKDGLIIGVHSAKFPNEKV	128
P.Troglodytes (XP_508046.2)	79	KIVVLDFFTYCCINCINCIIHLLPDLHALEHTYSDKDGLIIGVHSAKFPNEKV	128
M.Mulatta (XP_001091193.1)	79	KIVVLDFFTYCCINCINCIIHLLPDLHALEHTYSDKDGLIIGVHSAKFPNEKV	128
C.Lupus (XP_544027.2)	113	KVVILDFFTYCCINCINCIIHLLPDLHLEHTYSDKDGLIIGVHSAKFPNEKV	162
B.Taurus (NP_001077192.1)	79	KVVILDFFTYCCINCINCIIHLLPDLHALEHTYSDKDGLIIGVHSAKFPNEKV	128
M.Musculus (NP_080087.1)	79	KVVVLDFFTYCCINCINCIIHLLPDLHALEHTYSDKDGLIIGVHSAKFPNEKV	128
R.Norvegicus (NP_001100914.1)	79	KVVILDFFTYCCINCINCIIHLLPDLHALEHTYSDKDGLIIGVHSAKFPNEKV	128
G.Gallus (NP_001006504.1)	74	KVVVLDFFTYCCINCINCIIHLLPDLHALEHTYSDKDGLIIGVHSAKFPNEKV	123
D.Melanogaster (NP_001036460.1)	81	KVILDFFTYCCINCINCIIHLLPDLHALEHTYSDKDGLIIGVHSAKFPNEKV	130
A.Gambiae (XP_314572.4)	86	KVVVLDFFTYCCINCINCIIHLLPDLHALEHTYSDKDGLIIGVHSAKFPNEKV	135
A.Thaliana (NP_564718.2)	420	KVVILDFWTYCCINCINCIIHLLPDLHALEHTYSDKDGLIIGVHSAKFPNEKV	468
X.Tropicalis (XP_004919443.1)	75	KVVVLDFFTYCCINCINCIIHLLPDLHALEHTYSDKDGLIIGVHSAKFPNEKV	124

FIGURE 2

Multiple sequence misalignment of NHLRC2 spanning aa 79–128. p.L113R has been highlighted with a red box. Generated by MUSCLE (Edgar, 2004) version 3.6 (using option: -maxiters2) (Edgar, 2004).

and in the adult hippocampus, suggesting a role for dysregulated RNA metabolism in FINCA disease.

Altered *NHLRC2* or *NHLRC2* levels have been detected not only in association with FINCA disease, but also with idiopathic pulmonary fibrosis (IPF) (Boon et al., 2009; Kreus et al., 2022), lung adenocarcinoma (Ye et al., 2019), Parkinson's disease (van Dijk et al., 2012), Alzheimer's disease (AD) (Long et al., 2016), and sporadic amyotrophic lateral sclerosis (Andrés-Benito et al., 2020), suggesting that *NHLRC2* may indeed play a role in more common pathologies. Interestingly, increased levels of *NHLRC2* have been detected in the serum samples of AD patients, proposing *NHLRC2* as a potential serum biomarker for the disease (Long et al., 2016).

Here, we present clinical data on five new FINCA patients and expand the phenotype of the disease. Furthermore, we present data on neuropathology and *NHLRC2* expression in different brain regions in autopsy samples. We also provide pertinent details on hematological findings. Based on these data, we further delineate the clinical characteristics of FINCA disease.

## 2. Materials and methods

### 2.1. Patients and patient-derived samples

The clinical, laboratory and radiological data of five patients from three centers was collected (Clinic for Children and Adolescents, Oulu University Hospital, Oulu, Finland; St. Anna

Children's Hospital; Department of Paediatrics, Medical University of Vienna, Austria; and Starship Children's Hospital, Auckland, New Zealand). The patients were initially identified after whole exome sequencing (WES) revealed biallelic potentially pathogenic *NHLRC2* variants and with the clinical details suggestive of FINCA disease (Uusimaa et al., 2018); the respective clinicians contacted the corresponding author (J.U.). Studies on neuropathology and *NHLRC2* expression in different brain regions were performed on the available autopsy samples of three previously described deceased FINCA patients (Uusimaa et al., 2018). Written informed consent was obtained from all the parents or guardians of the patients participating in the study. The study was approved by the ethics committees of the participating centers.

### 2.2. Molecular genetic studies

Genomic DNA was extracted from peripheral blood or tissue samples of the probands, their affected siblings and available parental samples using standard methods. WES was performed at the Broad Institute of MIT and Harvard, Cambridge, MA, USA, for patient four (family three; post-mortem Sanger sequencing was performed from DNA extracted from the tissue sample of patient five), at the Department Medical Genetics, Medical University of Vienna for patient six (family four; post-mortem Sanger sequencing of DNA was performed from tissue sample for patient seven), and for patient eight (family five) as a part of

the Northern Finland Intellectual Disease project led by Professor Aarno Palotie (Kurki et al., 2019). The segregation of identified NHLRC2 variants within families three and four was confirmed, whereas parental DNA was not available in family five. More detailed data are provided in the [Supplementary material](#) on the case histories.

### 2.3. Histopathological analyses of brain autopsy samples

Autopsy samples were obtained from the brains of three previously described FINCA patients (Uusimaa et al., 2018). The tissue was fixed in buffered 4% formaldehyde, routinely processed into paraffin blocks and cut into 4.0  $\mu$ m sections. The autopsy samples of the patients and controls were prepared within a day after death. The control patient was 7 months old at the time of his death.

### 2.4. Histopathological analyses and immunohistochemistry of brain autopsy samples

Brain sections were stained with antibodies against NHLRC2 (Atlas antibodies, HPA038493, Bromma, Sweden). Samples were stained with a Flex-kit from Dako (Dako, Glostrup Denmark). Before application of the primary antibody, sections were heated in a microwave oven with Tris-EDTA, pH 9.0, for 15 min. After overnight incubation in +4°C with the primary antibody (1:500), a biotinylated secondary HRP Rabbit/mouse-antibody (Dako) was used. Negative control stainings were carried out by substituting non-immune rabbit or mouse primary antibody isotype control (Zymed Laboratories Inc. South San Francisco, CA, USA) and PBS for the primary antibody.

Whole-slide images were acquired with a NanoZoom S60 scanner (Hamamatsu, Hamamatsu City, Japan) in the Transgenic and Tissue Phenotyping core facility, Biocenter Oulu, University of Oulu at 40  $\times$  magnification.

## 3. Results

### 3.1. NHLRC2 variants in five novel FINCA patients

One patient was homozygous (patient eight), while the other four were compound heterozygote for the pathogenic variant c.442G > T (NM\_198514.4), leading to p.D148Y (rs201701259, NP\_940916.2) in the thioredoxin-like domain of NHLRC2. Patients four and five had a frameshift variant c.601\_602del (NM\_198514.4), leading to p.R201fs (rs757267294, NP\_940916.2), which is similar to the first FINCA patients reported by Uusimaa et al. (2018). Patients six and seven had a novel c.338T > G (NM\_198514.4) variant leading to p.L113R (NP\_940916.2) in the thioredoxin-like domain. The variant alters the highly conserved leucine amino acid residue and has been predicted as affecting

the function of NHLRC2 (SIFT 0.0) and possibly be damaging with a PolyPhen-2 score of 0.999 (sensitivity: 0.14; specificity: 0.99) (HumDiv, PolyPhen-2 v2.2.3r406). The identified variants and their location in the protein are illustrated in [Figure 1](#) and protein alignment in [Figure 2](#). The genetic findings are described in [Table 1](#).

### 3.2. Clinical, laboratory and radiological findings of the five novel FINCA patients

We identified five novel FINCA patients [these patients are numbered here chronologically as patients 4–8 based on our initial report on the first three FINCA patients (patients 1–3) described in Uusimaa et al. (2018)]. The clinical features of the new FINCA patients are summarized in [Table 1](#), with laboratory and radiological findings in [Table 2](#). All five patients presented at birth or during the first months (range from birth to 2 months) and their clinical phenotypes resembled the phenotypes of the first previously published FINCA patients (Uusimaa et al., 2018). The clinical features seen in all the patients included axial hypotonia, developmental delay, visual problems (including poor visual contact, decreased vision or strabismus), feeding problems, recurrent infections, respiratory symptoms, diarrhea/other intestinal symptoms and macrocytic anemia. The majority of the patients manifested poor weight gain and failure to thrive (4/5, 80%), epileptic seizures (3/5, 60%), and irritability (3/5, 60%), while transient liver dysfunction, transient kidney dysfunction, plexus paresis, Horner syndrome and abnormal carotenemia skin color were seen in individual patients. The eldest patient (currently 61 years old, patient eight) also has progressive muscular atrophy leading to neuromuscular scoliosis, pectus excavatum, ataxia and spastic diplegia. He had drug-resistant epileptic seizures and behavioral problems, including aggressive outbursts. Two patients with compound heterozygous NHLRC2 variants (patients five and seven) died because of progressive respiratory and multiorgan failure at the age of 10–11 months, whereas their siblings were alive, with current ages of 6 (patient six) and 19 years (patient four) and were relatively stable with fewer respiratory problems and infections since the age of 2.

Laboratory investigations ([Table 2](#)) revealed macrocytic anemia in all five patients, with the bone marrow aspirates in two patients (patients five and six, [Table 2](#)) showing increased erythropoiesis or dyserythropoiesis, marked bi- and multinuclearity of erythroblasts and increased eosinophils suggestive of congenital dyserythropoietic anemia (CDA type II) ([Figures 3A, B](#)). Four out of five patients needed several red blood cell transfusions in infancy. Furthermore, immunodeficiency with decreased immunoglobulin levels was detected in two patients.

Chest X-ray ([Figure 4](#)) and chest computed tomography demonstrated acute respiratory distress syndrome (ARDS) in patient six (at 4 months of age), widespread variable infections/pneumonitis in patient five and several pneumatoceles in patient four at the age of 17 years. Lung biopsy of patient six during infancy showed severely distorted lung architecture with severe septal thickening, foamy macrophages and markedly

TABLE 1 Genetic findings and clinical features of the five novel FINCA patients.

Patient number	4	5	6	7	8
Study center (Country)	New Zealand	New Zealand	Austria	Austria	Finland
NHLRC2 variant	p.Asp148Tyr, p.Arg201GlyfsTer6	p.Asp148Tyr, p.Arg201GlyfsTer6	p. Asp148Tyr, p. Leu113Arg	p. Asp148Tyr, p. Leu113Arg	p.Asp148Tyr, p.Asp148Tyr
Gender	Female	Female	Female	Male	Male
Ethnicity	Dutch/NZ	Dutch/NZ	Slovakian	Slovakian	Finn
Kinship	Siblings		Siblings		
Age at disease onset	1–2 months	5 weeks	2 months	At birth	At birth
Irritability	Yes	Yes	n.a.	n.a.	Yes, behavioral problems
Axial hypotonia/ muscle weakness, muscle atrophy	Yes	Yes, truncal hypotonia, generalized muscle weakness and atrophy	Yes	Yes	Yes, facial, truncal and proximal limb and shoulder muscle atrophy
Movement disorder	No	No	No	No	Yes, dystonia, ataxia, spastic diplegia
Developmental delay	Yes, since 3 years	Yes, since 6 months	Yes	Yes	Yes, since 3 years
Intellectual disability	Yes, profound intellectual disability	Yes, progressive encephalopathy	Yes	Yes	Yes, profound intellectual disability
Poor visual contact/decreased vision, strabismus	Yes	Yes	Yes	n.a.	Yes, variable eye contact, autistic features
Feeding problems	Yes	Yes	Yes, PEG since the age of 5 years	Yes	Yes, at birth
Poor weight gain, failure to thrive	Yes	Yes	Yes	Yes	No
Epileptic seizures	Yes	No	Yes	No	Yes, since 4 years
Respiratory symptoms	Yes, chronic infantile pneumonitis, tracheomalacia	Yes, chronic infantile pneumonitis, tracheomalacia	Yes, ARDS in infancy	Yes, ARDS as part of multiorgan failure	Yes, recurrent pneumonias
Recurrent infections	Yes, respiratory infections	Yes, respiratory infections	Recurrent pneumonias, but no severe pulmonary problems since infancy after initiation of antibiotic prophylaxis, transient IgG deficiency	Yes, recurrent severe infections (2x <i>E. coli</i> meningitis) at birth and in infancy	Yes, respiratory and urinary tract infections
Diarrhea/other intestinal symptoms	Yes, chronic diarrhea	Episodic diarrhea	Yes, recurrent episodes of diarrhea and vomiting	Febrile gastroenteritis before septic death	Ileal occlusion, appendicitis
Chronic anemia	Yes, several blood transfusions in infancy, CDA type II	Yes, several blood transfusions in infancy, CDA type II	Yes, hemolytic, macrocytic anemia, CDA type II like, several RBC transfusions in infancy	Yes, CDA type II like anemia, several RBC transfusions	Yes, transient macrocytic anemia
Hepatomegaly/liver dysfunction	No	Yes	No	No	No
Transient kidney dysfunction	No	Yes	No	Yes, renal failure as part of the multiorgan failure	No
Other symptoms/signs	Abnormal skin, carotenemia appearance	No	Progressive microcephaly (OFC 35 cm/+1 SD at birth, and 43 cm/-3.5 SD at the age of 2.5 years)	Plexus paresis, Horner syndrome	Pectus excavatum, neuromuscular scoliosis, recurrent accidents
Overall progressive disease course	Relatively stable, pulmonary problems improved and no severe infections since 2 years	Yes, progressive respiratory and multiorgan failure	Relatively stable, drug-resistant seizures	Yes, progressive respiratory and multiorgan failure	Yes, slight neurological progression
Current age/age at death	Alive 19 years	Deceased 11 months	Alive 6 years	Deceased 10 months	Alive 61 years

NZ, New Zealand; n.a., not available; PEG, percutaneous endoscopic gastrostomy; ARDS, acute respiratory distress syndrome; CDA, congenital dyserythropoietic anemia; RBC, red blood cell; OFC, occipitofrontal head circumference; SD, standard deviation.



TABLE 2 Laboratory and imaging findings of five FINCA patients with the *NHLRC2* variants.

Patient number	4	5	6	7	8
Study center (Country)	New Zealand	New Zealand	Austria	Austria	Finland
<b>Blood analyses</b>					
B-hemoglobin	88–130 g/l (ref. 117–155 g/l)	65–111 g/l (ref. 90–130 g/l)	65–109 g/dl (ref. 100–143 g/l)	88–130 g/l (ref. 100–155 g/l)	120–130 g/l (ref. 134–167 g/l)
E-MCV	95–105 fl (ref. 82–98 fl)	105–115 fl (rf. 71–87 fl)	85–108 fl (ref. 75–85 fl)	85–91 fl (ref. 74–106 fl)	101 fl (ref. 82–98 fl)
E-MCH	24–38 pg (ref. 27–33 pg)	28–40 pg (ref. 23–31 pg)	29–37 pg (ref. 25–35 pg)	29–32 pg (ref. 27–34 pg)	35 pg (ref. 27–33 pg)
E-MCHC	–	–	33–38 g/dl (ref. 30–37 g/dl)	33–36 g/dl (ref. 28–31 g/dl)	341 g/l (ref. 320–355 g/l)
<b>Immunoglobulins</b>					
IgG	n.a.	3.5 g/l (ref. 3–10 g/l)	2.29 g/l (ref. 2.44–11.8 g/l)	4.92 g/l (ref. 2.9–7.7 g/l)	n.a.
IgM	n.a.	0.05 g/l (ref. 0.1–1.2 g/l)	0.14 g/l (ref. 0.4–1.8 g/l)	0.35 g/l (ref. 0.11–0.76 g/l)	n.a.
IgA	n.a.	0.92 g/l	0.5 g/l (ref. 0.48–3.45 g/l)	0.37 g/l (ref. 0.33–1.25 g/l)	n.a.
<b>Imaging</b>					
X-rays/CT	CT chest at 17 years: a number of pneumatoceles especially in right lower lobe	Chest X-rays: widespread variable infections/ pneumonitis	ARDS at 4 months	n.a.	–
Brain MRI	At 17 years: severe generalized atrophy with fronto-temporal prominence, but affecting also parietal and occipital lobes and cerebellum; the corpus callosum is severely atrophyed	At 11 months: generalized atrophy with mild hyperintensity of the parieto-occipital white matter	At 2 years: arachnoidal cyst in the left temporal region and atrophy of the left temporal lobe	At 2 months: hydrocephalus, mesiotemporal atrophy	–
Tissues biopsy analyses	n.a.	Bone marrow aspirate: markedly increased erythropoiesis, marked binuclearity of erythroblasts. Marked increase in eosinophils > 15%-suggestive of CDA type II Muscle biopsy: normal–mild type II atrophy. Normal EM Liver biopsy: normal apart from some vacuolated cells, no fibrosis, cirrhosis Lung biopsy: severe distortion lung architecture, severe septal thickening, foamy macrophages, markedly hyperplastic type II pneumocytes (dx chronic pneumonitis of infancy) Normal ciliary biopsy	Bone marrow aspirate at age of 6 weeks: dyserythropoiesis, marked binuclearity (> 15%) and a few multinuclear erythroblasts; suggestive of CDA type II	n.a.	–

Ref, reference limits; n.a., not available; CT, computed tomography scan; ARDS, acute respiratory distress syndrome; CDA, congenital dyserythropoietic anemia; EM, electron microscopy; dx, dexter.

hyperplastic type II pneumocytes (chronic pneumonitis of infancy). Brain magnetic resonance imaging (MRI) revealed an arachnoid cyst in the left temporal region and atrophy of the left temporal lobe in patient six at 2 years of age (Figure 5), hydrocephalus and mesiotemporal atrophy in

patient seven at 2 months of age and severe generalized atrophy with fronto-temporal prominence, but also affecting the parietal and occipital lobes and cerebellum, and severely atrophyed corpus callosum in patient four at the age of 17 years (Figure 6).

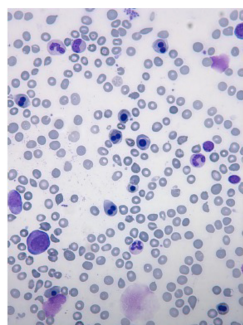
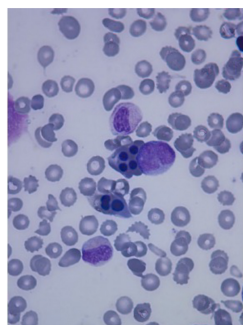
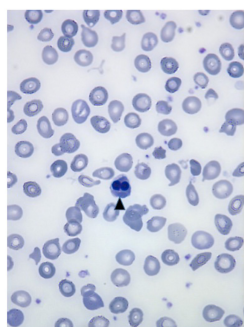


FIGURE 3

Peripheral blood smear of the patient six shows anisocytosis, poikilocytosis, fragmentocytes and binucleated normoblast (arrowhead). Bone marrow aspirates of the patient six show multinucleated erythroid precursors and dyserythropoiesis.

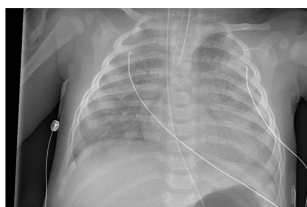
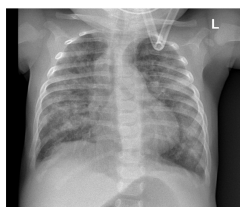


FIGURE 4

Chest X-ray of patient six at 4 months of age shows lung infiltrations and development of acute respiratory distress syndrome (ARDS, pneumocystis carinii and streptococcus pneumonia).

### 3.3. Histopathological findings in the brains of FINCA patients and NHLRC2 expression in humans

Immunohistochemical NHLRC2 expression was detected broadly in all the studied cells, excluding endothelial cells, where the expression was not seen in any tissues (Table 3). Expression was cytoplasmic in the neuronal, glial and meningotheial cells and in cells of the choroid plexus. In ependymal cells, the expression was apical. The strongest intensity of staining was found in neurons. In glial cells, the intensity was lower, but in both types of cells, the expression was widespread in different regions of the brains. Supplementary Figure 1 demonstrates the NHLRC2 expression in the patients' brain autopsy samples.

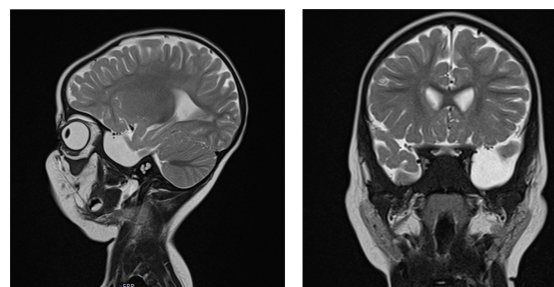


FIGURE 5

Brain MRI of patient six at the age of 2 years. T2 sagittal and coronal MRIs show an arachnoidal cyst in the left temporal region and atrophy of the left temporal lobe.

The intensity of the expression varied between the patients and between the patients and the control. Overall expression was wider and slightly stronger in the tissues of the control, but interestingly, it was the opposite in Purkinje cells, in which expression tended to be lower (Table 3). Furthermore, stronger expression in neuropil was occasionally observed in the control's tissues, particularly in the temporal and parietal lobes of the brain. A comparison of NHLRC2 expression in patient and control samples is demonstrated in Supplementary Figures 2, 3.

## 4. Discussion

We have reported on five novel patients from three unrelated families with FINCA disease. Furthermore, we present further data on neuropathology and, for the first time, NHLRC2 expression in different human brain regions in the autopsy samples of one control and the deceased FINCA patients originally described by Uusimaa et al. (2018).

### 4.1. Clinical phenotypes of novel FINCA patients compared with previously published cases

Based on the literature and novel FINCA patients described in the present study, all the patients with the NHLRC2 gene variants presented with developmental delay, along with variable axial hypotonia, muscle weakness, progressive muscular atrophy (leading to scoliosis), eating problems, poor eye contact, strabismus, seizures, behavioral problems and various types of movement disorders (ataxia, dystonia, cerebbral palsy, tremor and stereotypic hand movements). Thus, NHLRC2 is clearly essential for normal human nervous system function.

The present study, together with the so far reported FINCA cases, underlines how chronic macrocytic anemia, immunodeficiency, recurrent infections and pneumonias causing respiratory distress are the key clinical features of FINCA disease. Notably, recent work has identified NHLRC2 as a potent regulator of phagocytosis and filopodia formation (Haney et al., 2018). Furthermore, NHLRC2-deficient macrophages have been

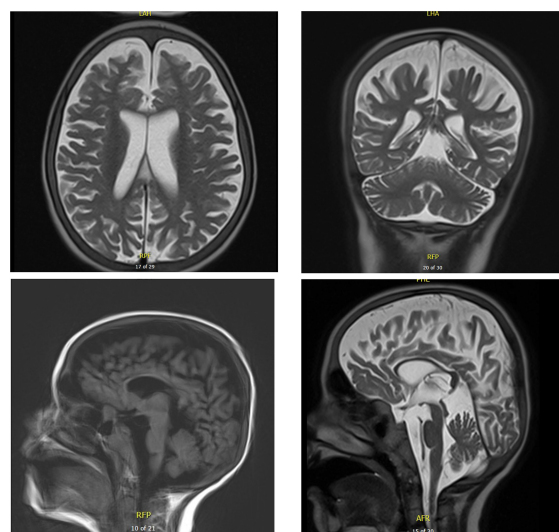


FIGURE 6

Brain MRI of patient five at the age of 17 years. T2 axial and coronal MRIs show general atrophy with normal white matter signal. Sagittal T1 and T2 brain MRIs show supra- and infratentorial cerebral atrophy, with marked thinning of the corpus callosum.

shown to undergo morphological changes and are resistant to certain bacteria *in vitro* (Yeung et al., 2019). Our patients suffered from chronic, partly lethal infections, but if this is related to the above-identified defect in macrophages, it has to be investigated further. In addition, NHLRC2 associates with p190RhoGAP and alters the activation levels of the cytoskeleton regulator RhoA (Haney et al., 2018). Erythroid-specific deletion of RhoA in mice was embryonic lethal because of severe anemia, and the primitive red blood cells were macrocytic, poikilocytes and frequently multinucleated (Konstantinidis et al., 2015). Binucleated and multinucleated erythroid cells are the key features in certain types of CDAs (King et al., 2022). Interestingly, we observed an erythroid lineage phenotype similar to congenital dyserythropoietic anemia type II (CDA II) in the two patients who had undergone bone marrow examinations (patients five and six) (Figure 3). Moreover, there was marked anisocytosis and poikilocytosis in the peripheral blood smear observed in patient six. It is also notable that four out of five patients required RBC transfusions because of severe anemia during infancy. Clearly, further investigations are necessary to elucidate the role of NHLRC2 in RBC development and membrane stability. In patient six, the initial lead-pathologies were severe anemia associated with feeding problems, failure to thrive and muscular hypotonia; hence, hematologists should keep ultra-orphan diseases like CDAs, FINCA syndrome and CAD-associated uridine responsive epileptic encephalopathy in the differential diagnostic repertoire.

Combining the clinical features of our five novel patients with the previously described 13 patients (Uusimaa et al., 2018; Brodsky et al., 2020; Rapp et al., 2021; Badura-Stronka et al., 2022) reveals the following: 10 patients have been reported as being alive (age between 4 and 61 years at the time of the publication), while eight were deceased (age at

death between 10 months and 2 years, 5 months). Eight of the 18 patients were male. All presented with axial hypotonia and developmental delay, usually severe. Most had recurrent infections, including recurrent pneumonias. Common presenting features included irritability (including impulsive behavior and aggressivity in older patients), movement disorders (dystonia/ataxia/tremor or stereotypic movements), failure to thrive, visual problems, feeding problems, episodic diarrhea or other intestinal problems, macrocytic anemia and an increased risk for respiratory distress and respiratory support during pneumonia. Epileptic seizures and immunodeficiency were also common features. Epilepsy phenotypes, electroencephalography (EEG) characteristics and brain MRI findings of FINCA patients have been presented in Supplementary Table 1. Furthermore, some patients exhibited transient liver dysfunction, hepatomegaly, transient kidney dysfunction and cardiac manifestations. Other features included hypothyroidism in two patients, pectus excavatum in two patients, tracheomalacia in one patient, cholelithiasis in one patient and an abnormal color of the skin in one patient. Chest radiography showed ARDS and chronic pneumonitis, with brain MRI revealing atrophy of the corpus callosum. A severe general cerebral and cerebellar atrophy in a patient at the age of 17 years suggested progressive neurodegeneration.

In previous publications, four patients were identified with homozygosity for the p.D148Y variant, as in our patient with the current age of 61 years (patient eight). All five patients were alive, and the ages of 4 previously reported cases varied between 7 and 14 years at the time of the publication (Rapp et al., 2021; Badura-Stronka et al., 2022). Thus, the phenotype could be differentially affected, depending on the loci of the rare damaging variants within the NHLRC2 gene. On the other hand, there was significant heterogeneity in the clinical presentation and outcome, even between the siblings with the same variants. Therefore, we conclude that the severity of disease seems to be modified by additional genetic and environmental factors, including exposure to infections and those related to developmental biology that need to be studied further.

## 4.2. Neuropathology of FINCA patients and NHLRC2 expression in the human brain

Autopsy samples of three previously described FINCA patients showed brain atrophy, white matter neuronal degeneration and angiomatosis such as vascularization and congestion (Uusimaa et al., 2018). The NHLRC2 expression data revealed that the control samples showed overall stronger NHLRC2 expression in neuronal and glial cells than in the patients (Table 3). On the other hand, we identified a clearly higher expression of NHLRC2 in the Purkinje cells of FINCA patients compared with the controls (Supplementary Figure 2). This finding is very interesting because Purkinje cells play a central role in cerebellar development and all cerebellar circuits. Because FINCA disease is a neuroimmunological disease, one hypothesis could be based on the link between progressive neurodegeneration and impaired peripheral immune responses, as exemplified by a recent study

TABLE 3 Expression of the NHLRC2 in different brain regions and cell types in the deceased FINCA patients and in the control samples.

	Neu	Gli	Men	End	Epe	Pil	Cho	Neu	Gli	Men	End	Epe	Pil	Cho	Neu	Gli	Men	End	Epe	Pil	Cho	Neu	Gli	Men	End	Epe	Pil	Cho
A					-		-					-		-					-		-					-	-	-
B					-		-					-		-					-		-					-		-
C					-		-					-		-	x	x	x	x	x	x	x	x	x	x	x	x	x	x
D					-		-							-	x	x	x	x	x	x	x					-		-
E					-		-					-		-	x	x	x	x	x	x	x	x	x	x	x	x	x	x
F					-		-					-		-					-		-					-		-
G																											-	
H			-											-	x	x	x	x	x	x	x	x	x	x	x	x	x	x
I														-	x	x	x	x	x	x	x			-			-	
J			-											-	x	x	x	x	x	x	x	x	x	x	x	x	x	x
K														-							-						-	
L			-											-							-						-	
M			-																								-	
N														-													-	
S	x	x	x	x	x	x	x							-							-						-	
	Patient 1							Patient 2							Patient 3							Control						

x No tissue available.  
- No representative cells.  
No expression.  
Low expression.  
Medium expression.  
Strong expression.

A, frontal lobe; B, temporal lobe; C, cingulate gyrus; D, parietal lobe; E, pre- and postcentral gyrus; F, occipital lobe; G, hippocampus; H, hypothalamus; I, basal ganglia; J, thalamus; K, middle brain; L, pons; M, medulla oblongata; N, cerebellum; S, spinal cord; Neu, neurons; Gli, glial cells; Men, meningotheelial cells; End, endothelial cells; Epe, ependymal cells; Pil, neuropil; Cho, choroid plexus.



demonstrating that the selective loss of Purkinje cells induces specific peripheral immune alterations by attracting leukocytes toward and into the cerebellum of a Purkinje cell degeneration mouse model (del Pilar et al., 2021). In their study, del Pilar et al. (2021) also suggested that this phenomenon could serve as an early biomarker of cerebellar degeneration and be responsible for an increased susceptibility to infections. Furthermore, the authors referred to several previous studies that have shown that the progression of neurodegenerative diseases has been reciprocally associated with impairments in peripheral immune responses and responsible for an increased susceptibility to infections, as exemplified by multiple sclerosis, AD, Huntington's disease, Parkinson's disease and amyotrophic lateral sclerosis (Scherzer et al., 2007; Björkqvist et al., 2008; Ciaramella et al., 2016; Fakhoury, 2016; Liu and Wang, 2017), and the identification of increased amounts of proinflammatory cytokines in cerebrospinal fluid and blood of patients with Alzheimer's and Parkinson's (Boyko et al., 2017; Chen et al., 2018).

The role of NHLRC2 in the function of the normal central nervous system and other organs remains unclear, but it is known to be involved in cytoskeletal organization and vesicle transport and has an important role in the maintenance of multiorgan homeostasis (Paakkola et al., 2018; Uusimaa et al., 2018). Additionally, NHLRC2 dysfunction contributes to the evolving neurodegeneration observed in the previously published FINCA patients and was clearly demonstrated in the current study. Our findings indicate that the pathological variants of *NHLRC2* influence protein expression in various regions of the human brain, hence causing variable neurological symptoms.

### 4.3. NHLRC2 variants associated with FINCA disease and disease models

In previous studies on NHLRC2, the thioredoxin-like domain was found to interact with a proenzyme form of caspase-8, and caspase-8 cleaves NHLRC2 *in vitro*. Excess reactive oxygen species (ROS) production led to a caspase-8-mediated decrease in NHLRC2 protein levels, leading to apoptotic cell death in colon cancer cells, suggesting an important role for NHLRC2 in the regulation of ROS-induced apoptosis (Nishi et al., 2017). NHLRC2 has been indicated as being a key regulator in phagocytosis and is suggested to act through controlling actin polymerization, cytoskeletal organization and filopodium formation (Haney et al., 2018; Paakkola et al., 2018; Yeung et al., 2019). Several genes involved in actin cytoskeletal arrangements were downregulated in the NHLRC2 mutant macrophages, and a co-immunoprecipitation experiment confirmed the interaction of NHLRC2 with FRYL-like transcription coactivator (FRYL), which is known to play a role in actin cytoskeleton regulation (Yeung et al., 2019).

A knockin mouse model for FINCA with pathogenic missense variant—c. G442T; p.D148Y—was generated in our research group by using the CRISPR/Cas9 technique (Hiltunen et al., 2020). This mouse line—C57BL/6N*Nhlrc2*<sup>em1Rthl</sup>—has been crossed with the *Nhlrc2* KO mouse line to mimic the compound heterozygous genotype of the FINCA patients. *in situ* hybridization (ISH) of *Nhlrc2* showed ubiquitous expression throughout the adult brain

of 32-week-old male mice, with the most prominent expression in cerebellar granule cells, followed by granule cells in the dentate gyrus and then by pyramidal cells in the hippocampal CA1 layer and layer 2 of the piriform cortex. ISH of FINCA/KO mice brain revealed a similar expression pattern of the mutated *Nhlrc2* mRNA to that of the wild-type (Hiltunen et al., 2020).

## 5. Conclusion

We report five new patients with FINCA disease, demonstrating strikingly similar key phenotypic features with the previously published FINCA patients (Brodsky et al., 2020; Rapp et al., 2021; Badura-Stronka et al., 2022). Furthermore, our data underline the importance of performing hematological and immunological studies on all patients with biallelic pathogenic NHLRC2 variants. Immunoglobulin treatment and additional vaccinations (e.g., pneumococcal vaccine and varicella immunoglobulin) and antibiotic prophylaxis (for pneumocystis carinii, etc.) are recommended if immunodeficiency is detected. Our results further demonstrate that biallelic *NHLRC2* gene variants cause infantile-onset FINCA disease, facilitate the early diagnosis and eventually provide clues how to improve the management of this severe multiorgan disease. Based on the current knowledge on the phenotypic spectrum of FINCA disease, we recommend considering WES analysis for patients with a history of infantile-onset cerebropulmonary manifestations as well as infantile-onset epileptic encephalopathies without pulmonary manifestations.

The clinical and histopathological characteristics of NHLRC2-related diseases, namely fibrosis, infection susceptibility/immunodeficiency/intellectual disability, neurodevelopmental disorder/neurodegeneration, and chronic anemia/cerebral angiomas can be summarized by the acronym FINCA.

## Data availability statement

The original contributions presented in this study are included in the article/**Supplementary material**, further inquiries can be directed to the corresponding author.

## Ethics statement

The studies involving human participants were reviewed and approved by the Ethics Committee of the Northern Ostrobothnia Hospital District, Oulu, Finland. Written informed consent to participate in this study was provided by the participants' legal guardian/next of kin.

## Author contributions

AT, HT, OK, JK, RK, RH, and JU contributed to the conception and design of the study. AT, LK, GO'G, JK, OK, ME, CW, JB, FL, KB, and JU collected and interpreted clinical, neuroradiological,

and laboratory data on patients. AT and HT performed neuropathological analyses. OK, EE, JB, FL, MK, and AP organized and performed molecular genetic analyses. AT, RH, and JU wrote the first draft of the manuscript. LK, GO'G, HT, and MH wrote sections of the manuscript. All authors contributed to manuscript revision, read, and approved the submitted version.

## Funding

This study was supported by the Academy of Finland Grants 266498, 273790, 303996, 317711, 311934, and 331436, the Sigrid Jusélius Foundation, the Foundation for Pediatric Research, Finland, the Emil Aaltonen Foundation, and the Alma and K. A. Snellman Foundation. Sequencing and analysis were provided by the Broad Institute of MIT and Harvard Centre for Mendelian Genomics (Broad CMG) and was funded by the National Human Genome Research Institute, the National Eye Institute, the National Heart, Lung, and Blood Institute grant UM1 HG008900 and in part by National Human Genome Research Institute grant R01 HG009141, and the Athlae Lyons Starship Research Trust and Starship Foundation.

## Acknowledgments

We thank all the families who participated in this study. Written informed consent from the parents or guardians was obtained. Furthermore, we acknowledge Pirjo Keränen, Riitta Vuento, Biocenter Oulu sequencing core, and the Biocenter Oulu Transgenic and Tissue Phenotyping Core Facility, University of Oulu, Finland; a member of Biocenter Finland and Infrafrontier-EMMA, for their excellent technical assistance. We thank the Scribendi proofreading team for the language editing. Some authors of this publication are members of the European Reference Network on Rare Neurological Diseases (ERN-RND), Rare and Complex Epilepsies (EpiCARE), Neuromuscular Diseases (ERN-EURO-NMD), and Rare Congenital Malformations and Rare Intellectual Disability (ERN-ITHACA).

## Conflict of interest

The authors declare that the research was conducted in the absence of any commercial or financial relationships that could be construed as a potential conflict of interest.

## References

Andrés-Benito, P., Povedano, M., Domínguez, R., Marco, C., Colomina, M. J., López-Pérez, Ó, et al. (2020). Increased c-x-c motif chemokine ligand 12 levels in cerebrospinal fluid as a candidate biomarker in sporadic amyotrophic lateral sclerosis. *Int. J. Mol. Sci.* 21:8680. doi: 10.3390/ijms21228680

## Publisher's note

All claims expressed in this article are solely those of the authors and do not necessarily represent those of their affiliated organizations, or those of the publisher, the editors and the reviewers. Any product that may be evaluated in this article, or claim that may be made by its manufacturer, is not guaranteed or endorsed by the publisher.

## Supplementary material

The Supplementary Material for this article can be found online at: <https://www.frontiersin.org/articles/10.3389/fnins.2023.1123327/full#supplementary-material>

The **Supplementary material** includes case histories of five novel FINCA patients, three figures on neuropathological findings in autopsy samples of the three previously published FINCA patients and a table presenting epilepsy phenotypes, EEG characteristics and brain MRI findings in novel and previously published FINCA patients.

### SUPPLEMENTARY FIGURE 1

Immunohistochemical NHLRC2 expression in brain autopsy samples of patients. **(A)** Strong expression in thalamic neurons. **(B)** Medium strength and widespread expression in the glial cells of the middle brain. Some glial cells are weakly positive or negative for NHLRC2. **(C)** Cerebellar overview and higher magnifications of the cell layers and Purkinje cells. Strong expression in Purkinje cells. **(D)** Meningothelial cells are weakly positive for NHLRC2. **(E)** Neurons of the inferior olivary nucleus have medium to strong expression. **(F)** Ependymal cells had apical expression and were weakly positive or negative for NHLRC2. **(G)** Dentate gyrus of the hippocampus and mild expression in neurons. **(H)** Expression in choroid plexus cells and periventricular neurons.

### SUPPLEMENTARY FIGURE 2

NHLRC2 expression was compared in different brain regions between patients and control. **(Frontal lobe):** Medium expression in neurons. There was no significant difference between the patients and control. **(Temporal lobe):** The intensity of the staining is stronger in the control compared with the patients. Medium to strong expression in the neuropils of the control. **(Pons):** Medium to strong expression in the neurons. The control group had slightly stronger expression compared with the patients. **(Cerebellum):** Strong expression in the Purkinje cells of the patients and mild in the cells of the control. **(Medulla oblongata):** Stronger expression in the neurons of the control group compared with the patients. **(Basal ganglia):** The expression and intensity of the staining is stronger in the control compared with the patients.

### SUPPLEMENTARY FIGURE 3

NHLRC2 expression was compared in different brain regions between the patients and control. **(Frontal lobe):** Mild-to-medium expression in the glial cells of the patients and medium expression in the glial cells of the control. **(Occipital lobe):** Mild to strong expression in the glial cells. Slightly stronger expression in the control group compared with the patients. **(Parietal lobe):** Stronger expression and more frequent occurrence of glial cells in the control. **(Spinal cord):** Strong expression in neurons in both the patients and control. **(Ependymal cells):** Negative to mild apical expression in the ependymal cells of the patients and medium apical expression in the ependymal cells of the control.

Badura-Stronka, M., Śmigiel, R., Rutkowska, K., Szymańska, K., Hirschfeld, A. S., Monkiewicz, M., et al. (2022). FINCA syndrome—Defining neurobehavioral phenotype in survivors into late childhood. *Mol. Genet. Genomic Med.* 10:e1899.

- Biterova, E., Ignatyev, A., Uusimaa, J., Hinttala, R., and Ruddock, L. W. (2018). Structural analysis of human NHLRC2, mutations of which are associated with FINCA disease. *PLoS One* 13:e0202391. doi: 10.1371/journal.pone.0202391
- Björkqvist, M., Wild, E. J., Thiele, J., Silvestroni, A., Andre, R., Lahiri, N., et al. (2008). A novel pathogenic pathway of immune activation detectable before clinical onset in Huntington's disease. *J. Exp. Med.* 205, 1869–1877. doi: 10.1084/jem.20080178
- Boon, K., Bailey, N. W., Yang, J., Steel, M. P., Groshong, S., Kervitsky, D., et al. (2009). Molecular phenotypes distinguish patients with relatively stable from progressive idiopathic pulmonary fibrosis (IPF). *PLoS One* 4:e5134.
- Boyko, A. A., Troyanova, N. I., Kovalenko, E. I., and Sapozhnikov, A. M. (2017). Similarity and differences in inflammation-related characteristics of the peripheral immune system of patients with Parkinson's and Alzheimer's diseases. *Int. J. Mol. Sci.* 18:2633. doi: 10.3390/ijms18122633
- Brodsky, N. N., Boyarchuk, O., Kovalchuk, T., Hariyan, T., Rice, A., Ji, W., et al. (2020). Novel compound heterozygous variants in NHLRC2 in a patient with FINCA syndrome. *J. Hum. Genet.* 65, 911–915. doi: 10.1038/s10038-020-0776-0
- Chen, X., Hu, Y., Cao, Z., Liu, Q., and Cheng, Y. (2018). Cerebrospinal fluid inflammatory cytokine aberrations in Alzheimer's disease, Parkinson's disease and amyotrophic lateral sclerosis: A systematic review and meta-analysis. *Front. Immunol.* 9:2122. doi: 10.3389/fimmu.2018.02122
- Ciamarella, A., Salani, F., Bizzoni, F., Orfei, M. D., Caltagirone, C., Spalletta, G., et al. (2016). Myeloid dendritic cells are decreased in peripheral blood of Alzheimer's disease patients in association with disease progression and severity of depressive symptoms. *J. Neuroinflammation* 13:18. doi: 10.1186/s12974-016-0483-0
- del Pilar, C., Lebrón-Galán, R., Pérez-Martín, E., Pérez-Revuelta, L., Ávila-Zarza, C. A., Alonso, J. R., et al. (2021). The selective loss of purkinje cells induces specific peripheral immune alterations. *Front. Cell. Neurosci.* 15:e773696.
- Edgar, R. C. (2004). Muscle: Multiple sequence alignment with high accuracy and high throughput. *Nucleic Acids Res.* 32, 1792–1797. doi: 10.1093/nar/gkh340
- Fakhoury, M. (2016). Immune-mediated processes in neurodegeneration: Where do we stand? *J. Neurol.* 263, 1683–1701. doi: 10.1007/s00415-016-8052-0
- Haney, M. S., Bohlen, C. J., Morgens, D. W., Ousey, J. A., Barkal, A. A., Tsui, C. K., et al. (2018). Identification of phagocytosis regulators using magnetic genome-wide CRISPR screens. *Nat. Genet.* 50, 1716–1727. doi: 10.1038/s41588-018-0254-1
- Hiltunen, A. E., Kangas, S. M., Ohlmeier, S., Pietilä, I., Hiltunen, J., Tanila, H., et al. (2020). Variant in NHLRC2 leads to increased hnRNP C2 in developing neurons and the hippocampus of a mouse model of FINCA disease. *Mol. Med.* 26:123. doi: 10.1186/s10020-020-00245-4
- Hiltunen, A. E., Vuolteenaho, R., Ronkainen, V. P., Miinalainen, I., Uusimaa, J., Lehtonen, S., et al. (2022). Nhlrc2 is crucial during mouse gastrulation. *Genesis* 60:e23470. doi: 10.1002/dvg.23470
- King, R., Gallagher, P. J., and Khoriaty, R. (2022). The congenital dyserythropoietic anemias: Genetics and pathophysiology. *Curr. Opin. Hematol.* 29, 126–136.
- Konstantinidis, D. G., Giger, K. M., Risinger, M., Pushkaran, S., Zhou, P., Dexheimer, P., et al. (2015). Cytokinesis failure in RhoA-deficient mouse erythroblasts involves actomyosin and midbody dysregulation and triggers p53 activation. *Blood* 126, 1473–1482. doi: 10.1182/blood-2014-12-616169
- Kreus, M., Lehtonen, S., Hinttala, R., Salonen, J., Porvari, K., and Kaarteenaho, R. (2022). NHLRC2 expression is increased in idiopathic pulmonary fibrosis. *Respir. Res.* 23:206. doi: 10.1186/s12931-022-02129-z
- Kurki, M. I., Saarentaus, E., Pietiläinen, O., Gormley, P., Lal, D., Kerminen, S., et al. (2019). Contribution of rare and common variants to intellectual disability in a sub-isolate of Northern Finland. *Nat. Commun.* 10:410.
- Liu, J., and Wang, F. (2017). Role of neuroinflammation in amyotrophic lateral sclerosis: Cellular mechanisms and therapeutic implications. *Front. Immunol.* 8:1005.
- Long, J., Pan, G., Ifeakor, E., Belshaw, R., and Li, X. (2016). Discovery of novel biomarkers for Alzheimer's disease from blood. *Dis. Markers* 2016:e4250480. doi: 10.1155/2016/4250480
- Nishi, K., Iwaihara, Y., Tsunoda, T., Doi, K., Sakata, T., Shirasawa, S., et al. (2017). ROS-induced cleavage of NHLRC2 by caspase-8 leads to apoptotic cell death in the HCT116 human colon cancer cell line article. *Cell Death Dis.* 8:3218. doi: 10.1038/s41419-017-0006-7
- Paakkola, T., Salokas, K., Miinalainen, I., Lehtonen, S., Manninen, A., Kaakinen, M., et al. (2018). Biallelic mutations in human NHLRC2 enhance myofibroblast differentiation in FINCA disease. *Hum. Mol. Genet.* 27, 4288–4302. doi: 10.1093/hmg/ddy298
- Polkoff, K. M., Lotti, S. N., Beever, J. E., and Wheeler, M. B. (2017). 206 CRISPR/Cas9-mediated repair of the NHLRC2 locus in beef cattle. *Reprod. Fertil. Dev.* 29, 212–212. doi: 10.1071/RDv29n1Ab206
- Rapp, C. K., van Dijk, I., Laugwitz, L., Boon, M., Briassoulis, G., Ilia, S., et al. (2021). Expanding the phenotypic spectrum of FINCA (fibrosis, neurodegeneration, and cerebral angiomas) syndrome beyond infancy. *Clin. Genet.* 100, 453–461. doi: 10.1111/cge.14016
- Scherzer, C. R., Eklund, A. C., Morse, L. J., Liao, Z., Locascio, J. J., Fefer, D., et al. (2007). Molecular markers of early Parkinson's disease based on gene expression in blood. *Proc. Natl. Acad. Sci. U.S.A.* 104, 955–960. doi: 10.1073/pnas.0610204104
- Uusimaa, J., Kaarteenaho, R., Paakkola, T., Tuominen, H., Karjalainen, M. K., Nadaf, J., et al. (2018). NHLRC2 variants identified in patients with fibrosis, neurodegeneration, and cerebral angiomas (FINCA): Characterisation of a novel cerebropulmonary disease. *Acta Neuropathol.* 135, 727–742. doi: 10.1007/s00401-018-1817-z
- van Dijk, K. D., Berendse, H. W., Drukarch, B., Fratantoni, S. A., Pham, T. V., Piersma, S. R., et al. (2012). The proteome of the locus ceruleus in Parkinson's disease: Relevance to pathogenesis. *Brain Pathol.* 22, 485–498. doi: 10.1111/j.1750-3639.2011.00540.x
- Ye, J., Liu, H., Xu, Z. L., Zheng, L., and Liu, R. Y. (2019). Identification of a multidimensional transcriptome prognostic signature for lung adenocarcinoma. *J. Clin. Lab. Anal.* 33:e22990. doi: 10.1002/jcla.22990
- Yeung, A. T. Y., Choi, Y. H., Lee, A. H. Y., Hale, C., Ponstingl, H., Pickard, D., et al. (2019). A genome-wide knockout screen in human macrophages identified host factors modulating *Salmonella* infection. *mBio* 8, e02169–19. doi: 10.1128/mBio.02169-19



## OPEN ACCESS

## EDITED BY

Subashika Govindan,  
Wellcome Trust DBT India Alliance, India

## REVIEWED BY

Michael Lodato,  
University of Massachusetts Medical School,  
United States  
Ashwin S. Shetty,  
Harvard University, United States

## \*CORRESPONDENCE

Sara Bizzotto  
✉ Sara.Bizzotto@icm-institute.org

RECEIVED 23 February 2023

ACCEPTED 25 April 2023

PUBLISHED 12 May 2023

## CITATION

Bizzotto S (2023) The human brain through the lens of somatic mosaicism.  
*Front. Neurosci.* 17:1172469.  
doi: 10.3389/fnins.2023.1172469

## COPYRIGHT

© 2023 Bizzotto. This is an open-access article distributed under the terms of the [Creative Commons Attribution License \(CC BY\)](#). The use, distribution or reproduction in other forums is permitted, provided the original author(s) and the copyright owner(s) are credited and that the original publication in this journal is cited, in accordance with accepted academic practice. No use, distribution or reproduction is permitted which does not comply with these terms.

# The human brain through the lens of somatic mosaicism

Sara Bizzotto\*

Sorbonne Université, Institut du Cerveau (Paris Brain Institute) ICM, Inserm, CNRS, Hôpital de la Pitié Salpêtrière, Paris, France

Every cell in the human brain possesses a unique genome that is the product of the accumulation of somatic mutations starting from the first postzygotic cell division and continuing throughout life. Somatic mosaicism in the human brain has been the focus of several recent efforts that took advantage of key technological innovations to start elucidating brain development, aging and disease directly in human tissue. On one side, somatic mutation occurring in progenitor cells has been used as a natural barcoding system to address cell phylogenies of clone formation and cell segregation in the brain lineage. On the other side, analyses of mutation rates and patterns in the genome of brain cells have revealed mechanisms of brain aging and disorder predisposition. In addition to the study of somatic mosaicism in the normal human brain, the contribution of somatic mutation has been investigated in both developmental neuropsychiatric and neurodegenerative disorders. This review starts with a methodological perspective on the study of somatic mosaicism to then cover the most recent findings in brain development and aging, and ends with the role of somatic mutations in brain disease. Thus, this review underlies what we have learned and what is still possible to discover by looking at somatic mosaicism in the brain genome.

## KEYWORDS

somatic mosaicism, human brain, neurodevelopment, brain aging, neurodevelopmental disorders, neurodegeneration

## Introduction

We have long believed that the human genome is the same in each cell of the body, and that rare somatic mutations occurring during life often due to the exposure to external agents such as smoke and UV light, are the cause of cancer. However, more recently, we have learned that the human body carries as many different genomes as the number of cells it is composed of, a phenomenon referred to as somatic mosaicism. This is due to the accumulation of somatic mutations (or variants) starting with the first postzygotic cell division and continuing during the whole life at rates and patterns that are specific to each tissue and cell type.

Somatic mutations, once occurred, permanently mark the genome. For this reason, the study of somatic mutation has proven effective at elucidating organism and tissue development but also disease predisposition and pathology insurgence. Several recent efforts have focused on somatic mutations in the human brain, revealing unique insights into development, aging and pathology. This review covers the latest findings in brain somatic mutation, and put them in perspective to underlie the unique insights somatic mutation is providing into the human brain, and the future potential of this field.



## Methods and technologies to study somatic mutation

The study of somatic mutation requires specific technologies and analytic tools. The choice of sample, the library preparation method and the sequencing technology must be adapted to the question(s) of interest. Indeed, different methodologies present specific detection limits that go from somatic mutations with >2% mosaicism in the sampled tissue to somatic mutations present in single-cell genomes (Figure 1).

Some of the studies conducted until now on the human brain have used deep (>200X) sequencing of bulk DNA extracted from biopsies made of thousands of cells (Baldassari et al., 2019a,b; Bizzotto et al., 2021; Fasching et al., 2021; Breuss et al., 2022). This approach allows detection of a wide range of variant allele frequencies (VAFs, calculated as the number of sequencing reads displaying the mutation over the total number of reads covering the mutant locus), and it is sensitive enough to detect somatic mutations present in >2% of the total cells in the biopsy (>1% VAF). However, the main limitation of this approach is the inability to detect extremely low (<1%) VAFs that represent rare mutations in the tissue, which might be relevant in polyclonal tissues such as the human brain, where many multiple progenitor cells contribute to a small tissue area. Bulk low-input

sequencing technologies can overcome such limitation by sequencing DNA extracted from as few as 100–1,000 cells (Ellis et al., 2021). However, these technologies require at least few cycles of DNA amplification, which can introduce DNA polymerase errors that can be difficult to discriminate from true somatic events during analysis. Duplex consensus sequencing technologies solve this problem by using a library preparation strategy that allows the recognition of the two strands of the same DNA molecule after sequencing (Schmitt et al., 2012; Kennedy et al., 2014; Abascal et al., 2021). By these means, PCR errors are recognized as those that are present in copies of the same strand. Furthermore, sequencing artifacts are discriminated as those present in individual reads associated with one strand. Such solutions allow to detect rare, low VAF somatic mutations, and can provide good measures of somatic variant rates and abundance in human tissues (Abascal et al., 2021; Coorens et al., 2021).

Bulk sequencing methods are used to identify mutations that are shared by multiple cells in the tissue (clonal somatic mutations). Although this is useful for studies that are interested in mutations that may have a bigger impact at the global tissue level, it is not sensitive enough to address the cumulative effect of somatic mutations in non-replicating differentiated cells such as neurons in the postnatal brain. For this, whole-genome amplification (WGA) methods have been developed for detection of somatic mutations at the single-cell

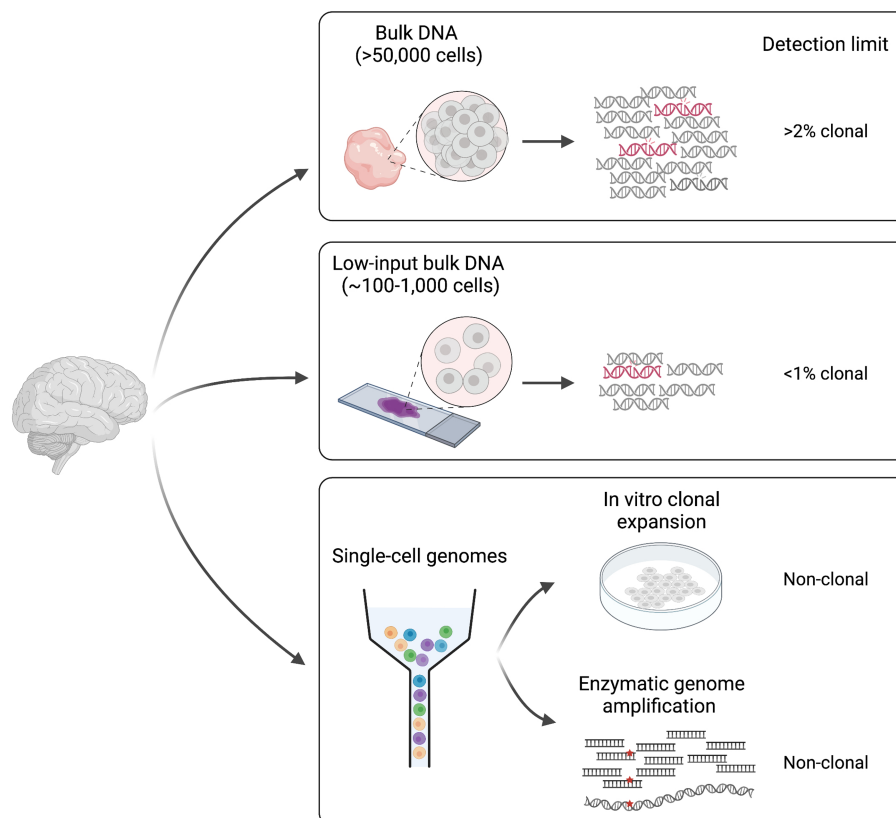


FIGURE 1

Different approaches for the study of somatic mutation. Methodologies can be divided in two main categories: (1) bulk DNA-sequencing (including low-input) and (2) single cell DNA-sequencing. Classic bulk DNA strategies use biopsies made of >50,000 cells and usually present a detection limit of >2% mosaicism (clonal). Low-input bulk methods start from as low as ~100–1,000 cells and have a lower detection limit of <1% clonal. Finally, single-cell technologies require genome amplification either through *in vitro* clonal expansion or through enzymatic genome amplification, and can detect non-clonal mutations present in single genomes. Figure created with BioRender.com.

level (Spits et al., 2006; Bae et al., 2018; Fasching et al., 2021; Gonzalez-Pena et al., 2021; Xing et al., 2021; Luquette et al., 2022). The main WGA strategies applied until now in the brain include: (1) clonal expansion in culture (Bae et al., 2018) and (2) enzymatic genome amplification (Spits et al., 2006; Gonzalez-Pena et al., 2021; Xing et al., 2021). The former can be applied to proliferating cells or embryonic stem cells after nuclear transfer from any other cell type however, it is subjected to cell culture somatic artifacts often associated with hypoxic conditions. Several methods exist for enzymatic genome amplification that can be applied to any cell type (Spits et al., 2006; Gonzalez-Pena et al., 2021; Xing et al., 2021). The main problem associated with these technologies is the introduction of artifact variants during amplification that need to be filtered during data analysis. One limitation common to all single-genome sequencing approaches is that they are still difficult to apply to many multiple replicates. While clonal expansion in culture is experimentally elaborate, enzymatic methods still have elevated costs, which has limited existing studies to sample sizes of less than 200 single-genomes.

Although next-generation sequencing (NGS)-based methods are effective in the study of somatic single-nucleotide variants (sSNVs) and small (less than ~40 bp) insertion/deletions (indels), detecting somatic structural variants (SVs) such as large copy number variants (CNVs) in NGS data is still challenging and requires sophisticated computational solutions. For this, long-read third-generation sequencing methods represent a valid alternative. However, although studies have been successful in identifying germline SVs in long-read data, somatic SVs have not been explored enough yet. Thus, application of long-read sequencing to such purpose requires further investigation (Jenko Bizjan et al., 2020; Fujimoto et al., 2021).

In parallel to library preparation and sequencing methods, detection of somatic mutations requires computational tools specifically adapted to discriminate between low-frequency artifacts, germline mutations, and true somatic events. A plethora of pipelines are now available, and most of the studies privilege consensus between different methods applied to the same data. Recently, the Brain Somatic Mosaicism Network (BSMN) has published a consensus of best practices for calling sSNVs in brain bulk DNA deep sequencing data that has 65% genome-wide detection sensitivity, and relies on multiple filtering steps to get rid of library and sequencing artifacts and germline variants (Wang et al., 2021). In non-cancer studies, where somatic mutations that are shared with other tissues are still relevant (e.g., lineage tracing of human development), the challenge is that there is no matched control available to filter non-somatic germline mutations. Several callers have recently been introduced that address this issue by using features obtained from raw data, machine learning or image-based representations coupled with convolutional neural network (CNN)-based classification to detect somatic mutations with high sensitivity and precision in the absence of a matched control (Huang et al., 2017; Dou et al., 2020; Yang et al., 2023). Callers specifically designed to detect somatic mutations in single-cell WGS were also introduced that use either read phasing or leveraging of mutation signatures and allele balance to discriminate between true somatic mutations and artifacts introduced during WGA (Bohrson et al., 2019; Luquette et al., 2022).

Finally, a major challenge associated to somatic mosaicism remains the ability to identify somatic mutations in specific cell types populating the same tissue. This is especially relevant in the human brain, since it contains hundreds of different cell types that have

specific developmental trajectories and properties. High-throughput single-cell transcriptomics and epigenomic data are now widely used to assign cell identities. However, genotyping of somatic mutations in such data is still limited by the sparse genome coverage given by these technologies (Bizzotto et al., 2021). Although identification of somatic mutations in specific cell types is now possible thanks to approaches such as cell-type sorting, G&T-seq (Genome and Transcriptome sequencing), PRDD-seq (Parallel RNA and DNA analysis after Deep-sequencing), GoT (Genotyping of Transcriptomes), and single-cell transcriptomics coupled with long-read sequencing, all these approaches still present several limitations (Macaulay et al., 2015; Nam et al., 2019; Huang et al., 2020; Bizzotto et al., 2021; Koboldt et al., 2021; Breuss et al., 2022; Townsend et al., 2023). While sorting is limited to broad and abundant cell types that can be targeted by specific known markers, G&T and PRDD-seq are still costly, time-consuming, low-throughput, or limited to targeted genes and genomic loci. GoT and long-read sequencing, on the other hand, have until now proven effective only for a subset of somatic mutations present in abundant transcripts. Thus, existing technologies are still very difficult to apply to low VAF somatic mutations and rare cell types, which underlies the need to develop more efficient high-throughput methods.

## Somatic mosaicism and human brain development

Since the first studies in 2015, somatic mutations have been shown to function as a tool to identify and track cellular clones in the human brain (Evrny et al., 2015; Lodato et al., 2015; Bizzotto and Walsh, 2022). The first study identified somatic endogenous retroelements in single-neurons and brain bulk DNA, and showed that spontaneous retrotransposition events that occur during human brain development can function as markers to analyze clone spreading in the cerebral cortex (Evrny et al., 2015). Retrotransposition events, however, are quite infrequent during development (<1 per terminally-differentiated neuronal genome), which limits their utility for the study of cell phylogenies (Evrny et al., 2012; Erwin et al., 2016). Indeed, more recent studies have focused on sSNVs that occur at a much higher frequency of at least 1–4 per genome per cell division (Bae et al., 2018; Ye et al., 2018; Rodin et al., 2021). sSNVs permanently label the genome of a cell and its descendence, except in the case of extremely rare events of somatic loss-of-heterozygosity. Furthermore, since the likelihood of the same rare mutation (excluding those frequent in the population) occurring twice in the same individual is extremely low, sSNVs act as unique markers. Thus, being frequent, unique, permanent and cumulative, sSNVs possess all the properties needed by a reliable lineage tracing tool. Since sSNVs label virtually every cell division of human brain development, they are ideal for studying cell phylogenies.

Studies conducted so far have managed to identify several clones and map their contributions to different brain regions and non-brain tissues, and have used this information to place in a temporal order some landmark steps of human brain development (Figure 2). We showed that ~50–100 founder progenitors of the human forebrain are produced by lineages that originate before gastrulation from the first cell divisions of the human embryo (Bizzotto et al., 2021; Bizzotto and Walsh, 2022). Another study suggested that brain lineage founder cells may segregate according to the antero-posterior axis of the central nervous system (CNS) primordium (formed by forebrain,

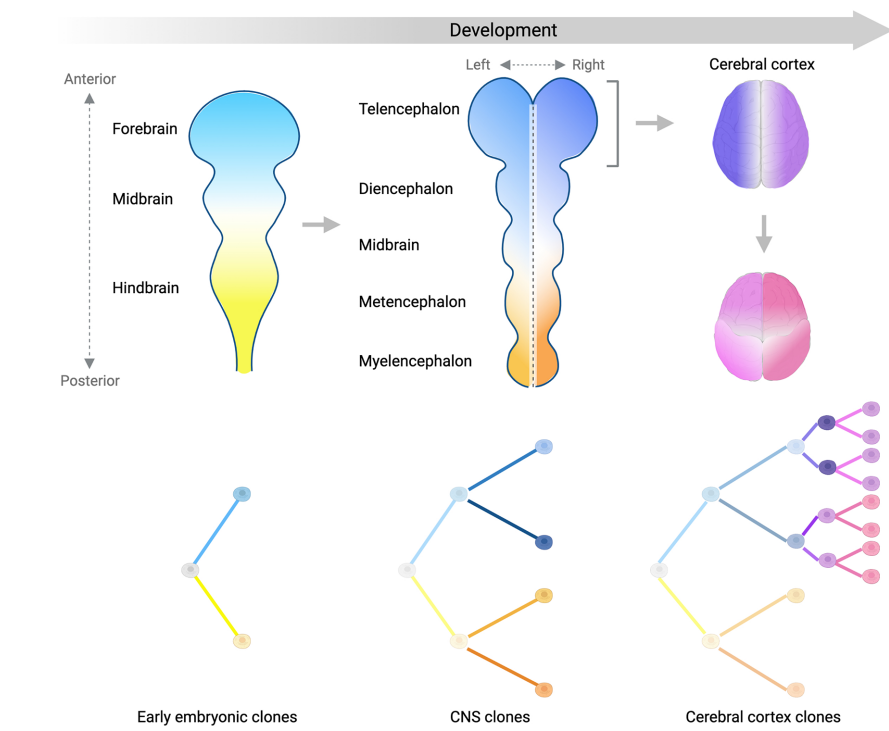


FIGURE 2

Lineage segregation during brain development. Schematic summarizing what we have learned so far about brain development from analyses of somatic mutation distribution patterns. Color gradients display the spatial distribution of separate (sub)-lineages in the developing central nervous system (CNS) over time. Trees in the bottom panels show the relationship between different (sub)-lineages. The antero-posterior axis is established first at early stages of embryonic development (left panel) and is represented by two lineages giving rise mostly to the anterior (light blue) or the posterior (light yellow) parts of the CNS primordium. As the CNS develops into more sub-regions, the left-right axis starts being established by sub-lineages of the blue and yellow clones (middle panel). Focusing on the forebrain (right panels), the left-right axis separating the two hemispheres (dark blue and purple) is established before the separation between the frontal lobe and more posterior lobes of the cortex (magenta and pink sub-lineages). Later on, the ventral-dorsal axis is established (not shown). Figure created with [BioRender.com](https://www.biorender.com).

midbrain and hindbrain) at very early stages of embryonic development (Fasching et al., 2021). The forebrain subsequently gives rise to the most anterior telencephalon and the diencephalon, while the hindbrain splits into metencephalon and myelencephalon. Analysis of clonal sSNVs showed that the forebrain and cerebellar primordia (metencephalon), likely split before the formation of the midline that separates the left and right hemispheres of the forebrain (Breuss et al., 2022), which means that the left-right axis is established after the specification of the neural tube into the most anterior forebrain and the most posterior hindbrain. Finally, within the forebrain, a first clone diffusion barrier seems to be established along the midline, while along the antero-posterior axis clones may be able to diffuse more freely until later stages (Coorens et al., 2021; Breuss et al., 2022) (Figure 2). Around 90–200 progenitors were estimated at the time of forebrain lateralization, consistent with the number of forebrain founder progenitors mentioned above (Breuss et al., 2022). sSNV distribution along the antero-posterior axis of the cortex showed that the frontal lobe and more posterior lobes constitute two broadly definable lineage clusters (Figure 2), probably due to the presence of the central sulcus and the Sylvian fissure, which may constitute a physical diffusion barrier limiting clonal spreading across regions (Bizzotto et al., 2021; Breuss et al., 2022). Finally, analyses of somatic mutations in sorted populations of glial cells (astrocytes, oligodendrocytes, and microglia) and excitatory and inhibitory

neurons strongly suggested that ventral and dorsal regions separate after the formation of the left-right and antero-posterior axes (Breuss et al., 2022). Despite these very interesting findings regarding the order in which different domains and axes are formed, our knowledge about segregation of progenitor cells in the brain lineage is still limited, and will require further, more in depth studies of somatic mutations across brain regions.

The human cerebral cortex is composed of ~170 billion cells and more than a 100 different cell types classified so far. This cellular complexity is reached through a huge number of cell divisions that involve different types of progenitor cells. For this reason, the clonal structure of the cortex is hard to decipher but somatic mutations are offering some interesting insights. Analyses of geographical distribution of clonal sSNVs in the cortex strongly suggested that younger clones arising later during development and presenting lower mosaicism distribute over narrower regions (Lodato et al., 2015; Bizzotto et al., 2021; Breuss et al., 2022). This observation suggests that each cortical region is a patchwork of cells that belong to independent intermingling clones. Although it has been difficult so far to reconstruct cell divisions of committed neural progenitors in the cortex due to the extremely low VAF (<1%) of somatic mutations that mark such divisions, few studies have managed to address how earlier, easier to identify, embryonic cell divisions contribute to the cortex. We and others showed that lineages

generated in the early embryo contribute asymmetrically on average to the cortex, with a high inter-individual variability that suggests that individual clones may undergo differential expansions and/or bottleneck events (Bizzotto et al., 2021; Coorens et al., 2021; Fasching et al., 2021; Breuss et al., 2022).

The mammalian cerebral cortex contains two broad cell type categories that are neuronal and non-neuronal glial cells, and we and others showed that in humans these two classes of cells are generated in different percentages from early pre-neurogenesis embryonic cell divisions (Bizzotto et al., 2021; Breuss et al., 2022). If we split these two main categories further, we find several cell types that are produced by distinct progenitor niches and follow characteristic migratory patterns. In the mouse, excitatory neurons, astrocytes and some oligodendrocytes are born from dorsal ventricular zone progenitors, while inhibitory neurons and other oligodendrocytes are derived from ventrally located progenitors. Somatic mutations characterized until now in different cell type populations seem to confirm this general pattern also in humans (Huang et al., 2020; Breuss et al., 2022). However, we know from a recent study that in humans a small proportion of inhibitory neurons might share dorsal cortical progenitors with excitatory neurons (Delgado et al., 2022), though this has not been confirmed yet by lineage tracing studies using somatic mutations in human tissue.

The cerebral cortex is a laminated structure composed of six identifiable layers that form in an inside-out manner. PRDD-seq studies managed to identify this inside-out order of formation of cortical layers in humans, showing at the same time that 10 or more excitatory neuron progenitors contribute to a specific cortical radial column. The same study also showed that medial, lateral and caudal ganglionic eminence (MGE, LGE, and CGE) interneurons are generated over the same developmental time window, except maybe for a proportion of CGE-derived LAMP5+ interneurons, and especially those co-expressing SST, that seem to be generated later. Similar to the mouse, PVALB+ and SST+ MGE-derived interneurons were enriched in infragranular cortical layers IV to VI and II to VI, respectively, while CGE-derived LAMP5+ and VIP+ interneurons tended to occupy upper layers (Huang et al., 2020). However, the study found no evidence for an inside-out pattern characterizing interneuron development, which is still debated in the mouse as well (Ang et al., 2003; Rudy et al., 2011; Huang et al., 2020). Future studies will need to characterize later more cell-type-restricted somatic mutations in order to reveal the finer properties of cell type production and distribution in the cortex.

## The aging human brain

The process of aging is accompanied by an increase in the predisposition to certain disorders such as neurodegeneration and cancer. In the aging brain, somatic mutations accumulate linearly in a process called *genosenium* (Lodato et al., 2018). The most recent estimates show that somatic mutations in aging human neurons accumulate at rates of ~16–17 sSNVs and 2–3 indels per genome per year such that while right after birth each neuron contains ~100–200 sSNVs and ~10–30 indels, at more advanced ages (>70 years old), sSNVs are on the order of ~1,000–2,000, and indels on the order of ~250–350 (Abascal et al., 2021; Luquette et al., 2022). Very recent data additionally characterized somatic mutations in aging oligodendrocytes, showing that these are surprisingly different from neurons and

accumulate sSNVs 69% faster (~27 per genome per year) and indels 42% slower (~1.8 per genome per year), probably due to different mechanisms of mutation (see below). Thus, oligodendrocytes in the brain of an 80 years old individual carry an order of 2,000–3,000 sSNVs and 150–200 indels, significantly different from the burden observed in neurons (Ganz et al., 2023).

The mechanisms of somatic mutation in the aging brain are not completely understood and vary between cell types. Recent studies have analyzed the genomic distribution of somatic mutations compared to several genomic co-variables (e.g., transcriptional activity, chromatin accessibility, replication timing, etc). Furthermore, mutation characteristics summarized in what are called signatures, were used to dissect mutation mechanisms. Signatures are spectra of somatic mutations obtained by the type of substitution and the trinucleotide context in the case of sSNVs, and the size, nucleotides affected and presence on repetitive and/or microhomology regions in the case of indels. Signatures are extracted and decomposed from a set of somatic mutations identified in tissue or single-cell genomes and can be fitted to signatures identified in many types of cancer as reported in the Catalogue Of Somatic Mutations In Cancer (COSMIC) (Tate et al., 2019). Such analyses have provided a way to understand the processes underlying somatic mutation in the brain. Analyses of genomic distribution of sSNVs and indels in aging neurons showed that somatic mutation seems to be driven mostly by transcriptional activity. Indeed, both sSNVs and indels were enriched in transcriptionally active functional regions and brain-specific regulatory regions (Lodato et al., 2018; Luquette et al., 2022; Ganz et al., 2023). Furthermore, both sSNVs and indels show highly significant enrichment in neuronal enhancers (Luquette et al., 2022). Mutational signatures identified in neurons resemble COSMIC single base substitution (SBS)5 and SBS89, and indel ID5 and ID8 (Luquette et al., 2022; Ganz et al., 2023). SBS5, ID5 and ID8 are clock-like signatures that accumulate with age independently of cell division, while SBS89 has no clear etiology. Consistent with the idea of neuronal somatic mutation being driven by transcription, the transcription-associated signatures SBS16 and ID4 were also found in aging neurons (Ganz et al., 2023). Recently, we found that oligodendrocytes accumulate mutations due to strikingly different mechanisms compared to neurons in the same brains (summarized in Figure 3). In oligodendrocytes, cell division seems to play an important role, consistent with the replenishment of oligodendrocytes by their precursor cells (OPCs) during the whole postnatal life. Oligodendrocyte sSNVs and indels are overall enriched in inactive genomic regions and although oligodendrocytes display accumulation of signatures also found in neurons such as SBS5, SBS89, ID5 and ID8, signatures specific to oligodendrocytes were identified such as the cell division signature SBS1 and SBS32, and signature ID9, usually found in a large fraction of gliomas and other brain tumors. Coherent with this, oligodendrocyte mutation density profiles across the genome correlated with those of glial-derived tumors (Ganz et al., 2023). Despite the association of neuronal somatic mutation with transcription levels, there is no data so far supporting the enrichment of somatic mutations in specific genes or gene networks and pathways. However, in our recent study we tested specifically cancer-associated genes in oligodendrocytes compared to neurons, and found that oligodendrocyte but not neuronal sSNVs were biased towards cancer-associated genes and even more towards



### Somatic mutation in the aging human brain


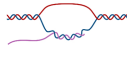


Cell type	Rates (genome/year)		Genomic enrichment	COSMIC signatures		Mechanism
 <b>Neurons</b>	sSNVs	indels	<ul style="list-style-type: none"> <li>Transcriptionally active regions</li> <li>Brain-specific regulatory regions</li> <li>Neuronal enhancers</li> </ul>	sSNVs	indels	 <b>Transcription</b>
	~16-17	~2-3		SBS5 SBS89 SBS16	ID5 ID4 ID8	
 <b>Oligodendrocytes</b>	sSNVs	indels	<ul style="list-style-type: none"> <li>Inactive genomic regions</li> </ul>	sSNVs	indels	 <b>Cell division (OPCs)</b>
	~27	~1-2		SBS5 SBS89 SBS1 SBS32	ID5 ID8 ID9	

FIGURE 3

Somatic mutation in different cell types in the aging human brain. The table summarizes what we have learned so far about somatic mutation in two different cell types (neurons and oligodendrocytes) in the aging human brain (Ganz et al., 2023). Figure created with BioRender.com.

genes mutated in CNS tumors, with the top tumors being oligodendroglioma and pilocytic astrocytoma (Ganz et al., 2023).

Accumulation of somatic mutations in aging brain cells informs on cell-type-specific disease predisposition. As we will see more in depth in the next section, somatic mutation in neurons is linked to neurodegeneration (Miller et al., 2022). In glial cells, however, somatic mutation may play a role in predisposing to tumor insurgence as we become older. A study investigating the burden of clonal somatic mutations in normal human brains found no correlation with age (Ganz et al., 2021). However, another study found that the proportion of brains carrying >100 sSNVs (hypermutable brains) raised with age (Bae et al., 2022). Hypermutability seems to be due to expansions of single or very few clones due to driver mutations that hitchhike all other mutations belonging to the same lineage. Indeed, hypermutable brains were enriched for damaging mutations in genes implicated in cancer (Bae et al., 2022). Since there is very little neuronal turnover in the postnatal brain, such clonal expansions are either congenital or the product of postnatal expansions within the glia lineage. Indeed, an increase in clonal oncogenic somatic mutations was observed in the white matter of the normal human cerebral cortex compared to the adjacent grey matter (Ganz et al., 2021). Despite these observations, contrary to other tissues (Genovese et al., 2014; Martincorena et al., 2015, 2018; Lee-Six et al., 2019; Yokoyama et al., 2019; Moore et al., 2020), oncogenic mutations in the human brain do not seem to increase with age (Ganz et al., 2021), maybe reflecting the fact that brain oncogenic clonal expansions over time can easily result in disease, thus eliminating the individuals carrying such clonal expansions from the control cohorts. It seems however important to underlie that studies conducted until now focused on relatively high VAFs, thus the increase with age of micro-clones carrying oncogenic mutations cannot be excluded at this time.

## Somatic mosaicism in neuropsychiatric and neurodegenerative disorders

Current estimates attribute 5–10% of the missing genetic heritability of more than 100 human disorders to somatic mutations (Yang et al., 2020). Somatic mutations are a known cause of, or have been implicated in several brain disorders from developmental

neuropsychiatric disorders such as focal epilepsy, autism spectrum disorders (ASD) and schizophrenia (SCZ) to neurodegeneration and Alzheimer's disease (AD) (Lim et al., 2015; D'Gama et al., 2017; Lim et al., 2017; Winawer et al., 2018; Baldassari et al., 2019a,b; Rodin et al., 2021; Sherman et al., 2021; Maury et al., 2022; Miller et al., 2022).

In the human genome, exons and areas of open chromatin are particularly vulnerable to somatic mutation during development (Rodin et al., 2021). Pathogenic somatic mutations in the mechanistic target of rapamycin (mTOR) pathway genes can cause focal cortical dysplasia (FCD) spectrum disorders that are associated with pharmaco-resistant epilepsy, such as FCD Type 2, hemimegalencephaly (HME) and tuberous sclerosis complex (TSC). Mutations identified so far cause hyperactivation of the mTOR pathway either through monoallelic gain-of-function (GoF) of an mTOR activator (*AKT3*, *PIK3CA*, *RHEB*, and *MTOR*), or through bi-allelic loss-of-function (LoF) of a repressor (*TSC1/2*, *NPRL2/3*, and *DEPDC5*) often due to a germline mutation followed by a somatic mutation in the second allele of the same gene (Poduri et al., 2012; Lim et al., 2015; D'Gama et al., 2017; Lim et al., 2017; Baldassari et al., 2019a,b; Lee et al., 2021). The mTOR pathway is a main regulator of cell growth and proliferation and indeed its hyperactivation causes hallmarks of the disease such as cortical dyslamination and presence of dysmorphic cells of abnormal size in the brain tissue (Blumcke et al., 2021). FCD mutations are often not found in patients' blood and are thus thought to occur in the brain lineage during cortical development. Although it has been shown that the size of the lesion correlates with the percentage of mutant cells, and that bigger lesions often involve both neurons and glial cells (D'Gama et al., 2017; Baldassari et al., 2019a,b), the exact time in development when FCD somatic mutations occur remains to be elucidated. Few studies have suggested that the excitatory neuron lineage, and especially outer radial glial cells (oRG) in the dorsal forebrain might be majorly affected in FCD (Pollen et al., 2019; Andrews et al., 2020; Chung et al., 2023) however, the exact cell types involved in the disorder pathophysiology remain unclear. Furthermore, even if a clear link between mTOR pathway genes and FCD spectrum disorders has been established, ~50–60% of cases have no clear genetic etiology. Recently, other genes and pathways have been implicated in focal brain malformations, such as genes involved in protein glycosylation (*SLC35A2*) or genes regulating

synaptic function and calcium dynamics (Winawer et al., 2018; Bonduelle et al., 2021).

FCD lesions are often found in extra-temporal locations in the cortex, with FCD type 2 preferentially affecting the frontal lobe (Kabat and Król, 2012) however, mesial temporal lobe epilepsy (MTLE), which is the most common focal epilepsy subtype, originates in the hippocampus (Lamberink et al., 2020). A very recent study addressed somatic mosaicism in this pathology by deep whole-exome sequencing (WES), and found mutations increasing the activity of the Ras/Raf/MAPK pathway in genes such as *PTPN11*, *KRAS*, *SOS1*, *BRAF*, and *NF1*. Such mutations were found in the hippocampus of lesional cases with visible mesial temporal sclerosis (MTS) but were undetectable in the adjacent temporal cortex and in non-lesional MTLEs. Low VAFs (0.8–3.3%) were found in cases without additional lesions such as low-grade epilepsy-associated tumors or FCD, suggesting later developmental occurrence (Khoshkhoo et al., 2022). These findings introduce the possibility of a pathway-specific susceptibility characterizing different brain regions, with the hippocampus being affected by mutations in the Ras/Raf/MAPK pathway and the frontal cortex by mutations in the PI3K/Akt/mTOR pathway. Although this remains purely speculative, we could hypothesize that this pathway-specific susceptibility has to do with the differential transcriptional activity of the two pathways in different brain regions during development or at early postnatal stages.

While developmental focal epilepsies are often monogenic disorders and thus their genetic etiology easier to investigate, the genetics underlying other developmental neuropsychiatric disorders such as ASD and SCZ is more difficult to elucidate due to their complex multigenic nature. Recent studies have shown a contribution of somatic mutations to these disorders (Dou et al., 2017; Krupp et al., 2017; Rodin et al., 2021; Sherman et al., 2021). Analyses of brain deep WGS data revealed an excess of mosaic sSNVs in ASD compared to neurotypical individuals in critical brain enhancers associated with genes specifically expressed in the brain (Rodin et al., 2021). A separate study also showed a significant contribution of large (>4 Mb) CNVs to ASD risk in 0.2% of probands (Sherman et al., 2021). Somatic mutation contribution to SCZ has been explored through deep WGS of purified neuronal populations, which identified two mechanisms contributing specifically to SCZ compared to control neurons, referred to as “*skiogenesis*” (Maury et al., 2022). A significant increase in sSNVs proximal (+/−1 Kb) to the midpoint of active transcription factor binding sites (TFBS) was observed, with enrichment seemingly related to fetal development but not brain-specific. Indeed, sSNV enrichment was seen at sites for many individual transcription factors (TFs) essential for early embryonic, craniofacial, and nervous system development. Signature analyses suggested a first mechanism generating these mutations as a consequence of prenatal oxidative damage that does not get effectively repaired due to TF binding that hinders the DNA repair machinery. A second mechanism was revealed by a 61.8-fold enrichment of CpG>GpG in active TFBS at promoters compared to the expected C>G genome-wide rate. C>G and C>A transversions at CpG sites reflect a footprint of enzymatic demethylation involving the creation of an abasic site through resection of oxidated methyl-cytosine. TF binding may similarly obstruct the repair of abasic sites before replication, thus leading to CpG transversions (Maury et al., 2022).

While developmental neuropsychiatric disorders and/or disorder risk are both associated with somatic mutations shared by multiple

cells (clonal mutations), non-clonal somatic mutations accumulating in aging neurons have been linked to neurodegenerative disorders such as Cockayne Syndrome (CS), Xeroderma Pigmentosum (XP) and AD (Lodato et al., 2018; Miller et al., 2022). CP and XP are caused by defects in DNA damage repair (DDR), and are associated with neurodegeneration and premature aging. Single neuron genomes from post-mortem brains of CS and XP individuals showed ~2.3-fold and ~2.5-fold excess of sSNV compared to age-matched neurotypical neurons, respectively (Lodato et al., 2018). A higher burden of sSNV accumulation during aging was also observed in PFC and hippocampal AD neurons compared to neurotypical controls. A signature showing a pronounced increase in AD compared to control included C>A substitutions associated with oxidative damage to guanine nucleotides and transcription-coupled nucleotide excision repair (TC-NER) deficiency (Jager et al., 2019; Kucab et al., 2019; Alexandrov et al., 2020; Miller et al., 2022). Thus, sSNVs in AD seem to increase due to the accumulation of high levels of inflammation-associated reactive oxygen species (ROS) that overwhelm the TC-NER. Although the exact mechanisms remain to be fully clarified, these studies highlight a clear link that appears to exist between increased burden of somatic mutation in neuronal genomes and neurodegeneration.

## Discussion

Somatic mutations in the human brain genome provide a record of each cell's history that we have started deciphering. While mutations occurring in progenitor cells offer a retrospective forensic lineage tree that describes cell divisions and clone formation (Bizzotto et al., 2021), post-mitotic non-clonal mutations represent a linear timer of the cell's life (Ganz et al., 2023). Recent studies have highlighted how different brain cell types accumulate somatic mutations with specific rates and patterns (Ganz et al., 2023). Further elucidating cell-type-specific rates of somatic mutation will greatly improve our understanding of human brain development but also postnatal cell phylogenies (e.g., glial cell replenishment or postnatal neurogenesis) by combining the unfolding of cell divisions with a temporal dimension of when any two cells split from a common ancestor (Ganz et al., 2023).

We now know that somatic mutations are linked to certain developmental brain pathologies such as FCD, ASD, and SCZ (D'Gama et al., 2017; Baldassari et al., 2019a,b; Rodin et al., 2021; Sherman et al., 2021; Maury et al., 2022). How somatic mutations impact development and brain function in these pathologies remains for the most part unclear. This is due to the limited knowledge of the normal developmental process of the human brain. Elucidating such aspects with further basic studies on the normal building of the clonal architecture of the human brain, including also cell type-specific patterns, will certainly contribute to clarify pathology insurgence. In addition to the developmental consequences of pathogenic mutations, the underlying causes of somatic mutation in these pathologies remain to be explored. Future studies will need to address this question. The same is true for the consequences of mosaic pathogenic mutations compared to their germline counterpart, and how different levels of mosaicism can impact brain function for distinct mutant genes and mutation types.

Recent studies have shown how certain pathological states are associated to increased somatic mutation rates in the human brain and

to disease-specific mechanisms (Lodato et al., 2018; Miller et al., 2022). Although current knowledge seems to suggest that increased somatic mutation in AD is due to oxidative damage due to the disorder, the exact role of increased rates of somatic mutation in neurodegeneration remains unclear, as well as the limit beyond which somatic mutations are not tolerated, thus leading to cell death.

The speed at which new technologies are introduced in the genetics field promises to boost many future studies that will contribute to further decipher human cells and tissues by dissecting the genome at unprecedented resolution. Somatic mutations provide a way of studying directly the human brain starting from available tissue. These studies are nicely complementing what we learn from animal and *in vitro* models by providing information on human brain development, aging, and pathology that is not accessible otherwise.

## Author contributions

The author confirms being the sole contributor of this work and has approved it for publication.

## References

- Abascal, F., Harvey, L. M. R., Mitchell, E., Lawson, A. R. J., Lensing, S. V., Ellis, P., et al. (2021). Somatic mutation landscapes at single-molecule resolution. *Nature* 593, 405–410. doi: 10.1038/s41586-021-03477-4
- Alexandrov, L. B., Kim, J., Haradhvala, N. J., Huang, M. N., Tian Ng, A. W., Wu, Y., et al. (2020). The repertoire of mutational signatures in human cancer. *Nature* 578, 94–101. doi: 10.1038/s41586-020-1943-3
- Andrews, M. G., Subramanian, L., and Kriegstein, A. R. (2020). mTOR signaling regulates the morphology and migration of outer radial glia in developing human cortex. *eLife* 9. doi: 10.7554/eLife.58737
- Ang, E. S. Jr., Haydar, T. F., Gluncic, V., and Rakic, P. (2003). Four-dimensional migratory coordinates of GABAergic interneurons in the developing mouse cortex. *J. Neurosci.* 23, 5805–5815. doi: 10.1523/JNEUROSCI.23-13-05805.2003
- Bae, T., Fasching, L., Wang, Y., Shin, J. H., Suvakov, M., Jang, Y., et al. (2022). Analysis of somatic mutations in 131 human brains reveals aging-associated hypermutability. *Science* 377, 511–517. doi: 10.1126/science.abm6222
- Bae, T., Tomasini, L., Mariani, J., Zhou, B., Roychowdhury, T., Franjic, D., et al. (2018). Different mutational rates and mechanisms in human cells at pregastrulation and neurogenesis. *Science* 359, 550–555. doi: 10.1126/science.aan8690
- Baldassari, S., Picard, F., Verbeek, N. E., van Kempen, M., Brilstra, E. H., Lesca, G., et al. (2019a). The landscape of epilepsy-related GATOR1 variants. *Genet. Med.* 21, 398–408. doi: 10.1038/s41436-018-0060-2
- Baldassari, S., Ribierre, T., Marsan, E., Adle-Biasette, H., Ferrand-Sorbets, S., Bulteau, C., et al. (2019b). Dissecting the genetic basis of focal cortical dysplasia: a large cohort study. *Acta Neuropathol.* 138, 885–900. doi: 10.1007/s00401-019-02061-5
- Bizzotto, S., Dou, Y., Ganz, J., Doan, R. N., Kwon, M., Bohrsen, C. L., et al. (2021). Landmarks of human embryonic development inscribed in somatic mutations. *Science* 371, 1249–1253. doi: 10.1126/science.abe1544
- Bizzotto, S., and Walsh, C. A. (2022). Genetic mosaicism in the human brain: from lineage tracing to neuropsychiatric disorders. *Nat. Rev. Neurosci.* 23, 275–286. doi: 10.1038/s41583-022-00572-x
- Blumcke, I., Coras, R., Busch, R. M., Morita-Sherman, M., Lal, D., Prayson, R., et al. (2021). Toward a better definition of focal cortical dysplasia: an iterative histopathological and genetic agreement trial. *Epilepsia* 62, 1416–1428. doi: 10.1111/epi.16899
- Bohrson, C. L., Barton, A. R., Lodato, M. A., Rodin, R. E., Luquette, L. J., Viswanadham, V. V., et al. (2019). Linked-read analysis identifies mutations in single-cell DNA-sequencing data. *Nat. Genet.* 51, 749–754. doi: 10.1038/s41588-019-0366-2
- Bonduelle, T., Hartlieb, T., Baldassari, S., Sim, N. S., Kim, S. H., Kang, H.-C., et al. (2021). Frequent SLC35A2 brain mosaicism in mild malformation of cortical development with oligodendroglial hyperplasia in epilepsy (MOGHE). *Acta Neuropathol. Commun.* 9.3. doi: 10.1186/s40478-020-01085-3
- Breuss, M. W., Yang, X., Schlachetzki, J. C. M., Antaki, D., Lana, A. J., Xu, X., et al. (2022). Somatic mosaicism reveals clonal distributions of neocortical development. *Nature* 604, 689–696. doi: 10.1038/s41586-022-04602-7
- Chung, C., Yang, X., Bae, T., Vong, K. I., Mittal, S., Donkels, C., et al. (2023). Comprehensive multi-omic profiling of somatic mutations in malformations of cortical development. *Nat. Genet.* 55, 209–220. doi: 10.1038/s41588-022-01276-9
- Coorens, T. H. H., Moore, L., Robinson, P. S., Sanghvi, R., Christopher, J., Hewinson, J., et al. (2021). Extensive phylogenies of human development inferred from somatic mutations. *Nature* 597, 387–392. doi: 10.1038/s41586-021-03790-y
- Coorens, T. H. H., Oliver, T. R. W., Sanghvi, R., Sovio, U., Cook, E., Vento-Tormo, R., et al. (2021). Inherent mosaicism and extensive mutation of human placentas. *Nature* 592, 80–85. doi: 10.1038/s41586-021-03345-1
- D’Gama, A. M., Woodworth, M. B., Hossain, A. A., Bizzotto, S., Hatem, N. E., LaCoursiere, C. M., et al. (2017). Somatic mutations activating the mTOR pathway in dorsal Telencephalic progenitors cause a continuum of cortical Dysplasias. *Cell Rep.* 21, 3754–3766. doi: 10.1016/j.celrep.2017.11.106
- Delgado, R. N., Allen, D. E., Keefe, M. G., Mancia Leon, W. R., Ziffra, R. S., Crouch, E. E., et al. (2022). Individual human cortical progenitors can produce excitatory and inhibitory neurons. *Nature* 601, 397–403. doi: 10.1038/s41586-021-04230-7
- Dou, Y., Kwon, M., Rodin, R. E., Cortes-Ciriano, I., Doan, R., Luquette, L. J., et al. (2020). Accurate detection of mosaic variants in sequencing data without matched controls. *Nat. Biotechnol.* 38, 314–319. doi: 10.1038/s41587-019-0368-8
- Dou, Y., Yang, X., Li, Z., Wang, S., Zhang, Z., Ye, A. Y., et al. (2017). Postzygotic single-nucleotide mosaicism contribute to the etiology of autism spectrum disorder and autistic traits and the origin of mutations. *Hum. Mutat.* 38, 1002–1013. doi: 10.1002/humu.23255
- Ellis, P., Moore, L., Sanders, M. A., Butler, T. M., Brunner, S. F., Lee-Six, H., et al. (2021). Reliable detection of somatic mutations in solid tissues by laser-capture microdissection and low-input DNA sequencing. *Nat. Protoc.* 16, 841–871. doi: 10.1038/s41596-020-00437-6
- Erwin, J. A., Paquola, A. C., Singer, T., Gallina, I., Novotny, M., Quayle, C., et al. (2016). L1-associated genomic regions are deleted in somatic cells of the healthy human brain. *Nat. Neurosci.* 19, 1583–1591. doi: 10.1038/nn.4388
- Evrny, G. D., Cai, X., Lee, E., Hills, L. B., Elhosary, P. C., Lehmann, H. S., et al. (2012). Single-neuron sequencing analysis of L1 retrotransposition and somatic mutation in the human brain. *Cells* 151, 483–496. doi: 10.1016/j.cell.2012.09.035
- Evrny, G. D., Lee, E., Mehta, B. K., Benjamini, Y., Johnson, R. M., Cai, X., et al. (2015). Cell lineage analysis in human brain using endogenous retroelements. *Neuron* 85, 49–59. doi: 10.1016/j.neuron.2014.12.028
- Fasching, L., Jang, Y., Tomasi, S., Schreiner, J., Tomasini, L., Brady, M. V., et al. (2021). Early developmental asymmetries in cell lineage trees in living individuals. *Science* 371, 1245–1248. doi: 10.1126/science.abe0981
- Fujimoto, A., Wong, J. H., Yoshii, Y., Akiyama, S., Tanaka, A., Yagi, H., et al. (2021). Whole-genome sequencing with long reads reveals complex structure and origin of structural variation in human genetic variations and somatic mutations in cancer. *Genome Med.* 13.65. doi: 10.1186/s13073-021-00883-1

## Funding

SB is supported by the Horizon2020 Research and Innovation Program Marie Skłodowska-Curie Actions (MSCA) Individual Fellowship (grant agreement no. 101026484—CODICES).

## Conflict of interest

The author declares that the research was conducted in the absence of any commercial or financial relationships that could be construed as a potential conflict of interest.

## Publisher’s note

All claims expressed in this article are solely those of the authors and do not necessarily represent those of their affiliated organizations, or those of the publisher, the editors and the reviewers. Any product that may be evaluated in this article, or claim that may be made by its manufacturer, is not guaranteed or endorsed by the publisher.



- Ganz, J., Luquette, L. J., Bizzotto, S., Bohrsen, C. L., Jin, H., Miller, M. B., et al. (2023). Contrasting patterns of somatic mutations in neurons and glia reveal differential predisposition to disease in the aging human brain. *bioRxiv* 2023.01.14.523958 doi: 10.1101/2023.01.14.523958
- Ganz, J., Maury, E. A., Becerra, B., Bizzotto, S., Doan, R. N., Kenny, C. J., et al. (2021). Rates and patterns of clonal oncogenic mutations in the normal human brain. *Cancer. Discovery* 12, 172–185. doi: 10.1158/2159-8290.CD-21-0245
- Genovese, G., Kahler, A. K., Handsaker, R. E., Lindberg, J., Rose, S. A., Bakhoum, S. F., et al. (2014). Clonal hematopoiesis and blood-cancer risk inferred from blood DNA sequence. *N. Engl. J. Med.* 371, 2477–2487. doi: 10.1056/NEJMoa1409405
- Gonzalez-Pena, V., Natarajan, S., Xia, Y., Klein, D., Carter, R., Pang, Y., et al. (2021). Accurate genomic variant detection in single cells with primary template-directed amplification. *Proc. Natl. Acad. Sci.* 118:e2024176118. doi: 10.1073/pnas.2024176118
- Huang, A. Y., Li, P., Rodin, R. E., Kim, S. N., Dou, Y., Kenny, C. J., et al. (2020). Parallel RNA and DNA analysis after deep sequencing (PRDD-seq) reveals cell type-specific lineage patterns in human brain. *Proc. Natl. Acad. Sci. U. S. A.* 117, 13886–13895. doi: 10.1073/pnas.2006163117
- Huang, A. Y., Zhang, Z., Ye, A. Y., Dou, Y., Yan, L., Yang, X., et al. (2017). Mosaic hunter: accurate detection of postzygotic single-nucleotide mosaicism through next-generation sequencing of unpaired, trio, and paired samples. *Nucleic Acids Res.* 45:e76. doi: 10.1093/nar/gkx024
- Jager, M., Blokzijl, F., Kuijk, E., Bertl, J., Vougioukalaki, M., Janssen, R., et al. (2019). Deficiency of nucleotide excision repair is associated with mutational signature observed in cancer. *Genome Res.* 29, 1067–1077. doi: 10.1101/gr.246223.118
- Jenko Bizjan, B., Katsila, T., Tesovnik, T., Sket, R., Debeljak, M., Matsoukas, M. T., et al. (2020). Challenges in identifying large germline structural variants for clinical use by long read sequencing. *Comput. Struct. Biotechnol. J.* 18, 83–92. doi: 10.1016/j.csbj.2019.11.008
- Kabat, J., and Król, P. (2012). Focal cortical dysplasia - review. *Pol. J. Radiol.* 77, 35–43. doi: 10.12659/PJR.882968
- Kennedy, S. R., Schmitt, M. W., Fox, E. J., Kohn, B. F., Salk, J. J., Ahn, E. H., et al. (2014). Detecting ultralow-frequency mutations by duplex sequencing. *Nat. Protoc.* 9, 2586–2606. doi: 10.1038/nprot.2014.170
- Khoshkhou, S., Wang, Y., Chahine, Y., Erson-Omay, E. Z., Robert, S., Kiziltug, E., et al. (2022). Somatic Ras/Raf/MAPK variants enriched in the Hippocampus in drug-resistant mesial temporal lobe epilepsy. *medRxiv* 2022.12.23.22283854 doi: 10.1101/2022.12.23.22283854
- Koboldt, D. C., Miller, K. E., Miller, A. R., Bush, J. M., McGrath, S., Leraas, K., et al. (2021). PTEN somatic mutations contribute to spectrum of cerebral overgrowth. *Brain* 144, 2971–2978. doi: 10.1093/brain/awab173
- Krupp, D. R., Barnard, R. A., Duffourd, Y., Evans, S. A., Mulqueen, R. M., Bernier, R., et al. (2017). Exonic somatic mutations contribute risk for autism spectrum disorder. *Am. J. Hum. Genet.* 101, 369–390. doi: 10.1016/j.ajhg.2017.07.016
- Kucab, J. E., Zou, X., Morganello, S., Joel, M., Nanda, A. S., Nagy, E., et al. (2019). A compendium of mutational signatures of environmental agents. *Cells* 177, 821–836.e16. doi: 10.1016/j.cell.2019.03.001
- Lamberink, H. J., Otte, W. M., Blumcke, I., Braun KPJ, European Epilepsy Brain Bank writing group et al. (2020). Seizure outcome and use of antiepileptic drugs after epilepsy surgery according to histopathological diagnosis: a retrospective multicentre cohort study. *Lancet Neurol.* 19, 748–757. doi: 10.1016/S1474-4422(20)30220-9
- Lee, W. S., Baldassari, S., Chipaux, M., Adle-Biassette, H., Stephenson, S. E. M., Maixner, W., et al. (2021). Gradient of brain mosaic RHEB variants causes a continuum of cortical dysplasia. *Ann. Clin. Transl. Neurol.* 8, 485–490. doi: 10.1002/actn.3.1286
- Lee-Six, H., Olafsson, S., Ellis, P., Osborne, R. J., Sanders, M. A., Moore, L., et al. (2019). The landscape of somatic mutation in normal colorectal epithelial cells. *Nature* 574, 532–537. doi: 10.1038/s41586-019-1672-7
- Lim, J. S., Gopalappa, R., Kim, S. H., Ramakrishna, S., Lee, M., Kim, W. I., et al. (2017). Somatic mutations in TSC1 and TSC2 cause focal cortical dysplasia. *Am. J. Hum. Genet.* 100, 454–472. doi: 10.1016/j.ajhg.2017.01.030
- Lim, J. S., Kim, W. I., Kang, H. C., Kim, S. H., Park, A. H., Park, E. K., et al. (2015). Brain somatic mutations in MTOR cause focal cortical dysplasia type II leading to intractable epilepsy. *Nat. Med.* 21, 395–400. doi: 10.1038/nm.3824
- Lim, E. T., Uddin, M., De Rubeis, S., Chan, Y., Kamumbu, A. S., Zhang, X., et al. (2017). Rates, distribution and implications of postzygotic mosaic mutations in autism spectrum disorder. *Nat. Neurosci.* 20, 1217–1224. doi: 10.1038/nn.4598
- Lodato, M. A., Rodin, R. E., Bohrsen, C. L., Coulter, M. E., Barton, A. R., Kwon, M., et al. (2018). Aging and neurodegeneration are associated with increased mutations in single human neurons. *Science* 359, 555–559. doi: 10.1126/science.aao4426
- Lodato, M. A., Woodworth, M. B., Lee, S., Evrony, G. D., Mehta, B. K., Karger, A., et al. (2015). Somatic mutation in single human neurons tracks developmental and transcriptional history. *Science* 350, 94–98. doi: 10.1126/science.aab1785
- Luquette, L. J., Miller, M. B., Zhou, Z., Bohrsen, C. L., Zhao, Y., Jin, H., et al. (2022). Single-cell genome sequencing of human neurons identifies somatic point mutation and indel enrichment in regulatory elements. *Nat. Genet.* 54, 1564–1571. doi: 10.1038/s41588-022-01180-2
- Macaulay, I. C., Haerty, W., Kumar, P., Li, Y. I., Hu, T. X., Teng, M. J., et al. (2015). G & T-seq: parallel sequencing of single-cell genomes and transcriptomes. *Nat. Methods* 12, 519–522. doi: 10.1038/nmeth.3370
- Martincorena, I., Fowler, J. C., Wabik, A., Lawson, A. R. J., Abascal, F., Hall, M. W. J., et al. (2018). Somatic mutant clones colonize the human esophagus with age. *Science* 362, 911–917. doi: 10.1126/science.aau3879
- Martincorena, I., Roshan, A., Gerstung, M., Ellis, P., Van Loo, P., McLaren, S., et al. (2015). Tumor evolution. High burden and pervasive positive selection of somatic mutations in normal human skin. *Science* 348, 880–886. doi: 10.1126/science.aaa6806
- Maury, E. A., Jones, A., Seplyarskiy, V., Rosenbluh, C., Bae, T., Wang, Y., et al. (2022). Enrichment of somatic mutations in schizophrenia brain targets prenatally active transcription factor bindings sites. *bioRxiv* 2022.02.23.481681 doi: 10.1101/2022.02.23.481681
- Miller, M. B., Huang, A. Y., Kim, J., Zhou, Z., Kirkham, S. L., Maury, E. A., et al. (2022). Somatic genomic changes in single Alzheimer's disease neurons. *Nature* 604, 714–722. doi: 10.1038/s41586-022-04640-1
- Moore, L., Leongamornlert, D., Coorens, T. H. H., Sanders, M. A., Ellis, P., Dentre, S. C., et al. (2020). The mutational landscape of normal human endometrial epithelium. *Nature* 580, 640–646. doi: 10.1038/s41586-020-2214-z
- Nam, A. S., Kim, K. T., Chaligne, R., Izzo, F., Ang, C., Taylor, J., et al. (2019). Somatic mutations and cell identity linked by genotyping of transcriptomes. *Nature* 571, 355–360. doi: 10.1038/s41586-019-1367-0
- Poduri, A., Evrony, G. D., Cai, X., Elhosary, P. C., Beroukhi, R., Lehtinen, M. K., et al. (2012). Somatic activation of AKT3 causes hemispheric developmental brain malformations. *Neuron* 74, 41–48. doi: 10.1016/j.neuron.2012.03.010
- Pollen, A. A., Bhaduri, A., Andrews, M. G., Nowakowski, T. J., Meyerson, O. S., Mostajo-Radji, M. A., et al. (2019). Establishing cerebral organoids as models of human-specific brain evolution. *Cells* 176, 743–756.e17. doi: 10.1016/j.cell.2019.01.017
- Rodin, R. E., Dou, Y., Kwon, M., Sherman, M. A., D'Gama, A. M., Doan, R. N., et al. (2021). The landscape of somatic mutation in cerebral cortex of autistic and neurotypical individuals revealed by ultra-deep whole-genome sequencing. *Nat. Neurosci.* 24:611. doi: 10.1038/s41593-021-00830-8
- Rudy, B., Fishell, G., Lee, S., and Hjerling-Leffler, J. (2011). Three groups of interneurons account for nearly 100% of neocortical GABAergic neurons. *Dev. Neurobiol.* 71, 45–61. doi: 10.1002/dneu.20853
- Schmitt, M. W., Kennedy, S. R., Salk, J. J., Fox, E. J., Hiatt, J. B., and Loeb, L. A. (2012). Detection of ultra-rare mutations by next-generation sequencing. *Proc. Natl. Acad. Sci. U. S. A.* 109, 14508–14513. doi: 10.1073/pnas.1208715109
- Sherman, M. A., Rodin, R. E., Genovese, G., Dias, C., Barton, A. R., Mukamel, R. E., et al. (2021). Large mosaic copy number variations confer autism risk. *Nat. Neurosci.* 24, 197–203. doi: 10.1038/s41593-020-00766-5
- Spits, C., Le Caignec, C., De Rycke, M., Van Haute, L., Van Steirteghem, A., Liebaers, I., et al. (2006). Whole-genome multiple displacement amplification from single cells. *Nat. Protoc.* 1, 1965–1970. doi: 10.1038/nprot.2006.326
- Tate, J. G., Bamford, S., Jubb, H. C., Sondka, Z., Beare, D. M., Bindal, N., et al. (2019). COSMIC: the catalogue of somatic mutations in Cancer. *Nucleic Acids Res.* 47, D941–D947. doi: 10.1093/nar/gky1015
- Townsend, S. E., Westfall, J. J., Navarro, J. B., Koboldt, D. C., Mardis, E. R., Miller, K. E., et al. (2023). Single-nuclei transcriptomics enable detection of somatic variants in patient brain tissue. *Sci. Rep.* 13:527. doi: 10.1038/s41598-023-27700-6
- Wang, Y., Bae, T., Thorpe, J., Sherman, M. A., Jones, A. G., Cho, S., et al. (2021). Comprehensive identification of somatic nucleotide variants in human brain tissue. *Genome Biol.* 22:92. doi: 10.1186/s13059-021-02285-3
- Winawer, M. R., Griffin, N. G., Samanamud, J., Baugh, E. H., Rathakrishnan, D., Ramalingam, S., et al. (2018). Somatic SLC35A2 variants in the brain are associated with intractable neocortical epilepsy. *Ann. Neurol.* 83, 1133–1146. doi: 10.1002/ana.25243
- Xing, D., Tan, L., Chang, C. H., Li, H., and Xie, X. S. (2021). Accurate SNV detection in single cells by transposon-based whole-genome amplification of complementary strands. *Proc. Natl. Acad. Sci. U. S. A.* 118:e2013106118. doi: 10.1073/pnas.2013106118
- Yang, X., Xu, X., Breuss, M. W., Antaki, D., Ball, L. L., Chung, C., et al. (2023). Control-independent mosaic single nucleotide variant detection with deep mosaic. *Nat. Biotechnol.* doi: 10.1038/s41587-022-01559-w
- Yang, X., Yang, C., Zheng, X., Xiong, L., Tao, Y., Wang, M., et al. (2020). Mosaic base: a knowledgebase of postzygotic mosaic variants in noncancer disease-related and healthy human individuals. *Genomics Proteomics Bioinformatics* 18, 140–149. doi: 10.1016/j.gpb.2020.05.002
- Ye, A. Y., Dou, Y., Yang, X., Wang, S., Huang, A. Y., and Wei, L. (2018). A model for postzygotic mosaicism quantifies the allele fraction drift, mutation rate, and contribution to de novo mutations. *Genome Res.* 28, 943–951. doi: 10.1101/gr.230003.117
- Yokoyama, A., Kakiuchi, N., Yoshizato, T., Nannya, Y., Suzuki, H., Takeuchi, Y., et al. (2019). Age-related remodelling of oesophageal epithelia by mutated cancer drivers. *Nature* 565, 312–317. doi: 10.1038/s41586-018-0811-x





## OPEN ACCESS

## EDITED BY

Esther Klingler,  
University of Geneva, Switzerland

## REVIEWED BY

Ricardo Scott,  
University of Alicante, Spain  
Yang Hui,  
Northwestern Polytechnical University, China

## \*CORRESPONDENCE

Adrien Roux  
✉ adrien.roux@hesge.ch

RECEIVED 19 March 2023

ACCEPTED 09 May 2023

PUBLISHED 15 June 2023

## CITATION

Loussert-Fonta C, Stoppini L,  
Neuenschwander Y, Righini O, Prim D,  
Schmidt C, Heuschkel MO, Gomez Baisac L,  
Jović M, Pfeifer ME, Extermann J and Roux A  
(2023) Opening the black box of traumatic  
brain injury: a holistic approach combining  
human 3D neural tissue and an *in vitro*  
traumatic brain injury induction device.  
*Front. Neurosci.* 17:1189615.  
doi: 10.3389/fnins.2023.1189615

## COPYRIGHT

© 2023 Loussert-Fonta, Stoppini,  
Neuenschwander, Righini, Prim, Schmidt,  
Heuschkel, Gomez Baisac, Jović, Pfeifer,  
Extermann and Roux. This is an open-access  
article distributed under the terms of the  
[Creative Commons Attribution License \(CC BY\)](https://creativecommons.org/licenses/by/4.0/).  
The use, distribution or reproduction in other  
forums is permitted, provided the original  
author(s) and the copyright owner(s) are  
credited and that the original publication in this  
journal is cited, in accordance with accepted  
academic practice. No use, distribution or  
reproduction is permitted which does not  
comply with these terms.

# Opening the black box of traumatic brain injury: a holistic approach combining human 3D neural tissue and an *in vitro* traumatic brain injury induction device

Céline Loussert-Fonta<sup>1</sup>, Luc Stoppini<sup>1</sup>, Yoan Neuenschwander<sup>2</sup>,  
Ophélie Righini<sup>3</sup>, Denis Prim<sup>3</sup>, Cédric Schmidt<sup>2</sup>,  
Marc O. Heuschkel<sup>1</sup>, Loris Gomez Baisac<sup>1</sup>, Milica Jović<sup>3</sup>,  
Marc E. Pfeifer<sup>3</sup>, Jérôme Extermann<sup>2</sup> and Adrien Roux<sup>1\*</sup>

<sup>1</sup>Tissue Engineering Laboratory, HEPIA HES-SO University of Applied Sciences and Arts Western Switzerland, Geneva, Switzerland, <sup>2</sup>Micro-Nanotechnology Group, HEPIA HES-SO University of Applied Sciences and Arts Western Switzerland, Geneva, Switzerland, <sup>3</sup>Diagnostic Systems Research Group, Institute of Life Technologies, School of Engineering, University of Applied Sciences and Arts Western Switzerland (HES-SO Valais-Wallis), Sion, Switzerland

Traumatic brain injury (TBI) is caused by a wide range of physical events and can induce an even larger spectrum of short- to long-term pathophysiological changes. Neuroscientists have relied on animal models to understand the relationship between mechanical damages and functional alterations of neural cells. These *in vivo* and animal-based *in vitro* models represent important approaches to mimic traumas on whole brains or organized brain structures but are not fully representative of pathologies occurring after traumas on human brain parenchyma. To overcome these limitations and to establish a more accurate and comprehensive model of human TBI, we engineered an *in vitro* platform to induce injuries via the controlled projection of a small drop of liquid onto a 3D neural tissue engineered from human iPS cells. With this platform, biological mechanisms involved in neural cellular injury are recorded through electrophysiology measurements, quantification of biomarkers released, and two imaging methods [confocal laser scanning microscope (CLSM) and optical projection tomography (OPT)]. The results showed drastic changes in tissue electrophysiological activities and significant releases of glial and neuronal biomarkers. Tissue imaging allowed us to reconstruct the injured area spatially in 3D after staining it with specific nuclear dyes and to determine TBI resulting in cell death. In future experiments, we seek to monitor the effects of TBI-induced injuries over a prolonged time and at a higher temporal resolution to better understand the subtleties of the biomarker release kinetics and the cell recovery phases.

## KEYWORDS

traumatic brain injury, optical projection tomography, 3D neural tissue, multiplex protein assays, biomarkers, electrophysiology, *in vitro* model

## Introduction

Traumatic brain injury (TBI) is the leading cause of mortality in young adults and a significant cause of death and disability across all countries, especially in low- and middle-income countries (Maas et al., 2017; Dewan et al., 2019; Schweitzer et al., 2019). TBI occurs when an external mechanical force is applied to the brain, possibly leading to permanent or temporary impairment of cognitive and physical functions. The severity of the trauma has been classified using the Glasgow Coma Scale (GCS). GCS scores of 13–15 represent mild brain injuries, 9–12 are moderate, and 3–8 are severe (Schweitzer et al., 2019). A recent report estimated the global incidence of all-severity and all-cause TBI at 939 cases per 100,000 people, representing 69 million worldwide. Mild TBI (mTBI) represents 740 cases per 100,000 people, representing 55.9 million people annually (Dewan et al., 2019). The spectrum of symptoms experienced by mTBI patients is vast, ranging from a slight headache to loss of consciousness (<30 min) and even post-traumatic amnesia (<24 h) (Blyth and Bazarian, 2010). At the brain tissue level, the impact leads to short-term primary injuries characterized by structural damages to blood–brain barrier (Cash and Theus, 2020), axonal injury (Tang-Schomer et al., 2012; Johnson et al., 2013), and microglial activation and microhemorrhages (Oppenheimer, 1968). Secondary injuries might develop over minutes to months after the primary lesions and are catalyzed by excessive excitatory neurotransmitter release and calcium influx, leading to apoptotic cell death or/and even early onset of neurodegenerative diseases, which can induce, in the long term, neurodegenerative diseases (Bramlett and Dietrich, 2015; Ng and Lee, 2019; Jarrahi et al., 2020; Dodd et al., 2022).

Despite the increasing awareness about the possible long-term damaging effects of mTBI, improvements in diagnosis and treatment are still insufficient. This concern is mainly due to the limited understanding of the primary and secondary injury mechanisms contributing to long-term sequels (Liaudanskaya et al., 2020). Therefore, to better understand the physiopathology of this type of trauma, various models have been developed, which mainly involve rodents or rodent tissues and can be categorized based on the type of injury sustained (focal or diffuse lesion) or the technique used (such as closed-skull weight drop or lateral fluid impact injury) (Kabadi et al., 2010; Arun et al., 2011; Morrison et al., 2011; Osier and Dixon, 2016). However, these models' lack of control over internal tissue and cell-level biomechanics may exacerbate animal-to-animal variability and do not fully illustrate human physiopathology (Azkona and Sanchez-Pernaut, 2022). Recent technological advancements have allowed the creation of 3D brainlike structures called cerebral organoids (Chiaradia and Lancaster, 2020), which resemble the cellular and anatomical composition of different regions of the human brain and can mimic disease pathways (Lancaster et al., 2013; Mariani et al., 2015; Garcez et al., 2016; Pollen et al., 2019; Velasco et al., 2019). Human brain organoids are becoming an emerging tool in TBI and mTBI as they provide a window into the injured tissues after trauma (Jgamadze et al., 2020; Ramirez et al., 2021a,b) and over time into the chronic phase of injury (Silvosa et al., 2022).

In this study, we developed an *in vitro* platform, termed “*in vitro* TBI,” inducing injury by a finely tunable (velocity and force) expulsion of liquid using a microvalve onto bioengineered human 3D neural tissues. In addition, we propose a correlative workflow to characterize in detail the traumatic area by combining electrical monitoring, imaging [confocal microscopy and optical projection tomography (OPT)], and circulating biomarkers analysis by multiplex assays (Jović et al., 2022).

With this approach, we could evaluate the significant changes occurring after the impact, such as electrophysiological dysregulation, tissue damage and loss, and temporal releases of multiple biomarkers. As a perspective, we hope to monitor TBI and mTBI with a higher temporal resolution to understand better the exact biomarker release kinetics and the tissue recovery processes. The ultimate objective was to design a rapid and sensitive diagnostic tool for mTBI and support the development of therapeutic and potentially neuroprotective agents while identifying appropriate dosing and toxicity levels.

## Materials and methods

### 3D neural tissue generation

Neural stem cells derived from induced pluripotent stem cells (NSChIPSC) (#A3890101 Thermo Fisher) were seeded with a density of 25,000 cells/cm<sup>2</sup> in six-well plates and processed for the generation of 3D neural tissue according to the protocol previously described in Govindan et al. (2021). For all the experiments, 1-year-old 3D neural tissues were used.

### TBI-induction platform: description and parameters

The developed instrument platform is based on a microvalve (#SMLD 300G, Fritz Gyger AG) that creates impacts on the neural tissue with either sterile air or culture medium. The microvalve is supplied with a continuous flow of compressed air (5 bars). The microvalve is mounted on a manual translation stage (#LT1, Thorlabs Inc.), which was fixed on an inverted microscope (#Axiovert 25, Zeiss). The position of the targeted 3D neural tissue, positioned on a Multi-Electrode Array (MEA) biochip or 24- or 96-well microplates, is reached due to an XY translation stage that is attached to the microscope's plate. This overall system allows to perform precise injuries on the targeted sample (Figure 1 and Supplementary Figure 1). In addition, we have developed a dedicated protocol to sterilize the entire system of the ejection of culture medium allowing the follow-up of the traumatized neural tissues during several days.

The microvalve is controlled by a programmable logic controller (#VC Mini, Fritz Gyger AG), and software (#MVC, Fritz Gyger AG) that allows the setting of the different parameters: Open time = the amount of time the microvalve is open; Cycle time = the total time required for one shot (ejection of culture medium or air); number of cycles = number of shots; the peak current = current that goes through the coil; and finally, the peak time =

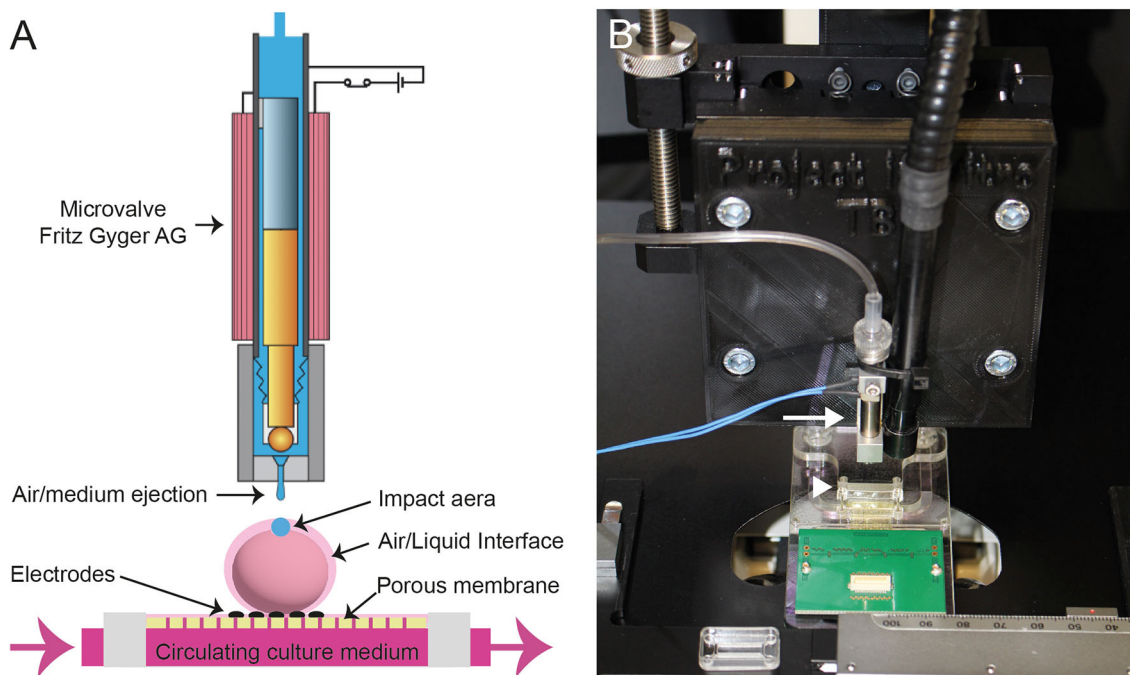


FIGURE 1

(A) Scheme of the Fritz Gyger microvalve (modified with the accord of Fritz Gyger AG) ejecting a drop of culture medium on a 3D neural tissue placed onto a porous Multi-Electrode Array (MEA) biochip. (B) Picture showing the microvalve (white arrow) attached to an XYZ translation stage mounted on an inverted microscope. The MEA is indicated with a white arrowhead.

time for which the valve is driven with an increased current for an instantaneous opening and corresponds to the time taken for the valve to open fully. For the experiments described in this work, we have used the following parameters: the open time was set at 1 ms and the cycle time at 100 ms with single shots.

## Electrophysiology data acquisition system and brain tissue interface

3D neural tissues used in this work were also monitored electrically to track the functional effect of mTBI. To interface the 3D neural tissue with recording electrodes, proprietary 32-channel MEA biochips and data acquisition systems have been used. MEA biochips were specifically adapted to allow air–liquid interface culture of the 3D neural tissue, providing optimal conditions for long-term tissue survival. MEA biochips were made of porous membranes incorporating thin film recording microelectrodes on which the 3D neural tissues are placed onto. A fluidic chamber below the membrane allows to feed the tissue with a culture medium sucked by capillary forces, thus allowing the tissue to remain supplied and humidified while staying at the air–liquid interface on the top of the membrane.

The MEA biochips were made of four microfabricated polyimide membrane strips (thickness of  $8\ \mu\text{m}$  and an equivalent porosity of 10% of the working area achieved by holes of  $\varnothing\ 7.5\ \mu\text{m}$  on a  $20\text{-}\mu\text{m}$  grid) that incorporate eight low-impedance platinum black electrodes ( $\varnothing\ 30\ \mu\text{m}$ , located on a  $200\text{-}\mu\text{m}$  grid, impedance below  $100\ \text{k}\Omega$  at  $1\ \text{kHz}$ ) in each. These strips were mounted using

conductive glue onto a printed circuit board that allows connection to external signal amplification and data acquisition electronics. The fluidic chamber below the membranes was made of several layers of laser-cut poly(methyl)methacrylate parts assembled using adhesive transfer tape (#467MP, 3M). The MEA biochips have been described previously (Ferlauto et al., 2018; Wertenbroek et al., 2021).

The functional neural electrical activity was amplified using two 16-channel Digital Electrophysiology Stimulator/Amplifier Chips (#RHS2116, Intan technologies), and data were acquired, displayed, and saved using the proprietary “Spike-on-Chip” platform (Wertenbroek et al., 2021). Data pre-analysis was performed using the Spike-on-Chip software, and home-made software was used to generate spike raster plots and signal figures from the acquired data.

## Electrophysiology experimental protocol

The 3D neural tissues sitting on a perforated Sterile Hydrophilic PTFE membrane of 2 mm diameter (named as confetti) (PTFE-005, HEPIA Biosciences) were plated onto porous MEA Biochips comprising four independent recording areas (Figure 2). The experiments were performed in triplicates to reach a total of 12 injured tissues analyzed. The selection of the 3D neural tissues was based on the number of active electrodes showing spontaneous activities with spike frequency  $> 0.1\ \text{Hz}$  before the induction of the trauma (at least present on 20–25 electrodes out of the total 32 electrodes). In total, eight electrodes were in direct contact with



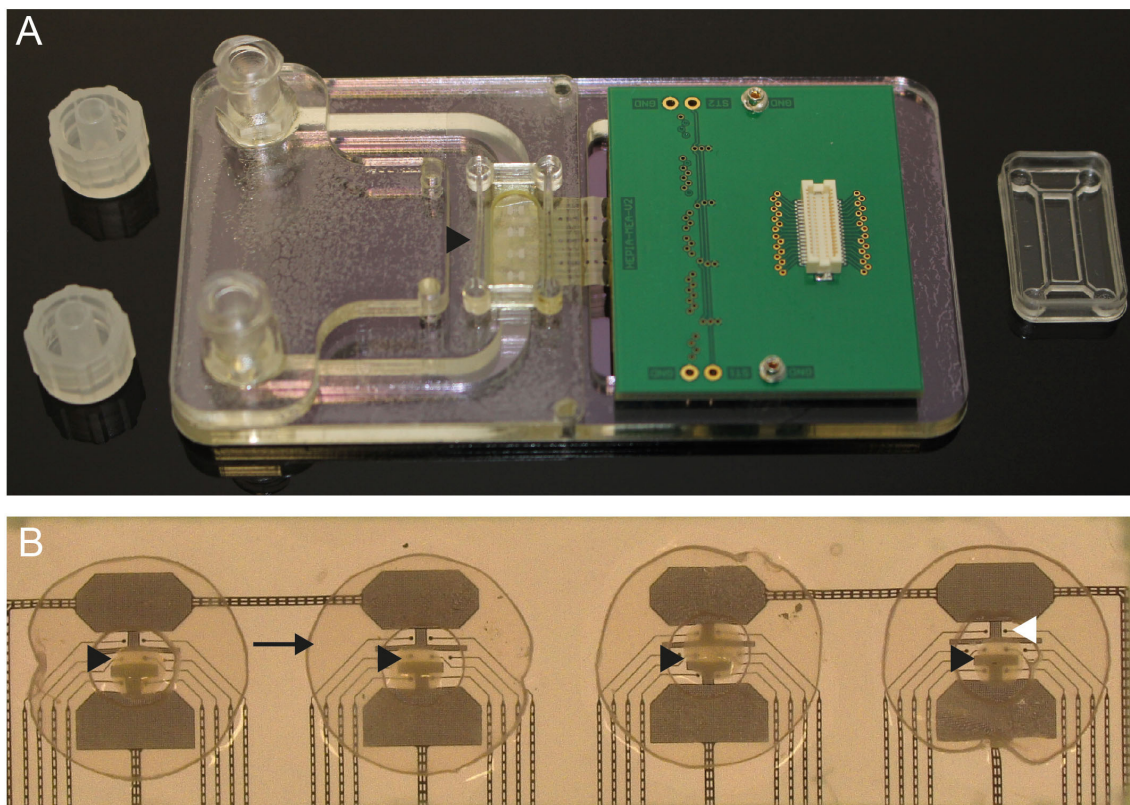


FIGURE 2

(A) Photo of the porous MEA where the black arrowhead shows the position of the recording chamber. (B) Close-up view of an MEA biochip where each of the four 3D neural tissues (black arrowheads) are placed onto four areas of eight recording electrodes (white arrowhead). The tissues are stabilized by a perforated "confetti" (black arrow).

each 3D neural tissue, and continuous acquisition and analyses of neural activities were performed using the Spike-on-Chips software. Recording of the spontaneous activity was started after 2 or 3 days to allow the activity of the neural networks to be stable. Control recordings were performed during 10–15 min within the incubator before the induction of the trauma. The MEA biochips were then transferred within the TBI-induction platform, and a single ejection of sterile culture medium was applied for each 3D neural tissue. MEA biochips were then put back into the incubator, and post-trauma recording of spontaneous activities was performed immediately and after 1 h, 24 h, and 48 h (10 min per recording). After the inductions of the traumas, we controlled that the tissues were always in the same position on the MEAs. Furthermore, to ensure that any changes in electrophysiological activity were the result of the trauma induction, we conducted "sham" experiments using the same protocol, e.g., the neural tissue samples were removed from the incubator and allowed to rest on the TBI-induction platform for 2 min without inducing trauma. A total of 12 control neural tissues were analyzed.

## Protein multiplex immunoassay materials

Antigens and antibodies were purchased from HyTest Ltd. Antigen GFAP human recombinant (#8G45); monoclonal

mouse anti-human glial fibrillary acidic protein (#4G25) clone 83cc (capture antibody) and clone 81cc (detection antibody); antigen FABP human (#8F65), monoclonal mouse anti-human fatty acid-binding protein (#4F29) clone 28cc (capture antibody) and clone 22 (detection antibody); antigen S100BB homodimer and S100A1B heterodimer human (#8S9h); monoclonal mouse anti-human S100 proteins (#4S37) clone 8B10cc (capture antibody) and clone 6G1cc (detection antibody).

Tau biomarker: Human Tau (total) Calibrator [#C018D-2, Meso Scale Discovery (MSD)]; biotin human Tau Antibody (#C21AGT-3, MSD) and SULFO-TAG anti-human Tau antibody (#D21AGT-3, MSD) were employed as capture and detection antibody, respectively.

## Sample preparation for immunoassays

Before the injury, the 3D neural tissues were individually placed inside the wells of a 24-well plate in a 200  $\mu$ l culture medium. Immediately before the injury and 2 h and 4 h after the injury, the conditioned culture medium was collected and replaced by a fresh one. After collection, the conditioned culture medium was frozen and stored at  $-20^{\circ}\text{C}$  until further processing.



## Protein multiplex immunoassay method

Conditions of the immunoassays: The antigen biomarkers, the samples, and the detection antibodies were diluted in 50 mM Tris with 0.1% BSA and 1 mM  $\text{CaCl}_2$ . The blocking solution for the singleplex assay contained 1% BSA and 1 mM  $\text{CaCl}_2$  in PBS 1X.

Protein Multiplex assay: The MSD U-PLEX Development Packs protocol was followed. The biotinylated capture antibodies of h-FABP, GFAP, and S100 $\beta$  were diluted 10 times in the same tube (0.286  $\mu\text{g/ml}$ ) with the U-PLEX Stop solution. The U-PLEX provided plate was coated with 50  $\mu\text{l}$  of capture antibody mix solution and incubated for 1 h at room temperature (RT) and 700 rpm. Then, the wells were washed with wash buffer (3x 300  $\mu\text{l}$  of PBS 1x with 0.06% Tween-20), and the mixture of antigen biomarkers or the samples or blank solutions (50  $\mu\text{l}$ ), respectively, were added to the wells and incubated (1 h, RT, 700 rpm). After the second washing step (3x 300  $\mu\text{l}$ ), 50  $\mu\text{l}$  of the detection antibody mixture was added and incubated (1 h, RT, 700 rpm). After the final washing step (6x 300  $\mu\text{l}$ ), 150  $\mu\text{l}$  of read buffer B was added to initiate the signal generation and read-out process (MESO QuickPlex SQ 120, MSD).

Singleplex assay: The MSD R-PLEX Antibody Set Singleplex assay protocol was followed. The GOLD 96-well Small Spot Streptavidin plate (Mesoscale, L45SA-1) was coated with 25  $\mu\text{l}$  of Tau biotinylated capture antibody (200  $\mu\text{l}$  diluted in 3.3 ml of PBS 1X) and incubated for 1 h at RT and 700 rpm. Then, the wells were washed with wash buffer (3x 150  $\mu\text{l}$  of PBS 1X with 0.06% Tween-20), 150  $\mu\text{l}$  of blocking solution was added to the wells, and the plate was incubated (1 h, RT, 700 rpm). The Human Tau Calibrator or the samples and blank solutions (50  $\mu\text{l}$ ) were added to the wells and incubated (1 h, RT, 700 rpm). After the third washing step (3x 150  $\mu\text{l}$ ), 50  $\mu\text{l}$  of the detection antibody was added and incubated (1 h, RT, 700 rpm). After the final washing step (4x 150  $\mu\text{l}$ ), 150  $\mu\text{l}$  of read buffer T 2X was added to initiate the signal generation and read-out process (MESO QuickPlex SQ 120, MSD).

Additional products description and methods are provided in the [Supplementary material](#) “Multiplex immunoassay materials” and “Multiplex immunoassay methods.”

## Sample preparation for imaging

Before the injury, the 3D neural tissues were individually placed inside the well of a 24-well plate in a 200  $\mu\text{l}$  culture medium. After the injury, the tissues were incubated for 2 h in a fresh culture medium containing Hoechst 33342 (#H3570, Invitrogen) and Propidium Iodide (PI) (#P5066, Invitrogen). After the staining, 3D neural tissues are fixed in 4% paraformaldehyde for 30 min at RT then washed in phosphate-buffered saline. For optimal imaging, all the samples are cleared by incubation in RapiClear 1.47 (SunJin Lab) for 2 days at RT. The samples were imaged directly within fresh clearing solution by confocal microscopy or embedded in 1% agarose aqueous solution within fluorinated ethylene propylene tubes for OPT. For the latter, the agarose was solidified on ice to limit the rehydration of the tissue and the reversibility of the clearing process. Intact 3D neural tissue was used as negative control and dead 3D neural tissue, e.g., chemically

killed by immersion in 4% paraformaldehyde for 12 h was used as positive control. All control samples were processed identically as described previously.

## Confocal imaging

All confocal images of 3D neural tissue were acquired with a TCS SPE microscope (Leica) equipped with an ACS APO 10X 0.3 NA dry objective using Leica LAS  $\times$  software (Leica). A 405-nm laser was used to excite Hoechst 33342 staining agent (all cell's nuclei), while a 532-nm laser was used to excite PI staining (dead cell nucleus). Z stacks were acquired with a voxel depth of 2.4  $\mu\text{m}$  and an average of 40 sections. In these conditions, the acquisition time was approximately 650 s. All the images are processed using Fiji software.

## 3D projection tomography and analysis

3D imaging was performed using OPT. The setup presented by [Schmidt et al. \(2021\)](#) was adapted to distinguish dead from healthy cells inside the 3D neural tissue. The optical lens was replaced with a commercial telecentric lens (#63-738, Edmund) providing 8  $\mu\text{m}$  spatial resolution. Hoechst staining of all nuclei was excited at 415 nm and acquired between 480 nm and 520 nm using a bandpass filter while PI staining of dead cells' nuclei was excited at 530 nm and acquired beyond 600 nm. The samples were imaged in the water acting as a refractive index matcher using a CMOS camera (#Chameleon3, Flir). Acquisition times for each sample were shorter than 180 s per spectral channel. Supplementary corrections have been implemented in the reconstruction algorithm to take residual mechanical instabilities ([Lu and Mackie, 2002](#)) and refractive index artifacts ([Liu et al., 2022](#)) into account.

3D visualization and data analysis were performed using the open-source 3D ImageJ Suite software ([Ollion et al., 2013](#)). The volumes of the 3D neural tissues were calculated by applying a threshold at 2% of the maximum pixel value and counting the number of voxels above it. The mean diameter of each organoid was deduced from volume assuming spherical geometries. The ratios of dead cells' nuclei into the tissues were calculated for each 3D neural tissue by isolating and counting the cells' nuclei from the two 3D images of the Hoechst and PI staining. We first applied a 3D Gaussian blur filter with a two-voxel kernel to denoise the signal and then used the 3D Maxima Finder plugin with a radius parameter of three voxels to identify the nucleus coordinates. The colocalization of peaks between the two channels was estimated using the 3D Distance Closest plugin with an exclusion distance parameter. This exclusion distance was adapted manually for each acquisition, and the uncertainty on the number of dead neurons was calculated by applying an (-5, +5) interval on this parameter.

## Statistical analysis

Data are presented as means and standard deviations unless indicated otherwise. Statistical differences comparing means were

analyzed using a two-tailed Student's *t*-test or ANOVA. Tukey's multiple comparisons test for ANOVA was used to determine the difference between groups and is indicated by an asterisk and black bar. All statistics were performed using GraphPad Prism 9.

## Results

### TBI-induction platform validation

We have developed an integrated platform for inducing traumas on *in vitro* human neural tissues (Figure 1 and Supplementary Figure 1). This platform has several main functionalities, including the precise positioning of samples (via X, Y adjustments) under the microvalve outlet (via Z adjustment), the control of parameters for liquid ejection to induce traumas, the visualization of tissues before, during, and after impact, and the maintenance of sterility for both the microvalve and tissues during injury.

Achieving a controlled induction of mTBI in 3D neural tissue specimens ranging from 0.5 to 1 mm requires precise dosing of force. To determine the optimal parameters for the ejection of culture medium onto 3D neural tissues, we performed a series of tests at varying pressures and distances between the sample and the microvalve nozzle (data not shown). The samples were then incubated in a fresh culture medium containing cell-permeant nuclear staining and cell-non-permeant nuclear staining for 1 h before chemical fixation for live/dead cell analysis. Based on preliminary results, we found that reproducible results were obtained when the samples were positioned 10 mm from the microvalve nozzle, with an open time of 1 ms for the ejection of the culture medium.

We found that the combination of a box enclosure around the TBI-induction platform and a protocol for sterilizing the pneumatic and liquid ejection system was effective in preventing contamination of the injured tissues and enabling analysis during the post-trauma recovery period. Moreover, due to a continuously supplied stock of culture medium in a 5 ml sterile syringe, numerous neural tissues could be injured in succession.

### Electrophysiology characterization of the injured tissue

Figure 3A shows an example of action potentials recorded from the same electrodes over a period of 30 s: before (control), 1 h, 24 h, and 48 h after the induction of the trauma. The control tissue is characterized by a spontaneous activity with amplitudes peak to peak around 200–250  $\mu$ V. Just after the induction of the injury, we observed a clear abolition of the electrophysiological spontaneous activities, followed by a progressive increase after 24 h, reaching nearly full recovery levels after 48 h. To assess the electrophysiological activity, we combined the number of MEA electrodes that exhibited recorded signals with the number of electrodes that displayed no detectable activity. This approach enabled the determination of the overall activity of the electrodes and the identification of potential alterations in electrophysiological activity (Figure 3B

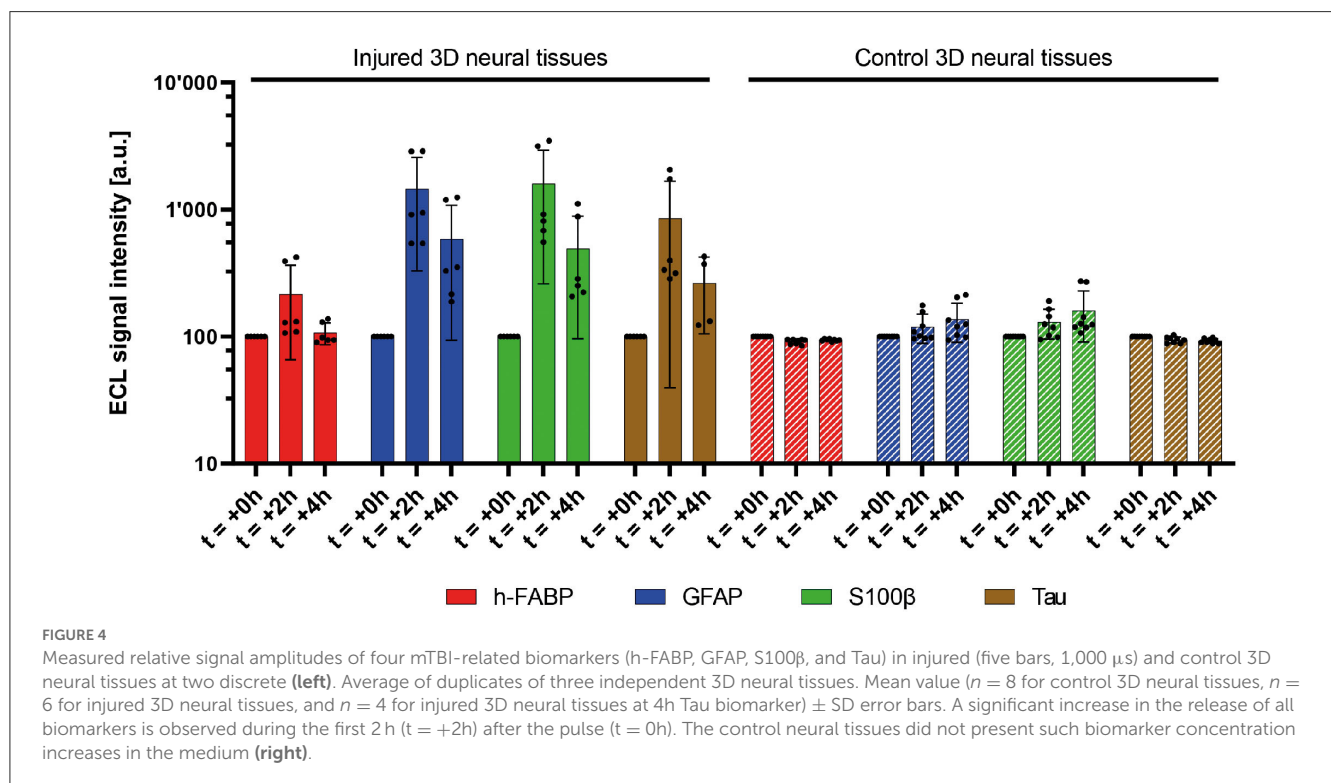
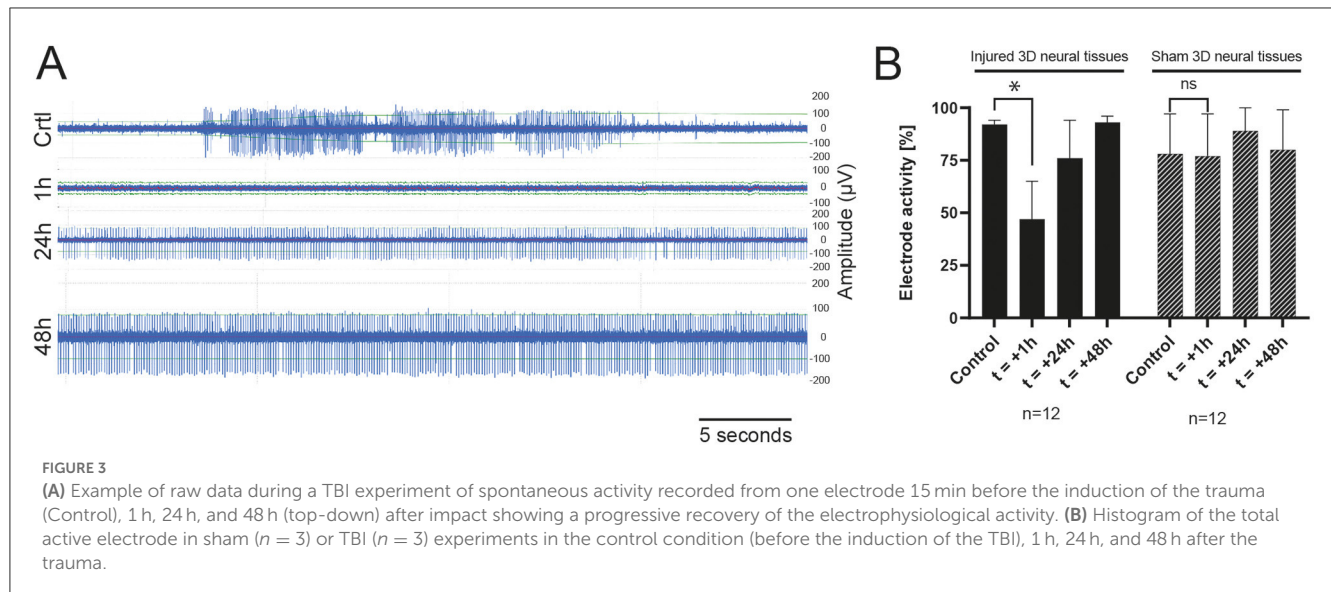
and Supplementary Figure 2). A decrease in activity 1 h after the induction of TBI was observed. Partial recovery was observed after 24 h, with a complete return to control levels obtained at 48 h. The right panel of Figure 3B shows the number of active electrodes recorded in the “sham” experiments. We did not measure any significant decrease in electrode activity under this condition.

### mTBI-related biomarkers released by injured tissue

In this study, multiplex and singleplex electrochemiluminescence immunoassays (ECLIA) were utilized to examine the release kinetics of four protein biomarkers, namely, h-FABP, GFAP, S100 $\beta$ , and Tau, associated with mild traumatic brain injury. Our findings, shown in Figure 4, revealed that the four protein biomarkers were detected in the culture medium after mTBI induction and demonstrated a statistically significant increase compared to the control samples that did not experience any injury or samples before the injury. Specifically, GFAP, Tau, and S100 $\beta$  exhibited a remarkable 15-fold increase at 2 h post-injury, while h-FABP showed a moderate 2-fold increase. Furthermore, 4 h after the injury, there was a sustained release of these three biomarkers into the culture medium, with levels eight times higher than before the injury. Notably, h-FABP concentrations returned to the original background level 4 h later. Additionally, it is worth mentioning that even in the control samples, there was a constant, yet significantly lower release of the four biomarkers into the culture medium. It is also important to mention that even in the control samples, there was a consistent, but significantly lower, release of the four biomarkers into the culture medium. This finding is not surprising since these circulating biomarkers can be detected at sub-pathological concentrations under normal human physiological conditions as well.

### Characterization of the injured neural tissue by optical microscopy

Figure 5 illustrates the comparison of 3D neural tissue imaged by OPT and confocal microscopy after a clarity step as described in the material sections. The sample was stained and chemically fixed 2 h after the injury as described in the methods section. All cell nuclei were stained using Hoechst staining (displayed in blue, Figures 5A, B second row), while dead cells were stained using PI staining (displayed in red, Figures 5A, B first row). Confocal microscopy was used as a gold standard to compare the signal of the OPT instrument. However, due to the penetration depth limitation of this imaging method (Pawley, 2006), we were only able to resolve virtual sections of tissue thinner than 200  $\mu$ m. OPT provided a high spatial resolution of 8  $\mu$ m and a field of view that enabled whole-tissue imaging. As a result, OPT allowed the identification of individual nuclei, as illustrated on an interactive model (Figure 5C), to calculate the ratio of dead cells, and to determine various structural parameters of both control and injured 3D neural tissues (see Table 1). Specifically, we estimated the mean volume and diameter of the 3D tissues to be  $0.15 \pm 0.06$  mm<sup>3</sup> and  $0.7 \pm 0.1$  mm,



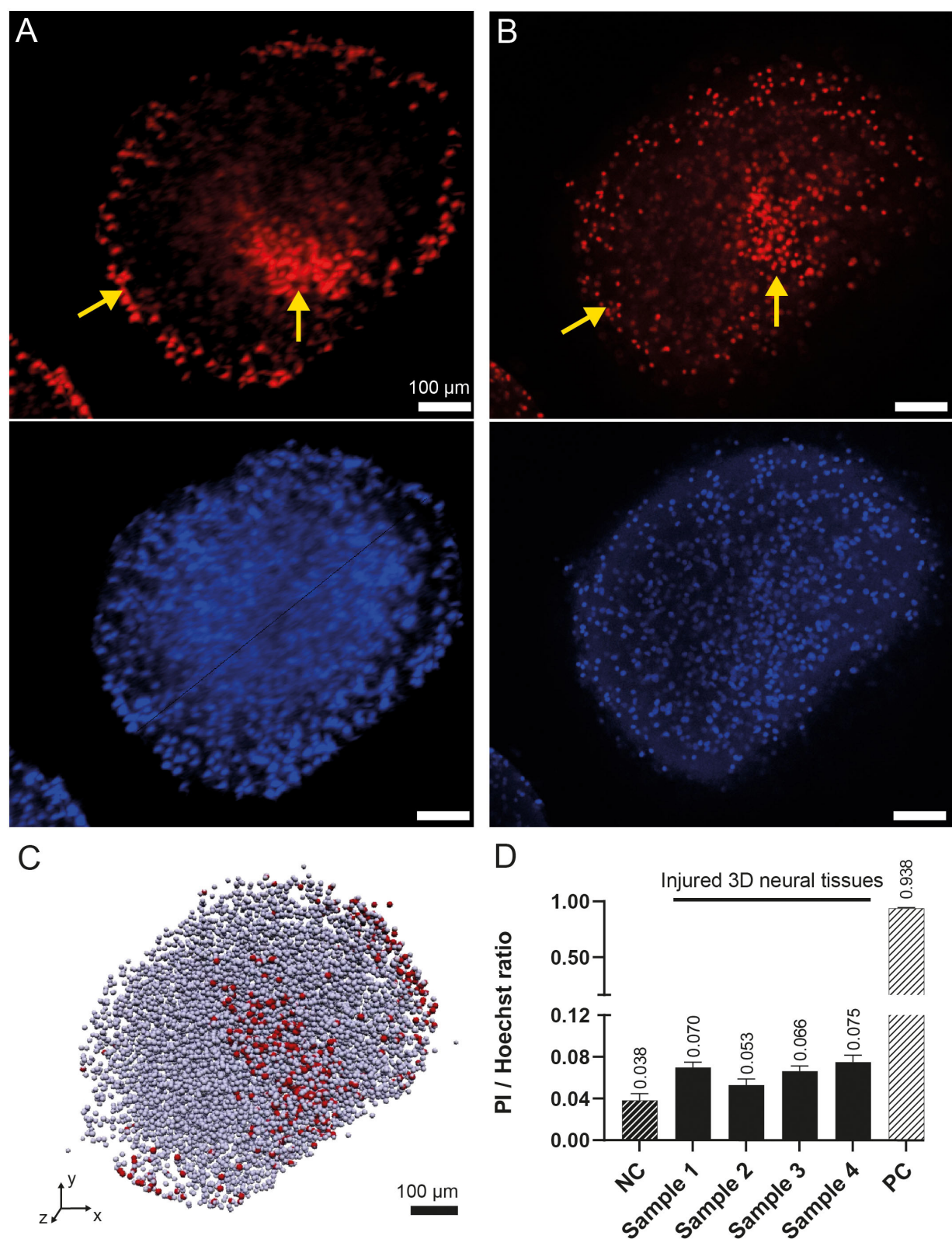
respectively. Additionally, the average nucleus density in the 3D neural tissues was calculated to be 58 kcells/mm<sup>3</sup>, demonstrating the ability of OPT to provide high-resolution imaging and accurate quantification of cellular features in 3D neural tissues.

To validate the Hoechst/PI staining method, an analysis of both positive and negative controls was performed. The positive control consisted of 3D neural tissue chemically fixed prior to staining with Hoechst/PI, while the negative control was intact tissue stained before chemical fixation. Analysis showed a live/dead cell ratio of  $0.938 \pm 0.006$  for the positive control, indicating that almost all cells (5,728 of 6,107) were stained with PI. In contrast, the negative

control had a much lower ratio of  $0.038 \pm 0.005$ . When we imaged the four impacted tissue samples, we observed a significantly higher mean dead cell ratio of  $0.07 \pm 0.01$ , compared to the negative control (Figure 5D). These results confirm the effectiveness of the staining method in identifying dead cells in 3D neural tissue.

Qualitatively, the imaging analysis of PI-stained 3D neural tissues revealed the presence of two denser regions, as shown in Figures 5A, B and indicated by yellow arrows. One of these regions was observed in the peripheral cell layer of the tissues, whereas the other was localized deeper within the tissue. While the peripheral signal of cell death was observed in all samples, including control,





**FIGURE 5**  
3D rendering of the human 3D neural tissues after TBI impacts. **(A)** Maximum intensity projection of the PI (top) and Hoechst (bottom) fluorescence signals acquired by OPT after integrating the signal over a 100- $\mu$ m-thick region. The color intensities are saturated to increase the ease of readability. **(B)** Similar view as in **(A)** acquired by confocal microscopy. The yellow arrows show the regions with higher densities of dead cells at the periphery of the tissue and around the main damaged area. **(C)** OPT 3D vectorized model representation of the identified cells. Dead cells are in red, whereas all other cells are in gray. **(D)** OPT computed PI/Hoechst ratios for four injured 3D neural tissue samples. A negative control (NC) organoid was imaged without TBI. A positive control (PC) was imaged after chemical fixation of PI.



TABLE 1 3D neural tissue parameters measured with OPT microscopy.

Parameters	Negative control	Positive control	Sample 1	Sample 2	Sample 3	Sample 4	Mean	Std
Volume (mm <sup>3</sup> )	0.2106	0.1127	0.2324	0.1759	0.1213	0.0726	0.15	0.06
Mean diameter (mm)	0.7382	0.5994	0.7628	0.6951	0.6142	0.5177	0.7	0.1
Number of total nuclei	10495	6107	17271	9625	7636	3734	9k	5k
Number of PI positive nucleus	401	5728	1205	509	507	280		
Nucleus density (nucleus/mm <sup>3</sup> )	49829	54169	74313	54729	62955	51412	58k	9k
Dead cells /total cells ratio	0.038	0.938	0.070	0.053	0.066	0.075	0.07	0.01

Both negative control and positive control were neither considered for ratio means nor for standard deviation (std).

positive control, and injured tissues, the deeper cell death area was only visible in the injured samples. By isolating the two regions from each other, it was possible to quantify the amount of PI staining in each region. The analysis showed that the mean total amount of signal coming from the main damaged area was nearly equivalent to the amount of signal coming from the tissue border (ratio 1/1.2).

## Discussion

Several *in vitro* and *in vivo* models have been developed to study the cellular and molecular events associated with TBI. Although 2D-based culture models are helpful, they lack the brain's complex 3D cellular organization and extracellular matrix composition. This is a significant weakness as traumatic brain injuries typically involve structural damage to the brain and affect different types of cells and networks of cellular interaction. To overcome this limitation, bioengineered tissues grown in 3D culture systems, mimicking native brain anatomy and physiological responses, are emerging as powerful *in vitro* models to investigate the pathophysiology of TBI (Ramirez et al., 2021b; Silvosa et al., 2022). This led to the development of a new *in vitro* model of TBI combining human cells organized in a 3D neural tissue subjecting to fluid percussion injury. During preliminary experiments, we calibrated the different parameters controlling the microvalve to perform a mild injury on the tissue. These parameters were kept constant for the entire study, and the tissue's response was analyzed with the different read-out modalities.

The occurrence of spontaneous action potentials in mature 3D neural tissues was reported previously (Quadrato et al., 2017), providing confidence in the utilization of electrophysiological recordings for tracking the functionality of neural networks following exposure to trauma. Although there was some variability observed among the various injured tissues, a distinct reduction in spontaneous activity recorded from most electrodes on the MEAs was noted. These observations are in accordance with previous studies carried out *in vivo* (Ding et al., 2011; Johnstone et al., 2013) and *in vitro* (Silvosa et al., 2022). Gradual restoration of spontaneous activity was also observed over time. Other authors reported a loss of activity followed by a slow activity decay to a stable, level plateau approximately 30–40% below reference when working with embryonic cortical tissue from mice (Rogers and Gross, 2019). For this work, we used MEA biochips made

of four areas incorporating eight electrodes each. Unfortunately, this MEA design was not fully adapted to the size of the 3D neural tissues. Therefore, different types of MEAs incorporating 32 recording electrodes adapted for a single tissue have been designed to get a more precise mapping of the entire neural network activity of the tissue. Those MEAs will provide the possibility to analyze the neural activity of the directly impacted region compared to activities from more distant areas. Beyond the current study, further electrophysiology experiments and data analysis using these improved MEA biochips are needed to characterize in more detail the effect of impacts on the whole neural network activities (frequency, amplitude, bursts, etc.) and provide valuable information regarding the functional impairment of neural tissue by TBI.

Tissue response to TBI is a mixture of molecular and cellular events. Biomarkers that can track these lesions and inflammatory processes are being explored for their potential to provide objective measures in the evaluation of the injury (Gutierrez et al., 2021). In this study, as a preliminary mTBI biomarker panel and based on the cell's distribution in the 3D neuronal tissues, we aimed to detect four proteins known for their clinically relevant relation with mTBI as previously described (Posti et al., 2019; Gutierrez et al., 2021). Glial fibrillary acid protein (GFAP) is a structural astrocyte protein while S100 $\beta$  is a calcium-binding protein expressed in cardiac muscles and astroglia among others. Axonal phosphoprotein Tau is expressed in axons and organs like kidneys and liver and, finally, heart fatty-acid-binding protein (h-FABP) is expressed in the heart but also in the brain. To confirm the validity of the presented *in vitro* TBI model, we conducted an analysis of the four protein biomarkers in the culture medium of 3D neural tissue both before and after injury. These biomarkers are not expected to be detectable at a high concentration, which was indeed confirmed in control experiments (Figure 4). Following a TBI impact, the concentration levels of the biomarkers increased and with a certain delay decreased again. So, at least qualitatively a similar kinetic observation is made compared to human *in vivo* TBI (Lagerstedt et al., 2018; Posti et al., 2019; Krausz et al., 2021). In the absence of a blood–brain barrier and vascular circulation (which would dilute/delay the release of biomarkers), a rapid increase in biomarker concentration is expected. A decrease in the concentration relatively soon after the injury, as shown in this study, suggests a minor (or moderate) as opposed to a major injury. However, this would have to be confirmed with more measurement time points (to generate a concentration profile)

and an extended observation period to characterize for instance when post-injury also GFAP, S100 $\beta$ , and Tau return to baseline concentrations. In fact, one would expect the slope of increase and decrease as well as the area under the curve to be different as a function of impact magnitude on the tissue. Repetitive vs. single trauma may also show different release kinetics. It is important to note that the high sensitivity of the ECLIA developed allows us to measure more subtle concentration changes, thus monitoring less significant injuries. It is also noteworthy that the injured 3D neural tissues seemed to release lower quantities of neuronal biomarkers, such as h-FABP, compared to glial ones (GFAP and S100 $\beta$ ) and axonal (Tau). Further investigations are necessary to improve the quantification of these biomarkers and to find out whether these observations are indeed due to the vulnerability of certain neuronal structures, the relative number of corresponding cell types, or a combination of both. The slight and steady rise of biomarkers in the controls may be correlated with OPT results obtained. It is indeed observed that, even in the absence of injury, a small fraction of the cells is dead at the periphery of the 3D neural tissues that could lead to the release of biomarkers and therefore increase the level of our studied proteins in the culture medium. Some experiments are ongoing to evaluate this effect.

Finally, to characterize the injured tissue, a mesoscopic imaging method, OPT, that was recently developed (Schmidt et al., 2021) to image millimetric tissue with a micrometric resolution, was used. With the 3D images acquired by OPT, it was possible to determine a mean 3D neural tissue diameter of  $0.7 \pm 0.1$  mm and a mean cell density of 58 kcells/mm<sup>3</sup>. This latter parameter is in good accordance with values found for the mouse brain organoid (Keller et al., 2018). In addition, the measured ratio of damaged cells 2 h after the impact ( $t = +2$ h) is significantly higher than what was measured without injury (negative control). As PI staining is membrane impermeant and should therefore be excluded from viable cells, we can assume that the cells detected as dead by OPT will not recover with time. Therefore, the extra dead cells ratio measured in the injured 3D neural tissues with respect to the negative control is attributed to the induced trauma. The spatial distribution of injured cells throughout the 3D neural tissue also allowed us to identify a main damaged area that is confined within the tissue or to the periphery, but within a limited solid angle. The observation of a permanent reduction of healthy cells after a head injury is in some ways at odds with the other results, which all show almost complete signal recovery over time. We explain this behavior by the fact that OPT measures the state of the entire sample at a specific time, whereas electrophysiological characterization only reads the signal from cells in contact or close to the electrodes and immunoassays measure protein diffusion over time and through the entire tissue. A better understanding of the diffusion process, in this case, requires more research and simulations.

## Conclusion

The *in vitro* TBI model we have developed in this study allows not only to reproducibly induce injuries on human 3D neural tissues but also a comprehensive characterization of injured tissue during the acute and recovery phases. Due to the versatility of the

developed platform, it was possible to show a clear abolition of electrophysiological spontaneous activities just after the induction of the injury, followed by a progressive increase in activity after 24 h and full recovery after 48 h. Additionally, four protein biomarkers associated with mild traumatic brain injury exhibited a statistically significant increase in their release into the culture medium compared to the control samples. Finally, the optical projection tomography provided images of injured areas with cellular resolution and allowed an accurate quantification of cellular features in 3D neural tissues.

In the next step, we plan to expand the range of data points after TBI induction to cover immediate and long-term responses, including data points that capture the first few minutes post-trauma and responses that occur over weeks or months. Finally, it is planned to further improve the system by the development of a more sophisticated biological model by the addition of different types of membrane-like structures on the surface of the brain parenchyma, to mimic the presence of a skull or meninges, which at least partially protects the brain from external forces. Therefore, the impacts of ejected culture medium will be more diffuse/distributed (as opposed to focusing on a small area) and would thus recreate more realistically concussion events such as the ones occurring in *in vivo* experiments.

## Data availability statement

The raw data supporting the conclusions of this article will be made available by the authors, without undue reservation.

## Author contributions

LS, AR, and MP designed the study. CL-F, YN, OR, DP, and CS collated the data, carried out data analyses, and produced the initial draft of the manuscript. MH, LG, MJ, JE, LS, AR, and MP helped perform the analysis with constructive discussions. All authors have read and approved the final submitted manuscript.

## Funding

HES-SO (project number 107078), HEPIA (internal funding), and a preliminary study has been funded by the Institute of Life Technologies of the HES-SO Valais-Wallis.

## Acknowledgments

The authors would like to thank Jonas Oppliger from Fritz Gyger AG for his support, Ousaamah Abidine for his Bachelor thesis on the TBI device, Alexandra Laszlo for her Master thesis on developing the staining method for injured 3D neural tissue, and Laetitia Nikles for her technical support.

## Conflict of interest

The authors declare that the research was conducted in the absence of any commercial or financial relationships that could be construed as a potential conflict of interest.

## Publisher's note

All claims expressed in this article are solely those of the authors and do not necessarily represent those of their affiliated organizations, or those of the publisher, the editors and the reviewers. Any product that may be evaluated in this article, or claim that may be made by its manufacturer, is not guaranteed or endorsed by the publisher.

## Multiplex immunoassay materials

All chemicals were used as received without further purification and all aqueous solutions were prepared with MQ water. U-PLEX Development Pack, 6-Assay (#K15231N-2), GOLD 96-well Small Spot Streptavidin Plate (#L45SA-1), GOLD SULFO-TAG NHS-Ester lyophilized (#R91AO-1), Gold read buffer B (#R60AM-2), read buffer T 4X (#R92TC), U-PLEX Stop Solution (#R50AO-1) were purchased from MSD. Other materials include Pierce Antibody Biotinylation Kit for IP (#90407, Thermo Scientific, Waltham), bovine serum albumin fraction V (#10735086001, Roche Diagnostics), PBS 10x pH 7.4 phosphate saline buffer (#70011-036, Gibco), Tween-20 (#P1379-100 mL, Merck (Sigma-Aldrich)),  $\text{CaCl}_2 \times 2\text{H}_2\text{O}$  (#223506, Fluka), Trizma base (#1002134476, Sigma-Aldrich), Zeba Spin desalting columns 7K MWCO, 0.5 mL (#89882, Thermo Fisher).

## Protein multiplex immunoassay method

Capture antibody biotinylation and linker-coupled antibody solutions: The capture antibodies (h-FABP, GFAP, and S100 $\beta$ ) were biotinylated with the EZ-Linker NHS-PEG4-Biotin antibody Biotinylation Kit from the Pierce<sup>TM</sup>. The concentration of the antibody solutions was 1 mg/mL, and 3.14  $\mu\text{L}$  of NHS-PEG4-Biotin solution was added to the diluted antibodies. The final concentrations of the biotinylated capture antibodies were measured at OD280 using the Nanodrop

OneC Microvolume UV-VIS Spectrophotometer (Thermo Fisher Scientific). Each biotinylated capture antibody was coupled with a determined linker from MSD to obtain a final antibody-linker concentration of 2.86  $\mu\text{g/mL}$  following the MSD protocol (MSD U-PLEX Development Pack). Tau capture antibody was diluted (200  $\mu\text{L}$  in 3.3 mL of PBS 1X) and used without further purification (MSD R-PLEX Antibody Sets Singleplex Assays).

Detection antibody labeling: Detection antibodies of all three biomarkers were conjugated with the  $\text{Ru}(\text{bpy})_3^{2+}$ -label using the GOLD SULFO-TAG NHS-Ester reagent provided by MSD (#MSD GOLD SULFO-TAG Conjugation Quick Guide). A challenge ratio of 50:1 was used for all detection antibodies (h-FABP, GFAP, and S100 $\beta$ ), while the labeling incorporation ratio was calculated by measuring the OD<sub>455</sub> values using the NanoDrop OneC Microvolume UV-VIS Spectrophotometer (Thermo Fisher Scientific). The calculated label ratio for h-FABP, GFAP, and S100 $\beta$  detection antibodies were 14:1, 13:1, and 19:1, respectively. The Tau detection antibody was used 100-fold diluted without further modification or purification.

## Supplementary material

The Supplementary Material for this article can be found online at: <https://www.frontiersin.org/articles/10.3389/fnins.2023.1189615/full#supplementary-material>

### SUPPLEMENTARY FIGURE 1

Picture showing the microvalve (white arrow) attached to an XYZ translation stage mounted on an inverted microscope. The 3D neural tissues are disposed in a 24-well plate to perform the injury.

### SUPPLEMENTARY FIGURE 2

Example of raster plots of 4 groups of eight electrodes. Each group of 8 electrodes, displayed in a different color (red, green, blue, and black), recorded one 3D neural tissue. The data were acquired during a TBI experiment. On the first row, one can observe the spontaneous and synchronous activity 15 min before the trauma induction (Control). After the trauma, e.g., 1 h, 24 h, and 48 h (top-down) after impact, one can observe a progressive recovery of the electrophysiological activity.

## References

- Arun, P., Spadaro, J., John, J., Gharavi, R. B., Bentley, T. B., Nambiar, M. P., et al. (2011). Studies on blast traumatic brain injury using *in-vitro* model with shock tube. *NeuroReport*. 22, 379–384. doi: 10.1097/WNR.0b013e328346b138
- Azkona, G., and Sanchez-Pernaute, R. (2022). Mice in translational neuroscience: What R we doing? *Prog Neurobiol*. 217:102330. doi: 10.1016/j.pneurobio.2022.102330
- Blyth, B. J., and Bazarian, J. J. (2010). Traumatic alterations in consciousness: traumatic brain injury. *Emerg. Med. Clin. North. Am.* 28, 571–594. doi: 10.1016/j.emc.2010.03.003
- Bramlett, H. M., and Dietrich, W. D. (2015). Long-term consequences of traumatic brain injury: current status of potential mechanisms of injury and neurological outcomes. *J. Neurotrauma*. 32, 1834–1848. doi: 10.1089/neu.2014.3352
- Cash, A., and Theus, M. H. (2020). Mechanisms of blood–brain barrier dysfunction in traumatic brain injury. *Int. J. Mol. Sci.* 21, 3344. doi: 10.3390/ijms21093344
- Chiaradia, I., and Lancaster, M. A. (2020). Brain organoids for the study of human neurobiology at the interface of *in vitro* and *in vivo*. *Nat. Neurosci.* 23, 1496–1508. doi: 10.1038/s41593-020-00730-3
- Dewan, M. C., Rattani, A., Gupta, S., Baticulon, R. E., Hung, Y. C., Punchak, M., et al. (2019). Estimating the global incidence of traumatic brain injury. *J. Neurosurg.* 130, 1080–1097. doi: 10.3171/2017.10.JNS17352
- Ding, M. C., Wang, Q., Lo, E. H., and Stanley, G. B. (2011). Cortical excitation and inhibition following focal traumatic brain injury. *J. Neurosci.* 31, 14085–14094. doi: 10.1523/JNEUROSCI.3572-11.2011
- Dodd, W. S., Panther, E. J., Pierre, K., Hernandez, J. S., Patel, D., Lucke-Wold, B., et al. (2022). Traumatic brain injury and secondary neurodegenerative disease. *Trauma. Care.* 2, 510–522. doi: 10.3390/traumacare2040042
- Ferlauto, L., D'Angelo, A. N., Vagni, P., Airaghi Leccardi, M. J. I., Mor, F. M., Cuttaz, E. A., et al. (2018). Development and characterization of PEDOT:PSS/alginate soft microelectrodes for application in neuroprosthetics. *Front. Neurosci.* 12, 648. doi: 10.3389/fnins.2018.00648
- Garcez, P. P., Loiola, E. C., and Madeiro, H. (2016). Zika virus impairs growth in human neurospheres and brain organoids. *Science*. 352, 816–818. doi: 10.1126/science.aaf6116

- Govindan, S., Batti, L., Osterop, S. F., Stoppini, L., and Roux, A. (2021). Mass generation, neuron labeling, and 3d imaging of minibrains. *Front. Bioeng. Biotechnol.* 8, 582650. doi: 10.3389/fbioe.2020.582650
- Gutierrez, M., Telles, J., Welling, L., Rabelo, N., Teixeira, M., Figueiredo, E., et al. (2021). Biomarkers for traumatic brain injury: a short review. *Neurosurg. Rev.* 44, 2091–2097. doi: 10.1007/s10143-020-01421-0
- Jarrahi, A., Braun, M., Ahluwalia, M., Gupta, R. V., Wilson, M., Munie, S., et al. (2020). Revisiting traumatic brain injury: from molecular mechanisms to therapeutic interventions. *Biomedicines* 8, 389. doi: 10.3390/biomedicines8100389
- Jgamadze, D., Johnson, V. E., Wolf, J. A., Cullen, D. K., Song, H., Ming, G., et al. (2020). Modeling traumatic brain injury with human brain organoids. *Curr. Opin. Biomed. Eng.* 14, 52–58. doi: 10.1016/j.cobme.2020.05.004
- Johnson, V. E., Stewart, W., and Smith, D. H. (2013). Axonal pathology in traumatic brain injury. *Exp. Neurol.* 246, 35–43. doi: 10.1016/j.expneurol.2012.01.013
- Johnstone, V. P. A., Yan, E. B., Alwis, D. S., and Rajan, R. (2013). Cortical hypoexcitation defines neuronal responses in the immediate aftermath of traumatic brain injury. *PLoS ONE* 8, 5. doi: 10.1371/journal.pone.0063454
- Jović, M., Prim, D., Saini, E., and Pfeifer, M. E. (2022). Towards a point-of-care (POC) diagnostic platform for the multiplex electrochemiluminescent (ECL) sensing of mild traumatic brain injury (mTBI). *Biomarkers* 2022, 21. doi: 10.3390/bios12030172
- Kabadi, S. V., Hilton, G. D., Stoica, B. A., Zapple, D. N., and Faden, A. I. (2010). Fluid-percussion-induced traumatic brain injury model in rats. *Nat. Protoc.* 5, 1552–1563. doi: 10.1038/nprot.2010.112
- Keller, D., Erö, C., and Markram, H. (2018). Cell densities in the mouse brain: a systematic review. *Front. Neuroanat.* 12, 83. doi: 10.3389/fnana.2018.00083
- Krausz, A. D., Korley, F. K., and Burns, M. A. (2021). The Current state of traumatic brain injury biomarker measurement methods. *Biosensors* 11, 319. doi: 10.3390/bios11090319
- Lagerstedt, L., Egea-Guerrero, J. J., Bustamante, A., Rodríguez-Rodríguez, A., El Rahal, A., Quintana-Díaz, M., et al. (2018). Combining H-FABP and GFAP increases the capacity to differentiate between CT-positive and CT-negative patients with mild traumatic brain injury. *PLoS ONE* 13, e0200394. doi: 10.1371/journal.pone.0200394
- Lancaster, M., Renner, M., Martin, C., Wenzel, D., Bicknell, L., Hurles, M., et al. (2013). Cerebral organoids model human brain development and microcephaly. *Nature* 501, 373. doi: 10.1038/nature12517
- Liaudanskaya, V., Chung, J. Y., Mizzoni, C., Rouleau, N., Berk, A. N., Wu, L., et al. (2020). Modeling controlled cortical impact injury in 3D brain-like tissue cultures. *Adv. Healthc. Mater.* 9, 2000122. doi: 10.1002/adhm.202000122
- Liu, Y., Dong, J., Schmidt, C., Boquet-Pujadas, A., Extermann, J., Unser, M., et al. (2022). Artifacts in optical projection tomography due to refractive-index mismatch: model and correction. *Opt. Lett.* 47, 2618. doi: 10.1364/OL.457144
- Lu, W., and Mackie, T. R. (2002). Tomographic motion detection and correction directly in sinogram space. *Phys. Med. Biol.* 47, 1267–1284. doi: 10.1088/0031-9155/47/8/304
- Maas, A. I. R., Menon, D. K., Adelson, P. D., Andelic, N., Bell, M. J., Belli, A., et al. (2017). Traumatic brain injury: integrated approaches to improve prevention, clinical care, and research. *Lancet. Neurol.* 16, 987–1048. doi: 10.1016/S1474-4422(17)30371-X
- Mariani, J., Coppola, G., Zhang, P., Abyzov, A., Provini, L., Tomasini, L., et al. (2015). FOXG1-dependent dysregulation of GABA/glutamate neuron differentiation in autism spectrum disorders. *Cell* 162, 375–390. doi: 10.1016/j.cell.2015.06.034
- Morrison, B., Elkin, B. S., Dollé, J. P., and Yarmush, M. L. (2011). *In vitro* models of traumatic brain injury. *Annu. Rev. Biomed. Eng.* 13, 91–126. doi: 10.1146/annurev-bioeng-071910-124706
- Ng, S. Y., and Lee, A. Y. W. (2019). Traumatic brain injuries: pathophysiology and potential therapeutic targets. *Front. Cell. Neurosci.* 13, 528. doi: 10.3389/fncel.2019.00528
- Ollion, J., Cochenne, J., Loll, F., Escudé, C., and Boudier, T. T. A. N. G. O. (2013). a generic tool for high-throughput 3D image analysis for studying nuclear organization. *Bioinformatics* 29, 1840–1841. doi: 10.1093/bioinformatics/btt276
- Oppenheimer, D. R. (1968). Microscopic lesions in the brain following head injury. *J. Neurol. Neurosurg. Psychiatry* 31, 299–306. doi: 10.1136/jnnp.31.4.299
- Osier, N., and Dixon, C. E. (2016). The controlled cortical impact model of experimental brain trauma: overview, research applications, and protocol. *Injury. Models. Central. Nervous. System* 1462, 177–192. doi: 10.1007/978-1-4939-3816-2\_11
- Pawley, J. B. (2006). *Fundamental Limits in Confocal Microscopy. Handbook Of Biological Confocal Microscopy*. Boston, MA: Springer US (2006).
- Pollen, A. A., Bhaduri, A., Andrews, M. G., Nowakowski, T. J., Meyerson, O. S., Mostajo-Radji, M. A., et al. (2019). Establishing Cerebral Organoids as Models of Human-Specific Brain Evolution. *Cell* 176, 743–756.e17. doi: 10.1016/j.cell.2019.01.017
- Posti, J. P., Takala, R. S. K., Lagerstedt, L., Dickens, A. M., Hossain, I., Mohammadian, M., et al. (2019). Correlation of blood biomarkers and biomarker panels with traumatic findings on computed tomography after traumatic brain injury. *J. Neurotrauma* 36, 2178–2189. doi: 10.1089/neu.2018.6254
- Quadrato, G., Nguyen, T., Macosko, E. Z., Sherwood, J. L., Min Yang, S., Berger, D. R., et al. (2017). Cell diversity and network dynamics in photosensitive human brain organoids. *Nature* 545, 48–53. doi: 10.1038/nature22047
- Ramirez, S., Mukherjee, A., Sepulveda, S., Becerra-Calixto, A., Bravo-Vasquez, N., Gherardelli, C., et al. (2021a). Modeling traumatic brain injury in human cerebral organoids. *Cells* 10, 2683. doi: 10.3390/cells10102683
- Ramirez, S., Mukherjee, A., Sepulveda, S. E., Gherardelli, C., Becerra-Calixto, A., Bravo-Vasquez, N., et al. (2021b). Protocol for controlled cortical impact in human cerebral organoids to model traumatic brain injury. *STAR. Protoc.* 2, 100987. doi: 10.1016/j.xpro.2021.100987
- Rogers, E. A., and Gross, G. W. (2019). Simultaneous electrophysiological and morphological assessment of functional damage to neural networks *in vitro* after 30–300 g impacts. *Sci. Rep.* 9, 14994. doi: 10.1038/s41598-019-51541-x
- Schmidt, C., Planchette, A. L., Nguyen, D., Giardina, G., Neuenschwander, Y., Franco, M. D., et al. (2021). High resolution optical projection tomography platform for multispectral imaging of the mouse gut. *Biomed. Opt. Express* 12, 3619. doi: 10.1364/BOE.423284
- Schweitzer, A. D., Niogi, S. N., Whitlow, C. J., and Tsiouris, A. J. (2019). Traumatic brain injury: imaging patterns and complications. *RadioGraphics* 39, 1571–1595. doi: 10.1148/rq.2019190076
- Silvosa, M. J., Mercado, N. R., Merlock, N., Vidhate, S., Mejia-Alvarez, R., Yuan, T. T., et al. (2022). Understanding primary blast injury: high frequency pressure acutely disrupts neuronal network dynamics in cerebral organoids. *J. Neurotrauma* 39, 1575–1590. doi: 10.1089/neu.2022.0044
- Tang-Schomer, M. D., Johnson, V. E., Baas, P. W., Stewart, W., and Smith, D. H. (2012). Partial interruption of axonal transport due to microtubule breakage accounts for the formation of periodic varicosities after traumatic axonal injury. *Exp. Neurol.* 233, 364–372. doi: 10.1016/j.expneurol.2011.10.030
- Velasco, S., Kedaigle, A. J., Simmons, S. K., Nash, A., Rocha, M., Quadrato, G., et al. (2019). Individual brain organoids reproducibly form cell diversity of the human cerebral cortex. *Nature* 570, 523–527. doi: 10.1038/s41586-019-1289-x
- Wertenbroek, R., Thoma, Y., Mor, F. M., Grassi, S., Heuschkel, M. O., Roux, A., et al. (2021). SpikeOnChip : a custom embedded platform for neuronal activity recording and analysis. *IEEE. Trans. Biomed. Circuits. Syst.* 15, 743–755. doi: 10.1109/TBCAS.2021.3097833





## OPEN ACCESS

## EDITED BY

Subashika Govindan,  
Wellcome Trust DBT India Alliance, India

## REVIEWED BY

Claire Cheetham,  
University of Pittsburgh, United States  
René Oliver Goral,  
National Institute of Environmental Health  
Sciences (NIH), United States

## \*CORRESPONDENCE

Nixon M. Abraham  
✉ nabraham@iiserpune.ac.in  
Sanjeev Galande  
✉ sanjeev@iiserpune.ac.in

<sup>†</sup>These authors have contributed equally to this work

RECEIVED 06 March 2023

ACCEPTED 15 May 2023

PUBLISHED 19 June 2023

## CITATION

Mahajan S, Sen D, Sunil A, Srikanth P, Marathe SD, Shaw K, Sahare M, Galande S and Abraham NM (2023) Knockout of angiotensin converting enzyme-2 receptor leads to morphological aberrations in rodent olfactory centers and dysfunctions associated with sense of smell.  
*Front. Neurosci.* 17:1180868.  
doi: 10.3389/fnins.2023.1180868

## COPYRIGHT

© 2023 Mahajan, Sen, Sunil, Srikanth, Marathe, Shaw, Sahare, Galande and Abraham. This is an open-access article distributed under the terms of the [Creative Commons Attribution License \(CC BY\)](https://creativecommons.org/licenses/by/4.0/). The use, distribution or reproduction in other forums is permitted, provided the original author(s) and the copyright owner(s) are credited and that the original publication in this journal is cited, in accordance with accepted academic practice. No use, distribution or reproduction is permitted which does not comply with these terms.

# Knockout of angiotensin converting enzyme-2 receptor leads to morphological aberrations in rodent olfactory centers and dysfunctions associated with sense of smell

Sarang Mahajan<sup>1,2†</sup>, Deepshikha Sen<sup>1,2†</sup>, Anantu Sunil<sup>1,3†</sup>, Priyadharshini Srikanth<sup>1,2</sup>, Shruti D. Marathe<sup>1,2</sup>, Karishma Shaw<sup>1,2</sup>, Mahesh Sahare<sup>2</sup>, Sanjeev Galande<sup>2,4,5\*</sup> and Nixon M. Abraham<sup>1,2\*</sup>

<sup>1</sup>Laboratory of Neural Circuits and Behaviour (LNCB), Department of Biology, Indian Institute of Science Education and Research (IISER), Pune, Maharashtra, India, <sup>2</sup>Department of Biology, Indian Institute of Science Education and Research (IISER), Pune, Maharashtra, India, <sup>3</sup>Indian Institute of Science Education and Research (IISER), Kolkata, West Bengal, India, <sup>4</sup>Laboratory of Chromatin Biology and Epigenetics, Department of Biology, Indian Institute of Science Education and Research (IISER), Pune, Maharashtra, India, <sup>5</sup>Center of Excellence in Epigenetics, Department of Life Sciences, Shiv Nadar University, Delhi-NCR, India

Neuronal morphological characterization and behavioral phenotyping in mouse models help dissecting neural mechanisms of brain disorders. Olfactory dysfunctions and other cognitive problems were widely reported in asymptomatic carriers and symptomatic patients infected with Severe Acute Respiratory Syndrome Coronavirus-2 (SARS-CoV-2). This led us to generate the knockout mouse model for Angiotensin Converting Enzyme-2 (ACE2) receptor, one of the molecular factors mediating SARS-CoV-2 entry to the central nervous system, using CRISPR-Cas9 based genome editing tools. ACE2 receptors and Transmembrane Serine Protease-2 (TMPRSS2) are widely expressed in the supporting (sustentacular) cells of human and rodent olfactory epithelium, however, not in the olfactory sensory neurons (OSNs). Hence, acute inflammation induced changes due to viral infection in the olfactory epithelium may explain transient changes in olfactory detectabilities. As ACE2 receptors are expressed in different olfactory centers and higher brain areas, we studied the morphological changes in the olfactory epithelium (OE) and olfactory bulb (OB) of ACE2 KO mice in comparison with wild type animals. Our results showed reduced thickness of OSN layer in the OE, and a decrease in cross-sectional area of glomeruli in the OB. Aberrations in the olfactory circuits were revealed by lowered immunoreactivity toward microtubule associated protein 2 (MAP2) in the glomerular layer of ACE2 KO mice. Further, to understand if these morphological alterations lead to compromised sensory and cognitive abilities, we performed an array of behavioral assays probing their olfactory subsystems' performances. ACE2 KO mice exhibited slower learning of odor discriminations at the threshold levels and novel odor identification impairments. Further, ACE2 KO mice failed to memorize the pheromonal locations while trained on a multimodal task implying the aberrations of neural circuits involved in higher cognitive functions. Our results thus provide the morphological basis for the sensory and cognitive disabilities caused by the deletion of ACE2 receptors and offer a potential experimental approach to study the neural circuit mechanisms of cognitive impairments observed in long COVID.

## KEYWORDS

ACE2 receptor, gene knockout, CRISPR-Cas9, olfactory system, sensory and cognitive deficits

## 1. Introduction

Angiotensin converting enzyme (ACE) 2 plays a critical role in maintaining physiological homeostasis (Donoghue et al., 2000; Hamming et al., 2004). It is widely expressed in different body systems and was identified as one of the molecular factors mediating Coronavirus disease 2019 (COVID-19) infection (Brann et al., 2020; Fodouliau et al., 2020; Hoffmann et al., 2020). Most of the mortality caused by COVID-19 infection have been reported to be due to severe respiratory problems. This was caused by malfunctioning of cardiovascular and respiratory systems (Crackower et al., 2002; Hoffmann et al., 2020). The defects associated with lung function can be a predictor for neurological impairments as well (Mahmmedi et al., 2021). Since the beginning of pandemic, autopsy studies reported the presence of viral particles in multiple organ systems including the nervous system (Puelles et al., 2020). Brain imaging data further confirmed the structural abnormalities caused by the viral infection (Douaud et al., 2022). Moreover, long-lasting brain dysfunctions have become a serious challenge in post-COVID-19 conditions (Pardasani and Abraham, 2022; Bhowmik et al., 2023). Therefore, probing the mechanisms underlying these deficits using animal models is a pressing need of global health.

The binding of viral particles on ACE2 receptors leads to the creation of a fusion pore that allows viral entry into the host cells. This is assisted by the priming of spike protein by host cell transmembrane protease, serine 2 (TMPRSS2) (Shang et al., 2020; Jackson et al., 2022). Although the routes of viral entry to the central nervous system (CNS) and the neurotropism of Severe Acute Respiratory Syndrome Coronavirus 2 (SARS-CoV-2) remain as debated topics, various cellular factors mediating virus entry are expressed in neuronal and non-neuronal cells in the brain (Pardasani and Abraham, 2022). ACE2 receptors are expressed in the non-neuronal supporting (sustentacular) cells of olfactory epithelium. This explains the prevalent olfactory deficits caused by different strains of SARS-CoV-2 (Bhattacharjee et al., 2020; Whitcroft and Hummel, 2020; Iravani et al., 2022), supported by the observations on presence of viral RNA and protein in the nasopharynx (Meinhardt et al., 2021). However, some studies did not find the presence of viral particles in the olfactory sensory neurons (OSNs) and olfactory bulb (OB), leading to the debate on the neurotropism of SARS-CoV-2 (Khan et al., 2021). Another receptor type that facilitates virus entry, Neuropilin-1 (NRP1) is expressed in the neurons, olfactory epithelial cells, and endothelial cells etc. (Cantuti-Castelvetri et al., 2020; Kyrou et al., 2021). Despite the above-mentioned evidence on molecular factors, studies dissecting the neural basis of olfactory and cognitive deficits using animal models are scarce.

Single cell sequencing studies of mouse olfactory epithelium revealed the expression of ACE2 and TMPRSS2 in the sustentacular cells, however not in the OSNs (Brann et al., 2020; Fodouliau et al., 2020; Hoffmann et al., 2020). Transnasal infusion of viral particles in Golden Syrian Hamsters provided the evidence for neuronal invasion.

Both neuronal and non-neuronal cell deaths were observed during the post-infection period (De Melo et al., 2021). As genetic approaches mimicking viral infection can provide stable readouts, we decided to generate ACE2 receptor knockout using CRISPR-Cas9 genome editing tools. The CRISPR-Cas9 technique has been successfully used in mouse and other mammalian species to generate genetically modified animals (Shao et al., 2014; Kang et al., 2019). The deletion of ACE2 gene was ensured by targeting the crucial translational start site of the exon 2 and verified by sequencing. On generating ACE2 KO mice, we carried out the morphological studies and the behavioral phenotyping focusing on the functioning of olfactory system. As olfactory problems of varying severity including hyposmia, anosmia and parosmia are observed during and post-COVID conditions, we used well-established and sensitive behavioral assays (Abraham et al., 2004, 2010, 2014; Bhattacharjee et al., 2019; Pardasani et al., 2021). The reduced thickness of OSN layer and the lowered MAP2 immunoreactivity in the glomerular region explained various olfactory problems including the detection, and discrimination deficits at the threshold levels and the lowered novel odor identification abilities. Further, ACE2 KO mice showed compromised pheromone location learning, which involved more than one sensory modality. Hence, our experimental approach would facilitate probing the neural mechanisms of long-COVID complications.

## 2. Materials and methods

### 2.1. Maintenance of animals

A total of 119 C57BL/6J and ACE2 KO male and female adult mice were used for all of the experiments in this study. The mice were between 6 to 8 weeks old at the beginning of the experiment. 12-h light/dark cycle was maintained and mice were grouped in individually ventilated cages in a temperature- and humidity-controlled animal facility. Mice had unlimited access to food, but were subjected to a water restriction schedule meant to keep them at >80% of their baseline body weight during Go/No-Go behavioral training. The schedule of water restrictions was never longer than 12h. All animal care and procedures were in accordance with the Institutional Animal Ethics Committee (IAEC) at IISER Pune and the Committee for the Purpose of Control and Supervision of Experiments on Animals (CPCSEA), Government of India.

### 2.2. Generation of ACE2 KO mouse model

Using CRISPR-Cas9 gene targeting technology, we generated a knockout mouse model for ACE2. The knockout was created by specifically targeting the translation start site (TSS), which lies in the exon 2 of the ACE2 gene (Figure 1A). Guide RNAs for the 5' and 3' ends of the targeted region were chosen to generate the knockout

(ATCAGCCTTTGAACTTGGGT; ATCAAAGTTCACCTTGCTTCT). SgRNAs were designed using the CRISPOR online tool<sup>1</sup> and synthesized by Sigma Aldrich.

### 2.3. Microinjection of one-cell embryos

C57BL/6J mice at 3–4 weeks of age were superovulated by intraperitoneal injection of 5 IU pregnant mare serum gonadotropin (PMSG), followed by injection of 5 IU human chorionic gonadotropin (Sigma Aldrich) after 48 h. Mouse zygotes were obtained by mating C57BL/6J stud males with superovulated C57BL/6J females. One-cell stage fertilized mouse embryos were injected with CRISPR components mixed in microinjection buffer. The final concentrations of Cas9 protein and sgRNA were 50 ng/μL and 25 ng/μL, respectively. The fertilized one cell embryos were isolated from superovulated female mice. Microinjection of the mixture was performed into pronuclei of fertilized eggs using FemtoJet 4i microinjector with manipulator (Eppendorf) attached to IX83 microscope (Olympus). The injected embryos were transferred into the oviduct of pseudo-pregnant females to allow further development. Microinjections and mouse transgenesis experiments were performed as described previously (Harms et al., 2014).

The resulting pups were genotyped for founder screening. The primers used for PCR were (ACE2-F1: 5'- ACCCTCCTCCTCCAGTG TAT -3' and ACE2-R1: 5'- AGGCAGTCACTCATCCTCAC -3'). PCR was conducted using the following conditions: Initial denaturation at 95°C for 4 min, 36 cycles with denaturation at 94°C (30 s), annealing at 60°C (30 s), and extension at 68°C (1 min). Final extension was performed at 68°C for 5 min. The deletion of the ACE2 gene's target site in mice was identified and confirmed by using polymerase chain reaction (PCR) and gene sequencing. The sequence confirmed founders were backcrossed to wild-type C57BL/6J mice for two consecutive generations and the founder line was established. Animals with confirmed ACE2 receptor gene knockout were used for breeding.

### 2.4. Western blotting

For Western Blotting (WB), 6–10 weeks old wild type and ACE2 KO animals were used. Mouse brains were dissected and stored at -80°C. Whole brain lysates were prepared in RIPA buffer supplemented with cOmplete protease inhibitor (Roche Cat # 04693116001). Protein estimation was performed using Pierce BCA protein assay kit (ThermoFisher Cat # 23225). Fifteen μg of the sample was loaded in each well of 12% acrylamide gel and SDS-polyacrylamide gel electrophoresis (PAGE) was performed. The proteins were then transferred to Immobilon-P PVDF membranes (Millipore Cat # IPVH00010). Blocking was performed with 5% milk/Tris-buffered saline-Tween 20 for 1 h at room temperature. The membranes were probed with primary anti-ACE2 antibody (Abcam Cat # 15348) and anti-GAPDH (Sigma Cat # G9545) at 1:1000 and 1:5000 dilutions, respectively at 4°C for 16 h. The secondary antibody used was peroxidase-conjugated AffiniPure Goat anti-rabbit IgG

(Jackson ImmunoResearch Cat # 111-035-003) at 1:5000 dilution for 1 h at room temperature. Bound antibody was detected using Clarity ECL Western Blotting Substrate (BioRad Cat # 1705061) with the image digitally captured using an ImageQuant LAS 4000 imager.

### 2.5. Hematoxylin and eosin staining of olfactory epithelium

The mice were initially perfused with 1 × Phosphate Buffer Saline (PBS) followed by 4% paraformaldehyde. The animal was decapitated, and the nasal cavity was dissected. After that, tissue was kept for a week in a 10% Ethylenediamine tetraacetic acid (EDTA) solution to decalcify the bones that surround the nasal cavity. After the removal of tissue from the EDTA solution, the nasal cavity was extracted by delicately removing the surrounding bones. Following the dissection of the nasal cavity, it was embedded in the paraffin wax. Briefly, the nasal cavity was kept in 60% isopropanol (90 min × 3 times), 80% isopropanol (45 min × 2 times), 90% isopropanol (30 min × 1 time followed by 15 min × 1 time), and then in xylene (15 min × 3 times). The dehydrated nasal cavity was then placed over previously melted paraffin wax and incubated overnight at 62°C in an oven. Following that tissue was embedded in a wax block and was incubated at -20°C overnight. Using microtome (RM2235, Leica Biosystems), 5–8 μm sections were obtained and were transferred to the poly-L-lysine coated slides. The slides were then incubated in a hybridization oven overnight at 62°C. Then, the slides were kept in xylene (5 min × 2 times) followed by varying concentrations of ethanol: 100, 90, 70, and 50% for 3 min each. The slides were then kept in distilled water for 3 min. The slides were removed from the water and left to air dry. A napkin was used to wipe away any excess water surrounding the tissue. Slides were positioned on the rails of the humidifying chamber, and a drop of hematoxylin was applied to the tissue and slides were left undisturbed for 15 min. The excess hematoxylin stain was removed with distilled water, and the slides were rinsed under running water for 15 min. The slides were then submerged for 10 s in 80% ethanol containing 1% Hydrochloric acid (HCl). To each tissue section, a drop of eosin was added. After 30 s of eosin application, slides were transferred to 70% ethanol for 1 min, 90% ethanol for 1 min, and 100% ethanol for 1 min. The slides were taken out of the ethanol and let to air dry. Following that slides were kept in xylene (15 min × 2 times). The slides were taken out, and before the slides dried fully, excess xylene was removed from the corners of the slides using a napkin and a drop of DPX medium was applied to the sections. The slides were mounted with a cover slip and edges of the cover slip were sealed. A brightfield microscope (BX43, Olympus) was next used to examine the sections and capture the images. We selected similar regions in the medio-lateral and antero-posterior axes on the nasal turbinates for both WT and KO mice. While calculating the cumulative distributions, 3–4 regions of interest (ROIs) from 18 to 24 sections per animal were selected to cover the nasal epithelium (Figure 2D). In addition, we have measured the epithelial thickness in different areas near to the septum (henceforth named as septal areas, dorsomedial and middle meatus areas) and other turbinate regions toward the lateral side (ethmoturbinate areas) in each section, with similar numbers from both locations (Supplementary Figure S1). The thickness of OE was measured across OSN layer at different locations (as marked in Figures 2B1,B2).

<sup>1</sup> <http://crispor.tefor.net/>

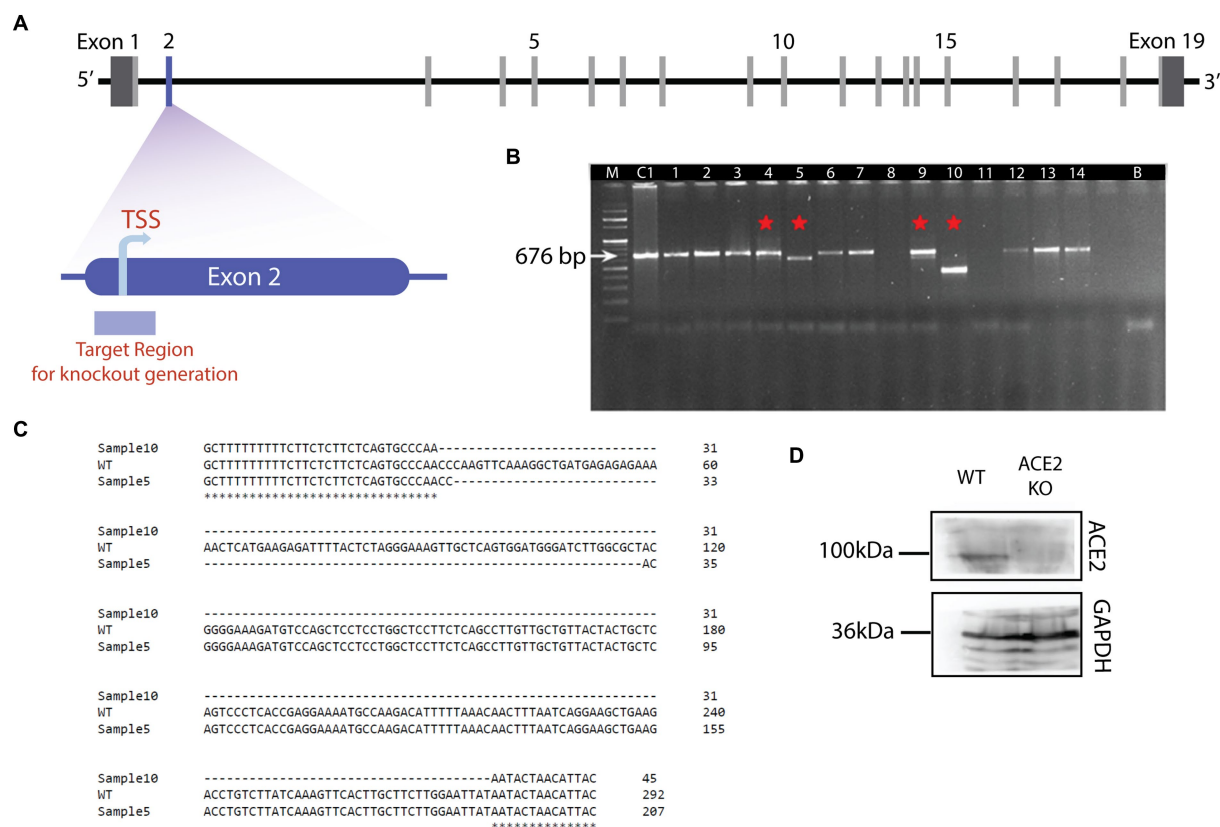


FIGURE 1

Generation of ACE2 knockout mouse model. **(A)** Schematic of the genetic structure of the ACE2 gene. ACE2 gene harbors 19 exons with the translation start site (TSS) in the exon 2. TSS is the target region to create the knockout using CRISPR-Cas9 mediated genome editing. **(B)** Agarose gel electrophoresis image of DNA samples isolated from the potential ACE2 KO animals. Sample C is the control (C57BL/6J) genomic DNA (676bp), Sample B is used as a negative control without any genomic DNA, and samples 1 to 14 are DNAs with genome editing. Samples 4, 5, 9, and 10 revealed the deletions and are depicted by red asterisk on the gel. Sample 10 showed the maximum deletion, hence selected for further breeding. **(C)** Sequence alignment showing deletions in samples 5 and 10. For the sample 5, 84bp deletion was observed, whereas for sample 10, a 246bp deletion occurred in the target region. These results confirmed the deletion of the ACE2 receptor gene in sample 10. **(D)** Western blot showing the expression of ACE2 protein in the brain of ACE2 KO and WT animals. The band corresponding to ACE2 protein was observed for WT animals, whereas in ACE2 KO animals, ACE2 expression was undetectable. Band corresponding to GAPDH protein is observed in brain lysates from both animals.

## 2.6. Immunohistochemistry using MAP2

ACE2 KO and WT animals were perfused, and their olfactory bulbs (OB) were dissected. The dissected brain was kept in 4% paraformaldehyde for 24 h before keeping it in 30% sucrose for 1 day for cryoprotection. For Microtubule associated protein 2 (MAP2) staining, 50  $\mu$ m thick sections were obtained using cryotome (CM1950, Leica Biosystems) and one section was selected for every five sections. Sections were washed three times in tris-buffered saline (1  $\times$  TBS) for 15 min on a rocker at 15 rpm. The permeabilization and blocking were done using TBST (0.2% Triton X-100 in 1  $\times$  TBS) with 5% bovine serum albumin (BSA) and 7.5% normal goat serum (NGS) for 1 h at room temperature. The sections were then incubated overnight at 4°C with primary antibody diluted in the respective blocking buffers. Chicken anti-MAP2 (Abcam, ab92434, 1:3000) was used as the primary antibody. Sections were then washed with 1  $\times$  TBS (10 min  $\times$  3 times) and incubated for 1 h at room temperature with secondary antibody diluted in TBST. Alexa Fluor 647-conjugated donkey anti-chicken IgG (Jackson ImmunoResearch, 703–605–155, 1:500) was used as the secondary antibody. The sections were

then given 1  $\times$  TBS (10 min  $\times$  3 times) washes and were incubated with DAPI (Sigma, 1:500) in 1  $\times$  TBS for 10 min. Following that, sections were washed once with 1  $\times$  TBS (10 min) and then mounted onto slides with glass coverslips using a mounting medium. The mounted sections were imaged using a confocal microscope (SP8, Leica Biosystems). All image acquisition parameters, such as the objective (40X oil immersion), zoom (1.0), pinhole diameter (1 AU), pixel format (1024  $\times$  1024), laser intensity (~5%), and scanned thickness of ~20  $\mu$ m (1  $\mu$ m step size), were kept constant during the imaging.

The area of the glomeruli and the MAP2 immunoreactivity were quantified from maximum intensity projection (MIP) images containing two channels: DAPI and MAP2 (Figure 2E, Blue and Green color, respectively). In the MIP images, each glomerulus representing an ROI was selected using the freehand selection tool in ImageJ/Fiji. The area and mean gray value (MAP2 channel) were measured for each glomerulus. To rule out any sampling bias that may result from the size distribution of glomeruli in the whole OB, we took every fifth coronal section of the OB (50  $\mu$ m sections, 12–14 sections of both OBs per mouse) covering the entire anterior–posterior axis.



Similar numbers of ROIs were selected in mediolateral and dorsoventral axes in both WT and ACE2 KO mice.

## 2.7. Go/no-go odor discrimination

### 2.7.1. Odors

For Go/No-Go discrimination task, following odors were used: Methyl Benzoate (MB), Limonene (+) (Li), Amyl acetate (AA), and Ethyl butyrate (EB). The odors were diluted in mineral oil (MO) and different dilution of the odors were used ( $10^{-4}$  to  $10^{-10}$  percent volume in MO). All odors had a purity level of above 99% and were purchased from Sigma-Aldrich, and the mineral oil was obtained from Oswal Pharmaceuticals in Pune, Maharashtra, India.

### 2.7.2. Odor pairs

Different sets of animals were trained to differentiate the following: Li vs. MO ( $10^{-10}$ ,  $10^{-9}$ , and  $10^{-8}$ % v/v), MB vs. MO ( $10^{-10}$ ,  $10^{-8}$ , and  $10^{-6}$ % v/v), and complex binary mixture of AA vs. EB [AA(60%) + EB(40%) vs. EB(60%) + AA(40%)] ( $10^{-8}$ ,  $10^{-6}$ , and  $10^{-4}$ % v/v).

### 2.7.3. Apparatus

For olfactory-based discrimination experiments, eight-channel olfactometer with custom modifications was used (Knosys). The apparatus consisted of an operant chamber where the animal was kept during the behavioral test. The operant chamber has a combined odor sampling and reward port on one side that is guarded by an IR beam. This allows for a tight association between odor presentation in a trial and the reward. A trial is initiated when the animal breaks the IR beam by poking its head into the sampling port. The odor valve connected to a flowmeter opens as the trial initiates and it controls the onset and flow of odor stream (airflow rate of 2 Liters per min). After 500 ms of odor valve opening, a final valve (diversion valve) that lies near to the sampling port, opens and the stimulus is delivered to the animal. The precise onset of the stimulation was ensured by a system of these solenoid valves that are controlled by custom written program in IGOR. The S+ (rewarded) or the S- (non-rewarded) odors were presented through a set of different valves.

### 2.7.4. Task-habituation phase

The animals were subjected to task habituation training three to 4 days after the beginning of the water deprivation schedule. Standard operant conditioning approaches were used to train the animals. The task habituation phase was performed for the animals to get acclimatized to the operant chamber, location of reward and sampling port, lick tube, sounds of the valves, and procedural aspects of the instrument. The task habituation consisted of nine phases (Phase 0–8). In the Phase 0, animal received water reward (3–5  $\mu$ L) simply by breaking the IR beam. This enabled the animals to locate the reward port and the water delivery tube. In the following phase, the animals were given water only when they made at least one lick. For the subsequent stages of this task-habituation training, the complexity level of the task increased gradually, and animals had to lick on the tube in order to receive the water reward. In the late stages of this phase, odor valve was introduced and animal received the odor stimulus for 2 s, wherein animal has to respond and lick to receive the

reward. All animals finished the task habituation phase in three to four sessions of 30 min.

### 2.7.5. Discrimination training phase

The odor-based discrimination tasks were performed using a Go/No-Go behavioral paradigm (Abraham et al., 2004). The mouse initiated a trial by breaking the IR beam that was guarding the sampling port. This enabled the opening of one of the solenoid valves, followed by the opening of a three-way diversion valve after 500 milliseconds. After diversion valve is opened the stimulus is presented to the animal for a 2 s duration. The use of a diversion valve reduced the period between the onset of the stimulus and the first contact with the animal. To obtain a reward, the animal has to meet the required reward criteria based on the reward contingency of the stimulus [Rewarded (S+)/ Non-Rewarded (S-)].

The time that was provided for animals to respond overlapped with the stimulus duration. The response time was virtually divided into four equal bins, i.e., for a response/stimulus duration of 2 s, divided into four 500 ms bins. Animals required to register a lick in at least three out of these four bins for a S+ trial to be considered correct. For a successful S+ trial, a water reward of 3–4  $\mu$ L was given to the animal after the stimulus ended [Reward Criteria: Animal needs to register a lick in at least three out of the four bins]. For an S- trial to be correct, animal was only allowed to lick for at most two bins. There was no punishment or reward for an incorrect or correct S- trial, respectively. Before the next trial could be initiated, a 5-s inter-trial interval (ITI) was kept. There were no rules requiring the mouse to smell the odor for a certain amount of time before making a choice and to prohibit licking prior to the odor. The mice received stimuli in blocks of 20 trials. Ten S+ trials and ten S- trials were present in each of these blocks. Within a block, the S+ and S- trials were pseudorandomized in order to prevent the delivery of more than two consecutive stimuli with the same reward condition. The preference for a particular stimulus was prevented by balancing the S+ and S- stimuli for a group of animals (for instance, in a group of 8 animals, 4 mice receive one stimulus as S+ while the other 4 animals receive another stimulus as S+). The animals were adequately motivated to finish 200–300 trials in a day, spaced out over 1–2 (30–40 min) sessions. Animal's motivation was measured using different instrumental readouts, including licking probability and inter-trial interval. The training session was terminated after the animal stopped licking for the rewarded trials. The data was collected using a custom-written software in IGOR-PRO that was compatible with the MCC-CIO-DIO 48 data acquisition card.

### 2.7.6. Behavioral readouts

#### 2.7.6.1. Learning curve

The learning curve measures the performance as the percentage of correct responses during the training. Each point on the learning curve indicates the average accuracy of 100 trials [50S+ and 50S-] across all animals.

#### 2.7.6.2. D-prime ( $d'$ )

Hit (correct S+) and false alarm (incorrect S-) probabilities were computed for  $d'$  over an average of 100 trials. The probabilities were used to calculate the z-score.  $d'$  was calculated as  $z(\text{hit}) - z(\text{false alarm})$  per 100 trials.

### 2.7.6.3. Discrimination time

The licking behavior of each mouse was monitored to assess the discrimination time. Animals' licking behavior was recorded with high temporal resolution and analyzed in time bins of 20 ms. The licking behavior changed as a result of learning and was considerably different between the early and late stages of learning. During the early phase of learning, when the animals were not able to discriminate the S+ and S- stimuli, they licked for both the stimuli. As a result, during the initial training phase, the animal's lick responses to S+ and S- stimuli were comparable. But as soon as they were able to differentiate between two stimuli, they began to selectively lick for S+ trials and avoid licking for S- trials, which caused a divergence in the lick responses between two stimuli. The statistical comparison of the lick responses between the S+ (150 trials) and S- (150 trials) trials was performed using one-tailed t-test. The t-test was performed for each time bin of the lick pattern between S+ and S- trials. This comparison yields a value of p curve as a function of time. In the value of p curve, the last time point where the value of p is  $<0.05$  is taken as the discrimination time. The discrimination time was measured task wise, i.e., for 300 trials.

### 2.7.6.4. Area under the curve (AUC)

The area under the curve (AUC) was also used to calculate the discrimination index of the animals. For AUC calculations, the lick probabilities for S+ and S- trials were used. The discrimination index was calculated as:  $AUC = (AUC_{S+} - AUC_{S-}) / AUC_{S+}$ .

## 2.8. Novel odor discrimination

To further compare the novel odor discrimination abilities of ACE2 KO mice with WT mice, a previously published olfactory habituation/dishabituation paradigm with slight modifications was adopted (Tillerson et al., 2006; Lehmkuhl et al., 2014). Before the experiment began, animals were kept in the experimental cage for 5 min for cage habituation. 50  $\mu$ L of distilled water or odor (diluted to 1% in mineral oil) was applied on a piece of Whatman filter paper and kept inside separate, identical boxes at the two ends of a cage. For the first trial, the box containing water was placed on one side of the cage, and the box containing the odor (cineole or eugenol) was placed on the opposite side. One trial continued for 3 min during which the behavior of animals was recorded. The boxes were removed from the cage after the trial finished. Inter-trial interval of 15 min were provided between the trials. In order to prevent any location-based bias of the animal, the cage was rotated around 180° between each trial. Only one odor was used for the first five trials to ensure the odor habituation, following which, on the 6<sup>th</sup> trial, this odor was replaced with a novel odor, e.g., if eugenol was used in the first five trials (habituated odor), it was replaced with cineole (novel odor) in the 6<sup>th</sup> trial. For each trial the behavior of animal was videotaped and the trial videos were analyzed using EthoVision software. The amount of time the animal spent sampling a particular box was determined by how long its nose tip was inside a region around 2 cm from the perimeter of the box. These areas were chosen as the zones in the software, while the entire cage served as the arena. The cage's length and width were used to calibrate the arena, and a sample rate of 30.00 samples per second was used. Dynamic subtraction was used to identify the mice's nose, center, and base of tail at a dark contrast of 50–60.

## 2.9. Pheromone detection

An open field pheromone detection experiment was used to examine the pheromone detecting capacities of ACE2 KO and wild type females. Before the experiment began, all females had attained sexual maturity. The behavioral apparatus used to assess pheromonal detectabilities comprised of a chamber with dimensions of 60 cm x 45 cm. Since non-volatile odorants are found in male-soiled bedding, and volatile odorants are found in urine, the test was conducted by placing a petri dish filled with male soiled bedding and urine (~100  $\mu$ L) at the center of the arena. Females were kept in the chamber for 10 min and were allowed to freely roam and explore the arena. A camera was used to record the animals' movements, and EthoVision software was used to track them. The amount of time the females spent in the vicinity of the petri dish was used to quantify the sampling behavior.

## 2.10. Multimodal pheromonal learning

### 2.10.1. Apparatus

Pheromone preference and odor association abilities in mice were tested using the multimodal pheromonal learning paradigm established in our lab (Pardasani et al., 2021). For this experiment, the same groups of females that were used for the pheromone detection experiment were used. The apparatus comprised of an arena with dimensions of 60 cm x 30 cm x 15 cm (length x width x height). The entire arena was divided into three spaced zones having equal areas with the help of two sliding partitions. Opening both the partitions allowed the females to explore the entire arena, whereas closing them allowed us to restrict the females in specific areas. At the opposite extremities of the arena, two 10 cm x 10 cm x 15 cm compartments with removable plates were positioned. In each chamber, a 55 mm petri dish held 100  $\mu$ L of either water (the neutral stimulus in chamber 2) or urine (the attractive pheromonal stimulus in chamber 1) was kept. These chambers were guarded by the lids having orifices with different diameters (5 mm and 10 mm). Due to this, the animal was restricted to sample the volatiles coming from the chamber's front side through the holes and they were able to associate the diameters with the volatile cues. To mitigate any bias toward the diameters of the holes, animals were counterbalanced for the association between the volatile cues and the different orifice sizes.

### 2.10.2. Paradigm

The experimental design included a 4-day initial testing phase, a 15-day training phase, and memory tests on the 15th day after the training. The purpose of the initial testing phase was to determine whether female mice have an intrinsic preference for the zones (zone 1 containing the volatile and non-volatile pheromones from male mice & zone 2 containing neutral stimuli, water). During the early testing and training phases, the equipment was rotated by 180° every day to eliminate any directional bias toward a specific zone. Following the initial testing phase, 15 days of training was performed. During the training phase, each day, the animal was only allowed in one of the zones for 15 min (alternating between the two zones after every 5 min, 3 times). Fifteen days after the end of training phase, memory test was performed. To test the memory, all volatile and

non-volatile pheromonal stimuli (urine and soiled bedding with non-volatile pheromonal traces) and neutral water stimuli were removed from the chambers of the apparatus while leaving the plates with specific diameter orifices undisturbed. Using the EthoVision program, the amount of time spent in each zone, particularly in front of chambers 1 and 2, was quantified. Animal tracks were visualized and time spent was calculated using EthoVision's nose point feature, which is used to track animals. The number of active attempts on the plates guarding chambers 1 and 2 was manually scored by counting each nose poke through the plate as one attempt. Memory index was calculated for both the time spent and number of active attempts as:  $\text{Memory Index} = (\text{Time spent or No. of active attempts in pheromone zone} - \text{Time spent or No. of active attempts in neutral stimulus zone}) / \text{Time spent or No. of active attempts in neutral stimulus zone}$ .

## 2.11. Behavioral tests for stress, anxiety, and motor control

Different tests were conducted to study the exploration, anxiety-like, and depression related behaviors and motor control of the animals. These tests were conducted in the following order:

### 2.11.1. Open field test

The set-up consisted of a pseudo home cage where mice belonging to the same cage were housed for about 15 min. The dimension of the cage was 42 cm x 26 cm x 18 cm and the top of the cage was covered with a grill. In order to prevent any initial hyperactivity, the animals were acclimated in this cage. During the test, a single mouse was permitted to pass from the cage into the main arena (60 cm x 45 cm) through a little opening for 10 min. A camera mounted on a tripod stand captured the exploratory behavior of the animal. Using EthoVision tracking software, the total distance traveled, time spent in the center of the arena, latency to the center, and total time spent in the four corners were calculated.

### 2.11.2. Elevated plus maze test

For EPM test, an elevated plus maze which was raised 50 cm above the ground was used. The apparatus constituted closed and open arms. The arms of the maze were 5 cm wide and 55 cm long. The closed arms consisted of walls that were 15 cm high. The middle zone at the junction of the four arms had a dimension of 5 cm x 5 cm. To initiate a trial, the animal was placed on this junction facing the open arm. The trials lasted for 5 min and animals were free to explore the EPM during this time. For quantitative analysis, the time spent in open vs. closed arms and the number of entries into the open and closed arms were calculated.

### 2.11.3. Tail suspension test

For TST, mouse was suspended by its tail using a 15 cm piece of tape attached to a horizontal rod at a height of 40 cm from the ground. Each trial lasted for 6 min, following which the animals were removed from the apparatus. For analysis, time spent mobile, where the animal tries to escape, and the time spent immobile were quantified manually with a resolution of 1 s.

### 2.11.4. Forced swim test

FST was performed using an acrylic cylinder of 15 cm diameter and 30 cm height that was filled with water (12 cm height). The mouse was placed in the water for 6 min. To prevent hypothermia after the experiment was finished, the mouse was placed in a cage covered with dry tissue which was kept on a heating pad for 15 min. The animal was then transferred to its native cage. Behavior of the animal was classified between the time spent mobile and immobile. The mobility and immobility were scored manually with a resolution of 1 s. Across ACE2 KO and wild type groups, time spent immobile was compared.

### 2.11.5. Rotarod test

The rotarod test was performed to evaluate the balance and motor coordination. The animals were placed on a rotating rod that rotates at a speed ranging from 1 to 4 revolutions per minute. The test was completed when the mouse fell off the rod and landed on the sponge bed that was kept at the base of the apparatus. Parameters such as total time spent by the animals on the rod and the distance traveled by them were quantified and compared between the two groups.

## 2.12. Statistical analysis

GraphPad Prism 9, Microsoft Excel, and Python were used for all data and statistical analyzes in this study. For image analysis ImageJ/Fiji was used. The data is presented as cumulative distributions and Mean  $\pm$  SEM. To determine the *p*-values and test for statistical significance, we used the Kolmogorov–Smirnov test (K-S test), student's *t*-test (Normally distributed data determined using Shapiro–Wilk test), Mann–Whitney test (Non-normally distributed data), one-way and two-way ANOVA, and associated post-hoc tests.

## 3. Results

### 3.1. Generation of ACE2 KO mice using CRISPR-Cas9 genome editing tools

The olfactory system of rodents is an attractive model to study the circuit mechanisms of many brain dysfunctions. The well-mapped anatomical organization, the ease of accessibility of different olfactory centers, and olfaction being the dominant sensory modality of rodents make it an efficient tool to modulate circuit functions which give rise to specific behavioral phenotypes mimicking brain disorders. Since the beginning of pandemic, olfactory system remained as the most studied sensory system due to prevalent olfactory and cognitive dysfunctions caused by SARS CoV-2 infection. As ACE2 receptor was one of the molecular factors mediating the virus entry (Klingenstein et al., 2020), ACE2 KO mouse model was generated using CRISPR-Cas9 by deleting the translation start site of the exon 2 of the ACE2 gene (Figure 1A). Guide RNAs for 5' and 3' end of the targeted region were chosen to generate the knockout. The mouse zygote was microinjected with the transcribed gRNA/Cas9 mRNAs, after the vectors that target ACE2 gene deletion were constructed using the guide RNAs. For confirmation of the deletion, the genomic DNA of



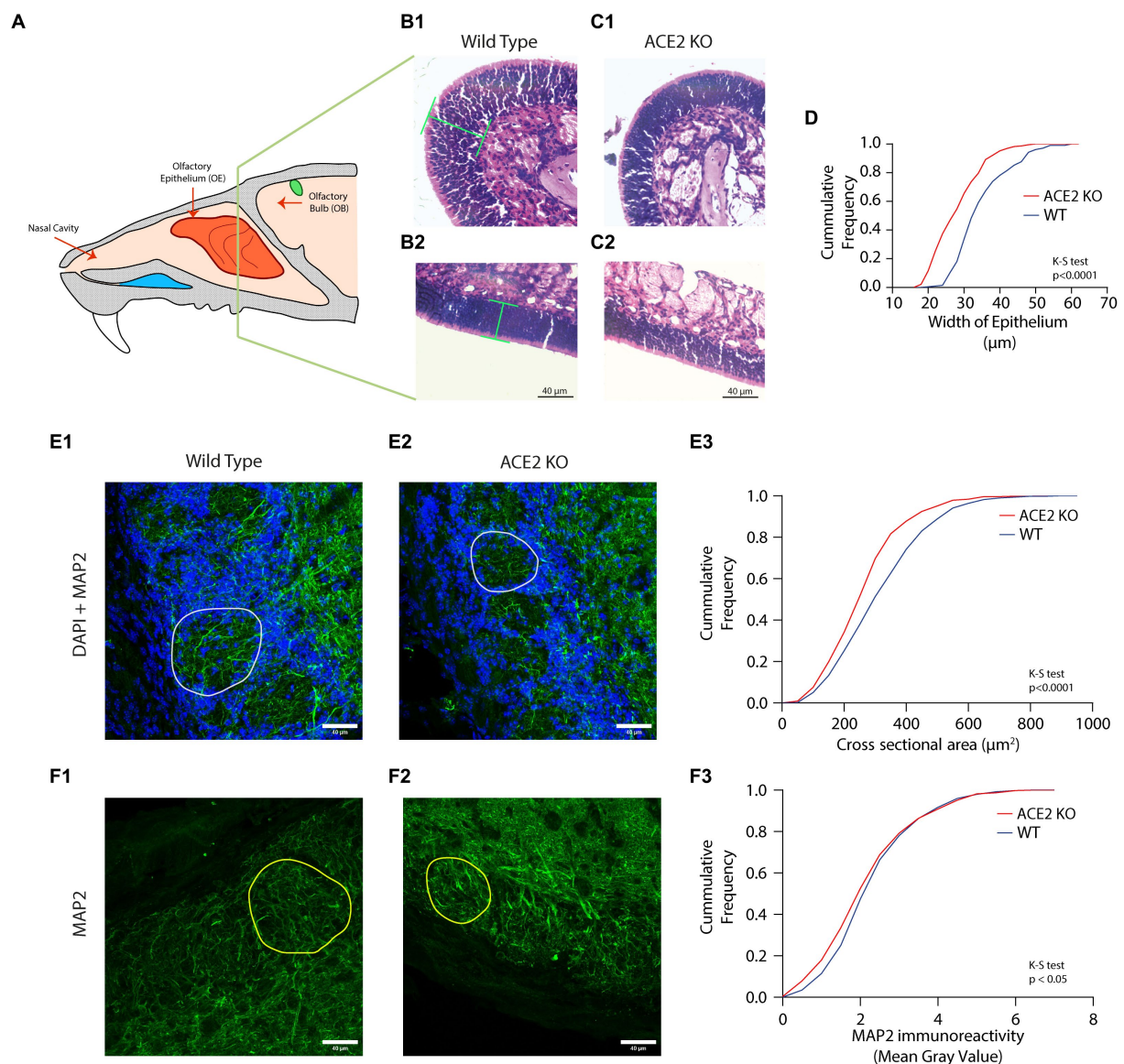


FIGURE 2

Morphological aberrations in the olfactory epithelium (OE) and olfactory bulb (OB) of ACE2 KO animals. **(A)** Schematic representation of the mouse olfactory system. The olfactory epithelium (OE) is present in the posterior region of the nasal cavity and harbors olfactory sensory neurons (OSNs). These OSNs express odor receptors. The signal from the OSNs is then transduced to the olfactory bulb (OB). **(B,C)** Representative images of different regions of OE stained with Hematoxylin and Eosin for WT **(B1,B2)** and ACE2 KO **(C1,C2)** animals, respectively. Green lines in the panel **B1** and **B2** represent the width of the epithelium. **(D)** Cumulative frequency distribution of epithelium width for ACE2 KO and WT animals. The width of epithelium for WT was  $35.39 \pm 0.5294 \mu\text{m}$ , ACE2 KO:  $28.67 \pm 0.4408$ , K-S test,  $p < 0.0001$ , number of animals:  $n_{\text{WT}} = 4$  and  $n_{\text{ACE2 KO}} = 4$ , number of region of interests (ROI): WT=211, ACE2 KO=232. **(E)** Representative images of the glomeruli pooled for WT and ACE2 KO animals. The cross-sectional area of the glomeruli pooled for WT and ACE2 KO animals. The cross-sectional area for WT was  $335.6 \pm 6.444 \mu\text{m}^2$ , for ACE2 KO was  $283.1 \pm 5.191 \mu\text{m}^2$  (K-S test,  $p < 0.0001$ , number of animals:  $n_{\text{WT}} = 3$  and  $n_{\text{ACE2 KO}} = 3$ , number of glomeruli: WT=496, ACE2 KO=558). **(F)** Representative images of the glomerular layer of the OB stained with MAP2 and green color. **(F3)** Cumulative frequency distributions of MAP2 immunoreactivity measured using mean intensity for WT and ACE2 KO animals. The MAP2 immunoreactivity for WT was  $2.490 \pm 0.0499$ , for ACE2 KO was  $2.357 \pm 0.0517$  (K-S test,  $p = 0.0349$ , number of animals:  $n_{\text{WT}} = 3$  and  $n_{\text{ACE2 KO}} = 3$ , number of glomeruli: WT=496, ACE2 KO=558).

the F0 mice was subjected to the PCR and was visualized using agarose gel electrophoresis. A shorter PCR product of the expected size was visible on the agarose gel. Visualization of the agarose gel revealed deletions in samples 4, 5, 9, and 10 with sample 10 showing the maximum deletion (band shown in sample 10 of Figure 1B). The deletions were further confirmed by performing the sequencing for samples 5 and 10 in which 84bp and 246bp deletions were observed,

respectively, (Figure 1C). F0 female mouse (sample 10) was further crossed with C57 BL6 males and the progenies were then backcrossed for three generations to obtain enough number of homozygous KO animals. The genotype of experimental mice were further confirmed by western blotting to check the ACE2 protein levels in the brains of ACE2 KO and WT animals. In contrast to WT animals, which showed prominent bands for ACE2, western blot analysis did not reveal any



band corresponding to ACE2 protein in the ACE2 KO animals. Bands for GAPDH, which acted as an internal control, were observed in both groups of animals (Figure 1D), thereby confirming the absence of ACE2 proteins in the brains of animals used in the experiments. These results therefore confirm the successful generation of the ACE2 KO mouse model. Further, morphological phenotypes of these mice were assessed using microscopic techniques and the behavioral phenotypes were studied using various assays.

### 3.2. ACE2 KO animals exhibit morphological alterations in the olfactory epithelium and olfactory bulb

Although there are mouse models available to study underlying mechanisms of brain dysfunctions caused by SARS CoV-2 infection, a detailed characterization of sensory as well as cognitive deficits using precise behavioral assays are lacking to date. In the olfactory system of rodents, ACE2 receptors are primarily found in supporting sustentacular cells of the olfactory epithelium (Bilinska et al., 2020; Butowt and Bilinska, 2020; Lechien et al., 2021). Due to the protective and supporting nature of sustentacular cells, the viral infection resulting in the internalization of receptors can cause neuroinflammatory changes leading to gradual decaying of OSN functions. To investigate the effect of ACE2 receptor knockout on the morphology of OSNs, we first quantified the OSN layer thickness and compared it to that of wildtype (WT) mice (Figure 2A). Coronal sections of the OE stained with Hematoxylin and Eosin were used to measure the OE thickness, which was assessed as the perpendicular distance from the basal membrane. For ACE2 KO, 232 regions of interest (ROIs), and for WT mice, 211 ROIs were analyzed along anterior–posterior and mediolateral axes for four mice in each group. The cumulative distributions of epithelium width measurements reveal smaller OE thickness in ACE2 knockout mice in comparison to that of the WT animals, indicating the role of supporting cells in maintaining the morphology of the OE (Figures 2B–D, WT:  $35.39 \pm 0.5294 \mu\text{m}$ , ACE2 KO:  $28.67 \pm 0.4408$ , K-S test,  $p < 0.0001$ ). In addition, we measured the epithelial thickness in different areas near to the septum (henceforth named as septal areas, dorsomedial and middle meatus areas) and other turbinate regions toward lateral side (ethmoturbinate areas) in each section, with similar numbers from both locations. On analyzing these areas separately, we observed lower thickness of olfactory epithelium in ACE2 KO animals in both locations, thereby confirming that reduction in epithelium thickness is independent of the location on the turbinates (Supplementary Figure S1, ACE2 KO vs. WT: K-S test,  $p < 0.0001$  for both septal and ethmoturbinate areas).

The OSNs project to glomeruli of OB in a receptor specific manner. In the glomeruli, these OSNs makes synapses with the Mitral/ Tufted cells, which are the output neurons of the OB. Since the morphological characteristics of OB glomeruli are dependent on the axonal inputs of OSNs (Potter et al., 2001), we hypothesized that the reduction observed in the OE thickness may result in the alterations of glomeruli morphology. To accomplish this, a quantitative analysis of the cross-sectional area of individual glomeruli was performed across ACE2 KO (558 glomeruli) and WT mice (496 glomeruli). The cumulative frequency distribution of the glomeruli area revealed a reduction in the cross-sectional area of olfactory glomeruli in ACE2

KO mice compared to WT, C57BL/6J animals (Figures 2E1–E3, WT:  $335.6 \pm 6.444 \mu\text{m}^2$ , ACE2 KO:  $283.1 \pm 5.191 \mu\text{m}^2$ , K-S test,  $p < 0.0001$ ). In addition to the cross-sectional area, we also analyzed the perimeter and minimum and maximum diameter. The perimeter and minimum and maximum diameter for glomeruli of the ACE2 KO animals were lower than that of the WT animals (Supplementary Figure S2). Further, to investigate the potential modifications in the neural circuits caused by the knockout of ACE2 receptors, we performed the immunostaining for the neuronal cytoskeletal protein MAP2, which stains the neurites. The qualitative analysis revealed a more prominent and discernible neurite projections in the glomeruli of WT animals. To quantify these changes, we calculated the mean gray value corresponding to MAP2 immunoreactivity in individual glomeruli of ACE2 and WT animals. A total of 558 glomeruli in ACE2 KO mice and 496 glomeruli in WT animals were analyzed and the cumulative distribution of intensities were compared across WT and ACE2 KO animals. This quantification revealed significantly lower MAP2 immunoreactivity in ACE2 KO compared to control mice implying severe alterations in neural circuits caused by the knockout of ACE2 receptors (Figures 2F1–F3, WT:  $2.490 \pm 0.0499$ , ACE2 KO:  $2.357 \pm 0.0517$ , K-S test,  $p = 0.0349$ ). Taken together, these results prove morphological aberrations in the sensory periphery (OE) as well as in the pre-cortical sensory area (OB) of ACE2 KO mice, which may cause alterations in the sensory and cognitive abilities of animals.

### 3.3. Altered odor detection and discrimination behavior in ACE2 KO mice

Having observed the morphological aberrations in ACE2 KO mice, we next asked how these aberrations are affecting their olfactory behavioral readouts. In asymptomatic carriers and symptomatic COVID-19 patients, we have observed compromised odor detection abilities more strikingly at the threshold levels (Bhattacharjee et al., 2020; Pardasani and Abraham, 2022; Bhowmik et al., 2023). Therefore, we investigated the detection abilities of ACE2 KO and WT mice using different batches of animals by training them on a go/no-go operant conditioning paradigm using different concentrations of specific odors vs. mineral oil (MO). On training mice to discriminate Methyl Benzoate from MO, ACE2 KO mice did not show any difference in the learning pace compared to WT animals (Figure 3A; MB,  $10^{-10}\%$ ,  $10^{-8}\%$ , and  $10^{-6}\%$ , diluted in MO, two-way ANOVA for each concentration, non-significant (ns) represents  $p > 0.05$ ). However, ACE2 KO mice showed slower learning pace for certain concentrations on training them to discriminate (+) Limonene ( $10^{-10}\%$ ,  $10^{-9}\%$ , and  $10^{-8}\%$ ) from MO (Figure 3B, two-way ANOVA for each concentration, \* represents  $p < 0.05$  and ns represents  $p > 0.05$ ). As these alterations can be dependent on the odorants used, a detailed screening using many odor pairs and more concentrations will be required to find out the changes in odor detectabilities.

As we observed varying detection abilities with ACE2 KO, we further studied odor discriminations using a complex binary mixture of Amyl acetate (AA) and Ethyl butyrate (EB) at varying concentrations (see methods). We quantified and compared various behavioral readouts from KO and WT animals to confirm the behavioral phenotypes caused by the knockout of ACE2 receptors. KO mice showed slower learning pace compared to control animals at different concentrations (Figure 3C, two-way ANOVA for each

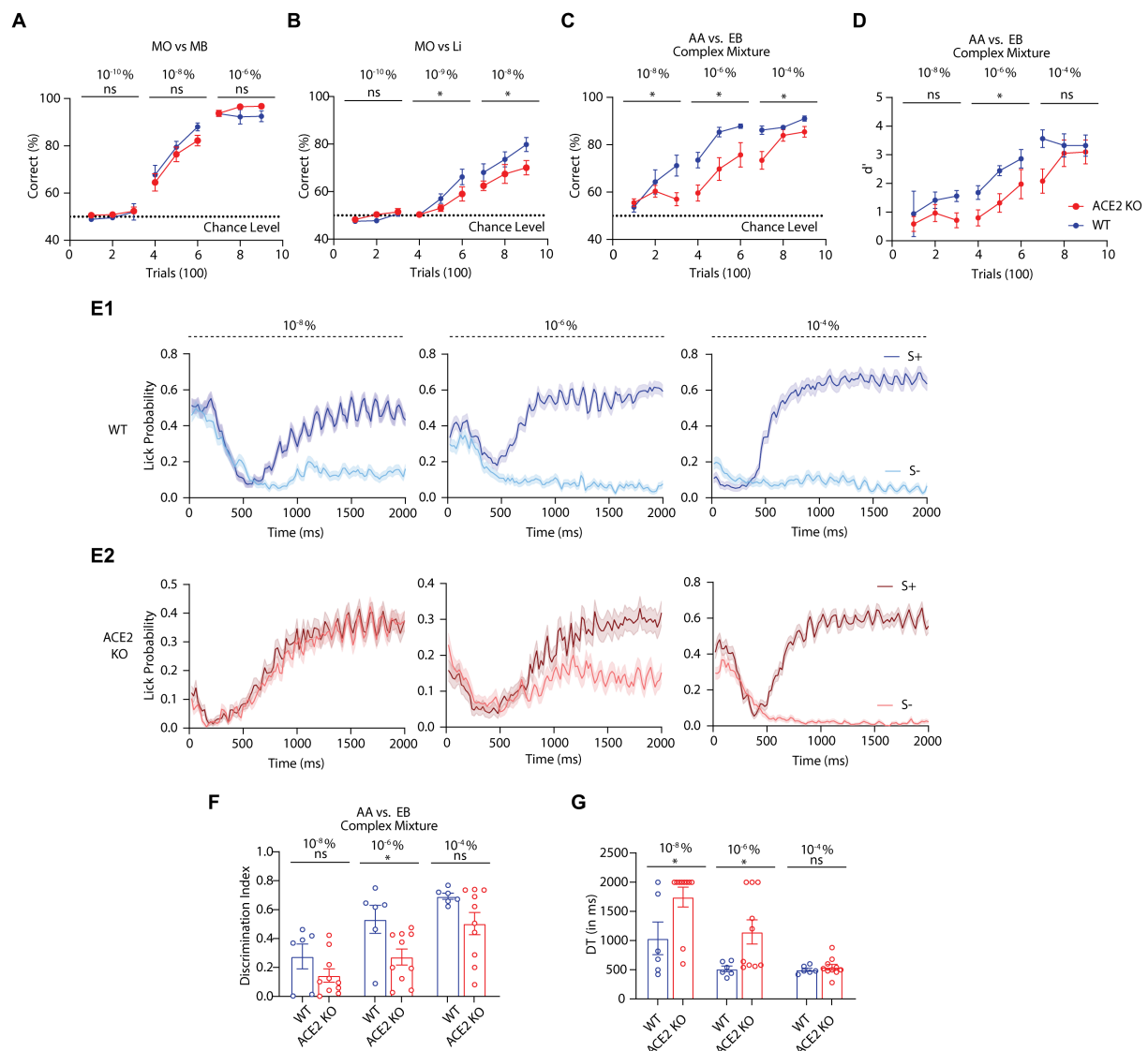


FIGURE 3

Odor detection and discrimination characteristics of WT and ACE2 animals. **(A)** Accuracy of performance shown by learning curves for WT and ACE2 KO animals when trained to discriminate mineral oil (MO) vs. Methyl Benzoate (MB) at different concentrations ( $10^{-10}\%$ ,  $10^{-8}\%$ , and  $10^{-6}\%$ ). Comparisons of learning curves: Two-Way ANOVA. For,  $10^{-10}\%$ : [ $F(1,45)=0.8053$ ,  $p=0.3743$ ],  $10^{-8}\%$ : [ $F(1,45)=2.495$ ,  $p=0.1212$ ], and  $10^{-6}\%$ : [ $F(1,45)=4.236$ ,  $p=0.0554$ ], number of animals:  $n_{ACE2KO}=10$ ,  $n_{WT}=7$ . **(B)** Learning curves of WT and ACE2 KO animals for mineral oil (MO) vs. Limonene (+) (Li) at different concentrations ( $10^{-10}\%$ ,  $10^{-9}\%$ , and  $10^{-8}\%$ ). Comparisons of learning curves: Two-Way ANOVA. For,  $10^{-10}\%$ : [ $F(1,66)=3.451$ ,  $p=0.0677$ ],  $10^{-9}\%$ : [ $F(1,63)=4.435$ ,  $p=0.0392$ ], and  $10^{-8}\%$ : [ $F(1,63)=7.574$ ,  $p=0.0077$ ], number of animals:  $n_{ACE2KO}=11$ ,  $n_{WT}=13$ . **(C)** Learning curves of WT and ACE2 KO animals for a complex odor discrimination task [60% Amyl acetate (AA)+40% Ethyl Butyrate (EB) vs. 60% EB+40% AA, at different concentrations ( $10^{-8}\%$ ,  $10^{-6}\%$ , and  $10^{-4}\%$ ). Comparisons of learning curves: Two-Way ANOVA. For,  $10^{-8}\%$ : [ $F(1,42)=4.605$ ,  $p=0.0377$ ],  $10^{-6}\%$ : [ $F(1,42)=15.09$ ,  $p=0.0004$ ], and  $10^{-4}\%$ : [ $F(1,42)=10.09$ ,  $p=0.0028$ ], number of animals:  $n_{ACE2KO}=10$ ,  $n_{WT}=6$ . **(D)**  $d'$  (d prime) of WT and ACE2 KO animals measured during a complex odor discrimination task, same as panel C, at different concentrations ( $10^{-8}\%$ ,  $10^{-6}\%$ , and  $10^{-4}\%$ ).  $d'$  were compared between WT and ACE2 KO animals using Two-Way ANOVA. For,  $10^{-8}\%$ : [ $F(1,42)=3.360$ ,  $p=0.0739$ ],  $10^{-6}\%$ : [ $F(1,42)=9.663$ ,  $p=0.0034$ ], and  $10^{-4}\%$ : [ $F(1,42)=3.277$ ,  $p=0.0774$ ], number of animals:  $n_{ACE2KO}=10$ ,  $n_{WT}=6$ . **(E)** Lick patterns of WT (**E1**) and ACE2 KO (**E2**) animals for different concentrations during the complex odor discrimination used in panel C and D. Y-axis represents the lick probability as a function of time (X-axis). **(F)** Discrimination index calculated using the lick probabilities at different concentrations. Comparison using two-tailed unpaired t-test: For,  $10^{-8}\%$ :  $p=0.1585$ ,  $10^{-6}\%$ :  $p=0.0235$ , and  $10^{-4}\%$ :  $p=0.5276$ . Number of animals:  $n_{ACE2KO}=10$ ,  $n_{WT}=6$ . **(G)** Comparison of discrimination times (DT) shown by WT and ACE2 KO animals for different concentrations, using two-tailed unpaired t-test: For,  $10^{-8}\%$ :  $p=0.0369$ ,  $10^{-6}\%$ :  $p=0.0367$ , and  $10^{-4}\%$ :  $p=0.0858$ . Number of animals:  $n_{ACE2KO}=10$ ,  $n_{WT}=6$ . In the figure \* indicates  $p<0.05$ , ns indicates: non-significant.

concentration, \* represents  $p<0.05$ ). To account for the hit and false alarm probabilities while learning the discrimination task, d-prime ( $d'$ ) was calculated for both KO and WT groups and significant differences were observed (Figure 3D, two-way ANOVA for each concentration, \* represents  $p<0.05$  and ns represents  $p>0.05$ ).

Further, on analyzing the lick behavior with high temporal precision, we observed the differences in their licking responses toward rewarded and non-rewarded odors (Figures 3E1,E2, see methods). Therefore, we calculated the discrimination index based on this and found significant differences between KO and WT groups (Figure 3F, see

methods, two-tailed unpaired *t*-test for each concentration, \* represents  $p < 0.05$  and ns represents  $p > 0.05$ ). Further, the difference in the reaction times, quantified by discrimination times (DT, see methods), showed slower times for the KO compared to control mice (Figure 3G, two-tailed unpaired *t*-test for each concentration, \* represents  $p < 0.05$  and ns represents  $p > 0.05$ ). In summary, this detailed behavioral phenotyping confirms the olfactory sensory and cognitive deficits due to the knockout of ACE2 receptors.

### 3.4. Impaired novel odor discrimination in ACE2 KO mice

Olfactory dysfunctions are reported as early symptoms in Parkinson's disease (PD) patients (Barresi et al., 2012; Doty, 2012; Fullard et al., 2017; Marin et al., 2018). In addition, a few cases of PD associated with COVID-19 infection have been reported (Li et al., 2020; Sulzer et al., 2020; Merello et al., 2021). As olfactory deficits and PD are strongly linked, we decided to test ACE2 KO mice on a habituation and novel odor discrimination task that is used to phenotype PD mouse models (Fleming et al., 2008; Lehmkuhl et al., 2014). Animals' ability to discriminate between a familiar odor and a novel odor was assessed by quantifying the time spent by them to sample the new odor after getting exposed to another stimulus (familiar odor) few times. In brief, mice were exposed to an odor for 3 min on one side of a cage while the opposite side had similar box without any odor. They were exposed five times rotating the cage 180 degrees for each trial (Figure 4A). The novel odor discrimination was assessed by comparing the time spent by animals in sampling the novel odor vs. the habituated odor. While WT mice spent a significantly longer time for exploring the novel odor compared to the habituated odor (Figure 4B, Habituated odor:  $3.753 \pm 0.7959$  s, Novel odor:  $6.908 \pm 1.514$  s, one-tailed paired *t*-test,  $p = 0.0132$ ), ACE2 KO animals spent a similar amount of time exploring both the odors (Figure 4C, Habituated odor:  $3.449 \pm 0.6708$  s, Novel odor:  $4.743 \pm 0.9469$  s, one-tailed paired *t*-test,  $p = 0.0965$ ). Hence, our results revealed impairments in novel olfactory discriminations in animals with knockout of ACE2 receptors.

### 3.5. ACE2 KO female mice display compromised multimodal pheromonal location memory

Rodent olfactory subsystems can process various types stimuli including pheromones. Volatile components of pheromones have been shown to be processed by main olfactory bulb (MOB) (Buck, 2000). As we observed morphological aberrations in the MOB, we studied the pheromone detection abilities of ACE2 KO mice. When presented with pheromonal cues from the opposite sex in form of the soiled bedding, sexually mature ACE2 KOs and control female mice explored these cues in a similar manner. This was quantified by measuring the time spent near to the soiled bedding kept at the center of an open arena (Figures 5A1-A4, WT:  $118.8 \pm 17.06$  s, ACE2 KO:  $138.8 \pm 26.19$  s, two-tailed unpaired *t*-test,  $p = 0.5143$ ). This result shows similar pheromonal detection abilities in ACE2 KO and control animals.

In nature, pheromone location information helps animals finding their mates and avoiding potential predators. This information can

also be carried by the substances where the semiochemicals are being sprayed. Therefore, involvement of whiskers along with the olfactory system is anticipated in enabling the multimodal association between pheromones and their locations. Hence, we investigated whether ACE2-KO mice show any deficits in the acquisition of this multimodal information. We employed an established behavioral paradigm to quantify the multimodal learning of pheromonal locations (Pardasani et al., 2021). When mice were allowed to explore both pheromone and neutral stimulus containing chambers (which were closed with lids having holes of different diameters, see Materials and Methods for the details, Figures 5B1,B2) in a three-chambered assay, no consistent preferences toward either of these chambers were observed. Both groups spent time in front of the chamber and displayed active attempts in sampling pheromonal cues, confirming their detection abilities (Figures 5C1-D2, two-way ANOVA with Bonferroni's multiple comparison test for time spent and number of active attempts for both groups of animals, \* represents  $p < 0.05$  and ns represents  $p > 0.05$ ). Both groups of mice were then trained for 15 days to associate pheromonal cues with varying orifice' diameters on the lid of the respective chambers (see methods). Their memory of multimodal association was assessed 15 days after the completion of training. The time spent in front of the urine chamber and the number of active attempts for sampling pheromonal cues were used to calculate the corresponding memory index. ACE2 KO females exhibited significantly lower memory index compared to the WT animals (Figures 5E1-F2, Memory index; Time Spent, WT:  $2.002 \pm 0.5185$ , ACE2 KO:  $0.4774 \pm 0.2123$ , two-tailed unpaired *t*-test,  $p = 0.0483$ ; Number of active attempts, WT:  $2.118 \pm 0.54$ , ACE2 KO:  $0.7249 \pm 0.5810$ , two-tailed Mann-Whitney test,  $p = 0.0186$ ). These results imply impaired cognitive abilities caused by the knockout of ACE2 receptors.

### 3.6. ACE2 KO mice did not display any anxiety or depression phenotypes

Having observed sensory as well as cognitive deficits in ACE2 KO mice, we further studied if these phenotypes were triggered by any anxiety-related or depressive behaviors that might be caused by the knockout of ACE2 receptors. This study was also prompted by the observations of long-term sensory and cognitive deficits (Bhattacharjee et al., 2020; Bhowmik et al., 2023) and mood disorders (Lamontagne et al., 2021) reported during and post-COVID conditions. We employed an array of commonly used behavioral paradigms to quantify these behaviors (Belovicova et al., 2017). On conducting open field test with experimental and control groups of mice, we did not observe any differences between the groups in the number and latency of entries to the center and the time spent in the center and the corners of the field (Figures 6A1-A4, two-tailed unpaired *t*-test for each parameter, ns represents  $p > 0.05$ ). In the elevated plus, we did not observe any differences in the time spent and number of entries in the open and closed arms (Figures 6B1-B4, two-tailed unpaired *t*-test for each parameter, ns represents  $p > 0.05$ ). These results indicate the absence of any anxiety-related behaviors due to the knockout of ACE2 receptors. To test for any depressive phenotypes, we conducted tail suspension and forced swim tests. Time of immobility was not different between the control and knockout groups of mice in the tail suspension test (Figure 6C, two-tailed

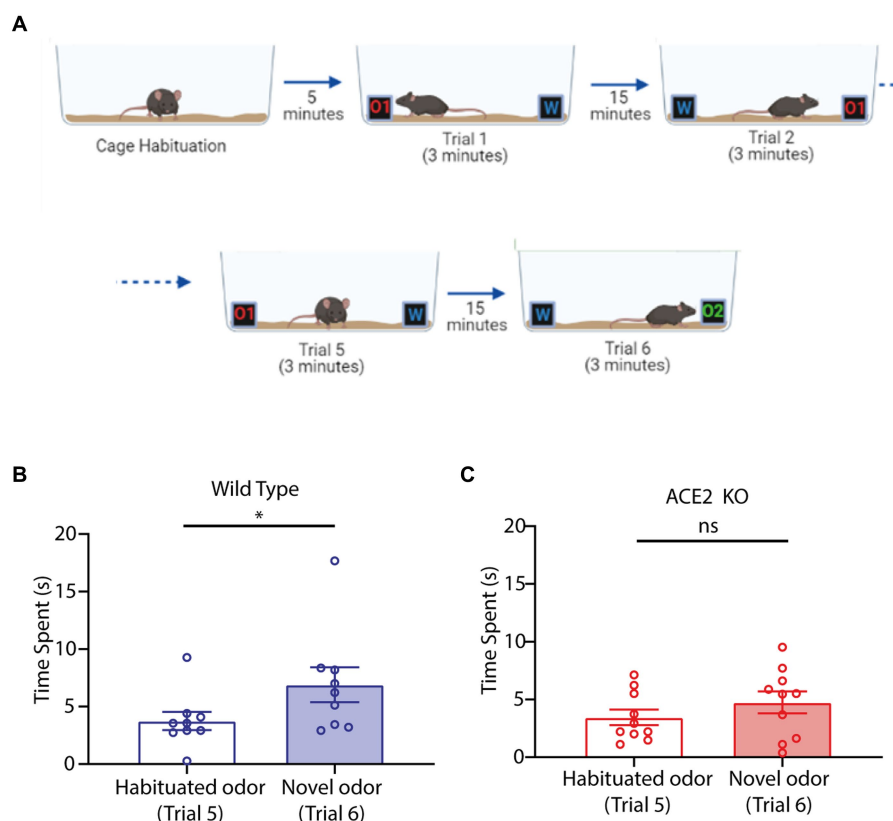


FIGURE 4

Novel odor discrimination is impaired in ACE2 KO animals. **(A)** Schematic of the novel discrimination task. The task begins with animals getting habituated with the cage followed by 5 trials of odor habituation wherein at one end an odorant (O1) was provided whereas on the other end there was water (W). For each trial the cage was rotated by 180° to mitigate any non-specific preference. Following habituation, the odor O1 was replaced by a novel odor (O2) and time spent by animals near the novel odor (Trial 6) vs. habituated odor (Trial 5) was used to assess the novel odor discrimination ability. **(B)** Comparison of time spent by WT animals during the task near the habituated and the novel odor. Time spent by animals near habituated odor ( $3.753 \pm 0.7959$ s) was significantly lower than that for novel odor ( $6.908 \pm 1.514$ s), one-tailed paired *t*-test,  $p = 0.0132$ ,  $n = 9$ . **(C)** Comparison of time spent by ACE2 KO animals during the task near the habituated and the novel odor. Time spent by animals near habituated odor ( $3.449 \pm 0.6708$ s) and novel odor ( $4.743 \pm 0.9469$ s) was similar, one-tailed paired *t*-test,  $p = 0.0965$ ,  $n = 10$ .

unpaired *t*-test,  $p = 0.3374$ ). In the forced swim test, immobility was slightly higher for the WT group, indicating the absence of any depressive symptoms in ACE2 KO mice (Figure 6D, two-tailed unpaired *t*-test,  $p = 0.0264$ ). Further, we carried out the rotarod test to see if there are any motor deficits in ACE2 KO mice and time spent on the rotarod and the distance covered by both groups of animals were found to be similar (Figures 6E1,E2, two-tailed unpaired *t*-test, ns represents  $p > 0.05$ ), indicating the absence of any motor dysfunctions due to the knockout of ACE2 receptors. All these tests provide the evidence for the absence of any mood disorder-related phenotypes in ACE2 knockout mice. Taken together, our results prove sensory and cognitive deficits in ACE2 KO mouse model, supported by the morphological aberrations we observed in these mice.

## 4. Discussion

Neurological complications of long-COVID may challenge the global health for many more years (Kay, 2022). Various olfactory problems including hyposmia, anosmia, and parosmia have been reported during infection and under long-COVID conditions (Bhattacharjee et al., 2020; Pardasani and Abraham, 2022; Bhowmik

et al., 2023). While infection at the olfactory periphery and the neuronal loss may explain the transient hyposmic and anosmic conditions, parosmia may result from the mis-targeting of regenerating OSNs during the recovery period (Costanzo, 2000; John and Key, 2003; Cooper et al., 2020). The expression of ACE2 receptors, that mediates virus infection in sustentacular cells of olfactory epithelium, explains the severe olfactory problems under COVID-19 infection. Therefore, we aimed to generate a complete ACE2 knockout mouse model using the CRISPR-Cas9 based genome editing method and investigate its function in modulating olfactory information processing. The deletion of ACE2 receptors may not lead to all pathophysiological conditions caused by SARS-CoV2 infection. However, the loss of ACE2 receptor function in the supporting sustentacular cells may ultimately result in the ionic imbalance in the epithelium, causing the cell death of olfactory sensory neurons, hence leading to various olfactory dysfunctions (Cooper et al., 2020).

Transgenic models can be created by different approaches. For example, in Cre-Lox recombination system, the expression specificity is achieved by crossing floxed mouse lines with Cre driver lines or by delivering Cre recombinase in a cell type-specific manner (Capecchi, 2005; Taniguchi et al., 2011). The generation of these mouse lines takes



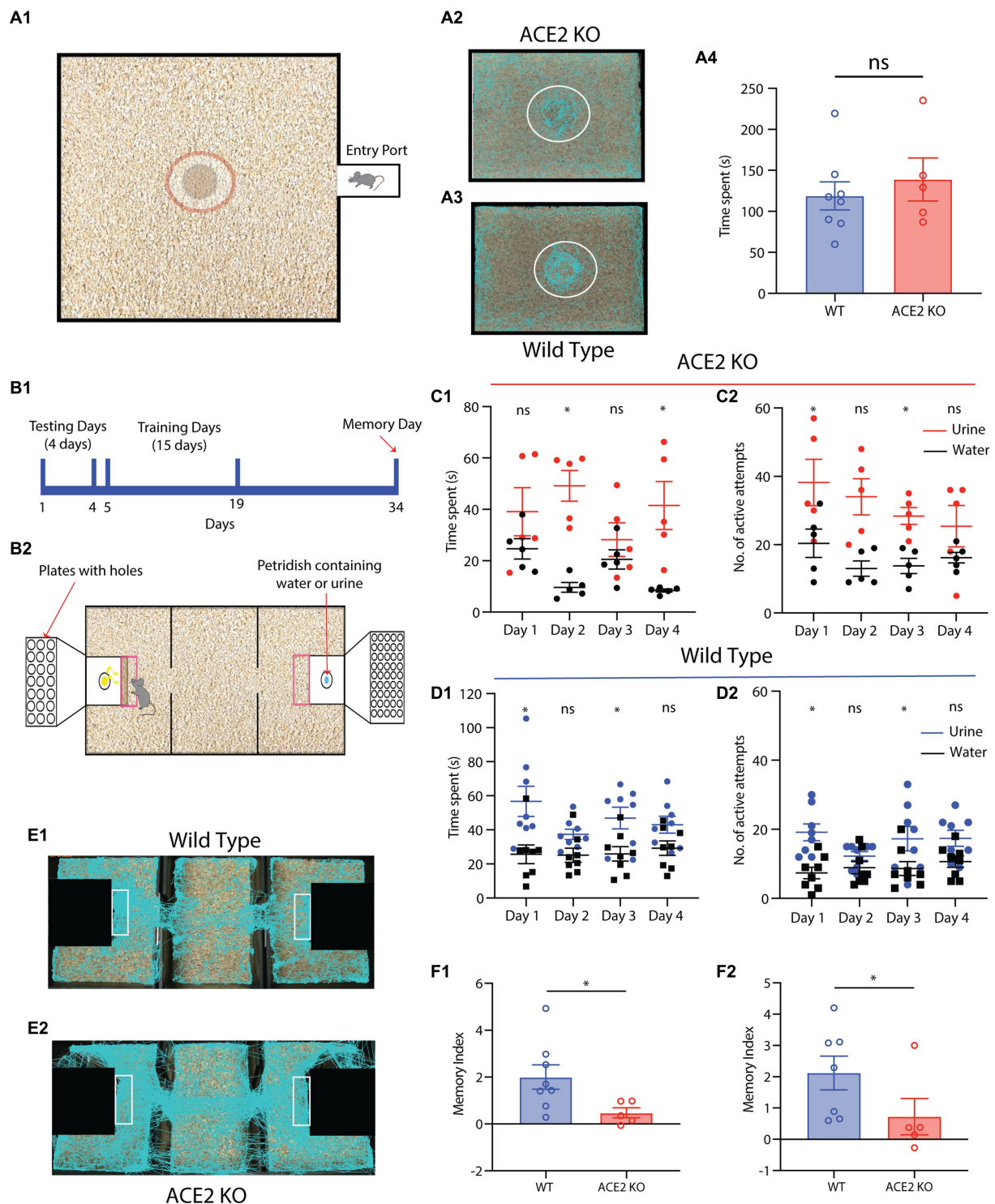


FIGURE 5

ACE2 KO animals show impaired memory in a multimodal pheromone learning task. **(A)** Pheromone detection abilities of ACE2 KO animals are similar to that of the WT animals. **(A1)** Diagrammatic representation of the setup used for pheromonal detection assay. The dimensions of the setup are 60cm x 45cm. A petri dish containing male soiled bedding and urine was placed at the center of the arena and females were introduced in this arena. The animals were tracked using EthoVision software while their motions were captured on camera. The time spent by females near to the petri dish was measured in order to gauge their pheromonal detection abilities. **(A2,A3)** Representative tracks taken by ACE2 KO and WT animals during the pheromone detection task, respectively. **(A4)** The pheromonal detection abilities of both groups of the animals was similar (WT:  $118.8 \pm 17.06$ s, ACE2 KO:  $138.8 \pm 26.19$ s, two-tailed unpaired *t*-test,  $p = 0.5143$ ,  $n_{ACE2KO} = 5$ ,  $n_{WT} = 8$ ). **(B)** **(B1)** Timeline of multimodal pheromone location learning task. Animals undergo testing for first 4 days, followed by 15 days training. Fifteen days post completion of the training, the memory of the animals was assessed. **(B2)** Illustration of the setup used for training the animals to associate the urine smell and neutral stimuli with specific orifice diameters. **(C,D)** Sampling parameters of ACE2 KO and Wildtype (WT) animals during first 4 days of testing, respectively. **(C1)** Time spent by ACE2 KO females near the water and urine zone during the testing days (two-way ANOVA with Bonferroni's multiple comparison test, \* represents  $p < 0.05$  and ns represents  $p > 0.05$ ). **(C2)**

(Continued)

FIGURE 5 (Continued)

Number of active attempts by ACE2 KO females near the water and urine zone during the testing days (two-way ANOVA with Bonferroni's multiple comparison test, \* represents  $p < 0.05$  and ns represents  $p > 0.05$ ,  $n_{ACE2KO} = 5$ ). (D) (D1) Time spent by WT females near the water and urine zone during the testing days (two-way ANOVA with Bonferroni's multiple comparison test, \* represents  $p < 0.05$  and ns represents  $p > 0.05$ ). (D2) Number of active attempts by WT females near the water and urine zone during the testing days (two-way ANOVA with Bonferroni's multiple comparison test, \* represents  $p < 0.05$  and ns represents  $p > 0.05$ ,  $n_{WT} = 8$ ). (E) (E1,E2) Representative tracks during the memory day for WT and ACE2 KO animals, respectively. (F) Comparison of Memory index between ACE2 KO and WT animals calculated using time spent and the number of active attempts. (F1) ACE2 KO females showed impaired memory (index calculated using time spent) compared to the WT animals (WT:  $2.002 \pm 0.5185$ , ACE2 KO:  $0.4774 \pm 0.2123$ , two-tailed unpaired  $t$ -test,  $p = 0.0483$ ). (F2) ACE2 KO females showed impaired memory (index calculated using number of active attempts) compared to the WT animals ( $2.118 \pm 0.54$ , ACE2 KO:  $0.7249 \pm 0.5810$ , two-tailed Mann–Whitney test (non-normal distribution),  $p = 0.0186$ ,  $n_{ACE2KO} = 5$ ,  $n_{WT} = 7-8$ ).

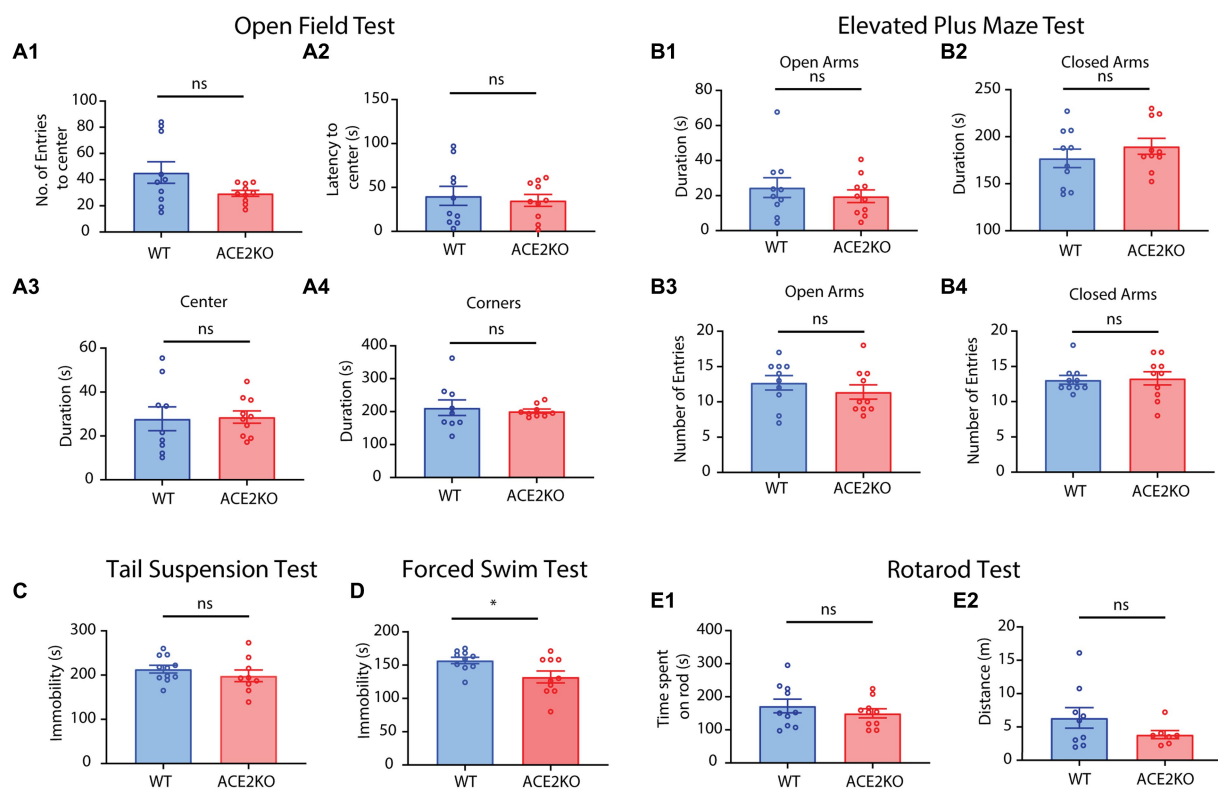


FIGURE 6

ACE2 KO and WT animals showed no differences in mood disorder-related behaviors. (A) Comparison of different parameters between ACE2 KO and WT animals for an open field test (OFT). (A1) Number of entries to the center between WT ( $45.40 \pm 8.224$ ) and ACE2 KO ( $29.50 \pm 2.296$ ) animals was similar (two-tailed unpaired  $t$ -test,  $p = 0.0790$ ). (A2) Latency to the center between WT ( $40.34 \pm 10.83s$ ) and ACE2 KO ( $35.17 \pm 6.170$ ) animals was similar (two-tailed unpaired  $t$ -test,  $p = 0.6895$ ). (A3) Time spent in the center between WT ( $27.81 \pm 5.448s$ ) and ACE2 KO ( $28.60 \pm 2.825$ ) animals was similar (two-tailed unpaired  $t$ -test,  $p = 0.8953$ ). (A4) Time spent in the corners between WT ( $212.0 \pm 23.80s$ ) and ACE2 KO ( $201.5 \pm 6.158s$ ) animals was similar (two-tailed unpaired  $t$ -test,  $p = 0.6774$ ). Number of animals:  $n_{ACE2KO} = 10$ ,  $n_{WT} = 9-10$ . (B) Comparison of different parameters between ACE2 KO and WT animals for an elevated plus maze test (EPM). (B1) Time spent in open arms between WT ( $177.1 \pm 9.792s$ ) and ACE2 KO ( $189.8 \pm 8.491$ ) animals was similar (two-tailed unpaired  $t$ -test,  $p = 0.3403$ ). (B2) Time spent in closed arms between WT ( $177.1 \pm 9.792s$ ) and ACE2 KO ( $189.8 \pm 8.491$ ) animals was similar (two-tailed unpaired  $t$ -test,  $p = 0.4747$ ). (B3) Number of entries in open arms between WT ( $12.70 \pm 1.023$ ) and ACE2 KO ( $11.40 \pm 1.013$ ) animals was similar (two-tailed unpaired  $t$ -test,  $p = 0.3784$ ). (B4) Number of entries in closed arms between WT ( $12.70 \pm 1.023$ ) and ACE2 KO ( $11.40 \pm 1.013$ ) animals was similar (two-tailed unpaired  $t$ -test,  $p = 0.8615$ ). Number of animals:  $n_{ACE2KO} = 10$ ,  $n_{WT} = 10$ . (C) Comparison of time immobile by ACE2 KO and WT animals for tail suspension test (TST). There was no significant difference in the time spent immobile between the groups (WT:  $213.5 \pm 8.628s$ , ACE2 KO:  $198.4 \pm 13.30s$ , two-tailed unpaired  $t$ -test,  $p = 0.3374$ , number of animals:  $n_{ACE2KO} = 9$ ,  $n_{WT} = 11$ ). (D) Comparison of time spent immobile by ACE2 KO and WT animals for forced swim test (FST). Time immobile by the ACE2 KO animals was significantly higher than that by the WT WT:  $0.1570 \pm 4.798s$ , ACE2 KO:  $132.3 \pm 9.017s$ , two-tailed unpaired  $t$ -test,  $p = 0.0264$ , number of animals:  $n_{ACE2KO} = 10$ ,  $n_{WT} = 10$ . (E) Comparison of different parameters between ACE2 KO and WT animals for rotarod test. (E1) There was no significant difference in the time spent on the rod between the groups (WT:  $172.2 \pm 20.61s$ , ACE2 KO:  $149.9 \pm 13.55s$ , two-tailed unpaired  $t$ -test,  $p = 0.3762$ ). (E2) There was no significant difference in the total distance covered between the groups (WT:  $6.356 \pm 1.544m$ , ACE2 KO:  $3.836 \pm 0.6166m$ , two-tailed unpaired  $t$ -test,  $p = 0.1935$ ).

longer than a year as it requires extensive backcrossing to screen for a homogenous background. The recent advancement in the CRISPR-Cas9 genome editing tools have enabled the researchers to

generate robust mouse models with targeted genetic background comparatively faster (Nishizono et al., 2020). The knockouts and knockins can be directly generated by injecting the guide RNA and

Cas9 into the pronucleus of fertilized mouse eggs (Yang et al., 2013). The existing ACE2 knockout mouse models created with CRISPR-Cas9 were mostly used to study the pulmonary and cardiovascular systems, and differences in knockout phenotypes are being reported. The genetic make-up of the models may attribute to the inconsistencies of the observed phenotypes, which can be considered as a drawback of the CRISPR-Cas9 approach (Jia et al., 2020). In this study, the deletion of ACE2 gene was ensured by targeting the crucial translational start site of the exon 2 and was confirmed by sequencing and western blotting.

The COVID-19 pandemic struck the world recording a high mortality rate and causing a decrease of human wellbeing globally. Since the start of the pandemic, numerous studies have been conducted to identify the various entry routes of SARS-CoV-2. The human angiotensin-converting enzyme 2 (hACE2) receptor was confirmed to be the target of the spike glycoprotein of the virus (Whittaker et al., 2021). After the viral glycoprotein binds to the ACE2 receptor, the TMPRSS2 protein cleaves the virus' S2 site, causing the internalization of the virus (Glowacka et al., 2011; Jackson et al., 2022). The widespread expression of ACE2 receptors indicates toward number of possible entry points for the invasion of virus (Mainland et al., 2015; Sungnak et al., 2020; Zhou et al., 2020; Boldrini et al., 2021; Casagrande et al., 2021; Huang N. et al., 2021; Pardasani and Abraham, 2022). Additionally, the virus can also enter the body through a breach of the blood-brain barrier (BBB), which is caused by the instability of the barrier by an increase in inflammatory cytokines following infection (Huang X. et al., 2021). Despite the debate over the virus's route of entry, it is recognized to be associated to the ACE2 receptors. As SARS-CoV2 entry into the cells through membrane fusion is thought to down-regulate the ACE2 receptors with a loss of these receptors' catalytic effect (Verdecchia et al., 2020), we created the ACE2 KO mouse model to mimic the effects of COVID-19 and studied its long-term effects. Even though it may not alter organ systems' functions as during or after COVID-19 infection, the ACE2 KO model offers a platform for the exploration of various parameters that can affect overall human well-being as a result of long-COVID-19.

The COVID-19 infection leads to morphological and functional alterations in the brain (Douaud et al., 2022; Du et al., 2023). Since the sustentacular cells of the olfactory epithelium contain the ACE2 receptor, we started by examining the impact of ACE2 deletion on the morphology of the olfactory epithelium (Brann et al., 2020). The width of the epithelium was considerably smaller in the ACE2 KO animals than in the control animals. Additionally, the glomeruli's cross-sectional area and MAP2 immunoreactivity were both reduced in the ACE2 KO animals. These findings demonstrate the changes brought about by the deletion of ACE2 in the olfactory epithelium and olfactory bulb. In humans, COVID-19 has been shown to increase apoptosis and decrease neurogenesis in the hippocampus (Bayat et al., 2022). In mouse models, it has been shown that ACE2 loss causes a reduction in the exercise-induced hippocampal neurogenesis (Klempin et al., 2018; Alenina and Bader, 2019). Given the relationship between ACE2 and COVID-19 and the fact that the olfactory epithelium is another part of the brain where

neurogenesis occurs (Crews and Hunter, 1994), it is probable that the decreased width of the OE is the result of increased apoptosis or reduced neurogenesis. Further studies investigating apoptosis and OSN turnover would be needed to confirm this.

The COVID-19 infection also causes learning and cognitive impairments that even persisted in the post-COVID conditions (Hampshire et al., 2021; Hugon et al., 2022; Bhowmik et al., 2023). Our observations of ACE2 KO animals having deficits in detection, discrimination, and novel odor recognition were similar to clinical observations made in patients. Humans' orbitofrontal cortex has extensive connections to other cortical areas and may help in processing of complex olfactory inputs (McGann, 2017). A decrease in the thickness of gray matter in the orbitofrontal cortex as a consequence of the COVID-19 may also contribute to severe olfactory and cognitive dysfunctions observed in humans (Douaud et al., 2022). In support of these clinical observations, earlier ACE2 KO mouse models exhibited learning impairments in Morris water maze and Y-maze tasks (Wang et al., 2016). In addition, ACE2 activation in the brain has been proven to have protective effects against the cognitive decline caused by amyloid pathology in a mouse model of Alzheimer's Disease (Evans et al., 2020). Despite these supporting evidence, the effect of CRISPR-Cas9 based disruption of ACE2 expression on other gene networks, may not mimic the exact pathophysiological conditions caused by COVID-19 (Stephan et al., 2022).

Rodents' olfaction is critical for their social and reproductive behaviors. During courtship behavior, olfactory system detects pheromones and recognizes their location (Pardasani et al., 2021). Here, we also investigated how ACE2 KO affected the animals' capacity for pheromone detection and the association of pheromones with their location. While the pheromonal detection abilities were unaffected, the ACE2 KO animals displayed poor memory of the pheromone location association, implying the impact of ACE2 deletion on rodents' social and reproductive behaviors. As a result of COVID-19 pandemic, a decline in sexual interest, and frequency were observed (Pascoal et al., 2021). In contrast, a few populations showed an increase in sexual desire, however with a reluctance toward conception (Yuksel and Ozgor, 2020). These findings emphasize the negative impact of the pandemic on human sexual health and success. These problems with reproductive health might be transient and may have resulted by COVID-19's detrimental effects on mental health. According to World Health Organization's assessment, the pandemic caused a 25% rise in the prevalence of anxiety and depression globally (WHO, 2022). However, over time, the behaviors linked to the deterioration of mood disorders such as anxiety and depression was diminishing, suggesting that these effects are transient and may have been attributed to a variety of factors during the pandemic (Manchia et al., 2022). In our analysis of mood disorder related behaviors, ACE2 KO animals did not show any depression or anxiety phenotypes.

In summary, our results demonstrate that knockout of ACE2 receptors leads to sensory and cognitive disabilities, which were similar to clinical observations made from COVID-19 patients. Further, our experimental strategy provides a potential method for

probing the neural mechanisms of cognitive deficits under long COVID conditions.

## Data availability statement

The original contributions presented in the study are included in the article/[Supplementary material](#), further inquiries can be directed to the corresponding authors.

## Ethics statement

The animal study was reviewed and approved by Institutional Animal Ethics Committee (IAEC), IISER Pune.

## Author contributions

NA and SG conceptualized the study. NA supervised all aspects of behavioral phenotyping and morphological analysis. SG supervised all aspects of knockout generation. NA carried out the experimental design. SM, DS, and AS performed behavioral, immunohistochemistry and microscopy experiments and analyzed the data. PS, SDM, and KS performed behavioral experiments and analyzed the data. MS performed knockout generation. SDM performed western blotting experiments. NA and SM wrote the manuscript with comments from others. All authors contributed to the article and approved the submitted version.

## Funding

This work was supported by the DBT/Wellcome Trust India Alliance intermediate grant (IA/I/14/1/501306 to NA), DST-Cognitive Science Research Initiative, Government of India (DST/CSRI/2017/271 to NA), JC Bose Fellowship from the Science and Engineering Research Board, Government of India (JCB/2019/000013 to SG), CSIR Fellowship, Government of India (SM and SDM) and UGC Fellowship, Government of India (KS) Part of the work was carried at the National

Facility for Gene Function in Health and Disease (NFGFHD) at IISER Pune, supported by a grant from the Department of Biotechnology, Government of India (BT/INF/22/SP17358/2016).

## Acknowledgments

The authors thank Laboratory of Neural Circuits and Behavior (LNCB) members for fruitful discussions. The authors also thank staff of National Facility for Gene Function in Health and Disease (NFGFHD) and IISER Biology- Leica microscopy facility for the technical support. This work was carried as part of the contribution of our Institute to the aims and output of the International Mouse Phenotyping Consortium (IMPC. [www.mousephenotype.org](http://www.mousephenotype.org)).

## Conflict of interest

The authors declare that the research was conducted in the absence of any commercial or financial relationships that could be construed as a potential conflict of interest.

## Publisher's note

All claims expressed in this article are solely those of the authors and do not necessarily represent those of their affiliated organizations, or those of the publisher, the editors and the reviewers. Any product that may be evaluated in this article, or claim that may be made by its manufacturer, is not guaranteed or endorsed by the publisher.

## Supplementary material

The Supplementary material for this article can be found online at: <https://www.frontiersin.org/articles/10.3389/fnins.2023.1180868/full#supplementary-material>

## References

- Abraham, N. M., Egger, V., Shimshek, D. R., Renden, R., Fukunaga, I., Sprengel, R., et al. (2010). Synaptic inhibition in the olfactory bulb accelerates odor discrimination in mice. *Neuron* 65, 399–411. doi: 10.1016/j.neuron.2010.01.009
- Abraham, N. M., Spors, H., Carleton, A., Margrie, T. W., Kuner, T., and Schaefer, A. T. (2004). Maintaining accuracy at the expense of speed: stimulus similarity defines odor discrimination time in mice. *Neuron* 44, 865–876. doi: 10.1016/j.neuron.2004.11.017
- Abraham, N. M., Vincis, R., Lagier, S., Rodriguez, I., and Carleton, A. (2014). Long term functional plasticity of sensory inputs mediated by olfactory learning. *Elife* 3:e02109. doi: 10.7554/eLife.02109
- Alenina, N., and Bader, M. (2019). ACE2 in brain physiology and pathophysiology: evidence from transgenic animal models. *Neurochem. Res.* 44, 1323–1329. doi: 10.1007/s11064-018-2679-4
- Barresi, M., Ciurleo, R., Giacompo, S., Foti Cuzzola, V., Celi, D., Bramanti, P., et al. (2012). Evaluation of olfactory dysfunction in neurodegenerative diseases. *J. Neurol. Sci.* 323, 16–24. doi: 10.1016/j.jns.2012.08.028
- Bayat, A.-H., Azimi, H., Moghaddam, M., Ebrahimi, V., Fathi, M., Vakili, K., et al. (2022). COVID-19 causes neuronal degeneration and reduces neurogenesis in human hippocampus. *Apoptosis* 27, 852–868. doi: 10.1007/s10495-022-01754-9
- Belovicova, K., Bogi, E., Csatosova, K., and Dubovicky, M. (2017). Animal tests for anxiety-like and depression-like behavior in rats. *Interdiscip. Toxicol.* 10, 40–43. doi: 10.1515/intox-2017-0006
- Bhattacharjee, A. S., Joshi, S. V., Naik, S., Sangle, S., and Abraham, N. M. (2020). Quantitative assessment of olfactory dysfunction accurately detects asymptomatic COVID-19 carriers. *EClinicalMedicine* 28:100575. doi: 10.1016/j.eclinm.2020.100575
- Bhattacharjee, A. S., Konakamchi, S., Turaev, D., Vincis, R., Nunes, D., Dingankar, A. A., et al. (2019). Similarity and strength of glomerular odor representations define a neural metric of sniff-invariant discrimination time. *Cell Rep.* 28, 2966–2978.e5. doi: 10.1016/j.celrep.2019.08.015
- Bhowmik, R., Pardasani, M., Mahajan, S., Magar, R., Joshi, S. V., Nair, G. A., et al. (2023). Persistent olfactory learning deficits during and post-COVID-19 infection. *Curr. Res. Neurobiol.* 4:100081. doi: 10.1016/j.crneur.2023.100081
- Bilinska, K., Jakubowska, P., Von Bartheld, C. S., and Butowt, R. (2020). Expression of the SARS-CoV-2 entry proteins, ACE2 and TMPRSS2, in cells of the olfactory epithelium: identification of cell types and trends with age. *ACS Chem. Neurosci.* 11, 1555–1562. doi: 10.1021/acscchemneuro.0c00210
- Boldrini, M., Canoll, P. D., and Klein, R. S. (2021). How COVID-19 affects the brain. *JAMA Psychiat.* 78, 682–683. doi: 10.1001/jamapsychiatry.2021.0500



- Brann, D. H., Tsukahara, T., Weinreb, C., Lipovsek, M., Van den Berge, K., Gong, B., et al. (2020). Non-neuronal expression of SARS-CoV-2 entry genes in the olfactory system suggests mechanisms underlying COVID-19-associated anosmia. *Sci. Adv.* 6:eabc5801. doi: 10.1126/sciadv.abc5801
- Buck, L. B. (2000). The molecular architecture of odor and pheromone sensing in mammals. *Cells* 100, 611–618. doi: 10.1016/S0092-8674(00)80698-4
- Butowt, R., and Bilinska, K. (2020). SARS-CoV-2: olfaction, brain infection, and the urgent need for clinical samples allowing earlier virus detection. *ACS Chem. Neurosci.* 11, 1200–1203. doi: 10.1021/acscchemneuro.0c00172
- Cantuti-Castelvetri, L., Ojha, R., Pedro, L. D., Djannatian, M., Franz, J., Kuivanen, S., et al. (2020). Neuropilin-1 facilitates SARS-CoV-2 cell entry and infectivity. *Science* 370, 856–860. doi: 10.1126/science.abd2985
- Capecchi, M. R. (2005). Gene targeting in mice: functional analysis of the mammalian genome for the twenty-first century. *Nat. Rev. Genet.* 6, 507–512. doi: 10.1038/nrg1619
- Casagrande, M., Fitzek, A., Spitzer, M. S., Püschel, K., Glatzel, M., Krasemann, S., et al. (2021). Presence of SARS-CoV-2 RNA in the cornea of Viremic patients with COVID-19. *JAMA Ophthalmol.* 139, 383–388. doi: 10.1001/jamaophthalmol.2020.6339
- Cooper, K. W., Brann, D. H., Farruggia, M. C., Bhutani, S., Pellegrino, R., Tsukahara, T., et al. (2020). COVID-19 and the chemical senses: supporting players take center stage. *Neuron* 107, 219–233. doi: 10.1016/j.neuron.2020.06.032
- Costanzo, R. M. (2000). Rewiring the olfactory bulb: changes in odor maps following recovery from nerve transection. *Chem. Senses* 25, 199–205. doi: 10.1093/chemse/25.2.199
- Crackower, M. A., Sarao, R., Oudit, G. Y., Yagil, C., Kozieradzki, I., Scanga, S. E., et al. (2002). Angiotensin-converting enzyme 2 is an essential regulator of heart function. *Nature* 417, 822–828. doi: 10.1038/nature00786
- Crews, L., and Hunter, D. (1994). Neurogenesis in the olfactory epithelium. *Perspect. Dev. Neurobiol.* 2, 151–161.
- De Melo, G. D., Lazarini, F., Levallois, S., Hautefort, C., Michel, V., Larrous, F., et al. (2021). COVID-19-related anosmia is associated with viral persistence and inflammation in human olfactory epithelium and brain infection in hamsters. *Sci. Transl. Med.* 13:eabf8396. doi: 10.1126/scitranslmed.abf8396
- Donoghue, M., Hsieh, F., Baronas, E., Godbout, K., Gosselin, M., Stagliano, N., et al. (2000). A novel angiotensin-converting enzyme-related carboxypeptidase (ACE2) converts angiotensin I to angiotensin 1–9. *Circ. Res.* 87, E1–E9. doi: 10.1161/01.res.87.5.e1
- Doty, R. L. (2012). Olfactory dysfunction in Parkinson disease. *Nat. Rev. Neurol.* 8, 329–339. doi: 10.1038/nrneurol.2012.80
- Douaud, G., Lee, S., Alfaro-Almagro, F., Arthofer, C., Wang, C., McCarthy, P., et al. (2022). SARS-CoV-2 is associated with changes in brain structure in UK biobank. *Nature* 604, 697–707. doi: 10.1038/s41586-022-04569-5
- Du, Y., Zhao, W., Huang, S., Huang, Y., Chen, Y., Zhang, H., et al. (2023). Two-year follow-up of brain structural changes in patients who recovered from COVID-19: A prospective study. *Psychiatry Res.* 319, 114969. doi: 10.1016/j.psychres.2022.114969
- Evans, C. E., Miners, J. S., Piva, G., Willis, C. L., Heard, D. M., Kidd, E. J., et al. (2020). ACE2 activation protects against cognitive decline and reduces amyloid pathology in the Tg2576 mouse model of Alzheimer's disease. *Acta Neuropathol.* 139, 485–502. doi: 10.1007/s00401-019-02098-6
- Fleming, S. M., Tetreault, N. A., Mulligan, C. K., Hutson, C. B., Masliah, E., and Chesselet, M.-F. (2008). Olfactory deficits in mice overexpressing human wildtype alpha-synuclein. *Eur. J. Neurosci.* 28, 247–256. doi: 10.1111/j.1460-9568.2008.06346.x
- Fodoulan, L., Tuberosa, J., Rossier, D., Boillat, M., Kan, C., Pauli, V., et al. (2020). SARS-CoV-2 receptors and entry genes are expressed in the human olfactory neuroepithelium and brain 23:101839. doi: 10.1016/j.isci.2020.101839
- Fullard, M. E., Morley, J. F., and Duda, J. E. (2017). Olfactory dysfunction as an early biomarker in Parkinson's disease. *Neurosci. Bull.* 33, 515–525. doi: 10.1007/s12264-017-0170-x
- Glowacka, I., Bertram, S., Müller, M. A., Allen, P., Soilleux, E., Pfeifferle, S., et al. (2011). Evidence that TMPRSS2 activates the severe acute respiratory syndrome coronavirus spike protein for membrane fusion and reduces viral control by the humoral immune response. *J. Virol.* 85, 4122–4134. doi: 10.1128/JVI.02232-10
- Hamming, I., Timens, W., Bulthuis, M. L. C., Lely, A. T., Navis, G. J., and van Goor, H. (2004). Tissue distribution of ACE2 protein, the functional receptor for SARS coronavirus. A first step in understanding SARS pathogenesis. *J. Pathol.* 203, 631–637. doi: 10.1002/path.1570
- Hampshire, A., Trender, W., Chamberlain, S. R., Jolly, A. E., Grant, J. E., Patrick, F., et al. (2021). Cognitive deficits in people who have recovered from COVID-19. *EClinicalMedicine* 39:101044. doi: 10.1016/j.eclinm.2021.101044
- Harms, D. W., Quadros, R. M., Seruggia, D., Ohtsuka, M., Takahashi, G., Montoliu, L., et al. (2014). Mouse genome editing using the CRISPR/Cas system. *Curr. Protoc. Hum. Genet.* 83, 15.7.1–15.7.27. doi: 10.1002/0471142905.hg1507s83
- Hoffmann, M., Kleine-Weber, H., Schroeder, S., Krüger, N., Herrler, T., Erichsen, S., et al. (2020). SARS-CoV-2 cell entry depends on ACE2 and TMPRSS2 and is blocked by a clinically proven protease inhibitor. *Cells* 181, 271–280.e8. doi: 10.1016/j.cell.2020.02.052
- Huang, X., Hussain, B., and Chang, J. (2021). Peripheral inflammation and blood-brain barrier disruption: effects and mechanisms. *CNS Neurosci. Ther.* 27, 36–47. doi: 10.1111/cns.13569
- Huang, N., Pérez, P., Kato, T., Mikami, Y., Okuda, K., Gilmore, R. C., et al. (2021). SARS-CoV-2 infection of the oral cavity and saliva. *Nat. Med.* 27, 892–903. doi: 10.1038/s41591-021-01296-8
- Hugon, J., Msika, E.-F., Queneau, M., Farid, K., and Paquet, C. (2022). Long COVID: cognitive complaints (brain fog) and dysfunction of the cingulate cortex. *J. Neurol.* 269, 44–46. doi: 10.1007/s00415-021-10655-x
- Iravani, B., Arshamian, A., and Lundström, J. N. (2022). Loss of olfactory sensitivity is an early and reliable marker for COVID-19. *Chem. Senses* 47:bjac022. doi: 10.1093/chemse/bjac022
- Jackson, C. B., Farzan, M., Chen, B., and Choe, H. (2022). Mechanisms of SARS-CoV-2 entry into cells. *Nat. Rev. Mol. Cell Biol.* 23, 3–20. doi: 10.1038/s41580-021-00418-x
- Jia, H., Yue, X., and Lazartigues, E. (2020). ACE2 mouse models: a toolbox for cardiovascular and pulmonary research. *Nat. Commun.* 11:5165. doi: 10.1038/s41467-020-18880-0
- John, J. A. S., and Key, B. (2003). Axon mis-targeting in the olfactory bulb during regeneration of olfactory neuroepithelium. *Chem. Senses* 28, 773–779. doi: 10.1093/chemse/bjg068
- Kang, Y., Chu, C., Wang, F., and Niu, Y. (2019). CRISPR/Cas9-mediated genome editing in nonhuman primates. *Dis. Model. Mech.* 12:dmm039982. doi: 10.1242/dmm.039982
- Kay, L. M. (2022). COVID-19 and olfactory dysfunction: a looming wave of dementia? *J. Neurophysiol.* 128, 436–444. doi: 10.1152/jn.00255.2022
- Khan, M., Yoo, S.-J., Clijsters, M., Backaert, W., Vanstapel, A., Speleman, K., et al. (2021). Visualizing in deceased COVID-19 patients how SARS-CoV-2 attacks the respiratory and olfactory mucosae but spares the olfactory bulb. *Cells* 184, 5932–5949.e15. doi: 10.1016/j.cell.2021.10.027
- Klempin, F., Mosienko, V., Matthes, S., Villela, D. C., Todiras, M., Penninger, J. M., et al. (2018). Depletion of angiotensin-converting enzyme 2 reduces brain serotonin and impairs the running-induced neurogenic response. *Cell. Mol. Life Sci.* 75, 3625–3634. doi: 10.1007/s00018-018-2815-y
- Klingenstein, M., Klingenstein, S., Neckel, P. H., Mack, A. F., Wagner, A. P., Kleger, A., et al. (2020). Evidence of SARS-CoV2 entry protein ACE2 in the human nose and olfactory bulb. *Cells Tissues Organs* 209, 155–164. doi: 10.1159/000513040
- Kyrou, I., Randeva, H. S., Spandidos, D. A., and Karteris, E. (2021). Not only ACE2—the quest for additional host cell mediators of SARS-CoV-2 infection: Neuropilin-1 (NRP1) as a novel SARS-CoV-2 host cell entry mediator implicated in COVID-19. *Signal Transduct. Target. Ther.* 6:21. doi: 10.1038/s41392-020-00460-9
- Lamontagne, S. J., Winters, M. F., Pizzagalli, D. A., and Olmstead, M. C. (2021). Post-acute sequelae of COVID-19: evidence of mood & cognitive impairment. *Brain Behav. Immun. Health* 17:100347. doi: 10.1016/j.bbih.2021.100347
- Lechien, J. R., Radulesco, T., Calvo-Henriquez, C., Chiesa-Estomba, C. M., Hans, S., Barillari, M. R., et al. (2021). ACE2 & TMPRSS2 expressions in Head & Neck Tissues: A systematic review. *Head Neck Pathol.* 15, 225–235. doi: 10.1007/s12105-020-01212-5
- Lehmkuhl, A. M., Dirr, E. R., and Fleming, S. M. (2014). Olfactory assays for mouse models of neurodegenerative disease. *JoVE* 90:e51804. doi: 10.3791/51804
- Li, W.-S., Chan, L.-L., Chao, Y.-X., and Tan, E.-K. (2020). Parkinson's disease following COVID-19: causal link or chance occurrence? *J. Transl. Med.* 18:493. doi: 10.1186/s12967-020-02670-9
- Mahammedi, A., Ramos, A., Bargalló, N., Gaskill, M., Kapur, S., Saba, L., et al. (2021). Brain and lung imaging correlation in patients with COVID-19: could the severity of lung disease reflect the prevalence of acute abnormalities on neuroimaging? A global multicenter observational study. *AJNR Am. J. Neuroradiol.* 42, 1008–1016. doi: 10.3174/ajnr.A7072
- Mainland, J. D., Li, Y. R., Zhou, T., Liu, W. L. L., and Matsunami, H. (2015). Human olfactory receptor responses to odorants. *Sci. Data* 2:150002. doi: 10.1038/sdata.2015.2
- Manchia, M., Gathier, A. W., Yapici-Eser, H., Schmidt, M. V., de Quervain, D., van Amelsvoort, T., et al. (2022). The impact of the prolonged COVID-19 pandemic on stress resilience and mental health: a critical review across waves. *Eur. Neuropsychopharmacol.* 55, 22–83. doi: 10.1016/j.euroneuro.2021.10.864
- Marin, C., Vilas, D., Langdon, C., Alobid, I., López-Chacón, M., Haehner, A., et al. (2018). Olfactory dysfunction in neurodegenerative diseases. *Curr. Allergy Asthma Rep.* 18:42. doi: 10.1007/s11882-018-0796-4
- McGann, J. P. (2017). Poor human olfaction is a 19th-century myth. *Science* 356:eaam7263. doi: 10.1126/science.aam7263
- Meinhardt, J., Radke, J., Dittmayer, C., Franz, J., Thomas, C., Mothes, R., et al. (2021). Olfactory transnucosal SARS-CoV-2 invasion as a port of central nervous system entry in individuals with COVID-19. *Nat. Neurosci.* 24, 168–175. doi: 10.1038/s41593-020-00758-5
- Merello, M., Bhatia, K. P., and Obeso, J. A. (2021). SARS-CoV-2 and the risk of Parkinson's disease: facts and fantasy. *Lancet Neurol.* 20, 94–95. doi: 10.1016/S1474-4422(20)30442-7

- Nishizono, H., Yasuda, R., and Laviv, T. (2020). Methodologies and challenges for CRISPR/Cas9 mediated genome editing of the mammalian brain. *Front. Genome Ed.* 2:602970. doi: 10.3389/fgeed.2020.602970
- Pardasani, M., and Abraham, N. M. (2022). "Neurotropic SARS-CoV-2: causalities and realities" in *COVID-19 pandemic, mental health and neuroscience - new scenarios for understanding and treatment*. eds. P. D. S. Palermo and P. B. Olivier (Rijeka: IntechOpen)
- Pardasani, M., Marathe, S. D., Purnapatre, M. M., Dalvi, U., and Abraham, N. M. (2021). Multimodal learning of pheromone locations. *FASEB J.* 35:e21836. doi: 10.1096/fj.202100167R
- Pascoal, P. M., Carvalho, J., Raposo, C. F., Almeida, J., and Beato, A. F. (2021). The impact of COVID-19 on sexual health: A preliminary framework based on a qualitative study with clinical sexologists. *Sex. Med.* 9:100299. doi: 10.1016/j.esxm.2020.100299
- Potter, S. M., Zheng, C., Koos, D. S., Feinstein, P., Fraser, S. E., and Mombaerts, P. (2001). Structure and emergence of specific olfactory glomeruli in the mouse. *J. Neurosci.* 21, 9713–9723. doi: 10.1523/JNEUROSCI.21-24-09713.2001
- Puelles, V. G., Lütgehetmann, M., Lindenmeyer, M. T., Sperhake, J. P., Wong, M. N., Allweiss, L., et al. (2020). Multiorgan and renal tropism of SARS-CoV-2. *N. Engl. J. Med.* 383, 590–592. doi: 10.1056/NEJMc2011400
- Shang, J., Wan, Y., Luo, C., Ye, G., Geng, Q., Auerbach, A., et al. (2020). Cell entry mechanisms of SARS-CoV-2. *Proc. Natl. Acad. Sci. U. S. A.* 117, 11727–11734. doi: 10.1073/pnas.2003138117
- Shao, Y., Guan, Y., Wang, L., Qiu, Z., Liu, M., Chen, Y., et al. (2014). CRISPR/Cas-mediated genome editing in the rat via direct injection of one-cell embryos. *Nat. Protoc.* 9, 2493–2512. doi: 10.1038/nprot.2014.171
- Stephan, M., Volkman, P., and Rossner, M. J. (2022). Assessing behavior and cognition in rodents, nonhuman primates, and humans: Where are the limits of translation? *Dialogues Clin. Neurosci.* 21, 249–259. doi: 10.31887/DCNS.2019.21.3/mrossner
- Sulzer, D., Antonini, A., Leta, V., Nordvig, A., Smeyne, R. J., Goldman, J. E., et al. (2020). COVID-19 and possible links with Parkinson's disease and parkinsonism: from bench to bedside. *NPJ Parkinsons Dis.* 6:18. doi: 10.1038/s41531-020-00123-0
- Sungnak, W., Huang, N., Bécavin, C., Berg, M., Queen, R., Litvinukova, M., et al. (2020). SARS-CoV-2 entry factors are highly expressed in nasal epithelial cells together with innate immune genes. *Nat. Med.* 26, 681–687. doi: 10.1038/s41591-020-0868-6
- Taniguchi, H., He, M., Wu, P., Kim, S., Paik, R., Sugino, K., et al. (2011). A resource of Cre driver lines for genetic targeting of GABAergic neurons in cerebral cortex. *Neuron* 71, 995–1013. doi: 10.1016/j.neuron.2011.07.026
- Tillerson, J. L., Caudle, W. M., Parent, J. M., Gong, C., Schallert, T., and Miller, G. W. (2006). Olfactory discrimination deficits in mice lacking the dopamine transporter or the D2 dopamine receptor. *Behav. Brain Res.* 172, 97–105. doi: 10.1016/j.bbr.2006.04.025
- Verdecchia, P., Cavallini, C., Spanevello, A., and Angeli, F. (2020). The pivotal link between ACE2 deficiency and SARS-CoV-2 infection. *Eur. J. Intern. Med.* 76, 14–20. doi: 10.1016/j.ejim.2020.04.037
- Wang, X.-L., Iwanami, J., Min, L.-J., Tsukuda, K., Nakaoka, H., Bai, H.-Y., et al. (2016). Deficiency of angiotensin-converting enzyme 2 causes deterioration of cognitive function. *NPJ Aging Mech. Dis.* 2:16024. doi: 10.1038/npjamd.2016.24
- Whitcroft, K. L., and Hummel, T. (2020). Olfactory dysfunction in COVID-19: diagnosis and management. *JAMA* 323, 2512–2514. doi: 10.1001/jama.2020.8391
- Whittaker, G. R., Daniel, S., and Millet, J. K. (2021). Coronavirus entry: how we arrived at SARS-CoV-2. *Curr. Opin. Virol.* 47, 113–120. doi: 10.1016/j.coviro.2021.02.006
- WHO. (2022). *COVID-19 pandemic triggers 25% increase in prevalence of anxiety and depression worldwide*. Geneva: World Health Organization.
- Yang, H., Wang, H., Shivalila, C. S., Cheng, A. W., Shi, L., and Jaenisch, R. (2013). One-step generation of mice carrying reporter and conditional alleles by CRISPR/Cas-mediated genome engineering. *Cells* 154, 1370–1379. doi: 10.1016/j.cell.2013.08.022
- Yuksel, B., and Ozgor, F. (2020). Effect of the COVID-19 pandemic on female sexual behavior. *Int. J. Gynaecol. Obstet.* 150, 98–102. doi: 10.1002/ijgo.13193
- Zhou, L., Xu, Z., Castiglione, G. M., Soiberman, U. S., Eberhart, C. G., and Duh, E. J. (2020). ACE2 and TMPRSS2 are expressed on the human ocular surface, suggesting susceptibility to SARS-CoV-2 infection. *Ocul. Surf.* 18, 537–544. doi: 10.1016/j.jtos.2020.06.007



## OPEN ACCESS

## EDITED BY

Subashika Govindan,  
Wellcome Trust DBT India Alliance, India

## REVIEWED BY

Bhavana Muralidharan,  
Institute for Stem Cell Science and  
Regenerative Medicine (inStem), India  
Antonio Galeone,  
National Research Council (CNR), Italy

## \*CORRESPONDENCE

Elena Taverna  
✉ elena.taverna@fht.org

RECEIVED 22 February 2023

ACCEPTED 31 July 2023

PUBLISHED 04 October 2023

## CITATION

Polenghi M and Taverna E (2023) Intracellular  
traffic and polarity in brain development.  
*Front. Neurosci.* 17:1172016.  
doi: 10.3389/fnins.2023.1172016

## COPYRIGHT

© 2023 Polenghi and Taverna. This is an open-  
access article distributed under the terms of  
the [Creative Commons Attribution License](#)  
(CC BY). The use, distribution or reproduction  
in other forums is permitted, provided the  
original author(s) and the copyright owner(s)  
are credited and that the original publication in  
this journal is cited, in accordance with  
accepted academic practice. No use,  
distribution or reproduction is permitted which  
does not comply with these terms.

# Intracellular traffic and polarity in brain development

Martina Polenghi and Elena Taverna\*

Human Technopole, Milan, Italy

Neurons forming the human brain are generated during embryonic development by neural stem and progenitor cells via a process called neurogenesis. A crucial feature contributing to neural stem cell morphological and functional heterogeneity is cell polarity, defined as asymmetric distribution of cellular components. Cell polarity is built and maintained thanks to the interplay between polarity proteins and polarity-generating organelles, such as the endoplasmic reticulum (ER) and the Golgi apparatus (GA). ER and GA affect the distribution of membrane components and work as a hub where glycans are added to nascent proteins and lipids. In the last decades our knowledge on the role of polarity in neural stem and progenitor cells have increased tremendously. However, the role of traffic and associated glycosylation in neural stem and progenitor cells is still relatively underexplored. In this review, we discuss the link between cell polarity, architecture, identity and intracellular traffic, and highlight how studies on neurons have shaped our knowledge and conceptual framework on traffic and polarity. We will then conclude by discussing how a group of rare diseases, called congenital disorders of glycosylation (CDG) offers the unique opportunity to study the contribution of traffic and glycosylation in the context of neurodevelopment.

## KEYWORDS

trafficking organelles, brain development, Golgi apparatus, neurodevelopmental disorders, epithelial polarity, neural stem and progenitor cells

## Introduction

Mammalian brain, and the human brain in particular, is a complex organ that needs high-level network-like organization for proper functioning. From an evolutionary point of view, the neocortex is the youngest part of the cerebral cortex responsible for higher order cognitive functions. The neocortex develops through a very precise sequence of symmetric and asymmetric division of neural progenitor cells (NPCs) (Noctor et al., 2004). NPCs proliferate or self-renew, and they generate—in a direct or indirect way—neurons. Neurons then migrate radially to the basal part of the cortex where they form, along with glial cells, the six-layered neocortex (Taverna et al., 2014). Neocortex development and evolution are linked to an increase in NPCs number and diversity (Rakic, 1995; Fish et al., 2008). Of note, NPCs morphological and functional diversity is mainly driven by difference in cellular polarity, defined as differential localization in space and time of cellular components and compartments (Arai and Taverna, 2017).

In this review we will first provide an overview on (i) NPCs classification and diversity (ii) the role of polarity in NPCs and discuss (iii) traffic from the endoplasmic reticulum (ER) and the Golgi apparatus (GA) in NPCs and (iv) how traffic diseases can inform us on the functional role of traffic in NPCs.

## Neural stem cell types in the developing brain

Neurons populating the neocortex are generated during embryonic development from two main classes of NPCs: apical progenitors (APs) and basal progenitors (BPs) (Figure 1). The broad classification between APs and BPs reflects the location where they undergo mitosis (Taverna and Huttner, 2010; Taverna et al., 2014). APs reside in the apical-most region of the developing neocortex, called ventricular zone (VZ) and they undergo mitosis at the apical surface of the VZ. BPs reside in a more basal area called subventricular zone (SVZ), where they undergo mitosis. APs and BPs show strikingly different cell biology and cellular architecture and make differential use of polarity cues, which is intimately linked to their function and balance between their proliferation and differentiation potential (Fietz and Huttner, 2011).

### Apical progenitors

APs are epithelial cells, with a very small apical plasma membrane (1%–2% of the total plasma membrane) lining the ventricle, and a very elongated basolateral plasma membrane reaching the basal lamina (Figure 1). APs elongation can be extreme, as in the case of the developing primate brain, where the distance between the apical surface and the basal lamina can be up to several millimeters. APs are further subdivided into neuroepithelial cells (NE) and apical radial glia cells (aRGs). NE are the founder cells of CNS, they are present during early neurogenesis, they occupy the VZ and they proliferate by dividing symmetrically, expanding the pool of NPCs (Götz and Huttner, 2005). aRGs appear at mid-neurogenesis, they occupy the VZ and contact the basal lamina via their basal process, that spans the SVZ and the forming cortical plate (Taverna et al., 2014). APs undergo interkinetic nuclear migration (INM). During INM the nucleus moves from the apical to the basal part of the VZ (and back) in concert with cell cycle progression, so that mitosis always happens at the apical surface, and S-phase in the basal most part of the VZ (Götz and Huttner, 2005; Taverna and Huttner, 2010; Taverna et al., 2014). INM confers to the VZ a pseudostratified appearance.

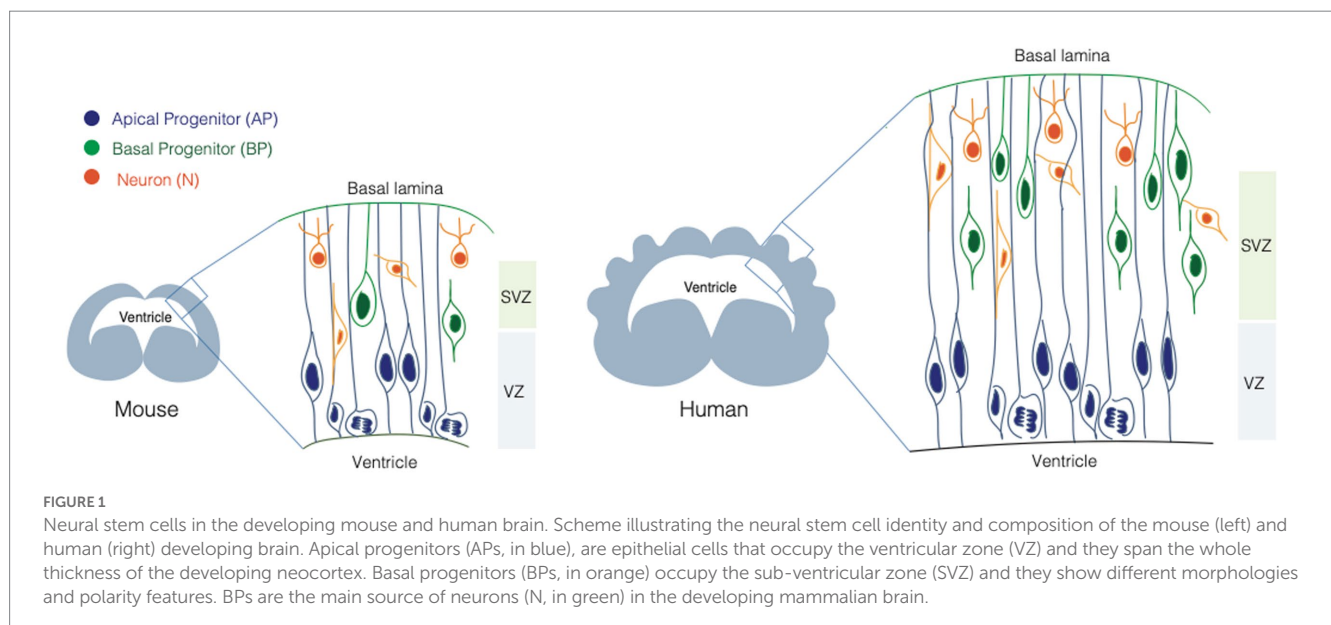
The division of APs is typically asymmetric self-renewing and generate a BP, that delaminates from the ventricular surface by losing the apical attachment. Delamination is strongly reminiscent of epithelial-to-mesenchymal transition, that is known to be mediated by a reorganization of the intracellular architecture (Wilsch-Bräuninger et al., 2012; Kawaguchi, 2021).

### Basal progenitors

BPs are a very heterogeneous class of progenitors, that divide basally in the SVZ (Figure 1). BPs differ in proliferative capacity, molecular landscape, and they typically lack apical attachment (Kriegstein and Alvarez-Buylla, 2009; Borrell and Reillo, 2012; Kalebic and Huttner, 2020). The occurrence and type of their basal polarity cues allow a further classification between intermediate progenitors (IPs) and basal radial glia cells (bRGs) (Florio and Huttner, 2014; Namba and Huttner, 2017; Kalebic and Huttner, 2020). IPs lack both apical and basal attachment and polarity, while bRGs can retain basal attachment, and can feature basal and/or apical polarity cues. The combinatorial presence of polarity cues is likely to expose BPs to a different subset of environmental signals compared to the ones reaching APs. The link between these cues and cell proliferation/differentiation potential is a very active area of research in the field of cell biology of neurogenesis (Kalebic and Huttner, 2020).

### Polarity in neural stem cells

The term polarity refers to the asymmetric distribution of cellular features, subcellular compartments and molecular components within the cell (Macara and Mili, 2008). Molecular and subcellular polarity allows compartmentalization of functions and it is instrumental for the ability of the cell to interact with and respond to the extracellular environment (Arai and Taverna, 2017). Notably epithelial cells are polar cells with at least two distinct compartments: an apical compartment facing a lumen and a basal compartment in contact with





the basal lamina. Compartmentalization of function is a shared feature between epithelial cells and neurons, that developed dedicated compartments to receive as well as to send signals from and to the extracellular environment or other cells they are in contact with. Changes in polarity features of single cells are often accompanied by whole tissue remodeling through migration of cells to different destinations, a process that can be observed from very early stages of development when cell identity and fate are determined by cell localization and by the repertoire of signals the cell is exposed to (Pinheiro and Heisenberg, 2020). But what about neural stem cells? In the context of brain development the link between cell identity and polarity is particularly intriguing as AP-to-BP fate switch, the central fate change in brain ontogeny and phylogeny, entails a major change in cell polarity.

## Polarity to sense and integrate signals from the extracellular environment

Apical progenitors possess an apical process contacting the apical surface and a basal process touching the pial surface. Differently, most BPs delaminate from the apical surface and only maintain contact with the basal membrane though some cells lose the basal process too. Delamination exposes BPs to only a subset of signals coming from the external environment, compared to the environmental cues that reaches both extremities of APs. The lumen of the ventricle is filled with CSF (Lehtinen et al., 2011) with signaling molecules such as FGF, IGF, Shh, retinoic acid, BMP and Wnts (Long et al., 2016; Wang et al., 2016); the action of these molecules is thought to happen via interaction with their receptors which are indeed localized at the plasma membrane of the apical process. An example of such interaction is provided by megalin, a glycoprotein enriched at the apical surface in the neuroepithelium, that interacts with BMPs and Shh; megalin mediates the endocytosis of Bmp4 and subsequent degradation, allowing Shh expression. Megalin KO mice display abnormal forebrain development following the increase in Bmp4 and loss of Shh. These mice show loss of ventrally derived oligodendroglial cells as well as interneuronal population. Megalin-triggered signaling pathway directly connects the extracellular environment with changes at the gene expression level in these neuroepithelial cells ultimately affecting brain developmental pathways (Willnow et al., 1996; Spoelgen et al., 2005).

At the level of the basal lamina APs receive signals from the meninges and the blood vessels that start developing. Interestingly, signals coming from meningeal cells, such as retinoic acid, were shown to have a role in cell identity switch from AP to BP (Siegenthaler et al., 2009; Janesick et al., 2015).

In the basal compartment, crucial players are laminin  $\alpha 2$  and  $\alpha 4$  and integrins (Taverna and Huttner, 2003; Fietz et al., 2010; Long et al., 2016; Kalebic et al., 2019). Integrins play a structural role by mediating the interaction of the basal process with the basal lamina as well as a functional role as they were shown to maintain the AP pool during development. Integrin  $\alpha v \beta 3$  is expressed by BPs and regulates their proliferation via its thyroid hormone receptor function. Loss of integrin  $\beta 1$  is accompanied by reduction in neural progenitor proliferation and their responsiveness to EGF, FGF and NGF signaling (Leone et al., 2005; Long and Huttner, 2019). BPs, lacking an apical contact, will receive a different subset of signals from the basal environment or from the surrounding cells in the developing neocortex. Interestingly, integrin  $\beta 1$  is involved in bRG proliferation

and expansion (Kalebic et al., 2019), a function tightly linked to the morphological features of bRG itself. These data suggest interesting avenues of investigations on how single neural stem cells do integrate signals during developmental time and in the tissue space, further expanding the concept of stem cell niche to the subcellular scale.

In conclusion, recent data suggest that cell polarity ultimately results in a differential way of sensing, integrating and responding to signals from the extracellular environment, which will influence cell identity. Of note, polarity also offers the structural and architectural basis for asymmetric partitioning of cellular components during cell division.

## Polarity and cell division

NPCs undergo either a symmetric or an asymmetric division: in the case of symmetric divisions NPCs divide and produce two daughter cells with the same identity of the mother cell ( $AP \rightarrow AP + AP$ , proliferative) or they can differentiate in two neurons ( $AP \rightarrow N + N$ , consumptive). In the case of asymmetric divisions instead, one daughter cell maintains the same identity of the mother cell while the other will acquire a different fate ( $AP \rightarrow AP + BP$ , self-renewing). The balance between these divisions is tightly controlled and alterations of this process lead to neurodevelopmental diseases, as in the case of microcephaly (Carpentieri et al., 2022). The degree of fate asymmetry can be driven by the asymmetric partitioning of cell biological components in the dividing mother cell.

For example, in *Drosophila*, Par-complex proteins, restricted to the apical domain, can either influence the daughter cells fate through indirect interaction with the spindle pole, or by restricting the transportation of proteins such as Miranda, Numb and Prospero selectively to the basal pole of the cell. Besides the well-known antagonism between Numb and Notch signaling and their involvement in maintaining cell identity vs. cell fate switch, Zhou et al. (2007) investigated the interaction between Numb and ACBD3 where the concerted presence of both proteins in the cytoplasm following Golgi apparatus disassembly during mitosis, leads to self-renewal pathway to be chosen by the dividing apical progenitor, at the expenses of neurogenesis.

Furthermore, different studies have demonstrated that inheritance of the apical membrane or of the basal membrane, has a role in driving the proliferation vs. differentiation decision. When having a perfectly apicobasal cleavage plane, the two daughter cells can inherit a portion each of the apical membrane, producing two progenitors that keep proliferating (symmetric proliferative division); conversely, a cleavage plane bypassing the apical PM will result into an asymmetric partitioning of cell biological components and in turn to an asymmetry in cell fate (Kosodo and Huttner, 2009; Taverna et al., 2016; Ayala and Colanzi, 2017). Given the central role of membrane receptors in sensing signals from the outside environment, one might speculate that differential inheritance of membrane(s) (apical and/or basal) might change, at least immediately after division in the G1 phase, the types of signals received by the cell, or the degree of signal integration. Intriguingly, G1 phase was reported as the cell cycle phase when developmental genes responsible for fate specification and switch are activated (Dalton, 2013, 2015).

Taken together, the available data call for a better understanding of the plasma membrane composition, biogenesis and dynamics in neural stem cells. Decades of seminal work on neurons has shown that

membrane traffic is one of the main cell biological processes shaping the composition and hence function of highly polarized cells (Bentley and Banker, 2016; Britt et al., 2016). We will here summarize and discuss the current status of knowledge on the role of membrane composition and traffic in neural stem cells, with a focus on the ER and GA.

## Polarity and intracellular architecture

### Plasma membrane

As all epithelial cells, APs feature an apical and a basolateral plasma membrane (PM) (Figure 2). The apical plasma membrane is subdivided into a planar portion and in the ciliary membrane, a specialized part of the apical plasma membrane that surrounds and delimits the cilium. Paridaen et al. (Paridaen et al., 2013; Paridaen and Huttner, 2014) elegantly showed that the ciliary membrane is internalized, partitioned during mitosis and inherited by one of the two daughter cells. The cell inheriting the ciliary remnant is more likely to have the fate of the mother cell and may in this way respond earlier to extracellular signaling from CSF (Wilsch-Bräuninger et al., 2012). These data suggest the idea that portions of the plasma membrane might endow the cell with the ability to differentially respond to extracellular signals, and again poses the interesting question as to which components and biochemical features confer unique properties to this small portion of the apical plasma membrane. The basolateral plasma membrane of APs is incredibly extended and traverse several functionally distinct zones, such as the SVZ and the CP. As for BPs, work conducted in bRGs (Kriegstein and Alvarez-Buylla, 2009; Fietz and Huttner, 2011; Borrell and Götz, 2014; Kalebic and Huttner, 2020; Kalebic and Namba, 2021) shows an astonishing level of structural and functional polarization and specialization. This is particularly clear for the apical and basal-directed processes of bRGs, whose presence correlates with the proliferative potential of the cell. The question arises as to which cell biological mechanisms are responsible for the structural, biochemical and functional specialization of the plasma membrane. In this review, we will focus on intracellular traffic.

### Conventional and unconventional trafficking routes

Lipids and proteins destined to the PM are first processed in the endoplasmic reticulum (ER) where a mannose-rich chain of sugars is added on asparagine residues, in a process called N-glycosylation. The maturation and elongation of the sugar chain is then operated in the GA where discrete units of monosaccharides are added to the protein (or lipid). An alternative to N-glycosylation is O-glycosylation, where sugars are added to the OH group of a serine or a threonine (D'Souza et al., 2021). The trafficking route ER → GA → PM is referred as to conventional secretion. This route is sometimes replaced by an alternative route that bypasses the GA (ER → PM), and that is referred to as the unconventional secretory pathway (USP) (Rabouille et al., 2012; Hanus et al., 2016; Nickel and Rabouille, 2018) (Figure 2). The unconventional routes have been extensively explored in flies, and, of note for this review, in neurons. Bowen et al. (2017) found that AMPA-type glutamate receptor GluA1 and neuroligin undergo ER processing and then accumulate in recycling endosomes at the level of dendrites and spines before being translocated to the plasma

membrane. This was found to occur even upon disruption of GA, that implies the presence of an alternative pathway for cargo delivery of proteins that bypasses the GA. In another work, Hanus et al. (2016) showed that numerous synaptic adhesion proteins, surface neurotransmitter receptors, voltage-dependent ion channels and growth factor receptors are largely N-mannose rich, lacking a complex sugar signature feature of Golgi processing. Nevertheless, these proteins are fully functional suggesting that USP is more common than previously thought.

The two classes of glycans can be recognized by concanavalin A (ConA), a lectin that binds to high mannose type glycans derived from the ER, and WGA that binds the complex type glycans derived from Golgi processing (Taverna et al., 2016). The intrinsic property of the glycosylation as a sequential process, already adds a complexity and heterogeneity to all possible modifications that can be added to proteins and lipids, without considering the other post translational modifications, such as sialylation and fucosylation which can be operated by Golgi and other PTMs that can be added before and after the Golgi processing. The fact that cells can also exploit different processing pathway elevates even more the complexity of the glycans and of plasma membrane composition.

## The endoplasmic reticulum

The ER is functionally and morphologically divided in two parts: the rough endoplasmic reticulum (RER) and the smooth endoplasmic reticulum (SER). In APs RER can be found in both apical and basal processes (Figure 2). ER is an interconnected tubular network of membranes that are in continuity with the nuclear envelope. This feature is relevant in the context of APs, as they move the nucleus in concert with cell cycle during INM (Taverna et al., 2016; Taverna and Huttner, 2019). It would therefore be interesting to know if any secretory or signaling functions of the ER show cell cycle-dependency as a consequence of nuclear movement. The RER is the starting point of the secretory pathway, where nascent proteins are transported while being translated by ribosomes (hence the name of rough ER).

Proteins undergo rounds of preliminary modifications and, if not correctly folded or modified, they are delivered back to the cytoplasm for proteasome degradation (Haynes et al., 2004; Ninagawa et al., 2021). Failure to degrade misfolded proteins causes ER stress which is in turn associated with apoptosis. There are several ways through which RER is actively involved in proteostasis; one is the unfolded protein response (UPR) that in mammals is mediated by three pathways that put the ER in communication with the nucleus: IRE1a, PERK and ATF6 are transmembrane receptors on the RER surface that sense misfolded proteins and after activation upon BiP/GRP78 dissociation, they trigger the UPR response through different pathways (Silvestre et al., 2009; Chao et al., 2014; Passemard et al., 2019).

### ER as sensor for stress

ER proteostasis revealed to be crucial during cortical development. Laguesse and colleagues showed that an upregulation of the UPR through the activation of the PERK-eIF2a-Atf4 signaling, caused by KO of Elp3 (a member of the elongator complex) leads to an increase in direct production of neurons from

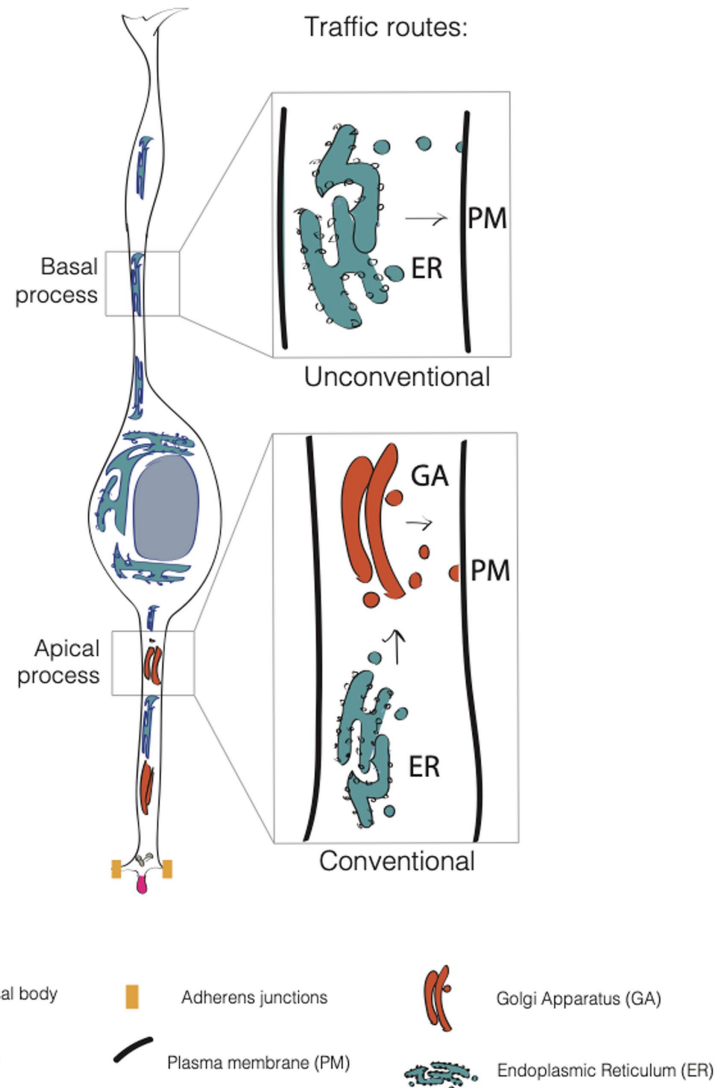


FIGURE 2

Conventional and unconventional trafficking routes in APs. In apical progenitors (APs), the apical process contains both the endoplasmic reticulum (ER, in blue) and the Golgi apparatus (GA, in dark orange). In contrast, the APs' basal process contains only the endoplasmic reticulum. Consequently, GA-derived glycoproteins are asymmetrically distributed in APs, as they are enriched only in the apical process. This suggests that the apical process relies on conventional traffic routes, while the basal process relies mainly on unconventional traffic routes.

APs, at the expenses of the indirect neurogenesis pathway (Laguesse et al., 2015). The depletion of IPs leads to a microcephalic phenotype in mice bearing the mutation (Laguesse et al., 2015). These observations elegantly highlight the relevance of ER stress response and proteostasis for cell fate specification and lineage progression in the developing brain.

Other ER stressors that come from the external environment, such as viruses can interfere with ER proteostasis and lead to aberrations in the development of the cortex. This is the case of Zika virus for example, that not only induces massive cell death but also causes ER stress, triggering UPR and contributing ultimately to primary microcephaly development in newborns (Wang and Ling, 2016). Another trigger for UPR is alcohol consumption by pregnant women, that directly exert an effect on the newborn developing brain, through epigenetic alterations, perturbation of calcium homeostasis and

generation of abnormal protein triggering UPR (Ji, 2012). Collectively, the involvement of the ER-related UPR response in microcephaly pathogenesis leads to interesting questions as to which is the role of UPR in cell fate switch in physiological conditions (Tomás et al., 2012; Casey et al., 2016; Passemard et al., 2019). One could speculate that during fate transition, in parallel to the radical changes in the transcriptional landscape, cells need to completely renew also their transcriptome and proteome repertoire. In that context, UPR might serve the purpose of implementing in an efficient and coordinated way those changes.

In NPCs, the ER has also been reported to form a diffusion barrier with a role in the asymmetric inheritance of mono- and polyubiquitylated proteins (Bin Imtiaz et al. 2022); though the relevance in terms of effect on progenitor cells identity following disruption has not been fully elucidated yet, future research on the

topic will help clarifying whether the ER could affect NPCs identity by regulating the partitioning and segregation between old or newly synthesized proteins.

## ER-Golgi intermediate compartment

The ER-Golgi intermediate compartment (ERGIC) is a vesiculotubular organelle that mediates the anterograde and retrograde transport between ER and GA. In polarized cells, such as neurons, the ERGIC compartment has been proposed to allow the GA derived-compounds to communicate with the most distant dendritic compartments (Breuza et al., 2004; Appenzeller-Herzog and Hauri, 2006; Zhang et al., 2009; de los Angeles Juricic Urzúa et al. 2021). Though in neurons it has been recently reported to be composed of both stationary and mobile compartments, the extent of ERGIC polarization in NPCs is currently not known.

Given the extreme elongation of APs (and bRG), one could speculate that the ERGIC compartment might have a role in helping the ER to sustain the complex process of protein maturation and modification that allows membranes and associated proteins to be delivered to distal locations, such as the basal process and/or the basal end foot.

## The Golgi apparatus

The GA is the first identified traffic organelle whose main function is adding glycan modifications to secretory pathway components. The GA is composed of multiple cisternae packed together to form a stack. Cisternae progress from the *cis*-Golgi, closer to the ER, through the *medial*- and then the *trans*-Golgi, where modified proteins or lipids enter the trans Golgi network (TGN) to be directed to their destination. Proteins arriving from the ER and ERGIC, are already partially modified by the ER with the addition of a core oligosaccharide chain. In the *medial*-Golgi a series of glycosyltransferase add sugars and by the time the protein reaches the exit site, the TGN, it is functional and ready to be delivered to the plasma membrane. In mammalian cells GA stacks are connected to form the Golgi ribbon (D'Souza et al., 2021). Interestingly, in APs the GA is not forming the typical Golgi ribbon but it exist as separated stacks (Figure 1) (Taverna et al., 2016), very much resembling the GA organization in *Drosophila* (Gosavi and Gleeson, 2017; Fujii et al., 2020).

The communication and transport of cargoes between the GA stacks and other trafficking organelles is dependent on the actin and microtubule cytoskeleton that interact with GA-resident structural proteins (Silvestre et al., 2009; Bowen et al., 2017; Passemard et al., 2019). GA interaction with the cytoskeletal elements is necessary not only for its integrity, but also for GA disassembly, a process that normally happens during the G2 phase of the cell cycle, when GA disassembly must occur to allow the cell to enter mitosis (Ayala and Colanzi, 2017). Blocking GA fragmentation results in G2 arrest, as a consequence of the so-called Golgi mitotic checkpoint (Sütterlin and Colanzi, 2010). Using depolymerizing drugs it is possible to actively induce fragmentation of GA at any time point of the cell cycle making the complex not functional anymore (Dinter and Berger, 1998; Breuza et al., 2004). In both situations, physiological or pharmacologically

forced, most proteins and enzymes that were resident of the Golgi stacks, move to the ER and ERGIC compartments (Kemal et al., 2022).

## Intracellular architecture of the Golgi apparatus: from neurons to NPCs

GA shows a polarized distribution in polarized cells, as beautifully shown in neurons, where it is found at the somatodendritic compartment while it is typically absent from the axon (Britt et al., 2016; Koppers and Farias, 2021). In pyramidal neurons the GA extends in the apical dendrite; this extension is crucial for cell polarization, axon specification and dendrite growth and is dependent on Ube3a, a gene found to be mutated in Angelman syndrome (AS) (Condon et al., 2013), a neurodevelopmental disease associated with severe learning disabilities. KD of Ube3a in mouse model of AS has been reported to be linked to defects in synaptic development and plasticity. Ube3a is a ubiquitin ligase that can target GA specific proteins. Interestingly, it has been hypothesized that in cortical neurons of AS mouse model, the link between Ube3a and GA resides in the under-acidification of GA cisternae leading to reduced protein sialylation (Condon et al., 2013).

Dendrites also contain Golgi outposts (GO), that ensure local and activity dependent modifications of proteins and lipids far away from the cell body (Bowen et al., 2017).

In APs the Golgi complex displays a non-canonical organization as (i) it shows a strong sub-compartmentalization, as it is only present in the apical process and it is dynamically reorganized during interkinetic nuclear migration (INM) (ii) it is not pericentrosomal (iii) it shows stacks but lacks the ribbon-like structure typically found in mammalian cells (iv) the stacks are organized perpendicular to the apicobasal axis, with the TGN surface parallel to the basolateral PM. Interestingly, GA is reorganized upon AP to BP fate transition, and in BPs GA is both pericentrosomal and perinuclear and shows a typical ribbon-like structure (Taverna et al., 2016; Taverna and Huttner, 2019) (Figure 2). These characteristics render the GA organization and re-organization quite unique and leave open several questions regarding the structure/function relation of such a peculiar architecture. We here discuss salient points and mention relevant questions that are still open.

## Mechanisms and dynamics of GA confinement in the apical process

The confinement of the GA to the apical process is of great interest in light of INM. INM is a process of nuclear movement that is cell cycle dependent: immediately after mitosis at the apical surface, an AP moves the nucleus from the apical to the basal side of the VZ during G1, undergoes S-phase at the basal most part of the VZ and then in G2 moves the nucleus back to the apical surface for a new round of mitosis. During all phases of the cell cycle the GA is apical to the nucleus, with a small portion localized close to it (Taverna et al., 2016; Xie et al., 2018; Brault et al., 2022). This dynamic organization poses two questions: which are the mechanisms that allow the apical confinement of the GA and which are the structural and functional effects of nucleokinesis on the GA. The apical confinement of the GA is maintained via the activity of PITPNA and PITPNB, two phosphatidylinositol 4-phosphate transfer proteins involved in the synthesis of PI4P on the Golgi membrane. The PI4P pool recruits GOLPH3 which serves as an adaptor to link the cisternae to the actin



cytoskeleton (Xie et al., 2018). As for the effect of nucleokinesis, live imaging experiments have shown that the GA in APs is stretched and elongated in G1, reaches its maximum apical-to-basal extension in S, and then it is compressed in G2, in concert with the basal-to-apical nuclear migration (Xie et al., 2018; Passemard et al., 2019). This accordion-like dynamics appears to be a peculiar feature of AP and they are intriguing in light of data linking mechanical forces applied on the GA to traffic from the GA (Guet et al., 2014). Indeed, since applying forces decreases vesicle budding from the GA, it would be interesting to understand if cycles of stretching and compression of the GA in AP in concert with the cell cycle result in a cell cycle dependent regulation of GA trafficking.

## GA distribution and plasma membrane architecture

The confinement of the GA to the apical process has consequences for the organization and sub-compartmentalization of the basolateral plasma membrane of APs. By using single cell labeling combined with ConA and WGA (two lectins that specifically recognize ER- and GA-derived glycans) it was found that the basolateral plasma membrane of APs is subdivided in two domains that differ in their glycosylation state (Taverna et al., 2016). The apical process traversing the VZ contains both ER and GA-derived glycans while the basal process traversing SVZ and CP contains ER-derived glycans only. Interestingly, the glycans polarization appears to mirror the organelle polarization and asymmetry along the apico-basal axis of the cell (Taverna et al., 2016) (Figure 2). The interesting question is if and how the differential localization of the organelles and PM components could influence cellular identity. An intriguing possibility to explore is that the type of glycosylation impacts the activation and functionality of receptors, their delivery to the plasma membrane (or to specific sub compartments) and/or their signaling pathway, thus affecting cellular behavior and fate choice.

## Intracellular architecture of fate transition

AP-to-BP fate transition closely resembles an epithelial to mesenchymal transition (EMT). As in EMT, the generation of a BP entails a deep reorganization of the intracellular compartments, in particular of the cilium/centrosome and of the GA. In newborn BPs before delamination, the cilium is re-positioned from an apical to a basolateral location (Wilsch-Bräuninger et al., 2012; Taverna and Huttner, 2019) (Figure 3). Interestingly, delamination is also paralleled by a reorganization of the GA, that became pericentrosomal (Taverna et al., 2016; Taverna and Huttner, 2019) (Figures 1, 3). It is not yet fully clear if this reorganization is a consequence of the fate transition, or if it can also be a cause driving fate transition. On the relation between traffic and fate specification, Brault and colleagues have demonstrated that post-Golgi traffic mediated by Rab6 is crucial for delamination and BP generation. The data show that interfering with Rab6 traffic increases the number of BPs, thus suggesting that traffic might directly influence fate (Brault et al., 2022).

## GA and centrosome: a long-lasting friendship story

In mammalian cells the GA is physically and functionally associated with the centrosome (Sütterlin and Colanzi, 2010). Despite the tight relationship, the pericentriolar positioning of the GA doesn't

appear to be fundamental for the secretory function of the organelle, in fact, organisms such as *Saccharomyces cerevisiae* or *Drosophila*, whose GA is not close to the centrosome still retain the ability to process and transfer proteins through the secretory pathway (Sütterlin and Colanzi, 2010). What is then the functional relevance for such an association? This association appears to be crucial for ciliogenesis, cell polarization and cell migration. As for ciliogenesis, the loss of GA proteins IFT20 and Rab8 impairs cilia formation. Of note, in the context of neurogenesis it has been demonstrated that in a portion of progenitors the ciliary membrane is asymmetrically inherited from the mother cell (Paridaen et al., 2013). This observation implies that at least half of newborn NPCs should rely on *de novo* ciliogenesis, that might depend on GA traffic routes, as suggested for work on cells in culture (Wilsch-Bräuninger et al., 2012; Witzgall, 2018; Diaz et al., 2020).

In general, APs offer an interesting paradigm regarding the centrosome/GA reciprocal regulation, as in interphase the GA and the centrosome are not physically associated (Taverna et al., 2016). The question arises as to whether they are still functionally associated, or if APs are lacking part of the regulation impinging on the GA/centrosome axis (Sütterlin and Colanzi, 2010).

## Function(s) of the Golgi apparatus

### Golgi as secondary microtubule organizing center

The GA can nucleate microtubules, thus serving as non-centrosomal microtubule organizing centre (MTOC) (Yanagida et al., 2012; Gavilan et al., 2018). The GA-MTOC was shown to be relevant for directional protein transport (Zhu and Kaverina, 2013). For example, in *Drosophila* sensory neurons GA and Golgi outposts, have been observed to be necessary for dendrite branching. Microtubules nucleating from GA are emanated in an anterograde direction providing a directionality to transport and trafficking (Ori-McKenney et al., 2012). MTOCs are of crucial importance in NPCs as they regulate and fine tune the architecture and function of the cytoskeleton, affecting spindle dynamics and orientation, and in turn fate choice. In APs the distance between the Golgi stacks and the basolateral PM is only few microns, it would therefore be interesting to understand if the GA in APs serves as MTOC, and is so, how the GA-MTOC affects the directionality and efficiency of traffic.

### Golgi as a stress sensor

In the last fifteen years GA emerged for its own role in proteostasis; it was already known the ability of the ER to respond to stressors and act as a cell sensor, triggering a response to restore homeostasis. It is now becoming clear that also the GA, in addition to its several roles, can act as a sensor to changes in pH that may affect its integrity and secretory functions, as well as to increased or decreased fraction of mature glycans. GA fragmentation-inducing drugs, such as brefeldin A, golgicide A or monensin, trigger a stress response mediated by ARF4 and CREB3. CREB3 is a leucine zipper transcription factor that, upon activation through proteolytic cleavage, translocates from the Golgi membranes to the nucleus, where it activates its target pro-apoptotic genes. CREB3 pathway is only one of the three Golgi-associated stress pathways known, the

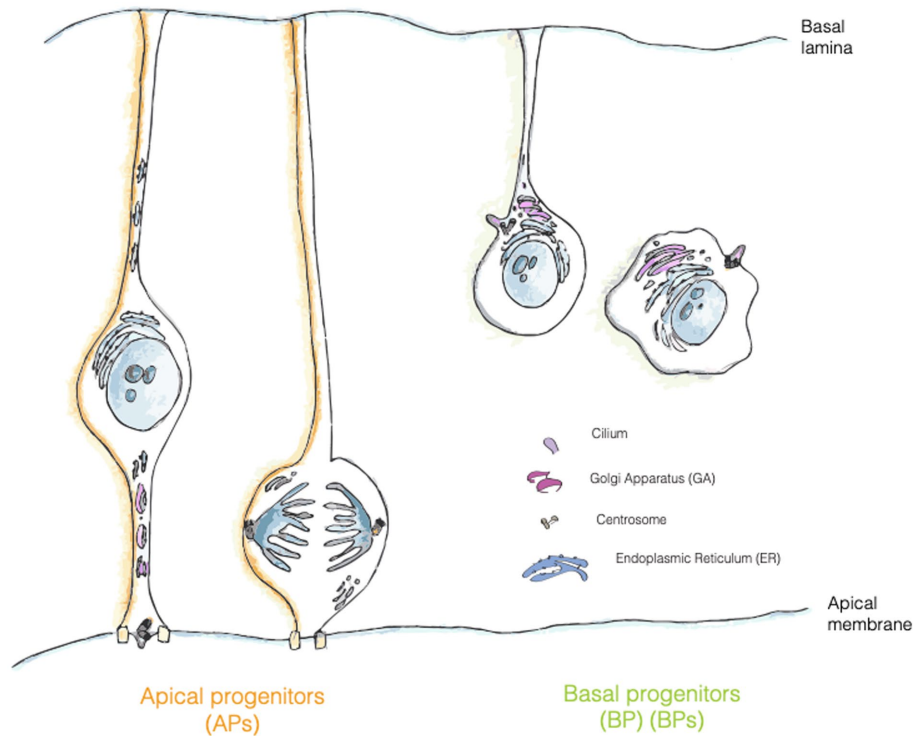


FIGURE 3

Localization of trafficking organelles in APs and BPs. Golgi apparatus (GA, pink) is formed by separate stacks localized in the apical process of APs and fragmented in mitotic AP, whereas in bRG and IPs it has a more canonical position and organization in the cell. Centrosome is represented in grey, RER in turquoise and ciliary membrane is painted in purple.

other two being TFE3 or HSP47 mediated. During stress responses TFE3 translocates to the nucleus, where it regulates, among others genes, glycosylation genes involved in sialylation and fucosylation (Sasaki et al., 2019; D'Souza et al., 2021). HSP47 pathway, identified by Miyata et al. (2013) and Sasaki et al. (2019), is activated by a different inducer of GA stress (BenzylGalNAc) which causes reduction of mucin-type glycosylation.

Recently, a fourth route that is triggered by increased or decreased proteoglycans capacity of the cell has been explored. Upon stress induced by the glycans themselves, GA starts a response ultimately leading to the activation of glycosylation enzymes for proteoglycans (Sasaki et al., 2019). GA has also been found to respond to DNA HR repair (Galea et al., 2022): in HeLa cells RAD51C, a regulatory HR protein, shuttles from the Golgi membranes to the perinuclear region following a DNA stress. RAD51 is linked to the golgin GM130, a multifunctional protein involved in GA structural maintenance. GM130 expression is under the control of TFE3 and was reported to be defective in some neuromuscular syndromes present in concert with microcephaly (Dinter and Berger, 1998; Passemard et al., 2019).

### GA as a central hub for glycosylation

Proteins and lipids traveling through the GA are modified via the addition of sugars, reflecting one of the main functions of the GA: glycosylation. Glycosylation is a post translational modification that is crucial for regulating proteins and lipids

function for signaling and/or structural purposes. Integrins are an excellent example of N-glycans in neurodevelopment; integrins are receptors found on the cell surface that require the presence of N-linked oligosaccharides to form functional dimers. These proteins are involved in a plethora of functions, such as cell migration and polarization in NPCs (Taverna and Huttner, 2003). Pathological changes in glycosylation are present in several diseases, ranging from neurodevelopmental and neurological disorders, to autoimmune diseases and cancer (Chang et al., 2018; Reily et al., 2019; Linders et al., 2020; D'Souza et al., 2021).

### Neurodevelopmental diseases associated with trafficking pathway defects

Golgiopathies is a term used to define all the diseases associated with defects in the trafficking pathway, in particular of the Golgi apparatus. Over 40% of GA-related genes known to be associated with diseases show central and peripheral nervous system clinical manifestations (Jaeken and Matthijs, 2001; Freeze et al., 2014, 2015) (see Table 1). This might be due to the extensive use of the trafficking pathway in neurons and glia, where traffic is used for synaptic transmission, for receiving signals or even to form the myelin sheet. Furthermore, evidences suggest that aberrations in ER- and GA-dependent trafficking could contribute to the pathophysiology and progression of

**TABLE 1** Trafficking-related structural proteins and enzymes found mutated in neurodevelopmental disorders.

Protein	Clinical manifestations	References
<b>Structural proteins</b>		
TRAPPC9	Autosomal recessive mental retardation MRT13	Mir et al. (2009)
TRAPPC12	Progressive childhood encephalopathy	Milev et al. (2017)
TRAPPC6B	Neurodevelopmental disorder with microcephaly, epilepsy and autistic features	Marin-Valencia et al. (2018)
CDC42	Takenouchi-Kosaki syndrome	Flynn et al. (2021)
LGALS3BP	Defects in neurodevelopment in de novo mutations	Kyrousi et al. (2021)
GM130	Neuromuscular syndrome with microcephaly	Shamseldin et al. (2016)
RABs	Several cancer types, Charcot Marie Tooth syndrome, Warburg micro syndrome	Banworth and Li (2018)
VPS13B	Cohen syndrome	Seifert et al. (2011)
ARF1	Brain abnormality	Ge et al. (2016)
ARF(3)	<i>De novo</i> mutation with developmental delay, epilepsy and brain abnormalities	Sakamoto et al. (2021)
ARFGEF	Autosomal recessive periventricular heterotopia with microcephaly	Xu et al. (2022)
COG complex	CDGII, mild to severe neurological impairment, microcephaly, mental retardation, cerebellar atrophy, hypotonia	Climmer et al. (2015)
<b>Enzymes</b>		
DPM2	CDG I, muscular dystrophy-dystroglycanopathy syndrome	Barone et al. (2012)
ALG1	CDG I, with broad clinical spectrum of neurodevelopmental disease	Ng et al. (2016)
ALG3	CDG I, severe developmental delay, epilepsy, cortical atrophy cerebellar vermis hypoplasia and ocular impairment	Farolfi et al. (2021)
ALG11	CDG I, neurodevelopmental defects, psychomotor disabilities and epilepsy	Haanpää et al. (2019)
SLC35A	CDG II, with severe ID and POM	Ng et al. (2013)
POMT1, POMT2	O-mannose disorders, Walker-Warburg syndrome	Vajsar and Schachter (2006)

several neurodegenerative diseases, however, in this case it is not yet clear if the aberrations are a cause or a consequence of disease (Caracci et al., 2019).

## Disease genes associated with GA structure, integrity and functional maintenance

The structural integrity of the GA and its organization in stacks are maintained thanks to proteins such as golgin-45, GM130 and Giantin, GRASPs and the small GTPases RABs, ARFs, ARLs and TRAPPs (see Table 1). The TRAPP complex activates RAB1 which in turn recruits golgins and GM130 at the cis-Golgi level, to ensure vesicle tethering; furthermore, TRAPPC9 is also involved in the association between COPII-coated vesicles and dynein for the movement of vesicles on the cytoskeleton. Loss of function mutations of TRAPPC9 have been identified in Autosomal recessive mental retardation 13 (MRT13), that shows as a clinical manifestation moderate to severe post-natal onset microcephaly (POM), thinning of the corpus callosum, a peculiar facial appearance, hypotonia and obesity (Mochida et al., 2009). TRAPPC12 mutations are associated with progressive childhood encephalopathy, progressive microcephaly and developmental defects. Another example is represented by Takenouchi-Kosaki syndrome, caused by mutations in the GTPase CDC42 which regulates bidirectional Golgi transport, cargo sorting and COPI formation; affected patients show a wide range of phenotypes, including ID, POM or congenital microcephaly (Rasika et al., 2018). Recent work showed the relevance of LGALS3BP in the generation and positioning of apical and basal NPCs (Kyrousi et al., 2021). LGALS3BP a cancer biomarker, is a galectin 3 binding protein, a secreted protein that interacts in the extracellular matrix with integrins, fibronectins and other components. Such example provides further evidence that the trafficking pathway, of which the GA is one of the central players, can influence brain development in multiple ways, affecting cellular components such as receptors, as well as the extracellular milieu (i.e., ECM components and interacting factors, secreted signals, etc.). Of note, receptors and ECM components are typically highly glycosylated proteins, suggesting the possibility that the change in the glycosylation state of these components might be one of the pathophysiological mechanisms underlying neurological manifestations.

## Disease genes associated with the GA glycosylation machinery

Though several diseases have been found to be associated with GA secretory and trafficking properties, we'd like to focus on one specific group of rare diseases called congenital disorders of glycosylation (CDGs). CDGs are a group of rare diseases associated with defects in glycosylation and aberrations on the ER and GA-trafficking pathways leading to (Jaeken and Casaer, 1997; Matthijs et al., 1997; Jaeken and Matthijs, 2001; Grunewald, 2002; Freeze and Ng, 2011; Freeze et al., 2015; Chang et al., 2018; Linders et al., 2020; Paprocka et al., 2021). CDGs are typically due to either mutations in ER and GA structural components or in ER and GA glycosylation enzymes. In the latter case traffic is indirectly affected most likely because of the activation of glycosylation quality check and/or because of defective protein folding (see also the section on UPR).

N-glycosylation associated CDGs, that are easier to identify, can be subdivided in Type I, caused by defects in the association of the first oligosaccharides to the lipid anchor at the level of the ER or in the cytoplasm; Type II CDGs are instead associated with defects at the level of the ER or Golgi in the glycosylation process or on the remodeling of N-glycans. Though CDGs affect usually different organs of the body, the most severe effects are quite often noticed in the

central nervous system at birth, probably because of the relevance of trafficking in neurodevelopment. This observation might not come to a surprise, as both neurons and progenitors are highly polarized cells, relying on heavy supply of membrane components, a feature that can make them particularly sensitive to any perturbation of the secretory pathway.

Severe congenital malformations associated with CDGs include microcephaly, macrocephaly, ventriculomegaly/hydrocephalus, myelination disorders, corpus callosum anomalies and brain atrophy (Paprocka et al., 2021) (see Table 1). On the contrary O-linked CDGs, conditions that affect secreted protein, are often associated with neuronal migration defects, as illustrated by muscular dystrophy-dystroglycanopathy (MDDG) syndrome (Nguyen et al., 2013). This could suggest that neuronal migration is dependent on accurate extracellular matrix deposition; on the other hand, plasma membrane-bound glycans seem to affect intrinsic transcriptional programs, thereby influencing cell identity probably because most membrane glycans are receptors involved in signaling pathways.

Indeed, defects on structural proteins of the ER or of the GA impair the whole trafficking pathway, resulting in aberrations in how and where enzymes are partitioned. Yet another way to perturb the glycosylation process is through alteration of the sugar supply or directly of the enzymes involved in glycosylation. Biosynthesis of N-glycans starts in the ER, where the family of ALG enzymes sequentially add sugar moieties to dolichol phosphate (Dol-P). Dol-P is synthesized from GDP-Mannose by the multi subunit complex DPM (Dol-P-Man) (Lauc and Trbojević-Akmačić, 2021). Consistently, microcephaly and neurodevelopmental defects are also present in CDG patients with mutations on DPM2, ALG11, SLC35A, ALG1 and ALG3. SLC35A2 belongs to the SLC35A family of sugar transporters and mutations in the X-linked UDP-galactose transporter gene leads to CDGs as they cause defective galactosylation of glycoconjugates in GA (Quelhas et al., 2021). ALG1, 3 and 11 enzymes are a b1,4 mannosyltransferase, a1,3 mannosyltransferase and an asparagine linked glycosylation protein 11 respectively, and as mentioned they are involved in the glycosylation process at the ER level (Rasika et al., 2018; Paprocka et al., 2021).

Along the glycosylation pathway, N-glycans are first transferred to the Asn residue of a protein by OST (oligosaccharyl-transferase) and then enter the GA, where further remodeling of the sugar chain is operated by mannosidase and/or fucosyltransferases (i.e., FUT). For example, mutations in the MGAT2 gene, that encodes for an acetylglucosaminyltransferase, is associated in CDG type II with neurological defects and hydrocephalus (Rasika et al., 2018). Cerebellar defects are instead observed related to mutations to another GA enzyme, INPP5E (Rasika et al., 2018). Ng et al. (2018) described three unrelated children with FUT8 mutations associated with growth and developmental retardation, neurological impairments and respiratory complications among the clinical manifestations.

At the level of GA complex-type glycans are formed. N-glycans can undergo further modification via addition of fucose, sialic acid, sulfate residues that increase the glycans' complexity (Lauc and Trbojević-Akmačić, 2021). Thus, disrupting GA at the structural or functional level can lead to several different outcomes that translate in different clinical manifestations of CDG.

Alternatively, the O-glycosylation pathway can happen in the GA, through a different set of glycosyltransferases (i.e., POMT1,2) (Vajsar

and Schachter, 2006) that allows the addition of sugars to the serine or threonine of molecules that are mainly destined to the extracellular environment. POMT1 and POMT2 mutations have been observed in patients with muscular dystrophy and intellectual disability. The number of congenital disorders with neurological manifestations classified as CDGs is steadily increasing in the last years, clearly highlighting the relevant connections between the homeostasis of trafficking pathway and neurodevelopment. Of note, a precise mechanistic explanation of how traffic and associated glycosylation affect neural stem cell behavior and in turn brain development is still lacking.

We think this class of diseases will provide an excellent opportunity for researchers to dig further into the deep secrets of the trafficking and Golgi dynamics in neurons and in neural progenitors where the journey of the nervous system development starts.

## Concluding remarks

In this review we summarize what is known up to date about the role of trafficking and in particular of Golgi apparatus in neurodevelopment. First of all, we summarized the basics of neurodevelopment, introducing the relevant cell types that concur in defining the neocortex in mammals. Lot of work has been done in unraveling the pathways underlying trafficking in neurons, but lot has still to be done in the context of neural progenitors and neurodevelopment. There is no doubt that research done on neurons provide a helpful access route to studies on NPCs, in particular on apical progenitors, as they (very much like neurons) are a case of extreme subcellular and architectural polarization and asymmetry. A question still left unanswered is the (possible) relation between cell identity and the Golgi complex, along with GA-dependent glycosylation, in light of the peculiarities of GA organization, localization and dynamics in APs. The occurrence of diseases, such as CDGs, where alterations in glycosylation are paralleled by strong neurodevelopmental manifestations, provide a real-life example of the functional link between the trafficking and glycosylation machinery and neurodevelopment. By leveraging CDG's genetics researchers might hope to unravel the basic principles linking sugar modifications with NPC behavior and brain development in health and disease. The existence of a second route for protein and lipid glycosylation, could direct future research to unravel yet unknown functions of trafficking organelles in different processes, including regulation of cell polarity cues in the context of neurodevelopment.

In a broader perspective, given that the heterogeneity and specificity of the sugar components of the added oligosaccharide chain make glycosylation highly combinatorial, it would be interesting to understand if a sugar-code exists, and if so, how it is exploited during brain development and evolution to affect and influence fate choice and cell identity. In this context is worth remembering that also lipids can be glycosylated, further increasing the level of complexity potentially reached by the sugar-code. A relevant step in this direction has been recently made by Lee et al. (2020) by showing that the glycome signature diverge spatially and temporally in mouse and human brain samples.



The advent of new techniques for lineage tracing and glycan analysis, along with the possibility to tightly control cell polarity and microenvironment using microfabrication, will certainly increase access and interest to this research field. At the same time, when considering pathological conditions, the possibility to use patient derived iPSC to grow brain organoids and organs on chip, will help recapitulating *in vitro* what happens *in vivo*, opening new avenues in our understanding of physiological processes and opening up, in future, to therapeutical interventions.

## Author contributions

All authors listed have made a substantial, direct, and intellectual contribution to the work and approved it for publication.

## Acknowledgments

The authors thank Salma Amin, Nereo Kalebic, Valentina Rava and Giulia Visani for discussion and constructive criticism on the manuscript. Martina Polenghi is a PhD student within the European School of Molecular Medicine (SEMM).

## References

- Appenzeller-Herzog, C., and Hauri, H.-P. (2006). The ER-Golgi intermediate compartment (ERGIC): in search of its identity and function. *J. Cell Sci.* 119, 2173–2183. doi: 10.1242/jcs.03019
- Arai, Y., and Taverna, E. (2017). Neural progenitor cell polarity and cortical development. *Front. Cell. Neurosci.* 11:384. doi: 10.3389/fncel.2017.00384
- Ayala, I., and Colanzi, A. (2017). Mitotic inheritance of the Golgi complex and its role in cell division: mitotic inheritance of the Golgi complex. *Biol. Cell.* 109, 364–374. doi: 10.1111/boc.201700032
- Banworth, M. J., and Li, G. (2018). Consequences of Rab GTPase dysfunction in genetic or acquired human diseases. *Small GTPases* 9, 158–181. doi: 10.1080/21541248.2017.1397833
- Barone, R., Aiello, C., Race, V., Morava, E., Foulquier, F., Riemersma, M., et al. (2012). DPM2-CDG: a muscular dystrophy-dystroglycanopathy syndrome with severe epilepsy. *Ann. Neurol.* 72, 550–558. doi: 10.1002/ana.23632
- Bentley, M., and Banker, G. (2016). The cellular mechanisms that maintain neuronal polarity. *Nat. Rev. Neurosci.* 17, 611–622. doi: 10.1038/nrn.2016.100
- Bin Imtiaz, M. K., Royall, L. N., Gonzalez-Bohorquez, D., and Jessberger, S. (2022). Human neural progenitors establish a diffusion barrier in the endoplasmic reticulum membrane during cell division. *Development* 149:dev200613. doi: 10.1242/dev.200613
- Borrell, V., and Götz, M. (2014). Role of radial glial cells in cerebral cortex folding. *Curr. Opin. Neurobiol.* 27, 39–46. doi: 10.1016/j.conb.2014.02.007
- Borrell, V., and Reillo, I. (2012). Emerging roles of neural stem cells in cerebral cortex development and evolution. *Dev. Neurobiol.* 72, 955–971. doi: 10.1002/dneu.22013
- Bowen, A. B., Bourke, A. M., Hiester, B. G., Hanus, C., and Kennedy, M. J. (2017). Golgi-independent secretory trafficking through recycling endosomes in neuronal dendrites and spines. *eLife* 6:e27362. doi: 10.7554/eLife.27362
- Brault, J.-B., Bardin, S., Lampic, M., Carpentieri, J. A., Coquand, L., Penisson, M., et al. (2022). RAB6 and dynein drive post-Golgi apical transport to prevent neuronal progenitor delamination. *EMBO Rep.* 23:e54605. doi: 10.15252/embr.202254605
- Breuza, L., Halbeisen, R., Jenö, P., Otte, S., Barlowe, C., Hong, W., et al. (2004). Proteomics of endoplasmic reticulum-Golgi intermediate compartment (ERGIC) membranes from brefeldin A-treated HepG2 cells identifies ERGIC-32, a new cycling protein that interacts with human Erv46. *J. Biol. Chem.* 279, 47242–47253. doi: 10.1074/jbc.M406644200
- Britt, D. J., Fariás, G. G., Guardia, C. M., and Bonifacio, J. S. (2016). Mechanisms of polarized organelle distribution in neurons. *Front. Cell. Neurosci.* 10:88. doi: 10.3389/fncel.2016.00088
- Caracci, M. O., Fuentealba, L. M., and Marzolo, M.-P. (2019). Golgi complex dynamics and its implication in prevalent neurological disorders. *Front. Cell Dev. Biol.* 7:75. doi: 10.3389/fcell.2019.00075
- Carpentieri, J. A., Di Cicco, A., Lampic, M., Andreau, D., Del Maestro, L., El Marjou, F., et al. (2022). Endosomal trafficking defects alter neural progenitor proliferation and cause microcephaly. *Nat. Commun.* 13:16. doi: 10.1038/s41467-021-27705-7
- Casey, C. A., Bhat, G., Holzapfel, M. S., and Petrosyan, A. (2016). Study of ethanol-induced Golgi disorganization reveals the potential mechanism of alcohol-impaired N-glycosylation. *Alcohol. Clin. Exp. Res.* 40, 2573–2590. doi: 10.1111/acer.13247
- Chang, I. J., He, M., and Lam, C. T. (2018). Congenital disorders of glycosylation. *Ann. Transl. Med.* 6:477. doi: 10.21037/atm.2018.10.45
- Chao, J. T., Wong, A. K. O., Tavassoli, S., Young, B. P., Chruscicki, A., Fang, N. N., et al. (2014). Polarization of the endoplasmic reticulum by ER-septin tethering. *Cells* 158, 620–632. doi: 10.1016/j.cell.2014.06.033
- Climer, L. K., Dobretsov, M., and Lupashin, V. (2015). Defects in the COG complex and COG-related trafficking regulators affect neuronal Golgi function. *Front. Neurosci.* 9:405. doi: 10.3389/fnins.2015.00405
- Condon, K. H., Ho, J., Robinson, C. G., Hanus, C., and Ehlers, M. D. (2013). The Angelman syndrome protein Ube3a/E6AP is required for Golgi acidification and surface protein sialylation. *J. Neurosci.* 33, 3799–3814. doi: 10.1523/JNEUROSCI.1930-11.2013
- D'Souza, Z., Sumya, F. T., Khakurel, A., and Lupashin, V. (2021). Getting sugar coating right! The role of the Golgi trafficking machinery in glycosylation. *Cells* 10:3275. doi: 10.3390/cells10123275
- Dalton, S. (2013). G1 compartmentalization and cell fate coordination. *Cells* 155, 13–14. doi: 10.1016/j.cell.2013.09.015
- Dalton, S. (2015). Linking the cell cycle to cell fate decisions. *Trends Cell Biol.* 25, 592–600. doi: 10.1016/j.tcb.2015.07.007
- de los Angeles Juricic Urzúa, M., Rojas, J. G., Correa, A. C., Cerda, M., Gründler, S. H., and González-Silva, C. (2021). The dendritic ERGIC: microtubule and actin cytoskeletons mediate stop-and-go movement of mobile carriers between stable structures. *Cell Biol.* doi: 10.1101/2021.03.31.437880
- Diaz, J., Gérard, X., Emerit, M.-B., Areias, J., Geny, D., Dégardin, J., et al. (2020). YIF1B mutations cause a post-natal neurodevelopmental syndrome associated with Golgi and primary cilium alterations. *Brain* 143, 2911–2928. doi: 10.1093/brain/awaa235
- Dinter, A., and Berger, E. G. (1998). Golgi-disturbing agents. *Histochem. Cell Biol.* 109, 571–590. doi: 10.1007/s004180050256
- Farolfi, M., Cechova, A., Ondruskova, N., Zidkova, J., Kousal, B., Hansikova, H., et al. (2021). ALG3-CDG: a patient with novel variants and review of the genetic and ophthalmic findings. *BMC Ophthalmol.* 21:249. doi: 10.1186/s12886-021-02013-2
- Fietz, S. A., and Huttner, W. B. (2011). Cortical progenitor expansion, self-renewal and neurogenesis—a polarized perspective. *Curr. Opin. Neurobiol.* 21, 23–35. doi: 10.1016/j.conb.2010.10.002

## Conflict of interest

The authors declare that the research was conducted in the absence of any commercial or financial relationships that could be construed as a potential conflict of interest.

## Publisher's note

All claims expressed in this article are solely those of the authors and do not necessarily represent those of their affiliated organizations, or those of the publisher, the editors and the reviewers. Any product that may be evaluated in this article, or claim that may be made by its manufacturer, is not guaranteed or endorsed by the publisher.

## Supplementary material

The Supplementary material for this article can be found online at: <https://www.frontiersin.org/articles/10.3389/fnins.2023.1172016/full#supplementary-material>

- Fietz, S. A., Kelava, I., Vogt, J., Wilsch-Bräuninger, M., Stenzel, D., Fish, J. L., et al. (2010). OSVZ progenitors of human and ferret neocortex are epithelial-like and expand by integrin signaling. *Nat. Neurosci.* 13, 690–699. doi: 10.1038/nn.2553
- Fish, J. L., Dehay, C., Kennedy, H., and Huttner, W. B. (2008). Making bigger brains—the evolution of neural-progenitor-cell division. *J. Cell Sci.* 121, 2783–2793. doi: 10.1242/jcs.023465
- Florio, M., and Huttner, W. B. (2014). Neural progenitors, neurogenesis and the evolution of the neocortex. *Development* 141, 2182–2194. doi: 10.1242/dev.090571
- Flynn, K., Feben, C., Lamola, L., Carstens, N., Krause, A., Lombard, Z., et al. (2021). Ending a diagnostic odyssey—the first case of Takenouchi-Kosaki syndrome in an African patient. *Clin. Case Rep.* 9, 2144–2148. doi: 10.1002/ccr3.3966
- Freeze, H. H., Chong, J. X., Bamshad, M. J., and Bobby, G. N. (2014). Solving glycosylation disorders: fundamental approaches reveal complicated pathways. *Am. J. Hum. Genet.* 94, 161–175. doi: 10.1016/j.ajhg.2013.10.024
- Freeze, H. H., Eklund, E. A., Ng, B. G., and Patterson, M. C. (2015). Neurological aspects of human glycosylation disorders. *Annu. Rev. Neurosci.* 38, 105–125. doi: 10.1146/annurev-neuro-071714-034019
- Freeze, H. H., and Ng, B. G. (2011). Golgi glycosylation and human inherited diseases. *Cold Spring Harb. Perspect. Biol.* 3:a005371. doi: 10.1101/cshperspect.a005371
- Fujii, S., Kurokawa, K., Tago, T., Inaba, R., Takiguchi, A., Nakano, A., et al. (2020). Sec71 separates Golgi stacks in *Drosophila* S2 Cells. *J. Cell Sci.* jcs.245571. doi: 10.1242/jcs.245571
- Galea, G., Kuodyte, K., Khan, M. M., Thul, P., Neumann, B., Lundberg, E., et al. (2022). The Golgi complex is a regulatory hub for homologous recombination-mediated DNA repair. *Cell Biol.* doi: 10.1101/2022.10.17.512236
- Gavilan, M. P., Gandolfo, P., Balestra, F. R., Arias, F., Bornens, M., and Rios, R. M. (2018). The dual role of the centrosome in organizing the microtubule network in interphase. *EMBO Rep.* 19:e45942. doi: 10.15252/embr.201845942
- Ge, X., Gong, H., Dumas, K., Litwin, J., Phillips, J. J., Waisfisz, Q., et al. (2016). Missense-depleted regions in population exomes implicate ras superfamily nucleotide-binding protein alteration in patients with brain malformation. *NPJ Genom. Med.* 1:16036. doi: 10.1038/npgenmed.2016.36
- Gosavi, P., and Gleeson, P. A. (2017). The function of the Golgi ribbon structure—an enduring mystery unfolds! *BioEssays* 39:1700063. doi: 10.1002/bies.201700063
- Götz, M., and Huttner, W. B. (2005). The cell biology of neurogenesis. *Nat. Rev. Mol. Cell Biol.* 6, 777–788. doi: 10.1038/nrm1739
- Grunewald, S. (2002). Congenital disorders of glycosylation: a review. *Pediatr. Res.* 52, 618–624. doi: 10.1203/01.PDR.0000031921.02259.55
- Guet, D., Mandal, K., Pinot, M., Hoffmann, J., Abidine, Y., Sigaut, W., et al. (2014). Mechanical role of actin dynamics in the rheology of the Golgi complex and in Golgi-associated trafficking events. *Curr. Biol.* 24, 1700–1711. doi: 10.1016/j.cub.2014.06.048
- Haanpää, M. K., Ng, B. G., Gallant, N. M., Singh, K. E., Brown, C., Kimonis, V., et al. (2019). ALG11-CDG syndrome: expanding the phenotype. *Am. J. Med. Genet. A* 179, 498–502. doi: 10.1002/ajmg.a.61046
- Hanus, C., Geptin, H., Tushev, G., Garg, S., Alvarez-Castelao, B., Sambandan, S., et al. (2016). Unconventional secretory processing diversifies neuronal ion channel properties. *eLife* 5:e20609. doi: 10.7554/eLife.20609
- Haynes, C. M., Titus, E. A., and Cooper, A. A. (2004). Degradation of misfolded proteins prevents ER-derived oxidative stress and cell death. *Mol. Cell* 15, 767–776. doi: 10.1016/j.molcel.2004.08.025
- Jaeken, J., and Casaer, P. (1997). Carbohydrate-deficient glycoconjugate (CDG) syndromes: a new chapter of neuropaediatrics. *Eur. J. Paediatr. Neurol.* 1, 61–66. doi: 10.1016/s1090-3798(97)80064-5
- Jaeken, J., and Matthijs, G. (2001). Congenital disorders of glycosylation.
- Janesick, A., Stephanie Cherie, W., and Blumberg, B. (2015). Retinoic acid signaling and neuronal differentiation. *Cell. Mol. Life Sci.* 72, 1559–1576. doi: 10.1007/s00018-014-1815-9
- Ji, C. (2012). Mechanisms of alcohol-induced endoplasmic reticulum stress and organ injuries. *Biochem. Res. Int.* 2012, 1–12. doi: 10.1155/2012/216450
- Kalebic, N., Gilardi, C., Stepien, B., Wilsch-Bräuninger, M., Long, K. R., Namba, T., et al. (2019). Neocortical expansion due to increased proliferation of basal progenitors is linked to changes in their morphology. *Cell Stem Cell* 24, 535–550.e9. doi: 10.1016/j.stem.2019.02.017
- Kalebic, N., and Huttner, W. B. (2020). Basal progenitor morphology and neocortex evolution. *Trends Neurosci.* 43, 843–853. doi: 10.1016/j.tins.2020.07.009
- Kalebic, N., and Namba, T. (2021). Inheritance and flexibility of cell polarity: a clue for understanding human brain development and evolution. *Development* 148:dev199417. doi: 10.1242/dev.199417
- Kawaguchi, A. (2021). Neuronal delamination and outer radial glia generation in neocortical development. *Front. Cell Dev. Biol.* 8:623573. doi: 10.3389/fcell.2020.623573
- Kemal, S., Richardson, H. S., Dyne, E. D., and Meng-meng, F. (2022). ER and Golgi trafficking in axons, dendrites, and glial processes. *Curr. Opin. Cell Biol.* 78:102119. doi: 10.1016/j.ceb.2022.102119
- Koppers, M., and Farias, G. G. (2021). Organelle distribution in neurons: logistics behind polarized transport. *Curr. Opin. Cell Biol.* 71, 46–54. doi: 10.1016/j.ceb.2021.02.004
- Kosodo, Y., and Huttner, W. B. (2009). Basal process and cell divisions of neural progenitors in the developing brain: basal process of neural progenitors. *Develop. Growth Differ.* 51, 251–261. doi: 10.1111/j.1440-169X.2009.01101.x
- Kriegstein, A., and Alvarez-Buylla, A. (2009). The glial nature of embryonic and adult neural stem cells. *Annu. Rev. Neurosci.* 32, 149–184. doi: 10.1146/annurev-neuro.051508.135600
- Kyrousi, C., O'Neill, A. C., Brazovskaja, A., He, Z., Kielkowski, P., Coquand, L., et al. (2021). Extracellular LGALS3BP regulates neural progenitor position and relates to human cortical complexity. *Nat. Commun.* 12:6298. doi: 10.1038/s41467-021-26447-w
- Laguesse, S., Creppe, C., Nedialkova, D. D., Prévot, P.-P., Borgs, L., Huysseune, S., et al. (2015). A dynamic unfolded protein response contributes to the control of cortical neurogenesis. *Dev. Cell* 35, 553–567. doi: 10.1016/j.devcel.2015.11.005
- Lauc, G., and Trbojević-Akmačić, I. (2021). *The role of glycosylation in health and disease: advances in experimental medicine and biology*. Cham: Springer.
- Lee, J., Ha, S., Kim, M., Kim, S.-W., Yun, J., Ozcan, S., et al. (2020). Spatial and temporal diversity of glycome expression in mammalian brain. *Proc. Natl. Acad. Sci. U.S.A.* 117, 28743–28753. doi: 10.1073/pnas.2014207117
- Lehtinen, M. K., Zappaterra, M. W., Chen, X., Yang, Y. J., Hill, A. D., Lun, M., et al. (2011). The cerebrospinal fluid provides a proliferative niche for neural progenitor cells. *Neuron* 69, 893–905. doi: 10.1016/j.neuron.2011.01.023
- Leone, D. P., Relvas, J. B., Campos, L. S., Hemmi, S., Brakebusch, C., Fässler, R., et al. (2005). Regulation of neural progenitor proliferation and survival by B1 integrins. *J. Cell Sci.* 118, 2589–2599. doi: 10.1242/jcs.02396
- Linders, P. T. A., Peters, E., ter Beest, M., Lefeber, D. J., and van den Bogaart, G. (2020). Sugary logistics gone wrong: membrane trafficking and congenital disorders of glycosylation. *Int. J. Mol. Sci.* 21:4654. doi: 10.3390/ijms21134654
- Long, K. R., and Huttner, W. B. (2019). How the extracellular matrix shapes neural development. *Open Biol.* 9:180216. doi: 10.1098/rsob.180216
- Long, K. R., and Huttner, W. B. (2022). The role of the extracellular matrix in neural progenitor cell proliferation and cortical folding during human neocortex development. *Front. Cell. Neurosci.* 15:804649. doi: 10.3389/fncel.2021.804649
- Long, K., Moss, L., Laursen, L., Boulter, L., and French-Constant, C. (2016). Integrin signalling regulates the expansion of neuroepithelial progenitors and neurogenesis via Wnt7a and decorin. *Nat. Commun.* 7:10354. doi: 10.1038/ncomms10354
- Macara, I. G., and Mili, S. (2008). Polarity and differential inheritance—universal attributes of life? *Cells* 135, 801–812. doi: 10.1016/j.cell.2008.11.006
- Marin-Valencia, I., Novarino, G., Johansen, A., Rosti, B., Issa, M. Y., Musaev, D., et al. (2018). A homozygous founder mutation in TRAPPC6B associates with a neurodevelopmental disorder characterised by microcephaly, epilepsy and autistic features. *J. Med. Genet.* 55, 48–54. doi: 10.1136/jmedgenet-2017-104627
- Matthijs, G., Schollen, E., Pardon, E., Veiga-Da-Cunha, M., Jaeken, J., Cassiman, J.-J., et al. (1997). Mutations in PMM2, a phosphomannomutase gene on chromosome 16p13 in carbohydrate-deficient glycoprotein Type I syndrome (Jaeken syndrome). *Nat. Genet.* 16, 88–92. doi: 10.1038/ng0597-88
- Milev, M. P., Grout, M. E., Saint-Dic, D., Cheng, Y.-H. H., Glass, I. A., Hale, C. J., et al. (2017). Mutations in TRAPPC12 manifest in progressive childhood encephalopathy and Golgi dysfunction. *Am. J. Hum. Genet.* 101, 291–299. doi: 10.1016/j.ajhg.2017.07.006
- Mir, A., Kaufman, L., Noor, A., Motazacker, M. M., Jamil, T., Azam, M., et al. (2009). Identification of mutations in TRAPPC9, which encodes the NIK- and IKK- $\beta$ -binding protein, in nonsyndromic autosomal-recessive mental retardation. *Am. J. Hum. Genet.* 85, 909–915. doi: 10.1016/j.ajhg.2009.11.009
- Miyata, S., Mizuno, T., Koyama, Y., Katayama, T., and Tohyama, M. (2013). The endoplasmic reticulum-resident chaperone heat shock protein 47 protects the Golgi Apparatus from the effects of O-glycosylation inhibition. *PLoS One* 8:e69732. doi: 10.1371/journal.pone.0069732
- Mochida, G. H., Mahajnah, M., Hill, A. D., Basel-Vanagaite, L., Danielle Gleason, R., Hill, S., et al. (2009). A truncating mutation of TRAPPC9 Is Associated with autosomal-recessive intellectual disability and postnatal microcephaly. *Am. J. Hum. Genet.* 85, 897–902. doi: 10.1016/j.ajhg.2009.10.027
- Namba, T., and Huttner, W. B. (2017). Neural progenitor cells and their role in the development and evolutionary expansion of the neocortex: neural progenitor cells' role in the development and evolutionary expansion of the neocortex. *Wiley Interdiscip. Rev. Dev. Biol.* 6:e256. doi: 10.1002/wdev.256
- Ng, B. G., Buckingham, K. J., Raymond, K., Kircher, M., Turner, E. H., He, M., et al. (2013). Mosaicism of the UDP-galactose transporter SLG35A2 causes a congenital disorder of glycosylation. *Am. J. Hum. Genet.* 92, 632–636. doi: 10.1016/j.ajhg.2013.03.012
- Ng, B. G., Gege, X., Chandy, N., Steyermark, J., Shinde, D. N., Radtke, K., et al. (2018). Biallelic mutations in FUT8 cause a congenital disorder of glycosylation with defective fucosylation. *Am. J. Hum. Genet.* 102, 188–195. doi: 10.1016/j.ajhg.2017.12.009
- Ng, B. G., Shiryayev, S. A., Rymen, D., Eklund, E. A., Raymond, K., Kircher, M., et al. (2016). ALG1-CDG: clinical and molecular characterization of 39 unreported patients. *Hum. Mutat.* 37, 653–660. doi: 10.1002/humu.22983

- Nguyen, H., Ostendorf, A. P., Satz, J. S., Westra, S., Ross-Barta, S. E., Campbell, K. P., et al. (2013). Glial scaffold required for cerebellar granule cell migration is dependent on dystroglycan function as a receptor for basement membrane proteins. *Acta Neuropathol. Commun.* 1:58. doi: 10.1186/2051-5960-1-58
- Nickel, W., and Rabouille, C. (2018). Unconventional protein secretion: diversity and consensus. *Semin. Cell Dev. Biol.* 83, 1–2. doi: 10.1016/j.semcdb.2018.03.007
- Ninagawa, S., George, G., and Mori, K. (2021). Mechanisms of productive folding and endoplasmic reticulum-associated degradation of glycoproteins and non-glycoproteins. *Biochim. Biophys.* 2021:129812. doi: 10.1016/j.bbagen.2020.129812
- Noctor, S. C., Martínez-Cerdeño, V., Ivic, L., and Kriegstein, A. R. (2004). Cortical neurons arise in symmetric and asymmetric division zones and migrate through specific phases. *Nat. Neurosci.* 7, 136–144. doi: 10.1038/nn1172
- Ori-McKenney, K. M., Jan, L. Y., and Jan, Y. N. (2012). Golgi outposts shape dendrite morphology by functioning as sites of centrosomal microtubule nucleation in neurons. *Neuron* 76, 921–930. doi: 10.1016/j.neuron.2012.10.008
- Paprocka, J., Jezela-Stanek, A., Tytki-Szymańska, A., and Grunewald, S. (2021). Congenital disorders of glycosylation from a neurological perspective. *Brain Sci.* 11:88. doi: 10.3390/brainsci11010088
- Paridaen, J. T. M. L., and Huttner, W. B. (2014). Neurogenesis during development of the vertebrate central nervous system. *EMBO Rep.* 15, 351–364. doi: 10.1002/embr.201438447
- Paridaen, J. T. M. L., Wilsch-Bräuninger, M., and Huttner, W. B. (2013). Asymmetric inheritance of centrosome-associated primary cilium membrane directs ciliogenesis after cell division. *Cells* 155, 333–344. doi: 10.1016/j.cell.2013.08.060
- Passemard, S., Perez, F., Gressens, P., and El Ghouzzi, V. (2019). Endoplasmic reticulum and Golgi stress in microcephaly. *Cell Stress* 3, 369–384. doi: 10.15698/cst2019.12.206
- Pinheiro, D., and Heisenberg, C.-P. (2020). Zebrafish gastrulation: putting fate in motion. *Curr. Top. Dev. Biol.* 136, 343–375. doi: 10.1016/bs.ctdb.2019.10.009
- Quelhas, D., Correia, J., Jaeken, J., Azevedo, L., Lopes-Marques, M., Bandeira, A., et al. (2021). SLC35A2-CDG: novel variant and review. *Mol. Genet. Metab. Rep.* 26:100717. doi: 10.1016/j.ymgmr.2021.100717
- Rabouille, C., Malhotra, V., and Nickel, W. (2012). Diversity in unconventional protein secretion. *J. Cell Sci.* 125, 5251–5255. doi: 10.1242/jcs.103630
- Rakic, P. (1995). A small step for the cell, a giant leap for mankind: a hypothesis of neocortical expansion during evolution. *Trends Neurosci.* 18, 383–388. doi: 10.1016/0166-2236(95)93934-P
- Rasika, S., Passemard, S., Verloes, A., Gressens, P., and El Ghouzzi, V. (2018). Golgiopathies in neurodevelopment: a new view of old defects. *Dev. Neurosci.* 40, 396–416. doi: 10.1159/000497035
- Reily, C., Stewart, T. J., Renfrow, M. B., and Novak, J. (2019). Glycosylation in health and disease. *Nat. Rev. Nephrol.* 15, 346–366. doi: 10.1038/s41581-019-0129-4
- Sakamoto, M., Sasaki, K., Sugie, A., Nitta, Y., Kimura, T., Gürsoy, S., et al. (2021). De Novo ARF3 variants cause neurodevelopmental disorder with brain abnormality. *Hum. Mol. Genet.* 31, 69–81. doi: 10.1093/hmg/ddab224
- Sasaki, K., Komori, R., Taniguchi, M., Shimaoka, A., Midori, S., Yamamoto, M., et al. (2019). PGSE is a novel enhancer regulating the proteoglycan pathway of the mammalian Golgi stress response. *Cell Struct. Funct.* 44, 1–19. doi: 10.1247/csf.18031
- Seifert, W., Kühnisch, J., Maritzen, T., Horn, D., Hauke, V., and Hennies, H. C. (2011). Cohen syndrome-associated protein, COH1, is a novel, giant Golgi matrix protein required for Golgi integrity. *J. Biol. Chem.* 286, 37665–37675. doi: 10.1074/jbc.M111.267971
- Shamseldin, H. E., Bennett, A. H., Alfaridhi, M., Gupta, V., and Alkuray, F. S. (2016). GOLGA2, encoding a master regulator of Golgi Apparatus, is mutated in a patient with a neuromuscular disorder. *Hum. Genet.* 135, 245–251. doi: 10.1007/s00439-015-1632-8
- Siegenthaler, J. A., Ashique, A. M., Zarbalis, K., Patterson, K. P., Hecht, J. H., Kane, M. A., et al. (2009). Retinoic acid from the meninges regulates cortical neuron generation. *Cells* 139, 597–609. doi: 10.1016/j.cell.2009.10.004
- Silvestre, D. C., Maccioni, H. J. F., and Caputto, B. L. (2009). Content of endoplasmic reticulum and Golgi complex membranes positively correlates with the proliferative status of brain cells. *J. Neurosci. Res.* 87, 857–865. doi: 10.1002/jnr.21915
- Spoelgen, R., Hammes, A., Anzenberger, U., Zechner, D., Andersen, O. M., Jerchow, B., et al. (2005). LRP2/megalin is required for patterning of the ventral telencephalon. *Development* 132, 405–414. doi: 10.1242/dev.01580
- Stenzel, D., and Huttner, W. B. (2013). Role of maternal thyroid hormones in the developing neocortex and during human evolution. *Front. Neuroanat.* 7:19. doi: 10.3389/fnana.2013.00019
- Stenzel, D., Wilsch-Bräuninger, M., Wong, F. K., Heuer, H., and Huttner, W. B. (2014). Integrin Avβ3 and thyroid hormones promote expansion of progenitors in embryonic neocortex. *Development* 141:1419. doi: 10.1242/dev.108902
- Sütterlin, C., and Colanzi, A. (2010). The Golgi and the centrosome: building a functional partnership. *J. Cell Biol.* 188, 621–628. doi: 10.1083/jcb.200910001
- Taverna, E., Götz, M., and Huttner, W. B. (2014). The cell biology of neurogenesis: toward an understanding of the development and evolution of the neocortex. *Annu. Rev. Cell Dev. Biol.* 30, 465–502. doi: 10.1146/annurev-cellbio-101011-155801
- Taverna, E., and Huttner, W. B. (2003). Role of integrins in the development of the cerebral cortex. *Cereb. Cortex* 13, 219–224. doi: 10.1093/cercor/13.3.219
- Taverna, E., and Huttner, W. B. (2010). Neural progenitor nuclei in motion. *Neuron* 67, 906–914. doi: 10.1016/j.neuron.2010.08.027
- Taverna, E., and Huttner, W. B. (2019). “The Golgi apparatus in polarized neuroepithelial stem cells and their progeny: canonical and noncanonical features” in *The Golgi apparatus and centriole: results and problems in cell differentiation*. ed. M. Kloc (Cham: Springer), 359–375.
- Taverna, E., Mora-Bermúdez, F., Strzyz, P. J., Florio, M., Icha, J., Haffner, C., et al. (2016). Non-canonical features of the Golgi apparatus in bipolar epithelial neural stem cells. *Sci. Rep.* 6:21206. doi: 10.1038/srep21206
- Tomás, M., Marín, M. P., Martínez-Alonso, E., Esteban-Pretel, G., Díaz-Ruiz, A., Vázquez-Martínez, R., et al. (2012). Alcohol induces Golgi fragmentation in differentiated PC12 cells by deregulating Rab1-dependent ER-to-Golgi transport. *Histochem. Cell Biol.* 138, 489–501. doi: 10.1007/s00418-012-0970-z
- Vajsar, J., and Schachter, H. (2006). Walker-Warburg syndrome. *Orphanet J. Rare Dis.* 1:29. doi: 10.1186/1750-1172-1-29
- Wang, L., Hou, S., and Han, Y.-G. (2016). Hedgehog signaling promotes basal progenitor expansion and the growth and folding of the neocortex. *Nat. Neurosci.* 19, 888–896. doi: 10.1038/nn.4307
- Wang, J.-N., and Ling, F. (2016). Zika virus infection and microcephaly: evidence for a causal link. *Int. J. Environ. Res. Public Health* 13:1031. doi: 10.3390/ijerph13101031
- Willnow, T. E., Hilpert, J., Armstrong, S. A., Rohlmann, A., Hammer, R. E., Burns, D. K., et al. (1996). Defective forebrain development in mice lacking Gp330/megalin. *Proc. Natl. Acad. Sci. U.S.A.* 93, 8460–8464. doi: 10.1073/pnas.93.16.8460
- Wilsch-Bräuninger, M., Peters, J., Paridaen, J. T. M. L., and Huttner, W. B. (2012). Basolateral rather than apical primary cilia on neuroepithelial cells committed to delamination. *Development* 139, 95–105. doi: 10.1242/dev.069294
- Witzgall, R. (2018). Golgi bypass of ciliary proteins. *Semin. Cell Dev. Biol.* 83, 51–58. doi: 10.1016/j.semcdb.2018.03.010
- Xie, Z., Hur, S. K., Zhao, L., Abrams, C. S., and Bankaitis, V. A. (2018). A Golgi lipid signaling pathway controls apical Golgi distribution and cell polarity during neurogenesis. *Dev. Cell* 44, 725–740.e4. doi: 10.1016/j.devcel.2018.02.025
- Xu, L., Zhou, Y., Ren, X., Chenlu, X., Ren, R., Yan, X., et al. (2022). Expanding the phenotypic and genotypic spectrum of ARFGEF1-related neurodevelopmental disorder. *Front. Mol. Neurosci.* 15:862096. doi: 10.3389/fnmol.2022.862096
- Yanagida, M., Miyoshi, R., Toyokuni, R., Zhu, Y., and Murakami, F. (2012). Dynamics of the leading process, nucleus, and Golgi apparatus of migrating cortical interneurons in living mouse embryos. *Proc. Natl. Acad. Sci. U.S.A.* 109, 16737–16742. doi: 10.1073/pnas.1209166109
- Zhang, Y. C., Zhou, Y., Yang, C. Z., and Xiong, D. S. (2009). A review of ERGIC-53: its structure, functions, regulation and relations with diseases. *Histol. Histopathol.* 24, 1193–1204. doi: 10.14670/HH-24.1193
- Zhou, Y., Atkins, J. B., Rompani, S. B., Bancescu, D. L., Petersen, P. H., Tang, H., et al. (2007). The mammalian Golgi regulates numb signaling in asymmetric cell division by releasing ACBD3 during mitosis. *Cells* 129, 163–178. doi: 10.1016/j.cell.2007.02.037
- Zhu, X., and Kaverina, I. (2013). Golgi as an MTOC: making microtubules for its own good. *Histochem. Cell Biol.* 140, 361–367. doi: 10.1007/s00418-013-1119-4

# Frontiers in Neuroscience

Provides a holistic understanding of brain  
function from genes to behavior

Part of the most cited neuroscience journal series  
which explores the brain - from the new eras  
of causation and anatomical neurosciences to  
neuroeconomics and neuroenergetics.

## Discover the latest Research Topics

See more →

### Frontiers

Avenue du Tribunal-Fédéral 34  
1005 Lausanne, Switzerland  
[frontiersin.org](https://frontiersin.org)

### Contact us

+41 (0)21 510 17 00  
[frontiersin.org/about/contact](https://frontiersin.org/about/contact)

